

Mechanistic Understanding of the Degradation Pathways of High-Value Organic Molecules

Jack Washington

Department of Pure and Applied Chemistry

University of Strathclyde/GlaxoSmithKline

PhD Thesis

2020

Author Declaration Form

This thesis is the result of the author's original research. It has been composed by the author and has not been previously submitted for examination which has led to the award of a degree.

The copyright of this thesis belongs to the author under the terms of the United Kingdom Copyright Acts as qualified by University of Strathclyde Regulation 3.50. Due acknowledgment must always be made of the use of any material contained in, or derived from, this thesis.

Signed:

Date:

Abstract

The chemistry of two classes of high value organic molecules has been explored through monitoring their degradation behaviours. Specifically, the degradation of *N,N,N*-trimethylanilinium salts and clavulanic acid has been examined systematically using a wide range of reaction monitoring techniques. Through understanding their respective degradation pathways, implications for *N,N,N*-trimethylanilinium salt use in synthetic organic chemistry, and the optimal manufacturing process of clavulanic acid have each been revealed.

Anilinium Salts in Synthesis

N,N,N-trimethylanilinium salts have been widely used as cross-coupling substrates, their application as methylating reagents is known but remains underexplored. A thorough mechanistic analysis herein delineates the factors that affect *N,N,N*-trimethylanilinium salt reactivity and describes resulting implications for both core synthetic use cases (methylation and cross-coupling). *N,N,N*-trimethylanilinium salts bearing nucleophilic halide counterions were shown to be less stable than those partnered with weakly coordinating anions. Regarding substituent effects, electron-deficient anilinium salts proved less stable than their electron-rich counterparts. Spectroscopic and thermal analyses provided evidence of *N,N,N*-trimethylanilinium iodide degradation to methyl iodide and the respective *N,N*-dimethylaniline. The methylating ability of a *N,N,N*-trimethylanilinium salt library was screened against a phenolic substrate and the scope of nucleophiles amenable to methylation was explored. Mechanistic experiments showed *N,N,N*-trimethylanilinium salts can act as a methyl iodide surrogate, react directly with nucleophiles, or partake in a solvent-assisted pathway.

Clavulanic Acid Production on the Manufacturing Scale

The degradation of the industrially and clinically important β -lactamase inhibitor clavulanic acid was explored in the context of its process-scale manufacture. A reliable method of monitoring clavulanic acid degradation with Reversed Phase HPLC in buffered aqueous solutions over the manufacturing-relevant pH range of 3-9 was developed. The most stable pH region for clavulanic acid was found to be between 5-

6. A pH profile was constructed which suggested different degradation mechanisms occur in high-pH and low-pH regimes. The effect of pH and temperature on the rate of clavulanic acid degradation was explored in samples from various points in the manufacturing process. The most stable pH for clavulanic acid was shown to vary at different stages of the process. A variety of spectroscopic techniques have been employed in the attempt to gain an insight into the degradation mechanism(s) of clavulanic acid.

Abbreviations

| | |
|---------|--|
| °C | Degrees Celsius |
| 3D | 3 Dimensional |
| 6-APA | 6-Aminopenicillanic acid |
| 7-ACA | 7-Aminocephalosporanic acid |
| APS | Acid precipitable solid |
| BArF | Tetrakis[3,5-bis(trifluoromethyl)phenyl]borate; B(C ₆ H ₃ C ₂ F ₆) ₄ |
| BE | Back extraction |
| BLS | β-lactam synthetase |
| CA | Clavulanic acid |
| CAD | Clavulanic acid dehydrogenase |
| CCE | Counter current extraction |
| CEA | N ² -(2-carboxyethyl)-arginine |
| CEAS | N ² -(2-carboxyethyl)-arginine synthase |
| cm | Centimetres |
| CNS | Central nervous system |
| COD | Cycloocta-1,5-diene |
| COPASI | Complex Pathway Simulator |
| COX-2 | Cyclooxygenase-2 |
| DBU | 1,8-Diazabicyclo[5.4.0]undec-7-ene |
| DCC | Dicyclohexylcarbodiimide |
| DCM | Dichloromethane; CH ₂ Cl ₂ |
| DF | Diafiltration |
| DIBAL-H | Diisobutylaluminium hydride |
| DLP | Dilauroyl peroxide |
| DMF | <i>N,N</i> -Dimethylformamide |
| DMSO | Dimethyl sulfoxide |
| DNA | Deoxyribonucleic acid |
| eq. | Equivalents |
| ESI | Electrospray ionisation |
| FDA | United States Food and Drug Administration |
| g | Grams |
| G3P | Glyceraldehyde 3-phosphate |

| | |
|------------------|--|
| GAPDH | Glyceraldehyde 3-phosphate dehydrogenase |
| GC | Gas chromatography |
| GSK | GlaxoSmithKline |
| h | Hours |
| HMW | High molecular weight |
| HOMO | Highest occupied molecular orbital |
| HPLC | High performance liquid chromatography |
| IC ₅₀ | Half maximal inhibitory concentration |
| IPA | Isopropyl alcohol |
| IR | Infrared |
| J | Joules |
| <i>J</i> | Coupling constant |
| KEH | Potassium 2-ethylhexanoate |
| L | Litres |
| LCMS | Liquid chromatography mass spectrometry |
| LMW | Low molecular weight |
| LUMO | Lowest unoccupied molecular orbital |
| M | mol dm ⁻³ |
| m/z | Mass to charge ratio |
| MBL | Metallo-β-lactamase |
| MDAP | Mass directed auto purification |
| Me | Methyl; -CH ₃ |
| MeCN | Acetonitrile |
| MeOH | Methanol |
| MHz | Megahertz |
| MiBK | Methyl isobutyl ketone |
| min | Minutes |
| mL | Millilitres |
| mmol | Millimoles |
| mol | Moles |
| MRSA | Methicillin resistant <i>Staphylococcus aureus</i> |
| MS | Mass spectrometry |
| NADPH | Nicotinamide adenine dinucleotide phosphate |
| NHC | <i>N</i> -Heterocyclic carbene |

| | |
|------------------------|--|
| nm | Nanometres |
| NMP | <i>N</i> -Methyl-2-pyrrolidone |
| NMR | Nuclear magnetic resonance |
| | s - singlet |
| | d – doublet |
| | t – triplet |
| | q - quartet |
| | m - multiplet |
| OTf | Trifluoromethanesulfonate |
| PAH | Proclavamate amidino hydrolase |
| PBP | Penicillin binding protein |
| pH | $-\log[\text{H}^+]$ |
| pK _a | pH at which 50% of molecule is protonated |
| ppm | Parts per million |
| RNA | Ribonucleic acid |
| RO | Reverse osmosis |
| RP | Reversed phase |
| <i>S. clavuligerus</i> | <i>Streptomyces clavuligerus</i> |
| SAM | <i>S</i> -adenosyl methionine |
| SAR | Structure activity relationship |
| SET | Single electron transfer |
| T1 _{ir} | T1 inversion-recovery |
| t-BA | tert-Butyl ammonium |
| TBACl | Tetrabutylammonium chloride |
| TBAF | Tetrabutylammonium fluoride |
| ^t Bu | <i>Tert</i> -Butyl; $-\text{C}(\text{CH}_3)_3$ |
| TEMPO | (2,2,6,6-Tetramethylpiperidin-1-yl)oxyl |
| <i>tert</i> | Tertiary |
| TFA | Trifluoroacetic acid |
| TGA | Thermal gravimetric analysis |
| THF | Tetrahydrofuran |
| TK | Tyrosine kinase |
| TLC | Thin layer chromatography |
| TMSO | <i>S,S,S</i> -Trimethylsulfoxonium |

| | |
|---------------|--|
| TP | Transpeptidase |
| UF | Ultrafiltration |
| UV | Ultraviolet |
| v/v% | Volume percent |
| μ | Ionic strength in mol dm^{-3} |
| μg | Micrograms |

Acknowledgments

I give sincere thanks to my PhD supervisors, Dr Marc Reid and Dr Sharon Baillie. Marc, thank you for welcoming me in to the group and sharing your infinite wisdom with me. The enthusiasm with which you have supported my PhD has opened up so many opportunities to me. For that, I am endlessly grateful. Sharon, thank you for taking me under your wing at GSK and showing me the world of process chemistry. Without your constant support and exceptional grammar policing, this thesis wouldn't exist.

Professor Harry Kelly, thank you for giving me the opportunity to join the programme and your support throughout my time on it. Professor Billy Kerr, thank you for allowing me to work so closely with your group at Strathclyde, for your restaurant reviews, and for noticing when I smell nice. Dr David Lindsay and Dr Laura Paterson, thank you for making me feel so welcome at your group meetings, and the invaluable advice you have given me over the last couple of years. Craig Irving, I am indebted to you for your help and patience with the NMR facilities, and thanks for letting me know when there is toast available.

I would like to thank all members of the Reid group, past and present, for their friendship and support. Chunhui, Ellis, Neil, Mhairi, Sam, Nathalie and Devanshi, you have all made the Reid group a wonderful place to work. Similarly, my thanks go to all members of the Kerr group, who have made me feel extremely welcome on Level 7. My fellow ex-dangerzone residents Gary and Giorgia, there has never been a dull moment in your presence. Raymond and Adele, thanks for making our ACS trip so fun. Adele, I'll never let you near my phone again, especially not after a Killer Karen.

I reserve my deepest thanks to my many friends and family who have supported me over the years and helped me have a life outside of chemistry. Megan, Alan, Teddy and Caitlyn, I can't imagine what my time in Glasgow would have been like without you all, and I don't want to. Brett and Oonagh, I wouldn't have made it through my Undergraduate degree, let alone PhD, without your friendship. I would be lost without the kindness, support and encouragement of my dear Mum, Dad and sister: Maggie, Martin and Jade. Finally, to my nieces Imogen and Edith, you bring so much light into my world, thank you both for everything.

Contents

| | |
|---|------------|
| Chapter 1 – Anilinium Salts in Synthesis..... | 1 |
| 1.1 Introduction..... | 1 |
| 1.1.1 Methyl Groups in Medicinal Chemistry..... | 1 |
| 1.1.2 Methylation Methodologies | 15 |
| 1.1.3 <i>N,N,N</i> -Trimethylanilinium Salts..... | 33 |
| 1.2 Proposed Work..... | 46 |
| 1.3 Results and Discussion..... | 50 |
| 1.3.1 Degradation of <i>N,N,N</i> -Trimethylanilinium Salts | 51 |
| 1.3.2 <i>N,N,N</i> -Trimethylanilinium Salts in Methylation Reactions | 86 |
| 1.4 Conclusions | 104 |
| 1.5 Future Work | 107 |
| 1.6 Experimental | 112 |
| 1.6.1 General Considerations | 112 |
| 1.6.2 Experimental Procedures..... | 113 |
| 1.7 References | 194 |
| Chapter 2 – Clavulanic Acid Production on the Manufacturing Scale..... | 206 |
| 2.1 Introduction..... | 206 |
| 2.1.1 Introduction to Antibiotics | 206 |
| 2.1.2 The Synthesis of Clavulanic Acid..... | 228 |
| 2.1.3 Degradation of Clavulanic Acid..... | 239 |
| 2.3 Results and Discussion..... | 251 |
| 2.3.1 Understanding the Effect of pH of Clavulanic Acid Degradation | 251 |
| 2.3.2 Degradation of Clavulanic Acid in Manufacturing Plant Samples | 266 |
| 2.3.3 Understanding the Aqueous Degradation Pathways of Clavulanic Acid... .. | 277 |
| 2.4 Conclusions | 294 |
| 2.5 Future Work | 296 |
| 2.6 Experimental | 298 |
| 2.6.1 General Considerations | 298 |
| 2.6.2 Experimental Procedures..... | 302 |
| 2.7 References | 317 |

Chapter 1 – Anilinium Salts in Synthesis

1.1 Introduction

1.1.1 Methyl Groups in Medicinal Chemistry

Methyl groups are ubiquitous in organic chemistry. The small CH₃ group is relatively inert, and its introduction to a molecule is often viewed as a mundane or trivial exercise. Despite this, the presence or absence of methyl groups in the molecular structure of numerous compounds has been demonstrated to remarkably affect their chemical and pharmacological properties.^{1,2,3} Many of the most compelling examples that highlight the importance of methyl groups can be found in medicinal chemistry.

The following introductory section aims to give an overview of the profound (and somewhat contested)^{4,5} effects that methyl groups can have on the chemical properties of their host molecules. Particular attention will be paid to the role of methyl groups in the pharmaceutical industry. A review of existing strategies to install methyl groups will then be presented, highlighting some of the challenges that are faced by methylation chemistry users.

The Importance of Methyl Groups

The methyl group is one of the most commonly occurring functionalities in biologically active molecules. Over 80% of the 200 best-selling small molecule drugs in 2018 contained one or more carbon- or heteroatom-bound methyl group.⁶ A selection of these top selling drugs is displayed (**Figure 1**), demonstrating the diverse range of environments in which these methyl groups can be found.

Though methyl groups are only able to participate in London dispersive interactions, the weakest form of intermolecular force, they exhibit significant stereoelectronic effects on small molecules and biological macromolecules. The addition of a methyl group to a drug compound can be used to fine tune its pharmacological activity, the effects have been shown to include: changes in potency, a reduction in off-target activity, increased solubility, and changes in drug metabolism.^{3,7} Specific examples of these phenomena will be discussed in this section of the introduction.

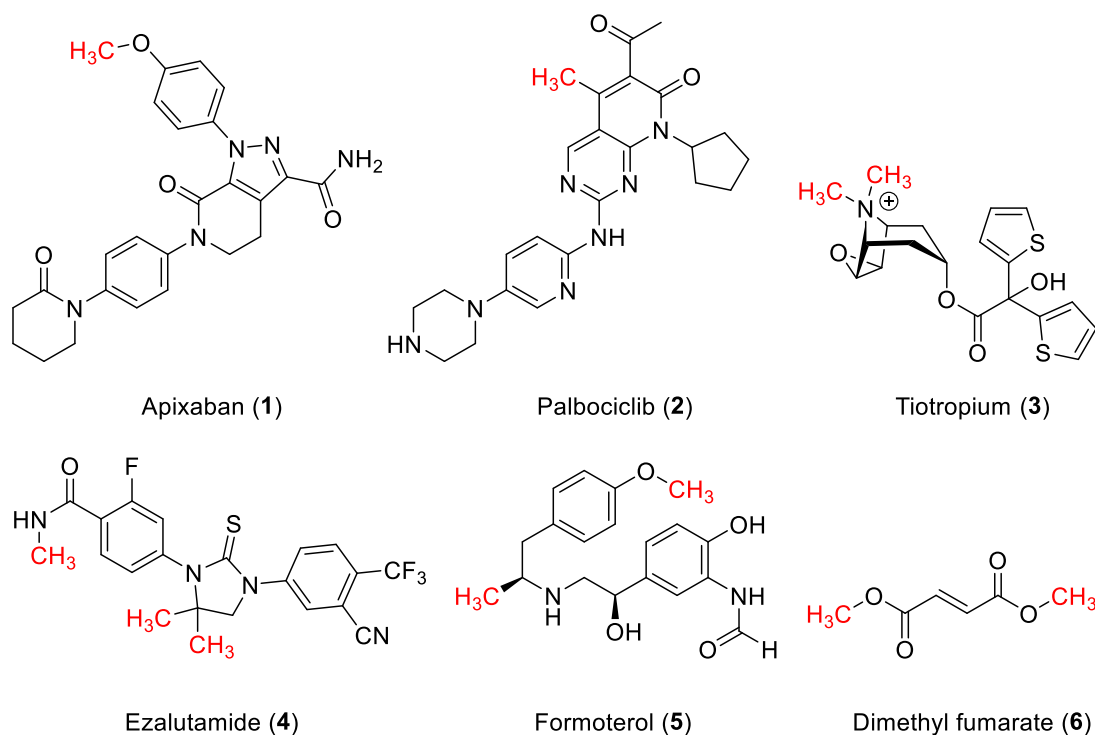


Figure 1. Six of the top 20 best-selling small molecule drugs in 2018 that contain one or more methyl groups.⁶

To comprehend the powerful effects that methyl groups have on drug properties, it is useful to first consider the role that they play in nature. One of the most fundamental classes of biomolecule that take advantage of the stereoelectronic changes promoted by methyl groups are the nucleic bases (**Figure 2**).² The nucleic bases consist of two structural types, the pyrimidine bases (**7-9**), and the purine bases (**10-11**). Of the pyrimidine bases, thymine (**7**) and uracil (**8**) vary only in the presence or absence of a methyl group in the C5-position; **7** is found in DNA, whilst **8** is found in RNA.⁸ A number of biological events involving DNA, such as transcription and nucleosome recognition, are dependent on its conformation. It is thought that DNA conformation is directly impacted by CH/ π interactions between purine bases and the thymine C5-methyl group, making it crucial for DNA function.⁹ Unlike the pyrimidine bases, purine nucleotides in DNA and RNA (**10-11**) do not have any methyl substituents present. There are, however, a number of purine alkaloid natural products whose methylation patterns govern their biological activity.

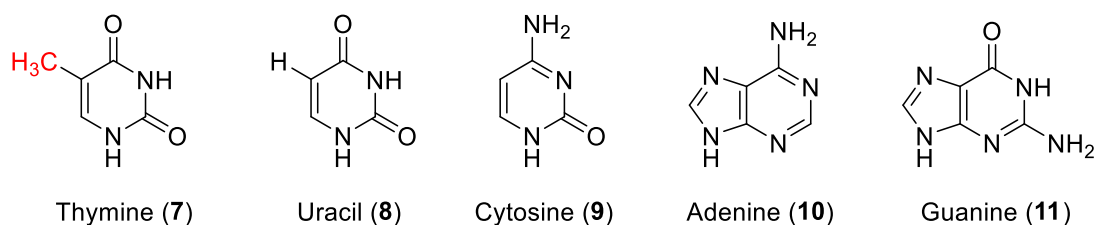


Figure 2. The structures of DNA and RNA nucleic bases (7-10), with the thymine C5-methyl group that differentiates it from uracil highlighted in red.⁹

Caffeine (13), theobromine (14) and theophylline (15) are purine alkaloids that derive from the S-adenosylmethionine (SAM) mediated di- or tri-methylation of Xanthine (12) (Figure 3).¹⁰⁻¹² Though the structures of 13-15 vary only in methylation pattern, they have remarkably different biological effects. The trimethylated 13 is the most lipophilic of the three and hence is the most effective central nervous system (CNS) stimulant, it is recognised by adenosine receptors which, upon uptake, ultimately cause an adrenaline release.^{2,11} 14 and 15 are less lipophilic and therefore have far less stimulatory activity, instead 14 acts as a pulmonary muscle relaxant whilst 15 is a powerful bronchodilator.^{11,12}

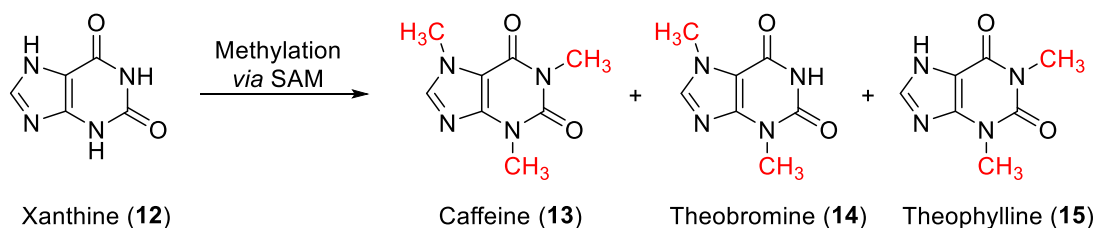


Figure 3. Purine alkaloids caffeine (13), theobromine (14) and theophylline (15) which are derived from various methylating patterns of xanthine (12).¹²

Another example from natural product chemistry that illustrates the potent effects of methyl substitution on biological activity is in the case of opium. Opium is the name given to mixture of more than 20 alkaloids that are derived from the latex of *Papaver somniferum*, a species of poppy plant.¹³ Of these alkaloids, morphine (16) is the most abundant and its largely responsible for its analgesic properties. Morphine acts against δ , κ , and μ opioid receptors within the CNS to give its pain-relieving therapeutic effects.^{13,14} Normorphine (17), codeine (18) and heterocodeine (19) are closely related

opium alkaloids which are differentiated from morphine by methylation patterns on the nitrogen atom and, C1-hydroxyl and C3-hydroxyl oxygen atoms (**Figure 4a**).

The four opioids (**16-19**) have unique biological activities. **17** has a 6-fold reduction in analgesic activity compared to **16**, despite its ability to maintain the same ionic ligation in the target bio-receptor.¹⁵ The nitrogen of **16** and **17** varies only slightly in pK_a so they would be expected to exist in the same ionisation state.¹⁶ Instead, the lower potency of **16** can be attributed to its more polar nitrogen which affects its physical-chemical properties and retards its ability to pass the blood-brain barrier to reach its target receptors. Codeine (**18**) on the other hand features a methoxy group in the C3 position and has a 200-fold decreased in receptor affinity compared to **16**. This loss of potency can be attributed to the reduced ability of **18** to form hydrogen-bonds with a histidine residue in the active site of the target opioid receptor (**Figure 4b**).¹⁷ Whilst the reduced potency may present itself as a disadvantage, it actually means that codeine can be made available as an over-the-counter medicine, used for treating less severe ailments.¹⁸ Heterocodeine (**19**) is twice as active as **16** *in vivo*. It can maintain the hydrogen bond with the target molecule *via* the C3 hydroxyl, whilst a methoxy group in the C6 position also increases its lipophilicity, giving it a facile entry into the CNS.¹⁹

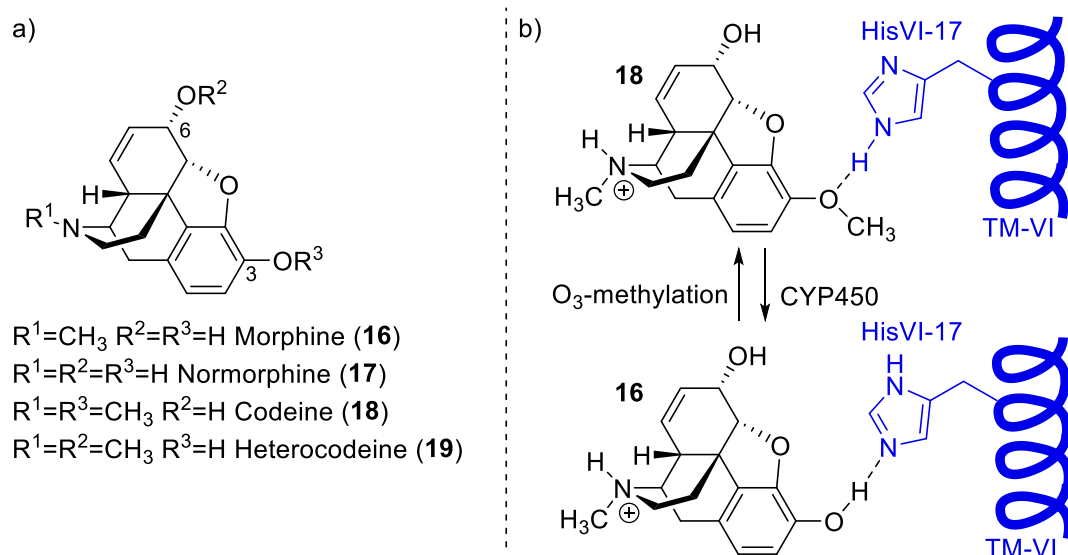


Figure 4. a) Generic structure of opium alkaloids with various methylation patterns to give morphine, normorphine, codeine and heterocodeine (**16-19**). b) A Representation of **16** and **18** binding to a histidine residue in the active site of an opioid receptor.

Effects of Methylation on Lipophilicity

Many of the improved properties of methylated drugs come from the increase in lipophilicity.³ The lipophilicity of a molecule is usually described by its Log *P* value, this is a logarithmic scale of the partition coefficient of a given molecule between *n*-octanol and water. A larger Log *P* value corresponds to a more lipophilic molecule i.e. it has a higher solubility in *n*-octanol than water. To illustrate the effect of methyl groups on lipophilicity, the comparison between benzene (**20**) and toluene (**21**) can be made (**Figure 5a**).²⁰ The introduction of a methyl group on the aromatic ring of **20** to form **21** increases the Log *P* value from 2.13 to 2.69. In general, the methylation of an aromatic compound can be expected to lead to a log *P* increase of approximately 0.52.^{21,22} The introduction of one or more methyl group to a molecule tends to make it more lipophilic, and thus increase its solubility in phospholipid-containing biomembranes. This can lead to a much higher bioavailability of a drug and thus improve its efficacy.^{23,24}

Though introducing methyl groups to a given molecule will generally cause an increase in its lipophilicity, it is worth noting that there are exceptions to the rule. One such exception can be observed in the case of aliphatic alcohols (**Figure 5b**).^{2,25} The addition of a methyl group on the C4-position of *n*-butanol (**22**) to give *n*-pentanol (**25**) causes an increase in lipophilicity from 0.84 to 1.40.²⁶ However, introducing methyl groups that make a molecule more compact, such as the change in structure from **25** to 2-pentanol (**26**) or, even more so neopentanol (**27**) causes a decrease in lipophilicity. Despite **27** having an additional carbon compared to **22**, it has a higher water solubility (122 g/L compared to 82 g/L). The increased water solubility as aliphatic alcohols become more globular can be rationalised by an entropic argument. In aqueous solutions, the solute (alcohols in this case) will be surrounded by a network of solvent water molecules (**Figure 5c**).^{27,28} More compact structures will require fewer water molecules to solvate them, therefore their dissolution in water is more energetically favourable.

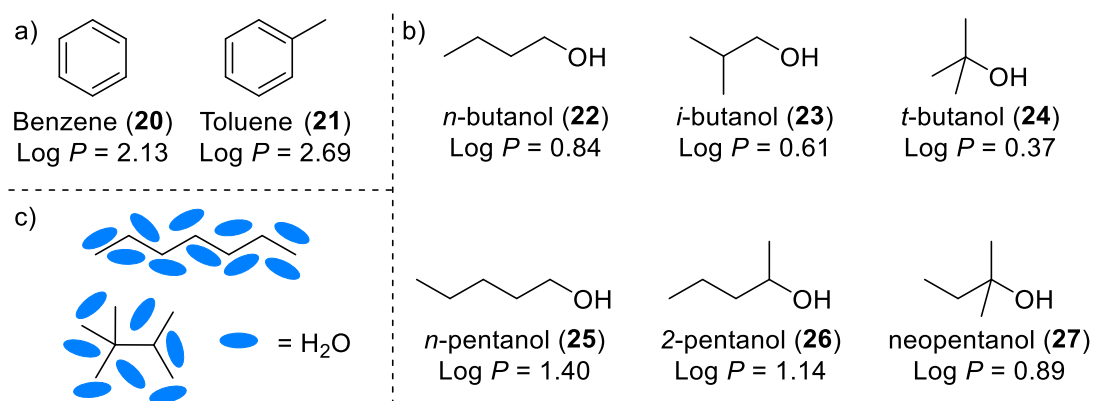


Figure 5. a) Comparison of benzene and toluene Log P values. b) Comparison of Log P values between aliphatic alcohols **22-27**. c) Stylistic representation of water molecules solvating linear and compact molecules.^{20,26-28}

Increased drug molecule lipophilicity through methylation doesn't only improve drug performance *via* an increased permeability through cell membranes, it can also lead to improvements in drug binding affinity. These improvements can be rationalised by desolvation effects.^{3,27,28} An increase in methylation reduces the desolvation energy required to remove the water molecules solvating a compound as it transfers from an aqueous environment to a more hydrophobic protein cavity.²⁹ When this desolvation energy is lowered, drug binding can become energetically favourable leading to a lower IC₅₀ of the drug. Furthermore, six of the twenty naturally occurring amino acids contain methyl groups (**Figure 6**).^{1,30} This results in proteins with various methylation patterns, so it is reasonable to predict that molecules with complementary methylation will interact favourably in these environments.

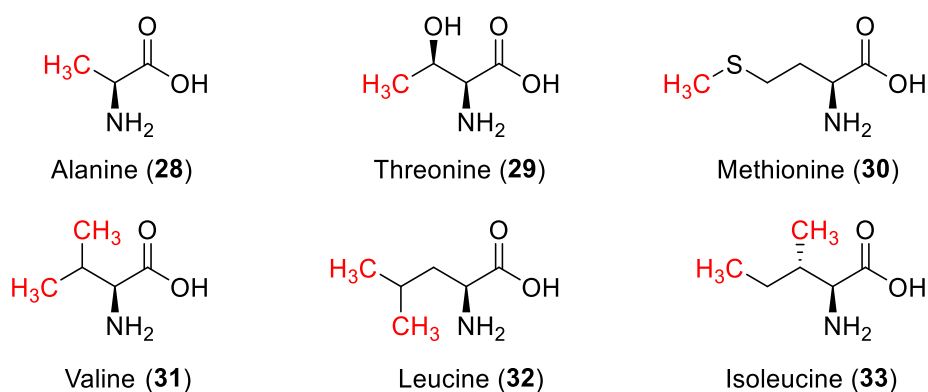
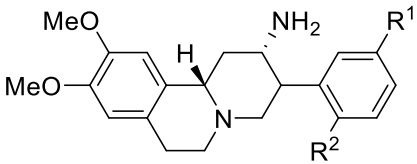


Figure 6. The six naturally occurring amino acids that contain one or more methyl group.³⁰

The change of free energy in transporting a molecule between two different solute environments (a polar aqueous environment to a non-polar greasy protein cavity, in this case) is known as the transfer free energy ($\Delta G^{\ominus}_{\text{transfer}}$).³¹ It is estimated that the change in transfer free energy that is gained by replacing a proton for a methyl group is about $\Delta\Delta G^{\ominus}_{\text{transfer}} \approx 0.8 \text{ kcal mol}^{-1}$ when moving from water to a protein.³² Based on this change in $\Delta G^{\ominus}_{\text{transfer}}$, a roughly 3.5-fold increase in drug potency can be approximated. Jorgensen *et al* conducted an extensive survey of over 2000 reported protein-ligand X-ray crystallographic structures to investigate this effect further.³³ Their empirical approach found that the potency of a drug could be boosted approximately 10-fold by the introduction of a single methyl group if it is well placed to interact favourably in a hydrophobic pocket of the protein active site.

An extreme case of improved drug potency arising from favourable hydrophobic interactions from methylation is shown in the case of a series of quinolizine-based dipeptidyl peptidase IV inhibitors (**Figure 7**).³⁴ Changing the R¹ group of **34** to the methyl group in **35** leads to a 43-fold decrease in IC₅₀ owing to favourable hydrophobic interactions. A second installation of a methyl group in the R² position to give **36** delivers a 117-fold increase in potency compared to **34**. Whilst these examples are very compelling, it is important to note that the active site of a drug target must be able to accommodate the methyl group spatially. Statistical analysis of the literature showed that replacing a proton with a methyl group is equally as likely to cause a decrease in ligand binding affinity as it is an increase.³³

| Compound | IC ₅₀ (nM) |
|-----------|-----------------------|
| 34 | 200 |
| 35 | 4.6 |
| 36 | 1.7 |



R¹=R²=H **34**
R¹=CH₃ R²=H **35**
R¹=R²=CH₃ **36**

Figure 7. An example of the effect that one or more hydrophobic methyl interactions can have on drug potency.³⁴

In the cases where drug binding efficiency is improved through hydrophobic interactions, the increase in potency is typically somewhere between 3- and 10-fold. There are rare cases where methylation can lead to potency improvements of two

orders of magnitude or more. This phenomenon can be so profound that it has been dubbed *the magic methyl effect*.¹ In these cases, desolvation effects alone cannot be used to rationalise the potency boost. There are usually more nuanced factors at play when such an improvement in drug efficiency is observed through methylation. Some examples where this has been evident are examined below.

Stereoelectronic effects of methyl groups

In addition to lowering the desolvation energy of a drug molecule, the addition of methyl groups can have remarkable effects on its electronic properties and its conformation. An electronic effect of methyl substituents is well demonstrated in the case of the proton pump inhibitor (PPI) Omeprazole (**37**).^{35,36} **37** is actually a prodrug used in the treatment of gastric ulcers (**Figure 8**).³⁷ It is activated in low pH environments to convert to the active cyclic sulfenamide species **38** which forms an irreversible covalent complex with the gastric H⁺-K⁺-ATPase enzyme (**Figure 9**). During the discovery programme to find suitable PPIs, the sulfoxide Timoprazole (**39**) was found to be an effective inhibitor of gastric H⁺-K⁺-ATPase enzyme, but significant side effects involving iodine recapture in the thyroid gland were observed.^{38,39}

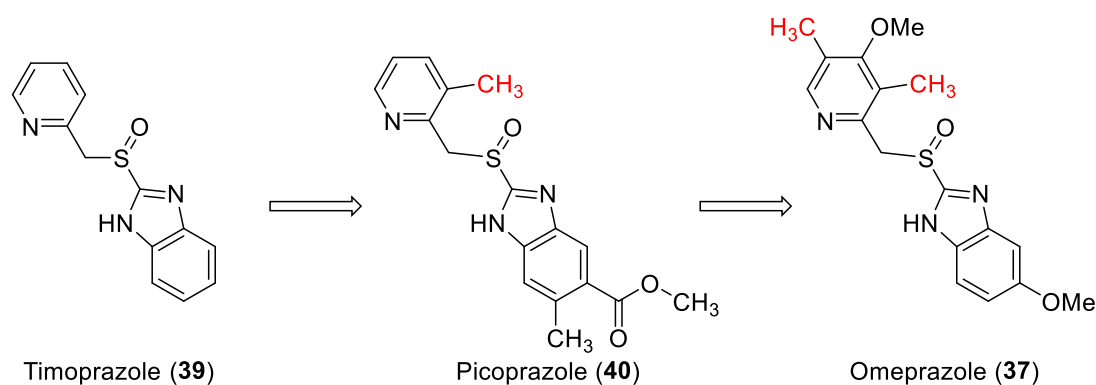


Figure 8. Chemical structures of proton pump inhibitors **39** and **40** leading to the discovery of Omeprazole (**37**).^{39,40}

Manipulation of the structure lead to the formation of Picoprazole (**40**) which was an effective PPI, but no longer had side effects in the thyroid gland. Through a structure-activity relationship (SAR) study, it was found that the additional methyl group on the

pyridine ring of **40** significantly improved the potency of the drug *via* its electron donating effects.⁴⁰ Further manipulation based on the SAR study eventually led to the discovery of structure **37**. Several mechanistic studies of gastric ATPase inhibition have shown that the electron-donating nature of the pyridine methyl substituents play two important roles in Omeprazole's success.³⁹

The methyl groups in **37** are responsible for fine tuning its pK_a . The electron-donating ability of these substituents increases the nucleophilicity of the pyridine nitrogen atom, which is a lipophilic weak base. **37** remains in its neutral state at physiological pH, which allows its passage through plasma membranes to reach its target tissue.^{37,38} Once inside parietal cells, the environment is much more acidic (\sim pH 1.0), the pyridine with its increased basicity is quickly protonated inside the cell, giving **37-H** which is no longer capable of passing the membrane to leave the cell (**Figure 9**).

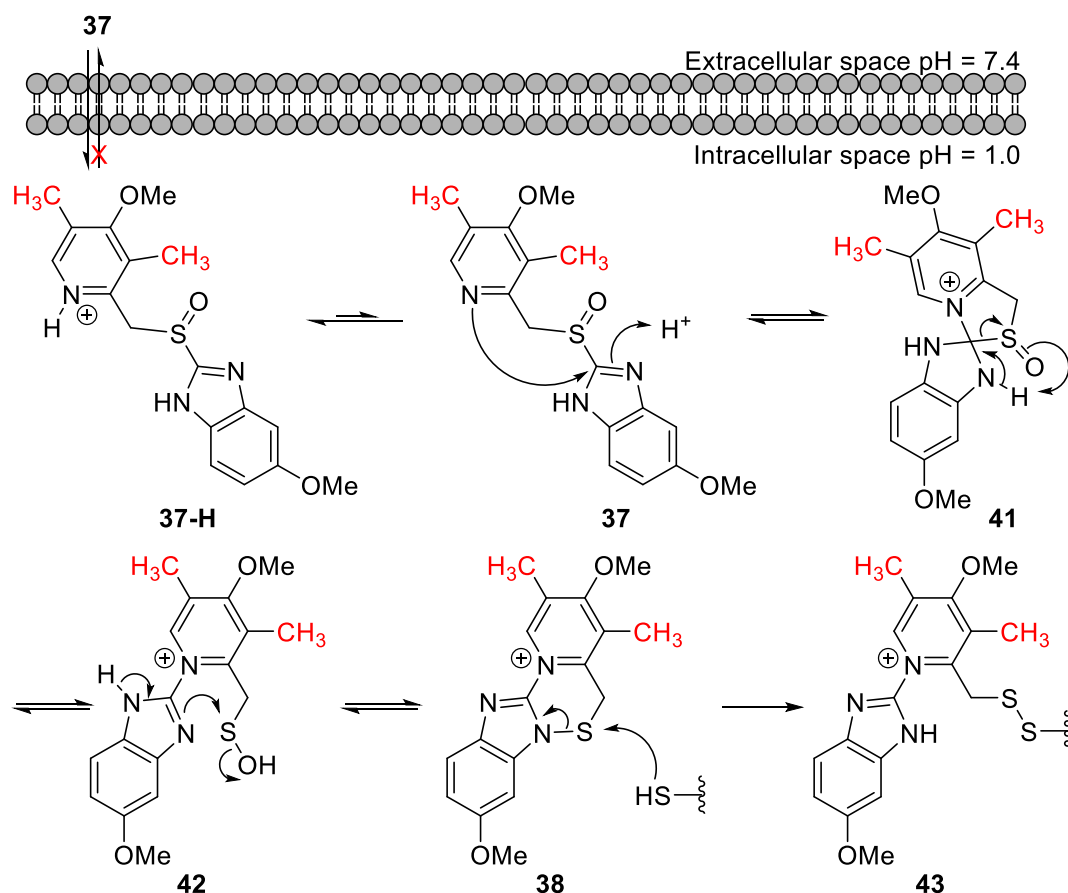


Figure 9. Activation mechanism of prodrug Omeprazole (**37**) leading to the active sulfenamide (**38**) and the inactive gastric ATPase adduct (**43**).^{37,39,40}

Once inside the cell, **37** can then undergo its activation process to the active drug form **38** (**Figure 9**). Nucleophilic addition of the pyridine nitrogen atom to the benzimidazole, followed by rearomatisation of the spirocyclic intermediate (**41**) gives the sulfenic acid (**42**).^{37,39,40} Dehydration of **42** produces the active form **38** which is intercepted by a cysteine residue in the gastric ATPase active site, generating a stable disulfide adduct, and thus irreversibly deactivating the enzyme. Both improved drug compartmentalisation in the desired cells, and the increased rate of drug activation, benefit from the increased nitrogen nucleophilicity brought about by the addition of methyl substituents.

The case of Omeprazole shows the powerful electronic effects that can be imparted on a drug molecule by the installation of methyl groups. Although relatively small, methyl groups can also have a drastic impact on drug potency and selectivity through steric effects that lead to desirable conformational changes.^{2,41} This has been demonstrated on numerous occasions, a few examples are presented here to illustrate the effect.

Imatinib (**46**) is a tyrosine kinase (TK) inhibitor that acts against the *Bcr-Abl* gene in the treatment of chronic myeloid leukemia (**Figure 10**).⁴²⁻⁴⁴ Initial efforts into the discovery of Imatinib used a high throughput screening and combinatorial chemistry approach to identify a diarylamine scaffold for the inhibition of TKs.⁴⁵⁻⁴⁷ Developing the scaffold further to improve the drug potency, **44** was discovered as an excellent inhibitor of the *Bcr-Abl* kinase; however, significant inhibition of other kinases was observed, leading to unacceptable off-target activity. It was found that the addition of a methyl substituent in the *ortho*- position of **44** to give **45** provided a compound with an improved potency against *Bcr-Abl* kinase, and a concomitant loss in activity against other kinases.⁴⁷⁻⁴⁹

The gain in selectivity for the desired TK could be explained by a conformational change brought into effect by the *ortho*-methyl group. The newly introduced methyl substituent in **45** causes the phenyl ring to rotate in such a manner that steric repulsion between the methyl group and the pyridazine nitrogen lone pair is minimised (**Figure 10**). This change in shape favoured binding in the *Bcr-Abl* kinase active site, whilst disfavouring other kinases.^{47,50} Final modifications to **45** to improve its

physicochemical properties eventually led to the discovery of Imatinib which is a highly potent and selective chemotherapeutic agent.^{50,51}

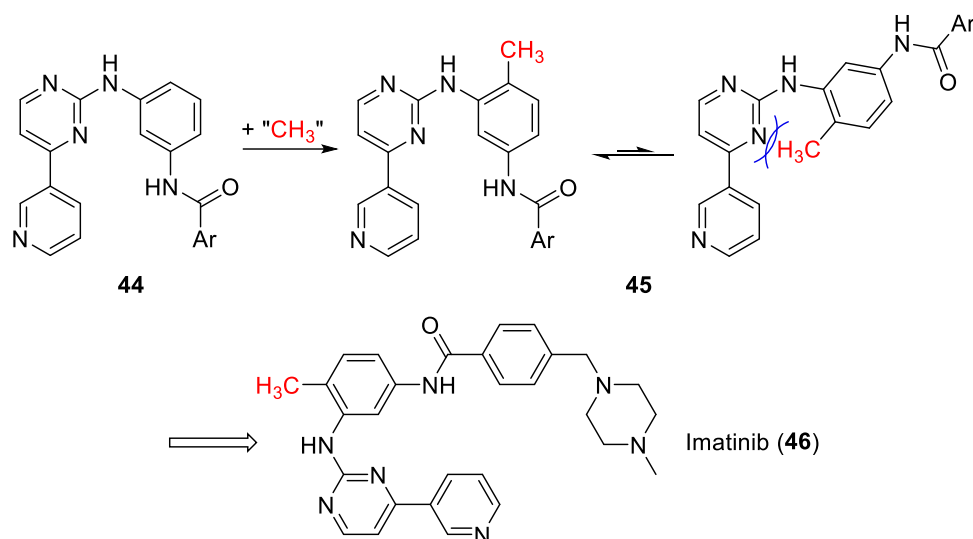


Figure 10. Conformational effects caused by *o*-methyl group in lead compound **45**, leading to the discovery of Imatinib (**46**).^{47,48,50}

Methyl-induced conformational changes are successful when they increase the shape complementarity between the shape of the unbound drug molecule and the active site of the target protein. When the drug has a similar conformation in its bound and unbound state, there will be a minimal energy cost involved with reordering the drug to bind to the active site.⁵² Compounds **47** and **48** were produced in an effort to discover p38 α kinase inhibitors (**Figure 11**). The dihedral angle of the biaryl bond in **47** is 50° , the addition of an *ortho*-methyl group in **48** twists the phenyl ring to give an increased dihedral angle of 65° .⁵³ The X-ray crystal structures of the protein-ligand bound complexes reveal that the dihedral angle of the biaryl bond in both **47** and **48** in their bound states is 85° . Therefore, the methylated drug **48** is 15° closer to its bound conformation in the resting state and has a favourable binding energy. This conformational effect manifests itself as a 208-fold increase in drug potency.^{33,53}

A similar effect is observed in the case of orexin receptor antagonists **49** and **50** used to treat insomnia (**Figure 11**).⁵⁴ Addition of an α -amino methyl group on the piperidine

core brings about a 480-fold potency increase.^{1,55} It is thought that the methyl group forces the ether substituent into an axial position, the amide is twisted to reduce the 1,3-diaxial interactions whilst holding the aryl rings in close proximity to allow π -stacking. The U-shaped conformation of **50** more closely resembles the bound state of these ligands than the equatorial conformation of **49**, which again gives it a lower binding energy.⁵⁵

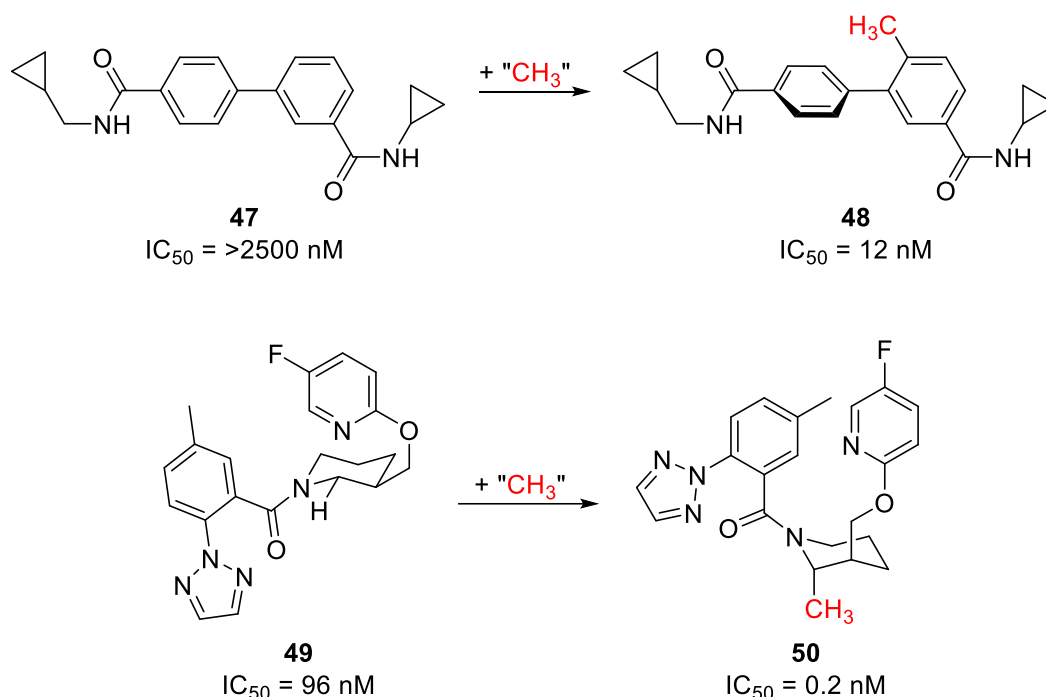


Figure 11. Conformational preorganisation of drug compounds induced by the addition of methyl groups.^{33,53,55}

It is noteworthy that methyl groups are not the only substituent capable of bringing about conformational biases in drug molecules, fluoro and trifluoromethyl substituents are often used to this effect. Fluoro substituents have a tendency to be unstable when positioned α to a heteroatom, which would make them unsuitable for optimisation of structures such as **49**.⁵⁶ The trifluoromethyl group is stable α to heteroatoms and also large enough that it can effectively bring about steric changes. However, compared to a simple methyl group, it brings a relatively large increase in the molecular weight (69 $gmol^{-1}$ for CF₃ vs 15 $gmol^{-1}$ for CH₃) and lipophilicity ($\Delta LogP \approx +0.88$ for CF₃ vs

$\Delta\text{Log}P = 0.56$ for CH_3) which can run the risk of violating Lipinski's rules if the drug candidate is already on the upper end of these limits.⁵⁷⁻⁵⁹

Changes in drug metabolism caused by methyl groups

Improving drug binding affinities through increased lipophilicity and stereoelectronic tuning has proven to be a powerful use of methyl groups in drug discovery efforts. Unfortunately, the binding affinity of a drug is only one of the many factors to take into consideration.⁶⁰ Drug metabolism also plays a significant role in the success of a drug; too fast and the bioavailability of the drug can be too low, too slow and the drug could take too long to clear to allow for the desired dosing regimen.

Lidocaine (**51**) is a drug used as a local anesthetic and an antiarrhythmic agent (**Figure 12**).⁶¹ It is part of a family of anesthetic drugs obtained through various structural modifications to cocaine. **51** was first discovered as a retroisostere of Procaine (**50**) and features two *ortho*-methyl substituents on its aromatic ring.⁶² There are two main pathways through which **51** could be metabolised. Oxidation *via* a hepatic cytochrome P450 enzyme leads to compound **54** which, followed by the expulsion of acetaldehyde, leaves **55** as a main metabolite.⁶³ Alternatively, a common metabolic pathway for this kind of drug (including **50**) is hydrolysis of the amide moiety *via* an amidase enzyme.^{64,65}

In the case of Lidocaine, the two electron-donating *ortho*-methyl substituents serve to make the amide less electrophilic which reduces its susceptibility to nucleophilic attack of an enzyme. Furthermore, a conformational twist in the benzene ring induced by the bis-*ortho*-methyl groups provides steric hindrance to protect against the approach of the amidase enzyme's catalytic residue. By blocking one of the metabolic pathways through methyl substitution, the metabolic stability of **51** was increased.^{61,66} As a testimony to its value, the bis-*ortho*-methylaryl moiety has since been included in a number of new compounds in this drug class.⁶¹

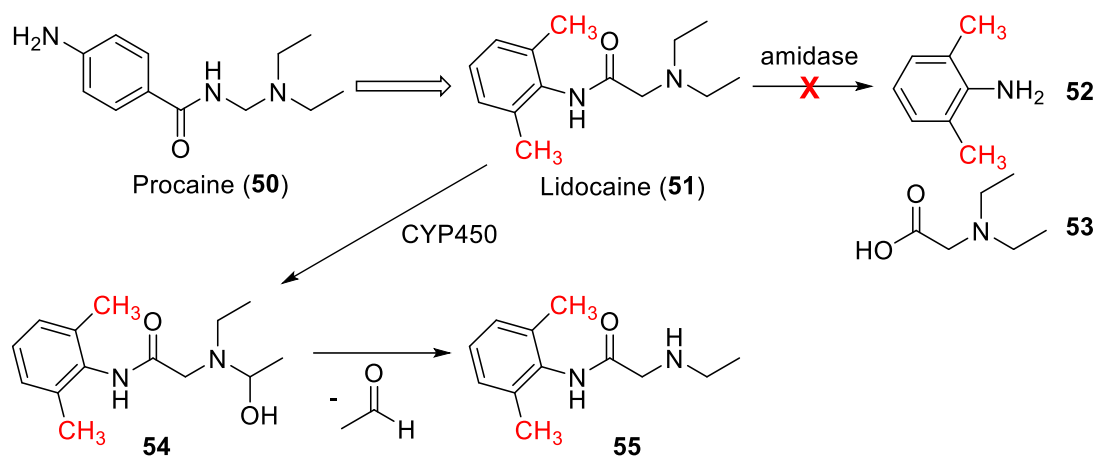


Figure 12. Anesthetics Procaine (**50**) and Lidocaine (**51**), and the main pathways for metabolism of **51**.^{63,64}

In the case of **51**, increasing the metabolic stability of the drug was a key objective in the drug discovery programme. There are however, cases where increasing drug metabolism can prove beneficial. This was evident in the case of Etoricoxib (**57**) a potent cyclooxygenase-2 (COX2) inhibitor used in the treatment of arthritis (**Figure 13**).^{1,67} During the drug discovery process, **56** was identified as a potent COX2 inhibitor.

In rats, 24 h after receiving a 20 mg/kg dose of **56**, its concentration in plasma was found to be in excess of 4 μM . This was deemed an unacceptably high concentration and was indicative of a very long metabolic half-life.⁶⁷ To combat this, analogues of **56** were synthesised to include various alkyl moieties on the pendant pyridine ring and thus, Etoricoxib (**57**) was discovered. **57** showed comparable potency against COX2 but also had a significantly shorter half-life of approximately 2 h, allowing adequate clearance from the body. **57** can be metabolised in two main ways, through the oxidation to form pyridine N-oxide **60**, or oxidation of the *ortho*-methyl substituent to secondary alcohol **58** and subsequently carboxylic acid **59** (**Figure 13**).⁶⁸ The formation of **60** is significantly slower than the alkyl oxidation to **58**, suggesting the long half-life of **56** is due to sluggish pyridine N-oxidation. By introducing the *ortho*-methyl group to **56**, the metabolic half-life of the drug was significantly reduced allowing for suitable clearance. This concept is known as introducing a *metabolic hotspot* to a drug.⁶⁹

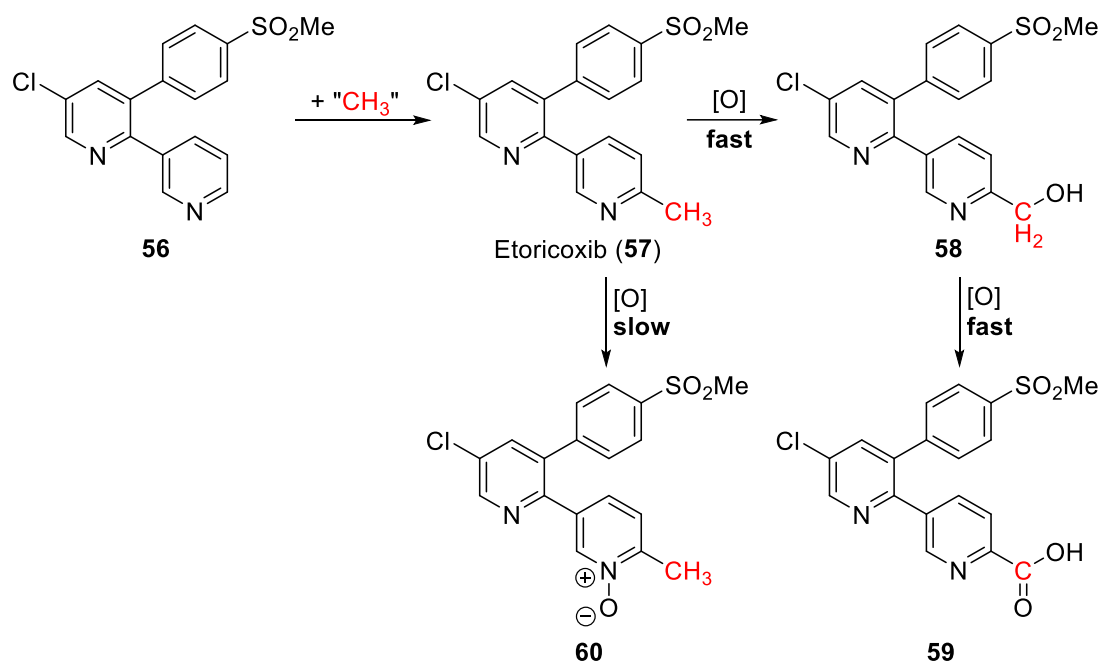


Figure 13. COX2 inhibitors **56** and **57**, and the major metabolic pathways of **57**.^{67,68}

Through a selection of examples in medicinal chemistry, this section demonstrates the powerful impact that adding a simple methyl group can have on the properties of a molecule. With this in mind, it is clear that methods to introduce methyl groups into molecules in a safe, efficient, and reliable manner are highly coveted by the synthetic chemical community. The next section of this introduction will present some commonly used protocols to methylate substrates. Owing to the diverse and extensive literature, the following section is not intended to be a comprehensive review of all methods available. Instead, it aims to give the reader an insight into the range of methodologies available for methylation, and points out some of the caveats involved with using each reagent. Where possible, recent advances in the field of methylation chemistry are given particular prominence.

1.1.2 Methylation Methodologies

The ability to install methyl groups into a molecule in a straight-forward manner is invaluable to synthetic chemists. There are a variety of methods available for

methylating a broad range of functionalities. For the purpose of this section, methylation strategies will be split into four main categories:

- (i) electrophilic methylations,
- (ii) nucleophilic methylations,
- (iii) radical-based methylations, and
- (iv) transition-metal catalysed C–H functionalisation.

Electrophilic methylating reagents

Electrophilic methylating reagents can be used to append methyl groups onto a diverse range of nucleophilic substrates. A selection of the most widely used electrophilic methylating reagents are shown (**Figure 14**).

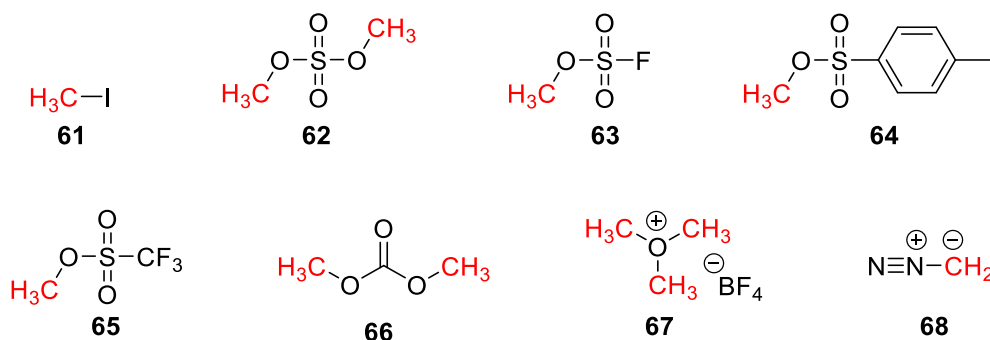


Figure 14. A selection of commonly used electrophilic methylating reagents.

Amongst the most widely known and commonly used methylating reagents is methyl iodide **61**.⁷⁰ **61** is an effective substrate for $\text{S}_{\text{N}}2$ reactions, owing to potential of the iodide ion to act as a good leaving group, and has been used for *O*-, *N*-, *S*-, and *C*-methylations (**Figure 15**).^{70–72} In addition, the softness of the iodide anion typically causes methylation at the softer part of an ambident nucleophile, for example *C*-methylation is usually observed when **61** reacts with an enolate, rather than reaction taking place at the harder *O*-nucleophile.^{70,73} Although analogous methyl halides can be used in alkylation reactions (i.e. methyl bromide and methyl chloride), **61** is

generally preferred as it is the most active towards methylation and it is a liquid at room temperature whereas the former two are gaseous. Despite the versatility of **61** in methylation reactions, there are some factors that can discourage its use. The major drawback associated with **61** is its toxicity as it is a known carcinogen that can enter the body through skin contact, ingestion and inhalation.^{74,75} Furthermore, despite being a liquid at room temperature, it is still relatively volatile with a boiling point of 42 °C, which exacerbates the safety concerns when used in a heated reaction.⁷⁰

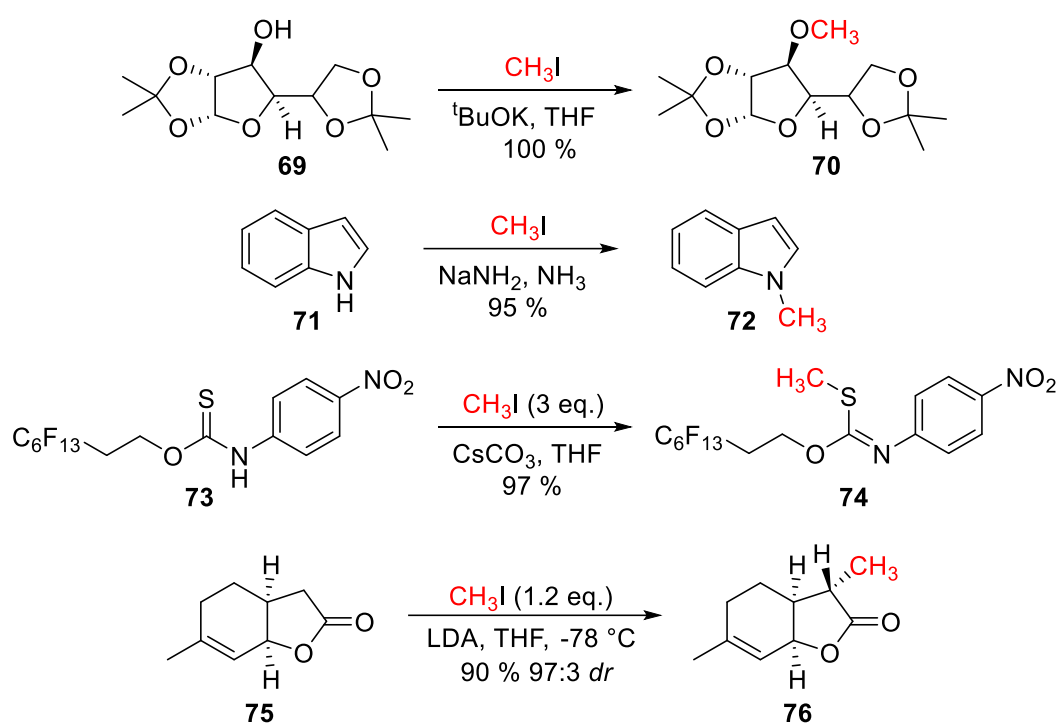


Figure 15. Examples of methyl iodide (**61**) being used in *O*-, *N*-, *S*-, and *C*-methylation reactions.⁷⁰⁻⁷²

Common alternatives to methyl iodide are the sulfates and sulfonates **62-65** (**Figure 14**).⁷³ Dimethyl sulfate (**62**) is a powerful methylating reagent that has been used in the methylation of a wide variety of nucleophiles, some examples include carboxylic acids, lactams and hydroxylamines (**Figure 16**).⁷⁶⁻⁷⁸ With a boiling point of 188 °C, exposure through inhalation is less of a risk for **62** than it is for **61**; however, it is still extremely toxic and carcinogenic so should be used with adequate precautions in place.⁷⁹

Of the sulfonates methyl fluorosulfonate (**63**) is the most active.⁷⁶ Although it is an excellent methylating reagent, it is also the most toxic with multiple deaths being reported after exposure.⁸⁰ Preferred reagents include methyl *p*-toluenesulfonate (**64**) and methyl trifluoromethanesulfonate (**65**). **64** has a slightly lower reactivity and a poor atom economy but is significantly less toxic.⁷³ **65** is comparative in terms of reactivity to **63**, though it does have a similarly poor safety profile.⁸¹

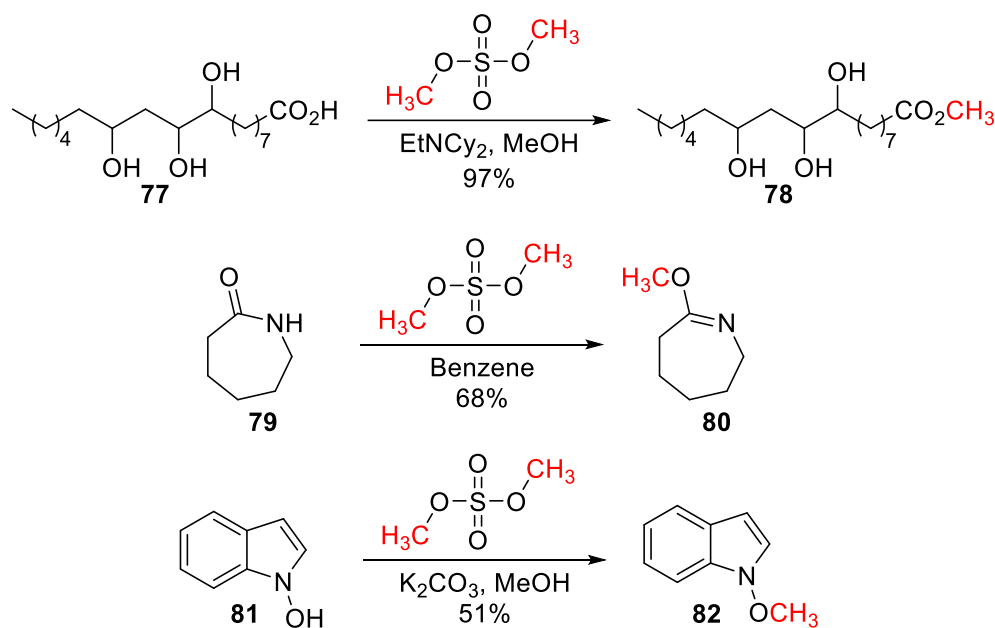


Figure 16. Examples of dimethyl sulfate (**62**) being used in carboxylic acid, lactam and hydroxylamine methylations.^{76–78}

Dimethylcarbonate (**66**) is often viewed as green alternative to methyl halides. It is non-toxic and biodegradable so has found applications as both a green solvent, and methylating reagent.^{82,83} **66** is used primarily as an *O*-, or *N*-methylating reagent. Though **66** has proven to be a competent methylating reagent, common drawbacks include long reaction times and high reaction temperatures.⁸⁴ These limitations were overcome in a report by Repic and co-workers who used **66** with DBU (**83**) as an activating catalyst under microwave radiation (**Figure 17**).⁸⁵ DBU activates **66** to carbamate intermediate **84**, this can then be intercepted by a phenoxide nucleophile to give an anisole, carbon dioxide and regenerate **83**. Under these conditions, a range of phenols and nitrogen-containing heterocycles could be methylated in yields of 91–99%.^{73,85}

The mono *N*-methylation of anilines has been achieved using **66** and **83** in a similar protocol (**Figure 18**).^{83,86} During this reaction, the aniline nucleophile had a tendency to undergo an unfavourable methoxycarbonylation side reaction which occurred at a temperature of around 90 °C, forming **87**. To combat this, high reaction temperatures of >130 °C were required to convert **87** to the desired product **86** in acceptable yields. It is unknown if **87** converts to **86** through intermediacy of **88**, or if it converts back to **85** and is then methylated directly.

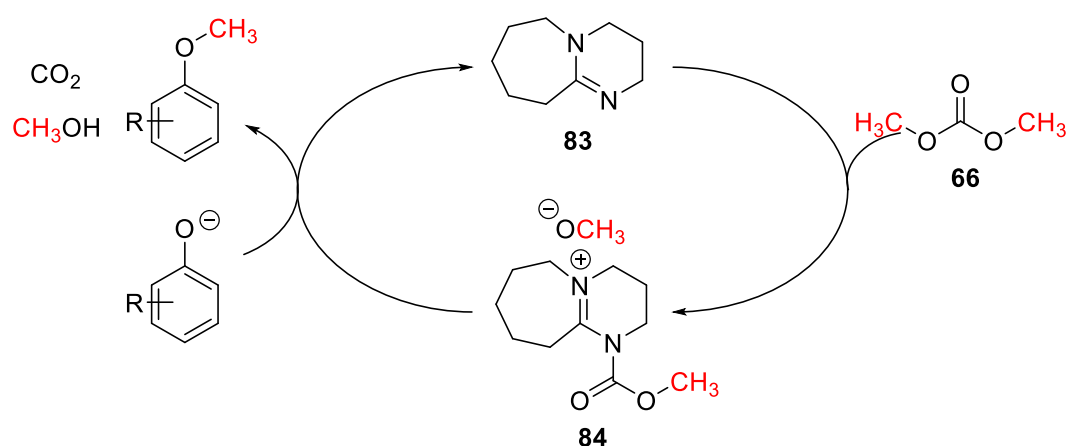


Figure 17. Methylation of phenols using dimethylcarbonate (**66**) and DBU (**83**) as a catalyst.⁸⁵

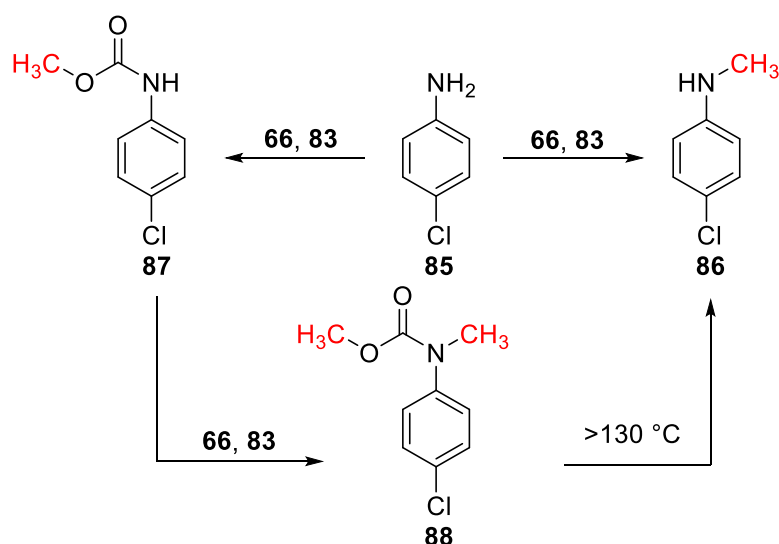


Figure 18. Mono *N*-methylation of aniline **85** using **66** and **83**, and the undesired methoxycarbonylation side reaction.^{83,86}

Trimethyloxonium tetrafluoroborate, or the *Meerwein Salt* (**67**), is another highly reactive electrophilic methylating reagent. It has been used in the alkylation of various anions and uncharged nucleophiles.⁸⁷ On account of its strong electrophilicity, it generally alkylates the site of an ambident nucleophile that has the highest electron density. It is typically used in cases where poly-alkylated products are desired, that are unobtainable through the use of more conventional electrophilic methylating reagents, for example in the synthesis of vinylidene disulfonium salt **90** (**Figure 19**).⁸⁸ **67** is a crystalline solid so despite its high toxicity and corrosiveness, is generally considered safer to handle than **61-65**. The major drawback associated with **67** is its low stability in air. It is stable enough to handle in air for a short period of time, but reactions must be carried out under an inert atmosphere, and storage is recommended under argon at a temperature below -15 °C.⁸⁷ The instability of **67** precludes its widespread use in large-scale manufacturing.

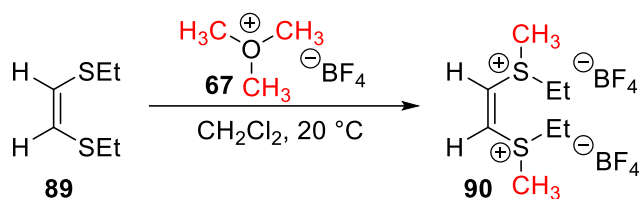


Figure 19. Preparation of vinylidene disulfonium salt (**89**) using trimethyloxonium tetrafluoroborate (**67**).⁸⁸

Diazomethane (**68**) is the last of the classical electrophilic methylating reagents that will be considered in this section. By far, the most common use of **68** is in the conversion of carboxylic acids to methyl esters, this is because **68** provides almost unrivalled selectivity in this kind of transformation.⁸⁹ The success of **68** in methylating acidic functionalities can be explained by its reaction mechanism (**Figure 20**).⁹⁰ **68** can be protonated by the carboxylic acid which simultaneously forms a highly reactive diazonium cation (**91**) and a carboxylate nucleophile. The carboxylate can then attack **91** in what is presumed to be a $\text{S}_{\text{N}}2$ reaction, which delivers the desired methyl ester product and the energetically favourable molecular nitrogen. Methylation of other, less

acidic, heteroatoms has been reported but generally an additional catalyst such as boron trifluoride etherate is required for suitable reactivity.^{89,91}

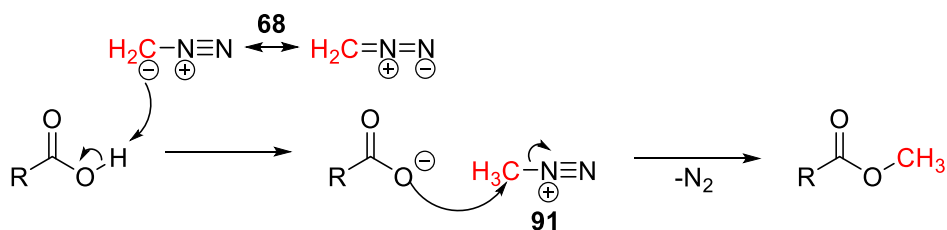


Figure 20. Mechanism of carboxylic acid esterification using diazomethane (**68**).⁹⁰

It has been shown that highly reactive methylating reagents usually have significant safety concerns associated with them, and diazomethane is no exception. **68** is a highly toxic and explosive gas which necessitates the use of rigorous safety protocols during its use. Its explosivity can be triggered *via* crystallisation, intense irradiation, and contact with rough surfaces or certain metal ions.^{89,92} Furthermore, during storage **68** has a tendency to undergo self-polymerisation reactions. To overcome safety issues related to its storage, **68** is often formed *in situ* from precursors such as *N*-methyl-*N*-nitroso-*p*-toluenesulfonamide (**92**), *N*-methyl-*N*-nitrosourea (**93**), or 1-methyl-3-nitro-1-nitrosoguanidine (**94**), then used immediately (**Figure 21**).⁹²⁻⁹⁴

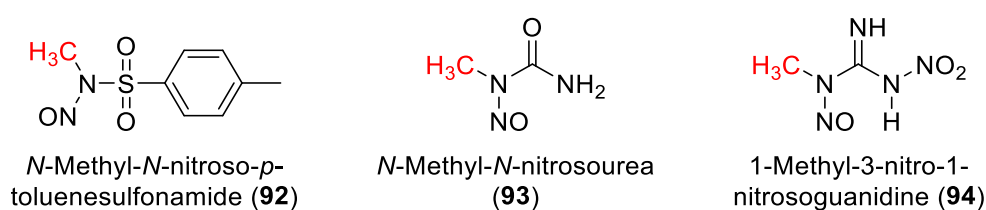


Figure 21. Common precursors used to generate diazomethane in situ.^{89,92,93}

Nucleophilic methylating reagents

Nucleophilic methylating reagents are largely outside the scope of this project; nonetheless, for completeness, a very brief introduction into their use is given below.

Nucleophilic methylating reagents can be thought of as synthetic equivalent of the methyl anion, CH_3^- . Due to the relatively electronegative nature of the methyl group in such reagents. Delivery of these anion equivalents is usually accomplished *via* alkyl-metal reagents (**Figure 22**). Organometallic methylating reagents are used to install methyl functionalities into electrophilic substrates such as ketones, carboxylic acids, esters, imines, and nitriles.

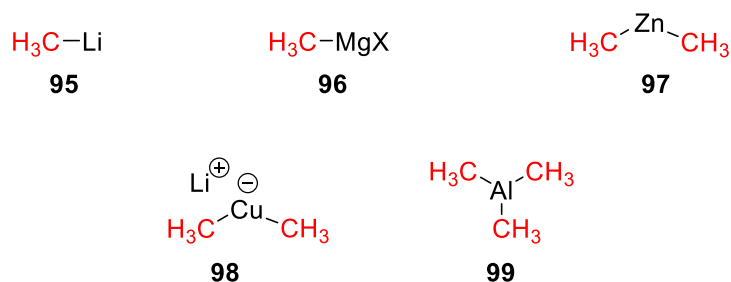


Figure 22. A selection of commonly used organometallic nucleophilic methylating reagents.

Methyl lithium (**95**) and methyl Grignard reagents (**96**) are two widely used nucleophilic methylating reagents, they are both viewed as hard nucleophiles and favour 1,2-addition when reacting with α,β -unsaturated systems (**Figure 23**).^{73,95,96} Dimethylzinc (**97**) has a similar reactivity profile to **95** and **96**. **97** is sometimes preferred to the latter two because it often has a better functional group tolerance; however, it is less stable and is highly flammable which can be a limiting factor in its usage.⁹⁷

Lithium dimethylcopper, also referred to as a *Gilman reagent* (**98**), provides a softer source of nucleophilic methyl group.⁹⁸ As such, reactions with **98** tend to favour the softer electrophilic site in a substrate, this is evident in its preference to undergo 1,4-conjugate additions in α,β -unsaturated systems (**Figure 23**). Trimethylaluminium (**99**) is another widely used organometallic methylating reagent. It is frequently employed alongside trimethylsilyl trifluoromethanesulfonate as seen in the transformation of **105** to **106** during the synthesis of (\pm)-Alstoscholarisine C.⁹⁹

Alkyl metal complexes are generally air and moisture sensitive which requires their usage under inert conditions. Solubility and stability issues also narrow the scope of solvents in which these reagents can be used. Due to their effectiveness at installing methyl groups, their employment is widespread nonetheless.⁷³

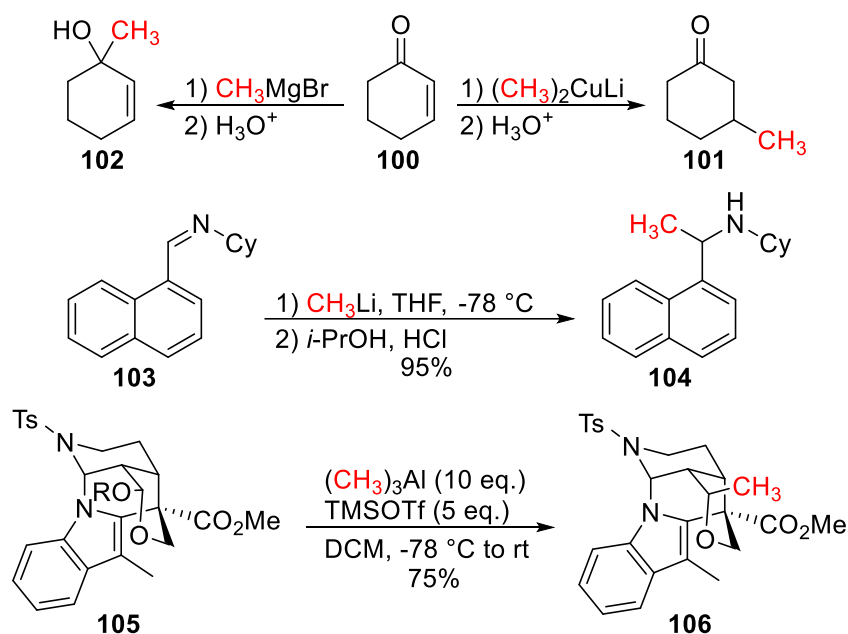


Figure 23. Examples of organometallic reagents being used in methylation reactions.^{96,98,99}

Radical-Based Methylation Reactions

In recent years, radical chemistry has undergone something of a renaissance.^{100,101} The ability of radicals to react with high selectivity, functional group tolerance, and under mild reaction conditions has made them a very attractive option to synthetic organic chemists. $\bullet\text{CH}_3$ radicals are relatively unstable which can present challenges with their usage; regardless, various protocols exist which have managed to harness them to methylate substrates effectively.¹⁰² Some of the recent developments in radical-mediated methylation reactions are documented in this section.

Peroxides are typically used in organic chemistry as either oxidants or radical initiators. Due to the relatively weak O-O bond in peroxides, under thermal or

photolytic conditions, they readily decompose to give a pair of alkoxide radicals.^{103,104} The alkoxide radicals can then undergo a subsequent bond fission to form a ketone and produce a $\bullet\text{CH}_3$ radical (**Figure 24a**). A number of carefully selected peroxides that can decompose in this manner have been used in a variety of methylative functionalisation reactions (**Figure 24b**).¹⁰⁴

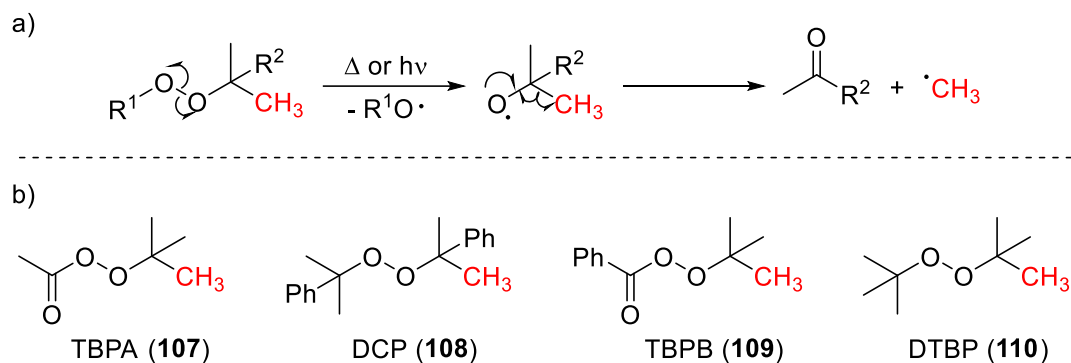


Figure 24. a) The generation of methyl radicals from peroxide precursors. b) Some common organic peroxides used in methylation methodologies.^{103,104}

The potential for peroxides to act as a reliable methyl source in methylation reactions was first reported in the C8 methylation of purine bases and related alkaloids by Zady and co-workers (**Figure 25**).¹⁰⁵ Under thermal (65-95 °C) or photolytic (>300 nm) conditions, *tert*-butyl peracetate (**107**) was used to produce methyl radicals that were able to methylate substrates such as caffeine (**13**) in the C8 position. The reaction was proposed to form the nitrogen based radical **112** which, following protonation from trifluoroacetic acid, delivered radical cation intermediate **113** which could then transform to the methylated product **111**. This early example of a radical methylation strategy has inspired a number of elegant methodologies in recent years.¹⁰⁴

A more recent example of CH methylation *via* dicumyl peroxide (**108**) produced radicals, is in the palladium-catalysed directed CH methylation reported by Li and co-workers.¹⁰⁶ A range of biaryl compounds were methylated in the *ortho*-aryl position in moderate to good yields with reasonable selectivity for monomethylated products (**Figure 26a**). The proposed catalytic cycle starts with the insertion of palladium(0) into the weak O-O bond of **114** to form a palladium (II) intermediate. Expulsion of acetophenone gives the methylpalladium intermediate **115**, which reacts with the

aromatic substrate to form α -cumyl alcohol and the palladium (II) species **116**. Finally, reductive elimination delivers the methylated aryl product and regenerates the palladium (0) catalyst. The proposed cycle was subject to limited mechanistic experiments so a Pd(II/IV) cycle could not be ruled out. This elegant approach to CH methylation sees palladium acting simultaneously as a peroxide initiator and a radical protector in this process.

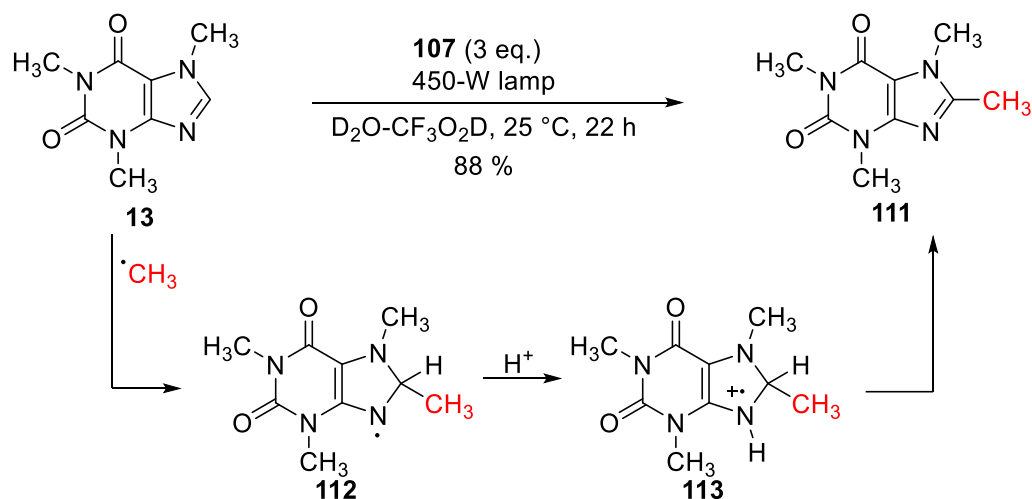


Figure 25. C8 methylation of caffeine using TBPA (**107**) and the proposed reaction mechanism.¹⁰⁵

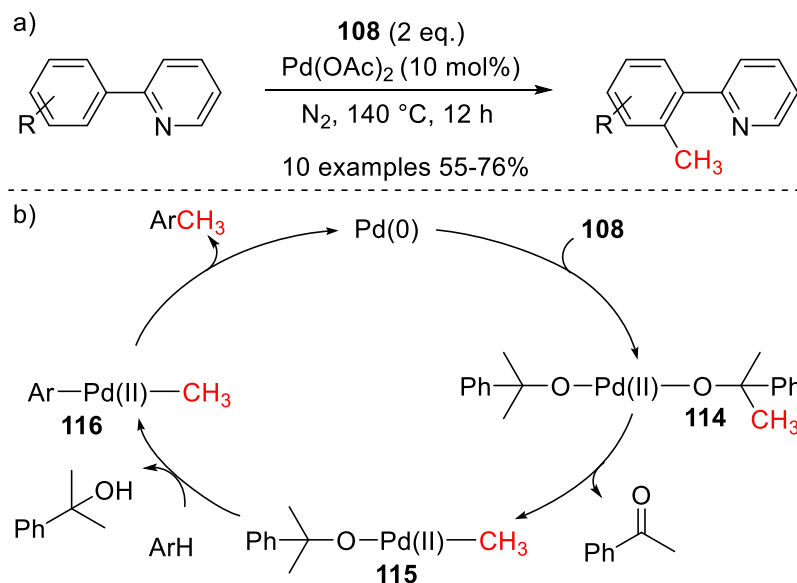


Figure 26. a) General scheme showing directed methylation of biaryl compounds using **108**. b) Proposed Pd(0/II) catalytic cycle of the methylation reaction.¹⁰⁶

Many of the reported methylation protocols using peroxides focus on the methylation of aromatic CH bonds. There has, however, been a number of methodologies that methylate different targets. These include *O*-methylation of carboxylic acids to form methyl esters, *N*-methylation of sulfoximines and a more unusual decarboxylative methylation of α,β -unsaturated carboxylic acids to form tertiary alkenes (**Figure 27**).¹⁰⁷⁻¹⁰⁹ Palladium, copper, or iron catalysts feature commonly in this type of reaction to activate the peroxides and to temper the radical intermediates.^{104,106} Major benefits of the use of peroxide in methylation reactions are that they are environmentally benign, fairly non-toxic, and easy to handle. However, the reported methodologies are often plagued with long reaction times and high temperatures which detract from the aforementioned green qualities.^{73,104}

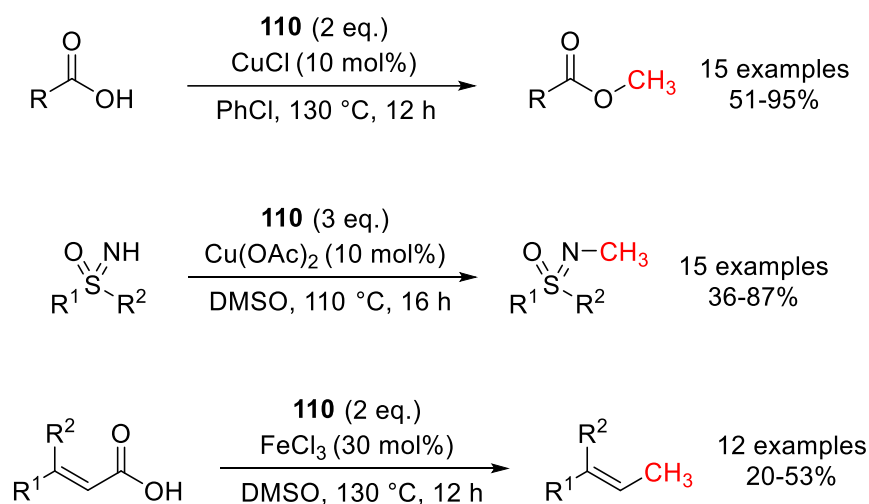


Figure 27. Various methylation protocols mediated by peroxides as a source of methyl radical.¹⁰⁷⁻¹⁰⁹

As demonstrated in the previous examples that used peroxides as methylating reagents, the inherent instability of the methyl radical often necessitates the use of a metal catalyst to placate its reactivity. Zard and co-workers took an alternative approach, where instead of directly generating methyl radicals, they sought to generate methyl radical equivalents that were more stable (**Figure 28**).

The researchers initially hoped that treating xanthate **117** with dilauroyl peroxide (DLP) as a radical initiator, they could generate radical intermediate **118** which would expel xanthate **119** and a methyl radical.¹¹⁰ Due to the instability of the methyl radical, the last part of this initiation reaction did not occur (**Figure 28a**). Instead, they took xanthate **120** and upon heating with DLP, the more stable carbon-centred radical **122** was generated through intermediacy of **121** (**Figure 28b**). This radical could then form an adduct with a range of heterocycles in a similar vein to the earlier work seen by Zady and co-workers.¹⁰⁵ In the example shown, caffeine (**13**) was the substrate, which lead to the intermediate **123**. The reaction was carried out in ethyl acetate at reflux which caused a thermal decarboxylation event, giving the desired methylated product **111** in 65% yield (**Figure 28c**). This methodology uses a creative approach, using a methyl radical surrogate to overcome its inherent instability. Unfortunately, many of the other heterocyclic substrates tested were reluctant to undergo the decarboxylation step, giving **123**-like acids as the major product.

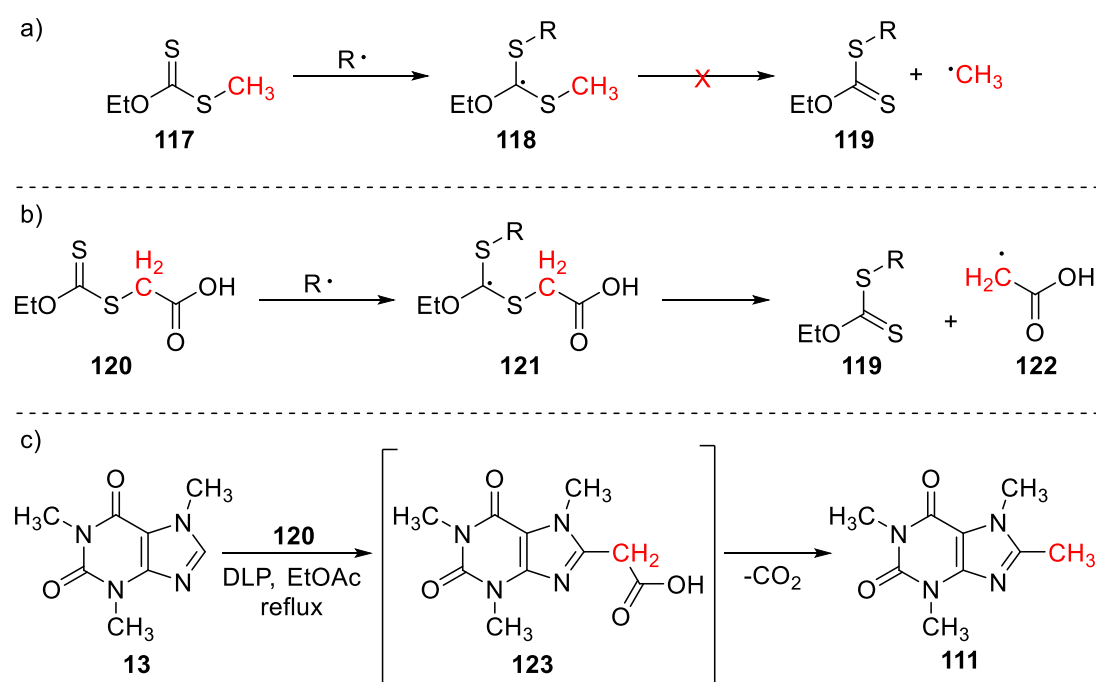


Figure 28. a) Attempt to generate methyl radicals from xanthate **117**. b) Formation of methyl radical equivalent **122** from xanthate **120**. c) Methylation of caffeine (**13**) using **120**.¹¹⁰

An alternative approach to generating methyl radical equivalents was published in a pioneering report by Li and co-workers.¹¹¹ Inspired by a photo-redox catalysed hydroxymethylation manifold designed by DiRocco and co-workers that yielded methylated side-products, the Li group sought to add methoxy radicals to heteroarenes that could undergo a dehydroxylation to deliver methylated products using a photo-induced, transition metal free approach.¹¹²

The generation of methoxy radical (**130**) from methanol (**126**) is typically slow, so the researchers proposed that its formation would be the rate limiting step in their process. Using **26** as the reaction solvent and dichloromethane (**131**) and trifluoroacetic acid (TFA) as additives, the group found that **130** could be adequately generated when the system was irradiated with UV light. Using 2-methylquinoline (**124**) as a substrate, the groups mechanistic study lead to the proposal of three pathways in which **130** could be formed (**Figure 29**).¹¹¹

The first pathway involves the photoinduced single electron transfer (SET) between solvent **126** and the cation **125** (**124** protonated by TFA), to form radical intermediate **127** and the methanol radical cation **128**. Intramolecular hydrogen transfer to give **129** and a subsequent deprotonation could deliver the desired methoxy radical **130** (**Figure 29a**). Alternatively, a similar pathway could be achieved by SET between **126** and **131**, to give dichloromethane radical anion **132** and **128** which could go on to become **130** in the aforementioned process (**Figure 29b**). The final pathway is initiated by the UV-light-induced heterolytic cleavage of **131** forming chlorine radical **133**. **133** could then abstract a hydrogen atom from **126** to deliver the desired methoxy radical and HCl (**134**) (**Figure 29c**).

Once generated, **130** can attack the C3 position of **125**, giving methoxy-substituted radical cation intermediate **135** which can exist between two resonance forms (**Figure 29d**). Loss of a water molecule leads to intermediate **136**. The strong nucleophilicity of the radical-cationic nitrogen atom in **136** should allow it to abstract a hydrogen atom from another equivalent of **126** forming a protonated amine, which after deprotonation would give **137**. Finally, tautomerisation of the enamine would deliver the desired product **138**.

This elegant approach to methylation was applied to a wide range of heterocycles, including a wide range of *S*-, and *N*-containing 5-, and 6-membered rings. The yields of methylated products were generally good (54-80%). This methodology presents some excellent advantages over a number of existing methods as it doesn't require handling of sensitive reagents, it is transition-metal free, and is carried out under operationally simple non-inert conditions.¹¹¹

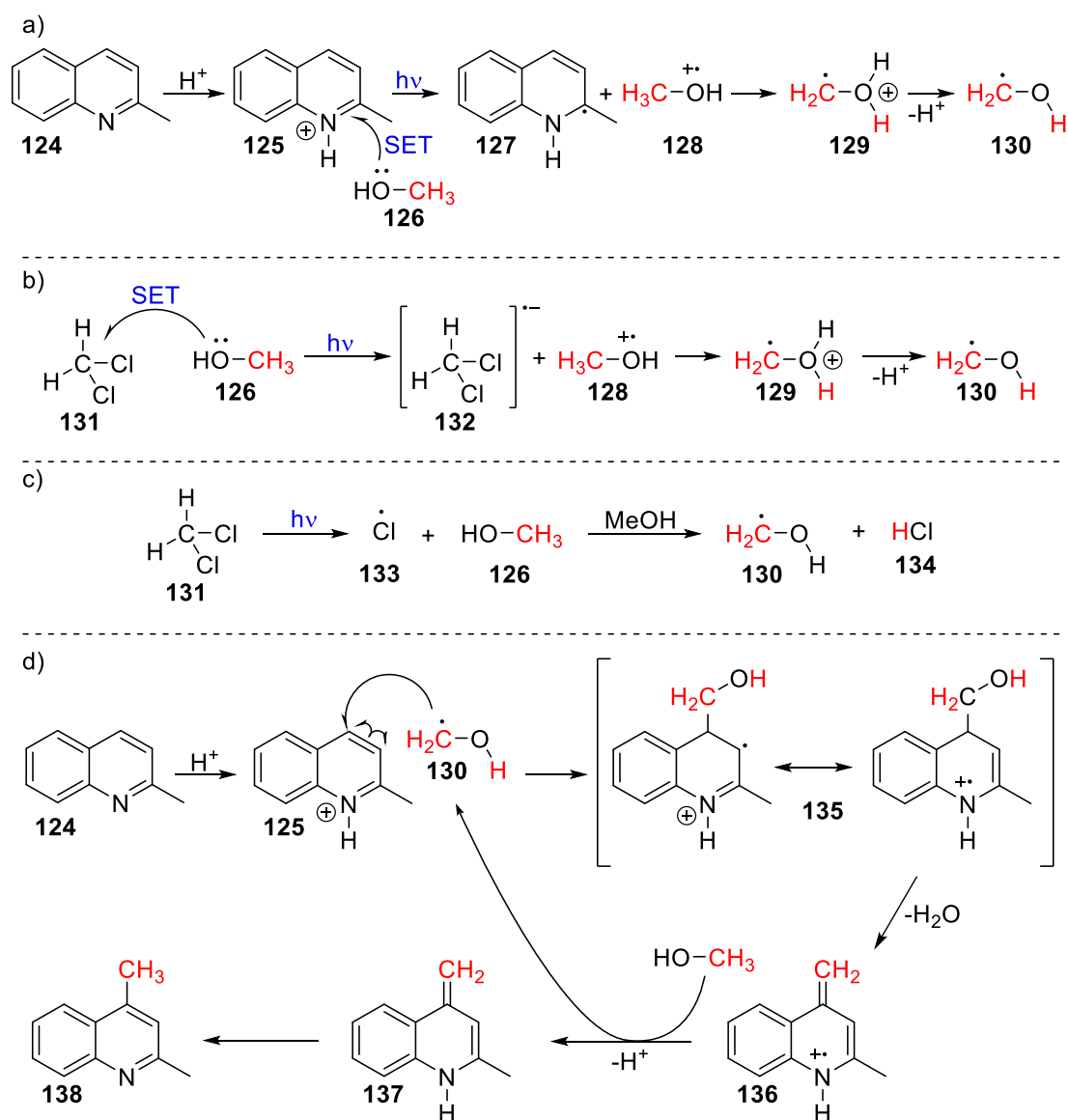


Figure 29. a) Formation of methyloxy radical (**130**) initiated by SET between methanol (**126**) and substrate (**124**). b) Formation of **130** initiated by SET between methanol (**126**) and dichloromethane (**131**). c) Formation of **130** initiated by photolysis of **131**. d) Proposed mechanism for addition of **130** to **124** and subsequent dehydroxylation to form methylated quinoline **138**.¹¹¹

Transition Metal Catalysed Methylation Reactions

The use of transition metal catalysis is ubiquitous in most realms of organic synthetic chemistry. With widespread applications it has helped chemists access a wealth of unexplored chemical space.^{113–115} The field of methylation chemistry is no exception, and has benefited greatly from the advancements in catalysis over recent years.^{73,116} This section aims to highlight some of the recent advancements in transition metal catalysed methylation reactions. Owing to the importance of methylation chemistry, research in this field has been very active; as such, the list of methods presented in this section is not intended to be exhaustive, but rather it will give an introduction to the techniques that methylation users can add to their toolkits.

Transition metal catalysis has significantly increased the number of chemicals that can act a source of methyl groups. Through the use of rhodium catalysis, *N,N*-dimethylformamide (**139**) has been used in the α -methylation of ketones (**Figure 30**).¹¹⁷ **139** can be oxidised *via* persulfate to form the iminium ion **140**, which can react with a ketone-derived enolate forming intermediate **141b**. An enolate mediated C-N bond scission gives α,β -unsaturated compound **142**. This process allows the transfer of a 1-carbon unit from **139** to the ketone substrate without the need for metal catalysis; however, the procedure delivers a methylene unit rather than the desired methyl. Here, rhodium catalyst **143** can form a metal-hydride (**145**) which can successfully reduce the unsaturated system to deliver the homologated ketone product.

This one pot reaction was applied to a broad scope of electron-rich and electron deficient aryl ketones, delivering α -methylated products in moderate to excellent yields (**Figure 30a**). Aside from the expensive rhodium catalyst, one of the major drawbacks associate with this methodology is the inability to reliably control over-alkylation. Furthermore, poor regioselectivity was obtained when substrates that had two α -hydrogen sites were tested under these conditions.¹¹⁷ As a cheap and abundant reagent *N,N*-dimethylformamide has been employed in a number of other methylation protocols; *N,N*-dimethylformamide dimethylacetal has been employed in similar reactions also.^{118,119}

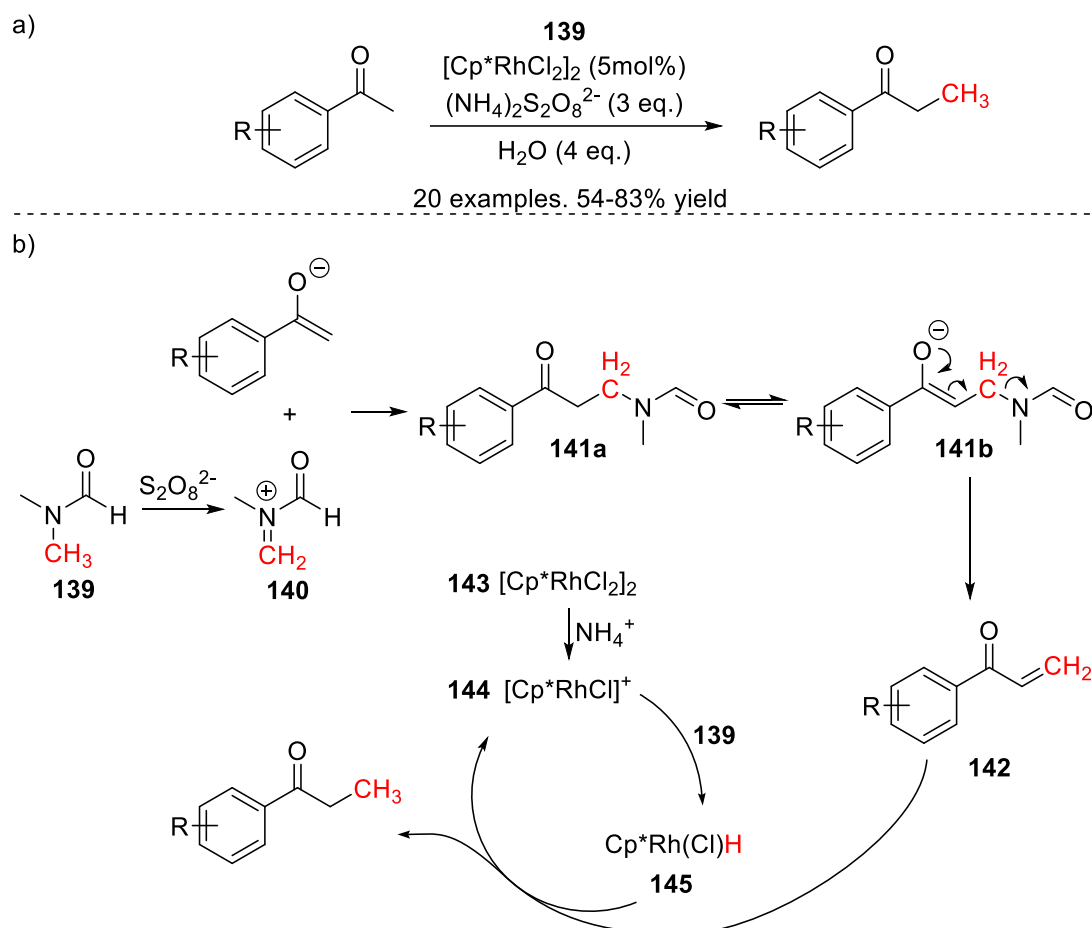


Figure 30. a) Rhodium catalysed α -methylation of aryl ketones using *N,N*-dimethylformamide (**139**). b) Proposed mechanism for the methylation reaction.¹¹⁷

Dimethyl sulfoxide (DMSO, **148**) has also found use as a methylating reagent under the catalytic influence of multiple transition metals.^{73,116,120–122} A recent report by Guo and co-workers used DMSO as a source of methyl group in a copper-catalysed synthesis of methyl esters from carboxylic acids (**Figure 31a**).¹²³ The broad substrate scope included aryl-, heteroaryl-, alkenyl-, and alkyl-carboxylic acids with yields ranging from 32-82% over 24 examples, though yields of around 60% and above were achieved in the cases of the benzoic acid derivatives. Though the exact mechanism is not known for this reaction, the group have proposed a pathway which mechanistic experiments point towards (**Figure 31b**). Hydrogen peroxide (**146**) can be homolysed by a Cu^{I} species to form two equivalents of hydroxyl radical (**147**), which can then add to **148** to form intermediate **149**. **149** then decomposes to methane sulfinic acid and a methyl radical. Meanwhile, in the presence of base, the acidic substrate can ligate to

the Cu^{II} catalyst. The copper-substrate complex can be intercepted by the methyl radical forming the desired methyl ester product.¹²³

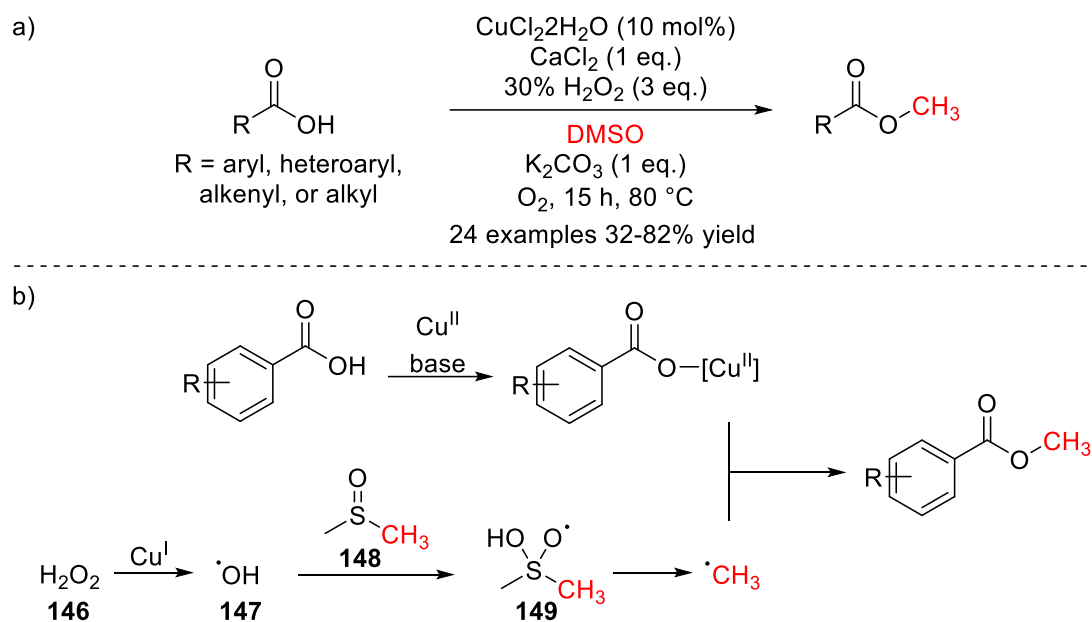


Figure 31. a) Copper catalysed methylation of carboxylic acids using DMSO (**148**).
b) Proposed mechanistic pathway for the methylation reaction.¹²³

Methanol (**126**), the simplest alkyl alcohol has found many uses as a source of methyl groups.^{124,125} Its abundance, low cost, and potential for atom-economical methylation reactions make it an attractive option. Methanol has been used in photoinduced methylation protocols (**Figure 29**),¹¹¹ and in multiple variations of the Mitsunobu reaction.¹²⁶ Here, the application of **126** in methylation reactions through a hydrogen-borrowing approach will be discussed.

Hydrogen-borrowing strategies that use **126** in the *N*-alkylation of amines follow the same general catalytic cycle (**Figure 32a**).^{73,127} Through a hydrogen transfer process, an appropriate metal catalyst oxidises **126** to generate formaldehyde (**150**) and a metal-hydride intermediate. The amine substrate condenses with **150** to form an aminoalcohol intermediate (**151**), a base mediated dehydration then gives the corresponding imine (**152**). The metal hydride species that was generated in the first step of the catalytic cycle can deliver the hydride to the imine, reducing it to the *N*-

methylated product (**153**). Liu and co-workers reported an efficient procedure for *N*-methylation of amines using a **126** and a relatively inexpensive cobalt catalyst (**Figure 32b**).¹²⁸ When primary alkyl amines were used as substrates, dimethylation was observed as the major product in all cases, conversely mono-methylation was observed when primary aromatic amines were used.

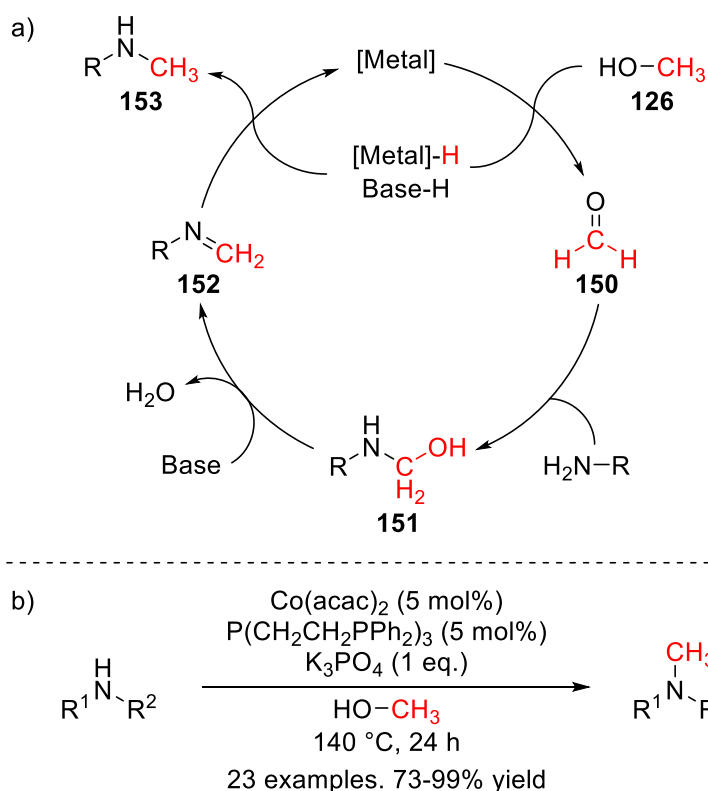


Figure 32. a) General catalytic cycle for the *N*-methylation of amines using **126** with a hydrogen borrowing approach. b) An example of a copper catalysed hydrogen-borrowing *N*-methylation of amines.^{127,128}

1.1.3 *N,N,N*-Trimethylanilinium Salts

Quaternary ammonium salts have found applications in most fields of chemistry. They can be found in the structures of drug molecules (**154**), asymmetric phase transfer catalysts (**155**) and in ionic liquids (**156**) (**Figure 33**).^{129–131} Further applications of quaternary ammonium salts can be found in the fields electrochemistry, material science and the textiles industry.^{132–134}

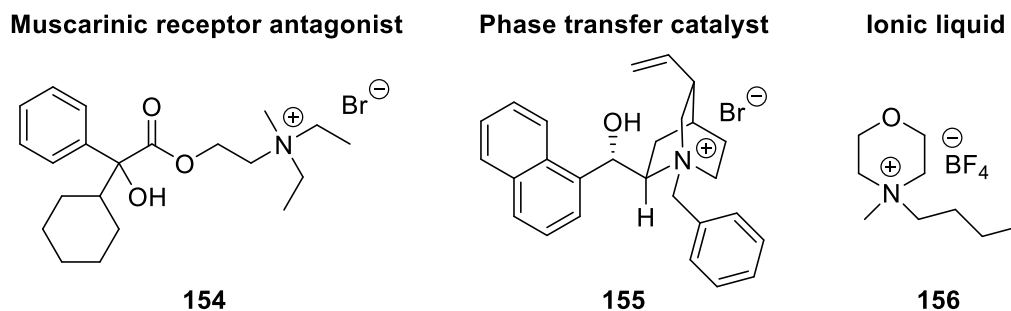


Figure 33. Quaternary ammonium salt moieties appearing in drug compounds (**154**), phase transfer catalysts (**155**), and ionic liquids (**156**).^{129–131}

This section will focus on the use of quaternary ammonium salts in synthetic organic chemistry. More specifically, it will look at molecules containing the aryltrimethylammonium moiety, also known as *N,N,N*-trimethylanilinium salts (**Figure 34**).

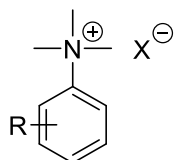


Figure 34. General structure of *N,N,N*-trimethylanilinium salts.

N,N,N-Trimethylanilinium Salts in Cross-Coupling Reactions

Arylamines are prevalent in pharmaceutical compounds and natural products. The ability to use the amino substituent as a handle for further functionalisation presents attractive opportunities to synthetic chemists. Due to the thermodynamic and kinetic stability of *N,N*-dialkyl arylamines, and their ability to coordinate strongly with metal centres, reports of their direct employment in cross-coupling reactions are extremely rare.^{135–138} Derivatization of the amine is normally carried out prior to cross coupling to weaken the C-N bond and facilitate oxidative addition to a metal centre.

Conversion of arylamines to aryl diazonium salts has been utilised in this manner in a number of cross-coupling methodologies (**Figure 35**).¹³⁹ The preparation of diazonium cross coupling partners is predicated on the arylamine being a primary

amine, the diazotisation process uses strongly acidic conditions, and the resulting diazonium salts carry the risk of explosion. These factors can discourage the use of a diazonium strategy.

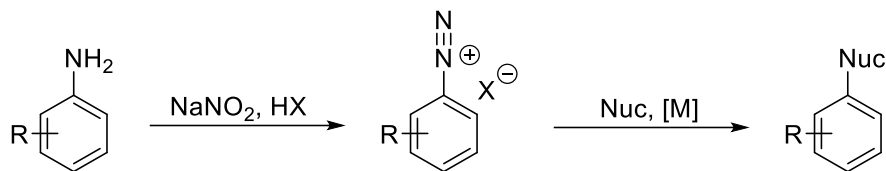


Figure 35. Diazotisation of primary arylamines and their use as electrophilic partners in cross-coupling reactions.¹³⁹

An alternative method for derivatising amines such that they can act as electrophilic partners in cross-coupling reaction is by quaternising the amine. This can be done through the a straight-forward alkylation of the arylamine, which can then be used in transition metal catalysed reactions. (**Figure 36**). The success of *N,N,N*-trimethylanilinium salts as cross-coupling electrophiles relies on the high polarity of the C-N bond and the thermodynamically favourable release of a neutral amine upon reaction.

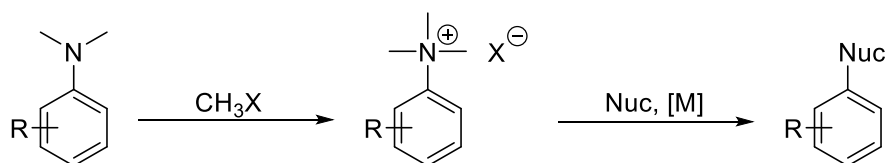


Figure 36. Quaternisation of a dialkyl arylamines and their subsequent use in cross-coupling reactions.

The first instance of *N,N,N*-trimethylanilinium salts being used in cross-coupling reactions was reported in the pioneering work of Wenkert and co-workers.¹⁴⁰ The group took a variety of aryl-substituted *N,N,N*-trimethylanilinium iodides and coupled them with Grignard reagents under nickel catalysed Kumada-type cross-coupling (**Figure 37a**). The yields of cross-coupled products varied significantly depending on

the substrate (methoxy and fluoro substituents were not well tolerated), and demethylation of the anilinium salts was a significant by-product in many cases.

The catalytic cycle resembles that of a typical Kumada cross-coupling (**Figure 37b**). The active nickel (0) catalyst (**157**) is proposed to react with the anilinium iodide to give the nickel (II) oxidative addition product (**158**) with extrusion of trimethylamine. A transmetalation step with the Grignard reagent give nickel (II) species **159**, which can then undergo a reductive elimination to deliver the cross-coupled product and regenerate **157**.^{140,141} Similar nickel catalysed cross couplings have been reported by the Wang group which use arylzinc or organoaluminium reagents as the nucleophilic coupling partners giving largely high yielding reactions (**Figure 38**).^{141,142}

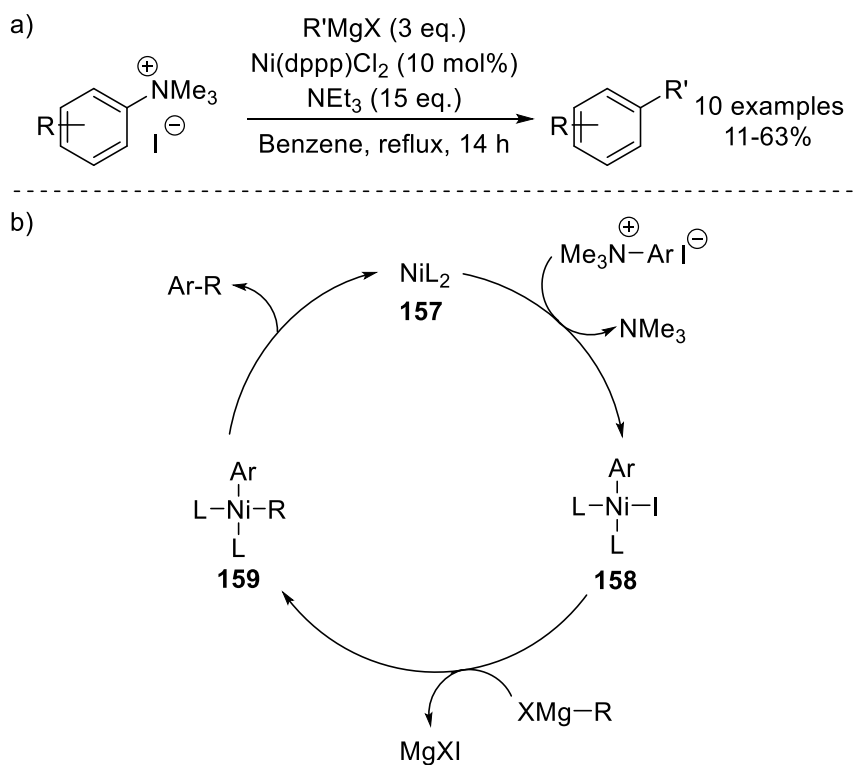


Figure 37. a) Nickel catalysed Kumada-type cross-coupling between *N,N,N*-trimethylanilinium iodides and Grignard reagents. b) Proposed mechanism of the Kumada-type cross-coupling.¹⁴⁰

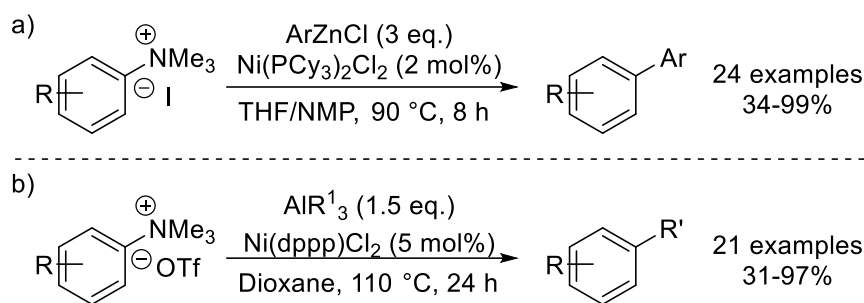


Figure 38. a) Kumada-type cross coupling with *N,N,N*-trimethylanilinium iodides and arylzinc reagents. b) Kumada-type cross-coupling of *N,N,N*-trimethylanilinium triflates and organoaluminium reagents.^{141,142}

The nickel catalysed Kumada-type cross-couplings shown above represent some of the early advancements in the use of *N,N,N*-trimethylanilinium cross-coupling reactions. Whilst good yields are achieved in many cases, long reaction times and high temperatures were often necessary. A report by Reeves and co-workers overcame some of these challenges (**Figure 39a**).¹⁴³ During their optimisation, they found that using anilinium triflate salts in the place of anilinium iodides allowed cross-coupling reactions to proceed smoothly. Furthermore, in screening some non-nickel catalysts, they found that $\text{PdCl}_2(\text{PPh}_3)_2$ was able to facilitate the Kumada coupling effectively. The operational ease of this methodology was demonstrated by carrying out a one pot quaternisation then Kumada coupling, directly from a dimethylaniline. The group also compared the reactivity of the anilinium triflate as an electrophile to some alternative aryl halides and aryl triflate, finding that the anilinium salt was inferior in reactivity only to the aryl iodide (**Figure 39b**).

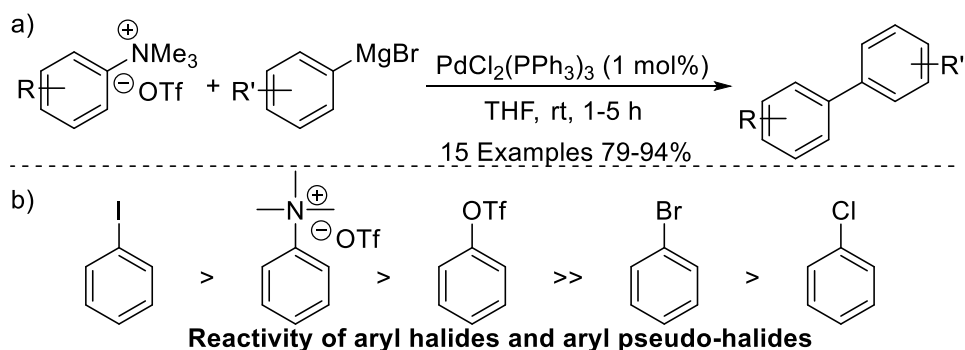


Figure 39. a) Reeves' palladium catalysed Kumada-type cross-coupling of *N,N,N*-trimethylanilinium triflate salts and Grignard reagents. b) Comparative reactivity of aryl halides and aryl pseudohalides under these conditions.¹⁴³

In an attempt to move away from Kumada-type cross-couplings that required the preparation of sensitive organometallic nucleophilic cross-coupling partners, MacMillan developed a Suzuki coupling that employed *N,N,N*-trimethylanilinium salts (**Figure 40**).¹⁴⁴ Palladium catalysts proved ineffective at facilitating these reactions whereas Ni(COD)₂ used with an NHC ligand (IMes) could readily insert into the aryl-ammonium bond and mediate cross-couplings with high yielding results. A wide range of readily-accessible electron-rich and electron-deficient boronic acids were employed in the study making this a versatile methodology to create substituted biaryl systems.

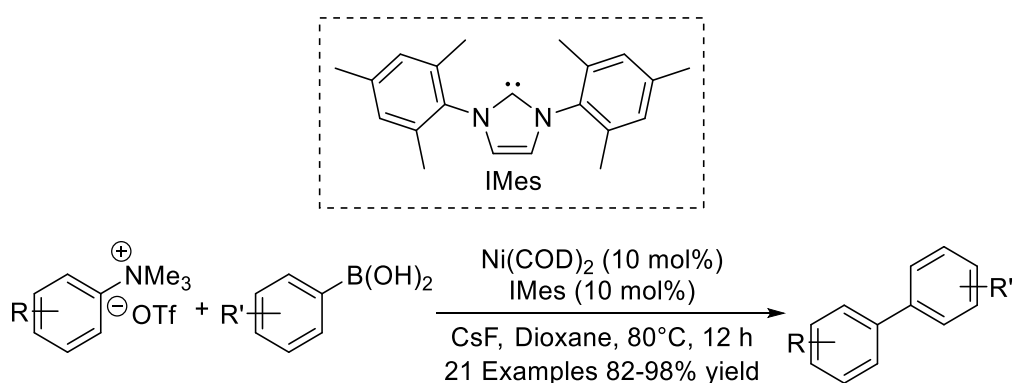


Figure 40. Suzuki cross-coupling of *N,N,N*-trimethylanilinium triflates and arylboronic acids.¹⁴⁴

A number of other notable cross-coupling methodologies that use *N,N,N*-trimethylanilinium salts as electrophilic cross coupling reactions have been reported. These include Sonogashira couplings, borylation reactions, oxazole and thiazole arylations and amination reactions (**Figure 41a-c**).¹⁴⁵⁻¹⁴⁸ This type of cross-coupling where the metal must insert itself in the aryl-ammonium bond seem to be exclusively catalysed by nickel or palladium. Also, it is notable that for arylative cross coupling reactions, the use *N,N,N*-trimethylanilinium triflates seems to be much more widespread than the halide analogues such as the iodide salts used in the pioneering report from Wenkert, though there has been no rigorous investigation into understanding the role that counterion plays in cross-coupling efficiency.¹⁴⁰

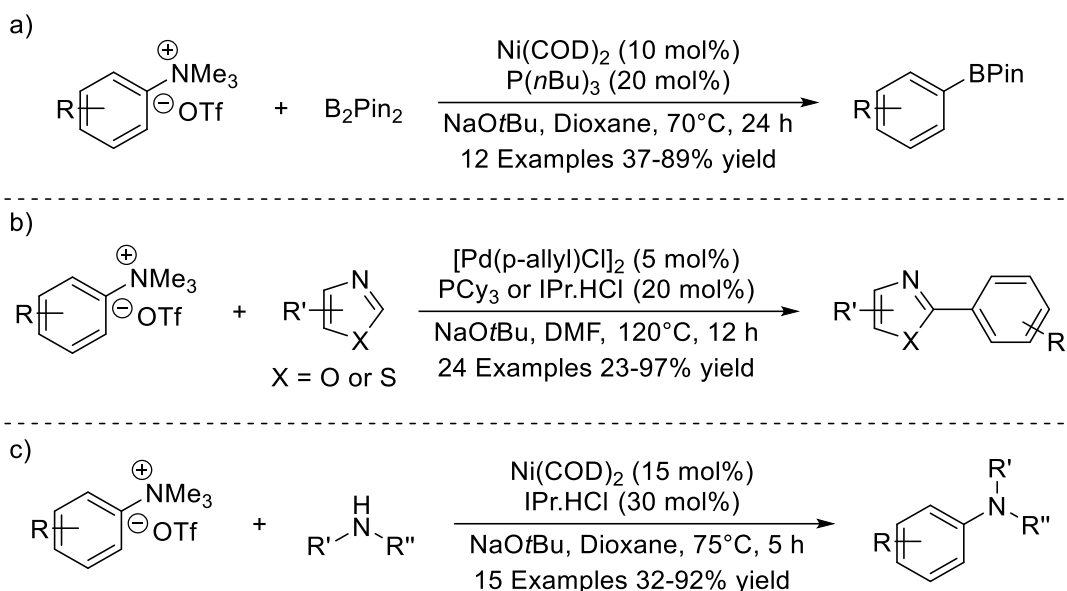


Figure 41. a) Borylation of *N,N,N*-trimethylanilinium triflates. b) Oxazole and thiazole arylation using *N,N,N*-trimethylanilinium triflates. c) Amination reactions using *N,N,N*-trimethylanilinium triflates.^{145–147}

A notable example of *N,N,N*-trimethylanilinium salts in cross-coupling reactions involves an elegant C-H borylation methodology reported by Phipps and co-workers (**Figure 42**).¹⁴⁹ Iridium catalysed aryl C-H borylation reactions typically use steric factors to control regioselectivity rather than electronics, as a result it is a useful method of introducing boron groups *ortho* to existing substituents.¹⁵⁰ However, when 1,2-disubstituted substrates are employed, regioselectivities are typically poor. This work sought to overcome these challenges by designing a catalytic system that could impart regio-control through ion-pair interactions.

Computational modelling led to the design of bi-functional anionic ligand **160** (**Figure 42a**). The modelling suggested that the anionic sulfonate on **160** could form favourable interactions with the cationic ammonium functionality of the substrate (**Figure 42b**). This interaction directed the *meta*-proton of the substrate towards the vacant site on the iridium catalyst, which allowed for regioselective CH functionalisation in this position. Running the reaction under the same conditions but replacing **160** with a neutral dtbpy ligand gave poor regioselectivity which was taken as strong evidence that the ion-pair directed control was taking place. Importantly, no reactivity resulting from iridium insertion into the aryl-ammonium bond was observed.¹⁴⁹

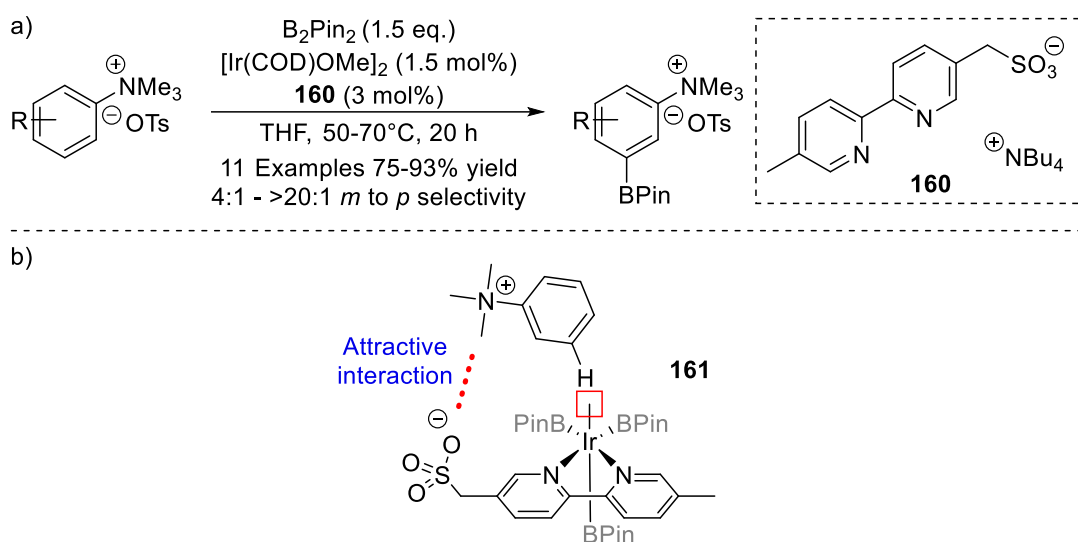


Figure 42. a) Iridium catalysed C-H borylation of *N,N,N*-trimethylanilinium tosylates. b) Ion-pair assisted meta-selective borylation.¹⁴⁹

N,N,N-Trimethylanilinium Salts in *S_NAr* Reactions

Transition metal catalysed functionalisation of *N,N,N*-trimethylanilinium salts has proven useful in organic chemistry. There has also been a number of reports that directly use anilinium salts as *S_NAr* substrates in the absence of any transition metal catalysts.

Uchiyama and co-workers reported the synthesis of aryl ethers through an *S_NAr* approach using *N,N,N*-trimethylanilinium salts in 2018 (**Figure 43**).¹⁵¹ An impressive range of aliphatic and aromatic alcohols were tolerated as nucleophiles under these conditions, giving consistently high yielding ether products. Numerous hydroxyl-containing pharmaceutical compounds and natural products were functionalised using this methodology. The triflate counterion was shown to be the most successful in this kind of reaction, and other conditions such as the species of base or solvent used were critical for reaction efficiency. A later report from the same group showed that this kind of methodology could be expanded for use with a broad range of heteroatomic nucleophiles. The powerful and general methodology is demonstrated through the late stage functionalisation of *N*-methyl-sulfadiazine (**162**) with germanium, silicon, aniline, thiol, selenium, and stannyl nucleophiles (**Figure 44**).¹⁵² Use of mercaptoethanol followed by a Smiles rearrangement gave a phenol product.

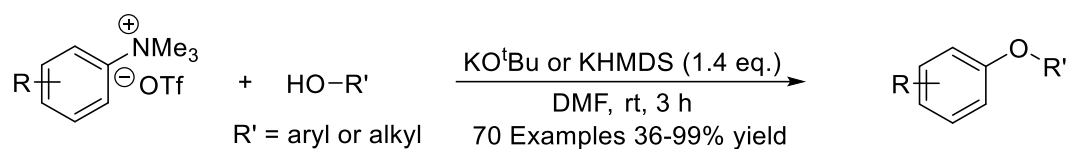


Figure 43. Synthesis of aryl ethers using *N,N,N*-trimethylanilinium triflates as $\text{S}_{\text{N}}\text{Ar}$ substrates.¹⁵¹

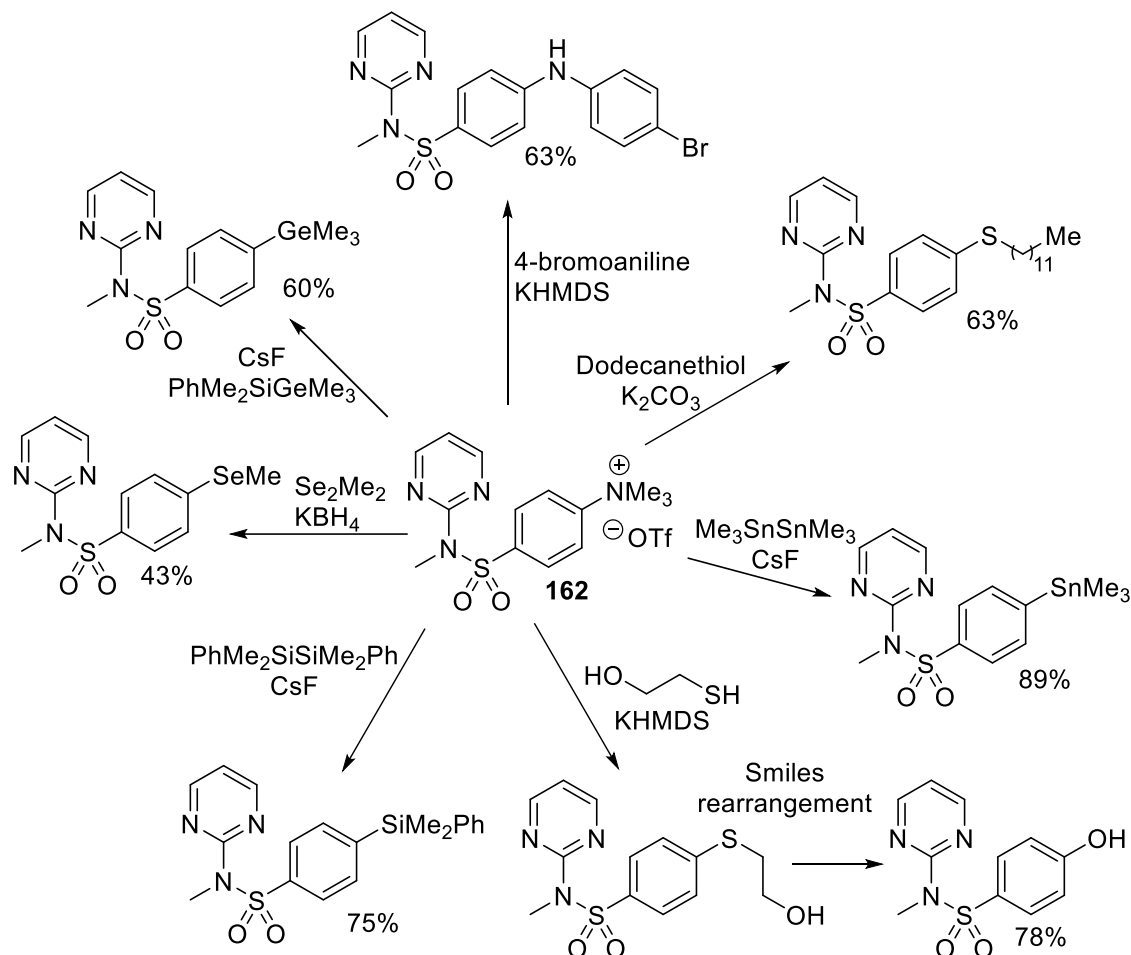
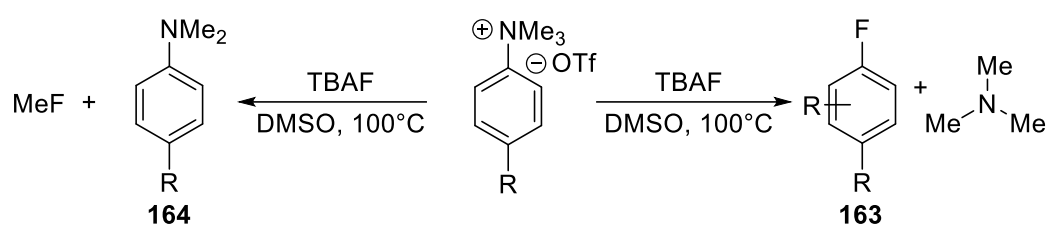


Figure 44. General $\text{S}_{\text{N}}\text{Ar}$ functionalisation of *N,N,N*-trimethylanilinium triflate (**162**) with a diverse range of nucleophiles.¹⁵²

A long-standing use of *N,N,N*-trimethylanilinium salts being used as $\text{S}_{\text{N}}\text{Ar}$ substrates is in the synthesis of aryl fluorides.¹⁵³ ^{18}F labelled aryl fluorides are often synthesised in this manner since the reactions generally proceed quickly and avoid the need for complex fluorinating reagents.¹⁵⁴

DiMagno and co-workers reported synthesis of aryl fluorides (**163**) by treating *N,N,N*-trimethylanilinium triflate with tetrabutylammonium fluoride (TBAF) in DMSO (**Figure 45**).¹⁵⁵ It was noticed during this study that with electron rich anilinium substrates, the competitive retro-Menschutkin demethylation from the fluoride anion to generate methyl fluoride and dimethylaniline (**164**) was dominant. ¹H-¹⁹F HOESY NMR studies conducted by the group suggests that a close ion pair exists between the fluoride anion and ammonium cation.



| Substituent | % 163 | % 164 |
|--------------------|--------------|--------------|
| NO ₂ | 99 | 1 |
| CHO | 99 | 1 |
| CN | 99 | 1 |
| Bz | 99 | 1 |
| CO ₂ Me | 96 | 4 |
| Br | 2 | 98 |
| H | 1 | 99 |
| Me | 1 | 99 |
| OMe | 1 | 99 |

Figure 45. Competitive S_NAr vs demethylation observed when treating *N,N,N*-trimethylanilinium triflate with TBAF.¹⁵⁵

N,N,N-Trimethylanilinium Salts in Methylation Reactions

In 2016, Chatani and co-workers published the first reported example of *N,N,N*-trimethylanilinium salts acting as a source of methyl group under a transition metal catalysed reaction manifold.¹⁵⁶ The study found that 8-aminoquinoline-derived benzamides could undergo a directed *ortho*-methylation with *N,N,N*-trimethylanilinium iodide under a nickel catalysed system (**Figure 46a**).

The proposed catalytic cycle for this reaction is as follows (**Figure 46b**). In the presence of a base, the benzamide substrate can coordinate to the nickel (II) active catalyst to give intermediate **166**. A base mediated ligand exchange can then activate an *ortho*-CH bond to form the five-membered-metallocyclic intermediate **167**. Oxidative addition of the anilinium iodide gives a four-coordinate nickel (IV) intermediate (**168**), which can then reductively eliminate back to a nickel (II) species (**169**). Protonation of **169** then causes the substrate to dissociate as its methylated derivative and regenerates the active nickel (II) catalyst (**165**).

Curiously, at no point in the groups' study was insertion of nickel into the aryl-ammonium C-N bond observed. Oxidative addition of anilinium salts to nickel in cross-coupling reactions is assumed to take place with nickel (0) species (see *N,N,N*-Trimethylanilinium Salts in Cross-Coupling Reactions). It is thought that the nickel (II) catalyst (**165**) used in this report will not be nucleophilic enough to oxidatively insert into the anilinium methylating reagent. Instead, the N-CH₃ bond appears to undergo addition to **165** in this reaction.

It cannot be ruled out that the *N,N,N*-trimethylanilinium iodide salt is thermally decomposing in toluene to produce the *N,N*-dimethylaniline and methyl iodide. Halide counterion-led demethylation of quaternary ammonium salts to form methyl halides is well precedented.^{155,157-159} Methyl iodide formed through decomposition could actually be undergoing the oxidative insertion step, with the anilinium salt acting a methyl iodide surrogate rather than directly as a methylating reagent. In fact, methylation of benzamides under a very similar reaction system using methyl bromide was reported by the Chatani group in 2013.¹⁶⁰ Whether the active methylating reagent is the anilinium salt or methyl iodide, the report demonstrates that anilinium salts can be used to replace methyl halides in methylation reactions.

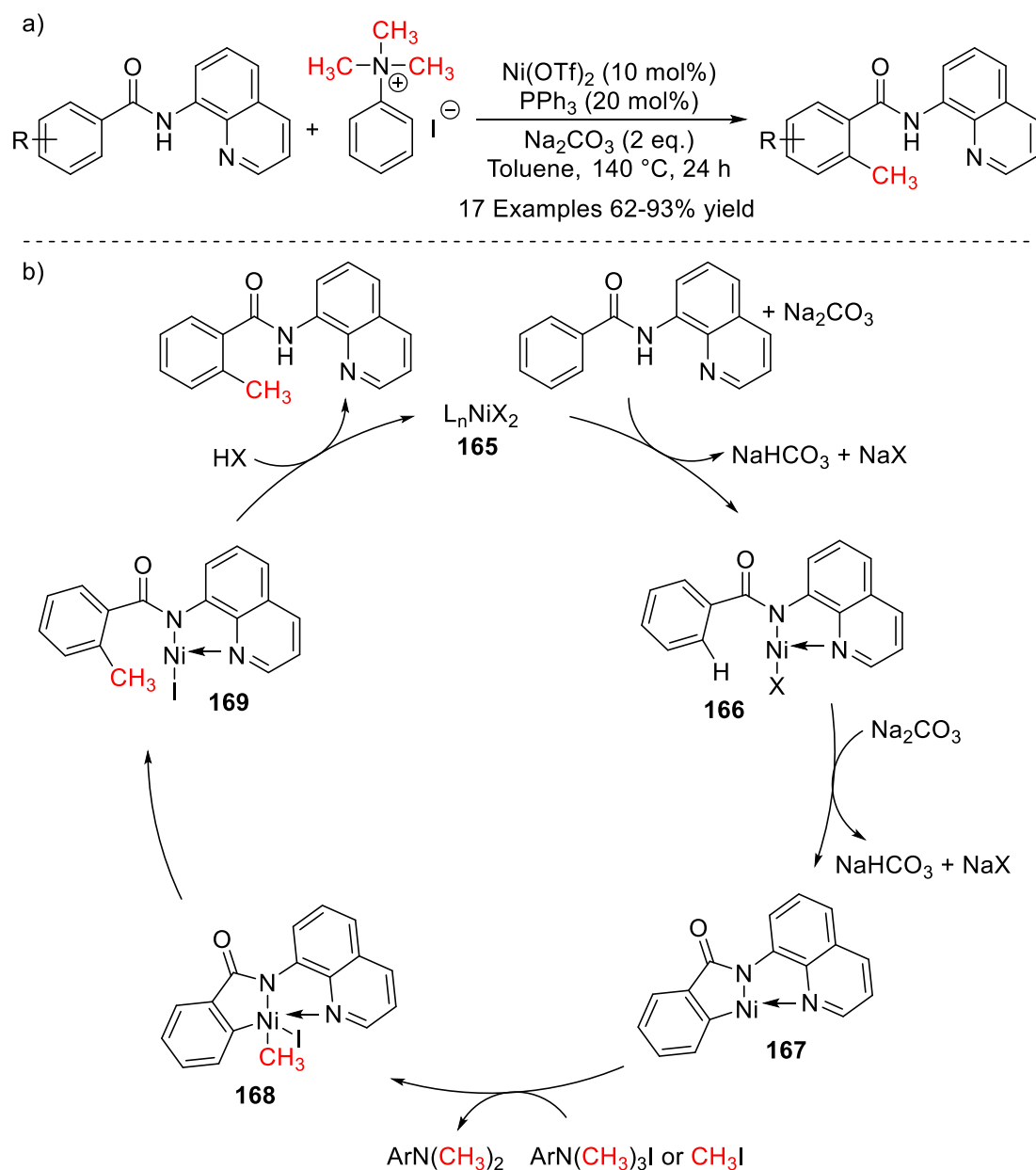


Figure 46. a) Nickel catalysed C-H methylation of benzamide derivatives. b) Proposed catalytic cycle for the C-H methylation reaction.¹⁵⁶

N,N,N-Trimethylanilinium salts have also been shown to act as methylating reagents without a transition metal catalyst. Carlsen and co-workers investigated the capacity of *N,N,N*-trimethylanilinium chloride to methylate a range of aryl-substituted phenols (**Figure 47**).¹⁶¹ In the phenols examined, moderate to good yields of the anisole product were obtained, with electron-rich phenols being more reactive. The reactions were carried out at high temperatures and for long periods of time, which is a drawback

to this methodology. There is also little understanding of whether the methylation occurs from a direct attack of phenol onto the anilinium salt, or *via* the *in situ* generation of methyl chloride.

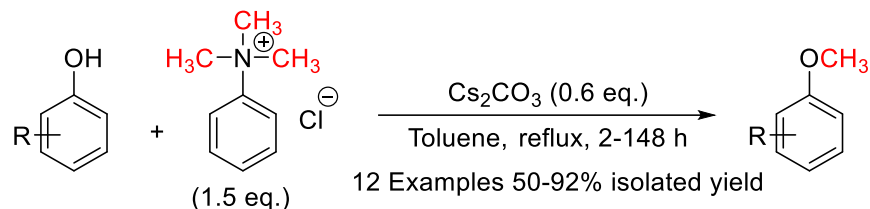


Figure 47. Methylation of phenols using *N,N,N*-trimethylanilinium chloride.¹⁶¹

Despite the potential of anilinium salts to act as methylating reagents, there has been little research into understanding their reactivity. The majority of reaction examples using anilinium salts can be found in patent literature. A selection of alcohols that have been methylated by *N,N,N*-trimethylanilinium salts on a process scale are given in **Figure 48**.¹⁶²⁻¹⁶⁴

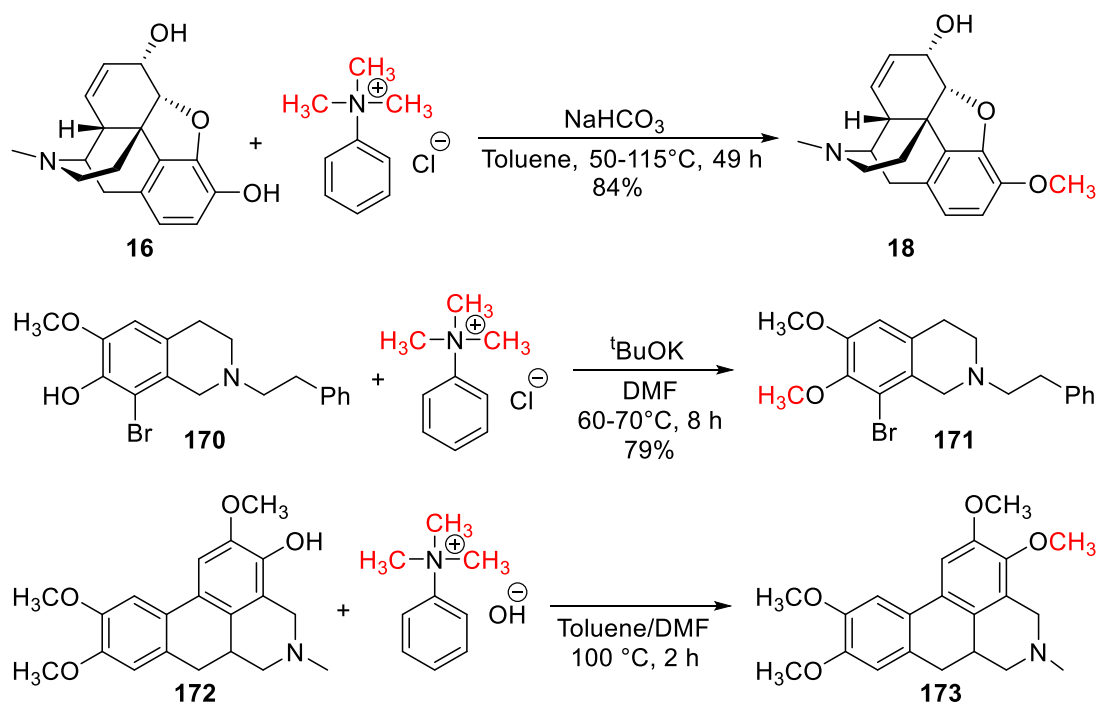


Figure 48. Examples of phenol methylation using *N,N,N*-trimethylanilinium salts.¹⁶²⁻¹⁶⁴

1.2 Proposed Work

Throughout the introduction to this chapter, several reported uses of *N,N,N*-trimethylanilinium salts have been discussed. The applications of these salts have been wide ranging and can mainly be split into two categories: arylation reactions and methylation reactions.

Arylation reactions occur when the *N,N,N*-trimethylanilinium acts as a source of aryl group for a nucleophile, these reactions are typically observed for transition metal catalysed cross coupling reactions and S_NAr reactions. Methylation reactions occur when the *N,N,N*-trimethylanilinium salt acts as a source of methyl groups. Methylation reactions have taken place through a transition metal catalysed reaction and also by direct reaction of nucleophiles with anilinium salts. The dichotomous reactivity of anilinium salts is summarised in **Figure 49**.

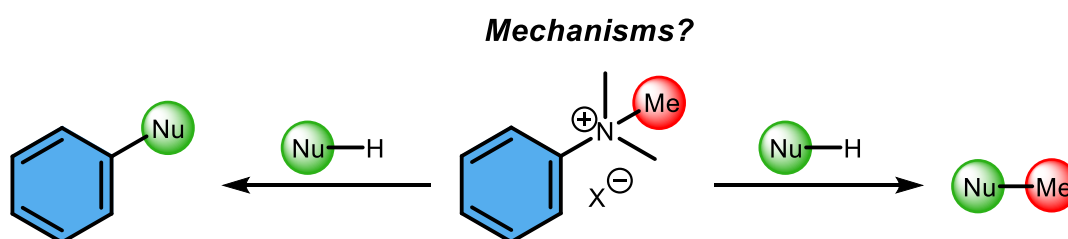


Figure 49. The dichotomous reactivity of *N,N,N*-trimethylanilinium salts.

Though *N,N,N*-trimethylanilinium salts have been used in both applications, arylations and methylations, there has been little work to understand the factors that govern their reactivity. This project aims to systematically investigate possible influences on the reactivity of *N,N,N*-trimethylanilinium salts, primarily through studying their degradation.

The first feature of *N,N,N*-trimethylanilinium salt structure that will be considered is the aryl substitution (**Figure 50**). To investigate this, a library of *N,N,N*-trimethylanilinium salts will be generated that represent a range of different aryl substitutions. This will include groups that are electron-donating and electron-withdrawing through both mesomeric and inductive effects. Substituents will be

included in the *ortho*-, *meta*-, and *para*- positions of the aromatic ring to examine the effect of substitution pattern and to investigate if steric influence is relevant to *N,N,N*-trimethylanilinium salt reactivity. It is proposed that measuring the thermal stability of each of the substituted *N,N,N*-trimethylanilinium salts will give insights into the substitution effect on reactivity.

The next factor that will be considered is the effect, if any, that the *N,N,N*-trimethylanilinium salt counterion species has on reactivity (**Figure 50**). Different halide counterions will be considered to observe any trends in reactivity with the halide series. The majority of *N,N,N*-trimethylanilinium salt applications in arylation methodologies have used triflate salts. Inspired by this, a range of non-nucleophilic counterions will also be considered. The effect of changing a halide counterion to a hexafluorophosphate, trifluoromethanesulfonate, or tetrakis(3,5-bis(trifluoromethyl)phenyl) borate anion will be examined. Again, this will primarily be investigated through looking at the effect of the counterion on thermal stability.

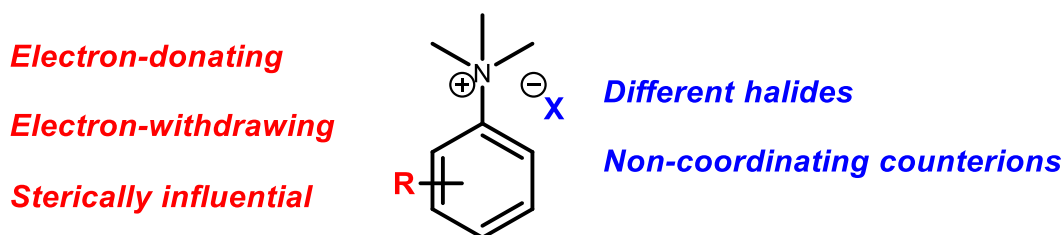


Figure 50. The effect of aryl substitution and counterion species on *N,N,N*-trimethylanilinium salt reactivity.

To gain an overview of the effects that aryl-substituents have on *N,N,N*-trimethylanilinium salt reactivity, the degradation of these salts will be monitored. The effect that these factors have on solid state stability of *N,N,N*-trimethylanilinium salts will be examined by the use of thermal gravimetric analysis (TGA). In solution, NMR spectroscopy will be used to measure the degradation of these salts over a fixed time period.

To gain a deeper insight into the reactivity of *N,N,N*-trimethylanilinium salts, their degradation will be monitored in real-time. Investigations will first be made to find a

suitable method to quantitatively analyse the degradation of these salts. Thereafter, it will be employed on a variety of *N,N,N*-trimethylanilinium salts to better understand the role of aryl substituents and counterions in their reactivity.

With the aid of a quantitative method to monitor degradation, kinetic analyses such as Hammett analysis and Eyring analysis can then be used to learn about the degradation in more detail. The mechanism by which *N,N,N*-trimethylanilinium salts degrade will be investigated through the kinetic analyses to gain an insight into how these salts can behave as reagents.

With an understanding of how *N,N,N*-trimethylanilinium salts degrade, attention will then turn to examining their applications in synthetic organic chemistry. Particular attention will be paid to the use of *N,N,N*-trimethylanilinium salts as methylating reagents since this potential is somewhat underexplored in the literature. The importance of methyl groups and accordingly methylative methodologies has been highlighted in this introduction. Furthermore, it has been shown that many existing electrophilic methylating reagents have significant safety risks associated with them. If *N,N,N*-trimethylanilinium salts can be employed as effective methylating reagents, they may offer some attractive benefits over existing reagents.

It is proposed that the understanding of *N,N,N*-trimethylanilinium reactivity gained through the degradation studies will guide the application of these salts in methylation reactions. The library of salts will be screened for their reactivity against a suitable nucleophile, such as a phenol to identify any trends between degradation and methylation. Any *N,N,N*-trimethylanilinium salts that prove effective in this methylation screen will be taken forward to examine their applicability to a broader range of nucleophiles.

Finally, the degradation and methylation studies will culminate in an attempt at elucidating methylation mechanism using *N,N,N*-trimethylanilinium salts. It is currently unknown how these salts react in existing applications. This uncertainty stems largely from the possibility of methylation to occur either from the salts directly, or through their decomposition methyl halide products (**Figure 51**).

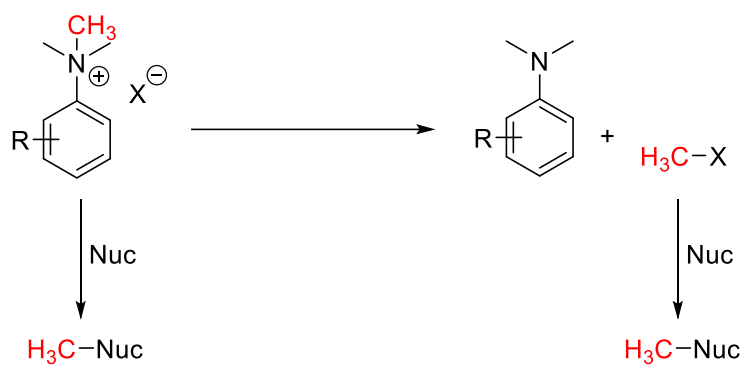


Figure 51. Methylation occurring from *N,N,N*-trimethylanilinium salts directly or their degradation products.

Understanding the mechanism(s) of the degradation and reactivity of *N,N,N*-trimethylanilinium salts will ultimately drive informed uses of these reagents in synthetic organic chemistry. It is expected that the information gained from these studies will be useful to both methylation and cross-coupling chemistry users.

1.3 Results and Discussion

Investigations into the degradation of *N,N,N*-trimethylanilinium salts began by determining the effects that aryl substitution had on the stability of anilinium salts in the solid state and in solution. To achieve this goal, it was first necessary to synthesise a library of anilinium salts that contained a representative range of electron-donating, electron-withdrawing, and sterically influential substituents in varying positions around the aromatic ring. Unsubstituted *N,N,N*-trimethylanilinium salts **174a-c** were commercially available and used as purchased. **175a-188a** were synthesised *via* methylation of the appropriate *N,N*-dimethylaniline with methyl iodide (**61**) (**Figure 52**).

N,N,N-trimethylanilinium iodides were chosen for this part of the study due to the simplicity of their synthesis with readily available starting materials. During the synthesis of the salt library, it was evident that *N,N*-dimethylanilines containing strongly electron-withdrawing groups in the *para*-position were generally more challenging to synthesise than their electron-rich counterparts. This is demonstrated by the low methylation yields (50 and 52%) obtained in the synthesis of **176a** and **177a**. Furthermore, attempts to synthesise 4-nitro- and 4-cyano-*N,N,N*-trimethylanilinium were extremely low yielding, which led to their exclusion from this study. Although optimising the synthesis of *N,N,N*-trimethylanilinium iodides was not a key focus of this project, it was found in general that an excess of **61** (3 eq.), high reaction concentration (2 M), long reaction times (*ca.* 16 h), and a sealed reaction vessel lead to satisfactory yields of the desired salts.

With a varied library of *N,N,N*-trimethylanilinium iodides in hand, attention then turned to understanding the effect that aryl-substituents had on their thermal stability in both the solid-state and solution phase. Studying the degradation of molecules can give a wealth of information about their stability and their reactivity. The data from these degradation studies and the implications that these are expected to have for their applications in synthetic organic chemistry are presented in the next section.

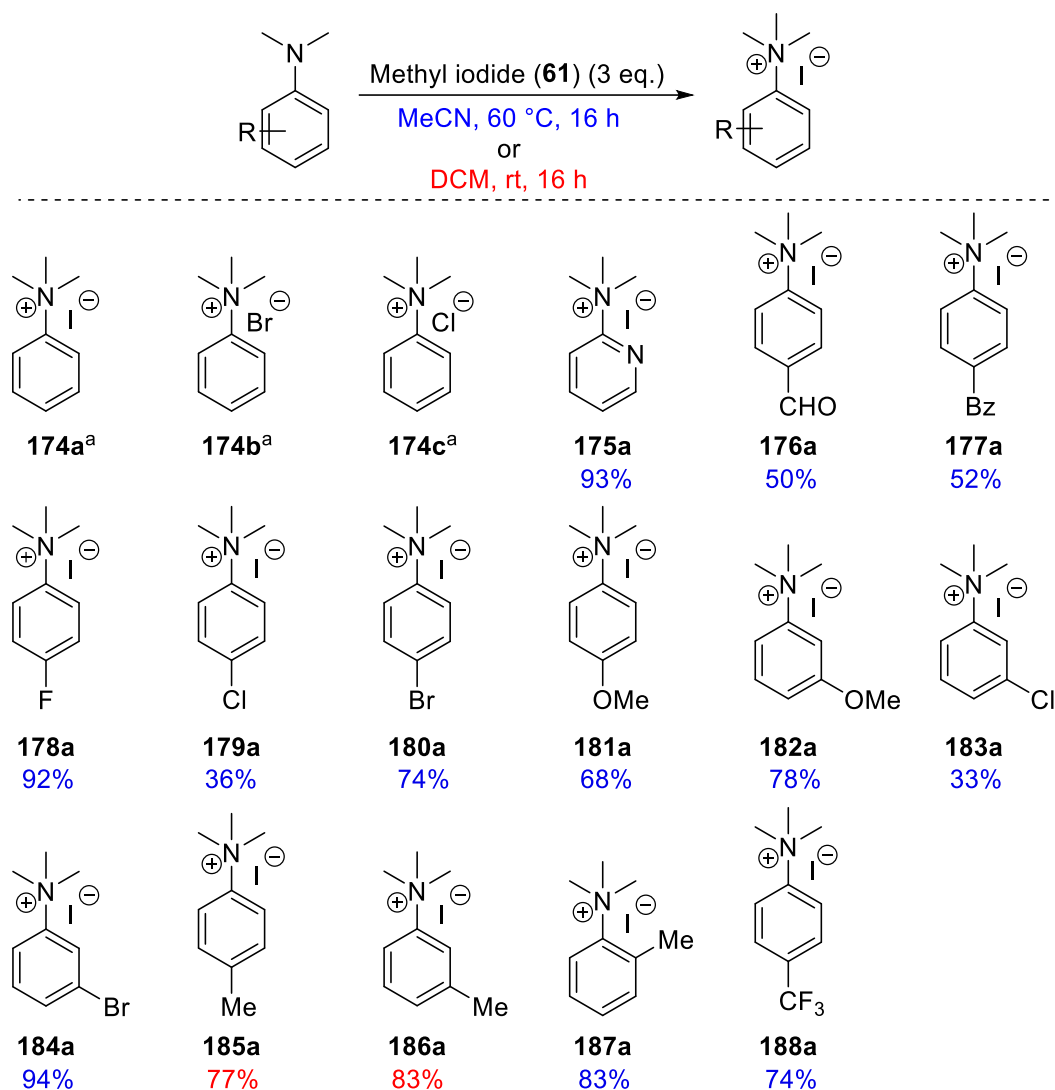


Figure 52. Library of *N,N,N*-trimethylanilinium salts synthesised for investigations into aryl-substituent effect of stability. ^aCommercially available.

1.3.1 Degradation of *N,N,N*-Trimethylanilinium Salts

Solid State Stability of N,N,N-Trimethylanilinium Salts

The stability of *N,N,N*-trimethylanilinium salts **174a-c** and **175a-187a** was investigated first in the solid state. Though it is not anticipated that these compounds would be used as directly as solids, there were two main motivations for carrying out this study. The first was to gain an insight into the stability and reactivity of these compounds in the absence of any solvent effects (though differences in the packing of ions within each crystal structure may have significant effects on reactivity). The

second motive considers the suitability of these salts as reagents for use in a research laboratory, or in a manufacturing facility.¹⁶⁵ In both settings, particularly the latter, reagents that have a high stability in the solid state are preferred, as this would allow their safe and convenient storage.

To assess the solid state stability of the *N,N,N*-trimethylanilinium salts, thermal gravimetric analysis (TGA) was employed. TGA monitors the mass of a sample whilst it is subjected to a temperature ramp (40-300 °C at a rate of 10 °C/min, in this case), which gives information about salt degradation and volatisation.¹⁶⁶ TGA analysis was carried out on the anilinium salt library under an atmosphere of argon in the first instance, the mass vs temperature traces are shown in **Figure 53**. All of the TGA traces, with the exception of **174a**, **174b**, **176a**, and **177a** show smooth curves. Based on existing literature around the degradation of quaternary ammonium salts, it seems likely the main degradation products would be the aryl-substituted *N,N*-dimethylaniline and methyl halide resulting from a retro-Menschutkin reaction (**Figure 54**).¹⁵⁷⁻¹⁵⁹ This hypothesis is further corroborated by experiments carried out previously within this research group.¹⁶⁷ Thermal volumetric analysis coupled with a sub-ambient distillation apparatus (TVA-SAD) was used to analyse the thermal degradation of **174a**, **180a** and **185a**; IR spectroscopy revealed evidence for the generation of methyl iodide upon the thermal degradation of each of these *N,N,N*-trimethylanilinium iodides.

The first observation to note from the TGA traces is that the halide counterion species appears to have an effect on the degradation temperature. This is evidenced by the varied peak degradation temperatures of **174a**, **b**, and **c** (184, 229, and 179 °C). The bromide salt (**174b**) degrades at a significantly higher temperature than both the iodide (**174a**) and chloride (**174c**) salts. In addition, **174a** and **c** do not show smooth TGA traces. The difference in degradation temperature could come from different nucleophilicities of the counterions in the absence of solvation, or could be an artefact of the crystal structure in the solid state. There is not a clear trend between the halides in the solid state, so the reason behind the differing degradation temperatures is unknown at this time.

There is a general trend of the more electron-deficient *N,N,N*-trimethylanilinium iodides (e.g. **176a** and **177a**) having a lower thermal stability than their electron-rich counterparts (e.g. **181a** and **185a**). A pseudo-Hammett plot is shown in **Figure 55** which supports the observation of lower onset degradation temperatures for *N,N,N*-trimethylanilinium iodides with increasing electron-deficiency. This is consistent with the proposed retro-Menschutkin degradation pathway where electron-withdrawing substituents would have a destabilising effect on the cationic nitrogen atom, thus favouring a transition towards the resulting neutral *N,N*-dimethylaniline species (**Figure 54**).

The final point to consider is that all of the *N,N,N*-trimethylanilinium salts analysed by TGA under an argon atmosphere were stable in the solid state up to temperatures of at least 170 °C. This suggests that these salts would be safe to store at room temperature.

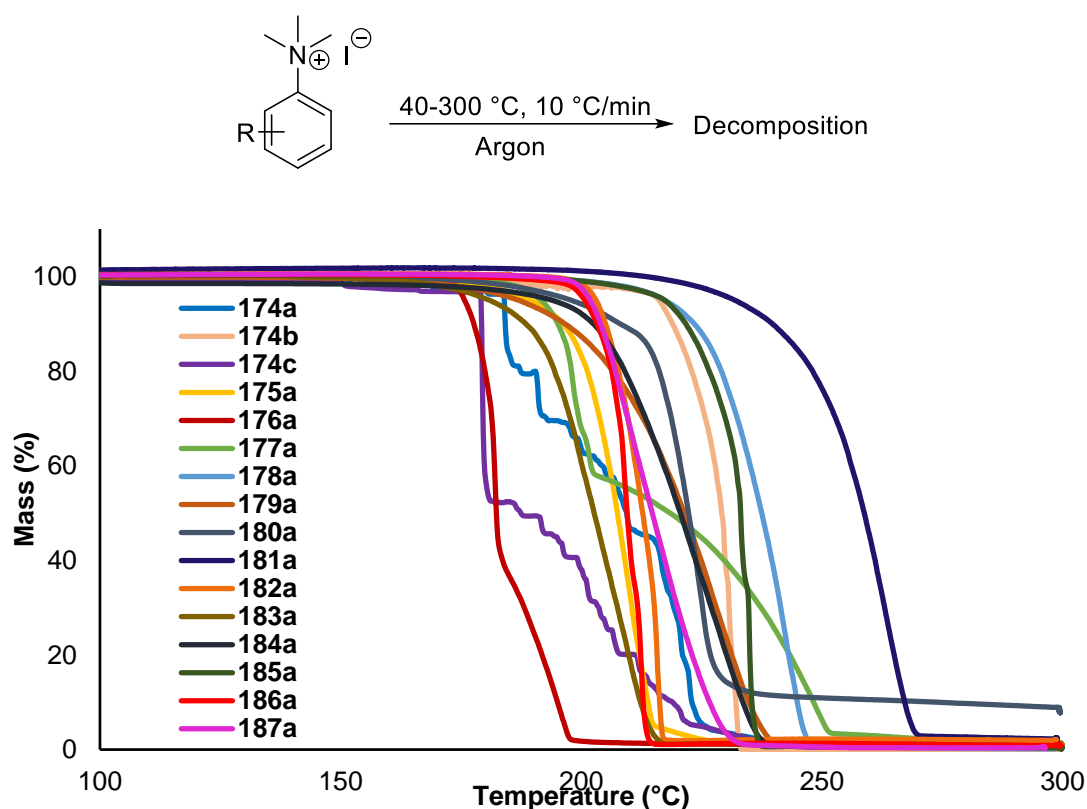


Figure 53. Mass vs temperature trace determined via thermal gravimetric analysis for salts **174a-c** and **175a-187a**. Temperature range: 40-300 °C. Temperature ramp: 10 °C/min. Gas: Argon. Temperatures between 40-100 °C have been omitted as no observable change in mass was measured for any of the salts in this temperature range.

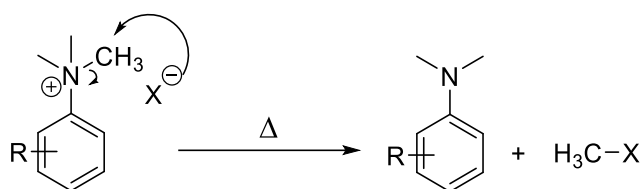


Figure 54. Proposed retro-Menshutkin degradation of *N,N,N*-trimethylanilinium salts.^{157–159}

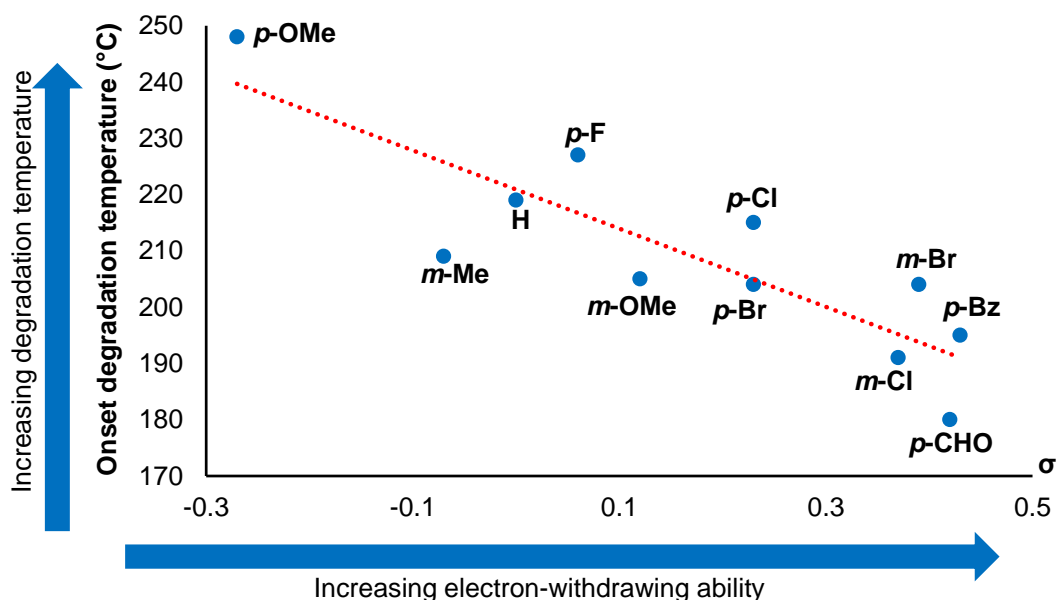


Figure 55. Hammett-derived analysis of TGA data for the degradation of anilinium iodides, supporting the role of electron-withdrawing aryl substituents in promoting thermal degradation at lower temperatures.

To supplement the suggestion that the *N,N,N*-trimethylanilinium salts analysed by TGA would be safe and convenient to store as solids, a selection of the salts with a range of degradation temperatures under argon were then tested in the presence of air (**Figure 56**). The onset and peak degradation temperatures for each of the salts tested in air were comparable to the values obtained under argon. Furthermore, each of the traces gave smooth curves with the exception, again, of **174c**, **176a** and **177a**. **176a** and **177a** appear to lose ~55% and ~40% of their original mass, respectively, before entering what appears to be a second phase in both argon and air. In each case the percentage of mass lost in the first step corresponds approximately to the mass of methyl iodide (142 g mol^{-1}). The boiling point of the resulting *N,N*-dimethylaniline of these carbonyl containing compounds is relatively high (177 and $245 \text{ }^\circ\text{C}$) which may

explain a slower rate of mass loss after an initial rapid loss of methyl iodide. Unfortunately, it was not possible to collect samples part-way through the analysis to test this hypothesis.

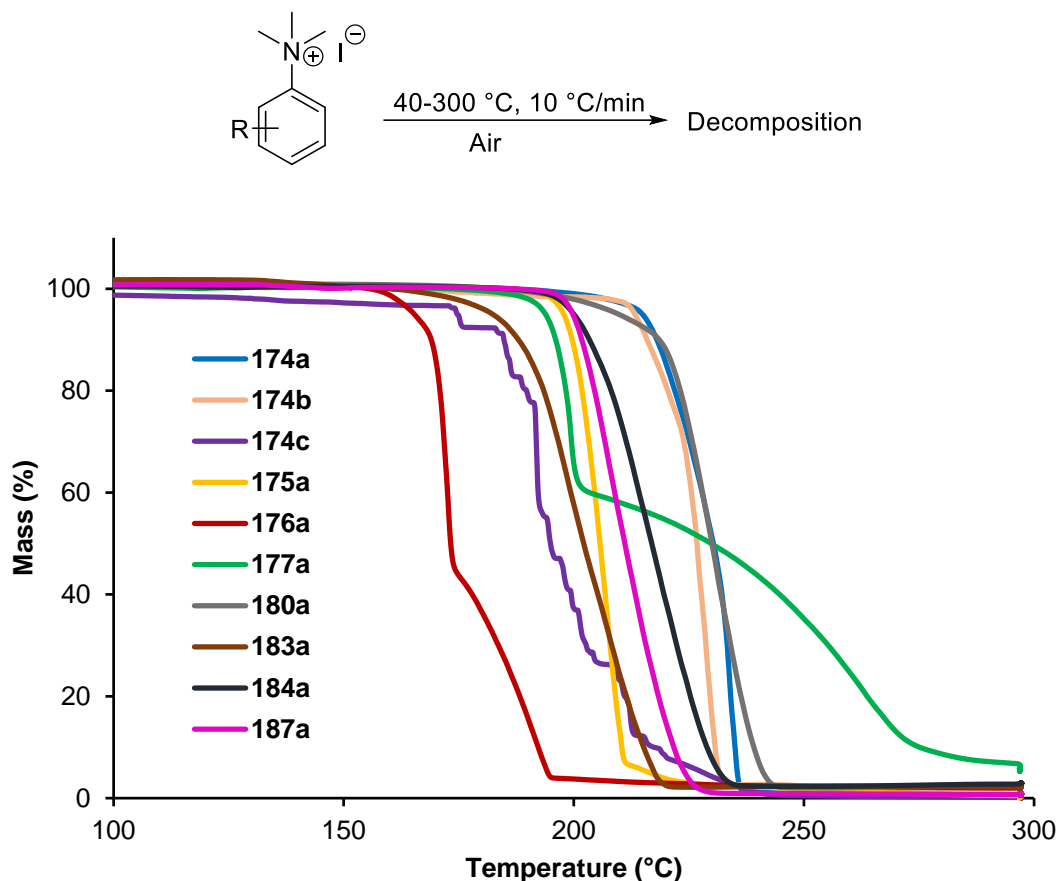


Figure 56. Mass vs temperature trace determined via thermal gravimetric analysis for salts **174a-c** and **175a-177a**, **180a**, **183a**, **184a**, and **187a**. Temperature range: 40-300 °C. Temperature ramp: 10 °C/min. Gas: Air. Temperatures between 40-100 °C have been omitted as no observable change in mass was measured for any of the salts in this temperature range.

Solution Phase stability of N,N,N-Trimethylanilinium Salts

After investigating the stability of the *N,N,N*-trimethylanilinium salts in the solid state, investigation into their thermal stability in solution began. DMSO was selected as an appropriate solvent due to its ability to solubilise the anilinium salts, enabling homogenous kinetic analysis; its high boiling point, allowing for flexible temperature

studies; and the availability of its inexpensive deuterated analogue which could be used in NMR experiments.

^1H NMR spectroscopy was used to obtain a quantitative overview of the substituent effect on the thermal stability of *N,N,N*-trimethylanilinium iodides **174a-188a** in DMSO-d_6 . Each salt was dissolved in DMSO-d_6 to a concentration of 0.06 M, and heated at 120 °C for 20 min. 1,2,4,5-tetramethylbenzene was used as an internal standard to calculate the concentration of anilinium salt before and after the heating period. The percentage degradation of each anilinium cation is shown in **Figure 57**.

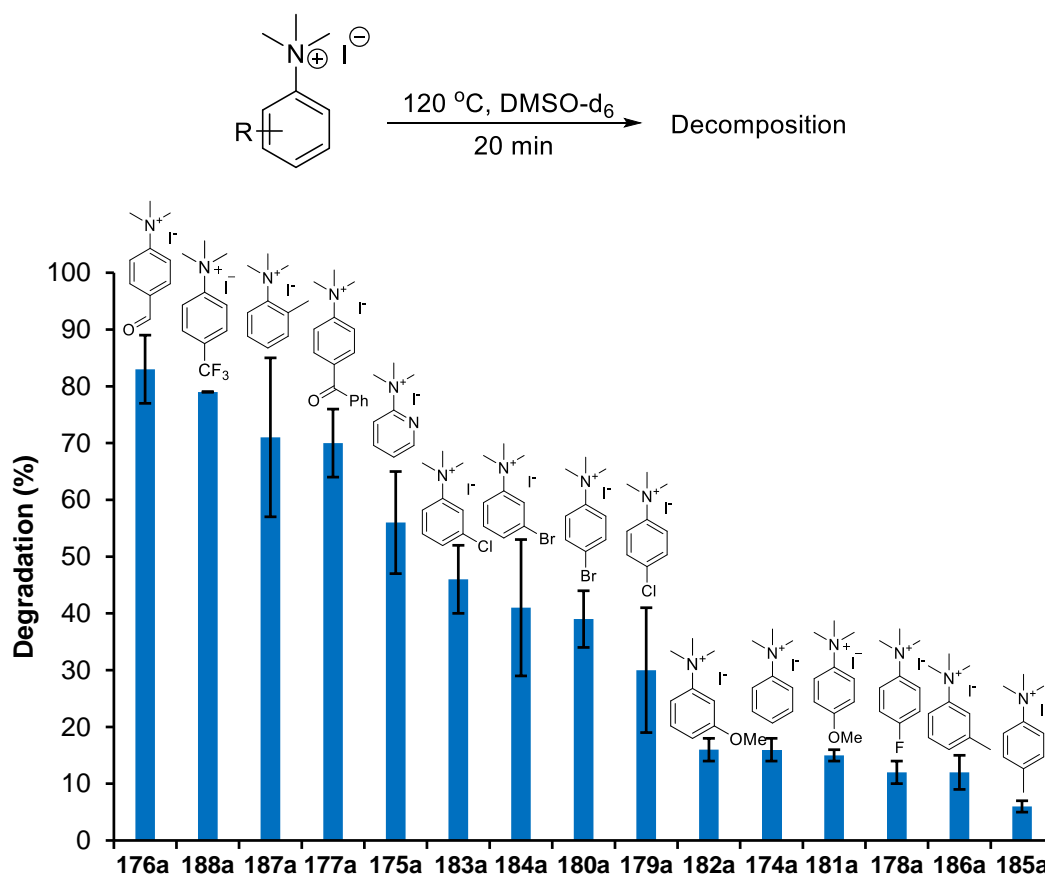


Figure 57. Relative degradation of a range of *N,N,N*-trimethylanilinium iodides upon heating in DMSO-d_6 (0.06 M) at 120 °C for 20 min; 1,2,4,5-tetramethylbenzene was used as an internal standard to calculate the concentration of the anilinium salt before and after heating. Results and associated errors are taken from triplicate runs.

The degradation study in DMSO-d_6 shows a similar overall trend to that which was observed in the solid state TGA analysis. Anilinium salts with electron-withdrawing

substituents were particularly susceptible to degradation upon heating in DMSO-d₆, for example *para*-formyl substituted (**176a**) and *para*-trifluoromethyl substituted (**188a**) anilinium salts showed 83±6 and 79±1% degradation, respectively. This is compared to electron-rich anilinium salts such as *para*-methyl (**185a**) or *meta*-methyl (**186a**) which only showed 6±1 and 12±3% degradation, respectively. The inductively-donating methyl substituent actually appears to stabilise **185a** and **186a** relative to the unsubstituted anilinium iodide (**174a**). This relationship between electron-deficiency and %degradation is illustrated with a pseudo-Hammett plot in **Figure 58**. The pseudo-Hammett plot shown uses σ values though σ^- values were also trialled giving an almost identical r^2 value (0.833 vs 0.832).

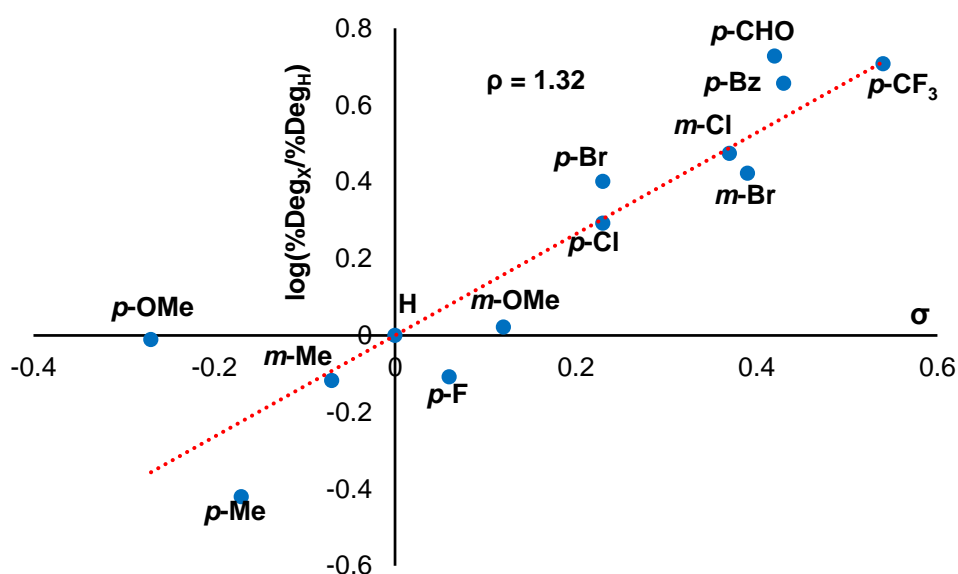


Figure 58. Pseudo-Hammett analysis of solution phase degradation experiments, supporting the observation that electron-deficient aryl substituents accelerate anilinium iodide degradation.

In terms of electronic properties, there is one apparent outlier to the trend. The *ortho*-methyl substituted *N,N,N*-trimethylanilinium iodide (**187a**) showed an average of 71±14% degradation over the heating period, despite the electron-donating nature of the methyl substituent. The experimental result can be justified with a steric argument. It is proposed that having the *ortho*-methyl substituent in close proximity to the quaternary nitrogen atom of the anilinium will provide a driving force for the

formation of a less strained *N,N*-dimethylaniline product (**189**) (**Figure 59**). Firstly, restricted rotation about the aryl C-N bond partially locks one N-CH₃ group planar to the aromatic ring, increasing 1,3-allylic-like interactions with the *ortho*-proton (highlighted in green). Furthermore, it is proposed that the methyl group being attacked from an incoming iodide should be approximately perpendicular to the aromatic plane. The locked conformation would lower the energy penalty required orient a methyl group in this position, thus lowering the energy barrier to reach the transition state. At the time of writing this thesis, computational work is being developed so the structures shown in **Figure 59** are for illustrative purposes only. This hypothesis that steric factors can influence the stability of *N,N,N*-trimethylanilinium iodides was supported by the fact that attempts to synthesise 2,6,*N,N,N*-pentamethylanilinium iodide and 2,6-diisopropyl-*N,N,N*-dimethylanilinium iodide were unsuccessful with the standard conditions shown in **Figure 52**.

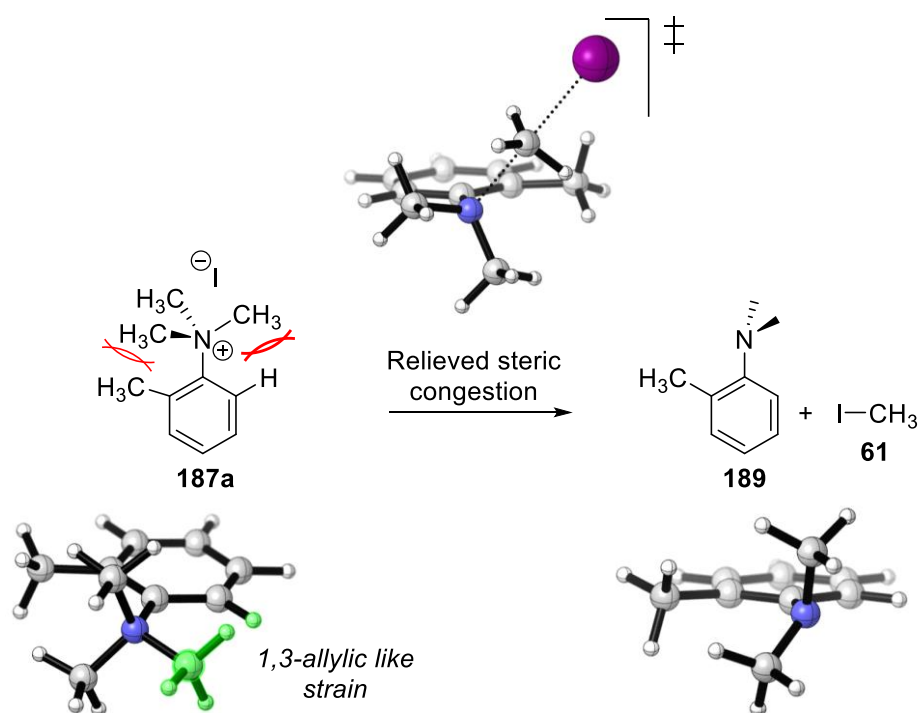


Figure 59. Relief of steric congestion as a driving force for the degradation of **187a**.

Interestingly, the *para*-fluoro substituted anilinium (**178a**) is stabilised, albeit slightly, with respect to the unsubstituted **174a** ($12\pm 2\%$ vs $15\pm 2\%$). The high electronegativity

of fluorine means that fluoro- aryl substituents are inductively highly electron-withdrawing; however, they also have the ability to donate electron density to the aromatic system through mesomeric effects. This explanation is corroborated by *para*-chloro (**179a**) and *para*-bromo (**180a**) which show a higher %degradation (30 ± 11 and $39\pm 5\%$), due to a lower ability to donate electron density through the π -system. *meta*-chloro (**183a**) and *meta*-bromo (**184a**) have higher %degradation values still (46 ± 6 and $41\pm 12\%$), where only a destabilising substituent effect through the halogens' inductive electron-withdrawing properties would be expected.¹⁶⁷

With an overview of the aryl-substituent effect on *N,N,N*-trimethylanilinium iodide stability in solution, efforts to understand the effects of counterion species began. The TGA studies (**Figure 53** and **Figure 56**), showed that **174a**, **174b**, and, **174c** degraded at different temperatures in the solid state so each of these salts were subjected to a degradation experiment in DMSO- d_6 . The percentage degradation of each anilinium after heating for 20 minutes at 120 °C is shown in **Figure 60**.

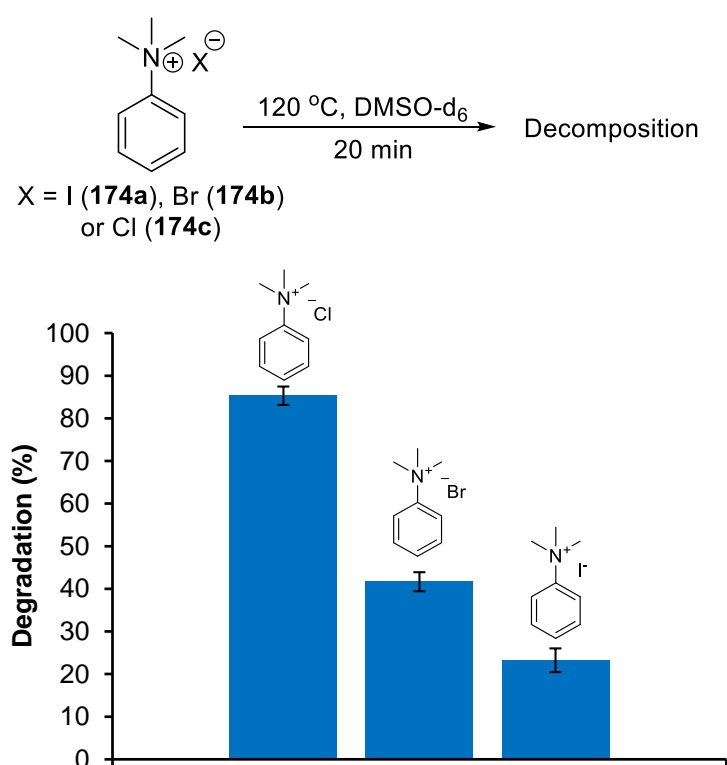


Figure 60. Relative degradation of **174a**, **174b**, and **174c** upon heating in DMSO- d_6 (0.06 M) at 120 °C for 20 min; 1,2,4,5-tetramethylbenzene was used as an internal standard to calculate the concentration of the anilinium salt before and after heating. Results and associated errors are taken from triplicate runs.

The experiment showed that halide counterion species has a marked effect on the thermal stability of *N,N,N*-trimethylanilinium salts in solution. The unsubstituted chloride salt **174c** degraded much more (85%) than the bromide **174b** (42%) and iodide **174a** (23%). This trend between halide species and degradation is consistent with the nucleophilicity of each halide ion in a polar aprotic solvent, which supports that hypothesis that the anilinium salts degrade through a nucleophilic attack of the counterion in a retro-Menschutkin reaction (**Figure 54**).^{168,169} It cannot be ruled out however, that ion-pairing effects could play a role in the stability difference. It is possible that a tighter ion pair between the ammonium moiety and the halide counterion could facilitate degradation by keeping the reactive partners in close proximity.^{155,170}

To investigate this further, initial attempts were made to generate fluoride, chloride, or bromide analogues of some aryl-substituted *N,N,N*-trimethylanilinium iodide salts using an ion-exchange resin. These were met with little success, so instead it was decided to investigate whether or not using halide additives (as opposed to isolated anion equivalents) would have an effect on degradation rate. The presence of halide additives is also relevant to some applications of anilinium salts in cross-coupling chemistry. **174a** was heated at 120 °C for 20 min in DMSO-*d*₆ with an equimolar amount of LiCl, KCl, TBACl, LiF, or TBAF and the concentration loss of **174a** was measured using ¹H NMR spectroscopy (**Figure 61**).

The addition of chloride salts to the degradation reaction mixtures increased the percentage degradation of **174a** in all cases, though the additive cation significantly affected the extent to which it was increased. The tetrabutylammonium chloride (TBACl) additive increased the degradation percentage to 92% (compared to 21% with no additive). Lithium chloride and potassium chloride accelerated the degradation less (69% and 24%), the difference is tentatively ascribed to a lower solubility of the metal chloride salts than TBACl which would give a lower effective concentration of chloride ions in solution.

A similar phenomenon was observed with tetrabutylammonium fluoride (TBAF) and lithium fluoride as the additives. The presence of TBAF promoted the degradation of **174a** to near completion (95%). LiF actually appeared to have a slight stabilising effect

on **174a**, though the margin of error makes this difficult to conclude with certainty. The solubility of LiF in DMSO is poor so it is likely that the concentration of fluoride in the degradation mixture is minimal (undissolved solids were visible in NMR tube). Furthermore, LiF is very hygroscopic and the solid became noticeably wet whilst weighing it out for the experiment. This prompted an investigation into the effect, if any, that water could be playing in this experiment.

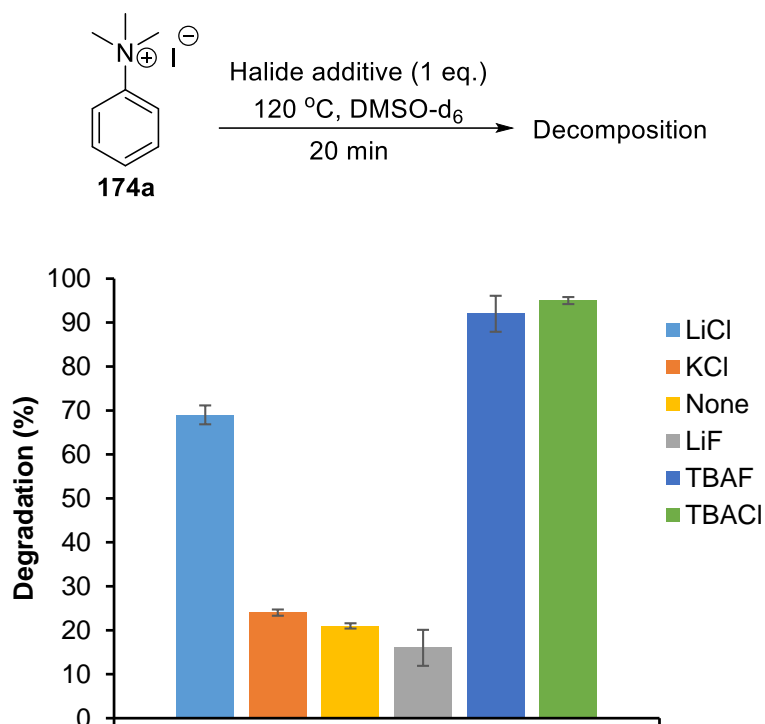


Figure 61. Relative degradation of **174a** upon heating in DMSO-d₆ (0.1 M) at 120 °C for 20 min in the presence of a halide additive (1 eq.).

174a and 1 equivalent of TBAF were heated in either DMSO-d₆, a 1:1 mixture of DMSO-d₆ and D₂O, or D₂O at 90 °C for 20 min. Using the maleic acid as an internal standard, the degradation of **174a** over the reaction time course was measured (**Figure 62**). Interestingly, the addition of water drastically retarded the degradation of **174a**. It is supposed that this occurs as a result of more effective halide solvation in water than in DMSO, thus making the halide counterions poorer nucleophiles.¹⁶⁸ The effect that water is shown to have on degradation through this experiment could be used to rationalise why the hygroscopic LiF additive appeared to reduce the degradation of

174a i.e. the LiF itself had little impact on degradation due to poor solubility, but the introduction of water to system lowered the rate of degradation.

Interested by the observation that water retarded anilinium degradation with TBAF present, it was then investigated whether or not this effect would be observed for anilinium iodides in the absence of any other halide additives. **174a**, **176a** and **187a** were each heated to 90 °C for 2 h in DMSO- d_6 with either 0, 10 or 20 v/v% D_2O added (**Figure 63**). It was clear from the experiments for all three *N,N,N*-trimethylanilinium iodides studied, that increasing the concentration of water lowered the degradation of anilinium salts. Again, this is presumed to occur due to the reduced nucleophilicity of the iodide anion in the presence of water, where it would be better solvated.

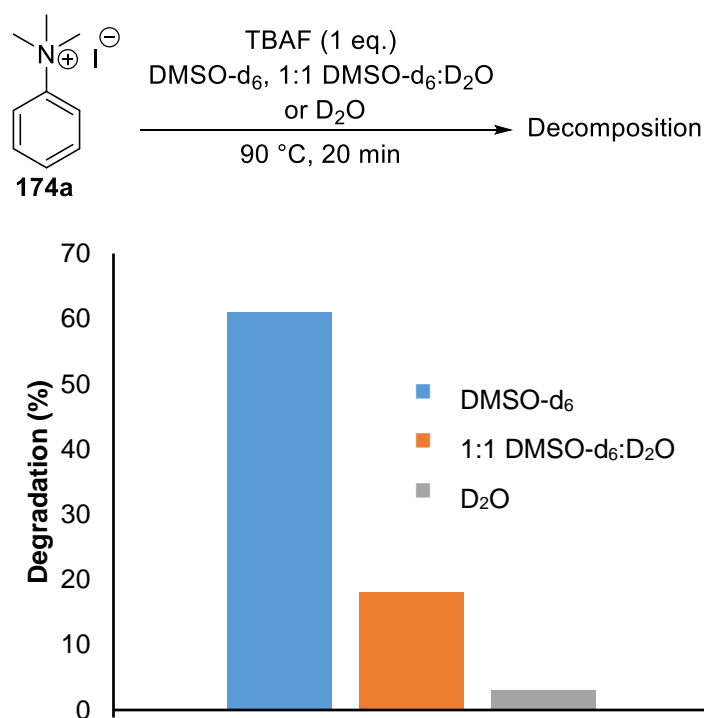


Figure 62. Degradation of **174a** with TBAF (1 eq.) in either DMSO- d_6 , D_2O , or 1:1 DMSO- d_6 : D_2O after heating at 90 °C for 20 min.

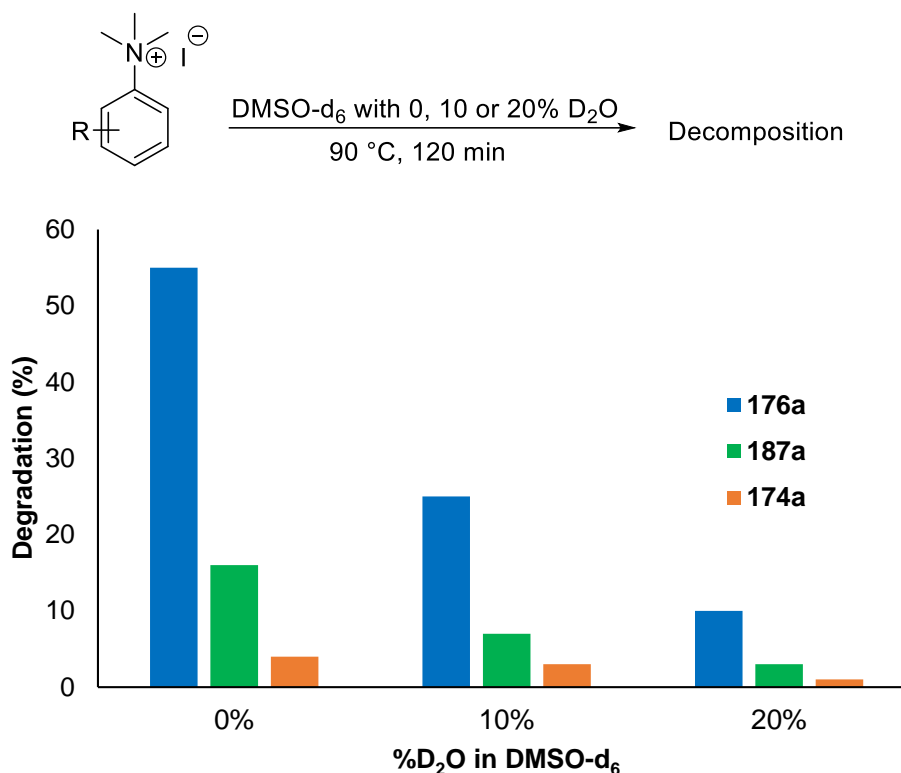


Figure 63. Degradation of **174a**, **176a** and **187a** in DMSO-d_6 with either 0, 10 or 20% D_2O added after heating at $90\text{ }^\circ\text{C}$ for 2 h.

Whereas the decomposition of an *N,N,N*-trimethylanilinium salt to generate the parent aniline and a methyl halide could be beneficial for methylation chemistry, it is conceivable that users may wish to minimise this degradative pathway. This would likely be the case for users of anilinium salts in $\text{S}_{\text{N}}\text{Ar}$ reactions or in transition metal catalysed cross couplings; both of which require the intact anilinium to act as an electrophilic reaction partner. It was hypothesised that the rate of anilinium degradation could be minimised by replacing nucleophilic halides with bulkier non-coordinating cations.

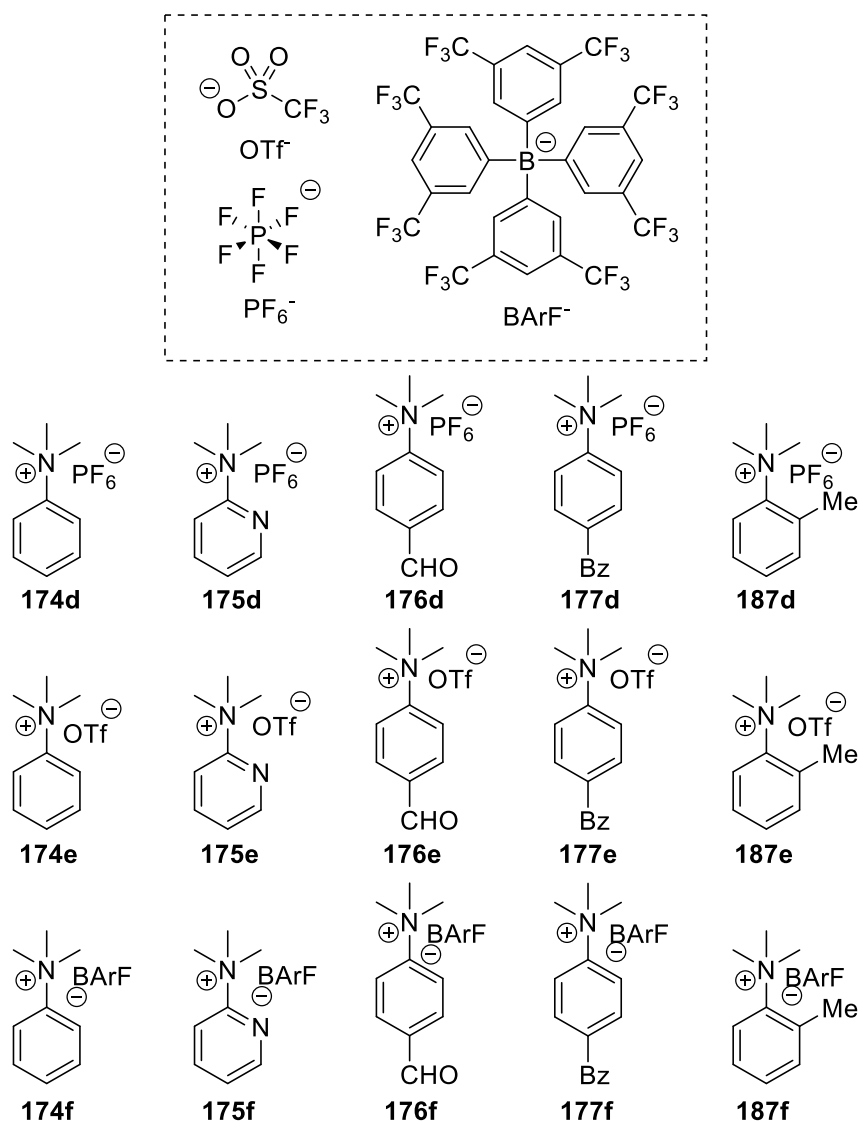


Figure 64. Library of *N,N,N*-trimethylanilinium hexafluorophosphate, triflate, and BArF salts synthesised to investigate the effects of non-nucleophilic counterions on anilinium degradation.

Hexafluorophosphate (PF₆⁻), trifluoromethanesulfonate or triflate (OTf), and tetrakis(3,5-bis-(trifluoromethyl)phenyl)borate (BArF⁻) were selected as suitably non-nucleophilic and weakly coordinating counterions to investigate this hypothesis.¹⁷¹ *N,N,N*-trimethylanilinium triflate salts were synthesised by methylation of the appropriately substituted *N,N*-dimethylaniline with methyl trifluoromethane sulfonate. *N,N,N*-trimethylanilinium hexafluorophosphate and BArF salts were made by an ion exchange from the appropriate *N,N,N*-trimethylanilinium iodide using KPF₆ and

NaBARF, respectively. The anilinium salts chosen to investigate with non-nucleophilic counterions are shown in **Figure 64**.

Once each of the hexafluoro phosphate, triflate, and BARF salts had been generated, they were subjected to similar degradation experiments in DMSO- d_6 as described above. Salts **174-177a,d,e** and **f** and **187a,d,e** and **f** were each heated in DMSO- d_6 at 120 °C for 1 h. The percentage of anilinium salt degradation in each case is shown in **Figure 65**. Changing an iodide counterion to a non-coordinating counterion drastically reduces the amount of anilinium degradation in all instances. For all BARF salts tested, the degradation of anilinium was almost negligible, except for the *para*-formyl *N,N,N*-trimethylanilinium cation, where the percentage degradation was reduced from 94% to 10% by replacing the iodide ion with a BARF ion.

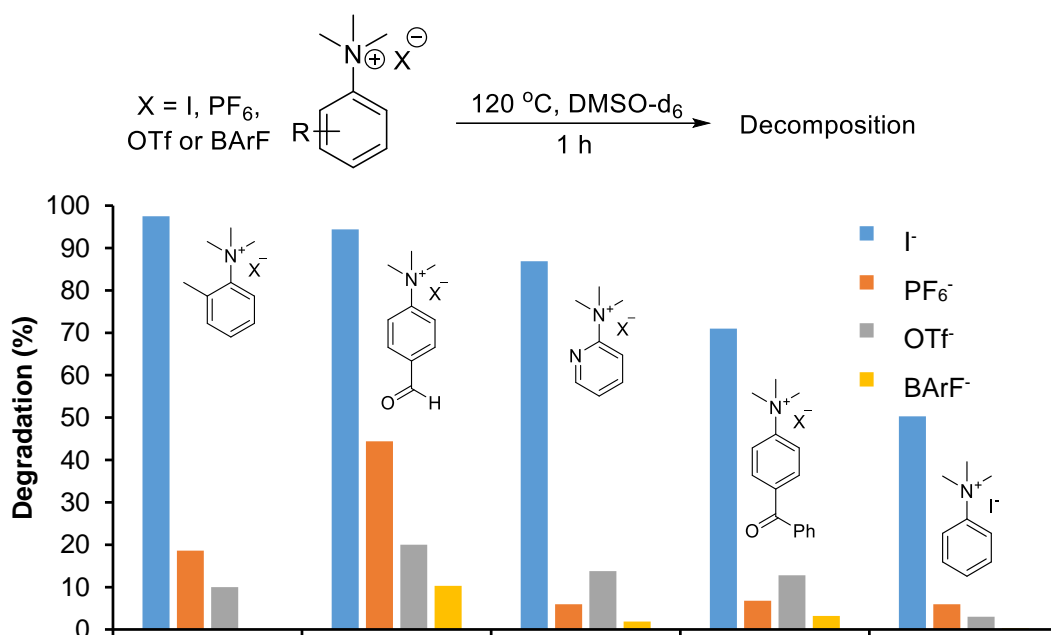


Figure 65. Degradation of **174-177a, d, e** and **f**, and **187a, d, e**, and **f**, upon heating in DMSO- d_6 at 120 °C for 1 h.

In addition to ^1H NMR spectra collected at the end of the heating period in these experiments, other heteronuclear (^{31}P , ^{19}F , and ^{11}B) spectra were collected where possible. These spectra showed that the triflate and BARF counterions remained intact throughout the heating experiment which suggests any observed degradation does not

directly involve these counterions. No methyl triflate was evident in the degradation mixtures of anilinium triflate salts, which could have arisen from an attack of the triflate anion onto an N-CH₃ group. In the case of the hexafluorophosphate salts however, an impurity was noticed in both the ³¹P and ¹⁹F NMR spectra in the degradation mixtures (**Figure 66**). The PF₆⁻ anion has been shown in the literature to have the capacity to degrade through a series of steps to form PO₂F₂⁻.¹⁷²

PO₂F₂⁻ appears to be present in our degradation mixtures which has two main implications. The first, is that the PF₆⁻ anion is unstable under these conditions, which would discourage the use of *N,N,N*-trimethylanilinium PF₆ salts in DMSO at high temperatures, particularly on a manufacturing scale where reaction impurities can be costly. The second is that the first step of the proposed PF₆⁻ degradation pathway is defluorination of PF₆⁻ to give PF₅ and F⁻. The halide additive experiments have shown that fluoride anions accelerate the rate of anilinium degradation, so the anion degradation will be detrimental to anilinium stability. This could explain why 44% of **176d** degraded upon heating despite there being no obvious way for the PF₆⁻ anion to interact directly with the anilinium cation.

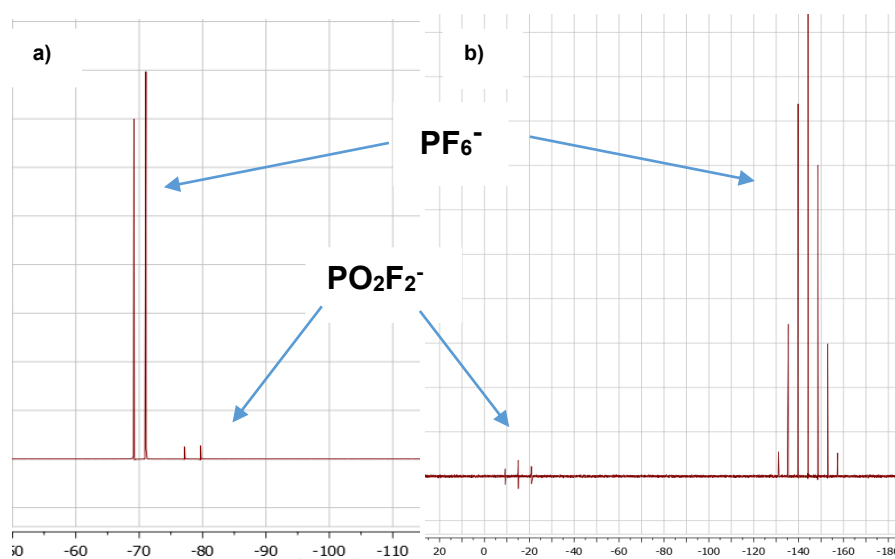


Figure 66a) ¹⁹F and **b)** ³¹P NMR spectra showing degradation of the PF₆⁻ anion.

The decomposition of the PF₆⁻ anion can explain some of the degradation of their anilinium salts. The apparent inertness of the triflate and BArF anions gives rise to the

question of how these anilinium salts are degrading. In order to gain a richer understanding of *N,N,N*-trimethylanilinium salt degradation in DMSO, the process was monitored in real time.

*Real Time Monitoring of *N,N,N*-trimethylanilinium Iodide Degradation*

Degradation studies up until this point had shown NMR spectroscopy to be a valuable analytical technique for monitoring the degradation *N,N,N*-trimethylanilinium salts. Accordingly, the suitability of ¹H NMR spectroscopy for the real time analysis of anilinium degradation was investigated to gain mechanistic insights into the degradation pathway(s). 4-formyl-*N,N,N*-trimethylanilinium iodide (**176a**) was selected as an appropriate salt for developing the kinetic analysis as its degradation is significantly developed over the proposed reaction time course (approximately three half-lives over 16 hours), and its protons are suitably resolved to allow accurate peak integrations. Furthermore, the formyl proton was easily identifiable from its downfield (~10.2 ppm) chemical shift, giving an additional handle for NMR analysis. To further ensure that spectra could be analysed quantitatively, the T1 relaxation time was determined for each of its proton environments using a T1IR experiment.

176a was dissolved in DMSO-d₆ to a concentration of 0.1 M, along with 1,2,4,5-tetramethyl benzene (0.06 M) as an internal standard. The solution was then heated to 80 °C in the probe of an NMR spectrometer, and a ¹H NMR spectrum was recorded approximately every 5 minutes over the course of around 16 hours. The delay time between scans (D1) was set to 25 seconds, this was chosen to be >5-times the longest T1 time which is generally accepted as the requirement for quantitative NMR analysis. The obtained spectra could then be stacked (**Figure 67**) and the concentration of **176a** and its degradants were calculated by comparison to the integrations obtained from the internal standard protons.

The concentrations of **176a** and 4-formyl-*N,N*-dimethylaniline (**189**) vs time were plotted; the concentration of each species was calculated *via* the integration of their aromatic protons (**Figure 68**). The stacked spectra and resulting time-course graph suggested that ¹H NMR analysis was a suitable technique for following the degradation of anilinium salts, but a more rigorous analysis of that assertion was required.

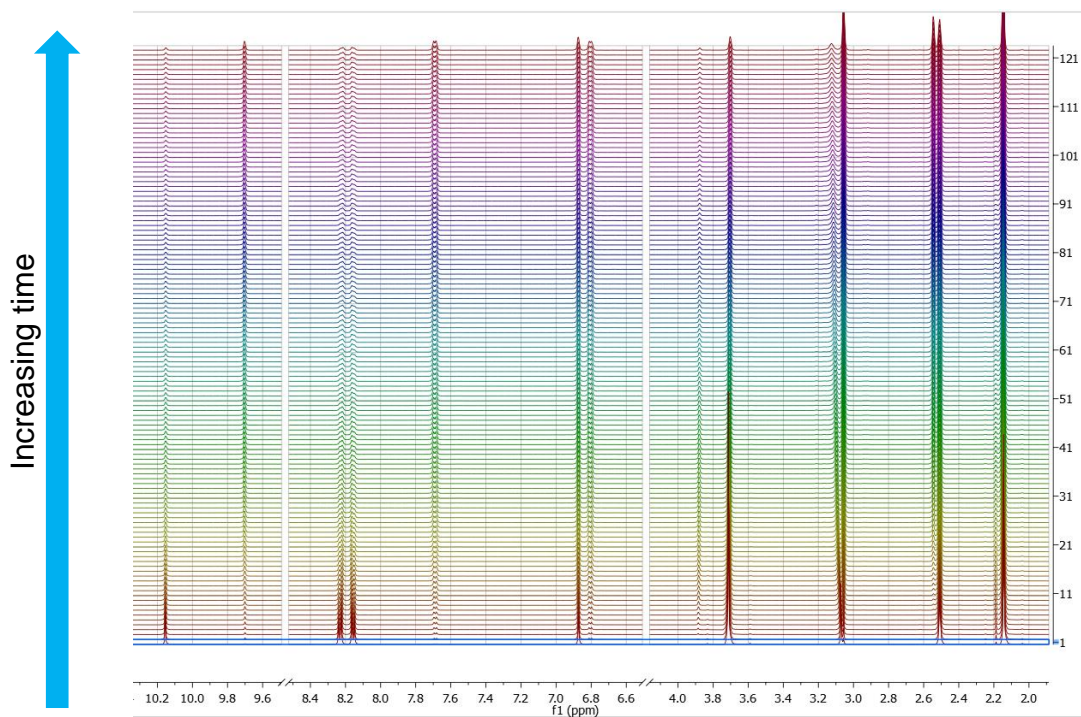


Figure 67. Stacked ^1H NMR spectra for the degradation of **176a** at $80\text{ }^\circ\text{C}$ in DMSO-d_6 .

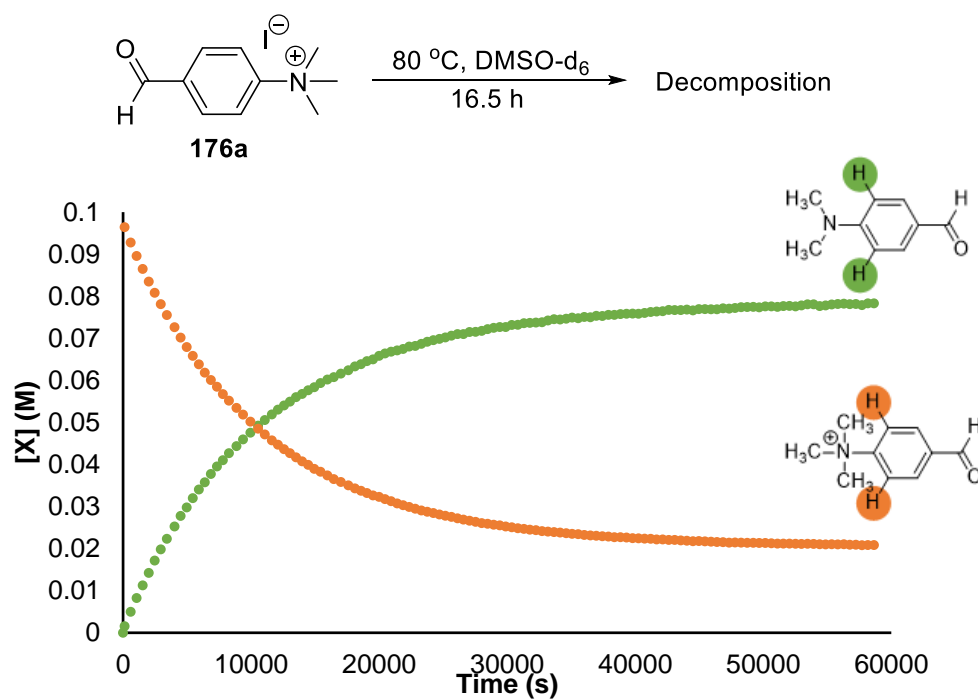


Figure 68. ^1H NMR time course for the degradation of **176a** determined by following aromatic proton shift of anilinium (orange) and aniline (green).

In order to test the validity of species concentrations calculated from the real-time ^1H NMR experiment, the concentrations of both **176a** and **189** were also calculated using their *N*-methyl group protons and their formyl protons (**Figure 69**). Curiously, the concentrations of **176a** calculated *via* its formyl proton (dark blue) and *ortho*-aryl protons (orange) were in close agreement, whilst the concentration calculated *via* the $-\text{N}(\text{CH}_3)_3^+$ protons (light blue) gave lower values. The disparity in concentration became more pronounced as the reaction progressed. Similarly, calculating the concentration of **189** *via* its $-\text{N}(\text{CH}_3)_2$ protons (yellow) gave lower values than those obtained from the *ortho*-aryl (yellow) or formyl (red) protons. Repeating the experiment with **176a** and other *N,N,N*-trimethylanilinium iodides showed that this phenomenon was genuine, which prompted an attempt at rationalising this result. Interestingly, the degradation of **176a** appears to reach an equilibrium, rather than go to completeness.

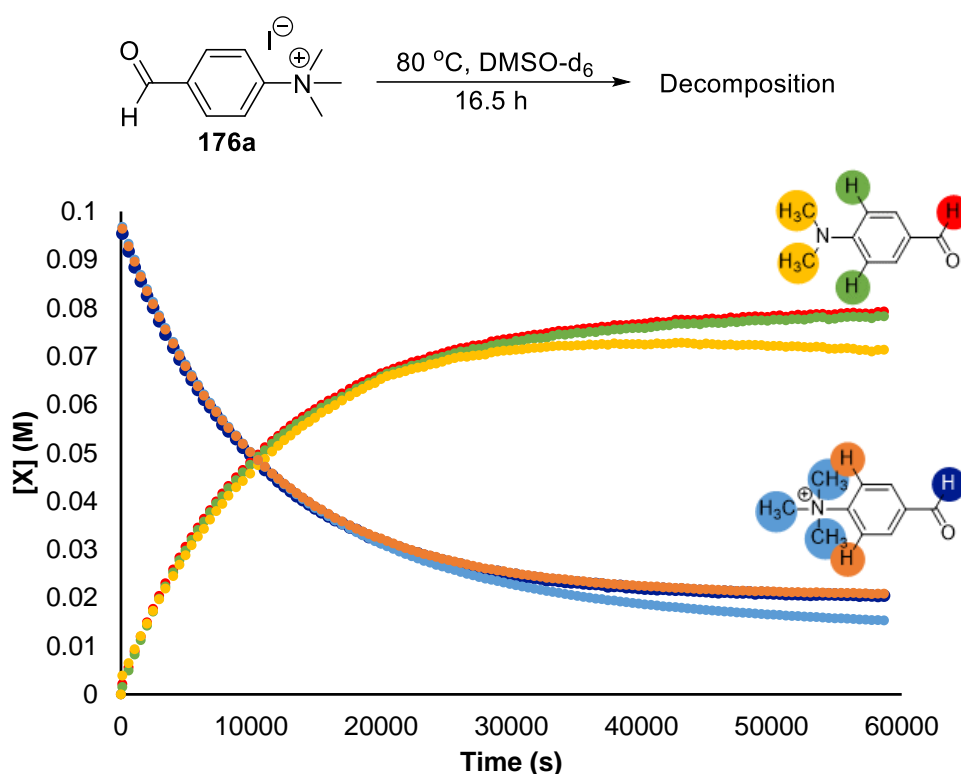


Figure 69. ^1H NMR time course showing the degradation of **176a** determined from aromatic (orange), *N*-methyl (light blue) and formyl (dark blue) protons, and the formation of **189** determined from aromatic (green), *N*-methyl (yellow) and formyl (red) protons.

The disparity between anilinium and aniline concentration measured by *ortho*-aryl and N-CH₃ protons could be rationalised by an isotopic scrambling event that exchanges N-CH₃ for N-CD₃ groups. It was hypothesised that the DMSO-d₆ solvent was acting non-innocently in the degradation reaction mixture (**Figure 70**). The *N,N,N*-trimethylanilinium iodide is proposed to decompose to the parent *N,N*-dimethylaniline and methyl iodide (**61**) through a retro-Menschutkin reaction, which is preceded and supported by the ¹H NMR monitoring.^{157–159} Alternatively, DMSO-d₆ (**193**) could demethylate the anilinium salt to give the aniline and trimethylsulfoxonium-d₆ iodide (TMSOI-d₆, **190**). **190** could also potentially be generated in the reaction degradation mixture through reaction of **61** with **189**.

190 could potentially directly re-methylate the dimethylaniline to the anilinium but with a CD₃ group in the place of a CH₃ group. Alternatively, **190** could decompose to give DMSO-d₃ (**191**) and methyl iodide-d₃ (**192**). The *in situ* generated **192** could then methylate the dimethyl aniline to the anilinium salt, again with a CD₃ group in the place of a CH₃ group. The consequence of the incorporation of CD₃ groups into **176a** and **189** is that a portion of the NMe groups on either molecule will be undetectable by ¹H NMR spectroscopy and thus give an artificially low concentration calculated *via* these protons. The proposed scrambling processes are corroborated by the fact that **176a** degradation appears to reach an equilibrium.

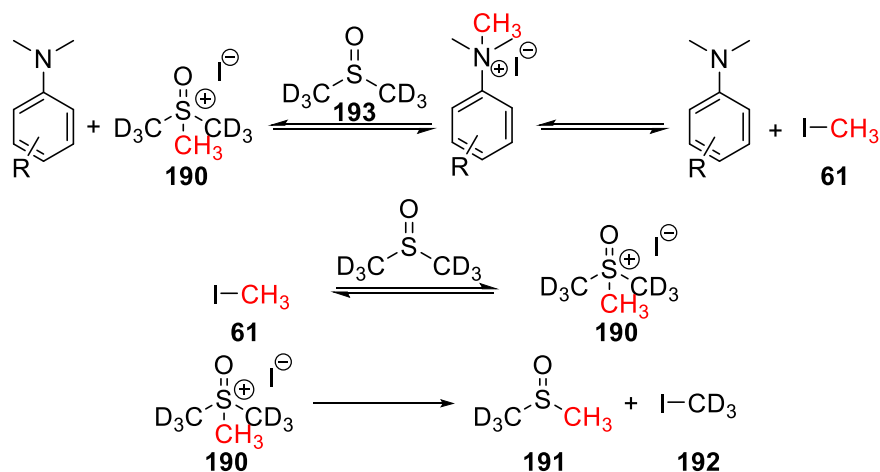


Figure 70. Proposed degradation pathway of *N,N,N*-trimethylanilinium iodide salts in DMSO-d₆.

In support of the proposed mechanism, **61**, **190** and **191** were all identified in the degradation ^1H NMR spectra (**Figure 71**). Methyl iodide (**61**, purple) appears to form initially at a rate which is consistent with the formation of dimethyl aniline **189** (green/yellow), whilst TMSOI (**190**, dark blue) formation appears to experience an induction period. This suggests that anilinium degradation led by the halide counterion occurs at a faster rate than the DMSO solvent-led degradation pathway, so majority of TMSOI will be formed by methylation from methyl iodide, rather than the anilinium cation directly. DMSO- d_3 (**191**) increases in concentration slowly throughout the course of the reaction.

The involvement of DMSO in the degradation of anilinium salts explains why OTf and BArF salts still degrade despite the lack of interaction from the non-nucleophilic counterions. The finding that iodide-led degradation is faster than DMSO-led degradation is supported by the drastically reduced degradation of the OTf, PF₆, and BArF salts in comparison to the iodide salts (**Figure 65**).

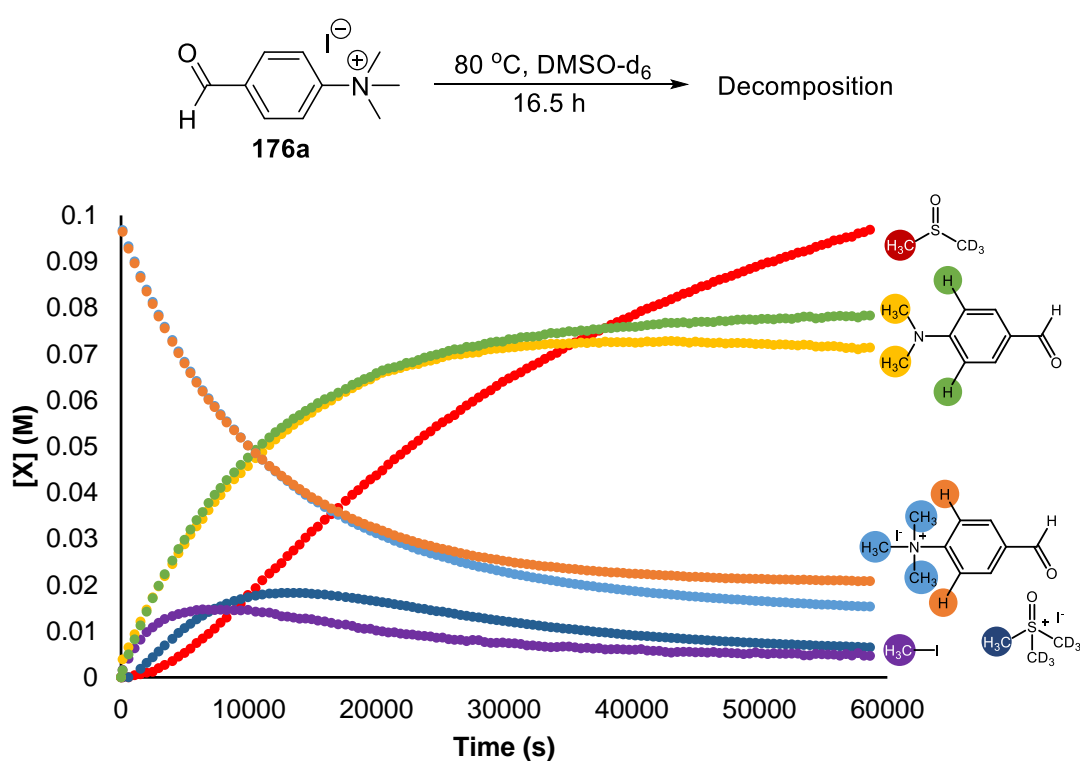


Figure 71. ^1H NMR time course for the degradation of **176a**, with colour-coded lines for **61**, **176a**, **189**, **190**, and **191**.

With a suitable method for monitoring the degradation of *N,N,N*-trimethylanilinium iodides in hand, the same technique was applied to a range of other aryl-substituted anilinium iodides. The T1 relaxation times were calculated for **174a-178a**, **180a**, **182a-184a**, **187a**, and **188a** and it was determined that a 25 s D1 time was appropriate for all of the samples. Each salt at a concentration of 0.1 M in DMSO-*d*₆ was then degraded at 80 °C as per the standard conditions. The concentration vs time curves calculated from aromatic protons for each of the salts tested are shown on one graph in **Figure 72**.

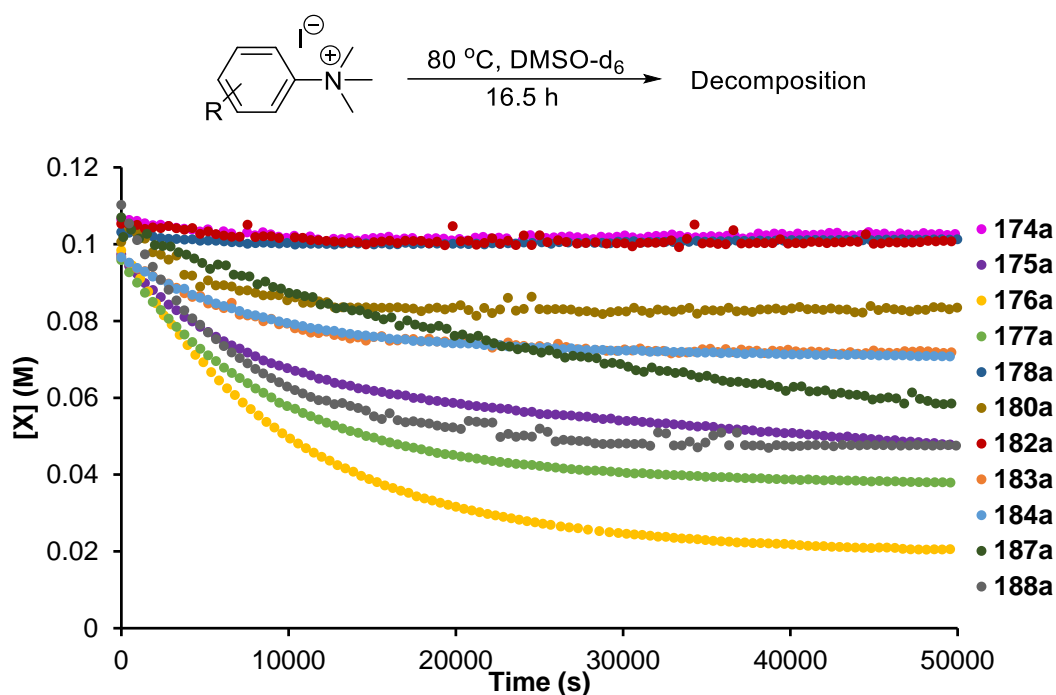


Figure 72. ¹H NMR time courses for the degradation of **174a-178a**, **180a**, **182a-184a**, **187a**, and **188a**.

From inspection of the degradation time course data, it is clear that electron-deficient anilinium salts such as *para*-formyl (**176a**, yellow), *para*-benzoyl (**177a**, light green), and *para*-trifluoromethyl (**188a**, grey) degrade at a much faster rate than the comparatively electron-rich anilinium salts such as unsubstituted (**174a**, pink) and *para*-fluoro (**178**, dark blue). This finding was in line with the data obtained from earlier single time-point experiments (**Figure 58**). The anilinium salts appear to reach an equilibrium concentration rather than full degradation. This could be rationalised by a build-up of TMSOI or methyl iodide in the sealed NMR tube that may methylate

the *N,N*-dimethylaniline through a Menshutkin reaction. There are two exceptions to this observation.

The first is in the case of the *ortho*-methyl salt (**187a**) which doesn't appear to reach an equilibrium concentration (at least not in the time-frame measured). The steric hindrance imposed by the methyl substituent may place a kinetic barrier on the reformation of its anilinium salt. It also degrades comparatively slowly to electron-deficient anilinium salts as could be expected from an electronic argument. This insight would not have been gained from the single time-point experiment alone, demonstrating the power of real-time degradation analysis. The second anomaly is the pyridinanium salt (**175a**) which appears not to reach equilibrium either. The cause for this is currently unknown, but it stands to reason that its unique aryl system could grant it reactivity pathways that are not available to the other samples.

After monitoring the degradation of various *N,N,N*-trimethylanilinium iodides that represented a range of electronic effects, and accordingly degradation rates, the concentration vs time could be converted to rate data to obtain further insights into the reactivity of the anilinium salts. To ensure that the proposed degradation model encompassed all of the relevant reactions, some additional experiments were carried out.

From the degradation experiments alone, there was no direct evidence that methyl iodide (**61**) could directly methylate DMSO- d_6 (**193**) to make TMSOI- d_3 (**190**). This is because **61** and **190** can both be made from attack of iodide or DMSO, respectively, onto the *N,N,N*-trimethylanilinium cation. Similarly, there was no direct evidence that **190** could decompose thermally back into **61** and **193**. To investigate whether or not **61** could methylate **193**, and if that reaction was reversible, a simplified kinetic NMR experiment was carried out.

A 0.1 M sample of commercially available TMSOI- d_0 was dissolved in DMSO- d_6 along with an internal standard, and heated to 80 °C in the NMR probe for approximately 1 h whilst ^1H NMR spectra were recorded at regular intervals. The concentration of TMSOI and methyl iodide vs time is plotted in **Figure 73**. It is evident that TMSOI decomposes thermally under these conditions, and that methyl iodide is the key degradation product.

Similarly, an experiment was conducted where methyl iodide was heated in DMSO-d₆ at 80 °C for 1 h (**Figure 74**). Here it can be seen that TMSOI is formed at a similar rate at which the methyl iodide is consumed. These experiments provide good evidence that the reaction of methyl iodide and DMSO occurs under the degradation reaction conditions, and that it is reversible. This reaction, which is independent of the anilinium cation or dimethyl aniline, is likely to facilitate isotopic scrambling.

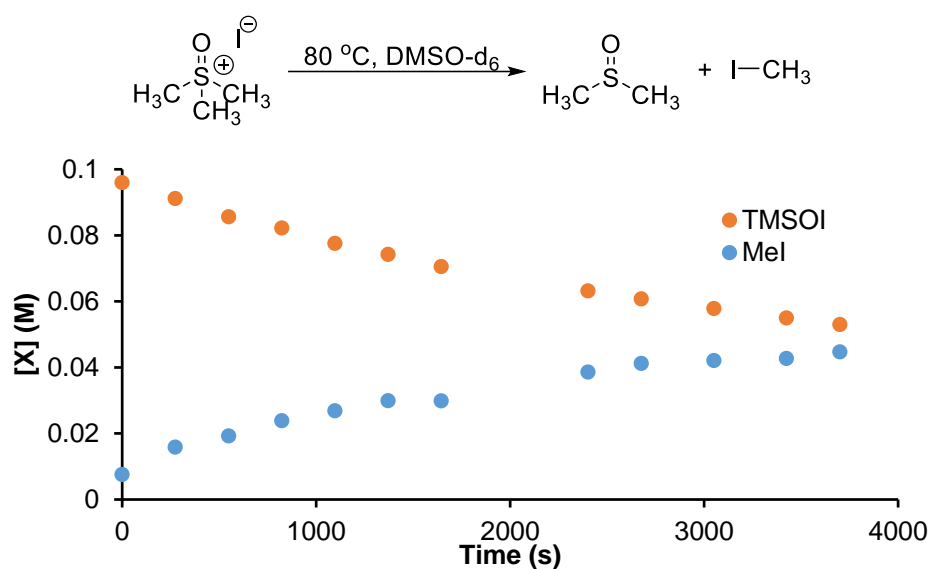


Figure 73. ¹H NMR time course for the thermal decomposition of TMSOI in DMSO-d₆ at 80 °C.

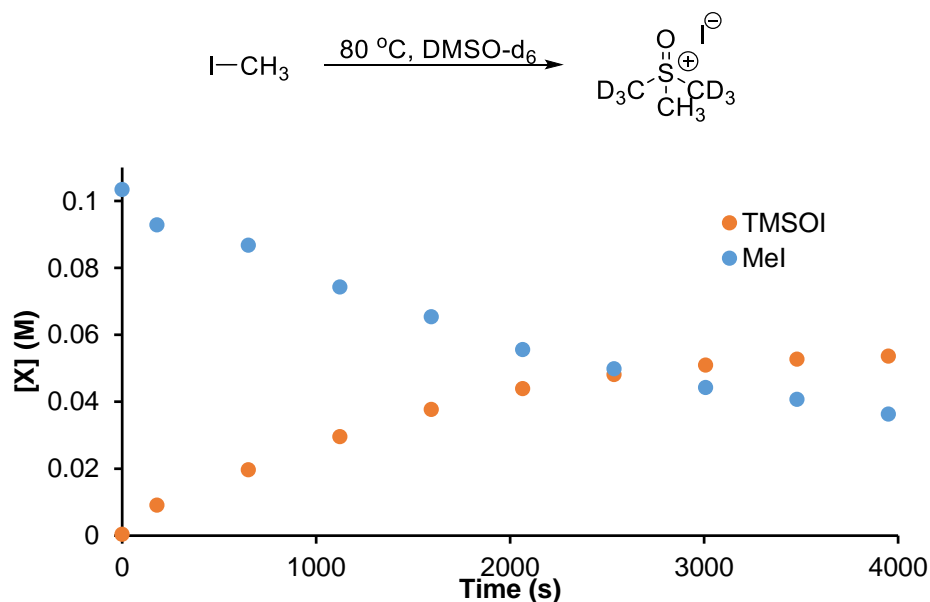
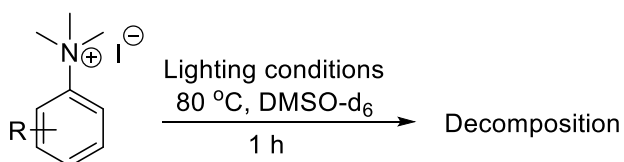


Figure 74. ¹H NMR time course for reaction of methyl iodide with DMSO-d₆ at 80 °C.

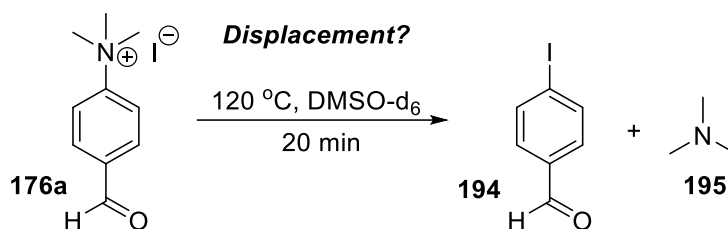
The proposed degradation pathway of the *N,N,N*-trimethylanilinium salts takes place *via* a series of 2-electron processes. In order to probe the possibility of any radical reactivity, some degradation experiments were carried out under exposure to different lighting conditions (**Figure 75**). **174a** was heated to 80 °C in DMSO-*d*₆ for 1 h either in darkness, under ambient light, under simulated sunlight, or under UV light. The average degradation from a triplicate of experiments under each of the conditions did not show a statistical difference. **176a** was then subjected to the same experiment under the two extremes of lighting condition (darkness and UV irradiation). The average percentage of degradation of **176a** under each of the lighting conditions was comparable again. These simple experiments suggest that single electron pathways are not present in the degradation process of *N,N,N*-trimethylanilinium iodides, or at least that they are negligible.

The final possible degradative pathway that was considered is the displacement of trimethylamine (**195**) with the iodide anion through an S_NAr-type process. To probe this **176a** was heated in DMSO-*d*₆ at 120 °C for 20 min in the presence of 4-I-benzaldehyde (**194**) (**Figure 76**). The concentration of each species was measured at the start and end of the heating period to see if there was any increase in the concentration of **194**, which would be the displacement product. The concentration of **194** was shown not to increase in this experiment, ruling out this reactive pathway.



| Anilinium Iodide | Lighting | Average Degradation (%) | Error (%) |
|------------------|----------|-------------------------|-----------|
| 174a | Darkness | 1.30 | 1.29 |
| 174a | Ambient | 1.73 | 0.34 |
| 174a | Sunlight | 1.51 | 1.51 |
| 174a | UV | 2.02 | 0.19 |
| 176a | Darkness | 20.59 | 1.02 |
| 176a | UV | 18.82 | 1.47 |

Figure 75. Average degradation of **174a** and **176a** upon heating for 1 h at 80 °C in DMSO-*d*₆ under a range of lighting conditions.



| Analyte | Time (min) | Average Concentration (M) | Concentration change (%) |
|-------------|------------|---------------------------|--------------------------|
| 176a | 0 | 0.103 | -89.4 ± 0.8 |
| | 20 | 0.011 | |
| 194 | 0 | 0.011 | -0.3 ± 0.3 |
| | 20 | 0.011 | |

Figure 76. Reaction probing the possibility of trimethylamine displacement in the degradation of **176a**.

With confidence that the earlier proposed degradation pathway encompassed all of the significant steps in *N,N,N*-trimethylanilinium iodide degradation, attention turned to estimating rate constants for the degradation reactions. For the purposes of kinetic modelling, the degradation process was separated into three distinct, reversible reactions (**Figure 77**). **Step 1**, the iodide-led degradation of *N,N,N*-trimethylanilinium was assigned rate constants k_1 and k_{-1} for the forward and reverse reactions, respectively. **Step 2**, the DMSO-led *N,N,N*-trimethylanilinium degradation was assigned rate constants k_2 and k_{-2} . **Step 3**, the reaction between methyl iodide and DMSO was assigned the rate constants k_3 and k_{-3} .

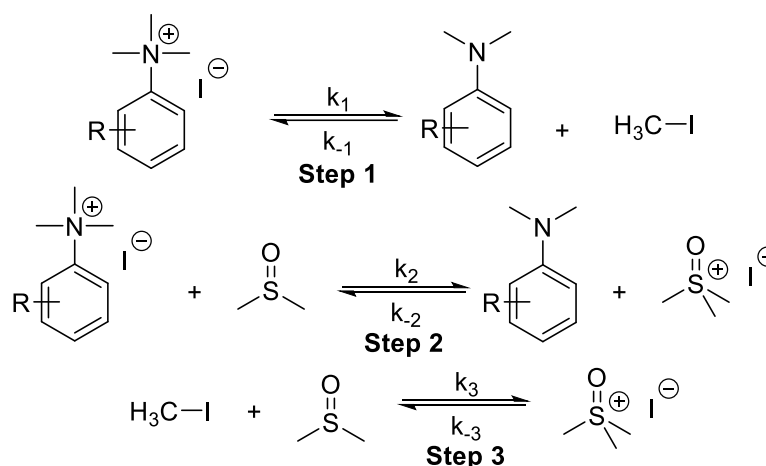


Figure 77. Proposed steps in the degradation of *N,N,N*-trimethylanilinium iodides.

Using the experimental data obtained through ^1H NMR degradation monitoring, rate constants for **steps 1-3** were estimated with a complex pathway simulator programme (COPASI). COPASI was configured with the three steps shown in **Figure 77**. Experimental concentration vs time data was then inputted into the programme for each salt. Rate constants k_1 , k_{-1} , k_2 , k_{-2} , k_3 , and k_{-3} were estimated by minimising the error between simulated concentration vs time plots with estimated rate constants, and the true experimental values. It was expected that evaporation of methyl iodide would affect some of the equilibria; however, the NMR tubes were sealed and the headspace volume was identical in each experiment so any error should be consistent across all experiments. Furthermore, the degradation experiments were found to be highly reproducible, suggesting that the parafilm seal was effective at keeping methyl iodide gas in the reaction tube.

For the purposes of the kinetic modelling, only the *N,N,N*-trimethylanilinium and *N,N*-dimethylaniline concentration data (both calculated from aromatic protons) were considered as these protons had well-resolved chemical shifts in all cases and are expected to be devoid of any isotopic scrambling effects. The model was also computed in such a way that priority was given to correlating simulating data with the anilinium concentration vs time curve. The estimated rate constants are shown in **Figure 78**.

| Salt | k_1 (s^{-1}) | k_{-1} ($\text{M}^{-1}\text{s}^{-1}$) | k_2 ($\text{M}^{-1}\text{s}^{-1}$) | k_{-2} ($\text{M}^{-1}\text{s}^{-1}$) | k_3 ($\text{M}^{-1}\text{s}^{-1}$) | k_{-3} (s^{-1}) |
|-------------|---------------------------|---|--|---|--|------------------------------|
| 174a | 1.11E-05 | 1.80E-95 | 1.60E-315 | 1.63E+07 | 1.81E-05 | 1.82E-04 |
| 175a | 4.47E-05 | 1.95E-03 | 3.74E-208 | 1.36E-172 | 1.94E-162 | 0.00E+00 |
| 176a | 7.95E-05 | 5.46E-04 | 1.71E-283 | 1.30E-13 | 5.53E-06 | 5.27E-05 |
| 177a | 6.41E-05 | 7.94E-276 | 6.96E-134 | 1.10E+08 | 2.95E-06 | 5.84E-23 |
| 178a | 9.45E-06 | 1.69E-02 | 2.85E-315 | 1.56E-02 | 1.79E-316 | 0.00E+00 |
| 180a | 1.85E-05 | 6.06E-03 | 1.58E-315 | 1.13E-306 | 6.34E-314 | 7.78E-04 |
| 182a | 4.46E-06 | 5.00E-259 | 1.82E-180 | 3.43E-02 | 1.66E-05 | 7.47E-212 |
| 183a | 2.53E-05 | 0.00E+00 | 4.74E-302 | 1.71E-02 | 7.70E-06 | 1.14E-04 |
| 184a | 3.09E-05 | 1.36E-145 | 4.75E-48 | 3.46E-02 | 6.39E-06 | 7.05E-05 |
| 187a | 1.89E-05 | 1.12E-85 | 9.96E-134 | 7.70E+11 | 1.59E-05 | 3.10E+11 |
| 188a | 8.08E-05 | 3.09E-81 | 1.23E-44 | 8.66E+09 | 4.40E-06 | 1.79E-04 |

Figure 78. Estimated rate constants k_1 , k_{-1} , k_2 , k_{-2} , k_3 , and k_{-3} estimated for a range of *N,N,N*-trimethylanilinium iodides using COPASI.

The estimated degradation rate constants show large variations in value for most steps of the reaction. In addition, equilibrium constants (K) calculated from the estimated k_1 and k_{-1} values (where $K = k_1/k_{-1}$) were not consistent with experimental observation. It is likely that many of these values are quite inaccurate due to the inability to accurately calculate the concentration of all intermediates in the degradation pathway (only the anilinium and aniline can be calculated free from isotopic scrambling effects). However, by weighting the simulated data towards the anilinium concentration curve, sensible values were obtained for k_1 , which corresponds to the iodide-led degradation.

Despite the reasonable k_1 values, there still remained large variations in values obtained for k_2 , k_{-2} , k_3 and k_{-3} . k_3 and k_{-3} both represent the reactions between methyl iodide and DMSO- d_6 , these reactions should proceed at the same rates regardless of the analyte species. Therefore, the kinetic data were remodelled in such a way that the values of k_3 and k_{-3} were fixed for all experiments. The rate constants obtained in this analysis are shown in **Figure 79**. In general, equilibrium constants calculated from k_1 and k_{-1} values using this model were more consistent with experimental values. However, the relative values for k_1 across these experiments did not correlate with the observed relative rates of degradation. Furthermore, the k_1 value obtained for **178a** was erroneously low, and large variations in k_2 and k_{-2} were still observed across experiments.

| Salt | k_1 (s ⁻¹) | k_{-1} (M ⁻¹ s ⁻¹) | k_2 (M ⁻¹ s ⁻¹) | k_{-2} (M ⁻¹ s ⁻¹) | k_3 (M ⁻¹ s ⁻¹) | k_{-3} (s ⁻¹) |
|-------------|--------------------------|---|--|---|--|-----------------------------|
| 174a | 1.30E-06 | 1.09E-08 | 6.41E-253 | 1.14E-169 | 2.00E-05 | 1.29E-04 |
| 175a | 7.68E-06 | 6.32E-08 | 7.60E-07 | 1.81E-258 | 2.00E-05 | 1.29E-04 |
| 176a | 7.20E-05 | 4.13E-09 | 2.82E-78 | 3.08E-04 | 2.00E-05 | 1.29E-04 |
| 177a | 7.55E-06 | 1.85E-27 | 1.33E-06 | 3.96E-212 | 2.00E-05 | 1.29E-04 |
| 178a | 6.89E-110 | 1.10E-288 | 1.48E-127 | 5.50E-94 | 2.00E-05 | 1.29E-04 |
| 182a | 1.34E-06 | 1.06E-08 | 9.96E-210 | 1.16E-19 | 2.00E-05 | 1.29E-04 |
| 183a | 7.96E-06 | 2.14E-08 | 7.04E-72 | 1.32E-149 | 2.00E-05 | 1.29E-04 |
| 184a | 8.48E-06 | 3.56E-08 | 1.37E-198 | 7.16E-119 | 2.00E-05 | 1.29E-04 |
| 187a | 1.32E-05 | 1.87E-08 | 2.43E-128 | 4.34E-61 | 2.00E-05 | 1.29E-04 |
| 188a | 1.04E-06 | 2.99E-08 | 1.78E-06 | 1.91E-238 | 2.00E-05 | 1.29E-04 |

Figure 79. Estimated rate constants k_1 , k_{-1} , k_2 , k_{-2} , k_3 , and k_{-3} estimated for a range of *N,N,N*-trimethylanilinium iodides, fixing k_3 and k_{-3} across all experiments.

Given the inconsistencies in estimated k_2 and k_{-2} values obtained with each model, and their generally low values, a further attempt was made to model the kinetic data such that k_2 and k_{-2} were removed (**Figure 77**, step 2). The values obtained for k_1 , k_{-1} , k_3 and k_{-3} with the simplified model are given in **Figure 80**. This model gave reasonable k_1 values consistent with observed relative degradation rates. In many cases reasonable K values could be calculated, but there was still some exceptions such as **178a** and **182a**.

| Salt | k_1 (s ⁻¹) | k_{-1} (M ⁻¹ s ⁻¹) | k_3 (M ⁻¹ s ⁻¹) | k_{-3} (s ⁻¹) |
|-------------|--------------------------|---|--|-----------------------------|
| 174a | 3.80E-06 | 6.16E-02 | 1.32E-05 | 1.19E-04 |
| 175a | 2.93E-05 | 3.26E-10 | 1.32E-05 | 1.19E-04 |
| 176a | 7.45E-05 | 5.71E-04 | 1.32E-05 | 1.19E-04 |
| 177a | 6.49E-05 | 1.90E-03 | 1.32E-05 | 1.19E-04 |
| 178a | 3.77E-06 | 3.36E+05 | 1.32E-05 | 1.19E-04 |
| 182a | 7.91E-06 | 1.52E+03 | 1.32E-05 | 1.19E-04 |
| 183a | 2.96E-05 | 9.27E-03 | 1.32E-05 | 1.19E-04 |
| 184a | 2.60E-05 | 6.78E-03 | 1.32E-05 | 1.19E-04 |
| 187a | 1.71E-05 | 8.09E-04 | 1.32E-05 | 1.19E-04 |
| 188a | 7.39E-05 | 2.22E-03 | 1.32E-05 | 1.19E-04 |

Figure 80. Estimated rate constants k_1 , k_{-1} , k_3 , and k_{-3} estimated for a range of *N,N,N*-trimethylanilinium iodides, fixing k_3 and k_{-3} across all experiments.

Despite best efforts to find a universal model to accurately estimate rate constants for all steps in proposed degradation pathway, there remained some uncertainty in each approach taken. Ideally, a model would be produced that takes into account the isotopic scrambling. Attempts in this vein were unsuccessful but should be continued in future work. Although the absolute predicted rate constants are not likely to be accurate, the k_1 values shown in **Figure 78** could at least be used comparatively to one another to gain further insights into aryl-substituent effects on anilinium degradation.

With approximated k_1 for the degradation across a range of aryl-substituted *N,N,N*-trimethylanilinium iodides, a Hammett plot could be produced for the iodide-led degradation (**Figure 81**). σ^- values were used for *para*-substituents as these would be expected to represent the increase of electron density on the nitrogen atom that could

be delocalised into the adjacent aryl system. The Hammett plot revealed a ρ value of 0.97. The positive value supports the hypothesis that more electron-deficient anilinium salts degrade at a faster rate than electron-rich anilinium salts. The data points fit reasonable well on the regression line with an r^2 value of 0.92. A plot was also produced with normal σ values, the plot gave a poorer fit with an r^2 value of 0.85, confirming the hypothesis that σ^- values would be more appropriate for the degradation of *N,N,N*-trimethylanilinium iodides.

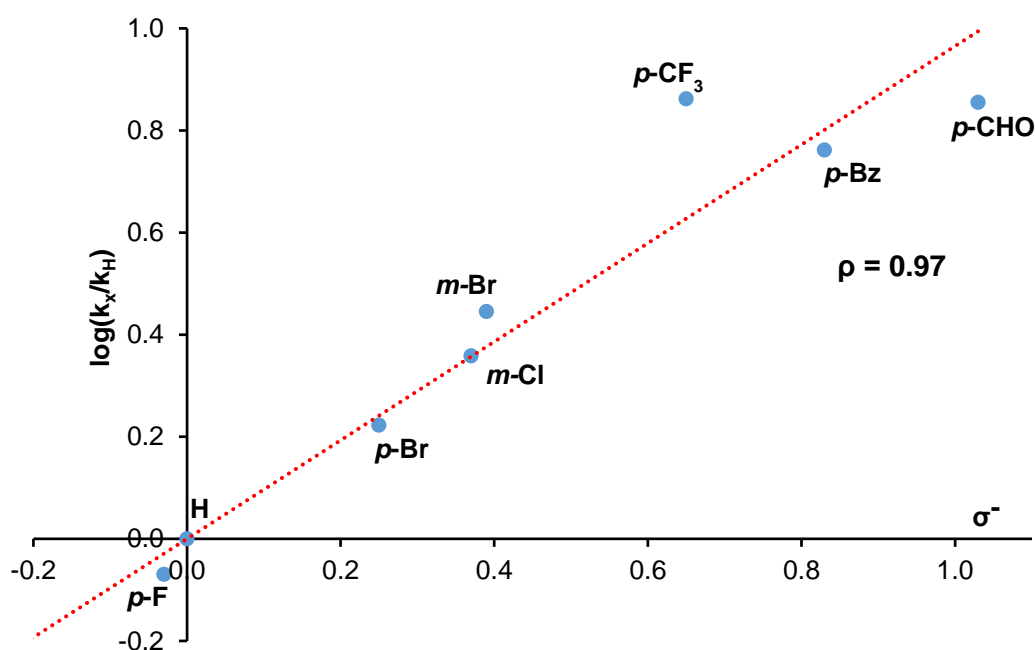


Figure 81. Hammett plot produced from estimated k_1 rate constants using σ^- values.

To gain an insight into the relative contributions from substituent field and resonance effects, a Swain-Lupton plot was also produced using the kinetic data available. The Swain-Lupton analysis creates a new σ value that is a weighted contribution of field effect (F) and resonance effects (R) for the aryl-substituents. The calculated Hammett parameter satisfies the equation $\sigma = fF + rR$, where f and r are coefficients that describe the relative contributions of field and resonance effect, and F and R are values of the field and resonance effects that each substituent has.¹⁷³ The plot revealed that field effects contribute 47% and resonance effects contribute 53% in the degradation of

N,N,N-trimethylanilinium iodides. The Swain-Lupton analysis gave an r^2 value of 0.95, which was marginally better than the 0.92 value obtained for a standard Hammett plot using σ^- values.

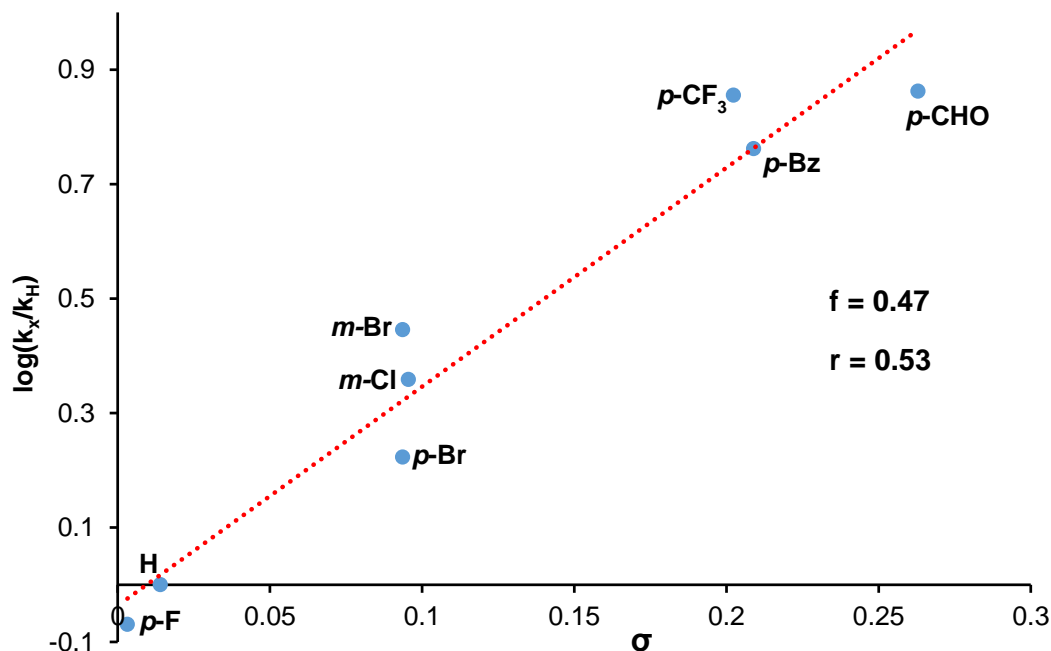


Figure 82. Swain-Lupton analysis using estimated k_1 values of *N,N,N*-trimethylanilinium iodide degradation.

Insights into the thermodynamic parameters associated with *N,N,N*-trimethylanilinium iodide degradation could be gained by considering the effect of temperature. To investigate this, ¹H NMR degradation monitoring was carried out on 0.1 M solutions of **176a** in DMSO-*d*₆ at a range of temperatures between 50 and 80 °C. The anilinium concentration vs time curves are shown in **Figure 83**. As would be expected, the rate of anilinium degradation increased at higher temperatures. Rate constants for the proposed degradation pathway (**Figure 77**) were estimated using COPASI for **176a** at 50, 60, 70, 75, and 80 °C with the same method used previously (**Figure 84**). Some notable issues with the kinetic modelling remain, such as inaccurate equilibrium constants calculated from k_1 and k_{-1} , but the relative k_1 values were consistent with the experimentally observed degradation rates.

The estimated values for k_1 at each of the temperatures could then be used with a linearised Eyring equation (**Equation 1**) to produce a plot (**Figure 85**) that would give values for the activation parameters of the iodide-led degradation pathway. The Eyring analysis revealed the standard activation enthalpy as $\Delta H^{\ddagger} = +127.0 \pm 4.0 \text{ kJmol}^{-1}$ and the standard activation entropy as $\Delta S^{\ddagger} = +34.8 \pm 11.7 \text{ Jmol}^{-1}\text{K}^{-1}$. ΔH^{\ddagger} and ΔS^{\ddagger} values for reactions involving a change in charge should be interpreted cautiously as the values can include solvation effects. In this case, the positive activation entropy is likely due to a reduced solvation demand as the two charged reactants proceed to neutral products (**Figure 86**).

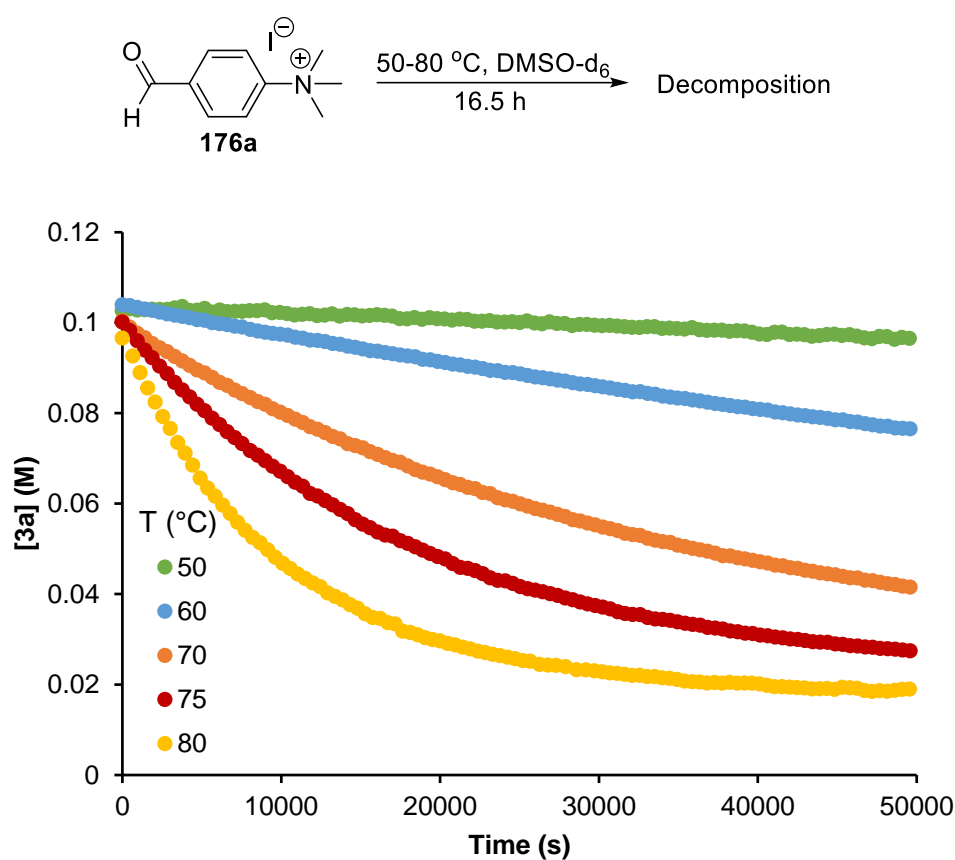


Figure 83. Concentration vs time data for the degradation of **176a** in DMSO-d₆ at 50, 60, 70, 75, and 80 °C.

| T (°C) | k ₁ (s ⁻¹) | k ₋₁ (M ⁻¹ s ⁻¹) | k ₂ (M ⁻¹ s ⁻¹) | k ₋₂ (M ⁻¹ s ⁻¹) | k ₃ (M ⁻¹ s ⁻¹) | k ₋₃ (s ⁻¹) |
|--------|-----------------------------------|--|---|--|---|------------------------------------|
| 50 | 1.17E-06 | 5.82E-295 | 1.53E-208 | 3.96E-181 | 1.67E-223 | 1.79E-114 |
| 60 | 6.28E-06 | 3.87E-130 | 7.12E-91 | 3.69E-229 | 3.94E-07 | 7.95E-153 |
| 70 | 2.21E-05 | 1.16E-236 | 1.59E-170 | 3.27E-03 | 4.03E+11 | 1.27E+14 |
| 75 | 4.06E-05 | 2.38E-236 | 3.26E-170 | 8.66E-03 | 2.46E+11 | 1.75E+14 |
| 80 | 7.42E-05 | 0.00E+00 | 1.63E-170 | 5.50E-03 | 9.48E+11 | 3.10E+14 |

Figure 84. Estimated rate constants k₁, k₋₁, k₂, k₋₂, k₃, and k₋₃ for the degradation of **176a** at temperatures of 50, 60, 70, 75, and 80 °C using COPASI.

$$\ln\left(\frac{kh}{k_b T}\right) = \left(\frac{-\Delta H^{\ddagger}}{R}\right)\frac{1}{T} + \frac{\Delta S^{\ddagger}}{R}$$

Equation 1

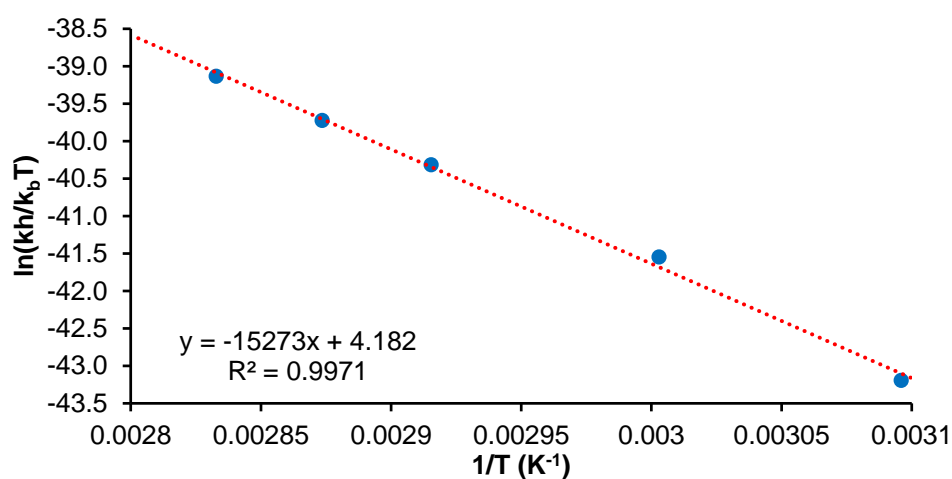


Figure 85. Linearised Eyring plot using k₁ values estimated for the degradation of **176a** at temperatures between 50-80 °C.

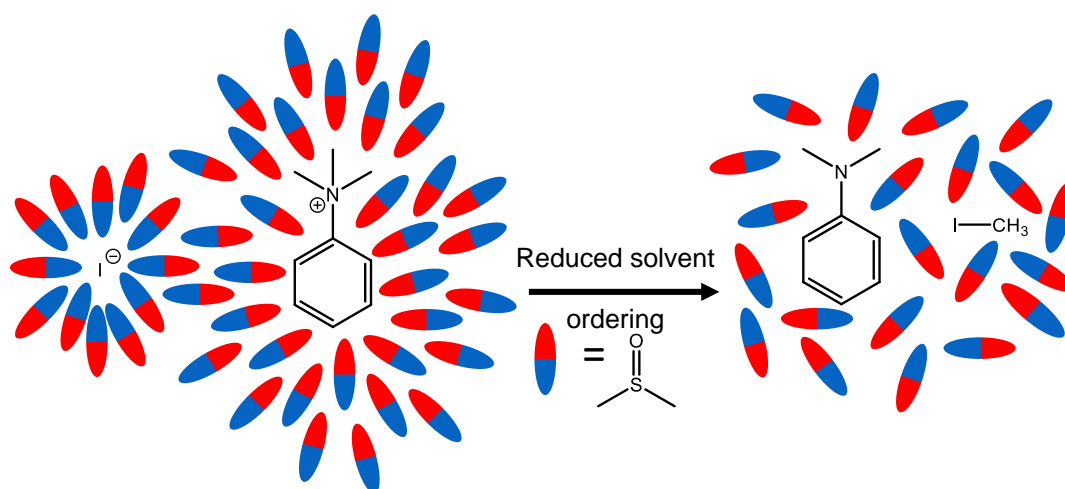


Figure 86. Stylised diagram showing the reduced solvation demand as *N,N,N*-trimethylanilinium iodides degrade to *N,N*-dimethylanilines and methyl iodide.

An important consideration for a reagent is the concentration at which it will be used. For comparability, all of the ^1H NMR monitoring experiments up until this point had been carried out with an *N,N,N*-trimethylanilinium iodide concentration of 0.1 M. In order to understand the effect that concentration has on the degradation rate, ^1H NMR spectroscopy was used to measure the degradation of **176a** in DMSO-d_6 at $80\text{ }^\circ\text{C}$ with initial concentrations between 0.025, 0.05, 0.10, 0.15, 0.20, and 0.25 M. The fraction degradation of **176a** vs time is reported on one graph for comparison (**Figure 87**). Upon visual inspection, it can be seen that at higher concentrations the rate of anilinium degradation increases. Rate constants for each step of the proposed degradation mechanism were calculated using COPASI (**Figure 88**). The calculated value of k_1 increases with increasing initial concentration of **176a**, which would not be expected for a true first order reaction.

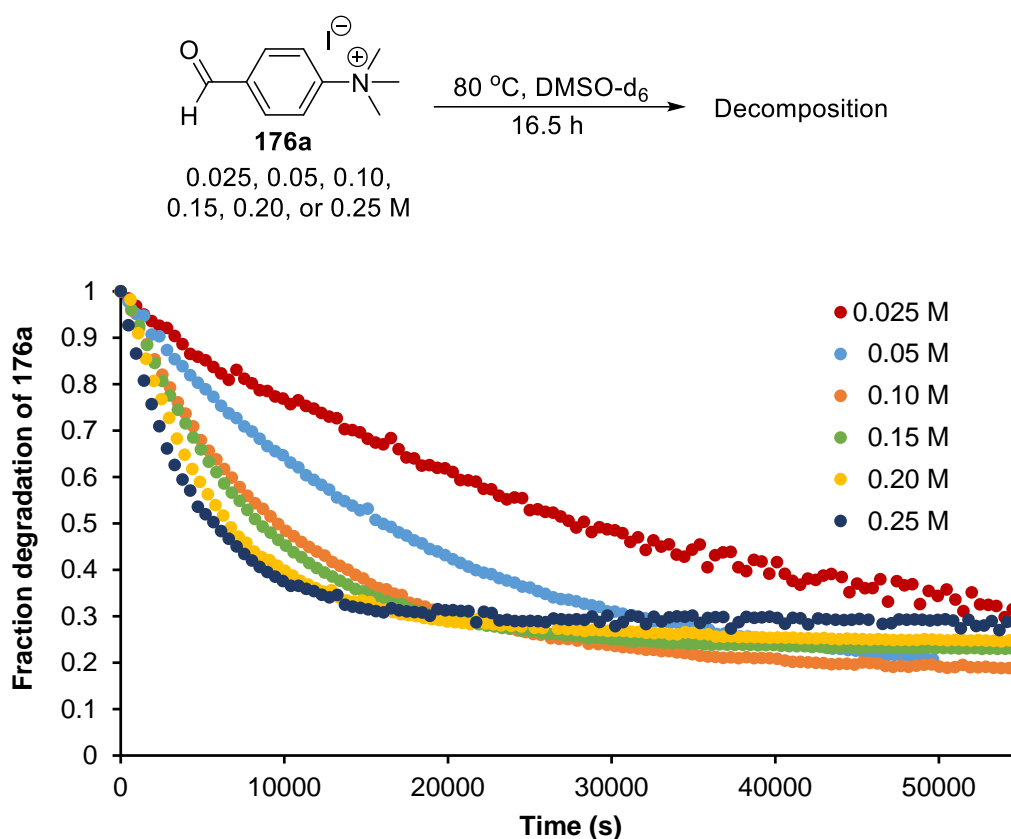


Figure 87. Fraction degradation of **176a** in DMSO-d_6 at $80\text{ }^\circ\text{C}$ with initial **176a** concentrations of 0.025, 0.05, 0.10, 0.15, 0.20, and 0.25 M.

| $[174]_0$ (M) | k_1 (s ⁻¹) | k_{-1} (M ⁻¹ s ⁻¹) | k_2 (M ⁻¹ s ⁻¹) | k_{-2} (M ⁻¹ s ⁻¹) | k_3 (M ⁻¹ s ⁻¹) | k_{-3} (s ⁻¹) |
|---------------|--------------------------|---|--|---|--|-----------------------------|
| 0.025 | 2.61E-05 | 0.00E+00 | 1.13E-170 | 5.53E-03 | 8.65E+11 | 1.98E+14 |
| 0.05 | 4.55E-05 | 8.34E-08 | 4.78E-171 | 4.06E-03 | 7.08E+11 | 1.75E+14 |
| 0.1 | 7.42E-05 | 0.00E+00 | 1.63E-170 | 5.50E-03 | 9.48E+11 | 3.10E+14 |
| 0.15 | 8.58E-05 | 9.05E-08 | 1.47E-171 | 1.64E-03 | 6.61E+11 | 5.62E+13 |
| 0.2 | 1.16E-04 | 8.86E-08 | 1.24E-171 | 1.86E-03 | 1.14E+12 | 7.87E+13 |
| 0.25 | 1.38E-04 | 8.77E-08 | 6.29E-172 | 1.84E-03 | 8.93E+11 | 6.65E+13 |

Figure 88. Estimated rate constants k_1 , k_{-1} , k_2 , k_{-2} , k_3 , and k_{-3} for the degradation of **176a** at initial concentrations of 0.025, 0.05, 0.10, 0.15, 0.20, and 0.25 M using COPASI.

Interested by the apparent non-first order nature of, initial degradation rates were estimated for the degradation reactions at each starting concentration of **176a** (**Figure 89**). Inspection of the data reveals an approximately linear trend between $[176a]_0$ and degradation rate, when $[176]_0 < 0.15$ M. However, at higher $[176]_0$ the relationship deviated more significantly from linearity which is suggestive of a reaction order greater than unity.

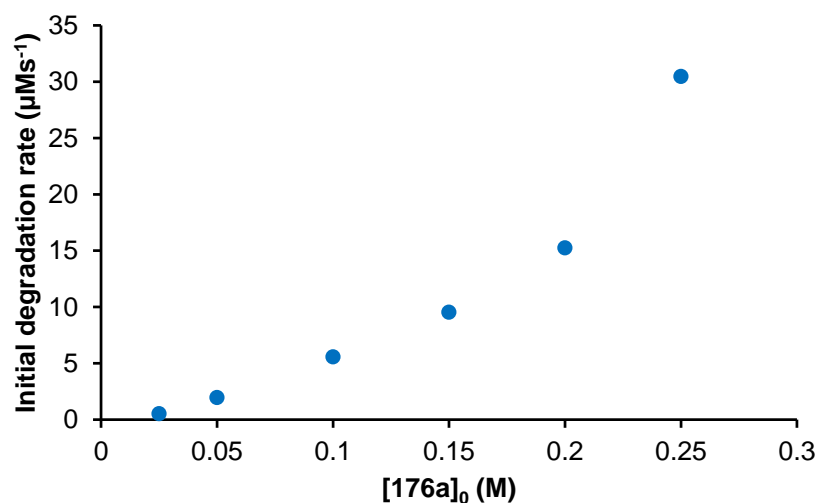


Figure 89. Initial concentration of **176a** vs calculated initial degradation rate.

It was initially thought that degradation of *N,N,N*-trimethylanilinium iodides occurred through the self-immolation of a single ion pair. However, the observation that the degradation is greater than first order with respect to anilinium suggests that this is not

necessarily the case. It is possible that at higher concentrations, inter-ion pair reactions can start to occur, leading to a mixture of first and second order reaction pathways. Second order rate constants, or first and second order rate constants for a mixed order reaction, that are consistent across experiments conducted for all concentrations of **176a** remain elusive. Adapting the kinetic model to account for the concentration dependence of anilinium degradation remains a problem for future investigation.

Alternatively, a possibility that has been considered (though largely unexplored experimentally) is that higher order aggregates may exist within solution. For example, it is plausible that the degradation of *N,N,N*-trimethylanilinium iodides could occur from an ion-pair dimer in solution (**Figure 90**). Further experiments are warranted to probe aggregation of *N,N,N*-trimethylanilinium iodides in solution.

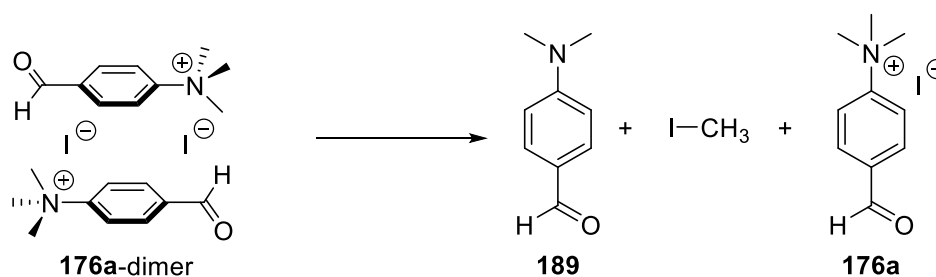


Figure 90. Possible degradation reaction of *N,N,N*-trimethylanilinium iodide ion pair.

1.3.2 *N,N,N*-Trimethylanilinium Salts in Methylation Reactions

With mechanistic insights into the degradation of *N,N,N*-trimethylanilinium salts in hand, their potential as methylating reagents was examined. As phenol *O*-alkylation represents one of the most used reactions in the pharmaceutical industry, the initial goal was to screen the methylating ability of the anilinium salt library on a particular phenol substrate in order to gain a comparison of reactivity.¹⁷⁴

4-^tBu-phenol (**194**) was selected as a suitable substrate for this study. In line with many of the reported uses of *N,N,N*-trimethylanilinium salts as methylating reagents, toluene was selected as a reaction solvent for comparing anilinium reactivity.^{162–164} Methylation reactions were carried out with potassium carbonate (4 eq.) for 3 h at 80 °C. *N,N,N*-trimethylanilinium salts **174a-c**, **174e**, **175a-180a**, **182a-184a**, and **187a**

were all screened for their ability to methylate **194** giving 4-^tBu-anisole (**195**). A chart showing the average conversion from a triplicate of experiments with each salt is shown in **Figure 91**.

From the methylation data it could be seen that the *N,N,N*-trimethylanilinium salt anion had a significant effect on methylating ability. The unsubstituted chloride (**174c**) gave higher average conversion of **194** to **195** (69±9%) than the bromide (**174b**, 39±15%), iodide (**174a**, 27±11%), and triflate (**174e**, 25±12%). The ability to methylate the phenol substrate appeared to be in line with degradation rate i.e. the chloride salt which was most prone to thermal degradation was the best methylating reagent. *Meta*-chloro (**183a**) and *meta*-bromo (**184a**) iodide salts performed well giving 62±26% and 52±25% conversion to **195**, respectively. Apart from these two main observations, there seemed to be no obvious trends in anilinium methylating ability in terms of substituent electronic effects.

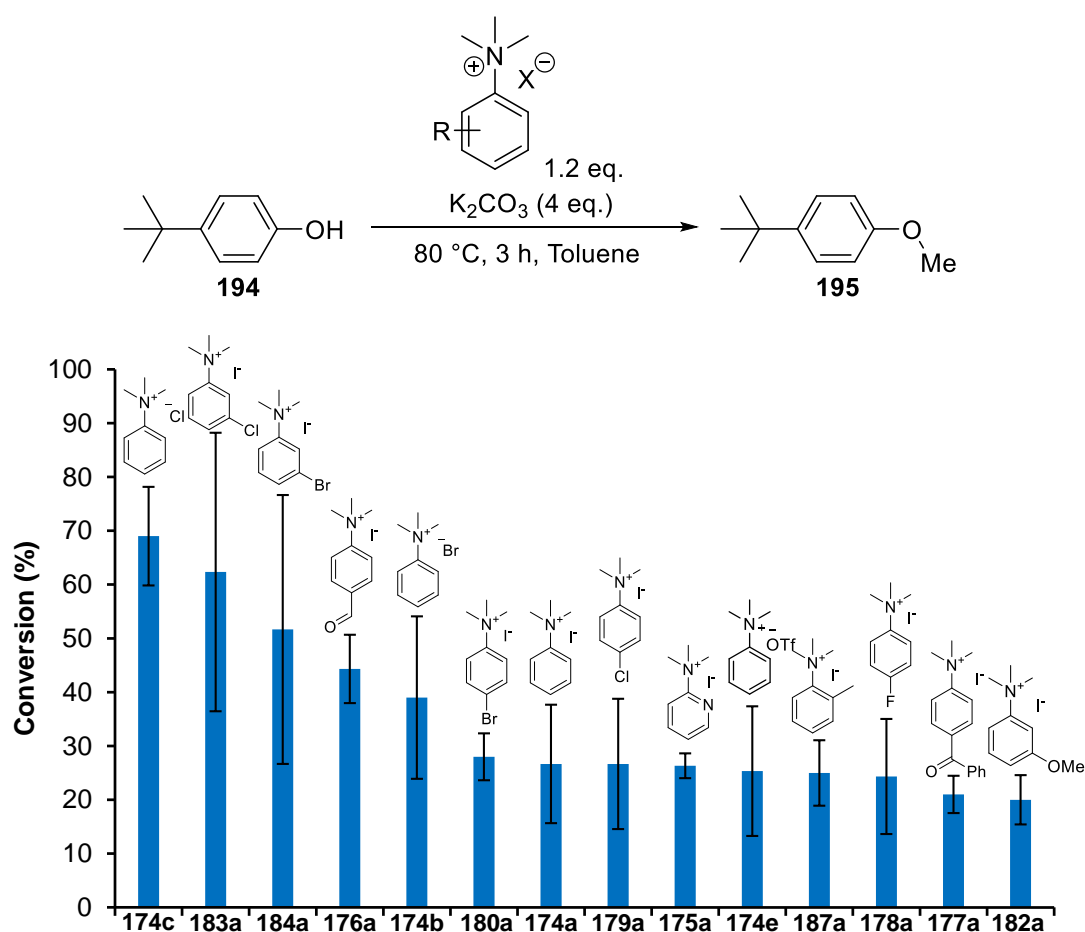


Figure 91. Average conversion of **194** to **195** in toluene with a range of *N,N,N*-trimethylanilinium salts.

The effect of reaction temperature on methylating ability in toluene was briefly investigated using **174a**, **174c**, **175a**, and **187a**. The methylation of **194** was carried out for each of these results under the standard reaction conditions with the exception of temperature which was set to 30, 50, or 80 °C (**Figure 92**). At 30 °C, no methylation product was observed for any of the anilinium salts tested. At 50 °C all salts tested gave some conversion to **195** albeit $\leq 5\%$ in each case. Significant conversions to **195** were only observed at reaction temperatures of 80 °C.

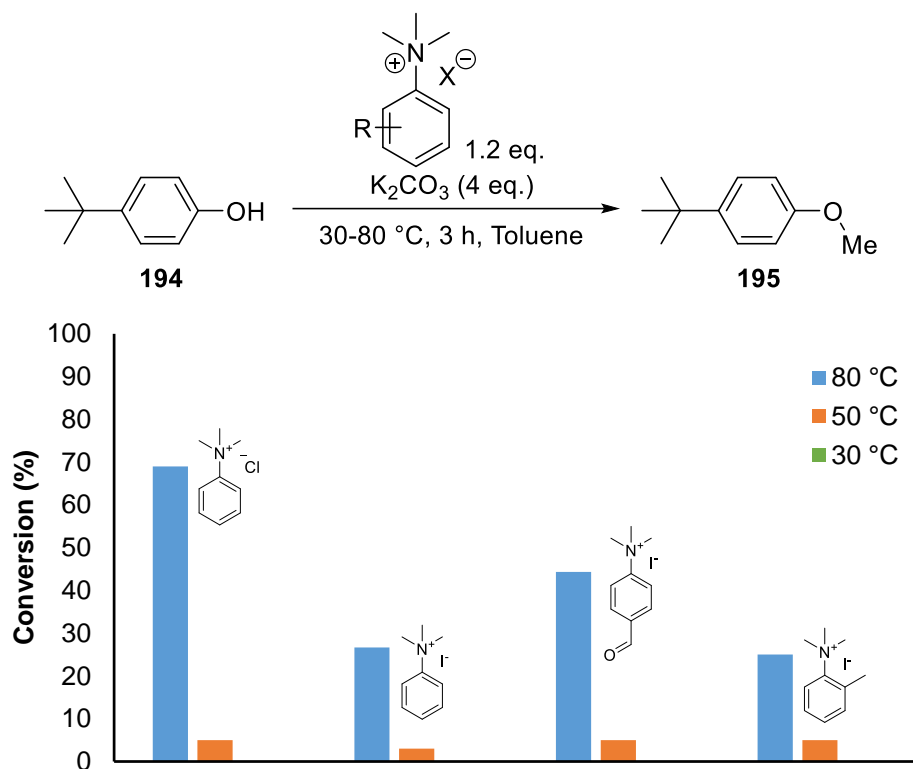


Figure 92. Conversion of **194** to **195** using **174a**, **174c**, **176a**, and **187a** at 30, 50, and 80 °C in toluene.

The methylation of **194** with a range of *N,N,N*-trimethylanilinium salts in toluene gave some information about anilinium methylating ability; however clear trends in reactivity were not observed. Many of the salts had low repeatability, giving rise to large errors e.g. $\pm 26\%$ for **183a** and $\pm 25\%$ for **184a**. It is possible that the lack of reproducibility could stem from the low solubility of *N,N,N*-trimethylanilinium iodides in toluene, where heterogeneous reactions could be more dependent on factors such as mixing efficiency. The large errors associated with the average conversion values could potentially mask genuine reactivity trends that the salts exhibit. Furthermore,

conversions in toluene under these reaction conditions were generally not useful in a preparative sense, the highest yielding reaction with **174c** was just 69%.

For the aforementioned reasons, it was decided to test the methylating ability of *N,N,N*-trimethylanilinium in an alternative solvent. To overcome the potential issues around insolubility of anilinium reagents, DMSO was selected as an appropriate solvent. Using DMSO would also allow parallels to be drawn between the existing degradation data and methylating ability. *N,N,N*-trimethylanilinium salts **174a-c**, **174e**, **175a-180a**, **182a-184a**, **187a**, and **188a** were screened for their ability to methylate **194** in DMSO at 80 °C for 3 h (**Figure 93**).

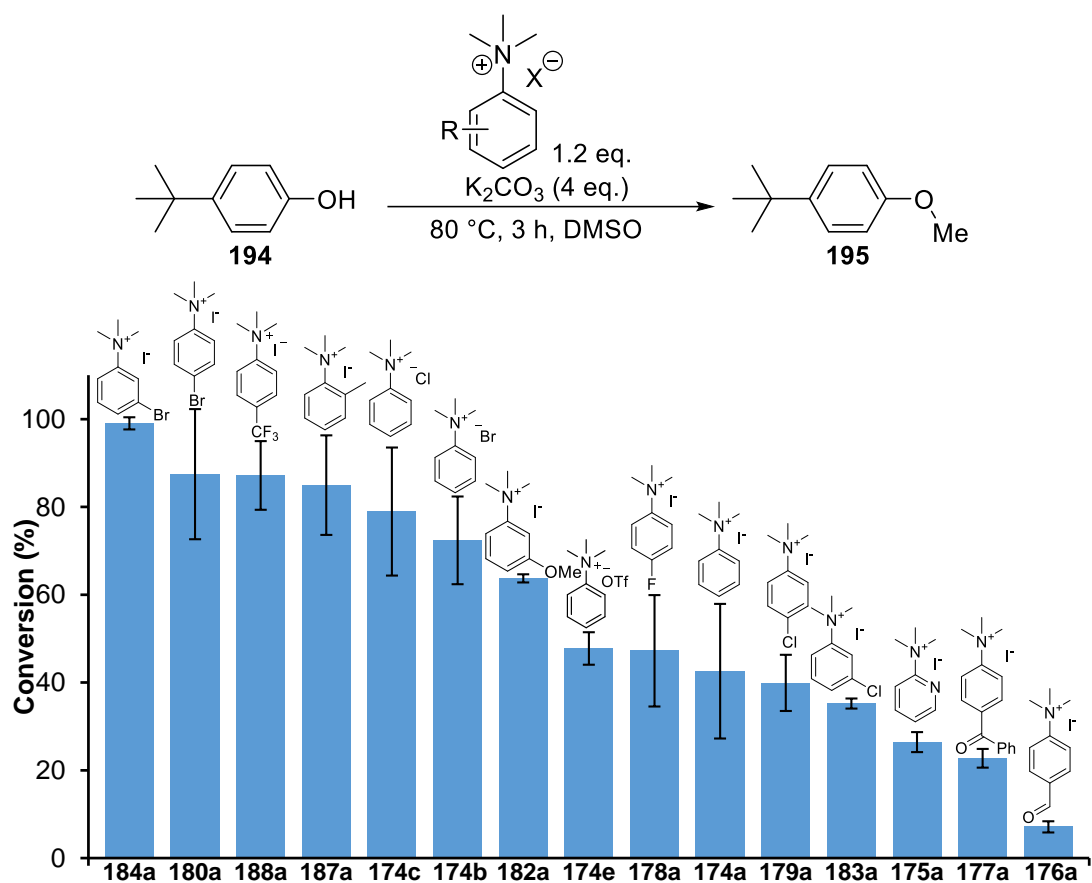


Figure 93. Average conversion of **194** to **195** in DMSO with a range of *N,N,N*-trimethylanilinium salts.

Overall, the *N,N,N*-trimethylanilinium salts appeared to be much more reactive as methylating reagents in DMSO than in toluene. The most reactive reagent towards methylation was shown to be the *meta*-bromo anilinium iodide (**184a**) giving an average conversion of 99% with minimal variance. Surprisingly, the *meta*-chloro

analogue (**183a**) which had a similar reactivity to **184a** in toluene and shares a similar degradation profile, was not very effective for methylation in DMSO giving just $35\pm 1\%$ conversion to **195**. The *para*-bromo anilinium iodide (**180a**) also gave a much higher average conversion ($87\pm 15\%$) to **195** compared to the fluoro ($47\pm 13\%$) and chloro ($40\pm 6\%$) analogues. Relatively high conversion ($85\pm 11\%$) to **195** was also observed in the case of the *ortho*-methyl salt (**187a**), this is consistent with the preference of **187a** to demethylate to its *N,N*-dimethylaniline.

The halide counterion was shown to have an effect on methylating ability, with the unsubstituted chloride salt (**174c**) giving a higher average conversion ($79\pm 15\%$) than the bromide (**174b**, $72\pm 10\%$), and iodide (**174a**, $43\pm 15\%$). The unsubstituted triflate salt (**174e**) gave a similar average conversion ($48\pm 4\%$) to the iodide, despite its slower anticipated degradation rate.

N,N,N-trimethylanilinium iodides with strongly electron-withdrawing groups such as **175a**, **176a**, and **177a** gave poor conversions to the anisole product (26 ± 2 , 7 ± 1 , $23\pm 2\%$). This result was initially surprising since the unstable anilinium salts might be expected to act efficiently in these reactions. Further investigation found that when these anilinium salts were used in the reaction, aryl ethers **196-198** were observed as the major product, which would arise from an S_NAr type reactivity (**Figure 94**). The respective yield of **196**, **197**, and **198**, were 61 ± 2 , 80 ± 3 , and $61\pm 3\%$. Interestingly, when *para*-trifluoromethyl (**188a**) was used, only $5\pm 1\%$ of the S_NAr product **199** was isolated. This is presumably due to the electron-withdrawing effect of the CF_3 group being completely inductive, giving it a diminished ability to stabilise the Meisenheimer intermediate that an S_NAr reaction could proceed through. No aryl ether products were detected for any of the *N,N,N*-trimethylanilinium iodides tested except for the aforementioned four.

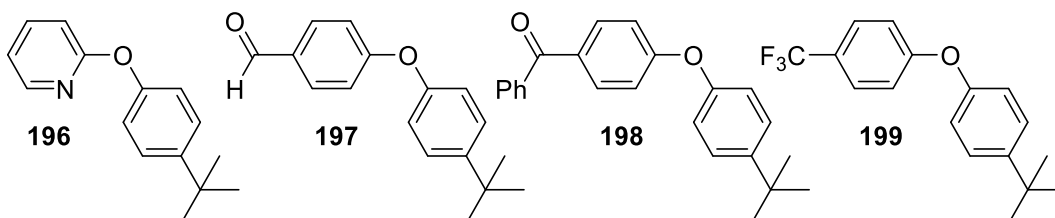


Figure 94. Aryl ethers resulting from S_NAr -type reaction of *N,N,N*-trimethylanilinium and **194**.

Overall, screening of *N,N,N*-trimethylanilinium salts for their methylation of **194** suggest that there is a play off in electronic factors where very electron rich salts will have low reactivity, but very electron deficient salts will start to favour arylation over methylation. **184a** gave repeatable high yielding reactions so it was decided to take this salt forward to test its methylating potential under the standard reaction conditions on a range of different nucleophiles. A substrate scope that consisted primarily of phenolic nucleophiles, but also thiophenol and benzoic acid was carried out (**Figure 95**). It is conceivable that the *meta*-bromo substituent of **184a** may be incompatible with other functionalities, so **187a** was also considered as an alternative for the synthesis of **200**, **210**, and **211**.

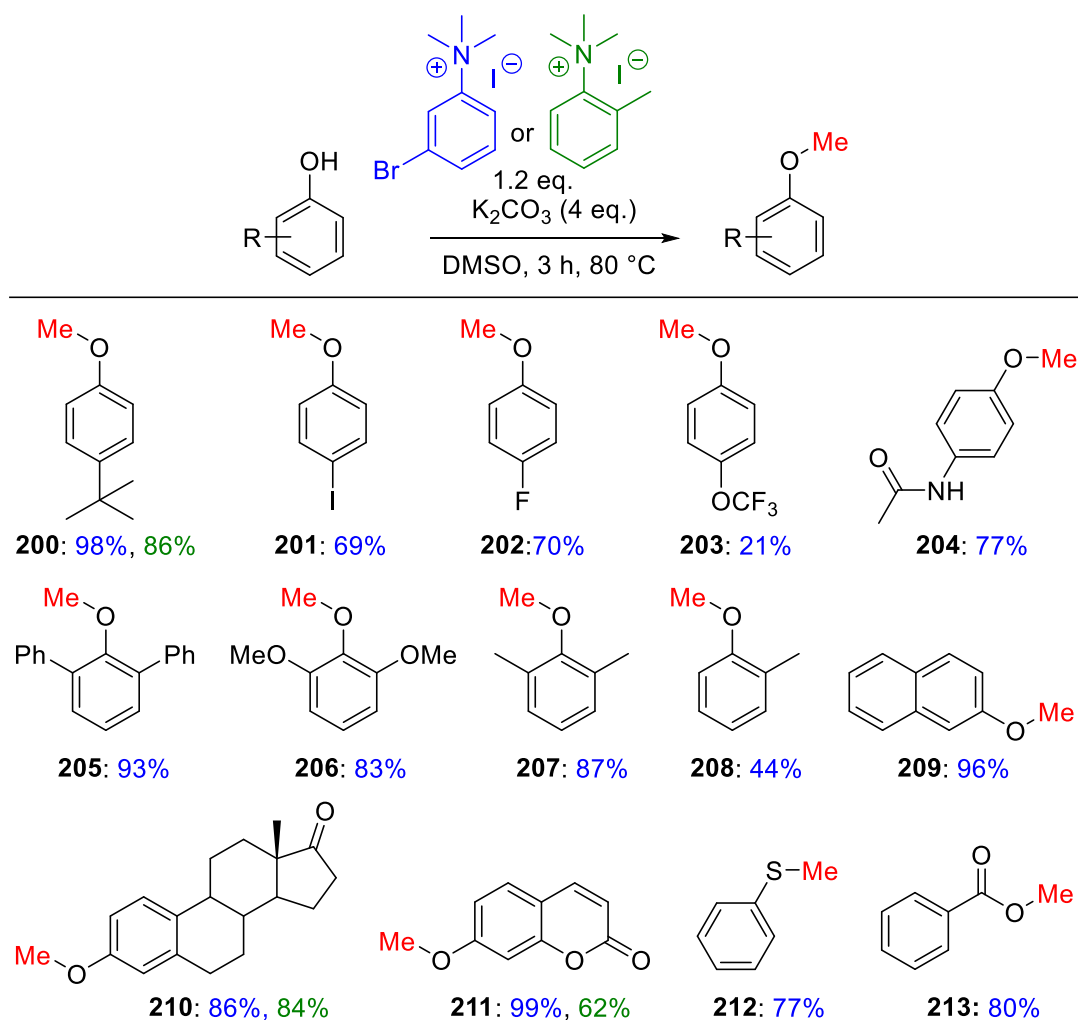


Figure 95. Methylation substrate scope of phenols, thiophenol and benzoic acid using **184a** (blue) or **187a** (green).

The substrate scope examined for methylation with **184a** represents a range of electronically and sterically differentiated phenols. Halogen substituted phenols gave anisole product **201** and **202** in 69% and 70% yield, respectively. Electron deficient phenols such as the starting material for **203** tended to give poorer conversions to the anisole. 4-acetamidophenol was effectively converted to the methylated product (**204**) in 77% yield, gratifyingly no *N*-methylation on the amide functionality was detected. Sterically encumbered 2,6-disubstituted phenols were amenable to methylation under these conditions delivering **205** (93%), **206** (83%), and **207** (87%), whereas the mono *ortho*-methylphenol only delivered **208** in 44% yield.

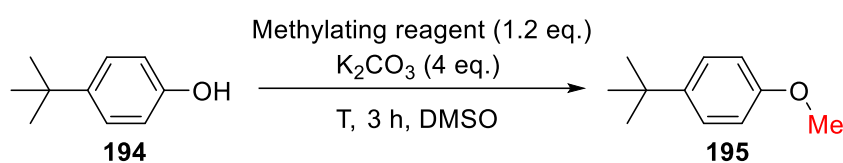
The phenyl ring could be extended to a naphthyl system, with 2-naphthanol being converted to its methyl ether in an excellent yield of 96%. Some slightly more complex substrates were then employed to demonstrate the utility of **184a** as a methylating reagent. Estrone could be converted to α -methoxyestrone (**210**) effectively, delivering the methyl ether product in 86% yield. 7-methoxycoumarin (**211**) was synthesised in an almost quantitative yield. Experiments showed that **184a** could be used for *S*-methylation, where thiophenol was converted to thioanisole in 77% yield. Finally, the esterification of benzoic acid to the methyl ester (**213**) also occurred giving a good yield of 80%.

Though the number of substrates examined was far fewer, the potential of **187a** as a methylating reagents was also demonstrated. 4-*t*-Bu-anisole (**200**) was delivered in 86% yield. Methyl ether products **210** and **211** were also generated in 84% and 62% yield, respectively. **187a** was generally lower yielding than **184a** as a methylating reagent but these initial experiments showed that it has potential as a reagent that could be improved through optimising the reaction conditions.

Comparison of 184a to common methylating reagents

With **184a** being revealed as an effective reagent for the methylation of phenol, it was then compared to some common existing methylating reagents in its reaction with **194**. Methyl iodide, methyl triflate, methyl tosylate, dimethyl sulfate and dimethylcarbonate were all tested in the place of **184a** under the standard methylation

reaction condition (**Figure 96**), the reaction with methyl iodide was also conducted at 40 °C. Our experiments showed that in DMSO at 80°C, **184a** was the most effective at synthesising **195** giving 98% of the anisole, in comparison to methyl iodide (79%), methyl triflate (2%), methyl tosylate (62%) and dimethyl sulfate (29%). Dimethylcarbonate did not deliver any of the methylated product though it is often employed alongside an activating catalyst such as DBU, or is used as the reaction solvent. The effectiveness of **184a** coupled with its potential advantages over other reagents e.g. reduced risk of exposure through inhalation and ease of handling as an air-stable solid, make it an attractive reagent to consider for the *O*-methylation of phenols.



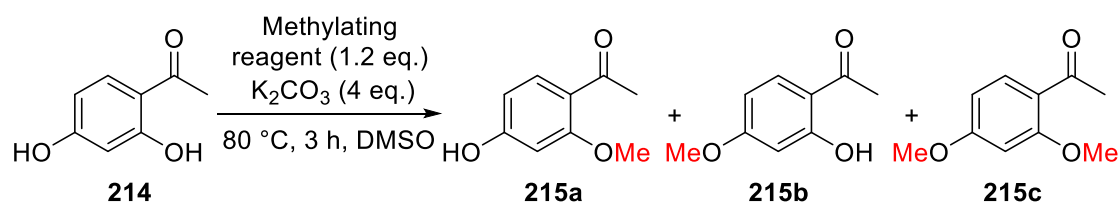
| Methylating reagent | T (°C) | Yield (%) |
|---------------------|--------|-----------|
| 184a | 80 | 98 |
| Methyl iodide | 40 | 70 |
| Methyl iodide | 80 | 79 |
| Methyl triflate | 80 | 2 |
| Methyl tosylate | 80 | 62 |
| Dimethyl sulfate | 80 | 29 |
| Dimethyl carbonate | 80 | 0 |

Figure 96. Comparison of methylation reagents for the conversion of **194** to **195**.

The lack of any observed *N*-methylation in the synthesis of **204** (**Figure 95**) when using **184a** suggested that using the anilinium salt as a methylating reagent could offer some reaction selectivity. In the case of **204**, complete chemoselectivity was observed for the *O*-nucleophile. A more challenging case of regioselectivity was investigated in

the methylation of **214** with **184a** as the methylating reagent (**Figure 97**). 2',4'-dihydroxyacetophenone (**214**) offers two potentially reactive phenolic nucleophiles. There is also potential for C-methylation α to the carbonyl but this would be highly unexpected. Assuming only O-methylation could occur, there are three potential products, the mono-methylated **215a** and **215b**, or the di-methylated **215c**.

Running the methylation of **214** under the standard reaction conditions revealed that no *ortho*-hydroxyl methylation product (**215a**) was observed. A mixture of 37% *para*-methylated product (**215b**) and 26% dimethylated product (**215c**) was observed when using **184a** as the methylating reagent. For comparison, methyl iodide was used in the same reaction. Again, no **215a** was seen and a mixture of **215a** and **215b** was obtained, though an improved selectivity for the monomethyl was seen using methyl iodide. Under the reaction conditions used in this preliminary reaction, a low regioselectivity was obtained using **184a** as the methylating reagent. However, the fact that **184a** and methyl iodide give different product distributions suggests that there could be an exploitable difference in the reactivity of each reagent. Further investigation, including reaction monitoring, could be used in the future to understand the reactivity differences between each reagent.



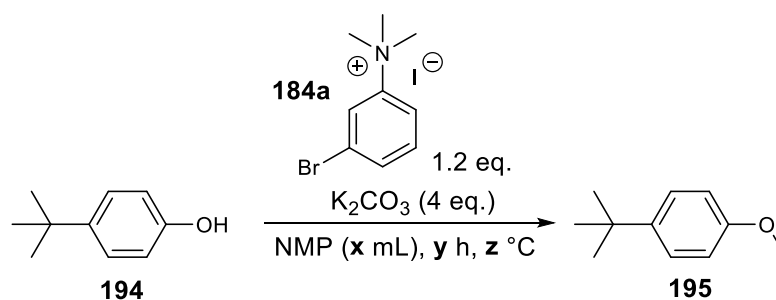
| Methylating reagent | 215a (%) | 215b (%) | 215c (%) |
|---------------------|----------|----------|----------|
| 184a | 0 | 37 | 26 |
| Methyl iodide | 0 | 57 | 20 |

Figure 97. Comparison of the regioselectivity when methylating **214** with either **184a** or methyl iodide.

Methylation Reactions in NMP

DMSO has proven to be a useful reaction solvent for the methylation of phenols with *N,N,N*-trimethylanilinium salts. However, due to its non-innocence and the proclivity for DMSO to decompose at high temperatures, it is conceivable that users of this chemistry (particularly process chemists) may wish to adopt a different solvent.^{175–177} It was thought that a similarly polar solvent would need to be used to solubilise the anilinium reagents. *N*-methyl-2-pyrrolidone (NMP) was chosen as an alternative solvent to consider as it is commonly used to replace DMSO in large-scale processes. Furthermore, it is not expected that NMP would be able to react directly with *N,N,N*-trimethylanilinium salts in the way that DMSO has been shown to.

The methylation of **194** was first carried out with **184a** in NMP under the standard conditions used for DMSO methylations (**Figure 98**, Entry 1), giving the methylation product in an 88% yield. A brief investigation into reaction temperature (Entry 2), reaction concentration (Entry 3), and reaction time (Entry 4) revealed that running the methylation in NMP under the existing conditions but for a longer period of time (8 h), the anisole product **195** could be isolated with a yield of 96%. Then, using the newly established reaction conditions, estrone and 7-hydroxycoumarin were also converted to their methyl ethers **210** and **211** with respective yields of 88% and 94% (**Figure 99**).



| Entry | x (mL) | y (h) | z (°C) | Yield (%) |
|----------|----------|----------|-----------|-----------|
| 1 | 2 | 3 | 80 | 88 |
| 2 | 2 | 3 | 50 | 62 |
| 3 | 5 | 3 | 80 | 83 |
| 4 | 2 | 8 | 80 | 96 |

Figure 98. Optimisation for the methylation of **194** in NMP using **184a**.

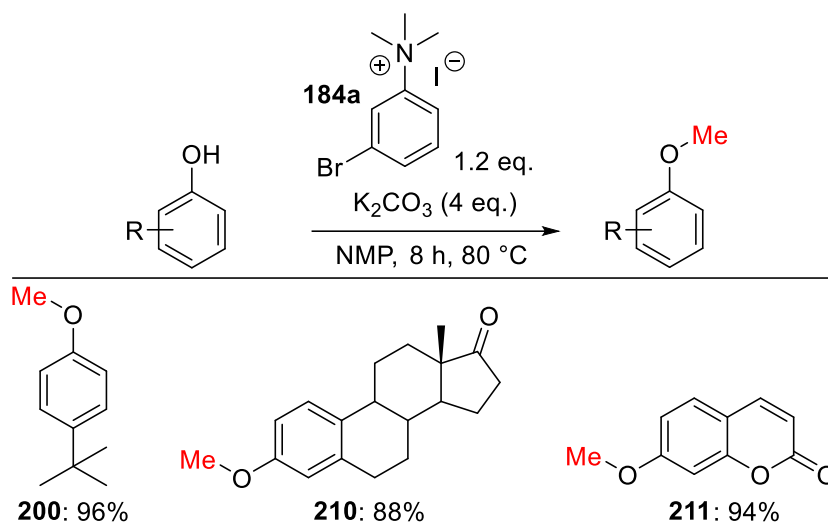


Figure 99. Methylation of phenols using **184a** in NMP.

With NMP proving to be a suitable alternative solvent to DMSO for the methylation of phenols, the following questions about the behaviour of anilinium salts in NMP were raised: Do *N,N,N*-trimethylanilinium iodides still decompose to *N,N*-dimethylanilines and methyl iodide in NMP? And if so, does the rate of degradation compare to that observed in DMSO-*d*₆?

To begin answering these questions, a suitable method to monitor the degradation of *N,N,N*-trimethylanilinium salts in NMP needed to be developed. Ideally ¹H NMR kinetic experiments analogous to those already carried out in DMSO-*d*₆ would be used. However, NMP-*d*₉ is less widely available than DMSO-*d*₆ which was a prohibiting factor in its use. It was thought that NMR spectroscopy could be used to follow an alternative nucleus to ¹H, allowing the non-deuterated solvent to be used in a degradation experiment. To put this hypothesis to the test, 4-trifluoromethyl-*N,N,N*-trimethylanilinium iodide (**188a**) was chosen as a substrate to monitor with ¹⁹F NMR spectroscopy.

A sequence was developed that allowed the NMR spectrometer to lock onto the N-CH₃ protons of NMP and carry out the shimming process, before obtaining a ¹⁹F NMR spectrum of the sample. With this sequence set up, the T1 delay times of each fluorine nucleus in **188a**, 4-trifluoromethyl-*N,N*-dimethylaniline, and α,α,α -trifluorotoluene (which would be used as an internal standard) were calculated *via* a T1ir experiment. A mixture of **188a** (0.1 M) and α,α,α -trifluorotoluene (0.1 M) was prepared in NMP

and heated at 80 °C for 16.5 h whilst ^{19}F NMR spectra were recorded at regular time intervals. The resulting spectra were stacked, which could be processed to calculate the concentrations of **188a** and 4-trifluoromethyl-*N,N*-dimethylaniline over the time course (**Figure 100**).

Unfortunately, the nature of the experiment meant that any non-innocence of NMP would not be observed (unless it involved the generation of a new fluorine-containing species). Though the assumption could not be tested, estimation of degradation rate constants were based solely on the reversible iodide-led degradation of **188a** (**Figure 101**). Using COPASI the estimated rate constants for this reaction were $k_1 = 4.44 \times 10^{-4} \text{ s}^{-1}$ and $k_{-1} = 4.78 \times 10^{-4} \text{ M}^{-1}\text{s}^{-1}$.

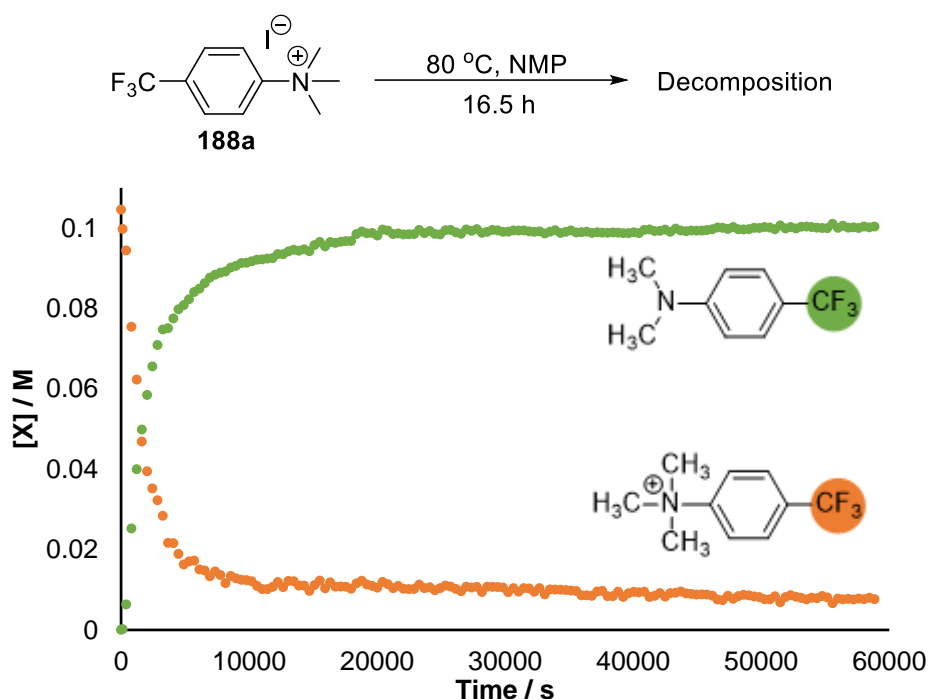


Figure 100. Degradation time course of **188a** (0.1 M) in NMP at 80 °C monitored in real-time by ^{19}F NMR spectroscopy. The concentrations of **188a** and 4-trifluoromethyl-*N,N*-dimethylaniline were determined from their trifluoromethyl groups with respect to the internal standard, α,α,α -trifluorotoluene.

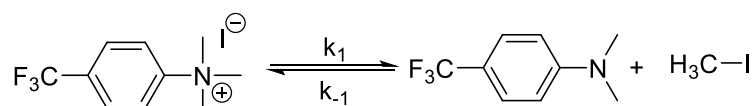


Figure 101. Proposed degradation reaction of **188a** in NMP with assigned rate constants k_1 and k_{-1} .

The monitoring of **188a** in NMP at 80 °C revealed that the *N,N,N*-trimethylanilinium iodide salt does thermally degrade. The rate constant for iodide-led degradation (k_1) was an order of magnitude higher than that observed for any of the anilinium salts tested in DMSO- d_6 . The concentration vs time plots for **188a** in both DMSO- d_6 and NMP are overlaid in **Figure 102**. The first observation here is the noticeable difference in degradation rate: $k_1 = 8.08 \times 10^{-5} \text{ s}^{-1}$ in DMSO- d_6 and $k_1 = 4.44 \times 10^{-4} \text{ s}^{-1}$ in NMP. The second point to consider is that, **188a** appears to reach an equilibrium concentration of about 0.05 M in DMSO- d_6 . In NMP, the salt almost completely degrades. Though DMSO and NMP largely have similar properties, differences in their physical parameters such as dielectric constant (74 vs 42) or viscosity (2.00 vs 1.66 mPas), may contribute to differences in *N,N,N*-trimethylanilinium salt stability in solution.¹⁷⁸ Alternatively, the ability of methyl iodide to react with DMSO to form TMSOI may act as a methyl iodide “sponge” to keep the volatile methylating reagent in solution. Without this mechanism in place for NMP, the methyl iodide could exist mainly in the NMR headspace which limits the rate of the backwards reaction. This cannot be probed with ^{19}F NMR.

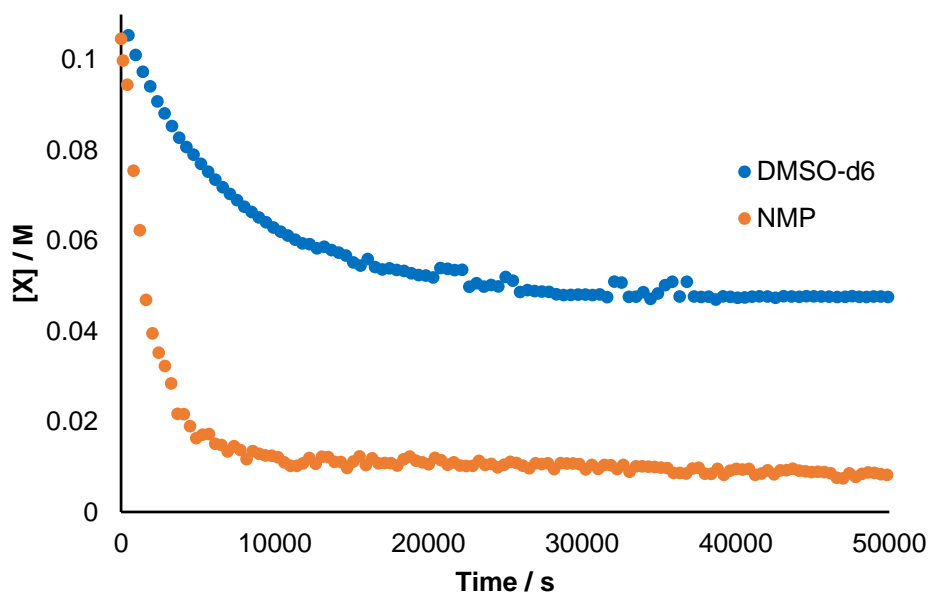


Figure 102. Comparison of the degradation of **188a** in DMSO- d_6 (blue) and NMP (orange).

Mechanism of Phenol Methylation using *N,N,N*-Trimethylanilinium Salts

Comprehensive degradation studies have shown that *N,N,N*-trimethylanilinium iodides readily decompose to *N,N*-dimethylanilines and methyl iodide when heated in DMSO and NMP. Synthetic studies have shown that *N,N,N*-trimethylanilinium iodides are capable of acting as competent reagents in the methylation of phenols.

The major remaining questions about the reactivity of *N,N,N*-trimethylanilinium salts revolve around the mechanism by which they act as methylating reagents (**Figure 103**). i.e. do they methylate phenols by direct attack of the nucleophile onto the anilinium salt (route **C**) or does the methyl iodide generated *in situ* from their decomposition act as the methylating reagent (route **D**). In DMSO, it is also uncertain if TMSOI plays a role in the methylation reactions (routes **A** and **B**). A series of experiments to delineate the reactive pathways are presented in this section.

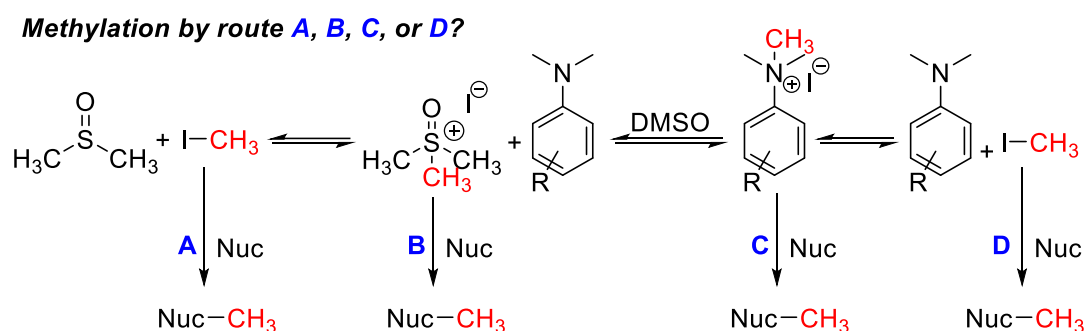


Figure 103. Possible pathways of nucleophile methylation using *N,N,N*-trimethylanilinium iodides in DMSO.

In order to gain mechanistic insights into the methylation reaction, it would be useful to follow the methylation process using real time ^1H NMR in the same way that the degradation was monitored. The use of potassium carbonate in the methylation reactions precluded this possibility as reaction mixtures were heterogeneous. Moving to a soluble base could potentially overcome this problem but finding a suitable soluble, non-nucleophilic base was challenging, and the obtained data would not have been representative of how these reactions proceed in practice. Therefore, a series of carefully designed experiments were carried out to systematically probe routes **A-D**.

The investigation first considered whether nucleophile attack occurs directly onto the anilinium salt (route **C**) or from the *in situ* generated methyl iodide (route **D**). PF₆ (**184d**) and BArF (**184f**) analogues of **184a** were used in the methylation of **194** to probe this (**Figure 104**). The direct question that can be answered from this set of experiments is: Is the generation of *in situ* generation of methyl iodide from anilinium decomposition necessary for methylation?

The answer to that question is no. **184d** and **184f** are able to methylate **194** with yields of 45% and 50% respectively, despite their inability to generate methyl iodide as a methylating reagent (*via* route **A** or route **D**). However, the yields obtained with the PF₆ and BArF salts are significantly lower than that obtained with the iodide (98%), which suggests that route **D** occurs at a faster rather than other methylation routes.

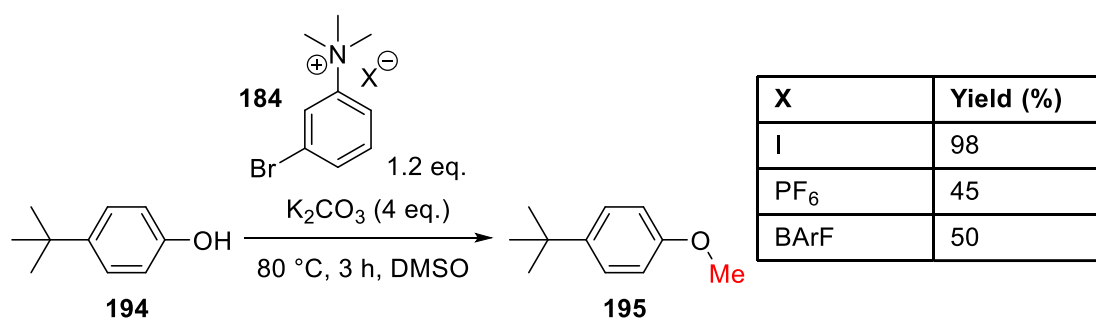


Figure 104. Methylation of **194** in DMSO using **184a, d, and f**.

Whilst the experiments in **Figure 104** show that decomposition to methyl iodide is not a prerequisite, they do not show conclusively that route **C** is occurring. This is because of the competing DMSO-led degradation which results in the synthesis of the TMSO cation. It is possible that the methylation occurring in the experiments above comes from TMSO rather than the anilinium directly i.e. methylation occurs *via* route **B**.

To gain a deeper insight into this uncertainty, the methylating potential of TMSO salts was investigated (**Figure 105**). TMSO iodide (**216a**), PF₆ (**216d**) and BArF (**216f**) were all used for the methylation of **194** in DMSO to see if methylation through route **B** was possible. **216a** methylated the phenol in 76%. This suggested TMSO could possibly react through route **B**; however, earlier experiments showed that TMSOI can

decompose to methyl iodide (**Figure 73**), meaning methylation through route **A** could be occurring.

Methylation with **216d** and **216f** occurred with 57% and 53% yields respectively. Neither of these reagents can decompose to methyl iodide so this suggests that direct reaction of the nucleophile with the TMSO cation (route **B**) is possible. Comparing the iodide case to the non-coordinating anions, it appears once again that where methyl iodide can be generated, methylation reactions are faster. i.e. methylation by methyl iodide (routes **A** and **D**) is faster than methylation by the TMSO or Anilinium cations (routes **B** and **C**).

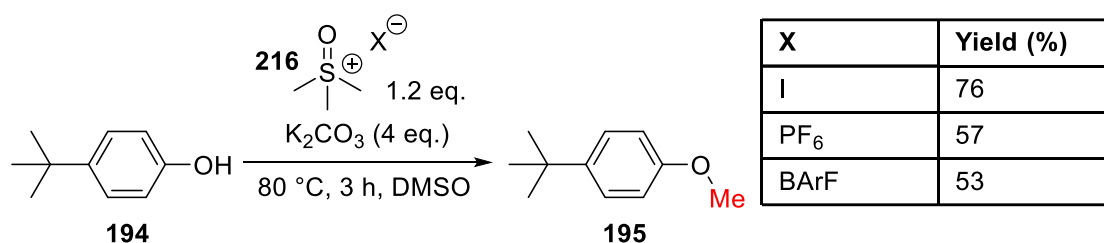


Figure 105. Methylation of **194** in DMSO using **216a**, **d**, and **f**.

The mechanistic experiments above show that methylation by route **B** is definitely possible. The higher methylation yields with the anilinium and TMSO iodides compared to PF₆ and BArF salts also suggest that routes **A** and **D** occur. The question that remained was if methylation directly from the anilinium (route **C**) could occur. To answer this question, changing the solvent away from DMSO was necessary, thus NMP was employed in the final reactions.

184a and **184d** were both used in the methylation of **194** in NMP (**Figure 106**). **184a** methylated the phenol effectively in 88% yield. Here routes **A** and **B** are not possible, so assuming NMP is innocent in this system, methylation must come entirely from the anilinium itself (route **C**) or methyl iodide (route **D**), anilinium salts were shown to decompose in NMP previously (**Figure 100**).

Finally, the methylation carried out with **184d** proceeded with a modest yield of 11%. With routes **A**, **B**, and **D** eliminated, it stands to reason that the methylation in this case

must be occurring directly from attack of **194** onto the anilinium cation *via* route **C**. The low methylation yield in this case suggests that methylation directly from the anilinium cation is inefficient.

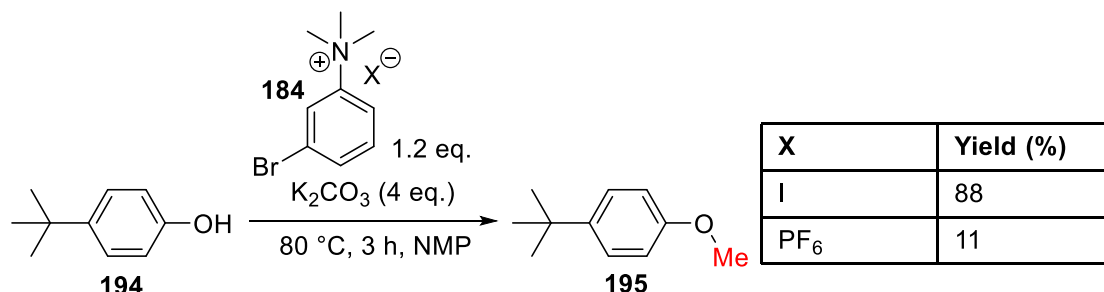


Figure 106. Methylation of **194** in NMP using **184a** and **184d**.

Taken together, the experiments carried out in this section gives a wealth of useful information about this methylation system. The key findings are as follows:

- Methylation of the nucleophile from methyl iodide, the anilinium cation, and the TMSO cation are all possible.
- Methylation *via* methyl iodide is the most efficient reaction pathway whenever methyl iodide can be generated.
- Methylation *via* the TMSO cation is more efficient than methylation from the anilinium directly.

Despite the absence of evidence for any single electron pathways occurring in the degradation reactions. For completeness, it was decided to probe the possibility of any radical mediated methylation. The methylation of **194** with **184a** was carried out in DMSO in the presence of 3 equivalents of TEMPO (**Figure 107**). The methylation proceeded with 65% yield, suggesting that the methylation reaction is not dominated by radical based pathways. Furthermore, no TEMPO adducts were detected by ¹H NMR or GCMS analysis. Although the reaction was not shut down, it did run with a

lower yield (65% compared to 98% in the absence of TEMPO), so without further investigation it is not possible to completely rule out any single electron pathways.

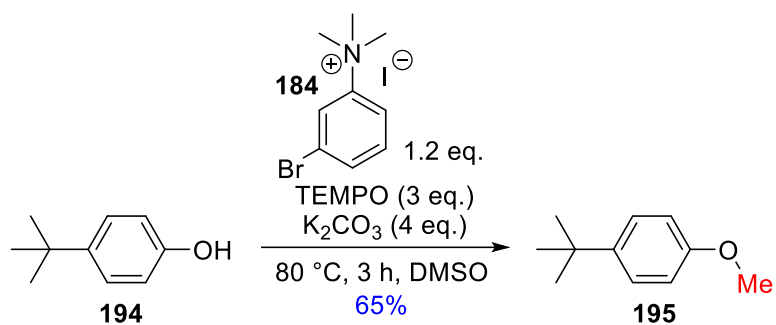


Figure 107. Methylation of **194** with **184a** in DMSO in the presence of TEMPO (3 eq.).

1.4 Conclusions

This project has focussed primarily on studying the degradation of *N,N,N*-trimethylanilinium salts to understand their reactivity. By monitoring the degradation of these salts, a wealth of information has been uncovered about their intrinsic stabilities and how they might be used as reagents. A range of analytical techniques has been employed in this study.

The effects on aryl substitution and counterion species on the reactivity of *N,N,N*-trimethylanilinium salts have been explored in great detail. A library of anilinium salts was synthesised to include aryl substituents in the *ortho*-, *meta*-, and *para*- positions of the anilinium aromatic ring, these substituents have represented electron-donating and electron withdrawing groups through both mesomeric and inductive effects, and also sterically influential groups. The effect of counterion species on salt stability was also studied. These investigations considered different halide species, and weakly coordinating anions such as hexafluorophosphate, trifluoromethanesulfonate and tetrakis(3,5-bis(trifluoromethyl)phenyl) borate.

Initial investigations considered the stability of *N,N,N*-trimethylanilinium salts in the solid state. Thermal gravimetric analysis was utilised in this part of the study. The data showed that halide counterion affects the stability of *N,N,N*-trimethylanilinium salts in the solid state, with the unsubstituted chloride salt decomposing at a lower temperature than both the analogous bromide and iodide. It was found that electron-withdrawing aryl substituents led to lower onset degradation temperatures than electron-donating substituents. The other key finding from the TGA experiments was that all of the *N,N,N*-trimethylanilinium salts tested were stable under both argon and air to temperatures of at least 165 °C. This suggests that the salts would be safe and convenient to store as reagents in a research laboratory or manufacturing plant setting.

The stability of the *N,N,N*-trimethylanilinium salt library was also investigated in DMSO. Initial investigations used single time point experiments to gain an insight into substituent and counterion effects on the thermal stability of these salts. As observed in the solid state, electron-deficient anilinium salts degraded more quickly than electron-rich anilinium salts. *N,N,N*-trimethylanilinium chloride salts were found to have a lower stability than bromides and iodides in turn. Changing the halide

counterion to non-coordinating hexafluorophosphate, trifluoromethanesulfonate, or tetrakis(3,5-bis(trifluoromethyl)phenyl) borate anions significantly reduced the degradation rate of the *N,N,N*-trimethylanilinium salts.

The degradation of a range of *N,N,N*-trimethylanilinium salts was monitored in real time using ^1H NMR spectroscopy. The findings from single time-point experiments with respect to substituent effects were consolidated. Quantitative kinetic analysis also revealed an interesting isotopic scrambling event that ultimately led to the assertion that DMSO acts non-innocently in these systems. The data led to the proposed mechanism shown in (**Figure 108**).

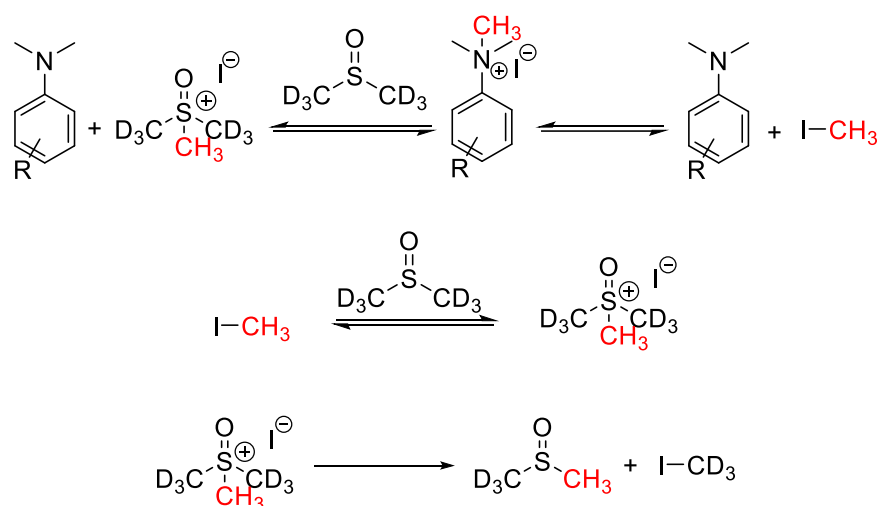


Figure 108. Proposed degradation mechanism of *N,N,N*-trimethylanilinium iodides in DMSO- d_6 .

With an understanding of *N,N,N*-trimethylanilinium salt degradation, attention turned to their synthetic applications. The methylating ability of a range of *N,N,N*-trimethylanilinium salts on 4- ^1Bu -phenol was screened in both toluene and DMSO. Generally, DMSO was better for reactivity which could stem from better anilinium salt solubility. Electron-rich anilinium salts reacted quite sluggishly towards methylation. Electron-deficient anilinium salts were shown in general to be more reactive; however, when substituents were strongly electron-withdrawing through resonance effects, $\text{S}_{\text{N}}\text{Ar}$ type reactivity became dominant. 3-Br-*N,N,N*-

trimethylanilinium iodide was shown to be the most effective methylating reagent under the conditions used.

3-Br-*N,N,N*-trimethylanilinium was then tested for its methylating ability on a range of substrates. These primarily included phenols which could be converted to anisole products in generally good yields. Thiophenol and benzoic acid could also be converted to thioanisole and methyl benzoate showing further potential for *N,N,N*-trimethylanilinium salts as methylating reagents. The methylation reactions were also shown to be feasible in NMP which could be more attractive to users of anilinium chemistry on scale.

Finally, the mechanism of phenol methylation was examined. A series of experiments designed to probe particular reactive pathways suggested that the primary methylating reagents in *N,N,N*-trimethylanilinium iodide reaction mixture was methyl iodide, which was generated *in situ* through anilinium degradation. The experiments show that in DMSO, non-innocence of the solvent can also promote methylation through the formation of trimethylsulfoxonium iodide and its subsequent decomposition to methyl iodide. It appears that direct attack of a nucleophile onto the *N,N,N*-trimethylanilinium moiety is possible but occurs at a slower rate than the aforementioned reactive pathways.

1.5 Future Work

It has been demonstrated in this project that gaining a mechanistic understanding of the degradation of *N,N,N*-trimethylanilinium salts can be used to guide their synthetic applications. It was shown that salts such as **184a** and **187a** are effective for the conversion of phenolic substrates to their respective anisole products. Much of the future work in this area should focus on furthering the synthetic utility of *N,N,N*-trimethylanilinium salts, by applying the mechanistic insights gained through this project. Mechanistic experiments showed that when using *N,N,N*-trimethylanilinium iodides for methylation reactions, the main methylation pathway is from the *in situ* generation of methyl iodide. Aside from obvious benefit of not having to directly handle toxic, volatile methyl iodide, the ability for *N,N,N*-trimethylanilinium iodides to slowly release methyl iodide into a reaction mixture may deliver some benefits to methylation chemistry users.

The in-depth investigation into *N,N,N*-trimethylanilinium salt degradation kinetics revealed a wealth of information about their reactivity. However, there are a few issues that should be addressed in the future. The kinetic modelling allowed the estimation of degradation rate constants that could be used in a comparative sense. Further refinements to the model should be made that take into account the observed isotopic scrambling such that each of the intermediates can be incorporated into the model to obtain more accurate rate constants. Further attempts to find a model that is more consistent with the apparent concentration dependence of anilinium degradation should also be explored. Monitoring the degradation of *N,N,N*-trimethylanilinium iodides with an added iodide salt may also give information about the degradation reaction order in anilinium.

Preliminary investigations into reaction selectivity with a substrate containing two potential methylation sites (2',4'-dihydroxyacetophenone) did not show any benefit of using *N,N,N*-trimethylanilinium iodides over methyl iodide. These experiments were, however, very limited and only considered the ratio of products after a set reaction time. This concept should be investigated further by studying the reaction kinetics to identify any differences in the rate of formation for any particular products. It is hoped that using *N,N,N*-trimethylanilinium salts to deliver a controlled release of methyl

iodide into the reaction mixture could be exploited to preferentially form the kinetically favoured methylation products (**Figure 109a**). Furthermore, changing the reaction conditions such as reaction temperature or the solvent, may deliver better selectivity. Aside from regioselectivity, it is envisaged that *N,N,N*-trimethylanilinium salts could react chemoselectively with ambident nucleophiles, such as 2-mercaptophenol, containing more than one different reactive centre (**Figure 109b**). Depending on the success of these proof of concept experiments, any regio- or chemoselectivity could be exploited for the selective methylation of drug compounds or natural products with multiple reactive sites, which would present attractive opportunities for using *N,N,N*-trimethylanilinium salts in synthetic organic chemistry.

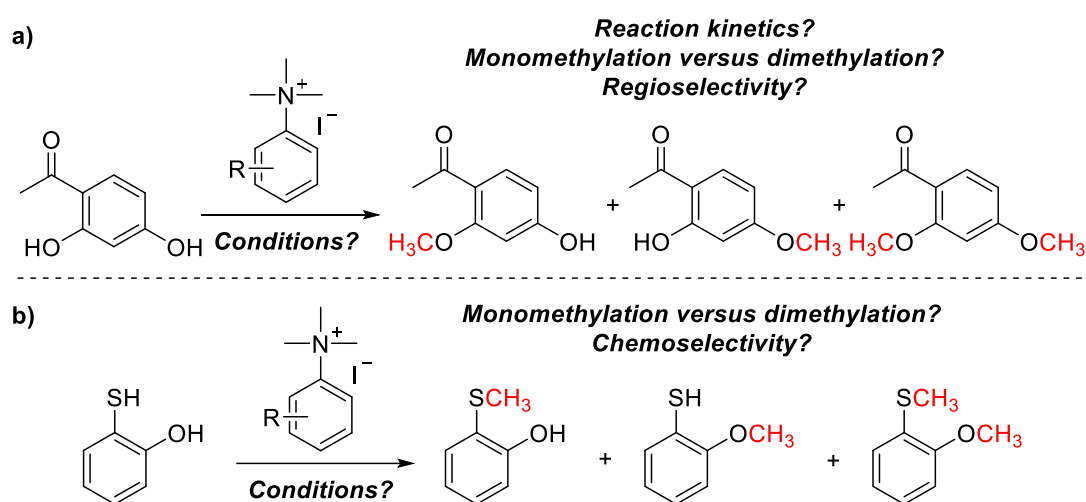


Figure 109. Potential investigation into methylation regioselectivity and chemoselectivity using *N,N,N*-trimethylanilinium iodides.

N,N,N-trimethylanilinium salts as methylating reagents could present numerous advantages over methyl iodide (or similar electrophilic methylating reagents) to users of methylation chemistries on a process-scale. The fact that *N,N,N*-trimethylanilinium salts are thermally stable solids at room temperature means that they are easier to handle and that they present a lower exposure risk than volatile compounds such as methyl iodide. However, the toxicity of *N,N,N*-trimethylanilinium salts should be investigated further before recommending their wide spread adoption.

Further safety benefits may be identified from thermal analysis of these methylation reactions. It is envisaged that a slow release of the active methylating reagent (methyl iodide) into a reaction mixture could allow reactions to proceed with a more controlled heat output compared to using methyl iodide directly (**Figure 110**). Various calorimetric methods such as reaction calorimetry or differential scanning calorimetry could be applied to these reaction systems to understand and safety advantages *N,N,N*-trimethylanilinium salts may offer.

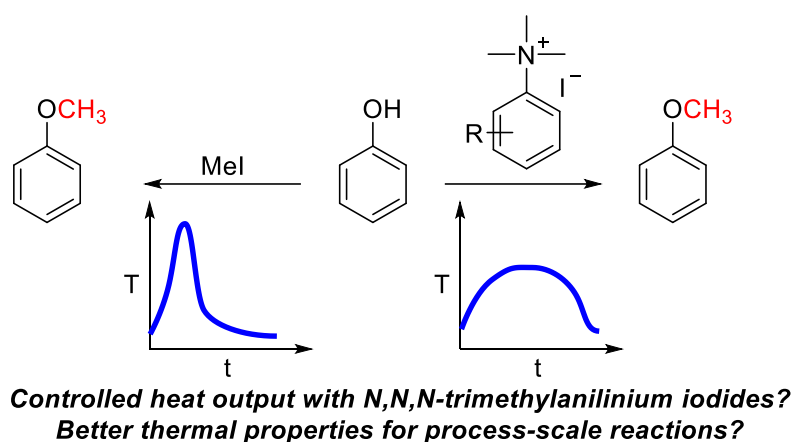
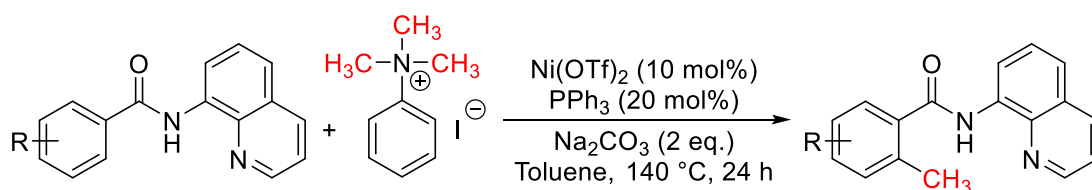


Figure 110. Potential investigations comparing reaction heat output with methyl iodide or *N,N,N*-trimethylanilinium iodides as methylating reagents.

The final area that should be considered for further investigation is the application of *N,N,N*-trimethylanilinium salts in cross coupling reactions. Whilst the applications of *N,N,N*-trimethylanilinium salts in cross coupling reactions are numerous, little understanding of the factors affecting their reactivity has been used to guide their usage. It is envisioned that insights into *N,N,N*-trimethylanilinium reactivity gained in this project could be used to increase the efficiency of cross coupling reactions using these reagents. Two select examples as a starting point for these investigations are identified below.

The CH-methylation protocol using *N,N,N*-trimethylanilinium iodide that was developed by Chatani and co-workers is not very well understood mechanistically (**Figure 46**, *vide infra*).¹⁵⁶ It is unclear from the original literature report if methylation

occurs directly from the *N,N,N*-trimethylanilinium cation or from methyl iodide that is generated *in situ*. The requirement for high reaction temperatures, the lack of reactivity using *N,N,N*-trimethylanilinium hexafluorophosphate, and the development of a very similar protocol from the group using methyl iodide directly, all suggest that methyl iodide generated from anilinium degradation is the effective source of methyl groups in this reaction manifold.¹⁶⁰ If the generation of methyl iodide is necessary for the reaction to occur, as suspected, the findings from this project may be applicable to improve reaction efficiency (**Figure 111**). It is envisaged that using an alternative reagent that is more susceptible to thermal degradation, such as *o*-methyl *N,N,N*-trimethylanilinium iodide (**187a**), in the place of the unsubstituted *N,N,N*-trimethylanilinium iodide (**174a**), could facilitate the generation of methyl iodide at lower temperatures or over shorter reaction times. **187a** would also be likely to have a higher solubility in toluene than **174a**, though any issues relating to reaction homogeneity are not mentioned in the original report.



Alternative *N,N,N*-trimethylanilinium salts to improve reaction efficiency?

Figure 111. Potential improvement of an existing cross-coupling methodology using the mechanistic findings from this project.¹⁵⁶

In many of the cross-coupling applications of *N,N,N*-trimethylanilinium salts, degradation to the *N,N*-dimethylaniline and methyl iodide represents an undesired reactive pathway. A selected methodology (**Figure 112**) uses *N,N,N*-trimethylanilinium iodides as the electrophilic coupling partners in a THF-NMP mixture at relatively high temperatures of 85 °C.¹⁷⁹ The substrate scope used in the investigation has a limited number of *N,N,N*-trimethylanilinium salts bearing electron withdrawing aryl substituents. Degradation of *N,N,N*-trimethylanilinium iodides to dimethylanilines and methyl iodide is not listed as a competing reaction, but findings

from this project suggest that this will be the case. Investigations into this reaction manifold, or similar, should be carried out that use the degradation understanding gained through this project to improve the efficiency of the cross-coupling. In particular, the use of OTf, PF₆ or BArF salts should be employed, and the reactions should be trialled at lower temperatures (potentially at the cost of longer reaction times), to minimise any competing demethylation of the *N,N,N*-trimethylanilinium substrates.

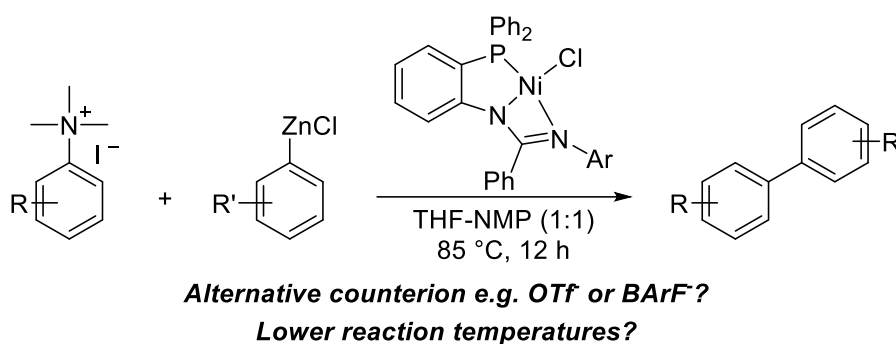


Figure 112. Potential investigations to utilise degradation understanding to promote cross coupling reaction efficiency.¹⁷⁹

1.6 Experimental

1.6.1 General Considerations

Solvents and Reagents

All reagents were obtained from commercial suppliers (Alfa Aesar, Fluorochem, Sigma-Aldrich, Thermofisher or VWR) and used without further purification unless otherwise stated.

Dimethylsulfoxide and *N*-methylpyrrolidone were dried over 4Å molecular sieves.

Tetrahydrofuran and toluene were obtained from a PureSolv SPS-400-5 Solvent Purification System.

Thin Layer Chromatography

Thin layer chromatography was carried out using Merck TLC Silica gel 60 F₂₅₄ plates. A Mineralight UVGL-25 lamp was used at 254 nm to visualise spots; when necessary vanillin or potassium permanganate dip was used to develop TLC plates.

Column Chromatography

Column chromatography was carried out using VWR silica gel (40-60 µm mesh).

IR spectroscopy

IR spectra were recorded on a Perkin Elmer Spectrometer 1. All spectra were taken from neat samples and absorptions are listed in cm⁻¹.

NMR Spectroscopy

¹H, ¹³C, ¹¹B ¹⁹F, and ³¹P NMR spectra for structural analysis and single point degradation studies were recorded on a Bruker AV3-400 spectrometer at 400 MHz and 101 MHz, 128 MHz, 376 MHz and 162 MHz, respectively. All spectra were recorded at ambient temperature using standard pulse methods. Chemical shifts are recorded in ppm with respect to residual solvent peak, and multiplicities are denoted as: singlet (s), doublet (d), triplet (t), quartet (q), quintet (quin) or multiplet (m). Coupling constant are reported in Hz and refer to H-H couplings, unless otherwise stated.

^1H NMR spectra for elevated temperature studies were recorded on a Bruker AV3-500HD spectrometer at 500 MHz. Chemical shifts are reported in ppm with respect to 1,2,4,5-tetramethylbenzene internal standard.

1.6.2 Experimental Procedures

*General Procedure A – Preparation of N,N -dimethylanilines from anilines*¹⁸⁰

To a flame dried two-necked 250 mL round bottom flask equipped with a stirrer bar was added the relevant aryl-substituted aniline (1 eq.), paraformaldehyde (5.4 eq.), sodium cyanoborohydride (5.4 eq.) and dry THF. Glacial acetic acid (5.4 eq.) was then added dropwise *via* syringe to the stirred solution at room temperature. The resultant mixture was heated to 50 °C and stirred under an atmosphere of argon for 18 h. After cooling to room temperature, the mixture was partitioned between a saturated sodium carbonate solution and diethyl ether. The layers were separated and the aqueous layer was extracted with two further portions of diethyl ether. The organic layers were collected and dried over anhydrous magnesium sulfate, filtered, then concentrated *in vacuo*. The resultant oil was purified by silica gel column chromatography (eluting with ethyl acetate/ petroleum ether 1:6) to give the corresponding dimethyl aniline.

General Procedure B – Preparation of N,N,N -trimethylanilinium iodide salts from N,N -dimethylanilines with methyl iodide

The relevant aryl-substituted N,N -dimethylaniline (1 eq.) was dissolved in acetonitrile to a concentration of 2 M in a sealed 25 mL round bottom flask equipped with a stirrer bar. Methyl iodide (3 eq.) was added dropwise *via* syringe to the stirred solution. The reaction mixture was stirred at 60 °C for 16 h and a white precipitate formed. Upon cooling, the solid was collected *via* vacuum filtration, and washed with diethyl ether (3 x 10 mL). The solid residue was then dried under high vacuum to give the corresponding N,N,N -trimethylanilinium iodide.

General Procedure C – Preparation of N,N,N -trimethylanilinium hexafluorophosphate salts from N,N,N -trimethylanilinium iodides with potassium hexafluorophosphate

The relevant aryl-substituted *N,N,N*-trimethylanilinium iodide (1 eq.) was dissolved in the minimum amount of deionised water to achieve dissolution. Potassium hexafluorophosphate (2 eq.) was added to the solution and stirred for 2 h causing a white precipitation to form. The solid was collected *via* vacuum filtration and washed with deionised water (3 x 10 mL), then dried in a vacuum oven overnight to give the corresponding *N,N,N*-trimethylanilinium hexafluorophosphate product.

General Procedure D – Synthesis of N,N,N-trimethylanilinium trifluoromethanesulfonate salts from N,N-dimethylanilines with methyl trifluoromethanesulfonate

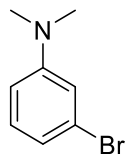
The relevant aryl-substituted *N,N*-dimethylaniline (1 eq.) was dissolved in dichloromethane to a concentration of 1 M in a sealed 50 mL round bottom flask equipped with a stirrer bar. Methyl trifluoromethanesulfonate (1.5 eq.) was added dropwise *via* syringe to the stirred solution. The reaction mixture was stirred at room temperature for 18 h. Diethyl ether (20 mL) was added to the resulting solution causing a precipitate to form. The solid was collected *via* vacuum filtration and washed with diethyl ether (3 x 10 mL) and dried under vacuum to give the *N,N,N*-trimethylanilinium trifluoromethanesulfonate product.

General Procedure E – Synthesis of N,N,N-trimethylanilinium tetrakis(3,5-bis(trifluoromethyl)phenyl) borate salts from N,N,N-trimethylanilinium iodides with sodium tetrakis(3,5-bis(trifluoromethyl)phenyl) borate

The relevant aryl-substituted *N,N,N*-trimethylanilinium iodide (1 eq.) and sodium tetrakis(3,5-bis(trifluoromethyl)phenyl) borate (1 eq.) were stirred in a 1:1 biphasic mixture of deionised water and dichloromethane at room temperature for 2 h. The organic layer was then collected, dried over anhydrous sodium sulfate and filtered. The filtrate was concentrated *in vacuo* then dried under high vacuum to give the corresponding *N,N,N*-trimethylanilinium tetrakis(3,5-bis(trifluoromethyl)phenyl) borate product.

Synthesis of *N,N*-dimethylanilines

Synthesis of 3-bromo-*N,N*-dimethylaniline



Prepared according to *General Procedure A*.

Amount of 3-Bromoaniline: 4.13 g, 23.9 mmol, 1 eq.

Amount of sodium cyanoborohydride: 7.90 g, 130 mmol, 5.4 eq.

Amount of paraformaldehyde: 3.91 g, 131 mmol, 5.4 eq.

Amount of acetic acid: 7.3 mL, 7.67 g, 128 mmol, 5.4 eq.

Volume of THF: 100 mL

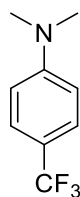
Product yield: 3.64 g, 18.2 mmol, 76 %

IR: ν_{\max} 2881, 2802, 1591, 1553, 1493, 1411, 1350, 1227, 1179, 1096, 1065, 982, 955, 827, 756, 679, 659 cm^{-1}

^1H NMR (400 MHz, CDCl_3): δ 2.98 (s, 6H, $\text{N}(\text{CH}_3)_2$), δ 6.67 (m, 1H, ArH), δ 6.87 (m, 1H, ArH), δ 7.11 (m, 1H, ArH)

^{13}C NMR (101 MHz, CDCl_3): δ 39.88, 110.44, 114.61, 118.60, 122.89, 129.76, 151.15

Synthesis of 4-trifluoromethyl-*N,N*-dimethylaniline



Prepared according to *General Procedure A*.

Amount of 4-trifluoromethylaniline: 3.87 g, 24.0 mmol, 1 eq.

Amount of sodium cyanoborohydride: 7.91 g, 130 mmol, 5.4 eq.

Amount of paraformaldehyde: 3.90 g, 131 mmol, 5.4 eq.

Amount of acetic acid: 7.3 mL, 7.67 g, 128 mmol, 5.4 eq.

Volume of THF: 100 mL

Product yield: 1.97 g, 10.4 mmol, 43 %

Melting point: 68-79 °C

IR: ν_{\max} 1614, 1553, 1368, 1323, 1231, 1195, 1157, 1096, 1065, 941, 816 cm^{-1}

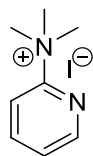
^1H NMR (400 MHz, CDCl_3): δ 3.04 (s, 6H, $\text{N}(\text{CH}_3)_2$), δ 6.73 (d, 2H, ArH, $J = 8.81$ Hz), δ 7.48 (d, 2H, ArH, $J = 8.81$ Hz)

^{13}C NMR (101 MHz, CDCl_3): δ 39.59, 110.66, 117.00 (q, $J_{\text{CF}^2} = 31.49$ Hz), 124.73 (q, $J_{\text{CF}^1} = 271.63$ Hz), 125.83 (m), 151.81

^{19}F NMR (376 MHz, CDCl_3): δ -60.87

Synthesis of N,N,N -trimethylanilinium salts

*Synthesis of N,N,N -trimethylpyridinaminium iodide, **175a***



Prepared according to *General Procedure B*.

Amount of N,N -dimethylpyridinamine: 1.22 g, 10.0 mmol, 1 eq.

Amount of methyl iodide: 1.87 mL, 4.26 g, 30.0 mmol, 3 eq.

Volume of acetonitrile: 5.0 mL

Product yield: 2.46 g, 9.3 mmol, 93 %

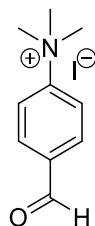
Melting point: 203-205 °C

IR: ν_{\max} 1490, 1466, 1151, 1060, 849 cm^{-1}

^1H NMR (400 MHz, DMSO-d_6): δ 3.60 (s, 9H, $\text{N}(\text{CH}_3)_3$), δ 7.73 (m, 1H, ArH), δ 8.11 (m, 1H, ArH), δ 8.25 (m, 1H, ArH), δ 8.68 (m, 1H, ArH)

^{13}C NMR (101 MHz, DMSO-d_6): δ 54.41, 115.28, 126.23, 141.07, 148.59, 156.67

Synthesis of 4-formyl-N,N,N-trimethylanilinium iodide, 176a



Prepared according to *General Procedure B*.

Amount of 4-formyl-*N,N*-dimethylaniline: 2.98 g, 20.0 mmol, 1 eq.

Amount of methyl iodide: 3.74 mL, 8.53 g, 60.1 mmol, 3 eq.

Volume of acetonitrile: 10.0 mL

Product yield: 2.90 g, 10 mmol, 50 %

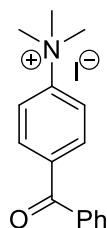
Melting point: 164-164 °C

IR: ν_{max} 3015, 1699, 1306, 1177, 827 cm^{-1}

^1H NMR (400 MHz, DMSO- d_6): δ 3.74 (s, 9H, $\text{N}(\text{CH}_3)_3$), δ 8.18 (m, 2H, ArH), δ 8.28 (m, 2H, ArH), δ 10.17 (s, 1H, CHO)

^{13}C NMR (101 MHz, DMSO- d_6): δ 56.40, 121.71, 130.84, 136.75, 151.01, 192.08

Synthesis of 4-benzoyl-N,N,N-trimethylanilinium iodide, 177a



Prepared according to *General Procedure B*.

Amount of 4-dimethylaminobenzophenone: 2.25 g, 10.0 mmol, 1 eq.

Amount of methyl iodide: 1.87 mL, 4.26 g, 30.0 mmol, 3 eq.

Volume of acetonitrile: 5.0 mL

Product yield: 1.90 g, 5.2 mmol, 52 %

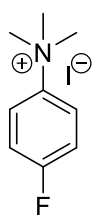
Melting point: 181-183 °C

IR: ν_{\max} 3007, 1655, 1597, 1288, 928 cm^{-1}

^1H NMR (400 MHz, DMSO- d_6): δ 3.70 (s, 9H, $\text{N}(\text{CH}_3)_3$), δ 7.61 (m, 2H, ArH), δ 7.72-7.79 (m, 3H, ArH), δ 7.95 (m, 2H, ArH), δ 8.19 (m, 2H, ArH)

^{13}C NMR (101 MHz, DMSO- d_6): δ 56.43, 121.14, 128.83, 129.78, 130.89, 133.46, 136.08, 138.47, 149.62, 194.47

Synthesis of 4-fluoro- N,N,N -trimethylanilinium iodide, 178a



Prepared according to *General Procedure B*.

Amount of 4-fluoro- N,N -dimethylaniline: 1.39 g, 10.0 mmol, 1 eq.

Amount of methyl iodide: 1.87 mL, 4.26 g, 30.0 mmol, 3 eq.

Volume of acetonitrile: 5.0 mL

Product yield: 2.60 g, 9.2 mmol, 92%

Melting point: 203-205 °C

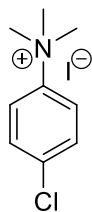
IR: ν_{\max} 3003, 1600, 1510, 1232, 1120, 948, 844 cm^{-1}

^1H NMR (400 MHz, DMSO- d_6): δ 3.66 (s, 9H, $\text{N}(\text{CH}_3)_3$), δ 7.54 (m, 2H, ArH), δ 8.09 (m, 2H, ArH)

^{13}C NMR (101 MHz, DMSO- d_6): δ 56.74, 116.65 (d, $J_{\text{CF}^2} = 23.6$ Hz), 123.44 (d, $J_{\text{CF}^3} = 8.6$ Hz), 143.32, 161.80 (d, $J_{\text{CF}^1} = 248$ Hz)

^{19}F NMR (376 MHz, DMSO- d_6): δ -111.5 (m)

Synthesis of 4-chloro-N,N,N-trimethylanilinium iodide, 179a



Prepared according to *General Procedure B*.

Amount of 4-chloro-*N,N*-dimethylaniline: 2.33 g, 15.0 mmol, 1 eq.

Amount of methyl iodide: 3.74 mL, 8.52 g, 60.1 mmol, 4 eq.

Amount of potassium carbonate: 8.29 g, 60.0 mmol, 4 eq.

Volume of acetonitrile: 15.0 mL

Product yield: 1.61 g, 5.4 mmol, 36%

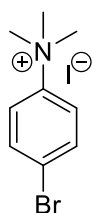
Melting point: 229-230 °C

IR: ν_{max} 1483, 1394, 1292, 1122, 1008, 945, 840 cm^{-1}

^1H NMR (400 MHz, DMSO- d_6): δ 3.66 (s, 9H, N(CH₃)₃), δ 7.75 (m, 2H, ArH), δ 8.05 (m, 2H, ArH)

^{13}C NMR (101 MHz, DMSO- d_6): δ 56.50, 122.83, 129.78, 134.62, 145.93

Synthesis of 4-bromo-N,N,N-trimethylanilinium iodide, 180a



Prepared according to *General Procedure B*.

Amount of 4-bromo-*N,N*-dimethylaniline: 1.0 g, 5.0 mmol, 1 eq.

Amount of methyl iodide: 0.94 mL, 2.14 g, 15.1 mmol, 3 eq.

Volume of acetonitrile: 2.5 mL

Product yield: 1.27 g, 3.7 mmol, 74%

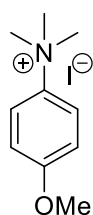
Melting point: 201-203 °C

IR: ν_{\max} 2361, 1479, 1464, 1408, 1395, 1123, 1078, 1005, 945, 926, 839, 814, 735, 710 cm^{-1}

^1H NMR (400 MHz, DMSO- d_6): δ 3.65 (s, 9H, $\text{N}(\text{CH}_3)_3$), δ 7.88 (m, 2H, ArH), δ 7.98 (m, 2H, ArH)

^{13}C NMR (101 MHz, DMSO- d_6): δ 56.44, 123.01, 123.26, 132.75, 146.42

Synthesis of 4-methoxy- N,N,N -trimethylanilinium iodide, 181a



Prepared according to *General Procedure B*.

Amount of 4-methoxy- N,N -dimethylaniline: 0.63 g, 5.0 mmol, 1 eq.

Amount of methyl iodide: 1.3 mL, 2.96 g, 20.0 mmol, 4 eq.

Amount of potassium carbonate: 2.71 g, 19.9 mmol, 4 eq.

Volume of acetonitrile: 5.0 mL

Product yield: 0.99 g, 3.4 mmol, 68%

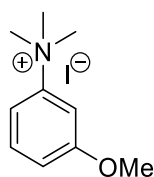
Melting point: 236-238 °C

IR: ν_{\max} 1605, 1512, 1261, 1188, 1026, 854 cm^{-1}

^1H NMR (400 MHz, DMSO- d_6): δ 3.64 (s, 9H, $\text{N}(\text{CH}_3)_3$), δ 3.83 (s, 3H, OCH_3), δ 7.12 (m, 2H, ArH), δ 7.93 (m, 2H, ArH)

^{13}C NMR (101 MHz, DMSO- d_6): δ 56.00, 56.67, 114.67, 121.98, 140.08, 159.53

Synthesis of 3-methoxy-N,N,N-trimethylanilinium iodide, 182a



Amount of 3-methoxy-*N,N*-dimethylaniline: 3.02 g, 20.0 mmol, 1 eq.

Amount of methyl iodide: 3.74 mL, 8.53 g, 60.1 mmol, 3 eq.

Volume of acetonitrile: 10.0 mL

Product yield: 4.55 g, 15.5 mmol, 78%

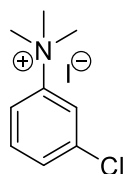
Melting point: 184-185 °C

IR: ν_{max} 3003, 1610, 1469, 1255, 1126, 1026, 904, 840 cm^{-1}

¹H NMR (400 MHz, DMSO-*d*₆): δ 3.67 (s, 9H, N(CH₃)₃), δ 3.88 (s, 3H, OCH₃), δ 7.17 (m, 1H, ArH), δ 7.49-7.59 (m, 3H, ArH)

¹³C NMR (101 MHz, DMSO-*d*₆): δ 56.26, 56.45, 107.17, 112.22, 115.35, 130.90, 148.30, 159.96

Synthesis of 3-chloro-N,N,N-trimethylanilinium iodide, 183a



3-chloroaniline (2.55 g, 20.0 mmol, 1 eq.) was dissolved in acetonitrile to a concentration of 2 M in a sealed 50 mL round bottom flask equipped with a stirrer bar and potassium carbonate (11.1 g, 80.4 mmol, 4 eq.) was added. Methyl iodide (5.0 mL, 11.4 g, 80.0 mmol, 4 eq.) was added dropwise *via* syringe to the stirred solution. The reaction mixture was stirred at 50 °C for 16 h. Upon cooling, the solid was collected *via* vacuum filtration. The white solid was then stirred in ethanol and 50 °C for 20 min, the resulting suspension was then filtered *via* vacuum filtration. Ethanol was removed

from the filtrate *via* rotary evaporation and then dried on a high vacuum line to yield 3-chloro-*N,N,N*-trimethylanilinium iodide as a white solid (1.95 g, 6.5 mmol, 33%).

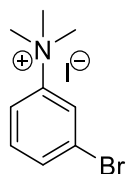
Melting point: 199-201 °C

IR: ν_{\max} 3004, 1591, 1481, 1178, 1097, 1082, 947, 866, 792 cm^{-1}

^1H NMR (400 MHz, DMSO- d_6): δ 3.63 (s, 9H, N(CH₃)₃), δ 7.69 (m, 2H, ArH), δ 7.97 (m, 1H, ArH), δ 8.17 (m, 1H, ArH)

^{13}C NMR (101 MHz, DMSO- d_6): δ 56.46, 119.60, 121.24, 130.24, 131.62, 134.23, 148.18

*Synthesis of 3-bromo-*N,N,N*-trimethylanilinium iodide, 184a*



Prepared according to *General Procedure B*.

Amount of 3-bromo-*N,N*-dimethylaniline: 4.10 g, 20.5 mmol, 1 eq.

Amount of methyl iodide: 3.8 mL, 8.73 g, 61.5 mmol, 3 eq.

Volume of acetonitrile: 10.0 mL

Product yield: 6.59 g, 19.3 mmol, 94%

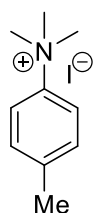
Melting point: 197-200 °C

IR: ν_{\max} 3003, 2922, 2361, 1584, 1449, 1422, 1180, 1078, 995, 947, 856, 792 cm^{-1}

^1H NMR (400 MHz, DMSO- d_6): δ 3.66 (s, 9H, N(CH₃)₃), δ 7.63 (m, 1H, ArH), δ 7.83 (m, 1H, ArH), δ 8.04 (m, 1H, ArH), δ 8.23 (m, 1H, ArH)

^{13}C NMR (101 MHz, DMSO- d_6): δ 56.46, 119.93, 122.54, 123.82, 131.82, 133.17, 148.21

Synthesis of N,N,N,4-tetramethylanilinium iodide, 185a



N,N,4-trimethylaniline (1.35, 10.0 mmol, 1 eq.) was dissolved in dichloromethane to a concentration of 1 M in a 25 mL round bottom flask equipped with a stirrer bar. Methyl iodide (3 eq.) was added dropwise to the stirred solution. The reaction mixture was stirred at room temperature for 16 h and a white precipitate formed. The precipitate was collected *via* vacuum filtration, and washed with diethyl ether (3 x 10 mL). The solid residue was then dried under high vacuum to give a white powder (2.13 g, 7.69 mmol, 77%).

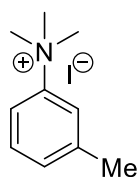
Melting point: 219-221 °C

IR: ν_{\max} 3009, 1512, 1394, 1122, 1018, 947, 813 cm^{-1}

^1H NMR (400 MHz, DMSO- d_6): δ 2.39 (s, 3H, Ar-CH₃), δ 3.62 (s, 9H, N(CH₃)₃), δ 7.45 (m, 2H, ArH), δ 7.78 (m, 2H, ArH)

^{13}C NMR (101 MHz, DMSO- d_6): δ 20.26, 56.40, 120.16, 130.23, 139.83, 144.93

Synthesis of N,N,N,3-tetramethylanilinium iodide, 186a



N,N,3-trimethylaniline (1.35, 10.0 mmol, 1 eq.) was dissolved in dichloromethane to a concentration of 1 M in a 25 mL round bottom flask equipped with a stirrer bar. Methyl iodide (3 eq.) was added dropwise to the stirred solution. The reaction mixture was stirred at room temperature for 16 h and a white precipitate formed. The precipitate was collected *via* vacuum filtration, and washed with diethyl ether (3 x 10 mL). The

solid residue was then dried under high vacuum to give a white powder (2.30 g, 8.29 mmol, 83%).

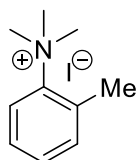
Melting point: 184-185 °C

IR: ν_{\max} 3009, 1614, 1487, 1296, 1182, 1095, 948, 896, 783 cm^{-1}

^1H NMR (400 MHz, DMSO- d_6): δ 2.44 (s, 3H, Ar-CH₃), δ 3.64 (s, 9H, N(CH₃)₃), δ 7.42 (m, 1H, ArH), δ 7.53 (m, 1H, ArH), δ 7.79 (m, 1H, ArH), δ 7.89 (m, 1H, ArH)

^{13}C NMR (101 MHz, DMSO- d_6): δ 21.04, 56.36, 117.36, 120.82, 129.74, 130.53, 139.95, 147.22

Synthesis of N,N,N,2-tetramethylanilinium iodide, 187a



Prepared according to *General Procedure B*.

Amount of *N,N,2*-trimethylaniline: 2.70 g, 20.0 mmol, 1 eq.

Amount of methyl iodide: 3.74 mL, 8.53 g, 60.1 mmol, 3 eq.

Volume of acetonitrile: 10.0 mL

Product yield: 4.58 g, 16.5 mmol, 83%

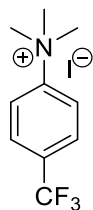
Melting point: Decomposes >187 °C

IR: ν_{\max} 1490, 1151, 1060, 948, 849, 756 cm^{-1}

^1H NMR (400 MHz, DMSO- d_6): δ 2.76 (s, 3H, Ar-CH₃), δ 3.73 (s, 9H, N(CH₃)₃), δ 7.43-7.55 (m, 3H, ArH), δ 7.88 (m, 1H, ArH)

^{13}C NMR (101 MHz, DMSO- d_6): δ 22.77, 56.47, 121.28, 127.85, 130.21, 130.30, 135.64, 146.16

Synthesis of 4-trifluoromethyl-N,N,N-trimethylanilinium iodide, 188a



Prepared according to *General Procedure B*.

Amount of 4-trifluoromethyl-*N,N*-dimethylaniline: 1.74 g, 9.21 mmol, 1 eq

Amount of methyl iodide: 1.71 mL, 3.89 g, 27.6 mmol, 3 eq

Volume of acetonitrile: 5.0 mL

Product yield: 2.25 g, 6.8 mmol, 74%

Melting point: 190-192 °C

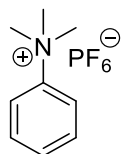
IR: ν_{\max} 3015, 2359, 1616, 1329, 1163, 1126, 1070, 1013, 926, 839 cm^{-1}

^1H NMR (400 MHz, DMSO- d_6): δ 3.68 (s, 9H, N-(CH₃)₃), δ 8.08 (m, 2H, ArH), δ 8.25 (m, 2H, ArH)

^{13}C NMR (101 MHz, DMSO- d_6): δ 56.44, 122.14, 126.09 (q, $J_{\text{CF}}^1 = 273.53$ Hz), 127.23 (m), 130.66 (q, $J_{\text{CF}}^2 = 30.08$ Hz), 150.09

^{19}F NMR (376 MHz, DMSO- d_6): δ -61.36

Synthesis of N,N,N-trimethylanilinium hexafluorophosphate, 147d



Prepared according to *General Procedure C*.

Amount of *N,N,N*-trimethylanilinium iodide: 0.25 g, 0.95 mmol, 1 eq

Amount of potassium hexafluorophosphate: 0.35 g, 1.9 mmol, 2 eq

Product yield: 0.20 g, 0.71 mmol, 73%

Melting point: 176-179 °C

IR: ν_{\max} 2990, 1786, 1263, 838 cm^{-1}

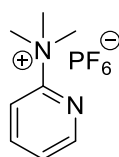
^1H NMR (400 MHz, DMSO- d_6): δ 3.61 (s, 9H, $\text{N}(\text{CH}_3)_3$), δ 7.65 (m, 3H, ArH), δ 7.96 (m, 2H, ArH)

^{13}C NMR (101 MHz, DMSO- d_6): δ 56.39, 120.32, 130.03, 131.10, 147.21

^{19}F NMR (376 MHz, DMSO- d_6): δ -70.15 (d, PF_6^- , $J = 710$ Hz)

^{31}P NMR (162 MHz, DMSO- d_6): δ -144.15 (hep, $J = 711$ Hz)

Synthesis of N,N,N -trimethylpyridinaminium hexafluorophosphate, 175d



Prepared according to *General Procedure C*.

Amount of N,N,N -trimethylpyridinaminium iodide: 0.14 g, 0.54 mmol, 1 eq.

Amount of potassium hexafluorophosphate: 0.20 g, 1.1 mmol, 2 eq.

Product yield: 0.09 g, 0.33 mmol, 62%

Melting point: 204-206 $^{\circ}\text{C}$

IR: ν_{\max} 3008, 1738, 1252, 1162 cm^{-1}

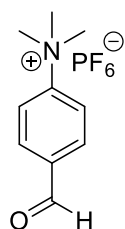
^1H NMR (400 MHz, DMSO- d_6): δ 3.59 (s, 9H, $\text{N}(\text{CH}_3)_3$), δ 7.73 (m, 1H, ArH), δ 8.09 (m, 1H, ArH), δ 8.25 (m, 1H, ArH), δ 8.68 (m, 1H, ArH)

^{13}C NMR (101 MHz, DMSO- d_6): δ 54.53, 115.11, 126.18, 141.03, 148.59, 156.67

^{19}F NMR (376 MHz, DMSO- d_6): δ -70.15 (d, PF_6^- , $J = 710$ Hz)

^{31}P NMR (162 MHz, DMSO- d_6): δ -144.17 (hep, $J = 711$ Hz)

Synthesis of 4-formyl-N,N,N-trimethylanilinium hexafluorophosphate, 176d



Prepared according to *General Procedure C*.

Amount of 4-formyl-*N,N,N*-trimethylanilinium iodide: 0.21 g, 0.73 mmol, 1 eq.

Amount of potassium hexafluorophosphate: 0.28 g, 1.5 mmol, 1.5 eq.

Product yield: 0.16 g, 0.51 mmol, 70%

Melting point: 184-186 °C

IR: ν_{\max} 941, 1180, 1217, 1492, 1605, 1703 cm^{-1}

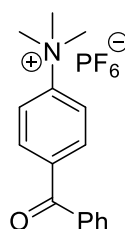
^1H NMR (400 MHz, DMSO- d_6): δ 3.65 (s, 9H, N(CH₃)₃), δ 8.16 (d, 2H, ArH, J = 9.1 Hz), δ 8.22 (d, 2H, ArH, J = 9.1 Hz), δ 10.12 (s, 1H, CHO)

^{13}C NMR (101 MHz, DMSO- d_6): δ 56.43, 121.64, 130.86, 136.80, 151.01, 192.02

^{19}F NMR (376 MHz, DMSO- d_6): δ -70.15 (d, PF₆⁻, J = 710 Hz)

^{31}P NMR (162 MHz, DMSO- d_6): δ -146.34 (hep, J = 709 Hz)

Synthesis of 4-benzoyl-N,N,N-trimethylanilinium hexafluorophosphate, 177d



Prepared according to *General Procedure C*.

Amount of 4-benzoyl-*N,N,N*-trimethylanilinium iodide: 95.5 mg, 0.26 mmol, 1 eq.

Amount of potassium hexafluorophosphate: 95.7 mg, 0.52 mmol, 2 eq.

Product yield: 67.1 mg, 0.17 mmol, 67%

Melting point: 238-240 °C

IR: ν_{\max} 2998, 1783, 1675, 1302, 832 cm^{-1}

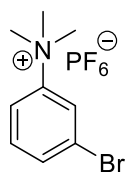
^1H NMR (400 MHz, DMSO- d_6): δ 3.68 (s, 9H, N(CH₃)₃), δ 7.61 (m, 2H, ArH), δ 7.76 (m, 3H, ArH), δ 7.96 (m, 2H, ArH), δ 8.16 (m, 2H ArH)

^{13}C NMR (101 MHz, DMSO- d_6): δ 56.44, 120.99, 128.79, 129.74, 130.86, 133.41, 136.21, 138.56, 149.59, 194.42

^{19}F NMR (376 MHz, DMSO- d_6): δ -70.16 (d, PF₆⁻, J = 711 Hz)

^{31}P NMR (162 MHz, DMSO- d_6): δ -144.16 (hep, J = 711 Hz)

Synthesis of 4-benzoyl-N,N,N-trimethylanilinium hexafluorophosphate, 184d



Prepared according to *General Procedure C*.

Amount of 3-bromo-N,N,N-trimethylanilinium iodide: 684.1 mg, 2.00 mmol, 1 eq.

Amount of potassium hexafluorophosphate: 73.6 g, 4.00 mmol, 2 eq.

Product yield: 64.9 mg, 0.17 mmol, 95%

Melting point: 172-174 °C

IR: ν_{\max} 2359, 1587, 1468, 1435, 1082, 949, 829, 785, 681 cm^{-1}

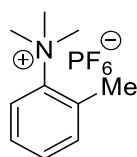
^1H NMR (400 MHz, DMSO- d_6): δ 3.63 (s, 9H, N(CH₃)₃), δ 7.61 (m, 1H, ArH), δ 7.82 (m, 1H, ArH), δ 8.01 (m, 1H, ArH), δ 8.26 (m, 1H, ArH)

^{13}C NMR (101 MHz, DMSO- d_6): δ 56.46, 119.93, 122.54, 123.82, 131.82, 133.17, 148.21

^{19}F NMR (376 MHz, DMSO- d_6): δ -70.15 (d, PF₆⁻, J = 711 Hz)

^{31}P NMR (162 MHz, DMSO- d_6): δ -144.19 (hep, J = 711 Hz)

Synthesis of N,N,N,2-tetramethylanilinium hexafluorophosphate, 187d



Prepared according to *General Procedure C*.

Amount of *N,N,N,2*-tetramethylaniliniumiodide: 0.33 g, 1.19 mmol, 1 eq.

Amount of ammonium hexafluorophosphate: 0.39 g, 2.38 mmol, 2 eq.

Product yield: 52.7 mg, 0.18 mmol, 15%

Melting point: Decomposes >190 °C

IR: ν_{\max} 1492, 1062, 943, 871 cm^{-1}

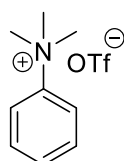
^1H NMR (400 MHz, DMSO- d_6): δ 2.73 (s, 3H, Ar-CH₃), δ 3.67 (s, 9H, N(CH₃)₃), δ 7.49 (m, 3H, ArH), δ 7.85 (d, 1H, J = 7.3 Hz)

^{13}C NMR (101 MHz, DMSO- d_6): δ 22.53, 56.52, 121.08, 127.82, 130.21, 130.36, 135.67, 145.22

^{19}F NMR (376 MHz, DMSO- d_6): δ -70.15 (d, PF₆⁻, J = 710 Hz)

^{31}P NMR (162 MHz, DMSO- d_6): δ -144.15 (hep, J = 710 Hz)

Synthesis of N,N,N-trimethylanilinium triflate, 174e



Prepared according to *General Procedure D*.

Amount of *N,N*-dimethylaniline: 2.42 g, 20.0 mmol, 1 eq.

Amount of methyl triflate: 3.30 mL, 4.94 g, 30.0 mmol, 1.5 eq.

Volume of dichloromethane: 20.0 mL

Product yield: 4.12 g, 14.4 mmol, 72%

Melting point: 82-84 °C

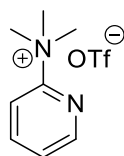
IR: ν_{\max} 3554, 3503, 2359, 1641, 1499, 1254, 1223, 1169, 1153, 1024, 951, 847, 756, 689, 624 cm^{-1}

^1H NMR (400 MHz, DMSO- d_6): δ 3.61 (s, 3H, N(CH₃)₃), δ 7.56-7.68 (m, 3H, Ar-H), δ 7.97 (m, 2H, ArH)

^{13}C NMR (101 MHz, DMSO- d_6): δ 56.38, 119.07, 120.27, 122.27, 130.03, 147.19

^{19}F NMR (376 MHz, DMSO- d_6): δ -77.75

Synthesis of N,N,N-trimethylpyridinium triflate, 175e



Prepared according to *General Procedure D*.

Amount of *N,N*-dimethylpyridinamine: 2.44 g, 20.0 mmol, 1 eq.

Amount of methyl triflate: 3.71 mL, 5.55 g, 33.8 mmol, 1.7 eq.

Volume of dichloromethane: 20.0 mL

Product yield: 5.04 g, 17.6 mmol, 88%

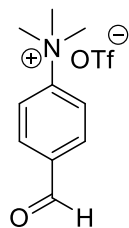
Melting point: 108-109 °C

IR: ν_{\max} 3003, 1473, 1259, 1226, 1147, 945 cm^{-1}

^1H NMR (400 MHz, DMSO- d_6): δ 3.59 (s, 9H, N(CH₃)₃), δ 7.73 (m, 1H, ArH), δ 8.09 (m, 1H, ArH), δ 8.24 (m, 1H, ArH), δ 8.68 (m, 1H, ArH)

^{13}C NMR (101 MHz, DMSO- d_6): δ 54.50, 115.08, 119.08, 126.17, 141.01, 148.58, 156.68

Synthesis of 4-formyl-N,N,N-trimethylanilinium triflate, 176e



Prepared according to *General Procedure D*.

Amount of 4-formyl-*N,N*-dimethylaniline: 1.49 g, 10.0 mmol, 1 eq.

Amount of methyl triflate: 1.7 mL, 2.54 g, 15.5 mmol, 1.5 eq.

Volume of dichloromethane: 10.0 mL

Product yield: 2.13 g, 6.8 mmol, 68%

Melting point: 107-119 °C

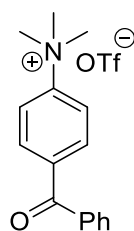
IR: ν_{max} 1259, 1147, 1026 cm^{-1}

^1H NMR (400 MHz, DMSO- d_6): δ 3.66 (s, 9H, N(CH₃)₃), δ 8.17 (d, 2H, ArH, J = 9.1 Hz), δ 8.22 (d, 2H, ArH, J = 9.1 Hz), δ 10.12 (s, 1H, CHO)

^{13}C NMR (101 MHz, DMSO- d_6): δ 56.43, 119.06, 121.66, 130.84, 136.80, 151.03, 192.03

^{19}F NMR (376 MHz, DMSO- d_6): δ -77.75

Synthesis of 4-benzoyl-N,N,N-trimethylanilinium triflate, 177e



Prepared according to *General Procedure D*.

Amount of 4-benzoyl-*N,N*-dimethylaniline: 1.13 g, 5.0 mmol, 1 eq.

Amount of methyl triflate: 0.85 mL, 1.27 g, 7.75 mmol, 1.55 eq.

Volume of dichloromethane: 5 mL

Product yield: 1.57 g, 3.0 mmol, 59%

Melting point: 128-130 °C

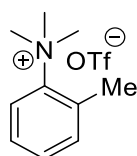
IR: ν_{\max} 1259, 1226, 1139, 1033 cm^{-1}

^1H NMR (400 MHz, DMSO- d_6): δ 3.68 (s, 9H, $\text{N}(\text{CH}_3)_3$), δ 7.62 (m, 2H, ArH), δ 7.76 (m, 3H, ArH), δ 7.96 (m, 2H, ArH), δ 8.17 (m, 2H, ArH)

^{13}C NMR (101 MHz, DMSO- d_6): δ 56.44, 119.08, 120.99, 128.77, 129.74, 130.86, 133.40, 136.12, 138.54, 149.60, 194.42

^{19}F NMR (376 MHz, DMSO- d_6): δ -77.74

Synthesis of N,N,N,2-tetramethylanilinium triflate, 187e



2-methylaniline (2.14 g, 20 mmol, 1 eq.) dissolved in dichloromethane (10 mL) and potassium carbonate (11.0 g, 80.0 mmol, 4 eq.) were added to a 50 mL round bottom flask equipped with a stirrer bar. Methyl triflate (9.0 mL, 13.5 g, 80.0, 4 eq.) was added dropwise to the stirred solution. The reaction mixture was stirred at room temperature for 18 h. The suspension was separated *via* vacuum filtration. Diethyl ether (20 mL) was added to the filtrate causing a precipitate to form. The solid was collected *via* vacuum filtration and washed with diethyl ether (3 x 10 mL) and dried under vacuum to give a white crystalline solid (1.62 g, 5.4 mmol, 27%).

Melting point: 88-90 °C

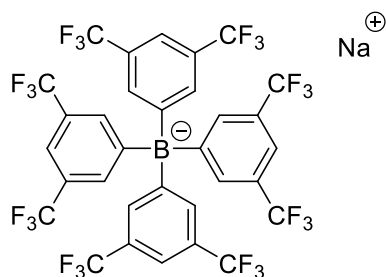
IR: ν_{\max} 2361, 1254, 1234, 1167, 1034, 762, 637, 559 cm^{-1}

^1H NMR (400 MHz, DMSO- d_6): δ 2.73 (s, 3H, Ar- CH_3), δ 3.67 (s, 9H, $\text{N}(\text{CH}_3)_3$), δ 7.49 (m, 3H, ArH), δ 7.85 (m, 1H, ArH)

¹³C NMR (101 MHz, DMSO-d₆): δ 22.52, 56.52, 119.06, 121.08, 122.26, 127.81, 130.18, 130.34, 135.65

¹⁹F NMR (376 MHz, DMSO-d₆): δ -77.75

Synthesis of sodium tetrakis(3,5-bis(trifluoromethyl)phenyl)borate (NaBAr^F)¹⁸¹



Magnesium turnings (5.00 g, 206 mmol, 12.6 eq.) were added to a flame dried 3-neck round bottom flask (250 mL) and ground under vacuum with a stir bar for 12 h. Iodine (0.500 g, 3.94 mmol) was added under argon, the system was then returned to vacuum and heated with a heat gun. Upon formation of iodine vapour, the mixture was allowed to cool to room temperature. Dry diethyl ether (25 mL) was added and the mixture was stirred vigorously under argon for 25 min giving a colourless liquid. 1,3-bis(trifluoromethyl)-5-bromobenzene (14 mL, 81 mmol, 5 eq.) in dry diethyl ether (25 mL) was added dropwise *via* a dropping funnel over the course of 65 min, resulting in a dark brown reaction mixture. The contents of the flask were stirred under argon at room temperature for a further 4 h. Boron trifluoride diethyl etherate (2 mL, 16.3 mmol, 1 eq.) in dry diethyl ether (12 mL) was added to the resulting Grignard reagent over the course of 1 h, once the addition was complete, the reaction mixture was refluxed under argon for 16 h. The reaction was then cooled to room temperature and transferred *via* cannula into an air-exposed aqueous sodium carbonate solution (1.5 M, 250 mL). The resulting suspension was stirred at room temperature for 1 h. The brown solid was collected *via* vacuum filtration, then extracted with diethyl ether (3 x 40 mL). The organic extracts were dried over sodium sulfate and the solvent was removed *via* rotary evaporation, giving the crude NaBAr^F salt as a brown oil.

The crude oil was dissolved in a 1:1 mixture of tetrahydrofuran and dichloromethane (15 mL), the solution was placed in a freezer for 48 h and a pale brown solid was

filtered. A second recrystallization of this solid from tetrahydrofuran and dichloromethane (15 mL) was performed yielding an off-white solid. The solid was dried under vacuum at 80 °C for 50 h to give NaBAr^F as a white solid (8.375 g, 9.45 mmol, 58%)

Melting point: Decomposed 330 °C

IR: ν_{\max} 2360, 1628, 1356, 1281, 1167, 1063, 931, 887, 837 710, 681, 670 cm⁻¹

¹H NMR (400 MHz, DMSO-d₆): δ 7.63 (s, 8H, ArH), δ 7.69 (s, 4H, ArH)

¹³C NMR (101 MHz, DMSO-d₆): δ 117.59 (m), 123.95 (q, $J_{\text{CF}}^1 = 273$ Hz), 128.60 (q, $J_{\text{CF}}^2 = 32$ Hz), 134.00, 160.90 (q, $J_{\text{CB}}^1 = 50.5$ Hz)

¹⁹F NMR (376 MHz, DMSO-d₆): δ -61.75

¹¹B NMR (128 MHz, DMSO-d₆): δ -6.83

Synthesis of N,N,N-trimethylanilinium tetrakis(3,5-bis-(trifluoromethyl)phenyl)borate, 174f



Prepared according to *General Procedure E*.

Amount of *N,N,N*-trimethylanilinium iodide: 0.263 g, 1.00 mmol, 1 eq.

Amount of tetrakis(3,5-bis(trifluoromethyl)phenyl) borate: 0.886 g, 1 mmol, 1 eq.

Product yield: 0.849 g, 0.85 mmol, 85%

Melting point: 150-152 °C

IR: ν_{\max} 1610, 1491, 1334, 1277, 1161, 1112 cm⁻¹

¹H NMR (400 MHz, DMSO-d₆): δ 3.61 (s, 9H, N(CH₃)₃), δ 7.63 (m, 11H, ArH anilinium and ArH BArF), δ 7.73 (s, 4H, ArH BArF), δ 7.97 (m, 2H, ArH anilinium)

¹³C NMR (101 MHz, DMSO-d₆): δ 56.34, 117.45, 120.33, 123.93 (q, J_{CF}¹ = 274 Hz), 128.43 (J_{CF}² = 31 Hz), 129.94, 134.00, 147.21, 160.93 (q, J_{CB}¹ = 51 Hz)

¹⁹F NMR (376 MHz, DMSO-d₆): δ -61.60

¹¹B NMR (128 MHz, DMSO-d₆): δ -6.83

Synthesis of N,N,N-trimethylpyridinium tetrakis(3,5-bis(trifluoromethyl)phenyl) borate, 175f



Prepared according to *General Procedure E*.

Amount of *N,N,N*-pyridinium iodide: 0.264 g, 1.00 mmol, 1 eq.

Amount of tetrakis(3,5-bis(trifluoromethyl)phenyl) borate: 0.886 g, 1 mmol, 1 eq.

Product yield: 0.911 g, 0.91 mmol, 91%

Melting point: 156-158 °C

IR: ν_{max} 1610, 1490, 1472, 1437, 1354, 1275, 1161, 1112 cm⁻¹

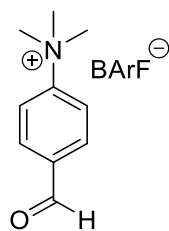
¹H NMR (400 MHz, DMSO-d₆): δ 3.59 (s, 9H, N(CH₃)₃), δ 7.62 (m, 8H, ArH BArF), δ 7.70 (m, 5H, ArH BArF and ArH anilinium), δ 8.09 (m, 1H, ArH anilinium), δ 8.25 (m, 1H, ArH anilinium), δ 8.68 (m, 1H, ArH anilinium)

¹³C NMR (101 MHz, DMSO-d₆): δ 54.47, 115.14, 117.50 (m), 119.87, 123.94 (q, J_{CF}¹ = 274 Hz), 126.12, 128.43 (q, J_{CF}² = 32 Hz), 134.00, 140.98, 148.53, 160.92 (q, J_{CB}¹ = 50.5 Hz)

¹⁹F NMR (376 MHz, DMSO-d₆): δ -61.91

¹¹B NMR (128 MHz, DMSO-d₆): δ -6.82

Synthesis of 4-formyl-N,N,N-trimethylanilinium tetrakis(3,5-bis(trifluoromethyl)phenyl) borate, 176f



Prepared according to *General Procedure E*.

Amount of 4-formyl-*N,N,N*-trimethylanilinium iodide: 0.146 g, 0.50 mmol, 1 eq.

Amount of tetrakis(3,5-bis(trifluoromethyl)phenyl) borate: 0.443 g, 0.50 mmol, 1 eq.

Product yield: 0.246 g, 0.24 mmol, 48%

Melting point: 159-161 °C

IR: ν_{\max} 1709, 1607, 1491, 1470, 1354, 1279, 1109, 1088 cm^{-1}

^1H NMR (400 MHz, DMSO- d_6): δ 3.66 (s, 9H, $\text{N}(\text{CH}_3)_3$), δ 7.63 (s, 8H, ArH BArF), δ 7.74 (s, 4H, ArH BArF), δ 8.19 (m, 4H, ArH anilinium), δ 10.12 (s, 1H, formyl)

^{13}C NMR (101 MHz, DMSO- d_6): δ 56.38, 117.56 (m), 121.68, 123.94 (q, $J_{\text{CF}^1} = 273$ Hz), 128.37 (q, $J_{\text{CF}^2} = 33$ Hz), 130.82, 134.00, 136.77, 151.01, 160.91 (q, $J_{\text{CB}^1} = 50$ Hz), 192.00

^{19}F NMR (376 MHz, DMSO- d_6): δ -61.90

^{11}B NMR (128 MHz, DMSO- d_6): δ -6.83

Synthesis of 4-benzoyl-N,N,N-trimethylanilinium tetrakis(3,5-bis(trifluoromethyl)phenyl) borate, 177f



Prepared according to *General Procedure E*.

Amount of 4-benzoyl-*N,N,N*-trimethylanilinium iodide: 0.367 g, 1 mmol, 1 eq.

Amount of tetrakis(3,5-bis(trifluoromethyl)phenyl) borate: 0.886 g, 1.00 mmol, 1 eq.

Product yield: 0.871 g, 0.79 mmol, 79%

Melting point: 151-152 °C

IR: ν_{\max} 1665, 1607, 1354, 1273, 1113 cm^{-1}

^1H NMR (400 MHz, DMSO- d_6): δ 3.68 (s, 9H, N(CH₃)₃), δ 7.62 (m, 10H, ArH BArF and ArH anilinium), δ 7.75 (m, 7H, ArH BArF and ArH anilinium), δ 7.96 (m, 2H, ArH anilinium), δ 8.17 (m, 2H, ArH anilinium)

^{13}C NMR (101 MHz, DMSO- d_6): δ 56.40, 117.60 (m), 121.05, 123.96 (q, $J_{\text{CF}}^1 = 273$ Hz), 128.31 (m), 128.74, 129.74, 130.85, 133.37, 134.02, 136.09, 138.52, 149.59, 160.88 (q, $J_{\text{CB}}^1 = 50$ Hz), 194.41

^{19}F NMR (376 MHz, DMSO- d_6): δ -61.61

^{11}B NMR (128 MHz, DMSO- d_6): δ -6.83

*Synthesis of 4-benzoyl-*N,N,N*-trimethylanilinium tetrakis(3,5-bis(trifluoromethyl)phenyl) borate, 184f*



Prepared according to *General Procedure E*.

Amount of 3-bromo-*N,N,N*-trimethylanilinium iodide: 0.367 g, 1.00 mmol, 1 eq.

Amount of tetrakis(3,5-bis(trifluoromethyl)phenyl) borate: 0.886 g, 1.00 mmol, 1 eq.

Product yield: 0.871 g, 0.79 mmol, 79%

Melting point: 154-155 °C

IR: ν_{\max} 2359, 1611, 1354, 1273, 1111, 885, 839, 710, 669 cm^{-1}

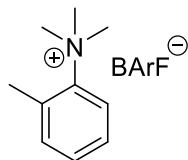
¹H NMR (400 MHz, DMSO-d₆): δ 3.62 (s, 9H, N(CH₃)₃), δ 7.57-7.65 (m, 9H, ArH BArF and ArH anilinium), δ 7.81 (m, 4H, ArH BArF), δ 8.01 (m, 2H, ArH anilinium), δ 8.27 (m, 2H, ArH anilinium)

¹³C NMR (101 MHz, DMSO-d₆): δ 56.44, 117.53 (m), 119.81, 122.48, 123.85, 123.96 (q, J_{CF}¹ = 271 Hz), 128.42 (q, J_{CF}² = 30 Hz), 131.73, 133.09, 133.99, 148.21, 160.91 (q, J_{CB}¹ = 50 Hz)

¹⁹F NMR (376 MHz, DMSO-d₆): δ -61.84

¹¹B NMR (128 MHz, DMSO-d₆): δ -6.83

Synthesis of N,N,N,2-tetramethylanilinium tetrakis(3,5-bis-(trifluoromethyl)phenyl) borate, 187f



Prepared according to *General Procedure E*.

Amount of *N,N,N,2*-tetramethylanilinium iodide: 0.277 g, 1.00 mmol, 1 eq.

Amount of tetrakis(3,5-bis(trifluoromethyl)phenyl) borate: 0.886 g, 1 mmol, 1 eq.

Product yield: 0.902 g, 0.89 mmol, 89%

Melting point: 132-134 °C

IR: ν_{max} 1610, 1490, 1355, 1276, 1136, 1112, 1088 cm⁻¹

¹H NMR (400 MHz, DMSO-d₆): δ 2.73 (s, 3H, Ar-CH₃), δ 3.68 (s, 9H, N(CH₃)₃), δ 7.47 (m, 3H, ArH anilinium), δ 7.62 (s, 8H, ArH BArF), δ 7.70 (s, 4H, ArH BArF), δ 7.85 (m, 1H, ArH anilinium)

¹³C NMR (101 MHz, DMSO-d₆): δ 22.48, 56.46, 117.44 (m), 121.11, 123.84 (q, J_{CF}¹ = 274 Hz), 127.99, 128.44 (q, J_{CF}² = 31 Hz), 130.09, 130.32, 134.00, 135.57, 145.19, 160.94 (q, J_{CB}¹ = 50.5 Hz)

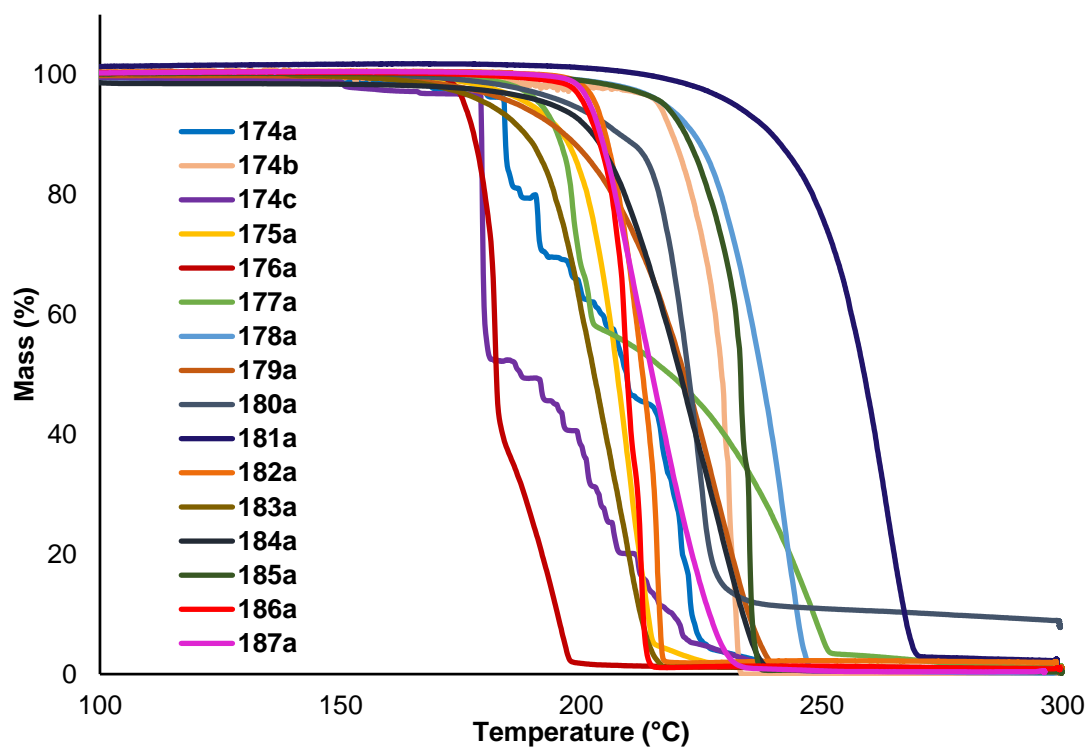
¹⁹F NMR (376 MHz, DMSO-d₆): δ -61.91

^{11}B NMR (128 MHz, DMSO- d_6): δ -6.83

Investigating Solid State Stability of N,N,N-trimethylanilinium Salts Using Thermal Gravimetric Analysis

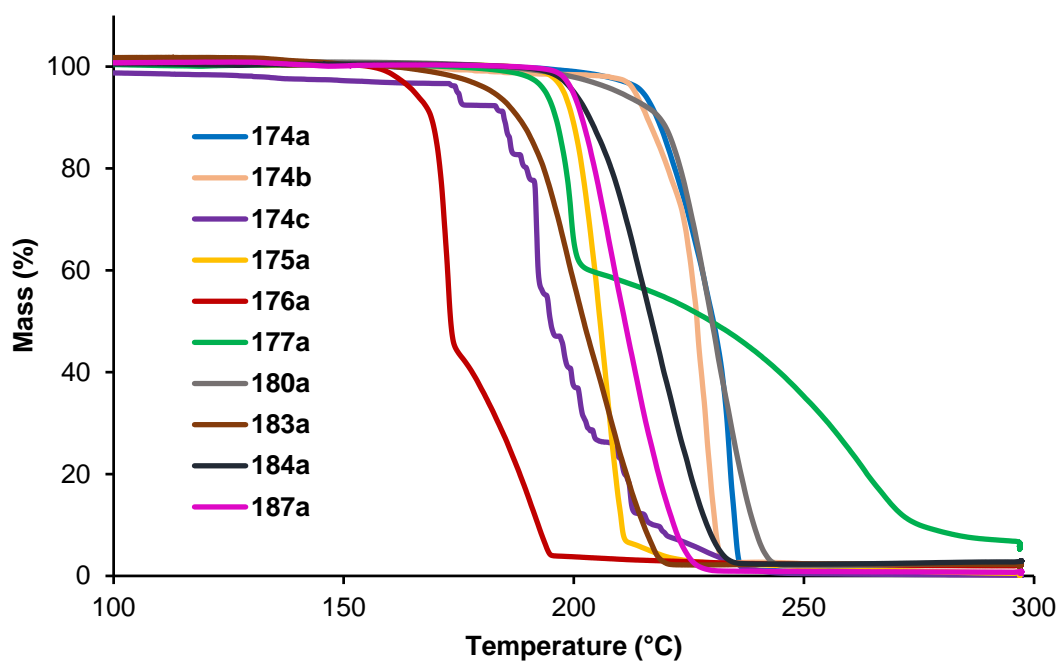
The relevant aryl-substituted *N,N,N*-trimethylanilinium salt (approx. 10 mg) was loaded into the TGA instrument. The sample was heated from 40-140 °C at a rate of 5 °Cmin⁻¹ then 140-300 °C at a rate of 10 °Cmin⁻¹ under an atmosphere of either argon or air.

TGA analysis under argon was performed for salts **174a-c**, and **175a-187a**. The TGA traces of temperature vs percentage of original mass are reported below. A table is also given which reports the onset and peak degradation temperatures for each of the *N,N,N*-trimethylanilinium salts tested. The peak temperature is the temperature at which mass-loss is the fastest. To calculate the onset temperature, a straight line fitted to the steepest part of each TGA trace and extrapolated back to find the temperature at which mass = 100%.



| Anilinium salt | Onset (°C) | Peak (°C) |
|-----------------------|-------------------|------------------|
| 174a | 184 | 184 |
| 174b | 221 | 229 |
| 174c | 179 | 179 |
| 175a | 199 | 210 |
| 176a | 180 | 182 |
| 177a | 195 | 198 |
| 178a | 227 | 242 |
| 179a | 204 | 229 |
| 180a | 214 | 225 |
| 181a | 248 | 261 |
| 182a | 205 | 212 |
| 183a | 191 | 210 |
| 184a | 204 | 227 |
| 185a | 230 | 235 |
| 186a | 209 | 223 |
| 187a | 187 | 203 |

TGA analysis under air was performed for salts **174a-c**, **175a**, **176a**, **177a**, **180a**, **183a**, **184a**, and **187a**. The TGA traces of temperature vs percentage of original mass are reported below. A table is also given which reports the onset and peak degradation temperatures for each of the *N,N,N*-trimethylanilinium salts tested.



| Anilinium salt | Onset (°C) | Peak (°C) |
|----------------|------------|-----------|
| 174a | 216 | 234 |
| 174b | 212 | 229 |
| 174c | 174 | 192 |
| 175a | 199 | 207 |
| 176a | 169,188 | 173 |
| 177a | 196, 237 | 199 |
| 180a | 220 | 231 |
| 183a | 188 | 198 |
| 184a | 203 | 217 |
| 187a | 200 | 208 |

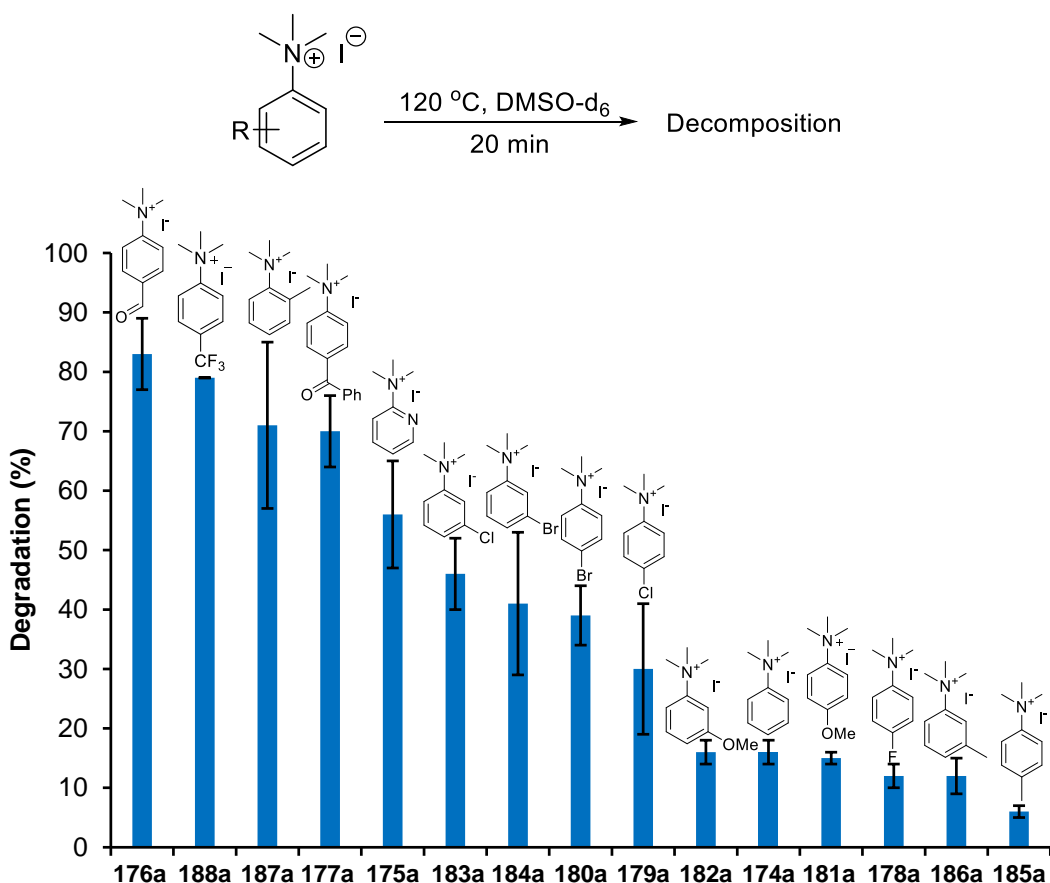
Investigating Solution Phase stability of N,N,N -trimethylanilinium Iodide Salts Using ^1H NMR Analysis

The relevant aryl substituted N,N,N -trimethylanilinium iodide (36.0 μmol) and 1,2,4,5-tetramethylbenzene internal standard (4.8 mg, 36.0 μmol) were dissolved in $\text{DMSO-}d_6$ (0.6 mL, 0.714 g), to give an anilinium concentration of 0.06 M and internal

standard concentration of 0.01 M. The solution was transferred to an NMR tube and a ^1H NMR spectrum was recorded as $t = 0$ min. The solution was heated to $120\text{ }^\circ\text{C}$ for 20 min in the NMR tube (using a DrySyn NMR heating block), then submerged in an ice bath to halt the degradation. A ^1H NMR spectrum was recorded of the degradation mixture and taken as $t = 20$ min.

The concentration of *N,N,N*-trimethylanilinium salt in solution was calculated *via* comparison of the integration of its selected aromatic protons against the aromatic protons of the internal standard appearing at δ 6.90 ppm. Each experiment was carried out in triplicate.

The thermal stability of *N,N,N*-trimethylanilinium iodide salts **174a-188a** in $\text{DMSO-}d_6$ was investigated in this manner. The degradation data is reported below as the percentage of anilinium salt degraded after heating at $120\text{ }^\circ\text{C}$ for 20 min.



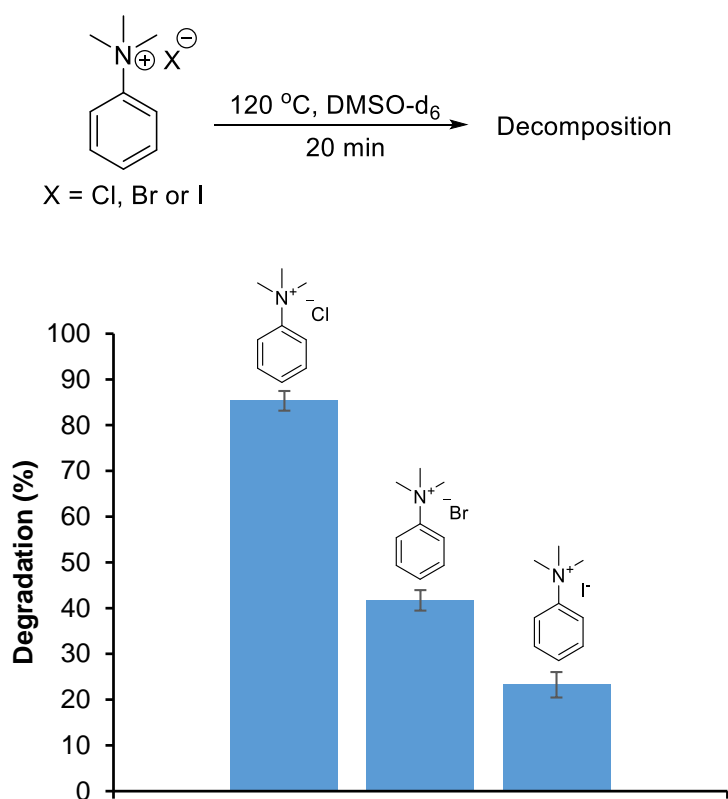
| Anilinium iodide | Degradation (%) | | | Average Degradation (%) | Error (%) |
|---------------------|-----------------|-------|-------|-------------------------|--------------|
| | Run 1 | Run 2 | Run 3 | | |
| 174a | 14.33 | 14.16 | 17.99 | 15.50 | 2.16 |
| 175a | 50.14 | 66.03 | 52.07 | 56.08 | 8.67 |
| 176a | 78.30 | 80.55 | 89.30 | 82.78 | 5.81 |
| 177a | 69.11 | 64.60 | 77.09 | 70.27 | 6.33 |
| 178a | 10.22 | 14.27 | 11.74 | 12.08 | 2.04 |
| 179a | 31.46 | 40.75 | 18.85 | 30.36 | 10.99 |
| 180a | 30.16 | 42.58 | 44.29 | 39.01 | 5.45 |
| 181a | 13.87 | 14.90 | 16.56 | 15.11 | 1.42 |
| 182a | 17.77 | 17.24 | 13.84 | 16.28 | 2.14 |
| 183a | 44.37 | 52.55 | 41.45 | 46.12 | 5.75 |
| 184a | 47.13 | 25.63 | 50.13 | 40.96 | 11.92 |
| 185a | 6.64 | 6.01 | 5.00 | 5.88 | 0.83 |
| 186a | 8.68 | 12.85 | 13.92 | 11.81 | 2.77 |
| 187a | 59.76 | 66.59 | 87.43 | 71.26 | 14.41 |
| 188a | 78.75 | 79.12 | 79.05 | 78.97 | 0.17 |

Investigating Solution Phase stability of N,N,N-trimethylanilinium Halide Salts Using ¹H NMR Analysis

The relevant unsubstituted *N,N,N*-trimethylanilinium halide (36.0 μ mol) and 1,2,4,5-tetramethylbenzene internal standard (4.8 mg, 36.0 μ mol) were dissolved in DMSO- d_6 (0.6 mL, 0.714 g), to give an anilinium concentration of 0.06 M and internal standard concentration of 0.06 M. The solution was transferred to an NMR tube and a ¹H NMR spectrum was recorded as $t = 0$ min. The solution was heated to 120 °C for 20 min in the NMR tube, then submerged in an ice bath to halt the degradation. A ¹H NMR spectrum was recorded of the degradation mixture and taken as $t = 20$ min.

The concentration of the *N,N,N*-trimethylanilinium cation in solution was calculated *via* comparison of the integration of its *meta*-protons at $\delta \sim 8.0$ ppm against the aromatic protons of the internal standard appearing at δ 6.90 ppm. Each experiment was carried out in duplicate.

The thermal stability of *N,N,N*-trimethylanilinium chloride, bromide, and iodide salts **174a-174c** was in DMSO- d_6 was investigated in this manner. The degradation data is reported below as the percentage of anilinium salt degraded after heating at 120 °C for 20 min.



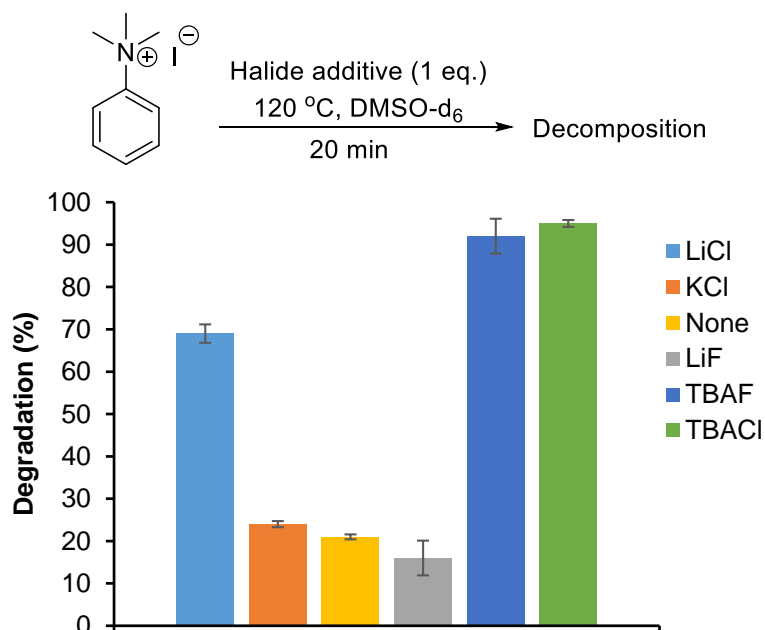
| Anilinium halide | Degradation (%) | | Average Degradation (%) | Error (%) |
|------------------|-----------------|-------|-------------------------|-----------|
| | Run 1 | Run 2 | | |
| 174a | 26.01 | 20.47 | 23.25 | 2.77 |
| 174b | 39.45 | 43.92 | 41.69 | 2.23 |
| 174c | 87.48 | 83.15 | 85.32 | 2.16 |

Investigating the Effect of Halide Additives on *N,N,N*-trimethylanilinium Iodide Stability Using ^1H NMR Analysis

N,N,N-trimethylanilinium iodide (9.5 mg, 36 μmol , 1 eq.), the relevant halide salt (36 μmol , 1 eq.), and 1,2,4,5-tetramethylbenzene internal standard (4.8 mg, 36 μmol) was dissolved in DMSO-d_6 (0.6 mL, 0.7140 g), to give an anilinium, additive, and internal standard concentration each of 0.06 M. The solution was transferred to an NMR tube and a ^1H NMR spectrum was recorded as $t = 0$ min. The solution was heated to 120 $^\circ\text{C}$ for 20 min in the NMR tube, then submerged in an ice bath to halt the degradation. A ^1H NMR spectrum was recorded of the degradation mixture and taken as $t = 20$ min.

The concentration of *N,N,N*-trimethylanilinium iodide in solution was calculated *via* comparison of the integration of its *meta*-protons at δ 8.0 ppm against the aromatic protons of the internal standard appearing at δ 6.90 ppm.

The thermal stability of *N,N,N*-trimethylanilinium DMSO-d_6 with lithium chloride, potassium chloride, tetrabutylammonium chloride, lithium fluoride, and tetrabutylammonium fluoride was investigated in this manner. The degradation data is reported below as the percentage of anilinium salt degraded after heating at 120 $^\circ\text{C}$ for 20 min.



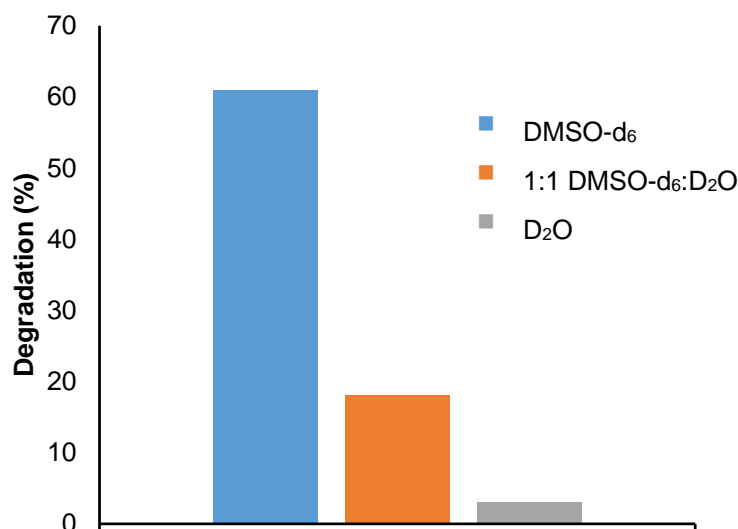
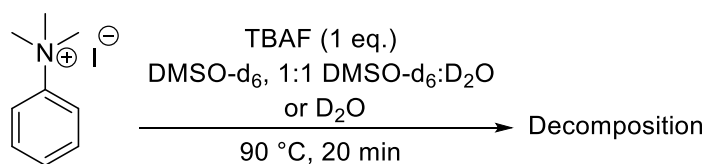
| Halide additive | Degradation (%) | | | Average Degradation (%) | Error (%) |
|-----------------|-----------------|-------|-------|-------------------------|-----------|
| | Run 1 | Run 2 | Run 3 | | |
| None | 20.81 | 21.15 | 22.21 | 21.38 | 0.60 |
| LiCl | 66.38 | 70.95 | 70.99 | 69.44 | 2.16 |
| KCl | 24.17 | 24.81 | 23.09 | 24.03 | 0.71 |
| TBACl | 93.76 | 95.36 | N/A | 94.56 | 0.80 |
| LiF | 11.63 | 19.84 | N/A | 15.73 | 4.10 |
| TBAF | 84.73 | 99.85 | N/A | 92.29 | 7.56 |

Investigating the Effect of Water on the Degradation of N,N,N-trimethylanilinium Iodide Using ¹H NMR Analysis

Stock solutions of maleic acid (7.0 mg, 36 μmol) in DMSO-d₆ (1.19 g, 1.0 mL), and maleic acid (4.2 mg, 36 μmol) in D₂O (1.11 g, 1 mL) were prepared.

To N,N,N-trimethylanilinium iodide (9.5 mg, 36 μmol) and tetrabutylammonium fluoride (10.0 mg, 36 μmol), either 0.6 mL DMSO-d₆ stock solution, 0.6 mL D₂O stock solution, or 0.3 mL of each stock solution, were added. The solution was transferred to an NMR tube and a ¹H NMR spectrum was recorded. The solution was heated to 90 °C for 20 min, then the NMR tube was placed in ice to halt the degradation. A ¹H NMR spectrum was recorded of the degradation mixture.

The concentration of the anilinium salt was calculated *via* the integration of its aromatic protons against the olefinic protons of the internal standard. The degradation data is reported below as a percentage of anilinium salt degraded after heating at 90 °C for 20 min.

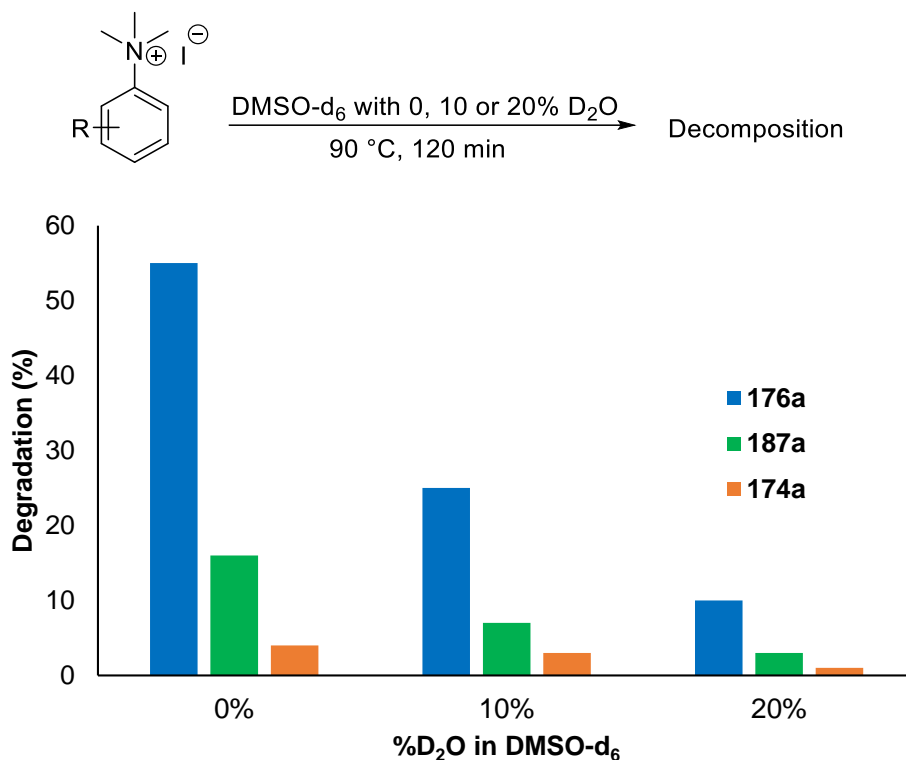


| Solvent | Degradation (%) |
|---|-----------------|
| DMSO-d ₆ | 61 |
| 1:1 DMSO-d ₆ :D ₂ O | 18 |
| D ₂ O | 3 |

The relevant aryl substituted *N,N,N*-trimethylanilinium iodide (60.0 μmol) and maleic acid internal standard (4.2 mg, 36.0 μmol) were dissolved in DMSO-d₆, 1:9 D₂O:DMSO-d₆, or 1:4 D₂O:DMSO-d₆ (0.6 mL), to give an anilinium concentration of 0.1 M and internal standard concentration of 0.06 M. The solution was transferred to an NMR tube and a ¹H NMR spectrum was recorded as t = 0 min. The solution was heated to 90 °C for 120 min in the NMR tube, then submerged in an ice bath to halt the degradation. A ¹H NMR spectrum was recorded of the degradation mixture and taken as t = 120 min.

The concentration of *N,N,N*-trimethylanilinium salt in solution was calculated *via* comparison of the integration of its selected aromatic protons against the aromatic protons of the internal standard appearing at δ 6.27 ppm.

The thermal stability of *N,N,N*-trimethylanilinium iodide salts **174a**, **176a** and **187a** in DMSO- d_6 with 0, 10 and 20% D_2O was investigated in this manner. The degradation data is reported below as the percentage of anilinium salt degraded after heating at 90 °C for 120 min.



| Anilinium iodide | Degradation (%) | | |
|------------------|---------------------|----------------------|----------------------|
| | 0% D ₂ O | 10% D ₂ O | 20% D ₂ O |
| 174a | 4 | 3 | 1 |
| 176a | 55 | 25 | 7 |
| 187a | 16 | 7 | 3 |

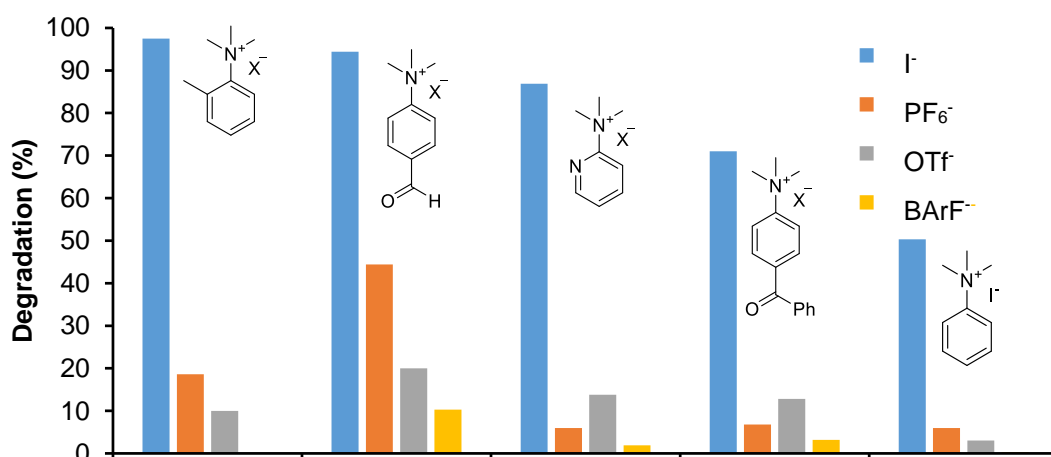
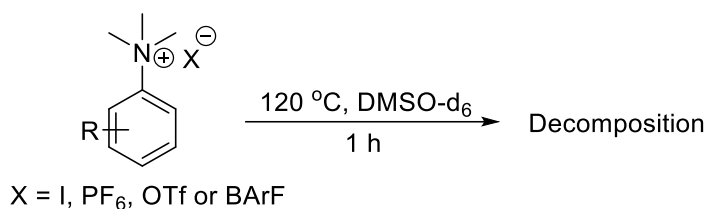
*Investigating the Effect of Non-nucleophilic Counter Ions *N,N,N*-trimethylanilinium Salt Stability Using ¹H NMR Analysis*

The relevant *N,N,N*-trimethylanilinium salt (36.0 μmol) and 1,2,4,5-tetramethylbenzene internal standard (4.8 mg, 36.0 μmol) were dissolved in DMSO- d_6 (0.6 mL, 0.714 g), to give an anilinium concentration of 0.06 M and internal standard concentration of 0.06 M. The solution was transferred to an NMR tube and a

^1H NMR spectrum was recorded as $t = 0$ min. The solution was heated to $120\text{ }^\circ\text{C}$ for 1 h in the NMR tube, then submerged in an ice bath to halt the degradation. A ^1H NMR spectrum was recorded of the degradation mixture and taken as $t = 1$ h.

The concentration of *N,N,N*-trimethylanilinium salt in solution was calculated *via* comparison of the integration of its selected aromatic protons against the aromatic protons of the internal standard appearing at δ 6.90 ppm.

The thermal stability of *N,N,N*-trimethylanilinium salts **174a,d,e,f**; **175a,d,e,f**; **176a,d,e,f**; **177a,d,e,f**; and **187a,d,e,f** in DMSO-d_6 was investigated in this manner. The degradation data is reported below as the percentage of anilinium salt degraded after heating at $120\text{ }^\circ\text{C}$ for 1 h.

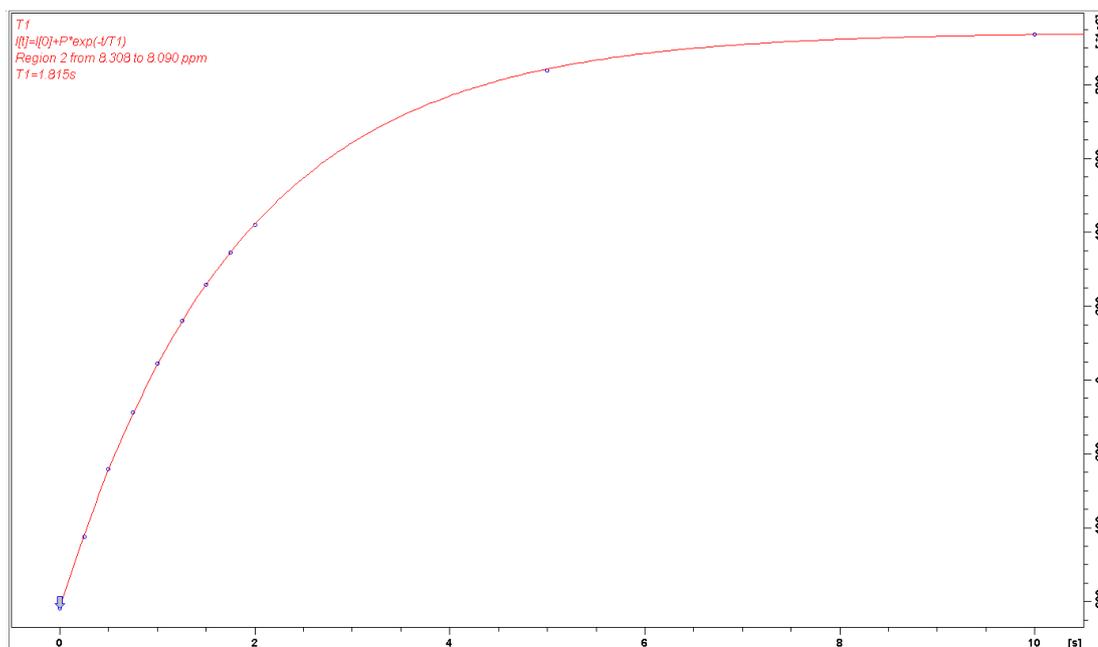


| Anilinium salt | Degradation (%) |
|----------------|-----------------|
| 174a | 97.5 |
| 175a | 94.4 |
| 176a | 86.9 |
| 177a | 71.0 |
| 187a | 50.3 |
| 174d | 18.6 |

| | |
|-------------|------|
| 175d | 44.4 |
| 176d | 5.95 |
| 177d | 6.80 |
| 187d | 5.96 |
| 174e | 10.0 |
| 175e | 20.0 |
| 176e | 13.8 |
| 177e | 12.8 |
| 187e | 3.03 |
| 174f | 0.0 |
| 175f | 10.3 |
| 176f | 1.9 |
| 177f | 3.2 |
| 187f | 0.3 |

Determination of T1 Relaxation Times for N,N,N-trimethylanilinium Iodides in DMSO-d₆

In order to gain reliable kinetic degradation data, it was necessary to calculate the T1 relaxation times for protons of interest on the *N,N,N*-trimethylanilinium salts investigated. A sample of 0.1 M of each *N,N,N*-trimethylanilinium iodide in DMSO-d₆ was prepared and subjected to a T1 inversion recovery (T1IR) sequence. The T1IR experiment uses a 180°- τ -90° pulse sequence which simultaneously inverts and measures peaks with a varied delay time (τ) to create a pseudo-2D NMR spectrum. Processing the spectrum on Bruker Topspin 4.0.7 allows the user to create a plot of τ vs area for each peak of interest, an exemplar plot is shown below.

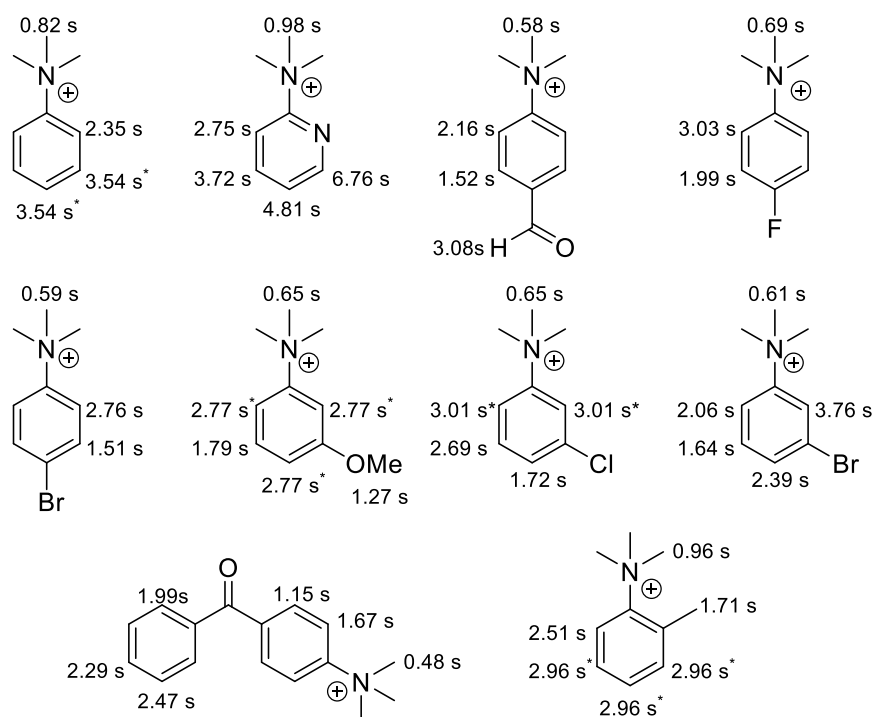


The following equation is fitted to the data where M_z is the magnetisation at $t = \tau$ s, and M_0 is the magnetisation at $t = 0$ s (maximum magnetisation).

$$M_z = M_0 \left(1 - e^{-\frac{\tau}{T_1}} \right)$$

Fitting the data to this equation is used to calculate T1, which corresponds to the time when magnetisation reaches $1 - 1/e$ (~63%) of its maximum value. Kinetic experiments were carried out with a delay time (D1) of at least 5x the longest calculated T1 time on each substrate. This ensured full relaxation of each nucleus, giving accurate peak area integrations for quantitative interpretation of spectra.

The calculated T1 relaxation times are displayed next to the relevant proton environment for each of the *N,N,N*-trimethylanilinium iodides investigated below. Values denoted with an asterisk represent proton signals that were too close to be integrated separately; therefore, the value will represent that T1 of proton with the longest relaxation time.



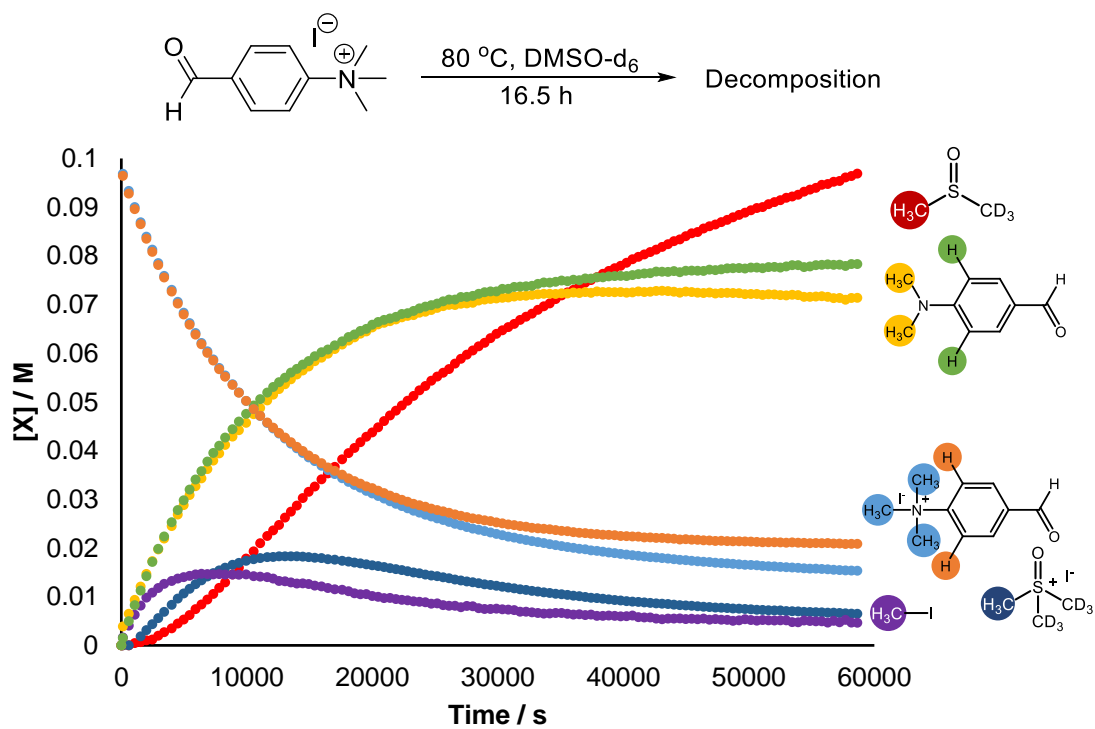
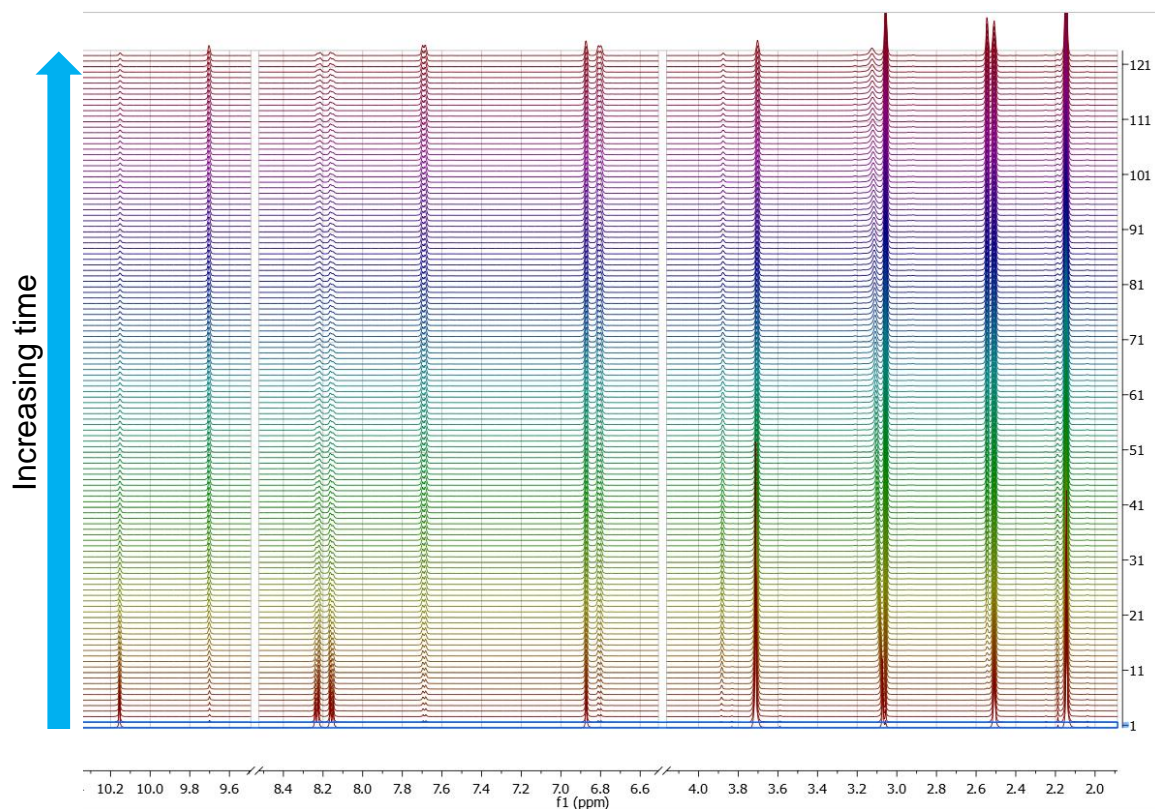
*Investigating Aryl Substitution Effect on the Degradation of *N,N,N*-trimethylanilinium Iodides in DMSO-*d*₆ Using ¹H NMR Spectroscopy*

The relevant aryl-substituted *N,N,N*-trimethylanilinium iodide (60.0 μmol) and 1,2,4,5-tetramethylbenzene internal standard (4.8 mg, 36 μmol) was dissolved in DMSO-*d*₆ (0.6 mL, 0.714 g), to give an anilinium concentration of 0.1 M, and an internal standard concentration of 0.06 M, then transferred to an NMR tube. A ¹H NMR spectrum (4 scans, 25 s relaxation time) was recorded every 5 min whilst the sample was heated to 80 °C in the NMR spectrometer probe.

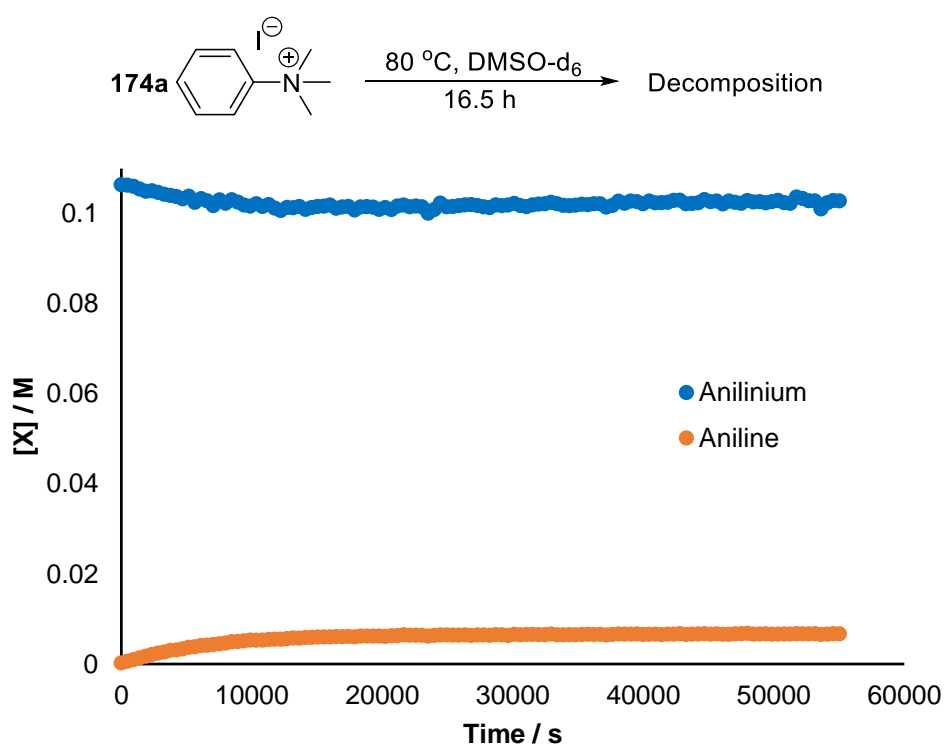
The concentration of the anilinium salt, aniline, methyl iodide, trimethylsulfoxonium-*d*₆ cation (TMSO-*d*₆), and dimethylsulfoxide-*d*₃ (DMSO-*d*₃) was calculated against the internal standard at each time point. The anilinium and aniline concentration was calculated from aromatic protons, N-methyl protons, and aryl-substituent protons where available.

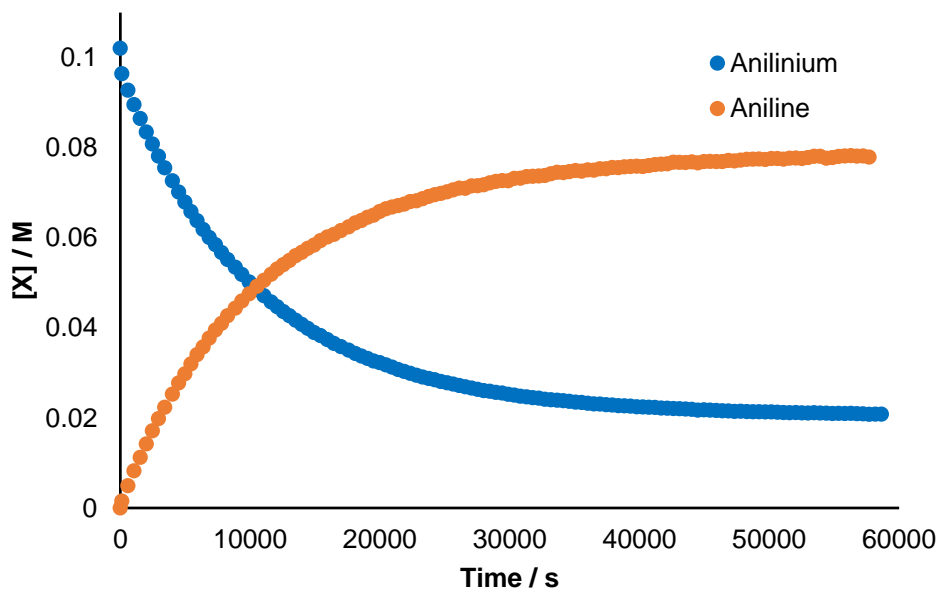
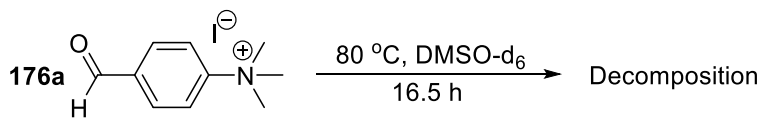
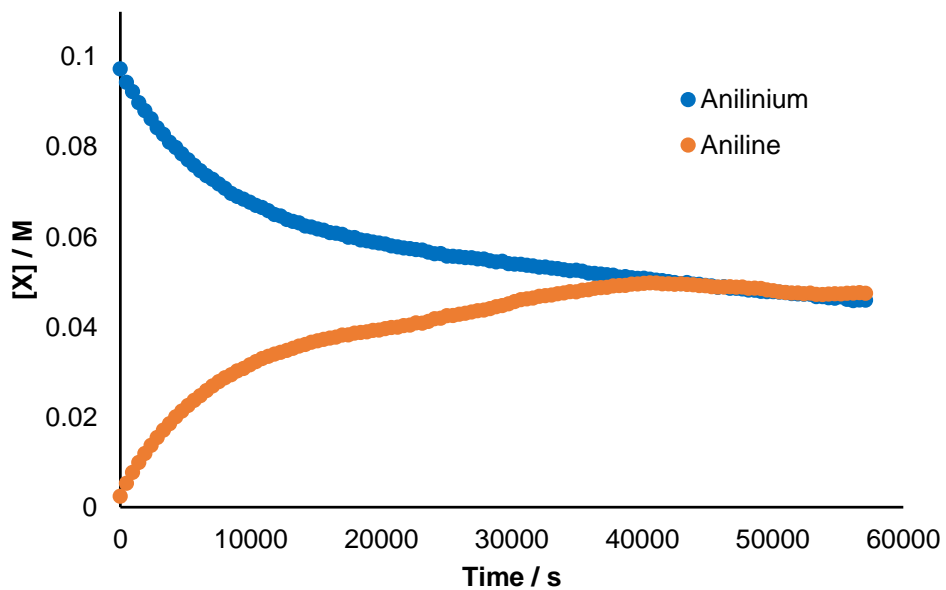
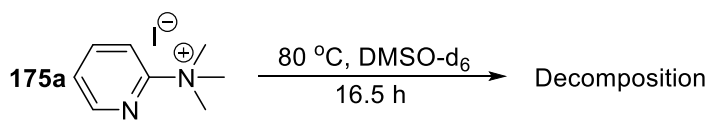
An exemplar stacked spectrum is shown below for the degradation of 3a, regions of the x-axis that do not contain any peaks have been omitted for clarity. Analysis of the stacked spectra, allows conversion of peak areas to species concentrations. A plot of

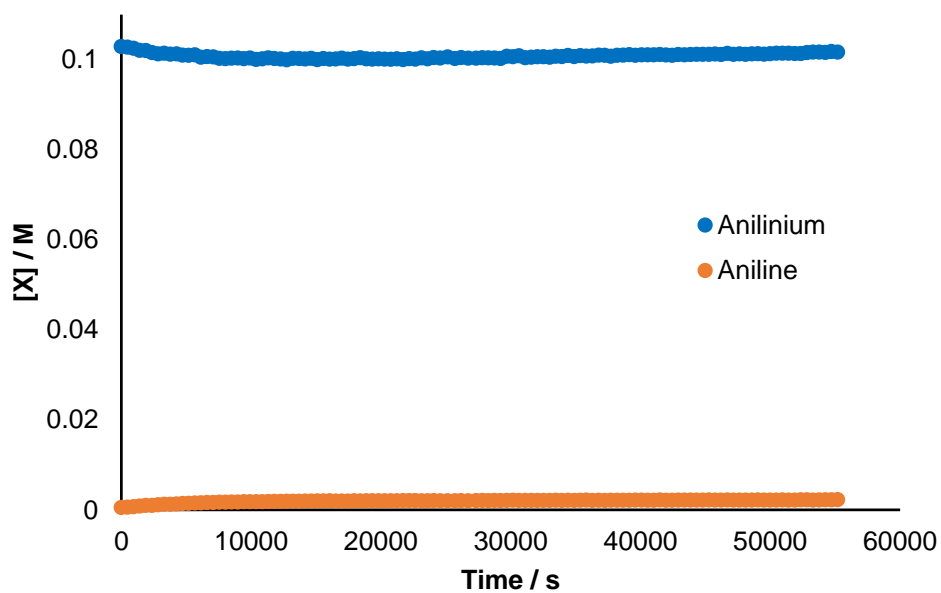
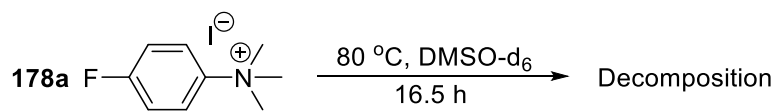
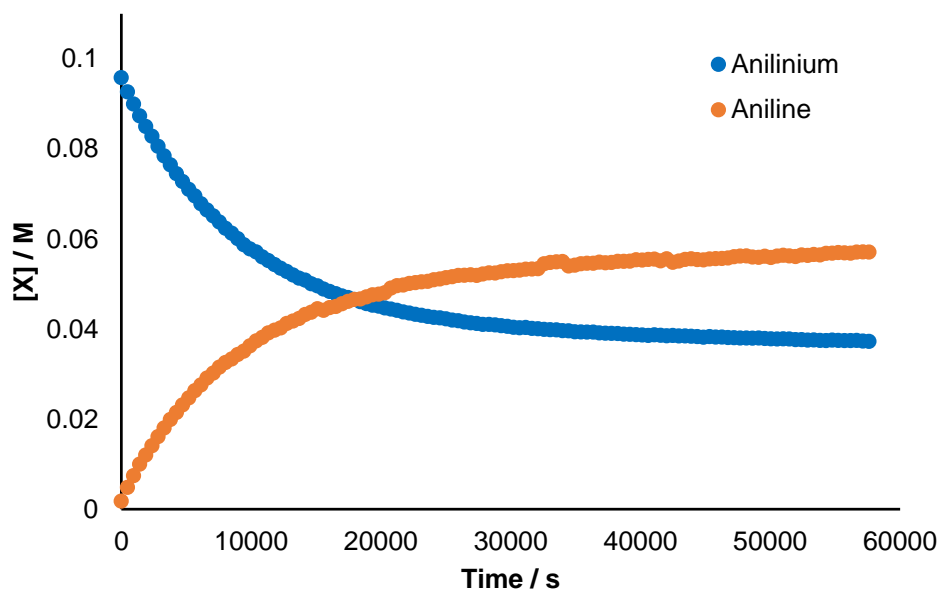
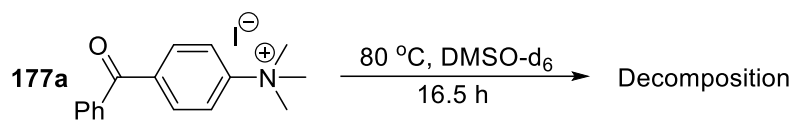
concentration vs time for **176a** is also shown below. Data points are colour coded to correspond to the proton environment from which the concentration was calculated.

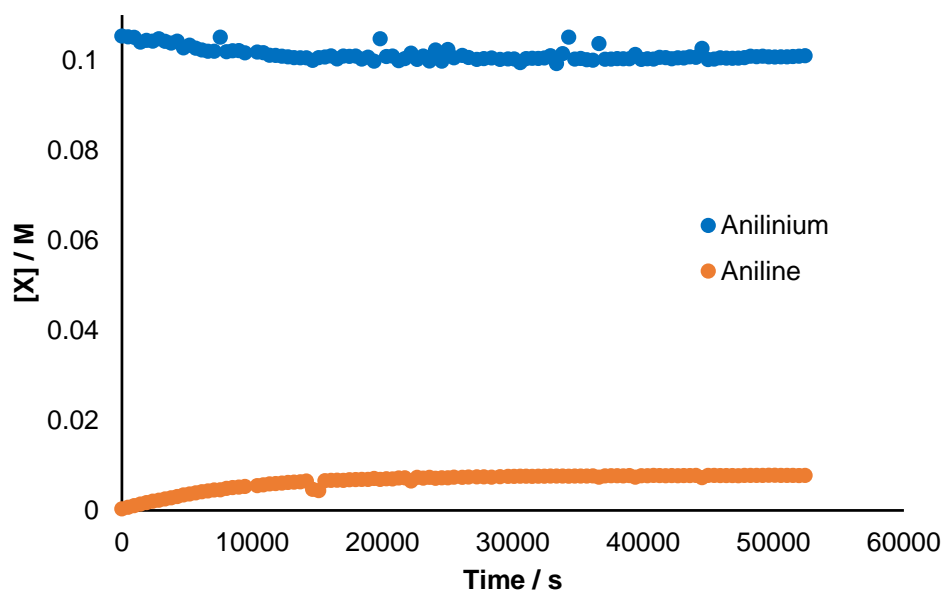
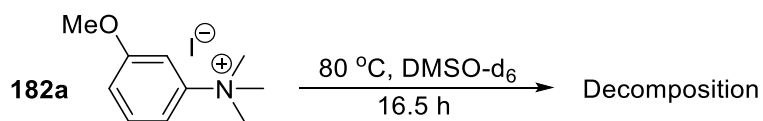
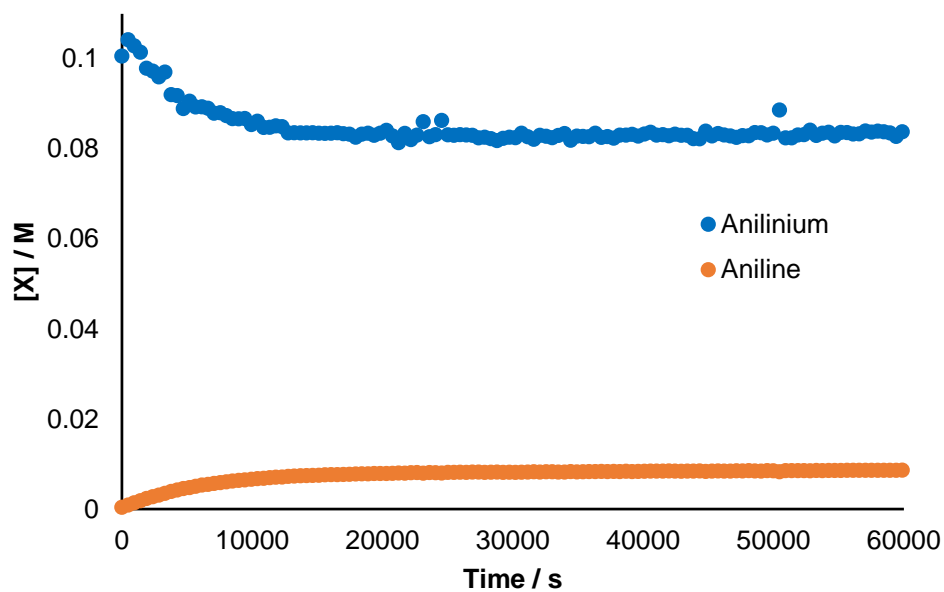
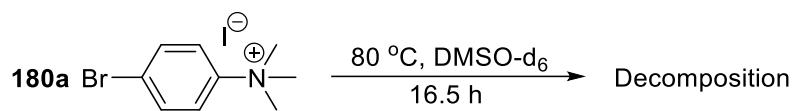


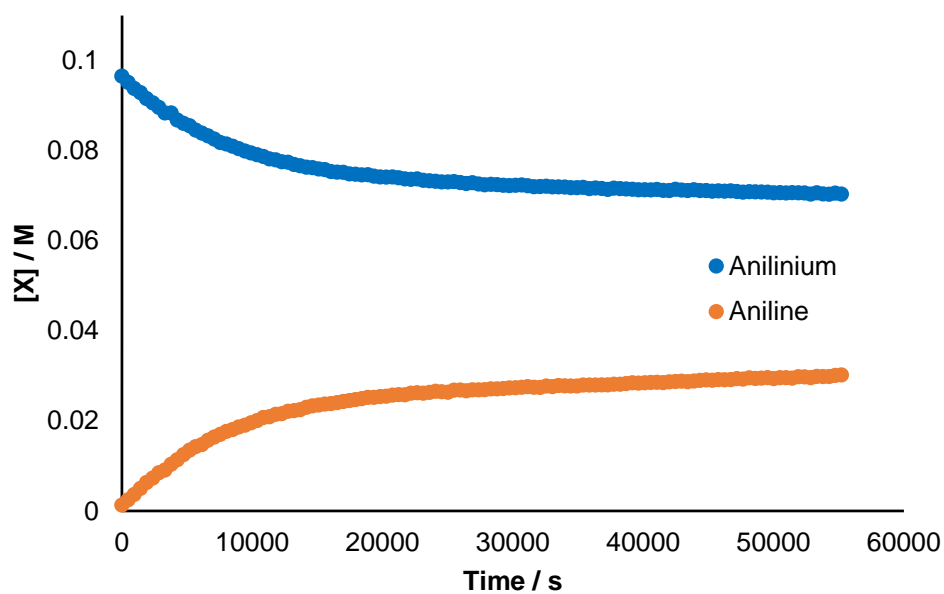
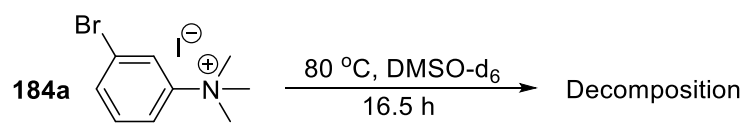
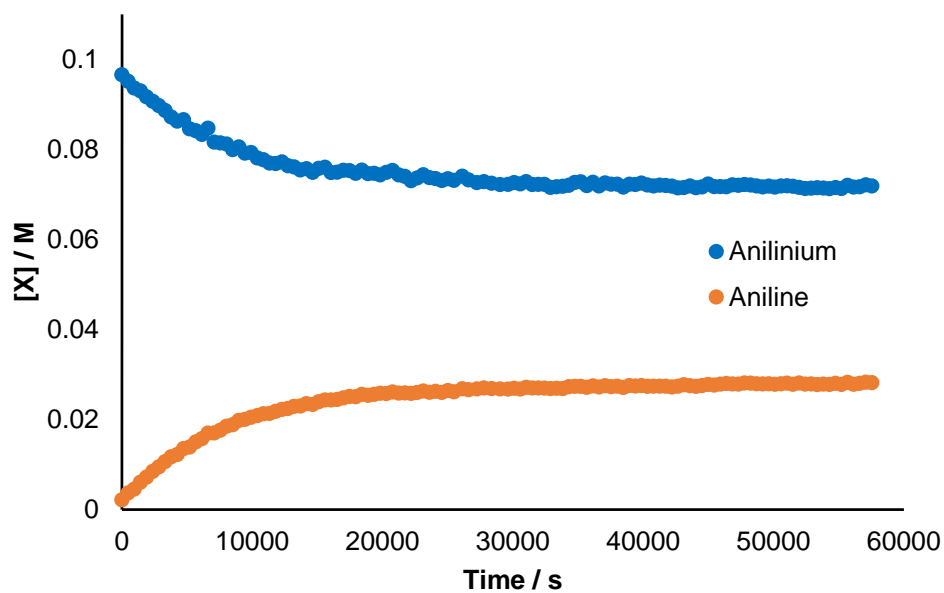
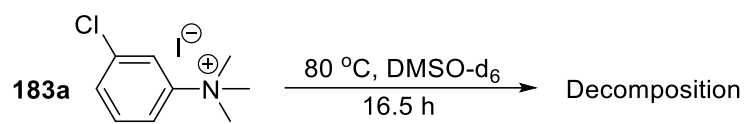
The degradation of a selection of *N,N,N*-trimethylanilinium iodides in DMSO- d_6 at 80 °C was monitored using this technique. Salts **174a-178a**, **180a**, **182a-184a**, **187a**, and **188a** were chosen to represent a range of anilinium degradation rates, as identified from the earlier single time point heating experiments. Below are the concentration *vs* time graphs constructed for each of the anilinium salts tested. Though the discrepancy between concentration calculated *via* integration of Ar-H *vs* N-(CH $_3$) $_3$ protons was observed in all cases, only the concentration of *N,N,N*-trimethylanilinium (blue) and *N,N*-dimethylaniline (orange) calculated *via* aromatic protons are shown in the following graphs for clarity.

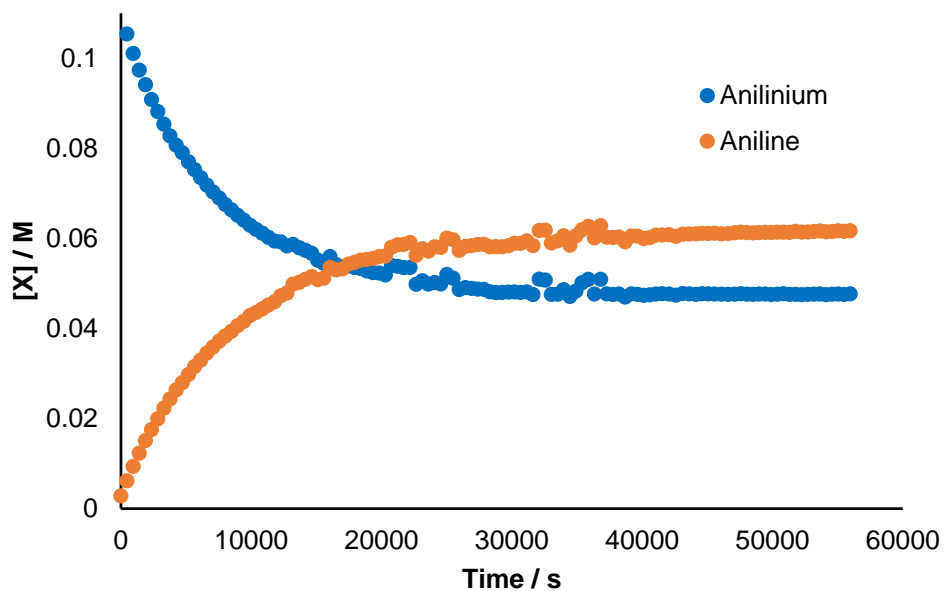
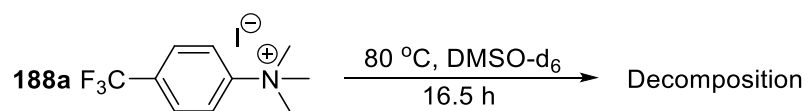
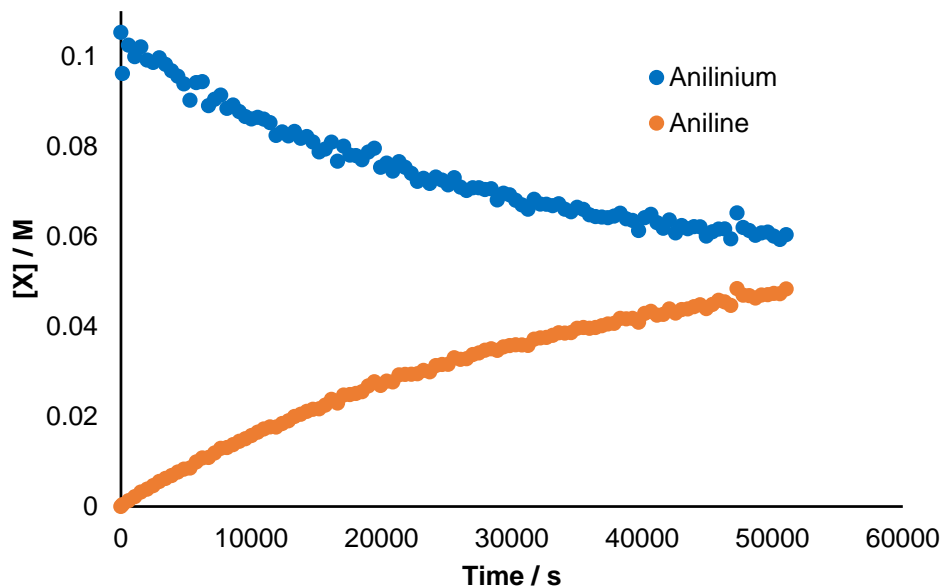
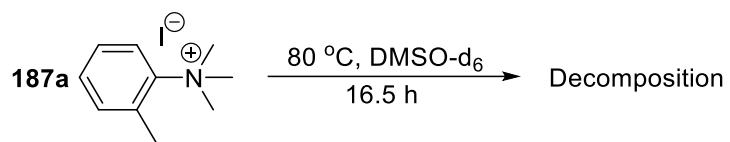




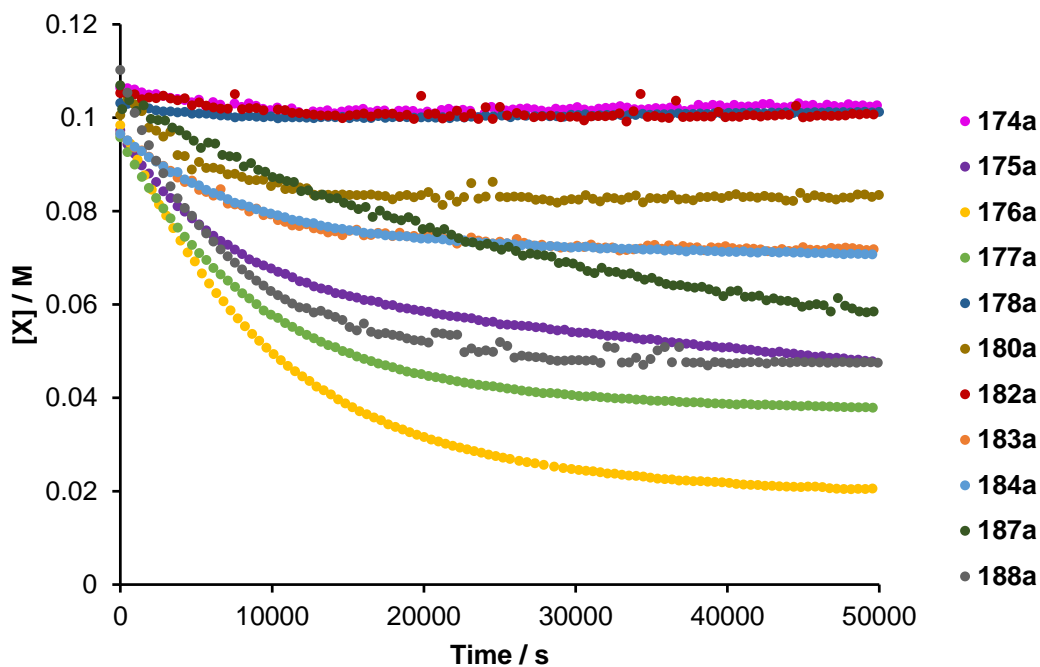




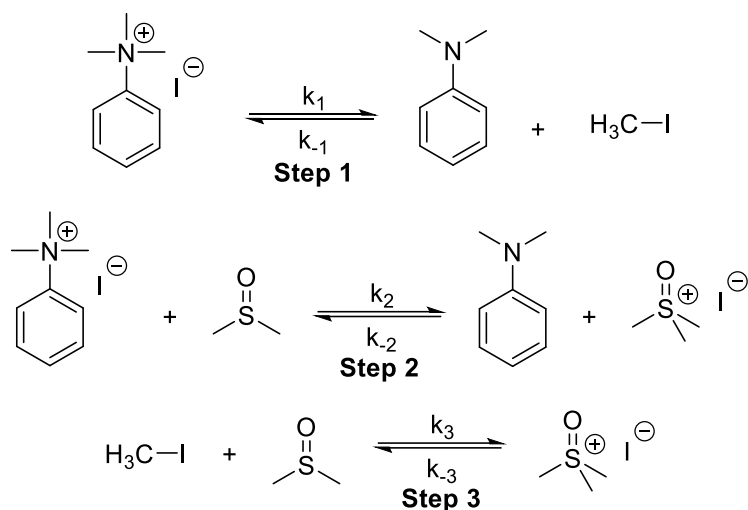




A graph compiling the anilinium degradation curves for each salt investigated is shown below.



According to the proposed degradation pathway, three separate reversible reactions were identified to occur in the degradation mixtures: iodide-led anilinium degradation, DMSO-led anilinium degradation, and reaction between methyl iodide and DMSO. The three reactions shown below have been assigned rate constants k_1 , k_{-1} , k_2 , k_{-2} , k_3 , and k_{-3} . Using COPASI v4.22 values for each rate constant in this reaction model were estimated. The modelling was programmed in such a way that priority would be given to correlating simulated data to the obtained anilinium concentration vs time curve. A summary of the rate constants also provided.

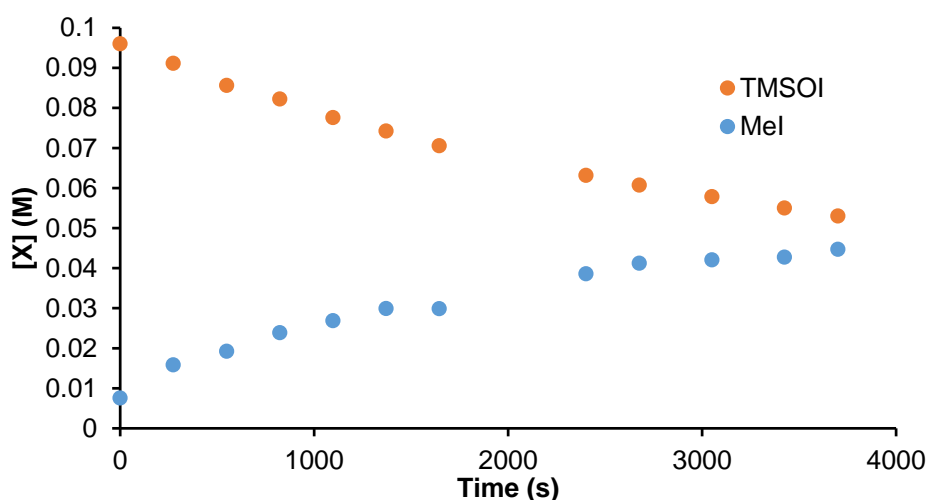


| Salt | k_1 (s ⁻¹) | k_{-1} (M ⁻¹ s ⁻¹) | k_2 (M ⁻¹ s ⁻¹) | k_{-2} (M ⁻¹ s ⁻¹) | k_3 (M ⁻¹ s ⁻¹) | k_{-3} (s ⁻¹) |
|-------------|--------------------------|---|--|---|--|-----------------------------|
| 174a | 1.11E-05 | 1.80E-95 | 1.60E-315 | 1.63E+07 | 1.81E-05 | 1.82E-04 |
| 175a | 4.47E-05 | 1.95E-03 | 3.74E-208 | 1.36E-172 | 1.94E-162 | 0.00E+00 |
| 176a | 7.95E-05 | 5.46E-04 | 1.71E-283 | 1.30E-13 | 5.53E-06 | 5.27E-05 |
| 177a | 6.41E-05 | 7.94E-276 | 6.96E-134 | 1.10E+08 | 2.95E-06 | 5.84E-23 |
| 178a | 9.45E-06 | 1.69E-02 | 2.85E-315 | 1.56E-02 | 1.79E-316 | 0.00E+00 |
| 180a | 1.85E-05 | 6.06E-03 | 1.58E-315 | 1.13E-306 | 6.34E-314 | 7.78E-04 |
| 182a | 4.46E-06 | 5.00E-259 | 1.82E-180 | 3.43E-02 | 1.66E-05 | 7.47E-212 |
| 183a | 2.53E-05 | 0.00E+00 | 4.74E-302 | 1.71E-02 | 7.70E-06 | 1.14E-04 |
| 184a | 3.09E-05 | 1.36E-145 | 4.75E-48 | 3.46E-02 | 6.39E-06 | 7.05E-05 |
| 187a | 1.89E-05 | 1.12E-85 | 9.96E-134 | 7.70E+11 | 1.59E-05 | 3.10E+11 |
| 188a | 8.08E-05 | 3.09E-81 | 1.23E-44 | 8.66E+09 | 4.40E-06 | 1.79E-04 |

Investigating the Thermal Degradation of Trimethylsulfoxonium Iodide in DMSO-d₆

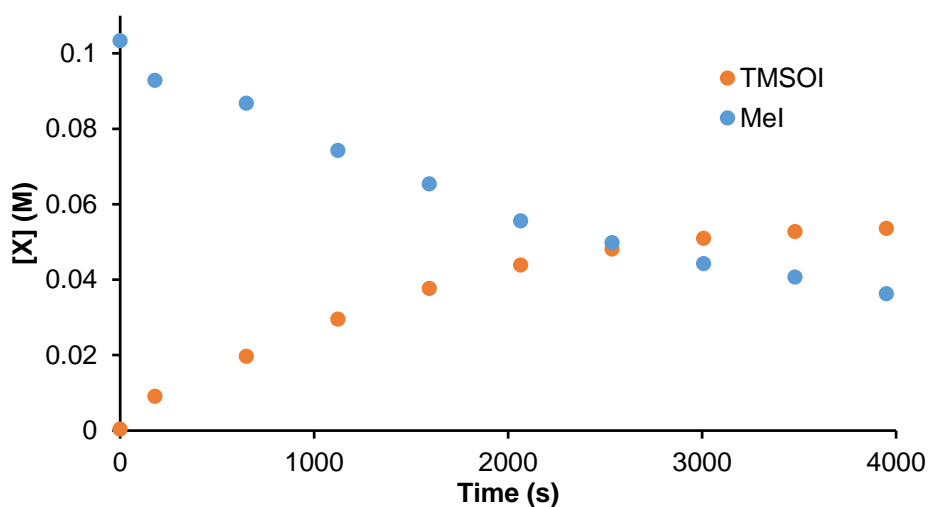
Trimethylsulfoxonium iodide (13.2 mg, 60 μmol) and 1,2,4,5-tetramethylbenzene internal standard (4.8 mg, 36 μmol) were dissolved in DMSO-d₆ (0.6 mL, 0.7140 g), to give trimethylsulfoxonium iodide concentration of 0.10 M, and an internal standard concentration of 0.06 M, then transferred to an NMR tube. A ¹H NMR spectrum (4 scans, 25 s relaxation time) was taken every 5 min whilst the sample was heated to 80 °C in the NMR spectrometer probe.

The concentration of the trimethylsulfoxonium salt and methyl iodide were calculated *via* their CH₃ protons at each time point against the internal standard. A graph showing the concentration of the trimethylsulfoxonium cation and methyl iodide *vs* time is given.



To investigate whether or not the degradation of trimethylsulfoxonium iodide was reversible, an analogous experiment was performed where methyl iodide was heated in DMSO- d_6 . For this reaction methyl iodide (8.79 mg, 62 μmol) and 1,2,4,5-tetramethylbenzene internal standard (4.8 mg, 36 μmol) were dissolved in DMSO- d_6 (0.6 mL, 0.7140 g), to give methyl iodide concentration of 0.10 M, and an internal standard concentration of 0.06 M, then transferred to an NMR tube. A ^1H NMR spectrum (4 scans, 25 s relaxation time) was taken every 5 min whilst the sample was heated to 80 $^\circ\text{C}$ in the NMR spectrometer probe.

The concentration of the trimethylsulfoxonium salt and methyl iodide were calculated *via* their CH_3 protons at each time point against the internal standard. A graph showing the concentration of the trimethylsulfoxonium cation and methyl iodide *vs* time is given.



Effect of Light Conditions on the degradation of N,N,N-trimethylanilinium Iodides in DMSO-d₆

The relevant *N,N,N*-trimethylanilinium iodide (60 μmol) and 1,2,4,5-tetramethylbenzene internal standard (4.8 mg, 36 μmol) was dissolved in DMSO-d₆ (0.6 mL, 0.714 g), to give an anilinium concentration of 0.1 M, and internal standard concentration of 0.06 M. The solution was transferred to an NMR tube and a ¹H NMR spectrum was recorded. The solution was heated to 80 °C in a water bath for 1 h either in darkness, exposed to ambient light, simulated sunlight (reptile lamp), or a UV lamp; then the NMR tube was placed in ice to halt the degradation. A ¹H NMR spectrum was recorded of the degradation mixture.

The concentration of the anilinium salt was calculated *via* the integration of its aromatic protons against those of the internal standard. Each experiment was performed in triplicate. **174a** and **176a** were investigated under these conditions, the degradation data are given below.

| Anilinium Iodide | Lighting Conditions | Degradation (%) | | | Average Degradation (%) | Error (%) |
|------------------|---------------------|-----------------|-------|-------|-------------------------|-----------|
| | | Run 1 | Run 2 | Run 3 | | |
| 174a | Darkness | 3.11 | 0.16 | 0.63 | 1.30 | 1.29 |
| 174a | Ambient | 2.17 | 1.69 | 1.34 | 1.73 | 0.34 |
| 174a | Sunlight | 1.39 | 2.39 | 0.74 | 1.51 | 1.51 |
| 174a | UV | 1.78 | 2.22 | 2.07 | 2.02 | 0.19 |
| 176a | Darkness | 22.03 | 19.84 | 19.90 | 20.59 | 1.02 |
| 176a | UV | 18.20 | 20.85 | 17.43 | 18.82 | 1.47 |

Investigating the Possibility of Trimethylamine Displacement from Iodide Counterion

To investigate the possibility that the iodide counter ion could displace the $-\text{NMe}_3^+$ moiety of *N,N,N*-trimethylanilinium salts to form trimethylamine and an aryl iodide, the formation of aryl iodide was probed in a degradation experiment.

176a (17.5 mg, 60.0 μmol) and 4-iodobenzaldehyde (1.4 mg, 6.0 μmol), and 1,2,4,5-tetramethylbenzene (4.8 mg, 36 μmol) were dissolved in DMSO-d_6 (0.6 mL, 0.714 g), to give an anilinium concentration of 0.1 M, a 4-iodobenzaldehyde concentration of 0.01 M, and internal standard concentration of 0.06 M. The solution was transferred to an NMR tube and a ^1H NMR spectrum was recorded as $t = 0$ min. The solution was heated to 120 $^\circ\text{C}$ for 20 min in the NMR tube, then submerged in an ice bath to halt the degradation. A ^1H NMR spectrum was recorded of the degradation mixture and taken as $t = 20$ min.

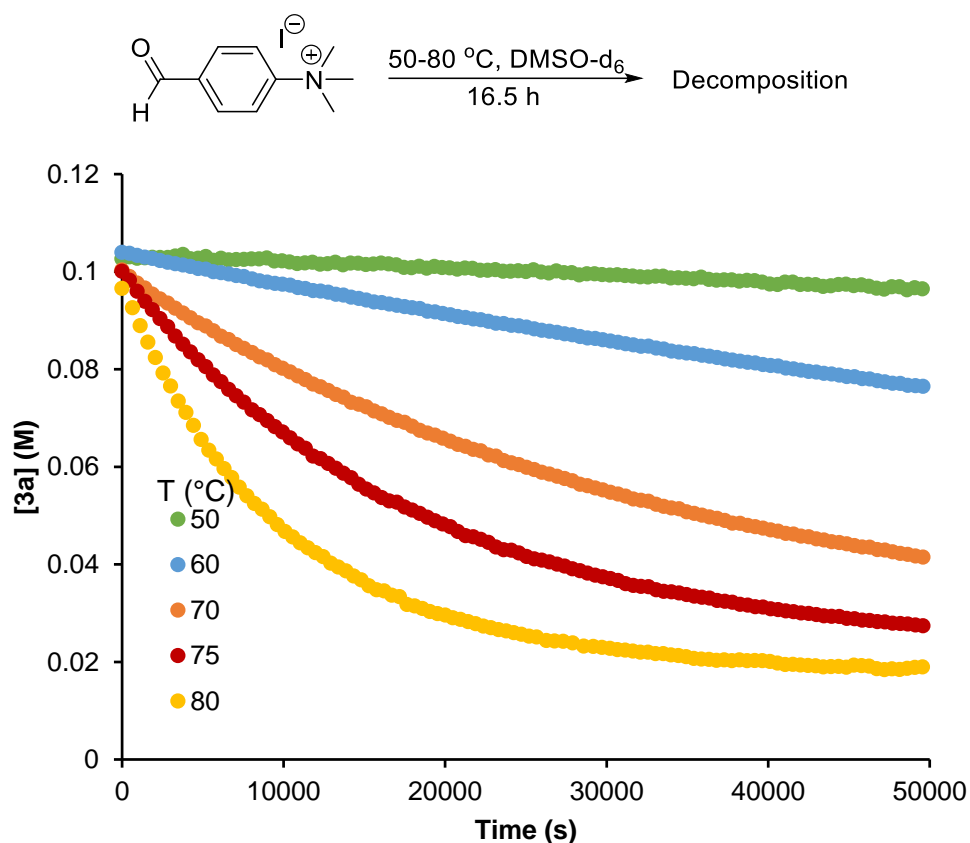
The concentration of *N,N,N*-trimethylanilinium salt and 4-iodobenzaldehyde in solution were calculated against the internal standard. The concentration of **176a** and 4-iodobenzaldehyde at $t = 0$ and $t = 20$ min are shown reported in the table below. On 89.4 ± 0.8 % of **3a** degraded over the time course, whilst there was a 0.3 ± 0.3 % calculated decrease in the concentration of 4-iodobenzaldehyde. This shows that there was no detectable change in the increase of the proposed iodide displacement product.

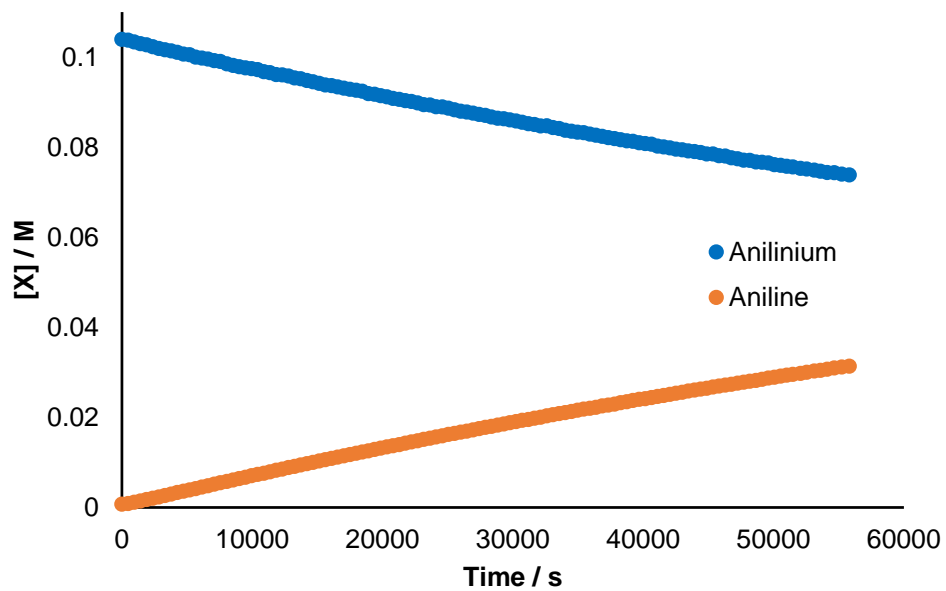
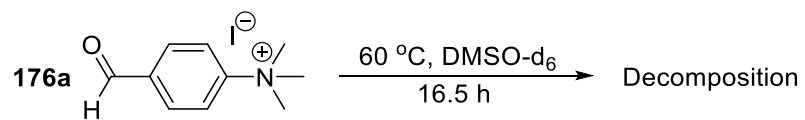
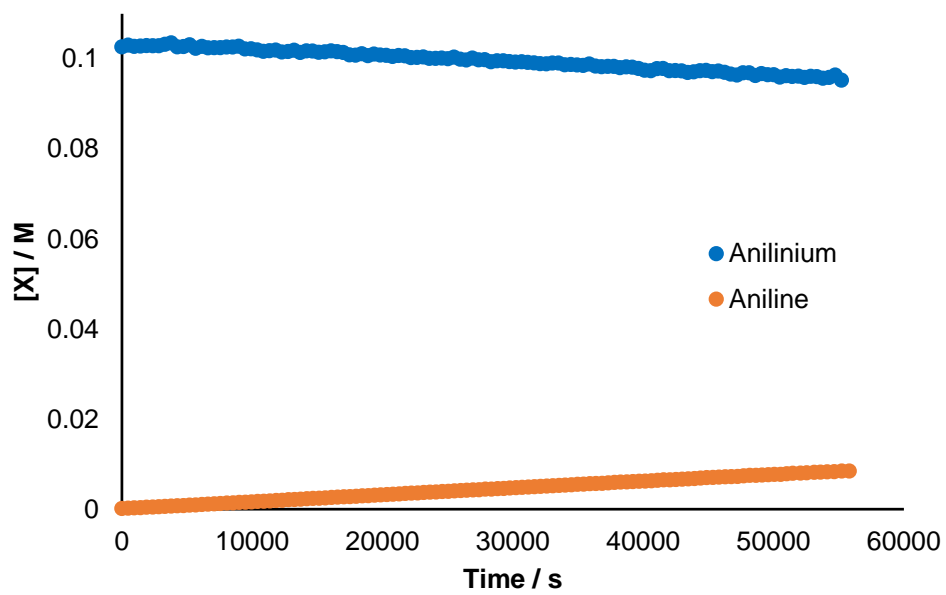
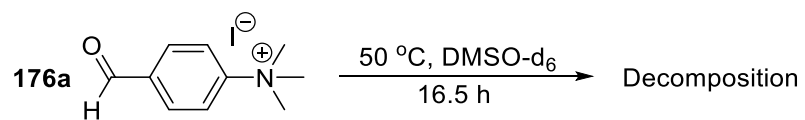
| Analyte | Time (min) | Concentration (M) | | | Average Concentration (M) | Concentration change (%) |
|------------------|------------|-------------------|-------|-------|---------------------------|--------------------------|
| | | Run 1 | Run 2 | Run 3 | | |
| 176a | 0 | 0.098 | 0.105 | 0.105 | 0.103 | -89.4 ± 0.8 |
| | 20 | 0.009 | 0.012 | 0.012 | 0.011 | |
| 4-I-benzaldehyde | 0 | 0.011 | 0.011 | 0.011 | 0.011 | -0.3 ± 0.3 |
| | 20 | 0.011 | 0.010 | 0.011 | 0.011 | |

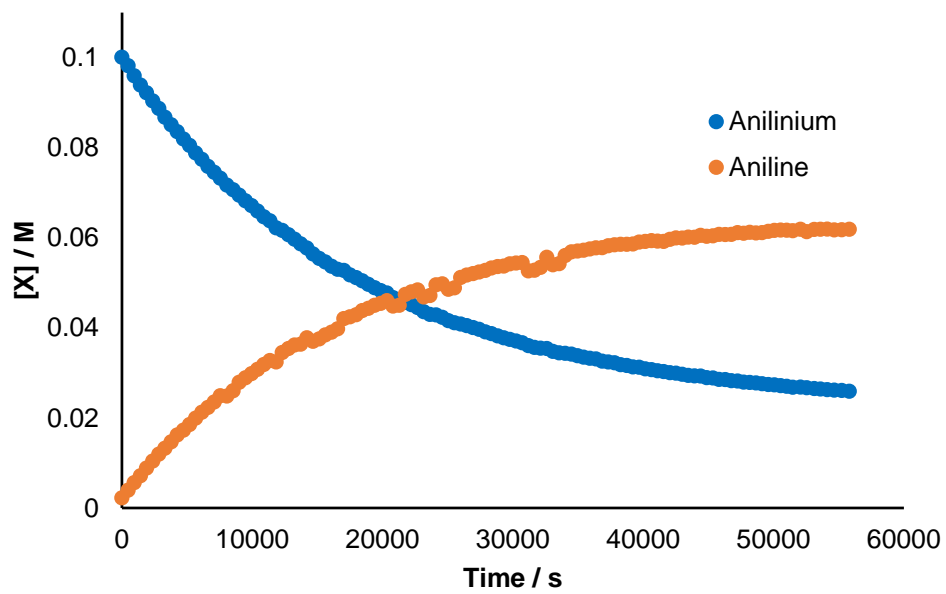
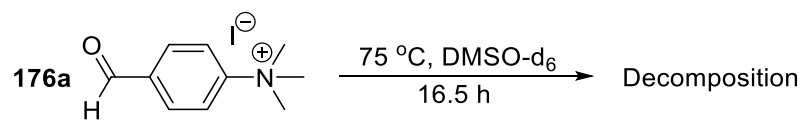
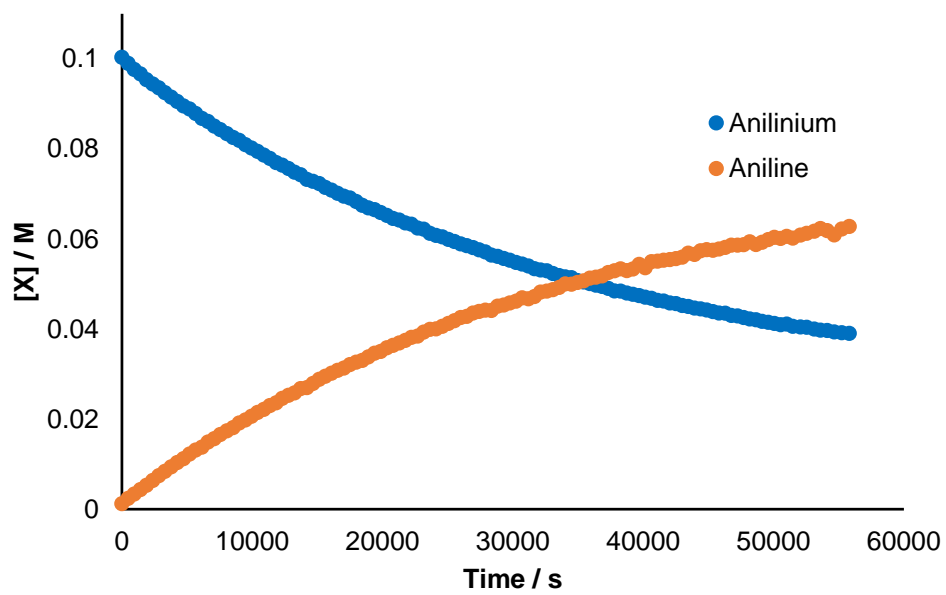
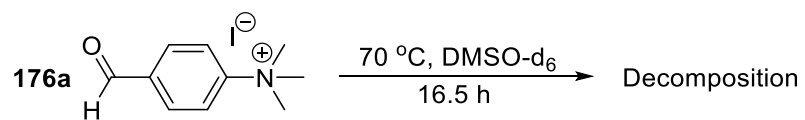
Investigating Temperature Effect on the Degradation of 176a in DMSO-d₆ Using ¹H NMR Spectroscopy

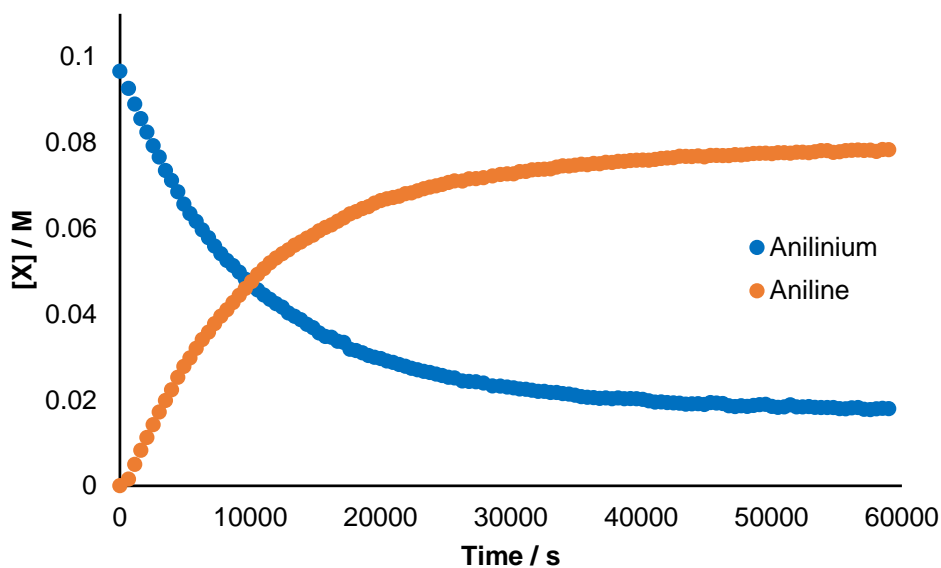
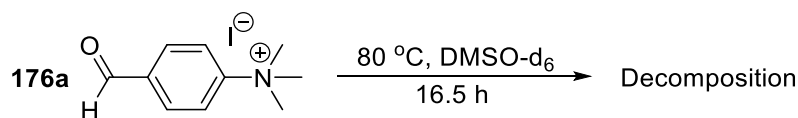
3a (17.5 mg, 60.0 μmol) and 1,2,4,5-tetramethylbenzene internal standard (4.8 mg, 36 μmol) were dissolved in DMSO-d₆ (0.6 mL, 0.714 g), to give an anilinium concentration of 0.10 M, and an internal standard concentration of 0.06 M, then transferred to an NMR tube. A ¹H NMR spectrum (4 scans, 25 s relaxation time) was recorded every 5 min whilst the sample was heated to 50, 60, 70, 75, or 80 °C in the NMR spectrometer probe.

The concentration of the anilinium (blue) and aniline (orange) was calculated against the internal standard at each time point. The concentration vs time curves are shown all on one graph and graphs for each temperature studied are shown below.









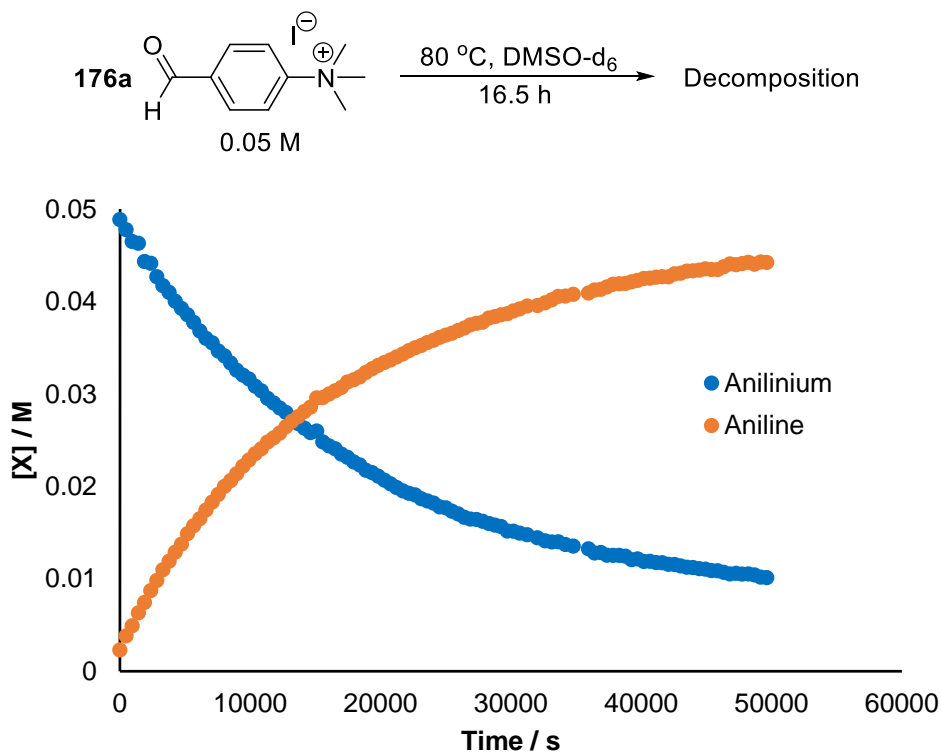
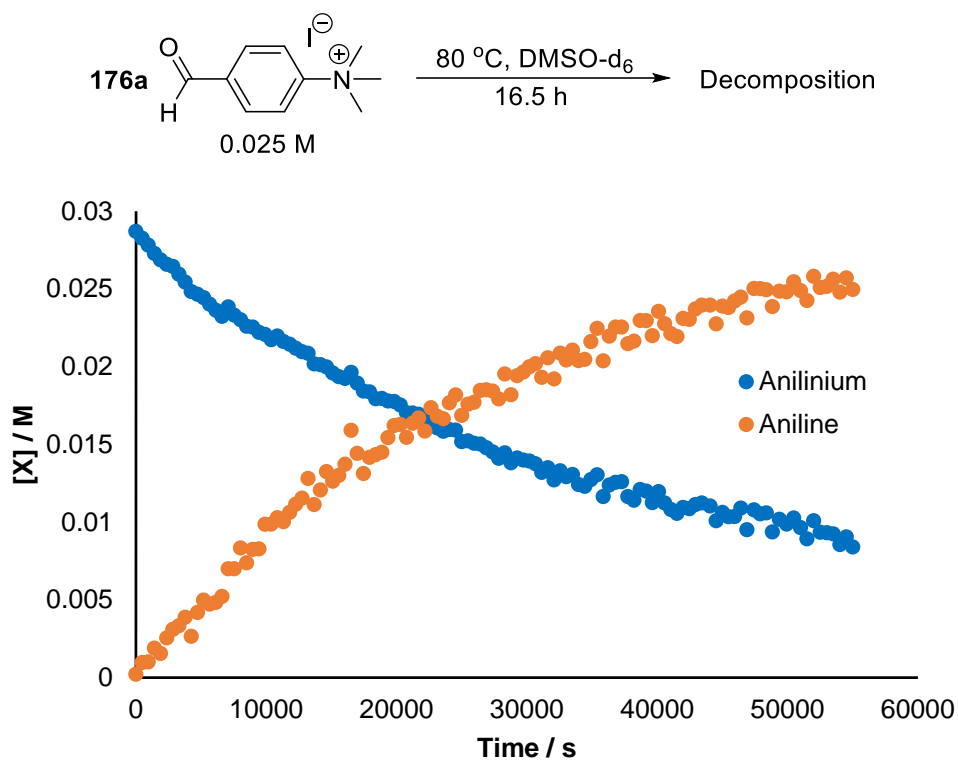
Rate constants were determined for each step of the proposed degradation pathway at each temperature studied, estimated value are shown below.

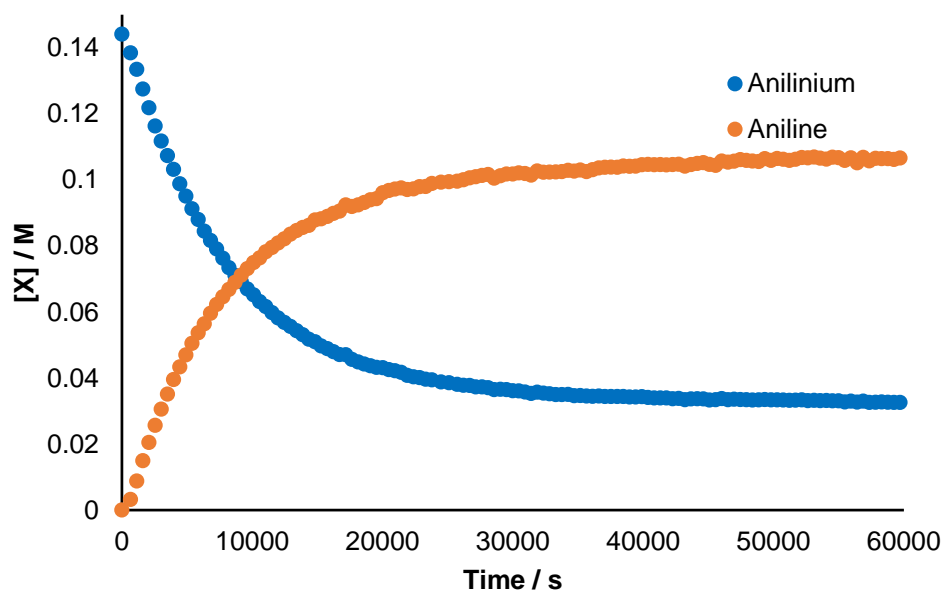
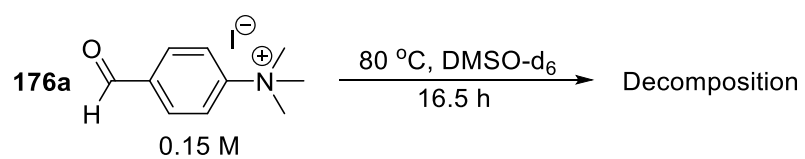
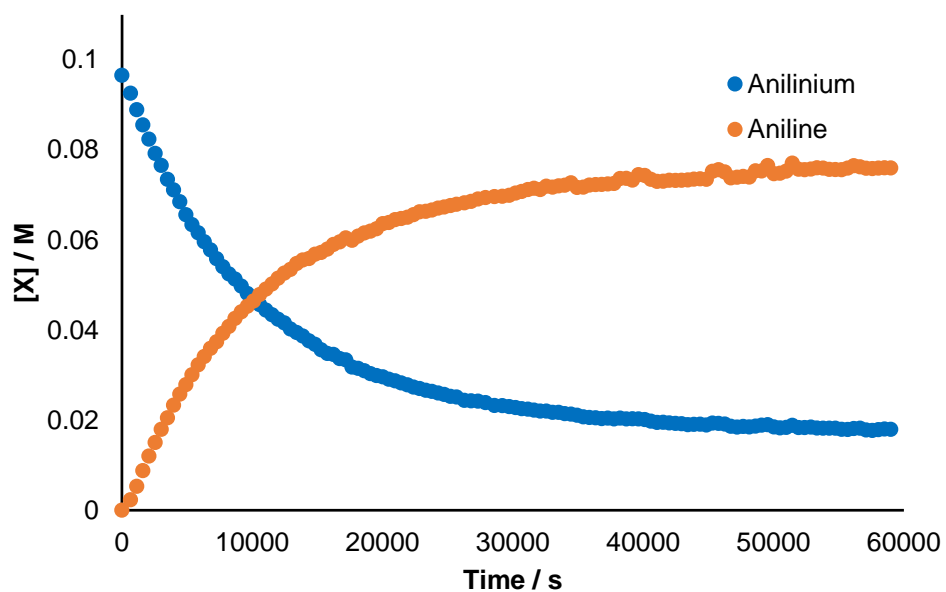
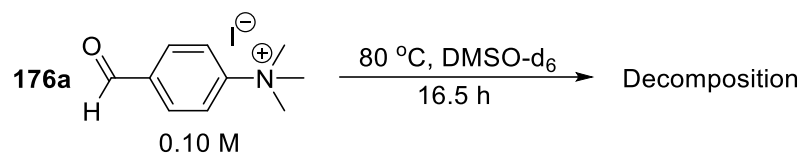
| T (°C) | k ₁ (s ⁻¹) | k ₋₁ (M ⁻¹ s ⁻¹) | k ₂ (M ⁻¹ s ⁻¹) | k ₋₂ (M ⁻¹ s ⁻¹) | k ₃ (M ⁻¹ s ⁻¹) | k ₋₃ (s ⁻¹) |
|--------|-----------------------------------|--|---|--|---|------------------------------------|
| 50 | 1.17E-06 | 5.82E-295 | 1.53E-208 | 3.96E-181 | 1.67E-223 | 1.79E-114 |
| 60 | 6.28E-06 | 3.87E-130 | 7.12E-91 | 3.69E-229 | 3.94E-07 | 7.95E-153 |
| 70 | 2.21E-05 | 1.16E-236 | 1.59E-170 | 3.27E-03 | 4.03E+11 | 1.27E+14 |
| 75 | 4.06E-05 | 2.38E-236 | 3.26E-170 | 8.66E-03 | 2.46E+11 | 1.75E+14 |
| 80 | 7.42E-05 | 0.00E+00 | 1.63E-170 | 5.50E-03 | 9.48E+11 | 3.10E+14 |

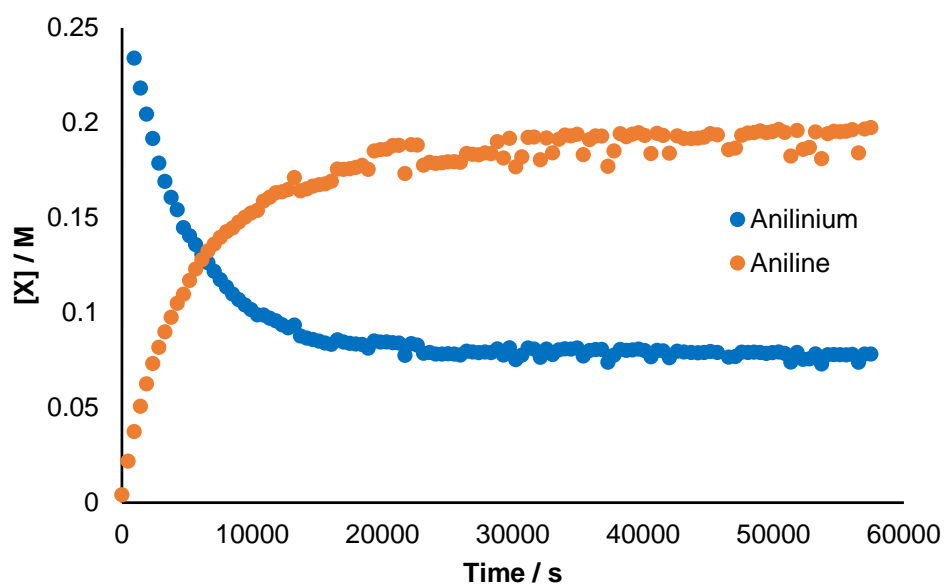
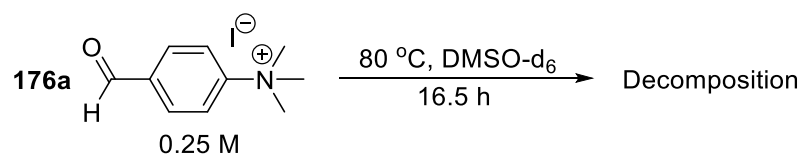
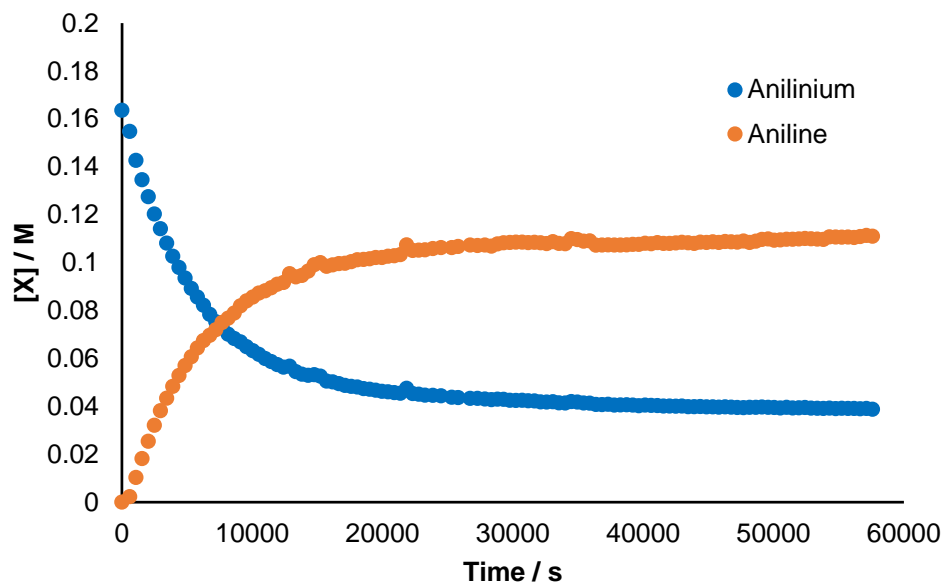
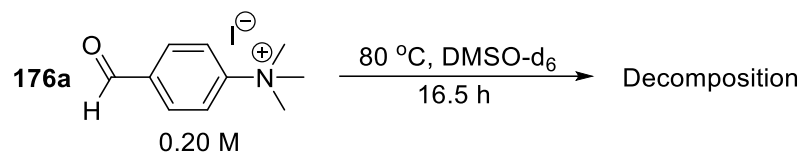
Investigating the Effect Concentration on the Degradation of 3a in DMSO-d₆ Using ¹H NMR Spectroscopy

174a and 1,2,4,5-tetramethylbenzene internal standard (4.8 mg, 36 μmol) were dissolved in DMSO-d₆ (0.6 mL, 0.714 g), to give an anilinium concentration of 0.025, 0.05, 0.10, 0.15, 0.20, or 0.25 M, and an internal standard concentration of 0.06 M, then transferred to an NMR tube. A ¹H NMR spectrum (4 scans, 25 s relaxation time) was recorded every 5 min whilst the sample was heated to 80 °C in the NMR spectrometer probe.

The concentration of the anilinium (blue) and aniline (orange) was calculated against the internal standard at each time point. The concentration vs time graphs for each temperature studied are shown below.







Rate constants were determined for each step of the proposed degradation pathway, at each concentration, estimated value are shown below.

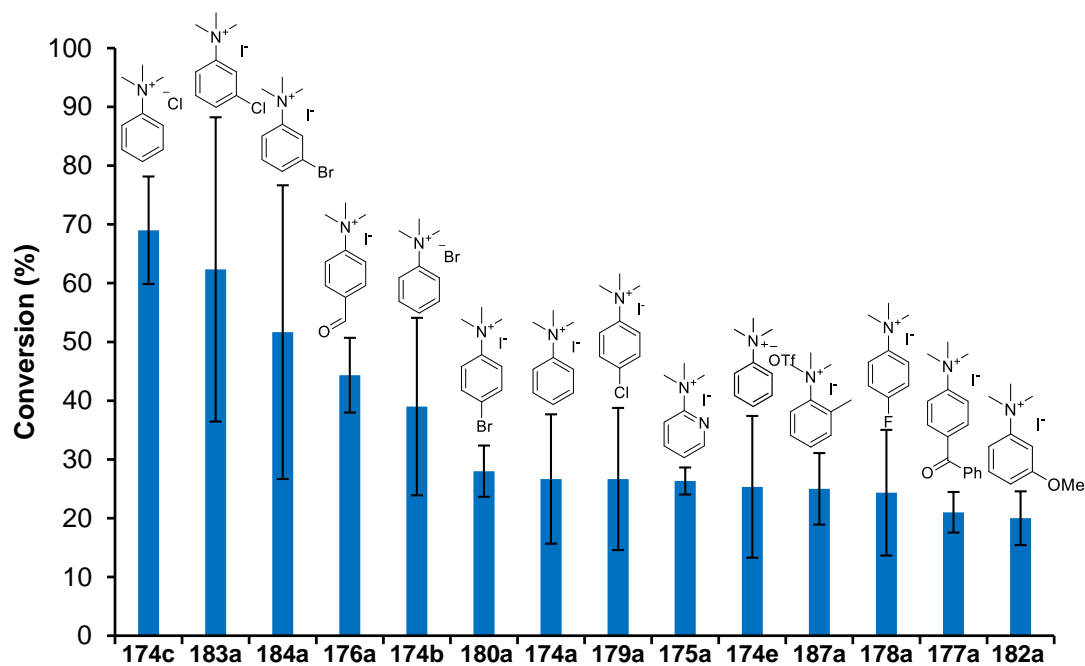
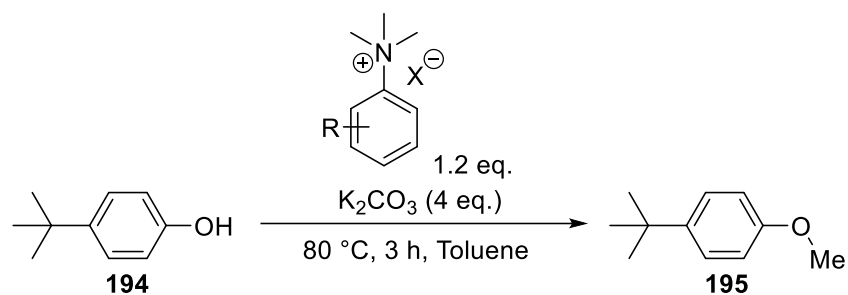
| [174] ₀ (M) | k ₁ (s ⁻¹) | k ₋₁ (M ⁻¹ s ⁻¹) | k ₂ (M ⁻¹ s ⁻¹) | k ₋₂ (M ⁻¹ s ⁻¹) | k ₃ (M ⁻¹ s ⁻¹) | k ₋₃ (s ⁻¹) |
|------------------------|-----------------------------------|--|---|--|---|------------------------------------|
| 0.025 | 2.61E-05 | 0.00E+00 | 1.13E-170 | 5.53E-03 | 8.65E+11 | 1.98E+14 |
| 0.05 | 4.55E-05 | 8.34E-08 | 4.78E-171 | 4.06E-03 | 7.08E+11 | 1.75E+14 |
| 0.1 | 7.42E-05 | 0.00E+00 | 1.63E-170 | 5.50E-03 | 9.48E+11 | 3.10E+14 |
| 0.15 | 8.58E-05 | 9.05E-08 | 1.47E-171 | 1.64E-03 | 6.61E+11 | 5.62E+13 |
| 0.2 | 1.16E-04 | 8.86E-08 | 1.24E-171 | 1.86E-03 | 1.14E+12 | 7.87E+13 |
| 0.25 | 1.38E-04 | 8.77E-08 | 6.29E-172 | 1.84E-03 | 8.93E+11 | 6.65E+13 |

Methylation of 4-¹Bu-phenol using N,N,N-trimethylanilinium Salts in Toluene

4-¹Bu-phenol (0.300 g, 2 mmol, 1 eq.), the relevant N,N,N-trimethylanilinium salt (2.4 mmol, 1.2 eq.), potassium carbonate (1.106 g, 8 mmol, 4 eq.), and Toluene (3 mL) were added to an Asynt DrySyn Octo reaction carousel tube equipped with a stirrer bar. The reaction mixture was heated to 80 °C with stirring for 3 h.

After cooling, an aliquot of the supernatant was taken and the conversion of 4-¹Bu-phenol to 4-¹Bu-anisole was calculated *via* ¹H NMR analysis of the crude reaction mixture. Each experiment was conducted in triplicate.

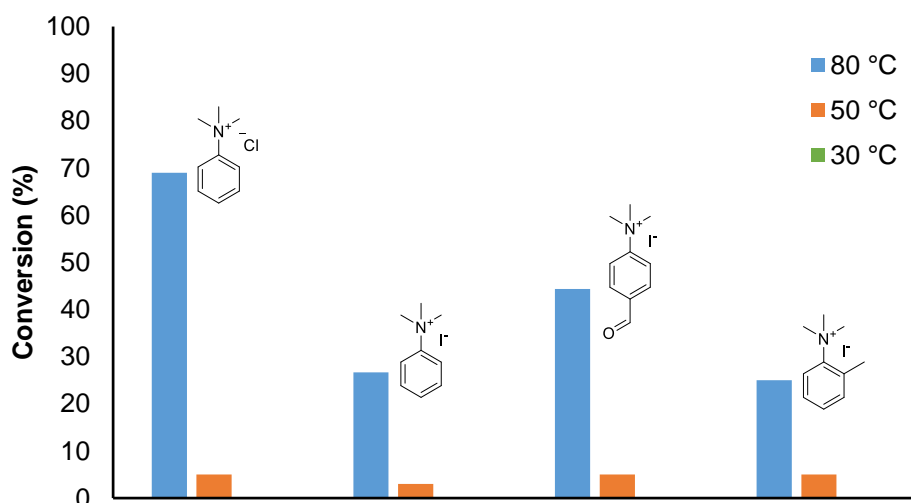
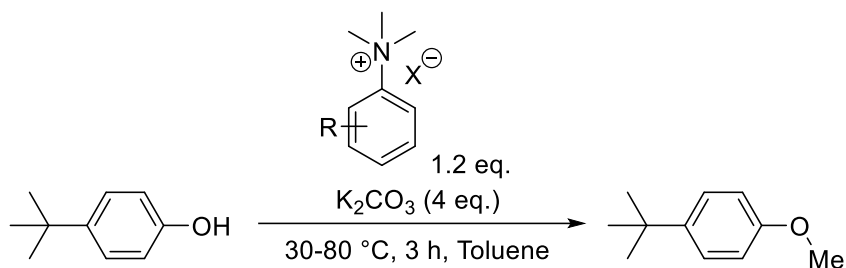
N,N,N-trimethylanilinium salts **174a-c**, **174e**, **175a-180a**, **182a-184a**, and **187a** were all screened for their ability to methylate 4-¹Bu-phenol in this manner. A chart showing the average conversion to the anisole product of each anilinium salt tested is shown below. A table showing the values for each of the three runs, the average and the error is also provided.



| Anilinium salt | Conversion (%) | | | Average Conversion (%) | Error (%) |
|----------------|----------------|-------|-------|------------------------|-----------|
| | Run 1 | Run 2 | Run 3 | | |
| 174a | 16 | 26 | 38 | 26.67 | 11.02 |
| 174b | 53 | 41 | 23 | 39.00 | 15.10 |
| 174c | 61 | 67 | 79 | 69.00 | 9.17 |
| 174e | 38 | 24 | 14 | 25.33 | 12.06 |
| 175a | 25 | 25 | 29 | 26.33 | 2.31 |
| 176a | 37 | 48 | 48 | 44.33 | 6.35 |
| 177a | 19 | 25 | 19 | 21.00 | 3.46 |
| 178a | 31 | 30 | 12 | 24.33 | 10.69 |
| 179a | 36 | 31 | 13 | 26.67 | 12.10 |

| | | | | | |
|-------------|----|----|----|-------|-------|
| 180a | 33 | 26 | 25 | 28.00 | 4.36 |
| 182a | 25 | 16 | 19 | 20.00 | 4.58 |
| 183a | 72 | 82 | 33 | 62.33 | 25.89 |
| 184a | 79 | 30 | 46 | 51.67 | 24.99 |
| 187a | 22 | 32 | 21 | 25.00 | 6.08 |

An investigation into the effect of temperature on the ability of a selection of *N,N,N*-trimethylanilinium salts to methylate 4-^tBu-phenol in toluene was then investigated. The experimental procedure was identical to the procedure mentioned above, with the exception that the reaction was carried out at either 30 or 50 °C. Anilinium salts **174a**, **174c**, **176a**, and **187a** were screened for their methylating ability at these temperatures. A graph showing the conversion to the anisole product for each salt at each temperature is shown below. A table containing the conversion to anisole at 30 and 50 °C is also provided.



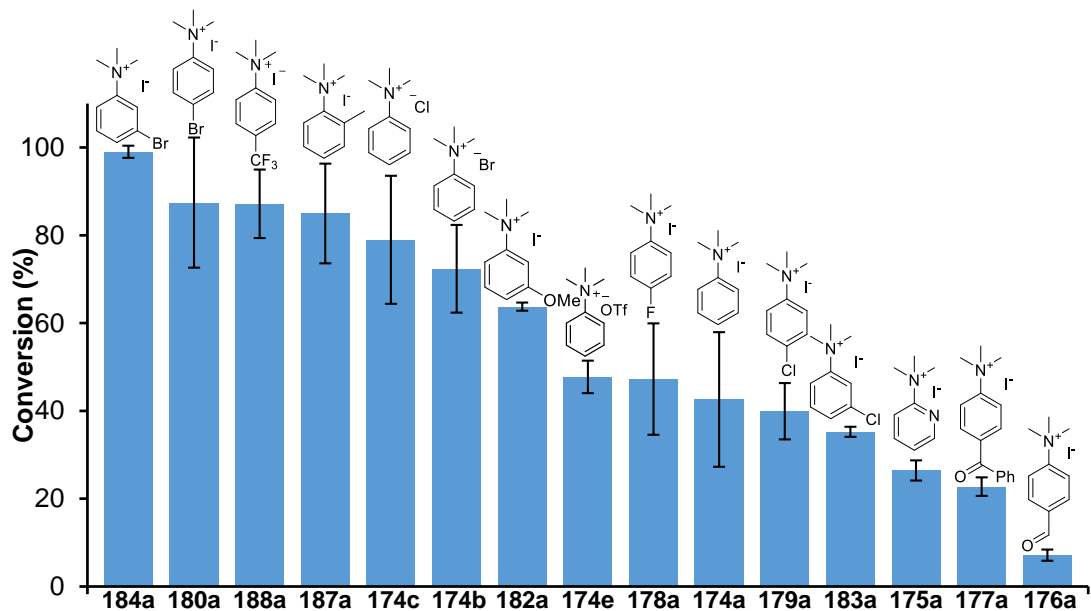
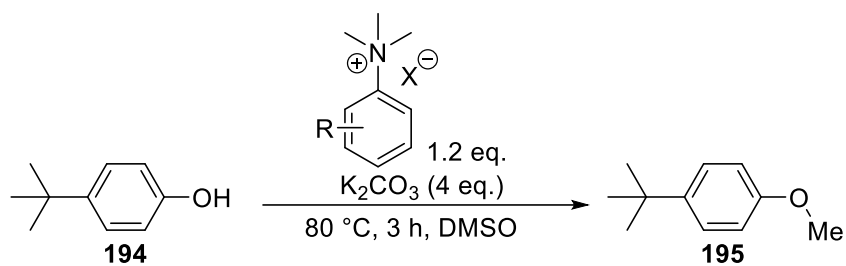
| Anilinium salt | Conversion (%) | | |
|----------------|----------------|-------|-------|
| | 30 °C | 50 °C | 80 °C |
| 174a | 0 | 3 | 27 |
| 174a | 0 | 5 | 69 |
| 176a | 0 | 5 | 44 |
| 187a | 0 | 5 | 25 |

Methylation of 4-¹Bu-phenol using N,N,N-trimethylanilinium Salts in DMSO

4-¹Bu-phenol (0.150 g, 1 mmol, 1 eq), the relevant *N,N,N*-trimethylanilinium salt (1.2 mmol, 1.2 eq), potassium carbonate (0.553 g, 4 mmol, 4 eq), and DMSO (2.5 mL) were added to a 25 mL round bottom flask equipped with a stir bar. The reaction mixture was heated to 80 °C with stirring for 3 h in the sealed round bottom flask.

After cooling, an aliquot of the supernatant was taken and the conversion of 4-¹Bu-phenol to 4-¹Bu-anisole was calculated *via* ¹H NMR analysis of the crude reaction mixture. Each experiment was performed in triplicate

N,N,N-trimethylanilinium salts **174a-c**, **174e**, **175a-180a**, **182a-184a**, **187a**, and **188a** were all screened for their ability to methylate 4-¹Bu-phenol in this manner. A chart showing the average conversion to the anisole product is shown below. A table containing conversions for each run, the average and the error is also provided.

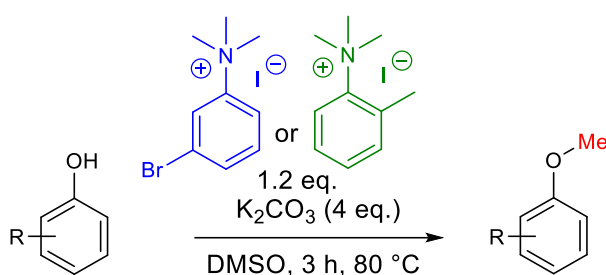


| Anilinium salt | Conversion (%) | | | Average Conversion (%) | Error (%) |
|----------------|----------------|-------|-------|------------------------|-----------|
| | Run 1 | Run 2 | Run 3 | | |
| 174a | 27.00 | 63.43 | 37.35 | 42.59 | 15.33 |
| 174b | 86.49 | 65.72 | 64.90 | 72.37 | 9.99 |
| 174c | 67.90 | 61.59 | 96.61 | 75.37 | 15.24 |
| 174d | 52.63 | 46.91 | 43.69 | 47.74 | 3.70 |
| 175a | 23.30 | 27.32 | 28.68 | 26.43 | 2.28 |
| 176a | 5.85 | 6.69 | 8.87 | 7.14 | 1.27 |
| 177a | 25.55 | 22.24 | 20.44 | 22.74 | 2.12 |
| 178a | 48.52 | 31.09 | 62.09 | 47.24 | 12.69 |
| 179a | 34.26 | 48.87 | 36.63 | 39.92 | 6.40 |
| 180a | 66.50 | 98.39 | 97.48 | 87.46 | 14.82 |

| | | | | | |
|-------------|--------|--------|--------|-------|-------|
| 182a | 64.12 | 62.45 | 64.63 | 63.73 | 0.93 |
| 183a | 34.57 | 34.27 | 36.84 | 35.22 | 1.15 |
| 184a | 100.00 | 97.07 | 100.00 | 99.02 | 1.38 |
| 187a | 72.57 | 100.00 | 82.32 | 84.96 | 11.35 |
| 188a | 90.87 | 76.30 | 94.35 | 87.17 | 7.82 |

Methylation of phenols in DMSO using 3-Br-N,N,N-trimethylanilinium iodide

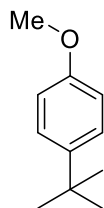
General procedure F - Methylation of nucleophiles in DMSO using 11a



The relevant nucleophile (1 mmol, 1 eq.), 3-Br-*N,N,N*-trimethylanilinium iodide (**184a**, 0.4104 g, 1.2 mmol, 1.2 eq.) or 2-*N,N,N*-tetramethylanilinium iodide (**187a**, 0.3326 g, 1.2 mmol, 1.2 eq.), potassium carbonate (0.553 g, 4 mmol, 4 eq.), and DMSO (2 mL) were added to a 25 mL round bottom flask equipped with a stir bar. The reaction mixture was heated to 80 °C with stirring for 3 h in the sealed round bottom flask. After cooling, the reaction was diluted with water (10 mL) and extracted with dichloromethane (3 x 15 mL). The organic layers were then combined, washed with 1M HCl (3 x 20 mL), dried over MgSO₄, and filtered. The solvent was then removed *in vacuo* to give the crude methylated product. Column chromatography on silica gel was used to deliver the methylated product.

A range of phenolic substrates, thiophenol, and benzoic acid were subjected to these conditions. Details for the synthesis of each substrate are given below.

Synthesis of 4-*t*-Bu-anisole **200**¹⁸²



Prepared according to *General Procedure F*

Amount of 4-*t*-Bu-phenol: 0.1502 g, 1.00 mmol

Product yield using **184a**: 0.1608 g, 0.979 mmol, 98%

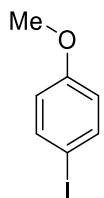
Product yield using **187a**: 0.1411 g, 0.859 mmol, 86%

IR: ν_{\max} 2959, 2361, 1612, 1514, 1464, 1364, 1298, 1246, 1183, 1036, 827, 793 cm^{-1}

¹H NMR (400 MHz, CDCl₃): δ 1.33 (s, 9H, C(CH₃)₃), δ 3.82 (s, 3H, OCH₃), δ 6.87 (m, 2H, ArH), δ 7.33 (m, 2H, ArH)

¹³C NMR (101 MHz, CDCl₃): δ 30.98, 33.54, 54.70, 112.84, 125.71, 142.83, 156.79

Synthesis of 4-*I*-anisole **201**¹⁸³



Prepared according to *General Procedure F*

Amount of 4-*I*-phenol: 0.2340 g, 1.00 mmol

Product yield using **184a**: 0.1615 g, 0.691 mmol, 69%

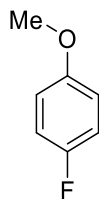
Melting point: 47-48 °C

IR: ν_{\max} 2361, 1584, 1481, 1285, 1238, 1172, 1026, 997, 831, 808, 583 cm^{-1}

¹H NMR (400 MHz, CDCl₃): δ 3.79 (s, 3H, OCH₃), δ 6.71 (m, 2H, ArH), δ 7.58 (m, 2H, ArH)

¹³C NMR (101 MHz, CDCl₃): δ 54.88, 82.33, 115.94, 137.73, 158.99

Synthesis of 4-F-anisole **202**¹⁸⁴



Prepared according to *General Procedure F*

Amount of 4-F-phenol: 0.1122 g, 1.00 mmol

Product yield using **184a**: 0.0877 g, 0.696 mmol, 70%

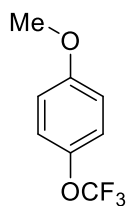
IR: ν_{\max} 3055, 3001, 2953, 2934, 2837, 2355, 2335, 1721, 1668, 1601, 1296, 1250, 1210, 1120, 1034, 887, 723 cm^{-1}

¹H NMR (400 MHz, CDCl₃): δ 3.81 (s, 3H, OCH₃), δ 6.86 (m, 2H, ArH), δ 7.00 (m, 2H, ArH)

¹³C NMR (101 MHz, CDCl₃): δ 55.23, 114.25 (d, $J_{\text{CF}^3} = 7.51$ Hz), 115.25 (d, $J_{\text{CF}^2} = 22.89$), 155.37, 157.91 (d, $J_{\text{CF}^1} = 234.30$)

¹⁹F NMR (376 MHz, CDCl₃): δ -124.40

Synthesis of 4-trifluoromethoxy-anisole **203**¹⁸⁵



Prepared according to *General Procedure F*

Amount of 4-trifluoromethoxy-phenol: 0.1781 g, 1.00 mmol

Product yield using **184a**: 0.0403 g, 0.210 mmol, 21%

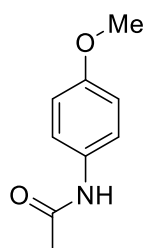
IR: ν_{\max} 2361, 1584, 1481, 1285, 1238, 1172, 1026, 997, 831, 808, 583 cm^{-1}

^1H NMR (400 MHz, CDCl_3): δ 3.83 (s, 3H, OCH_3), δ 6.92 (m, 2H, ArH), δ 7.18 (m, 2H, ArH)

^{13}C NMR (101 MHz, CDCl_3): δ 54.97, 114.11, 120.19 (q, $J_{\text{CF}^1} = 255.7$ Hz), 121.86, 142.23, 157.63

^{19}F NMR (376 MHz, CDCl_3): δ -58.53

*Synthesis of 2,6-diphenylanisole 204*¹⁸⁶



Prepared according to *General Procedure F*

Amount of 4-acetamidophenol: 0.1548 g, 1.01 mmol

Product yield using **184a**: 0.1279 g, 0.774 mmol, 77%

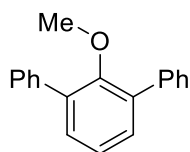
Melting point: 129-131 °C

IR: ν_{max} 2359, 1650, 1609, 1560, 1056, 1437, 1370, 1327, 1257, 1225, 1171, 835, 806, 683 cm^{-1}

^1H NMR (400 MHz, CDCl_3): δ 2.12 (s, 3H, CH_3), δ 3.78 (s, 3H, OCH_3), δ 6.83 (d, 2H, ArH, $J = 8.77$ Hz), δ 7.39 (d, 2H, ArH, $J = 8.77$ Hz), δ 7.99 (broad s, 1H, NH)

^{13}C NMR (101 MHz, CDCl_3): δ 23.88, 54.98, 113.66, 121.39, 130.42, 155.98, 167.59

Synthesis of 2,6-diphenylanisole 205



Prepared according to *General Procedure F*

Amount of 2,6-diphenylphenol: 0.2460 g, 1.00 mmol

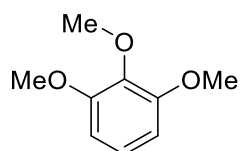
Product yield using **184a**: 0.2411 g, 0.926 mmol, 93%

IR: ν_{\max} 1497, 1462, 1441, 1406, 1227, 1177, 1084, 1028, 1005, 804, 762, 748, 696, 611, 582 cm^{-1}

^1H NMR (400 MHz, CDCl_3): δ 3.34 (s, 3H, OCH_3), δ 7.39 (dd, 1H, ArH, $J = 7.00$, 8.14 Hz), δ 7.52 (m, 4H, ArH), δ 7.60 (m, 4H, ArH), δ 7.80 (m, 4H, ArH)

^{13}C NMR (101 MHz, CDCl_3): δ 60.07, 123.90, 126.78, 127.84, 129.00, 130.03, 135.42, 138.39, 154.63

*Synthesis of 1,2,3-trimethoxybenzene 206*¹⁸⁷



Prepared according to *General Procedure F*

Amount of 2,6-methoxyphenol: 0.1542 g, 1.00 mmol

Product yield using **184a**: 0.1395 g, 0.831 mmol, 83%

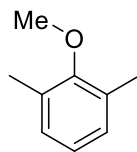
Melting point: 41-42 $^{\circ}\text{C}$

IR: ν_{\max} 2940, 2835, 2359, 1593, 1498, 1475, 1435, 1296, 1254, 1229, 1172, 1103, 1094, 1001, 901, 777, 739, 696 cm^{-1}

^1H NMR (400 MHz, CDCl_3): δ 3.85 (s, 3H, O- CH_3) δ 3.89 (s, 6H, O- CH_3), δ 6.61 (d, 2H, ArH, $J = 8.39$ Hz), δ 7.02 (t, 1H, ArH, $J = 8.39$ Hz)

^{13}C NMR (101 MHz, CDCl_3): δ 55.58, 60.33, 104.75, 123.12, 137.68, 153.05

Synthesis of 2,6-dimethylanisole **207**¹⁸⁸



Prepared according to *General Procedure F*

Amount of 2,6-methylphenol: 0.1222 g, 1.00 mmol

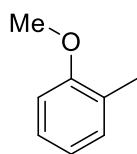
Product yield using **184a**: 0.1185 g, 0.870 mmol, 87%

IR: ν_{\max} 2943, 1475, 1416, 1263, 1213, 1170, 1091, 1018, 811, 769 cm^{-1}

¹H NMR (400 MHz, CDCl₃): δ 3.80 (s, 6H, Ar-CH₃) δ 3.81 (s, 3H, O-CH₃), δ 6.53 (d, 2H, ArH, $J = 8.43$ Hz), δ 6.93 (t, 1H, ArH, $J = 8.43$ Hz)

¹³C NMR (101 MHz, CDCl₃): δ 55.45, 60.16, 104.73, 123.11, 137.61, 152.97

Synthesis of 2-methylanisole **208**¹⁸⁹



Prepared according to *General Procedure F*

Amount of 2-methylphenol: 0.1082 g, 1.00 mmol

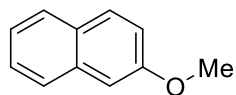
Product yield using **184a**: 0.0541 g, 0.442 mmol, 44%

IR: ν_{\max} 2999, 2941, 2916, 2833, 2357, 1601, 1585, 1489, 1460, 1435, 1288, 1260, 1190, 1165, 1151, 1043, 897, 843 cm^{-1}

¹H NMR (400 MHz, CDCl₃): δ 2.32 (s, 3H, Ar-CH₃) δ 3.90 (s, 3H, O-CH₃), δ 6.93 (m, 2H, ArH), δ 7.23 (m, 2H, ArH)

¹³C NMR (101 MHz, CDCl₃): δ 15.74, 54.73, 109.44, 119.81, 126.12, 126.34, 130.15, 157.28

*Synthesis of 2-methoxynaphthalene 209*¹⁹⁰



Prepared according to *General Procedure F*

Amount of 2-naphthol: 0.1444 g, 1.00 mmol

Product yield using **184a**: 0.1525 g, 0.964 mmol, 96%

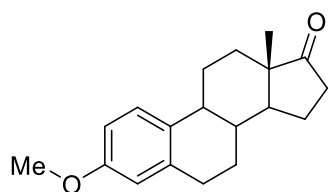
Melting point: 69-70 °C

IR: ν_{\max} 2361, 1628, 1589, 1473, 1439, 1389, 1258, 1213, 1169, 1115, 949, 897, 835, 816, 741, 698, 621 cm^{-1}

¹H NMR (400 MHz, CDCl₃): δ 3.90 (s, 3H, O-CH₃), δ 7.14 (d, 1H, ArH, $J = 2.57$ Hz), δ 7.18 (dd, 1H, ArH, $J = 8.86$ Hz), δ 7.35 (ddd, 1H, ArH, $J = 8.15, 6.83, 1.24$), δ 7.46 (ddd, 1H, ArH, $J = 8.15, 6.86, 1.24$), δ 7.72 (m, 3H, ArH)

¹³C NMR (101 MHz, CDCl₃): δ 54.82, 105.37, 118.31, 123.18, 126.34, 127.26, 128.57, 128.99, 134.19, 157.20

*Synthesis of estrone 3-methyl ether 210*¹⁹¹



Prepared according to *General Procedure F*

Amount of α -estrone: 0.2704 g, 1.00 mmol

Product yield using **184a**: 0.2432 g, 0.856 mmol, 86%

Product yield using **187a**: 0.2400 g, 0.844 mmol, 84%

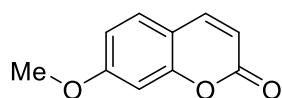
Melting point: 169-170 °C

IR: ν_{\max} 2913, 2361, 1736, 1503, 1452, 1316, 1236, 1165, 1107, 910, 245, 822, 575 cm^{-1}

^1H NMR (400 MHz, CDCl_3): δ 0.93 (s, 3H, C- CH_3), δ 1.38-1.72 (m, 6H), δ 1.93-2.58 (m, 7H), δ 2.93 (m, 2H), δ 3.80 (s, 3H, O- CH_3), δ 6.67 (d, 1H, ArH, $J = 2.78$ Hz), δ 6.75 (dd, 1H, ArH, $J = 2.78, 8.59$ Hz), δ 7.22 (d, 1H, ArH, $J = 8.59$ Hz)

^{13}C NMR (101 MHz, CDCl_3): δ 13.39, 21.12, 25.48, 26.10, 29.21, 31.14, 35.37, 37.91, 43.48, 47.48, 49.92, 54.68, 111.08, 113.41, 125.83, 131.51, 137.22, 157.13, 220.19

*Synthesis of 7-methoxycoumarin 211*¹⁹²



Prepared according to *General Procedure F*

Amount of 7-hydroxycoumarin: 0.1619 g, 1.00 mmol

Product yield using **184a**: 0.174 g, 0.986 mmol, 99%

Product yield using **187a**: 0.109 g, 0.616 mmol, 62%

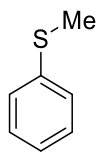
Melting point: 115-116 °C

IR: ν_{\max} 2361, 1701, 1611, 1504, 1398, 1350, 1281, 1231, 1123, 1024, 980, 891, 826, 750, 615 cm^{-1}

^1H NMR (400 MHz, CDCl_3): δ 3.79 (s, 3H, O- CH_3), δ 6.16 (d, 1H, C=C-H, $J = 9.49$ Hz), δ 6.69 (d, 1H, ArH, $J = 2.47$ Hz), δ 6.76 (dd, 1H, ArH, $J = 8.60, 2.47$ Hz), δ 7.30 (d, 1H, ArH, $J = 8.60$ Hz), δ 7.58 (d, 1H, C=C-H, $J = 9.49$ Hz)

^{13}C NMR (101 MHz, CDCl_3): δ 55.18, 100.25, 111.88, 111.95, 112.37, 128.30, 142.96, 155.27, 160.56, 162.26

*Synthesis of thioanisole 212*¹⁹³



Prepared according to *General Procedure F*

Amount of thiophenol: 0.1100 g, 1.00 mmol

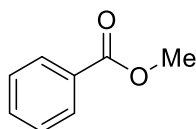
Product yield: 0.0958 g, 0.773 mmol, 77%

IR: ν_{\max} 3057, 2918, 2359, 1582, 1479, 1439, 1315, 1088, 1024, 966, 893, 135, 669 cm^{-1}

¹H NMR (400 MHz, CDCl₃): δ 2.54 (s, 3H, S-CH₃), δ 7.20 (m, 1H, ArH), δ 7.35 (m, 4H, ArH)

¹³C NMR (101 MHz, CDCl₃): δ 15.39, 124.56, 126.18, 128.36, 138.01

*Synthesis of methylbenzoate 213*¹⁹⁴



Prepared according to *General Procedure F*

Amount of benzoic acid: 0.1222 g, 1.00 mmol

Product yield: 0.1085 g, 0.797 mmol, 80%

IR: ν_{\max} 2951, 2361, 1719, 1600, 1452, 1435, 1315, 1273, 1176, 1109, 1023, 964, 822, 708 cm^{-1}

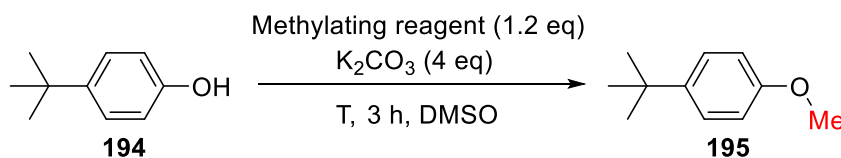
¹H NMR (400 MHz, CDCl₃): δ 3.90 (s, 3H, O-CH₃), δ 7.43 (m, 2H, ArH), δ 7.53 (m, 1H, ArH), δ 8.05 (m, 2H, ArH)

¹³C NMR (101 MHz, CDCl₃): δ 51.50, 127.82, 129.03, 129.66, 132.36, 166.51

Comparison of 184a to Common Methylating Reagents

4-^tBu-phenol (0.150 g, 1 mmol, 1 eq), potassium carbonate (0.553 g, 4 mmol, 4 eq), and DMSO (2.5 mL) were added to a 25 mL round bottom flask equipped with a stirrer bar. The relevant methylating reagent (1.2 mmol, 1.2 eq) was added *via* syringe or as a solid. The reaction mixture was heated to 40 or 80 °C with stirring for 3 h in the sealed round bottom flask.

After cooling, the reaction was diluted with water (10 mL) and extracted with dichloromethane (3 x 15 mL). The organic layers were then combined, washed with 1M HCl (3 x 20 mL), dried over MgSO₄, and filtered. The solvent was then removed *in vacuo* to give the crude methylated product. Column chromatography on silica gel was used to deliver the anisole product. The yield of anisole for under each of the methylation conditions is given below.

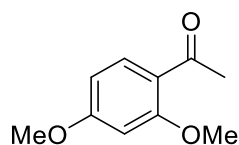


| Methylating reagent | T (°C) | Yield (mg, %) |
|---------------------|--------|---------------|
| 184a | 80 | 161, 98 |
| Methyl iodide | 40 | 115, 70 |
| Methyl iodide | 80 | 129, 79 |
| Methyl triflate | 80 | 4.0, 2 |
| Dimethyl carbonate | 80 | 0.0, 0 |

Comparison of Selectivity Methylating 2',4'-dihydroxyacetophenone with 184a and Methyl Iodide

2',4'-dihydroxyacetophenone (0.076 g, 0.50 mmol, 1 eq.), potassium carbonate (0.276 g, 2.0 mmol, 4 eq.), 184a or methyl iodide (1.2 eq.), and DMSO (1 mL) were added to a 25 mL round bottom flask equipped with a stirrer bar. The reaction mixture was heated to 80 °C with stirring for 3 h in the sealed round bottom flask.

¹³C NMR (101 MHz, CDCl₃): δ 25.70, 55.06, 100.34, 107.12, 113.41, 131.78, 164.77, 165.62, 202.05



¹H NMR (400 MHz, CDCl₃): δ 2.59 (s, 3H, C(O)CH₃), δ 3.88 (s, 3H, OCH₃), δ 3.91 (s, 3H, OCH₃), δ 6.48 (d, 1H, ArH, *J* = 2.30 Hz), δ 6.54 (dd, 1H, ArH, *J* = 8.71, 2.31 Hz), δ 7.85 (d, 1H, *J* = 8.71 Hz, ArH)

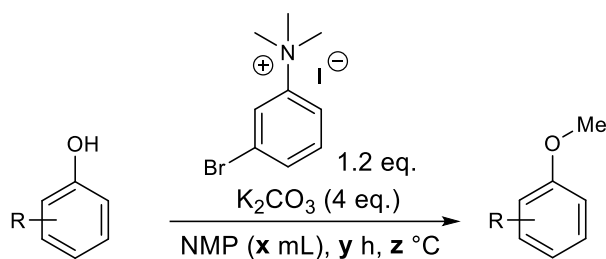
¹³C NMR (101 MHz, CDCl₃): δ 31.32, 54.94, 55.02, 97.83, 104.53, 120.07, 132.19, 160.57, 164.02, 197.24

Reaction Optimisation for the Methylation of Phenols using 11a in NMP

Based on the standard conditions used to methylate phenols with 11a in DMSO, a brief screen of conditions was carried out for the reaction in NMP. The general procedure was as follows.

4-^tBu-phenol (0.150 g, 1 mmol, 1 eq.), **184a** (1.2 mmol, 1.2 eq.), potassium carbonate (0.553 g, 4 mmol, 4 eq.), and NMP (**x** mL) were added to a 25 mL round bottom flask equipped with a stir bar. The reaction mixture was heated to **z** °C with stirring for **y** h in the sealed round bottom flask.

After cooling, the reaction was diluted with water (10 mL) and extracted with dichloromethane (3 x 15 mL). The organic layers were then combined, washed with 1M HCl (3 x 20 mL), dried over MgSO₄, and filtered. The solvent was then removed *in vacuo* to give the crude methylated product. Column chromatography on silica gel was used to deliver the anisole product. The yield of anisole for under each of the methylation conditions is given below.



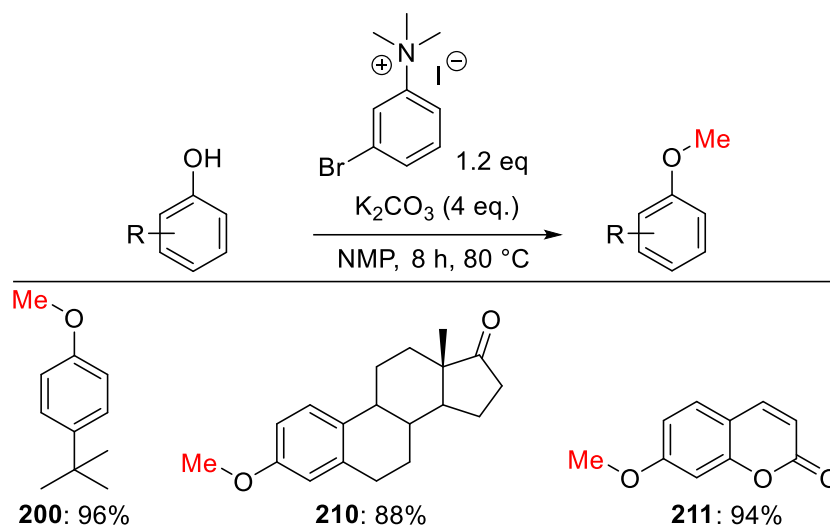
| Entry | x (mL) | y (h) | z (°C) | Yield (mg, %) |
|-------|--------|-------|--------|---------------|
| 1 | 2 | 3 | 80 | 145, 88 |
| 2 | 2 | 3 | 50 | 102, 62 |
| 3 | 5 | 3 | 80 | 136, 83 |
| 4 | 2 | 8 | 80 | 158, 96 |

Methylation of Phenols using 184a in NMP

4-^tBu-phenol, α -estrone, and 4-hydroxycoumarin were converted to their corresponding methyl ethers in NMP using the following general procedure.

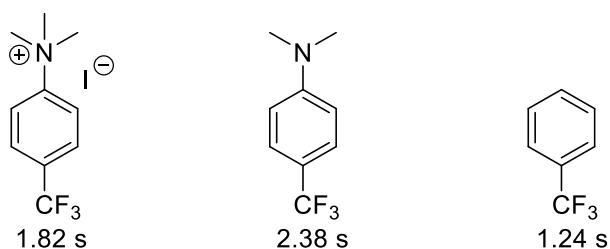
The relevant nucleophile (1 mmol, 1 eq), **184a** (0.4104 g, 1.2 mmol, 1.2 eq.), potassium carbonate (0.553 g, 4 mmol, 4 eq.), and NMP (2 mL) were added to a 25 mL round bottom flask equipped with a stir bar. The reaction mixture was heated to 80 °C with stirring for 8 h in the sealed round bottom flask. After cooling, the reaction was diluted with water (10 mL) and extracted with dichloromethane (3 x 15 mL). The organic layers were then combined, washed with 1M HCl (3 x 20 mL), dried over MgSO₄, and filtered. The solvent was then removed *in vacuo* to give the crude methylated product. Column chromatography on silica gel was used to deliver the methylated product.

The yield of each anisole product is shown in the scheme below. For brevity, readers are directed to *Methylation of phenols in DMSO using 3-Br-N,N,N-trimethylanilinium iodide* section for spectroscopic data and nucleophile stoichiometries.



Determination of T1 Relaxation Times for N,N,N -trimethylanilinium Iodides in $DMSO-d_6$

In order to gain quantitative ^{19}F NMR data to follow the degradation of **188a** in NMP, the T1 times of each ^{19}F were determined using the procedure described in section X. The calculated T1 relaxation times for **188a**, 4-trifluoromethyl- N,N -dimethylaniline, and α,α,α -trifluorotoluene are shown below.

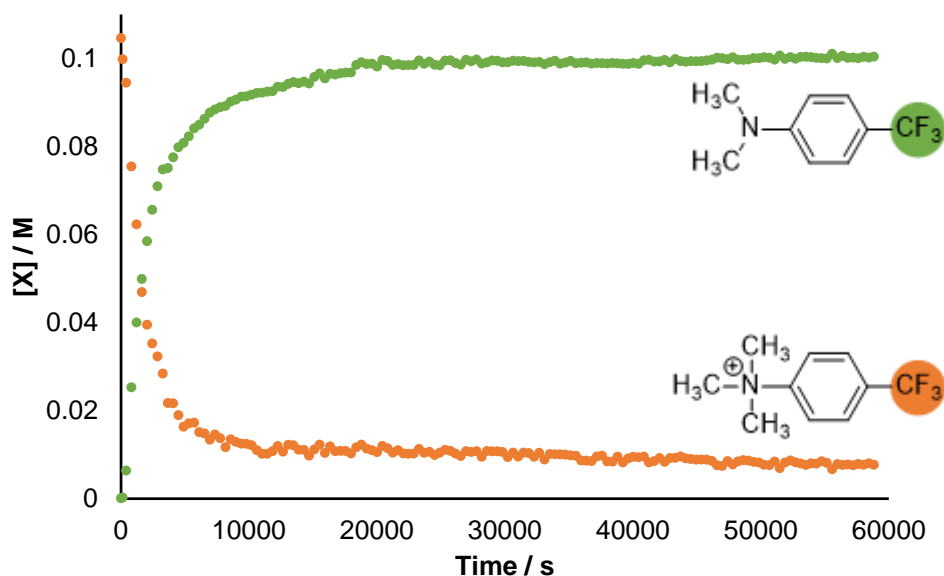


Monitoring the Degradation of **188a** in NMP Using ^{19}F NMR Spectroscopy

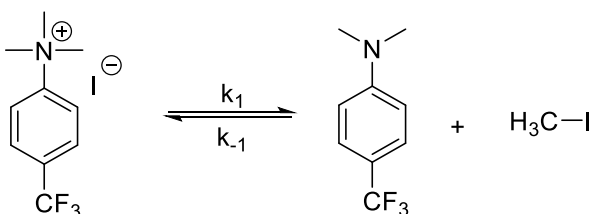
188a (19.9 mg, 60.0 μmol) and α,α,α -trifluorotoluene internal standard (8.8 mg, 60 μmol) were dissolved in NMP (0.6 mL, 0.618 g), to give an anilinium and internal standard concentration of 0.1 M, then transferred to an NMR tube. A ^{19}F NMR spectrum (4 scans, 25 s relaxation time) was recorded every 5 min whilst the sample was heated to $80\text{ }^\circ\text{C}$ in the NMR spectrometer probe.

The concentration of the anilinium salt and aniline was calculated against the internal standard at each time point.

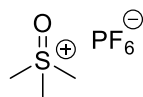
A plot of concentration vs time for **188a** and 4-trifluoromethyl-*N,N*-dimethylaniline is shown below. Data points are colour coded to correspond to the fluorine environment from which the concentration was calculated.



Assuming no reaction between the solvent and **188a**, the degradation would consist only of the following reversible step, which has been assigned rate constants k_1 and k_{-1} . Using COPASI v4.22 values for each rate constant in this reaction model were estimated. The modelling was programmed in such a way that priority would be given to correlating simulated data to the obtained anilinium concentration vs time curve. The estimated rate constant for this reaction were $k_1 = 4.44 \times 10^{-4} \text{ s}^{-1}$ and $k_{-1} = 4.78 \times 10^{-4} \text{ M}^{-1} \text{ s}^{-1}$.



Synthesis of trimethylsulfoxonium hexafluorophosphate, 216d



Trimethylsulfoxonium iodide (0.6602 g, 3 mmol, 1 eq.) was dissolved in the minimum amount of deionised water to achieve dissolution. Potassium hexafluorophosphate (0.5522 g, 3 mmol, 1 eq.) was added and the resulting mixture was stirred at room temperature for 3 h causing a white precipitation to form. The solid was collected *via* vacuum filtration and washed with deionised water (3 x 5 mL), then dried in a vacuum oven overnight to give a white powder (0.5671 g, 79%).

Melting point: Decomposed at 256 °C

IR: ν_{\max} 3003, 2914, 2359, 1412, 1233, 1040, 845, 822 cm^{-1}

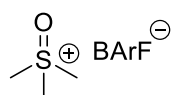
^1H NMR (400 MHz, DMSO- d_6): δ 3.83 (s, 9H, S-(CH₃)₃)

^{13}C NMR (101 MHz, DMSO- d_6): δ 38.95

^{19}F NMR (376 MHz, DMSO- d_6): δ -70.09 (d, PF₆⁻, J = 711 Hz)

^{31}P NMR (162 MHz, DMSO- d_6): δ -146.39 (hep, J = 711 Hz)

Synthesis of trimethylsulfoxonium tetrakis(3,5-bis-(trifluoromethyl)phenyl) borate, 216f



The trimethylsulfoxonium iodide (0.3756 g, 1.707 mmol, 1 eq.) and sodium tetrakis(3,5-bis(trifluoromethyl)phenyl) borate (1 eq.) were stirred in a 1:1 biphasic mixture of deionised water and dichloromethane. The organic layer was collected and dried over sodium sulfate. The solvent was removed *in vacuo* to give a white powder.

Melting point: Decomposed at 237 °C

IR: ν_{\max} 2631, 2331, 1609, 1352, 1271 1144, 1113, 1028, 885, 837, 726, 710, 669 cm^{-1}

¹H NMR (400 MHz, DMSO-d₆): δ 3.83 (s, 9H, S-(CH₃)₃), δ 7.62 (m, 8H, ArH BArF), δ 7.69 (s, 4H, ArH BArF)

¹³C NMR (101 MHz, DMSO-d₆): δ 38.91, 117.66, 123.97 (q, J_{CF}¹ = 271.9 Hz), 128.43 (J_{CF}² = 30 Hz), 134.02, 147.21, 160.89 (q, J_{CB}¹ = 49 Hz)

¹⁹F NMR (376 MHz, DMSO-d₆): δ -61.75

¹¹B NMR (MHz, DMSO-d₆): δ -6.82

General procedure for methylation of 4-^tBu-phenol for mechanistic experiments

4-^tBu-phenol (0.1502 g, 1 mmol, 1 eq.), methylating reagent (1.2 mmol, 1.2 eq.), potassium carbonate (0.553 g, 4 mmol, 4 eq.), and solvent (2 mL) were added to a 25 mL round bottom flask equipped with a stir bar. The reaction mixture was heated to 80 °C with stirring for 3 h open to air. After cooling, the reaction was diluted with water (10 mL) and extracted with dichloromethane (3 x 15 mL). The organic layers were then combined, washed with 1M HCl (3 x 20 mL), dried over MgSO₄, and filtered. The solvent was then removed *in vacuo* to give the crude methylated product. Column chromatography on silica gel was used to deliver **17** as a brown oil.

| Entry | Methylating reagent | Solvent | Yield 17 (mg, %) |
|-------|---------------------|---------|-------------------------|
| 1 | 184d | DMSO | 73.9, 45 |
| 2 | 184f | DMSO | 82.1, 50 |
| 3 | 216a | DMSO | 125, 76 |
| 4 | 216d | DMSO | 93.6, 57 |
| 5 | 216f | DMSO | 87.0, 53 |
| 6 | 184a | NMP | 14.5, 88 |
| 7 | 184d | NMP | 18.1, 11 |

1.7 References

- (1) Schönherr, H.; Cernak, T. *Angew. Chem. Int. Ed.* **2013**, *52*, 12256.
- (2) Barreiro, E. J.; Kümmerle, A. E.; Fraga, C. A. M. *Chem. Rev.* **2011**, *111*, 5215.
- (3) Wermuth, C. G. In *Optical Isomerism in Drugs*; Academic Press: San Diego, **2015**.
- (4) Lukac, I.; Zarnecka, J.; Griffen, E. J.; Dossetter, A. G.; St-Gallay, S. A.; Enoch, S. J.; Madden, J. C.; Leach, A. G. *J. Chem. Inf. Model.* **2017**, *57*, 2424.
- (5) Burns, M.; Essafi, S.; Bame, J. R.; Bull, S. P.; Webster, M. P.; Balieu, S.; Dale, J. W.; Butts, C. P.; Harvey, J. N.; Aggarwal, V. K. *Nature*, **2014**, *513*, 183.
- (6) McGrath, N. A.; Brichacek, M.; Njardarson, J. T. *J. Chem. Educ.* **2010**, *87*, 1348.
- (7) Biron, E.; Chatterjee, J.; Ovadia, O.; Langenegger, D.; Brueggen, J.; Hoyer, D.; Schmid, H. A.; Jelinek, R.; Gilon, C.; Hoffman, A. *Angew. Chem. Int. Ed.* **2008**, *47*, 2595.
- (8) Vértessy, B. G.; Tóth, J. *Acc. Chem. Res.* **2009**, *42*, 97.
- (9) Umezawa, Y.; Nishio, M. *Nucleic Acids Res.* **2002**, *30*, 2183.
- (10) Cantoni, G. L. *J. Biol. Chem.* **1953**, *204*, 403.
- (11) Nehlig, A.; Daval, J.-L.; Debry, G. *Brain Res. Rev.* **1992**, *17*, 139.
- (12) Snyder, S. H.; Katims, J. J.; Annau, Z.; Bruns, R. F.; Daly, J. W. *Proc. Natl. Acad. Sci.* **1981**, *78*, 3260.
- (13) Casey, A.; Parfitt, R. Opioid Analgesics, Chemistry and Receptors. *Trends Pharmacol. Sci.* 1987, *8* (1), 39.
- (14) Raynor, K.; Kong, H.; Chen, Y.; Yasuda, K.; Yu, L.; Bell, G. I.; Reisine, T. *Mol. Pharmacol.* **1994**, *45*, 330.
- (15) Beckett, A. H.; Casy, A. F. *J. Pharm. Pharmacol.* **1954**, *6*, 986.
- (16) Liao, C.; Nicklaus, M. C. *J. Chem. Inf. Model.* **2009**, *49*, 2801.
- (17) Mignat, C.; Wille, U.; Ziegler, A. *Life Sci.* **1995**, *56*, 793.

- (18) Eddy, N. B.; Friebel, H.; Hahn, K.-J.; Halbach, H. *Bull. World Health Organ.* **1969**, *40*, 639.
- (19) Eddy, N. B. *J. Pharmacol. Exp. Ther.* **1935**, *55*, 127.
- (20) van De Waterbeemd, H. *Quant. Struct. Relationships*, **1993**, *12*, 269.
- (21) Leo, A.; Hansch, C.; Elkins, D. *Chem. Rev.* **1971**, *71*, 525.
- (22) Fujita, T.; Iwasa, J.; Hansch, C. *J. Am. Chem. Soc.* **1964**, *86*, 5175.
- (23) Testa, B.; Carrupt, P.-A.; Gaillard, P.; Billois, F.; Weber, P. *Pharm. Res.* **1996**, *13*, 335.
- (24) Mälkiä, A.; Murtomäki, L.; Urtti, A.; Kontturi, K. *Eur. J. Pharm. Sci.* **2004**, *23*, 13.
- (25) Ginnings, P. M.; Baum, R. *J. Am. Chem. Soc.* **1937**, *59*, 1111.
- (26) Souza, E. S.; Zaramello, L.; Kuhnen, C. A.; Junkes, B. da S.; Yunes, R. A.; Heinzen, V. E. F. *Int. J. Mol. Sci.* **2011**, *12*, 7250.
- (27) Némethy, G. *Angew. Chem. Int. Ed. Eng.* **1967**, *6*, 195.
- (28) Southall, N. T.; Dill, K. A.; Haymet, A. D. J. *J. Phys. Chem. B.* **2002**, *106*, 521.
- (29) Hansch, C.; Hoekman, D.; Gao, H. *Chem. Rev.* **1996**, *96*, 1045.
- (30) Andrew, E. R.; Hinshaw, W. S.; Hutchins, M. G.; Sjöblom, R. O. I.; Canepa, P. C. *Mol. Phys.* **1976**, *32*, 795.
- (31) Serafin, J. M. *J. Chem. Educ.* **2003**, *80*, 1194.
- (32) Andrews, P. R.; Craik, D. J.; Martin, J. L. *J. Med. Chem.* **1984**, *27*, 1648.
- (33) Leung, C. S.; Leung, S. S. F.; Tirado-Rives, J.; Jorgensen, W. L. *J. Med. Chem.* **2012**, *55*, 4489.
- (34) Boehringer, M.; Fischer, H.; Hennig, M.; Hunziker, D.; Huwyler, J.; Kuhn, B.; Loeffler, B. M.; Luebbers, T.; Mattei, P.; Narquizian, R.; et al. *Bioorg. Med. Chem. Lett.* **2010**, *20*, 1106.
- (35) Walt, R. P.; Gomes, M. D.; Wood, E. C.; Logan, L. H.; Pounder, R. E. *Br. Med. J. (Clin. Res. Ed.)* **1983**, *287*, 12.

- (36) Larsson, H.; Carlsson, E.; Junggren, U.; Olbe, L.; Sjöstrand, S. E.; Skånberg, I.; Sundell, G. *Gastroenterology*, **1983**, *85*, 900.
- (37) Wallmark, B.; Brändström, A.; Larsson, H. *Biochim. Biophys. Acta - Biomembr.* **1984**, *778*, 549.
- (38) Olbe, L.; Carlsson, E.; Lindberg, P. *Nat. Rev. Drug Discov.* **2003**, *2*, 132.
- (39) Lindberg, P.; Brändström, A.; Wallmark, B.; Mattsson, H.; Rikner, L.; Hoffmann, K.-J. *Med. Res. Rev.* **1990**, *10*, 1.
- (40) Lindberg, P.; Carlsson, E. In *Analogue-based Drug Discovery*; Wiley-VCH: Weinheim, **2006**.
- (41) Kuntz, K. W.; Campbell, J. E.; Keilhack, H.; Pollock, R. M.; Knutson, S. K.; Porter-Scott, M.; Richon, V. M.; Sneeringer, C. J.; Wigle, T. J.; Allain, C. J.; et al. *J. Med. Chem.* **2016**, *59*, 1556.
- (42) Lugo, T. G.; Pendergast, A. M.; Muller, A. J.; Witte, O. N. *Science*, **1990**, *247*, 1079.
- (43) Druker, B. J.; Talpaz, M.; Resta, D. J.; Peng, B.; Buchdunger, E.; Ford, J. M.; Lydon, N. B.; Kantarjian, H.; Capdeville, R.; Ohno-Jones, S. *N. Engl. J. Med.* **2001**, *344*, 1031.
- (44) Goldman, J. M.; Melo, J. V. *N. Engl. J. Med.* **2001**, *344*, 1084.
- (45) Schuhmacher, A.; Gassmann, O.; Hinder, M. *J. Transl. Med.* **2016**, *14*, 105.
- (46) Silverman, L.; Campbell, R.; Broach, J. R. *Curr. Opin. Chem. Biol.* **1998**, *2*, 397.
- (47) Capdeville, R.; Buchdunger, E.; Zimmermann, J.; Matter, A. *Nat. Rev. Drug Discov.* **2002**, *1*, 493.
- (48) Zimmermann, J.; Buchdunger, E.; Mett, H.; Meyer, T.; Lydon, N. B. *Bioorg. Med. Chem. Lett.* **1997**, *7*, 187.
- (49) Zimmermann, J.; Buchdunger, E.; Mett, H.; Meyer, T.; Lydon, N. B.; Traxler, P. *Bioorg. Med. Chem. Lett.* **1996**, *6*, 1221.
- (50) Lin, Y.-L.; Meng, Y.; Jiang, W.; Roux, B. *Proc. Natl. Acad. Sci.* **2013**, *110*, 1664.

- (51) Schindler, T.; Bornmann, W.; Pellicena, P.; Miller, W. T.; Clarkson, B.; Kuriyan, J. *Science*, **2000**, 289, 1938.
- (52) Mobley, D. L.; Dill, K. A. *Structure*, **2009**, 17, 489.
- (53) Angell, R.; Aston, N. M.; Bamborough, P.; Buckton, J. B.; Cockerill, S.; deBoeck, S. J.; Edwards, C. D.; Holmes, D. S.; Jones, K. L.; Laine, D. I. *Med. Chem. Lett.* **2008**, 18, 4428.
- (54) Gamble, M. C.; Katsuki, F.; McCoy, J. G.; Strecker, R. E.; McKenna, J. T. *Sleep*, **2019**, 1.
- (55) Cox, C. D.; McGaughey, G. B.; Bogusky, M. J.; Whitman, D. B.; Ball, R. G.; Winrow, C. J.; Renger, J. J.; Coleman, P. J. *Bioorg. Med. Chem. Lett.* **2009**, 19, 2997.
- (56) Mei, H.; Han, J.; Fustero, S.; Medio-Simon, M.; Sedgwick, D. M.; Santi, C.; Ruzziconi, R.; Soloshonok, V. A. *Chem.: Eur. J.* **2019**, 25, 11797.
- (57) Lipinski, C. A. *J. Pharmacol. Toxicol. Methods*, **2000**, 44, 235.
- (58) Hann, M. M.; Keserü, G. M. *Nat. Rev. Drug Discov.* **2012**, 11, 355.
- (59) Jeffries, B.; Wang, Z.; Graton, J.; Holland, S. D.; Brind, T.; Greenwood, R. D. R.; Le Questel, J.-Y.; Scott, J. S.; Chiarparin, E.; Linclau, B. *J. Med. Chem.* **2018**, 61, 10602.
- (60) Caldwell, Z. Y.; Cadwell, G. W. *Curr. Top. Med. Chem.* **2001**, 403.
- (61) Ruetsch, Y. A.; Borgeat, T. B.; Borgeat, A. *Curr. Top. Med. Chem.* **2001**, 175.
- (62) Bowdle, T. A.; Knutsen, L. J. S.; Williams, M. In *Local and Adjunct Anesthesia*; Taylor, J. B., Triggle, D. J., Eds.; Elsevier: Oxford, **2007**.
- (63) Bill, T. J.; Clayman, M. A.; Morgan, R. F.; Gampper, T. J. *Aesthetic Surg. J.* **2004**, 24, 307.
- (64) Weber, B. W.; Kimani, S. W.; Varsani, A.; Cowan, D. A.; Hunter, R.; Venter, G. A.; Gumbart, J. C.; Sewell, B. T. *J. Biol. Chem.* **2013**, 288, 28514.
- (65) Licea-Perez, H.; Evans, C. A.; Summerfield, S. G. *Bioanalysis*, **2018**, 11, 85.
- (66) Hondeghem, L. M.; Katzung, B. G. *Annu. Rev. Pharmacol. Toxicol.* **1984**, 24, 387.

- (67) Friesen, R. W.; Brideau, C.; Chan, C. C.; Charleson, S.; Deschênes, D.; Dubé, D.; Ethier, D.; Fortin, R.; Gauthier, J. Y.; Girard, Y. *Bioorg. Med. Chem. Lett.* **1998**, *8*, 2777.
- (68) Rodrigues, A. D.; Halpin, R. A.; Geer, L. A.; Cui, D.; Woolf, E. J.; Matthews, C. Z.; Gottesdiener, K. M.; Larson, P. J.; Lasseter, K. C.; Agrawal, N. G. B. *Drug Metab. Dispos.* **2003**, *31*, 224.
- (69) Llona-Minguez, S.; Ghassemian, A.; Baranczewski, P.; Desroses, M.; Koolmeister, T.; Artursson, P.; Scobie, M.; Helleday, T. *Medchemcomm*, **2017**, *8*, 1553.
- (70) Sulikowski, G. A.; Sulikowski, M. M.; Haukaas, M. H.; Moon, B. *Iodomethane. Encyclopedia of Reagents for Organic Synthesis.*; John Wiley and sons: New Jersey, **2005**.
- (71) Chniti, I.; Maouati, H.; Sanhoury, M. A. K.; Merlet, D.; Chehidi, I. *Synth. Commun.* **2017**, *47*, 15.
- (72) Wuts, P. G. M. *Protection for the Carbonyl Group. Greene's Protective Groups in Organic Synthesis*; John Wileys and sons: New Jersey, **2014**.
- (73) Chen, Y. *Chem.: A Eur. J.* **2019**, *25*, 3405.
- (74) Mileson, B. E.; Sweeney, L. M.; Gargas, M. L.; Kinzell, J. H. *Inhal. Toxicol.* **2009**, *21*, 583.
- (75) Bolt, H. M.; Gansewendt, B. *Crit. Rev. Toxicol.* **1993**, *23*, 237.
- (76) Merriman, G. *Dimethyl Sulfate. Encyclopedia of Reagents for Organic Synthesis.*; John Wiley and sons: New Jersey, **2001**.
- (77) Benson, R. E.; Cairns, T. L. *J. Am. Chem. Soc.* **1948**, *70*, 2115.
- (78) Stodola, F. H. *J. Org. Chem.* **1964**, *29*, 2490.
- (79) Rippey, J. C. R.; Stallwood, M. I. *Emerg. Med. J.* **2005**, *22*, 878.
- (80) Hite, M.; Rinehart, W.; Braun, W.; Peck, H. *Am. Ind. Hyg. Assoc. J.* **1979**, *40*, 600.

- (81) Alder, R. W.; Phillips, J. G. E.; Huang, L.; Huang, X. *Methyltrifluoromethanesulfonate*. *Encyclopedia of Reagents for Organic Synthesis*; John Wiley and sons: New Jersey, **2005**.
- (82) Selva, M.; Perosa, A. *Green Chem.* **2008**, *10*, 457.
- (83) Tundo, P.; Selva, M.; Memoli, S. *Dimethylcarbonate as a Green Reagent*. In *Green Chemical Syntheses and Processes; ACS Symposium Series; American Chemical Society*, **2000**; 767, 8.
- (84) Schöffner, B.; Schöffner, F.; Verevkin, S. P.; Börner, A. *Chem. Rev.* **2010**, *110*, 4554.
- (85) Shieh, W.-C.; Dell, S.; Repič, O. *Org. Lett.* **2001**, *3*, 4279.
- (86) Tundo, P.; Selva, M. *Acc. Chem. Res.* **2002**, *35*, 706.
- (87) Stahl, I.; Seapy, D. G. *Trimethyloxonium Tetrafluoroborate*. *Encyclopedia of Reagents for Organic Synthesis*; John Wiley and sons: New Jersey, **2008**.
- (88) Braun, H.; Amann, A. *Angew. Chem.* **1975**, *87*, 773.
- (89) Sammakia, T. *Diazomethane*. *Encyclopedia of Reagents for Organic Synthesis*; John Wiley and sons: New Jersey, **2001**.
- (90) Kühnel, E.; Laffan, D. D. P.; Lloyd-Jones, G. C.; Martínez del Campo, T.; Shepperson, I. R.; Slaughter, J. L. *Angew. Chemie Int. Ed.* **2007**, *46*, 7075.
- (91) Neeman, M.; Caserio, M. C.; Roberts, J. D.; Johnson, W. S. *Tetrahedron*, **1959**, *6*, 36.
- (92) Barkawi, L. S.; Cohen, J. D. *Nat. Protoc.* **2010**, *5*, 1619.
- (93) Proctor, L. D.; Warr, A. J. *Org. Process Res. Dev.* **2002**, *6*, 884.
- (94) Halket, J. M.; Zaikin, V. V. *Eur. J. Mass Spectrom.* **2004**, *10*, 1.
- (95) Rathman, T. L.; Araki, S.; Hirashita, T. *Methylolithium*. *Encyclopedia of Reagents for Organic Synthesis*; John Wiley and Sons: New Jersey, **2006**.
- (96) Shindo, M.; Koga, K.; Asano, Y.; Tomioka, K. *Tetrahedron* **1999**, *55*, 4955.
- (97) Tollefson, E. J.; Dawson, D. D.; Osborne, C. A.; Jarvo, E. R. *J. Am. Chem. Soc.* **2014**, *136*, 14951.

- (98) Jastrzebski, J. T. B. H.; van Koten, G. *Structures and Reactivities of Organocopper Compounds. Modern Organocopper Chemistry.*; John Wiley and Sons: New Jersey, **2002**.
- (99) Mason, J. D.; Weinreb, S. M. *Angew. Chem.* **2017**, *129*, 16901.
- (100) Stephenson, C. R. J.; Studer, A.; Curran, D. P. *Beilstein J. Org. Chem.* **2013**, *9*, 2778.
- (101) Yan, M.; Lo, J. C.; Edwards, J. T.; Baran, P. S. *J. Am. Chem. Soc.* **2016**, *138*, 12692.
- (102) Tsang, W. *J. Am. Chem. Soc.* **1985**, *107*, 2872.
- (103) Gray, P.; Williams, A. *Chem. Rev.* **1959**, *59*, 239.
- (104) Dai, Q.; Jiang, Y.; Yu, J.-T.; Cheng, J. *Synthesis.* **2016**, *48*, 329.
- (105) Zady, M. F.; Wong, J. L. *J. Am. Chem. Soc.* **1977**, *99*, 5096.
- (106) Zhang, Y.; Feng, J.; Li, C.-J. *J. Am. Chem. Soc.* **2008**, *130*, 2900.
- (107) Xia, Q.; Liu, X.; Zhang, Y.; Chen, C.; Chen, W. *Org. Lett.* **2013**, *15*, 3326.
- (108) Teng, F.; Cheng, J.; Yu, J.-T. *Org. Biomol. Chem.* **2015**, *13*, 9934.
- (109) Rong, G.; Liu, D.; Lu, L.; Yan, H.; Zheng, Y.; Chen, J.; Mao, J. *Tetrahedron* **2014**, *70*, 5033.
- (110) Huang, Q.; Zard, S. Z. *Org. Lett.* **2018**, *20*, 1413.
- (111) Liu, W.; Yang, X.; Zhou, Z.-Z.; Li, C.-J. *Chem.* **2017**, *2*, 688.
- (112) Huff, C. A.; Cohen, R. D.; Dykstra, K. D.; Streckfuss, E.; DiRocco, D. A.; Krska, S. W. *J. Org. Chem.* **2016**, *81*, 6980.
- (113) Beaumier, E. P.; Pearce, A. J.; See, X. Y.; Tonks, I. A. *Nat. Rev. Chem.* **2019**, *3*, 15.
- (114) Zhou, Q.-L. *Angew. Chem. Int. Ed.* **2016**, *55*, 5352.
- (115) Crabtree, R. H.; Lei, A. *Chem. Rev.* **2017**, *117*, 8481.
- (116) Yan, G.; Borah, A. J.; Wang, L.; Yang, M. *Adv. Synth. Catal.* **2015**, *357*, 1333.
- (117) Li, Y.; Xue, D.; Lu, W.; Wang, C.; Liu, Z.-T.; Xiao, J. *Org. Lett.* **2014**, *16*, 66.
- (118) Le Bras, J.; Muzart, J. *Molecules.* **2018**, *28*, 1939.

- (119) Borah, A.; Goswami, L.; Neog, K.; Gogoi, P. *J. Org. Chem.* **2015**, *80*, 4722.
- (120) Prousek, J. *Pure and Appl. Chem.* **2007**, *79*, 2325.
- (121) Kawai, K.; Li, Y.-S.; Song, M.-F.; Kasai, H. *Bioorg. Med. Chem. Lett.* **2010**, *20*, 260.
- (122) Jiang, X.; Wang, C.; Wei, Y.; Xue, D.; Liu, Z.; Xiao, J. *Chem.: A Eur. J.* **2014**, *20*, 58.
- (123) Jia, J.; Jiang, Q.; Zhao, A.; Xu, B.; Liu, Q.; Luo, W.-P.; Guo, C.-C. *Synthesis*, **2016**, *48*, 421.
- (124) Obora, Y. *Top. Curr. Chem.* **2016**, *374*, 11.
- (125) Obora, Y. *ACS Catal.* **2014**, *4*, 3972.
- (126) Aurelio, L.; Brownlee, R. T. C.; Hughes, A. B. *Chem. Rev.* **2004**, *104*, 5823.
- (127) Reed-Berendt, B. G.; Polidano, K.; Morrill, L. C. *Org. Biomol. Chem.* **2019**, *17*, 1595.
- (128) Liu, Z.; Yang, Z.; Yu, X.; Zhang, H.; Yu, B.; Zhao, Y.; Liu, Z. *Adv. Synth. Catal.* **2017**, *359*, 4278.
- (129) Zhou, Z.-B.; Matsumoto, H.; Tatsumi, K. *Chem.: A Eur. J.* **2006**, *12*, 2196.
- (130) Hendrickx, R.; Johansson, J. G.; Lohmann, C.; Jenvert, R.-M.; Blomgren, A.; Börjesson, L.; Gustavsson, L. *J. Med. Chem.* **2013**, *56*, 7232.
- (131) Denmark, S. E.; Gould, N. D.; Wolf, L. M. *J. Org. Chem.* **2011**, *76*, 4260.
- (132) Xue, Y.; Xiao, H.; Zhang, Y. *Int. J. Mol. Sci.* **2015**, *16*, 3626.
- (133) Latlief, M. A.; Goldsmith, M. T.; Friedl, J. L.; Stuart, L. S. *J. Pediatr.* **1952**, *40*, 599.
- (134) Mousavi, M. P. S.; Kashefolgheta, S.; Stein, A.; Bühlmann, P. *J. Electrochem. Soc.* **2016**, *163*, 74.
- (135) Xu, R.; Xu, Y. *Modern Inorganic Synthetic Chemistry*; Elsevier Science: Amsterdam, **2017**.
- (136) Cao, Z.-C.; Xie, S.-J.; Fang, H.; Shi, Z.-J. *J. Am. Chem. Soc.* **2018**, *140*, 13575.
- (137) Wu, X.-F.; Neumann, H.; Beller, M. *Angew. Chemie Int. Ed.* **2011**, *50*, 11142.

- (138) Oderinde, M. S.; Jones, N. H.; Juneau, A.; Frenette, M.; Aquila, B.; Tentarelli, S.; Robbins, D. W.; Johannes, J. W. *Angew. Chemie Int. Ed.* **2016**, *55*, 13219.
- (139) Roglans, A.; Pla-Quintana, A.; Moreno-Mañas, M. *Chem. Rev.* **2006**, *106*, 4622.
- (140) Wenkert, E.; Han, A.-L.; Jenny, C.-J. *J. Chem. Soc., Chem. Commun.* **1988**, *14*, 975.
- (141) He, F.; Wang, Z.-X. *Tetrahedron*, **2017**, *73*, 4450.
- (142) Xie, L. G.; Wang, Z. X. *Angew. Chemie - Int. Ed.* **2011**, *50*, 4901.
- (143) Reeves, J. T.; Fandrick, D. R.; Tan, Z.; Song, J. J.; Lee, H.; Yee, N. K.; Senanayake, C. H. *Org. Lett.* **2010**, *12*, 4388.
- (144) Blakey, S. B.; MacMillan, D. W. C. *J. Am. Chem. Soc.* **2003**, *125*, 6046.
- (145) Zhang, X.-Q.; Wang, Z.-X. *Org. Biomol. Chem.* **2014**, *12*, 1448.
- (146) Zhang, H.; Hagihara, S.; Itami, K. *Chem.: A Eur. J.* **2015**, *21*, 16796.
- (147) Zhu, F.; Tao, J.-L.; Wang, Z.-X. *Org. Lett.* **2015**, *17*, 4926.
- (148) Chen, Q.; Gao, F.; Tang, H.; Yao, M.; Zhao, Q.; Shi, Y.; Dang, Y.; Cao, C. *ACS Catal.* **2019**, *9*, 3730.
- (149) Davis, H. J.; Mihai, M. T.; Phipps, R. J. *J. Am. Chem. Soc.* **2016**, *138*, 12759.
- (150) Hartwig, J. F. *Chem. Soc. Rev.* **2011**, *40*, 1992.
- (151) Wang, D.; Yang, Z.; Wang, C.; Zhang, A.; Uchiyama, M. *Angew. Chemie Int. Ed.* **2018**, *57*, 3641.
- (152) Wang, D.-Y.; Wen, X.; Xiong, C.-D.; Zhao, J.-N.; Ding, C.-Y.; Meng, Q.; Zhou, H.; Wang, C.; Uchiyama, M.; Lu, X.-J. *iScience* **2019**, *15*, 307.
- (153) Angelini, G.; Speranza, M.; Wolf, A. P.; Shiue, C.-Y. *J. Fluor. Chem.* **1985**, *2*, 177.
- (154) Haka, M. S.; Kilbourn, M. R.; Leonard Watkins, G.; Toorongian, S. A. *J. Label. Compd. Radiopharm.* **1989**, *27*, 823.
- (155) Sun, H.; DiMagno, S. G. *J. Fluor. Chem.* **2007**, *128*, 806.
- (156) Uemura, T.; Yamaguchi, M.; Chatani, N. *Angew. Chemie Int. Ed.* **2016**, *55*, 3162.

- (157) Burns, J. T.; Leffek, K. T. *Can. J. Chem.* **1969**, *47*, 3725.
- (158) Sawicka, M.; Storoniak, P.; Skurski, P.; Blazejowski, J.; Rak, J. *Chem. Phys.* **2006**, *324*, 425.
- (159) Storoniak, P.; Rak, J. *J. Therm. Anal. Calorim.* **2000**, *60*, 927.
- (160) Aihara, Y.; Chatani, N. *J. Am. Chem. Soc.* **2013**, *135*, 5308.
- (161) Per H J Carlsen, Katerina Liberkova, Rachel Harrex, J. R. *Acta Chem. Scand.* **1997**, *51*, 343.
- (162) Francis, C. US20050261500A1, **2004**.
- (163) Yu, Linda; Hsin, Ling-Wei; Lee, T.-C. WO/2018/157233, **2018**.
- (164) Hartenstein, Johannes; Fritschi, E. US4425350A, **1980**.
- (165) Noonan, G.; Leach, A. G. *Org. Biomol. Chem.* **2015**, *13*, 2555.
- (166) Levi, D. W.; Reich, L.; Lee, H. T. *Polym. Eng. Sci.* **1965**, *5*, 135.
- (167) Castillo, N.; Boyd, R. J. *J. Chem. Theory Comput.* **2006**, *2*, 271.
- (168) Rodewald, R. F.; Mahendran, K.; Bear, J. L.; Fuchs, R. *J. Am. Chem. Soc.* **1968**, *90*, 6698.
- (169) Weaver, W. M.; Hutchison, J. D. *J. Am. Chem. Soc.* **1964**, *86*, 261.
- (170) Pregosin, P. S. *Magn. Reson. Chem.* **2017**, *55*, 405.
- (171) Strauss, S. H. *Chem. Rev.* **1993**, *93*, 927.
- (172) Plakhotnyk, A. V; Ernst, L.; Schmutzler, R. *J. Fluor. Chem.* **2005**, *126*, 27.
- (173) Hansch, C.; Leo, A.; Taft, R. W. *Chem. Rev.* **1991**, *91*, 165.
- (174) Brown, D. G.; Boström, J. *J. Med. Chem.* **2016**, *59*, 4443.
- (175) Wang, Z.; Richter, S. M.; Gates, B. D.; Grieme, T. *Org. Process Res. Dev.* **2012**, *16*, 1994.
- (176) Lam, T. T.; Vickery, T.; Tuma, L. *J. Therm. Anal. Calorim.* **2006**, *85*, 25.

- (177) Yang, Q.; Sheng, M.; Henkelis, J. J.; Tu, S.; Wiensch, E.; Zhang, H.; Zhang, Y.; Tucker, C.; Ejeh, D. E. *Org. Process Res. Dev.* **2019**, *23*, 2210.
- (178) Smith, P. W. G.; Thatchell, A. R.; Hannaford, A. I.; Furniss, B. S. *Textbook of Practical Organic Chemistry*; John Wiley and Sons: New York, **1996**.
- (179) Zhang, X.-Q.; Wang, Z.-X. *J. Org. Chem.* **2012**, *77*, 3658
- (180) Reed, H.; Paul, T. R.; Chain, W. J. *J. Org. Chem.* **2018**, *83*, 11359.
- (181) Martínez-Martínez, A. J.; Weller, A. S. *Dalt. Trans.* **2019**, *48*, 3551.
- (182) Verkerk, U.; Fujita, M.; Dzwiniel, T. L.; McDonald, R.; Stryker, J. M. *J. Am. Chem. Soc.* **2002**, *124*, 9988.
- (183) Chen, J.; Ko, S.; Liu, L.; Sheng, Y.; Han, H.; Li, X. *New. J. Chem.* **2015**, *39*, 3736.
- (184) Glasnov, T. N.; Holbrey, J. D.; Kappe, C. O.; Seddon, K. R.; Yan, T. *Green Chem.* **2012**, *14*, 3071.
- (185) Huang, C.; Liang, T.; Harada, S.; Lee, E.; Ritter, T. *J. Am. Chem. Soc.* **2011**, *133*, 13308.
- (186) Patel, P.; Borah, G. *Chem. Commun.* **2017**, *53*, 443.
- (187) Groombridge, B. J.; Goldup, S. M.; Larrosa, I. *Chem. Commun.* **2015**, *51*, 3832.
- (188) Routasalo, T.; Helaja, J.; Kavakka, J.; Koskinen, A. M. P. *European J. Org. Chem.* **2008**, *18*, 3190.
- (189) Cetin, M. M.; Hodson, R. T.; Hart, C. R.; Cordes, D. B.; Findlater, M.; Casadonte, D. J.; Cozzolino, A. F.; Mayer, M. F. *Dalt. Trans.* **2017**, *46*, 6553.
- (190) Magnin, L. P.; Zargarian, D. *Organometallics.* **2019**, *38*, 4687.
- (191) Smith, A. B.; Kurti, L.; Davulcu, A. H.; Cho, Y. S.; Ohmoto, K. *J. Org. Chem.* **2007**, *72*, 4611.
- (192) Iqbal, P. F.; Bhat, A. R.; Azam, A. *Eur. J. Med. Chem.* **2009**, *44*, 2252.
- (193) Chowdhury, S.; Samuel, P. M.; Das, I.; Roy S. *J. Chem. Soc. Chem. Commun.* **1994**, *17*, 1993.

- (194) Sajiki, H.; Mori, A.; Mizusaki, T.; Ikawa, T.; Maegawa, T.; Hirota, K. *Org. Lett.* **2006**, *8*, 987.

Chapter 2 – Clavulanic Acid Production on the Manufacturing Scale

2.1 Introduction

This chapter-specific introduction aims to provide a brief account of the chemistry of antibiotics from their initial discovery through to modern day developments; particular focus will be made upon β -lactam containing compounds such as penicillins and cephalosporins. The pertinent issue of antibiotic resistance will be highlighted, leading to a discussion of the β -lactamase inhibitor, clavulanic acid.

2.1.1 Introduction to Antibiotics

Antibiotics are a type of pharmacological agent used in treating bacterial infections.¹⁹⁵ Differences between bacterial cells and cells belonging to the host organism are exploited in order to kill bacteria without causing damage to the mammalian host cells. Bactericidal antibiotics are capable of killing bacteria whilst bacteriostatic antibiotics work by preventing the growth of bacteria and thus aid, rather than replace the immune system in clearing a bacterial infection. Some antibiotic drugs are capable of killing a wide range of bacteria, these are known as *broad spectrum antibiotics*; conversely, antibiotics that are active against a small variety of bacteria are known as *narrow spectrum antibiotics*.^{196,197}

Though the terms aforementioned can be used to categorise antibiotics into two separate classes, a more common method of classifying antibiotics is *via* their chemical structure; each of these classifications having different modes of action and being active against different bacterial species. Four of the antibiotic classes with the largest market shares are given with their general structure in **Figure 1**. The β -lactam containing *cephalosporins* and *penicillins* are the two most widely prescribed antibiotics. *Fluoroquinolones* and *tetracyclines* are both used less commonly than β -lactam antibiotics, but they represent a significant portion of the antibiotic market share nonetheless. *Macrolides* are 12-16 membered lactone rings with one or more deoxy sugar attached via glycosidic linkages. *Aminoglycosides* are glycosides modified with amino groups. Both macrolides and aminoglycosides are amongst the highest revenue antibiotic classifications but due to the immense variability within

each classification, neither type can be depicted effectively with a single structural motif.¹⁹⁸

Although there is a vast range of antibiotic types available, this project focuses specifically on penicillin and β -lactam compounds. The discovery of penicillin is widely regarded as one of the biggest breakthroughs in modern medicine and its discovery in 1928 revolutionised the medical field.¹⁹⁹

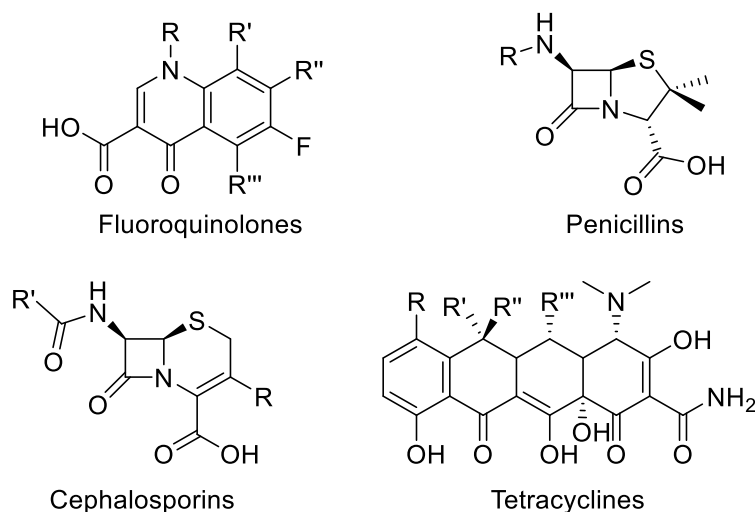


Figure 1. General chemical structure of fluoroquinolones, penicillins, cephalosporins and tetracyclines.^{196,200–202}

The Discovery of Penicillin

Germ theory was first proposed by Girolamo Fracastoro in 1546 and it suggested that disease could be caused by microorganisms such as bacteria, fungi and viruses. The theory started to gain acceptance throughout the 19th century but it was not until a series of pioneering experiments carried out by Robert Koch and Louis Pasteur that the necessary compelling evidence was collated.^{196,197,203} The acceptance of germ theory by the scientific community inspired a wealth of bacteriological research which led to the identification of bacteria responsible for a variety of diseases that were prevalent at the time such as cholera, tuberculosis, and anthrax.²⁰⁴

One of the first practical applications of germ theory was work carried out by the surgeon Joseph Lister at the Glasgow Royal Infirmary. After becoming aware of the

work carried out by Pasteur, Lister sought to develop antiseptic techniques that could be used on surgical wards to reduce the chances of patient infection and disease. Phenol, then known as carbolic acid, was applied to patient wounds and was used to clean surgical equipment before usage. The rate of death caused by infection saw a large decrease after Joseph Lister started to employ these antiseptic techniques on his ward. Whilst phenol is effective at killing bacteria, it also has a range of undesirable side effects on human patients such as corrosiveness through protein-degeneration, killing white blood cells resulting in a diminished immune system, and causing damage to the central nervous system.²⁰⁵

During this period of intensive bacteriological research, scientists began to search for a so called “magic bullet”. The term “magic bullet” was coined by the German biochemist Paul Ehrlich; in this context it refers to a drug that can kill a desired bacterium (one responsible for a particular disease) without causing any harm to the patient hosting the bacteria.²⁰⁶ A particular strain of bacteria named *Treponema pallidum* was discovered to be the cause of the disease syphilis (one which was particularly prevalent during this era). Ehrlich was investigating the effects of various chemical compounds on *Treponema pallidum* with the aim of finding a chemotherapeutic agent capable of killing the bacteria and thus eradicating syphilis. In 1909, an arsenic containing compound arsphenamine, later marketed as Salvarsan, was found to be an effective candidate and was the most efficacious cure for syphilis up until the early 1940s. At the time, it was believed to exist as an As=As double bonded dimer but a recent study by Lloyd *et al.* showed through mass spectrometry that it actually exists primarily as the As single bonded trimer and pentamer (**Figure 2**).^{196,197,207}

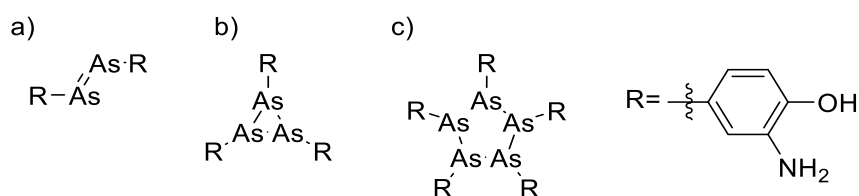


Figure 2. Salvarsan was believed to exist as the As=As double bonded dimer (a) during its time of use; a 2005 mass spectrometry study showed that it actually exists primarily as a mixture of the As-As single bonded trimer (b) and pentamer (c).²⁰⁷

In 1921, a scientist named Alexander Fleming who was a bacteriologist working in St. Mary's hospital in London, discovered a substance in his own mucus that had bactericidal properties.²⁰⁸ He named this substance lysozyme due to its lytic properties and his belief (which would later prove to be correct) that lysozyme was an enzyme of some kind.²⁰⁹ Further research showed that lysozyme was found in various other human secretions; although it had antibacterial properties, it was not effective in killing any of the bacteria that were known to be harmful so it had no practical applications and the scientific community took little notice of the discovery.^{210,211}

Fleming, upon returning from a vacation in 1928, was washing up old cell cultures when he noticed that one of the plates had been contaminated with spots of mould. He noticed that, around the perimeter of these mould contaminations, the colonies of *Staphylococci* that were intentionally grown on the plate were translucent and smaller than everywhere else on the plate. From this observation, he deduced that the mould was producing a substance capable of killing the bacteria in the petri dish.^{199,203} The mould in question was *Penicillium notatum* and the chemical responsible for the bactericidal properties of its secretion was named penicillin. The findings of this research were published in 1929 by Alexander Fleming; however, the therapeutic potential of penicillin was not immediately recognised.²⁰⁹ Fleming and his co-workers attempted to isolate penicillin from the mould's secretion but had limited success due to the instability of penicillin and the small quantities produced by the mould. For many years, penicillin remained little more than a curiosity with its main application being the isolation of penicillin-sensitive bacteria from penicillin-insensitive bacteria.^{209,211,212}

In order to try and progress his research, Fleming passed on some of his cultures to Howard Florey and Ernst Chain at the University of Oxford.^{197,199} In 1939, the group started to produce penicillin on a larger scale, *via* fermentation of *Penicillin notatum*, with the intention to carry out animal experiments and clinical trials. Norman Heatley, a biochemist in the group, developed a novel method of extracting penicillin from the fermentation filtrate *via* liquid-liquid extraction (**Figure 3**). Penicillin-containing aqueous fermentation filtrate was acidified to pH 2 with phosphoric acid immediately before being extracted into amyl-acetate; the penicillin is then reported to have been transferred back into phosphate-buffer solution or water *via* a counter-current

extraction process.²¹³ The initial clinical trials showed that penicillin was capable of preventing death from an otherwise lethal dose of *Streptococci* in mice.²¹⁴ Similar promising results were observed in human patients but clinical trials were hindered by low drug supplies.²¹⁵

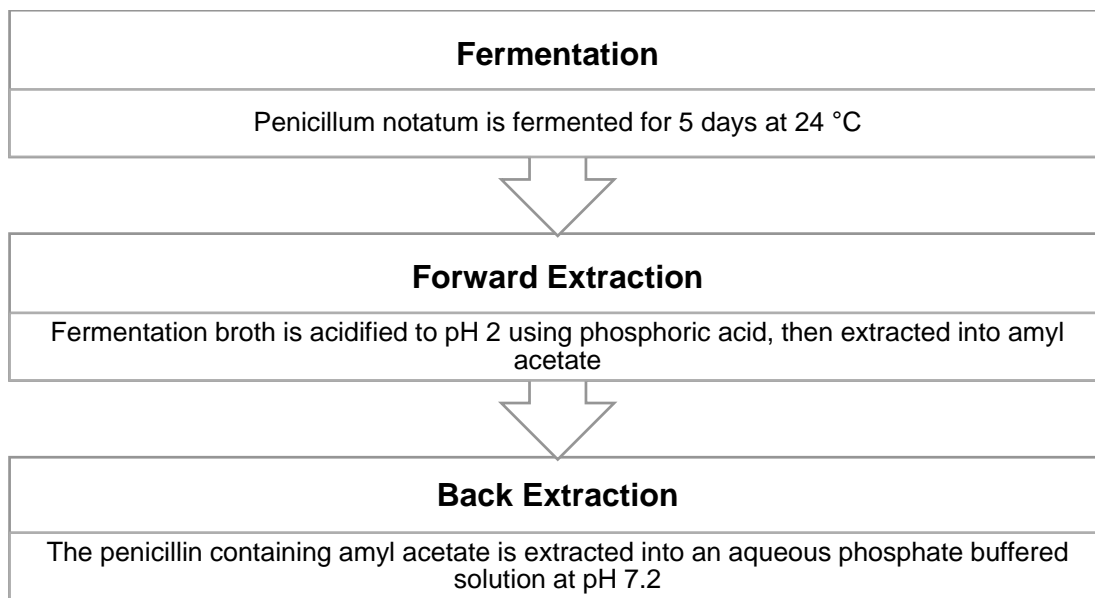


Figure 3. Flow diagram of the penicillin extraction process developed by Heatley.²¹³

Once the potential of penicillin as a chemotherapeutic agent was recognised, and with the high demand for antibacterial agents arising from the war, intensive efforts were put in to producing penicillin on a large scale. Part of this research was carried out at the Northern Regional Research Laboratory in Illinois, USA. By using corn-steep liquor (a by-product from their milling process) and penicillin precursors in the fermentation medium, a ten-fold increase in yield was observed versus that which was obtained with the fermentation medium used by Heatley *et al.*¹⁹⁹ A vast number of other *Penicillium* strains were also tested in order to find strains that were more productive than *Penicillium notatum*. Eventually, the strain *Penicillium chrysogenum* was discovered inside a mouldy cantaloupe from a food market in Illinois which was capable of producing penicillin titres of 60-150 µg/mL (compared to *ca.* 1.2 µg/mL from *Penicillium notatum*).^{216,217} Through exposure to high energy radiation and multiple rounds of mutagenesis, the yields of penicillin were increased further still;

strains currently used in industry are capable of producing titres of up to 50,000 $\mu\text{g/mL}$.²¹⁷⁻²²¹

With clinical trials showing promising results for penicillin, in conjunction with increasingly efficient methods of producing penicillin and governmental subsidies, pharmaceutical industries started to invest their efforts into producing penicillin on a commercial scale. The first commercial penicillin production plant was opened by Pfizer in 1944 producing 1.66 trillion units of penicillin in its first year of operation, the rate of production continued to rise exponentially over the following few years and in 1946 penicillin became available to the general public as a prescription drug.^{199,218} When penicillin was first discovered, the antibiotic market was virtually non-existent; since then the drug market has seen vast amount of growth and has evolved beyond recognition. Despite the turbulent nature of the pharmaceutical industry, penicillin remains an important and competitive drug type worldwide.

The Structure of Penicillin

Fermentation was, and is still today, the most efficient way of producing penicillin; however, during early research efforts, fermentation methods still gave relatively low yields and limited techniques were available to isolate penicillin from the fermentation broth.²¹⁹ These factors led scientists working in the area to try and determine the chemical structure of penicillin in hopes that a more fruitful total synthesis could then be devised.²²² The task was very difficult due to the limited, low purity samples of penicillin available, as well as the limited number of analytical techniques compared to those available in the 21st century.

Information about the structure of penicillin came from a series of systematic retrosynthetic disconnections and tests for particular functional groups.^{222,223} It was found that the addition of acid to aqueous penicillin solutions would liberate CO_2 gas and the penicillin yielded its nitrogen atoms as ammonium chloride and an amino acid; this amino acid was isolated in its crystalline form and named penicillamine (**Figure 4**).^{224,225} The presence of sulfur was detected in penicillin through a sodium fusion test, and a geminal dimethyl group was predicted then later proven via synthesis. Mercuric chloride was used to identify the presence of a thiazolidine ring.^{222,226,227}

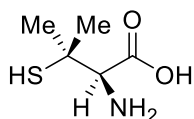


Figure 4. Structure of penicillamine.²²⁵

The information that was obtained about penicillin led to the proposal of two different thiazolidine-containing structures from different people within the team working on this project. Robert Robinson deduced that the structure of penicillin was an oxazolone-thiazolidine (**Figure 5**).²²⁶

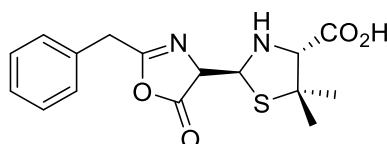


Figure 5. Oxazolone-thiazolidine structure of penicillin proposed by Robinson.^{222,226}

Through electrometric titration studies, Edward Abraham noticed a lack of a weak basic group that would be expected from the nitrogen atom on the thiazolidine ring proposed by Robinson. This data led Abraham to propose a structure for penicillin that included a β -lactam moiety fused to a thiazolidine ring (**Figure 6**); the β -lactam functional group had not previously been found in a naturally occurring product and the structure was not well received by his senior colleague, Robinson. Despite conflict within the group, both structures had a significant amount of support within the field, neither Abraham nor Robinson was able to prove their prediction to be the correct one.^{196,222,226}

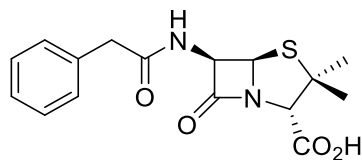


Figure 6. β -Lactam containing structure of penicillin proposed by Abraham.^{222,226}

Dorothy Hodgkin was a pioneer of X-ray crystallography working at the University of Oxford. She had, during the 1940s, been gaining recognition for her work on

elucidating the structure of Sterol. Hodgkin gathered X-ray diffraction data and interpreted it to solve the three-dimensional crystal structure of penicillin.²²⁸ The technique was still in its infancy and the task of determining the structure *via* crystallography was one that required a lot of patience and ingenuity from Hodgkin. By comparing the diffraction patterns of sodium, potassium, and rubidium salts of penicillin, Hodgkin was able to conclusively prove the structure of the molecule.^{229,230} The structure proposed by Abraham which includes the conformationally strained β -lactam motif (**Figure 6**) was shown to be correct. The 3D structural model presented by Hodgkin was crafted from wire and corks. Modern digital representations of the structure have also been generated (**Figure 8**, *vide infra*).

Rather than referring to one particular structure, the term penicillin can be used to classify a range of molecules. Penicillins all contain the same β -lactam-thiazolidine bicyclic core structure and vary only by the side chain appended to the β -lactam ring. There are five natural penicillin structures known, the two most common amongst these are penicillin G and penicillin V. The core structure with a simple primary amine in place of the side chain is called 6-aminopenicillanic acid (6-APA) and is commercially important as it is a precursor to semi-synthetic penicillins (**Figure 7**). The structure that was elucidated by Hodgkin was that of benzylpenicillin which is more commonly referred to as penicillin G.^{229,231,232}

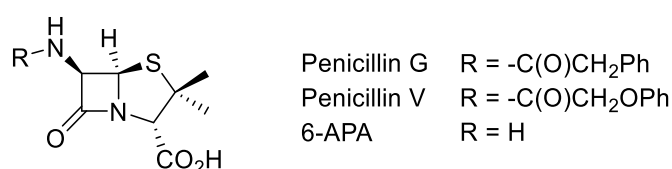


Figure 7. Generic structure of penicillin molecules with side chain groups for penicillin G, penicillin V and 6-APA shown.^{231,232}

The β -lactam moiety in the structure of penicillin plays an important role in defining the characteristics of the molecule as a whole. Lactams can be described as cyclic amides; amides tend to be resistant to nucleophilic addition and hydrolysis due to a resonance stabilisation energy obtained from delocalisation of nitrogen's lone pair of electrons over the carbonyl group. In order to maximise this resonance stabilisation energy, amides will typically adopt a planar geometry. Penicillins are unstable over a

range of conditions, and crystallography has shown that the amide group within the penicillin core is not planar (**Figure 8**).²³³

The lack of planarity arises from the conformation of the fused β -lactam and thiazolidine rings. The strain introduced to the β -lactam ring by the thiazolidine means that the lactam nitrogen has more sp^3 character than sp^2 character.^{234,235} The extent to which electrons can delocalise across the N-C(O) bond is reduced and thus the amide bond no longer has as much π -bonding character as would be observed in a linear (i.e. acyclic) analogue. The lower C-N bond order in the β -lactam ring means that the C=O bond behaves more like a ketone carbonyl than an amide carbonyl, and thus is more electrophilic than would be expected of an amide carbonyl. The reduced ability of bridgehead nitrogen atoms to donate electron density across amide bond was demonstrated by Tani and Stoltz through the analysis of 2-quinuclidonium salts.²³⁶ It has been estimated that a β -lactam fused to a thiazolidine is more reactive than a lone β -lactam by approximately two orders of magnitude. The lone β -lactam is, in turn more reactive than a linear amide by a further two orders of magnitude.²³⁷ Aside from the lack of stabilisation through resonance, there is also an inherent instability associated with small rings arising from torsional and angular ring strain.²³⁸ The susceptibility of the β -lactam moiety to nucleophilic addition contributes to the instability of penicillins but, concurrently, it is also instrumental to its mode of action, and will be discussed later in this introduction.

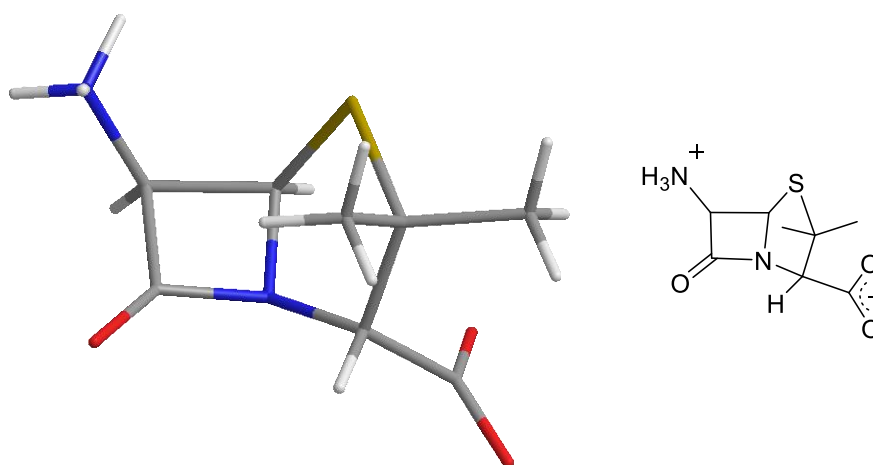


Figure 8. Conformational structure of 6-APA in its zwitterionic form determined by X-ray crystallography which displays the non-planar nature of the β -lactam arising from the fused ring system.²³³

The Synthesis of Penicillin

Once the chemical structure of penicillin was confirmed, intensive efforts were made to devise a total synthesis of the antibiotic. The desire to come up with a synthesis was driven by the potential for a more efficient and controllable production method than fermentation. More importantly, synthetic efforts towards penicillin were driven by harnessing the ability to create analogues of the naturally occurring penicillins. Though the structure of penicillin was confirmed by Hodgkin in 1945, it wasn't until 1957 that a synthesis was successfully formulated by J. C. Sheehan at Massachusetts Institute of Technology.^{196,239}

The major synthetic challenge faced when making penicillin V was the incorporation of a β -lactam ring. The sensitivity of this functional group to a range of conditions required the ring to be formed during the last step of the synthesis.²⁴⁰ Methods of making amide bonds prior to the work carried out by Sheehan required harsh conditions that were disruptive to the rest of the molecule.²⁴¹ In the research leading up to this synthesis, it was discovered by Sheehan that aliphatic carbodiimides such as dicyclohexylcarbodiimide (DCC) were effective as coupling reagents between carboxylic acids and amines under mild conditions.^{239,242} It was hypothesised that the treatment of a suitably functionalised thiazolidine precursor with an amide coupling reagent would afford the β -lactam-containing penicillin V target.

In the original total synthesis of penicillin V (**Figure 9**), the thiazolidine ring was formed by reacting racemic *tert*-butyl phthalimidomalonaldehyde (**1**) with D-penicilloic acid (**2**), a good yield was achieved by isomerising the undesired products and recrystallizing them. The required stereoisomer (**3**) was deprotected with hydrazine then subsequently reacted with phenoxyacetyl chloride to attach the phenoxy side chain which is characteristic of penicillin V. The *tert*-butyl ester (**5**) was deprotected with HCl to afford a penicilloic acid (**6**) in high yield then DCC was used to perform an intramolecular cyclisation to form the β -lactam ring and complete the synthesis of penicillin V (**7**).^{239,243}

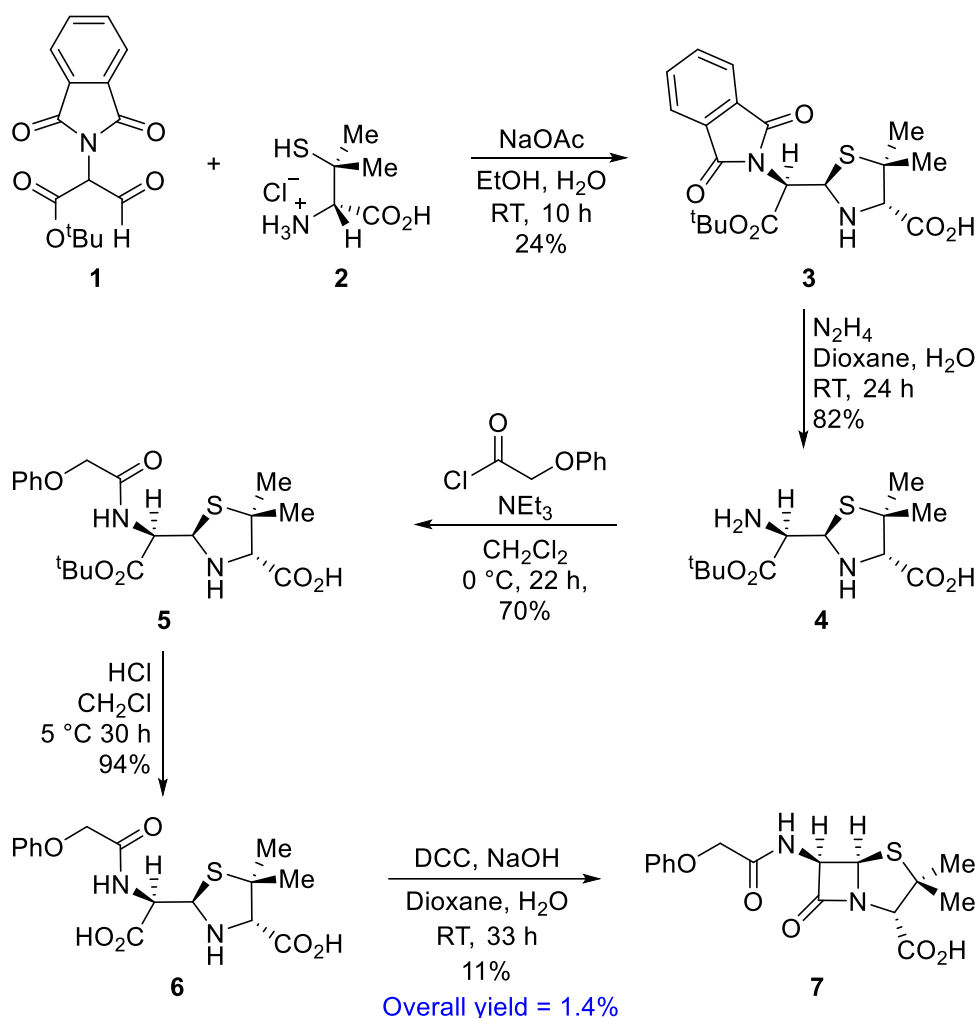


Figure 9. Reaction scheme for the total synthesis of penicillin V designed by J. C. Sheehan.^{239,243}

The total synthesis of penicillin is not as efficient as fermentation methods so it is not used to produce penicillin industrially. Although the synthesis itself is not industrially applicable, the research efforts spanning over a decade facilitated the development of new synthetic technologies such as amide coupling reagents which are widely used in both an academic and industrial setting.^{242,244} Furthermore, the total synthesis of penicillin created the potential for synthetic analogues of naturally occurring penicillins to be discovered. Penicillins with different side chains were created to combat problems with instability or antibiotic resistance.²⁴⁵ New penicillin products are often made by semi-synthetic means; penicillin G or V are produced by fermentation, their respective side chains are then cleaved via chemical or enzymatic

means to form 6-APA.²³¹ The use of penicillin acylase enzymes tends to be preferred in the process of manufacturing semi-synthetic penicillins as they are environmentally and economically favoured.^{245,246} 6-APA is then *N*-acylated with the desired side chain, this was classically carried out through formation of a mixed anhydride but modern industrial methods use an enzymatic process.^{247,248}

Penicillin is known to degrade rapidly in acidic conditions which is attributed, in part, to the ability of the side chain carbonyl to act as a nucleophile, opening the β -lactam ring.²⁴⁵ By adding electron-withdrawing groups such as phenol or carboxyl substituents on to the side chain, the electron density on the carbonyl is reduced along with its nucleophilic tendency.²³² Amoxicillin, ampicillin, and ticarcillin are all semi-synthetic penicillins with improved pharmacological properties owing to acid resistance from these modifications (**Figure 10**).²⁴⁹

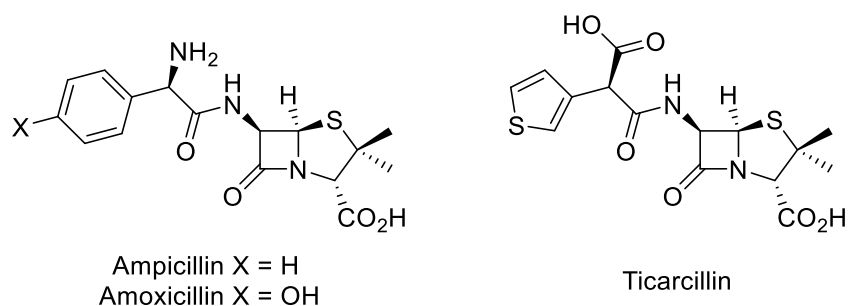


Figure 10. Structures of acid resistant semi-synthetic antibiotics ampicillin, amoxicillin and ticarcillin. Each contains an electron withdrawing group to reduce nucleophilicity of the side chain carbonyl.²⁴⁹

A similar approach has been taken to produce β -lactamase resistant antibiotics, incorporating sterically bulky groups to hinder the approach of nucleophilic residues of β -lactamase enzymes; methicillin, flucoxacillin, and oxacillin were all designed in this way (**Figure 11**).^{245,250}

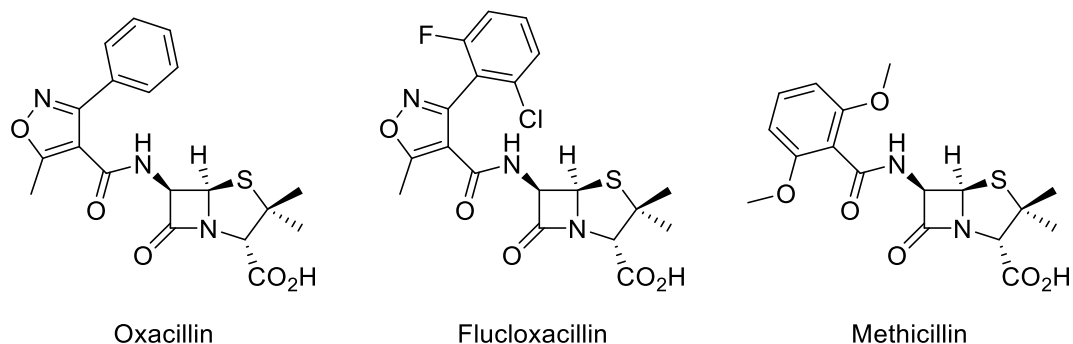


Figure 11. Structures of oxacillin, flucloxacillin and methicillin, semi-synthetic antibiotics that are active against β -lactam resistant bacteria due to the incorporation of a bulky group in their side arm.²⁵⁰

Cephalosporins are a family of β -lactam antibiotics closely related to penicillins and are widely used in the antimicrobial industry.²⁵¹ The structure of cephalosporins comprise of a β -lactam ring fused with a dihydrothiazine ring and are adorned with side chains analogous to penicillins (**Figure 12**).²⁰⁰ Cephalosporin C is produced by *Cephalosporium acremonium*; an acylase enzyme is used to cleave the side chain to afford 7-aminocephalosporanic acid (7-ACA).²⁵² 7-ACA is then acylated to and make semi-synthetic cephalosporin analogues in a strategy similar to that of penicillins *via* 6-APA.²⁵³ The mechanism by which cephalosporins work against bacteria is the same as penicillin and other β -lactam antibiotics, this will be discussed in the next section of this introduction.

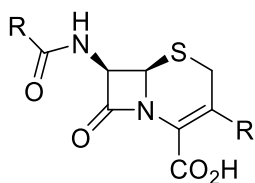


Figure 12. General structure of cephalosporins.²⁰⁰

β-Lactam Antibiotic Mechanism of Action

β-Lactam antibiotics target the cell wall in order to kill bacteria. A cell wall is a mesh-like structure of biopolymers that envelopes the cell to impart structural rigidity and to prevent osmotic pressure from rupturing the cell.^{254,255} The main polymer present in cell walls is named peptidoglycan which consists of alternating sugars *N*-acetylglucosamine and *N*-acetylmuramic acid, cross-linked by small peptide chains. Early experiments showing that bacteria adopted filamentous shapes when exposed to penicillin and that radioactively labelled penicillin G accumulated on the cell wall made it clear to investigators that bacterial cell walls were the target of β-lactam antibiotics.^{254,256} It was not until the later identification of peptidoglycan and subsequent insights into its biosynthetic pathway that the way in which the antibiotics disabled the cell wall was fully understood.

The cross-linking between peptidoglycan chains occurs between stem pentapeptides on neighbouring strands, the process is called *transpeptidation* and is carried out *via* transpeptidase enzymes (TP) which are also known as penicillin binding proteins (PBP). The cross-linking is essential for the cell wall to have the necessary structural integrity to withstand the high osmotic pressure a bacterial cell experiences.²⁵⁵ There is a large number of known PBPs in existence, these are divided into two broad categories,,: High molecular weight (HMW) and low molecular weight (LMW). Further subclasses A, B and C, are also used to describe PBPs based on domain organisation; most bacterial species possess at least 2 different classes of PBP.^{257,258}

PBPs contain a catalytic serine residue and general lysine base, the serine residue covalently binds to the *D*-alanine-*D*-alanine terminus of a donor pentapeptide strand. An amino group of an acceptor strand can then attack this acyl-enzyme intermediate to release the cross-linked peptidoglycan. β-lactam groups are conformationally very similar to the terminal *D*-alanine-*D*-alanine of peptidoglycan stem pentapeptides (**Figure 13**), this allows the drugs to access the active site of PBPs.²⁵⁸

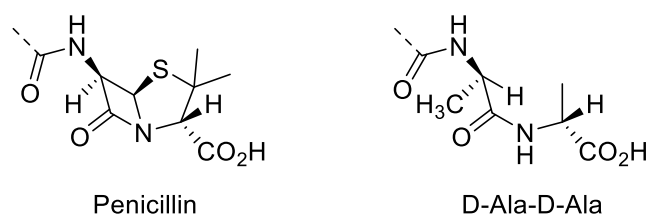


Figure 13. 3D depiction of penicillin and a D-Ala-D-Ala portion of a peptide chain highlighting the conformational similarity between the two structures.^{233,258}

The serine residue, upon deprotonation from a lysine base, cleaves the β -lactam ring of the antibiotic open, forming a stable covalently bonded enzyme-drug complex (**Figure 14**).^{256,258,259} The resulting adduct that is formed has a long lifetime which means the PBP is not available for transpeptidation and thus, cannot perform its function. With the inability to cross-link peptidoglycan strands, defects start to arise across the cell wall; cells will first start to elongate as osmotic pressure rises and then bulges form along the cell wall until it eventually ruptures and the cell dies.²⁶⁰

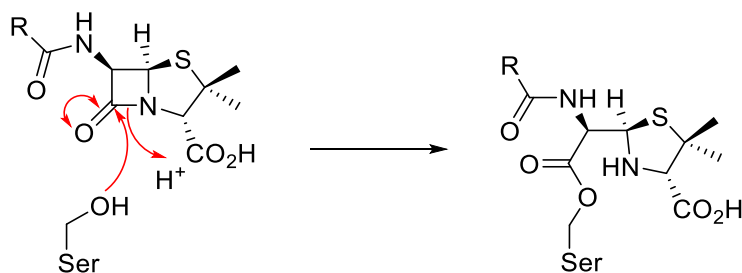


Figure 14. A simplified mechanism showing a serine residue in the active site of PBP forming a covalent adduct with a penicillin molecule by opening the β -lactam ring.^{256,258,259}

β -Lactam Antibiotic Resistance

From the moment a drug reaches the market, its lifetime starts to diminish due to evolved drug resistance.²⁰⁶ Resistance to penicillin was noted within two years of its commercial use. However, more alarmingly, clinically significant resistance to drugs

can be apparent just months after their widespread use.²⁶¹ Antibiotic resistance is a growing problem in 21st century society and pharmaceutical researchers are under increasing pressure to combat the global issue.^{196,262}

One way in which cells can develop resistance to a drug is to prohibit the drug from entering the cell. Over producing membrane proteins can create a so called efflux pump that has the ability to pump drugs out of the cell such that their concentration is too low to take effect.²⁶² Similarly, mutations in the structure of the cell can serve to reduce cell membrane permeability and thus stop drugs from reaching the intended target.²⁶³ Another mechanism of drug resistance is changing the receptor of a drug target such that the antibiotic is no longer recognised. In the context of β -lactam antibiotics, mutated forms of PBP have been discovered that have a lower affinity to the pharmaceutical agent than typically observed.²⁶⁴ The PBP2' enzyme is one such mutated transpeptidase that is present in some antibiotic resistant bacteria, it has a low binding affinity for all known β -lactam antibiotics and is the molecular basis for the Methicillin-resistant *Staphylococcus aureus* (MRSA) phenotype, a widely spread antibiotic resistant bacteria.²⁶²

The most prevalent resistance mechanism of β -lactam antibiotics and in the context of this project, the most relevant, is drug inactivation. Through evolutionary processes, cells often develop methods of modifying drugs to render them inactive before they can reach their target. Many bacteria produce a type of enzyme named β -lactamase that have such an effect on β -lactam containing antibiotics.²⁶⁵ β -Lactamases open the β -lactam ring of antibiotics using a nucleophilic serine residue, the resulting acyl-enzyme complex is easily cleaved with a water molecule from the active site to regenerate the enzyme. The effect of this is that β -lactam antibiotics are catalytically decomposed before they can reach their PBP targets. There are over 2500 β -lactamases that have currently been discovered and the number is still increasing.^{266,267}

There are three main ways in which antibiotic resistance is combated. Whilst not eradicating the problem, taking care not abuse antibiotics by unnecessary use can help to significantly slow down the rate in which resistance spreads.²⁶⁸ Another method is to design novel drugs that can circumvent the resistance mechanisms by changing the drug target.^{269,270} Vancomycin for instance is a synthetic glycopeptide antibiotic used

as a last resort against antibiotic resistant bacteria (**Figure 15**). Like β -lactam antibiotics, vancomycin affects the cell wall transpeptidation; however, rather than blocking the active site of PBPs, it takes effect by binding to the peptidoglycan substrate to stop it from reaching the PBP.²⁷¹ β -Lactam antibiotics themselves have also been altered in order to become less prone to β -lactamase facilitated degradation, this can be a fairly effective approach but, given the highly mutagenic nature of bacteria, resistance to new drug analogues is normally developed.^{249,250}

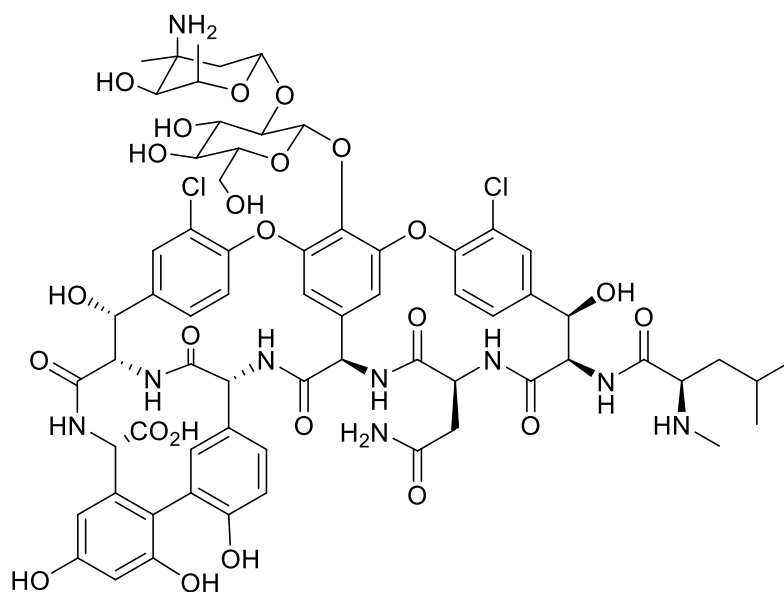


Figure 15. Structure of vancomycin, a synthetic glycopeptide antibiotic.²⁵³

The final way in which antibiotic resistance can be retarded is by combination therapy of a working antibiotic with an agent that combats the resistance mechanism. In the case of β -lactam antibiotics, chemicals that can inhibit the β -lactamase enzyme allow the antibiotics to persist for enough time to exhibit their bactericidal properties. There are 3 different β -lactamase inhibitors currently available on the drug market that are each co-administered with a different β -lactam antibiotic (**Figure 16**). Tazobactam is administered alongside piperacillin, sulbactam with either ampicillin or cefoperazone, and clavulanic acid with amoxicillin. Of these combinations, clavulanic acid and amoxicillin is the most commonly prescribed; it first reached the market with the brand

name Augmentin under the production of Beechams which, over time became GlaxoSmithKline.²⁷² Clavulanic acid is administered in the form of its potassium clavulanate salt as this has more desirable pharmacological properties than the free acid.

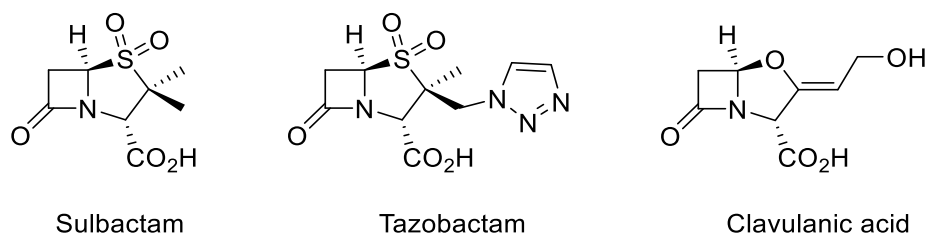


Figure 16. Structures of the three β -lactamase inhibitors that are currently available on the drug market, sulbactam, tazobactam and clavulanic.²⁷³

The Discovery of Clavulanic Acid

Since resistance to β -lactam antibiotics was first observed, scientists set about discovering analogues of penicillin with a lower susceptibility to β -lactamases. During a screening experiment of β -lactam producers, *Streptomyces clavuligerus* was found to produce clavam metabolites that showed resistance to β -lactamases. Clavulanic acid (CA) was isolated and identified as the molecule responsible for activity against β -lactamase.^{196,273} Clavam molecules are those which contain a bicyclic β -lactam-oxazolidinone nucleus that can be functionalised in the 2 and 3 positions (**Figure 17**).²⁷⁴ The chirality of the carbon atom at the ring junction plays an important part in the biological activity of the clavam molecule.²⁷⁵

The structure of CA is very similar to that of penicillins varying only in the lack of acylamino side chain, an oxygen atom in place of sulphur to give an oxazolidinone ring rather than a thiazolidine ring, and the inclusion of a hydroxyethylidene chain (**Figure 17**).²⁷⁶⁻²⁷⁸ The *5R,3R* stereochemistry of clavulanic acid which was determined by X-ray crystallography is essential for its activity as a β -lactamase inhibitor.^{275,279,280} $5S$ -Clavams can exhibit a bactericidal effect by inhibiting bacterial homoserine-O-

succinyl transferase.^{276,279} Clavulanic acid itself has antibiotic properties against a wide range of Gram-positive and Gram-negative bacteria; however, its potency is too low to be of practical use administered alone. Instead, clavulanic acid is co-administered with a more active antibiotic, namely amoxicillin (*vide supra*).^{265,273,281}

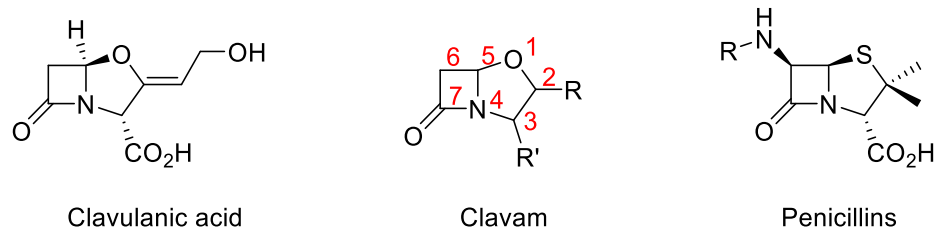


Figure 17. The structure of clavulanic acid (left) and the general structures of clavam compounds (middle) and penicillins (right).^{273,274}

Historically, there have been multiple attempts to classify the varied family of β -lactamase enzymes according to substrate, isoelectric focus, inhibitory properties, and molecular structure.^{277,282–285} Each of the classification systems have their merits and the most useful system in each particular case is dependent on the context. One of the most widely used classification systems is the Ambler system which categorises β -lactamases into two groups: serine enzymes and zinc enzymes.²⁷⁷ The serine enzymes all use serine residues to catalyse the antibiotic inactivation; these are separated into classes A, C, and D depending on their amino acid sequence. The serine hydroxyl group acts as a nucleophile to facilitate the opening of the β -lactam ring (**Figure 18**). Class B enzymes, also known as metallo- β -lactamases (MBLs) contain zinc atoms that assist the opening of the β -lactam ring (**Figure 19**).

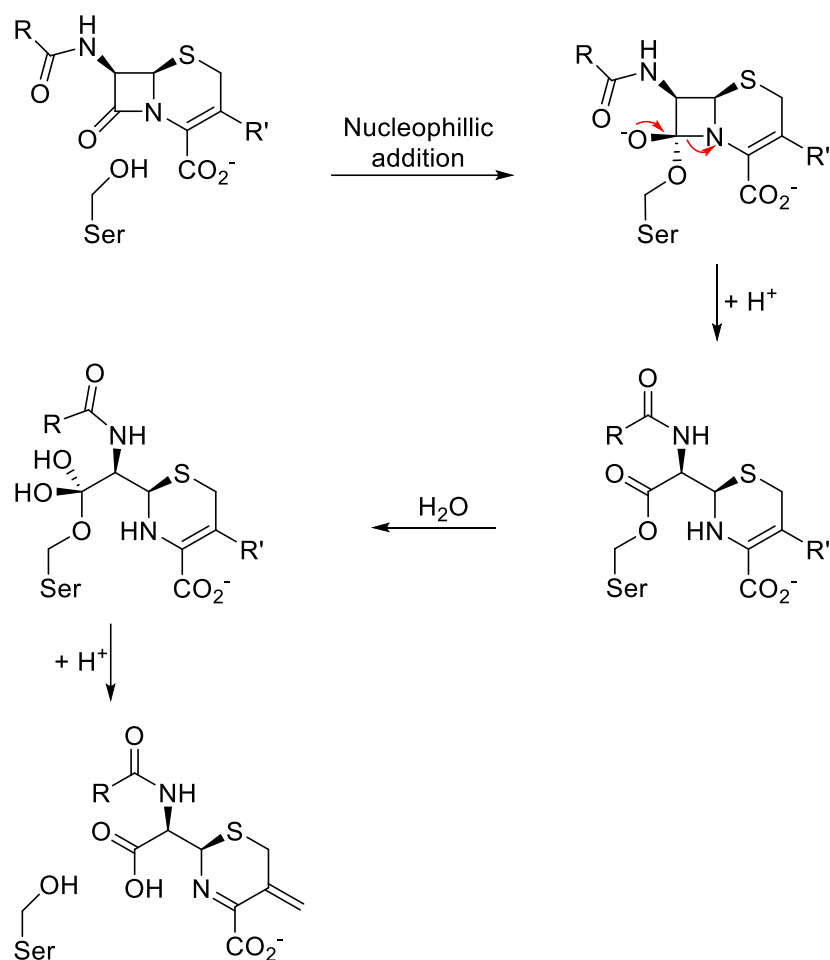


Figure 18. Simplified mechanism of a serine enzyme catalysing the degradation of a cephalosporin β -lactam antibiotic.²⁸⁶

The MBL enzymes are of particular concern because they are able to catalyse the degradation of all existing classes of β -lactam antibiotic with the exception of monobactams.²⁸⁷ Current chemotherapeutic agents such as clavulanic acid do not exhibit any inhibitory effect on MBLs.^{288,289} There is much structural diversity within the MBL family and in a similar fashion to serine enzymes, they are broken down into three subclasses: B1, B2, and B3; the assigned classification is dependent on the amino acid sequence within each enzyme.²⁸⁷ The active site of an MBL contains either one or two zinc atoms that are necessary for its activity; the exact catalytic mechanism of these metallo-enzymes remains somewhat ambiguous and appears to vary between individual members of the MBL family.^{287,289} Though the exact mechanism is not

known, extensive studies have discovered that zinc atoms in the MBL active site can serve two key roles to assist in the catalysis of β -lactam antibiotics.

Zinc atoms within an MBL active site carry an effective positive charge and have the ability to act as Lewis acids. The β -lactam carbonyl oxygen atom has been shown to coordinate to zinc in the active site, this serves to generate a more electron-deficient neighbouring carbon and thus increases its susceptibility to nucleophilic attack.²⁸⁶ Furthermore, the coordination of oxygen to zinc helps to stabilise the developing negative charge on the anionic tetrahedral intermediate that is formed upon nucleophilic attack (**Figure 19**).²⁸⁹

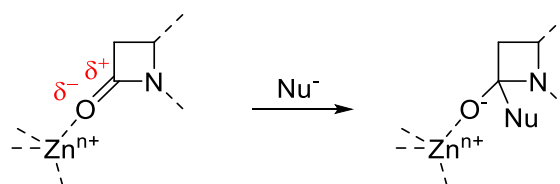


Figure 19. Facilitation of nucleophilic attack on β -lactam carbonyl through coordination of carbonyl oxygen to zinc in the MBL active site.²⁸⁹

The ligands associated with zinc vary between each enzyme but are typically a combination of histidine, aspartic acid, cysteine, asparagine, and/or glycine residues, and one or more water molecule.²⁹⁰ The pK_a of the associated water molecule is lowered from its coordination to zinc which means it can easily be deprotonated to form a metal-bound hydroxide species. This coordinated hydroxide ion has the ability to act as a nucleophile and catalyse the breakdown of β -lactam antibiotics through addition onto the carbonyl (**Figure 20**).²⁸⁹

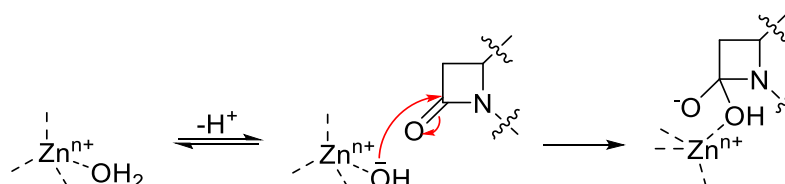


Figure 20. Ligation to zinc lowers the pK_a of water molecules allowing the facile formation of metal-bound hydroxide species, these can then act as nucleophiles to degrade β -lactam rings.²⁸⁹

The β -lactam functional group of clavulanic acid is responsible for its action as a β -lactamase inhibitor; the lactam ring is opened in a mechanism similar to that of penicillins at the PBP active site. Whereas β -lactam antibiotics undergo a ring opening reaction catalysed by β -lactamase followed by a rapid cleavage of the acyl-enzyme complex to regenerate the enzyme (*vide supra*), the clavulanic acid acyl-enzyme complex persists for a longer period of time (**Figure 21**).^{286,291} The long lifetime of this complex means that the enzyme is inhibited for enough time that the co-administered antibiotic can reach the PBP to kill the bacterial cells. Clavulanic acid can be described as a suicide inhibitor as it is itself degraded in order to inhibit the enzyme.²⁹²

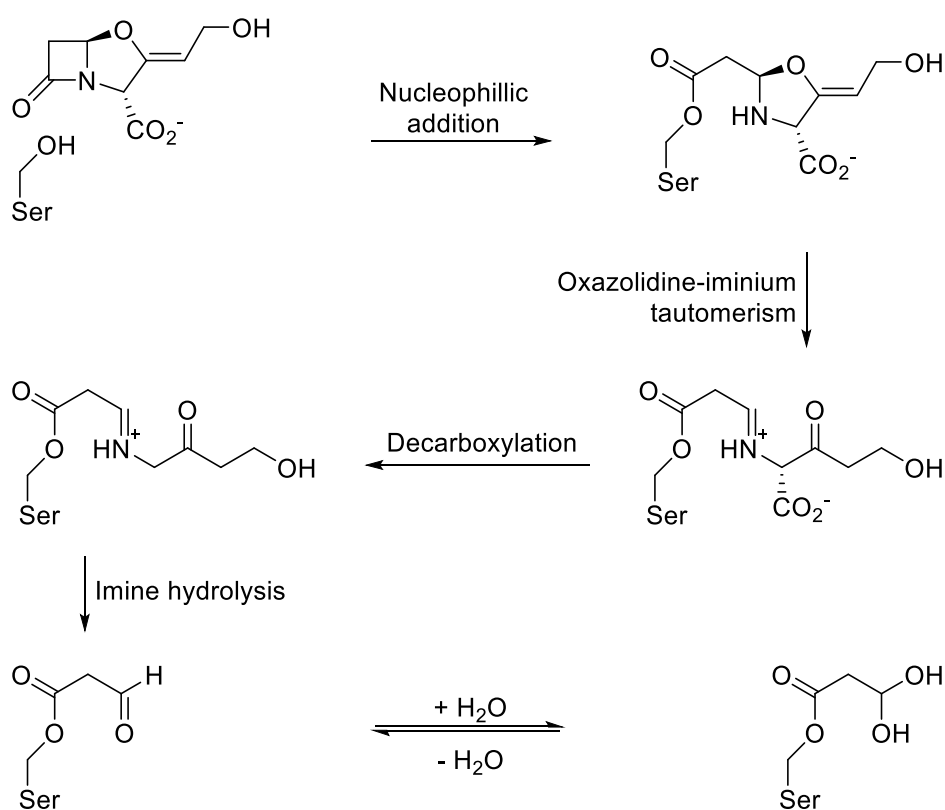


Figure 21. Mechanism of β -lactamase inhibition by clavulanic acid.²⁹¹

2.1.2 The Synthesis of Clavulanic Acid

Total Synthesis of Clavulanic Acid

As with β -lactam antibiotics, there are several challenges which must be overcome in order to devise a total synthesis of clavulanic acid. To date, there has been only two reported total syntheses of clavulanic acid, both of which were reported by Peter Bentley and co-workers at Beechams, and each route affords a racemic mixture of clavulanic acid.^{293–295}

The first total synthesis designed by the Bentley group was in 1977 (**Figure 22**).²⁹⁵ The first step of the synthesis was the N-alkylation of 4-(methylthio)azetidin-2-one (**8**) with dimethyl 2-bromo-3-oxoglutarate and 2 equiv. sodium hydride in dimethylformamide; the reaction afforded the β -ketodiester (**9**), which was largely in the enol form, in 29 % yield. The chlorine derivative of **9** was formed by treating it with an excess of chlorine in carbon tetrachloride, a base induced cyclization in dimethylformamide followed by an aqueous work up afforded the racemic bicyclic diester (**10**) in 34 % yield. An alkene isomerisation of the diester was achieved by irradiating **10** with UV light from a low pressure mercury lamp in benzene; the Z isomer (**11**) was gained in a 2:3 mixture. Diisobutyl aluminium hydride was used to reduce the diester to (\pm)-methyl clavulanate (**12**); the reaction yield is reported to be low but the exact yield is not quoted. It is stated that (\pm)-methyl clavulanate is convertible to (\pm)-clavulanic acid (**13**) although a procedure and yield for this step was not reported by the group.²⁹⁵

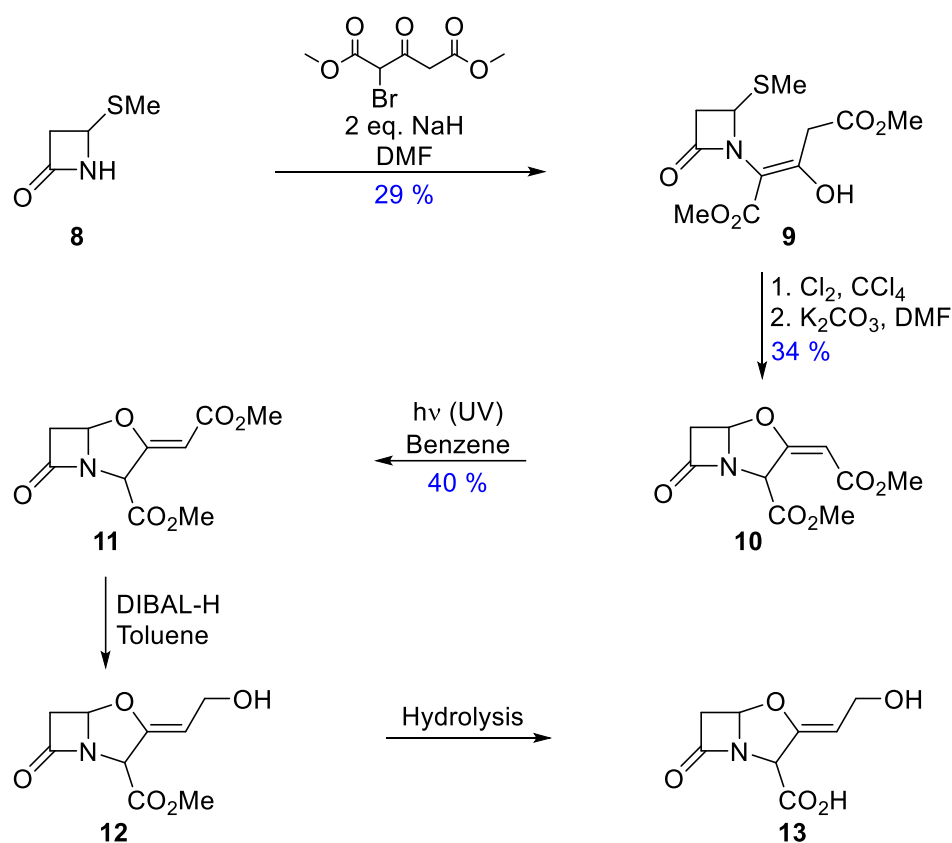


Figure 22. Reaction scheme for the first total synthesis of clavulanic acid designed by Bentley *et al.*²⁹⁵

A second total synthesis of clavulanic acid was carried out by Bentley *et al.* in 1979 (**Figure 23**).²⁹⁴ The synthesis started by acylating the starting material (**14**) with vinyl acetyl chloride in THF in the presence of lithium bis(trimethylsilyl)amide to give an enolic ester (**15**) in 64% yield. A chlorinolysis using chlorine in carbon tetrachloride was performed followed by a base catalysed cyclization with triethylamine to afford the racemic bicyclic diene (**16**). Treatment of the diene with ozone in ethylacetate formed the ozonide (**17**) in 65% yield. The final step was a hydrogenation of the ozonide using 10% Pd/C to give (\pm)-methyl clavulanate (**18**) in 9% yield. As with the previous synthesis, the elaboration of (\pm)-methyl clavulanate to (\pm)-clavulanic acid is not directly reported; the racemic methyl clavulanate product was obtained in an overall yield of 0.86%.²⁹⁴

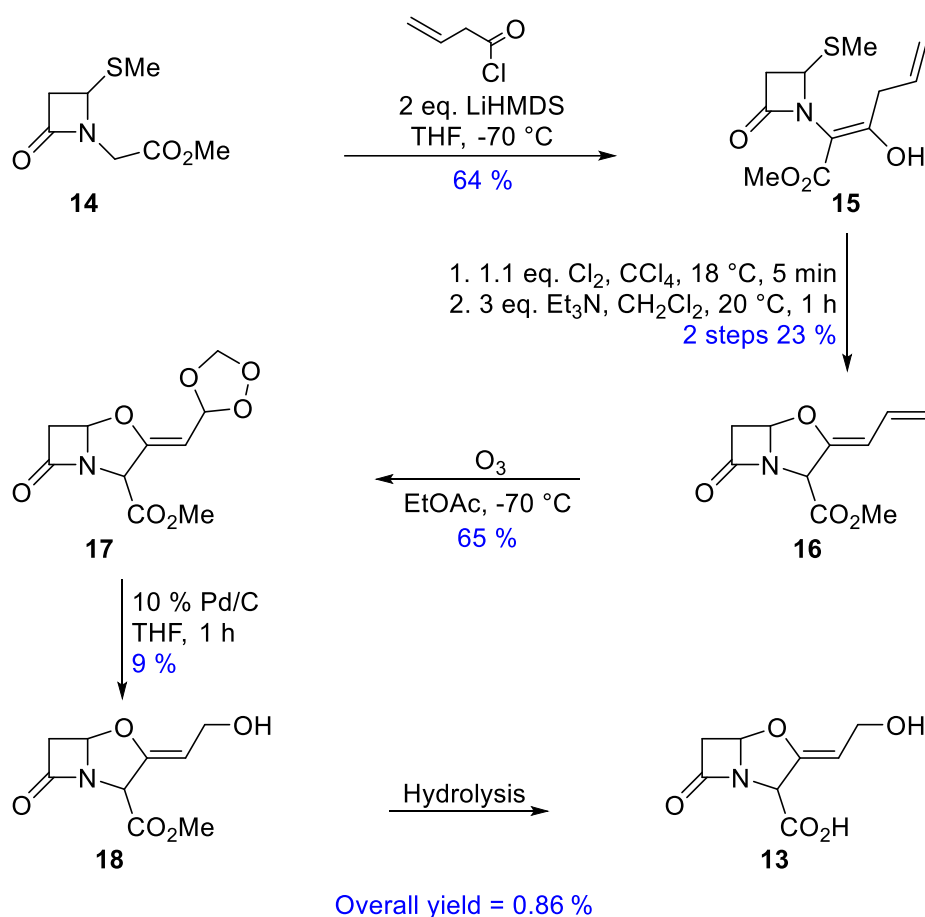


Figure 23. Reaction scheme for the second total synthesis of clavulanic acid designed by Bentley *et al.*²⁹⁴

Both of the total syntheses designed by Bentley *et al.* are low yielding and do not proceed with stereocontrol.^{294,295} Furthermore, the conditions used for a number of steps (such as carbon tetrachloride solvent) would not be suitable on a process scale. Given the large quantities of clavulanic acid prescribed across the globe, it would not be feasible to meet this demand by synthetic means.

Fermentative Synthesis of Clavulanic Acid

As with most other β -lactam containing antibiotics, fermentation methods are the most efficient way of producing clavulanic acid on a commercial scale; particularly by the fed-batch method due to its operational simplicity and superior productivity.²⁹⁶ *Streptomyces clavuligerus* is the species of bacterium that is used to produce clavulanic

acid industrially, though other species of the *Streptomyces* genus have been shown to produce CA.²⁹⁷ The biosynthetic pathway for clavulanic acid production via *S. clavuligerus* has not been fully characterised but studies have been carried out that give a reasonably comprehensive insight as to how the metabolite is made in nature.²⁹⁸

S. clavuligerus does not exclusively produce CA, a range of other primary and secondary metabolites are formed. These metabolites include, but are not limited to, penicillin N, cephamycin C and a host of other clavams (5S clavams) that do not possess the 3R, 5R geometry that is essential for β -lactamase inhibitory properties.²⁹⁷ The biosynthetic pathway followed to make CA is shared in part with other clavams produced; however, the biosynthesis of CA is different to that of conventional antibiotics such as cephalosporins and penicillins.^{298,299} It was initially speculated that the biosynthetic pathway of clavulanic acid was shared with other bicyclic β -lactam antibiotics such as cephalosporins based on the fact both compounds can be produced by the same species of bacterium.²⁹⁷ The conventional β -lactam antibiotics are produced via the tripeptide precursor δ -(L- α -aminoadipyl)-L-cysteinyl-D-valine (**Figure 24**), more commonly known as the Arnstein peptide.³⁰⁰

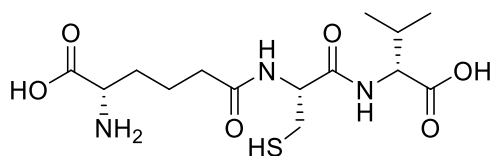


Figure 24. Structure of the δ -(L- α -aminoadipyl)-L-cysteinyl-D-valine, a tripeptide precursor in the biosynthesis of penicillins and cephalosporins.³⁰⁰

A lack of evidence for an intermediate analogous to the Arnstein peptide suggested that CA may be produced via a different pathway to conventional β -lactam antibiotics.³⁰¹ Enzymes known to be responsible for penicillin and cephalosporin synthesis were shown to have an incompatible substrate-specificity to CA precursors which further opposed the credibility of a shared pathway. Initial feeding studies suggested amino acids such as arginine or ornithine condensed with an intermediate in

a 3C glycolytic pathway in the early stages of CA synthesis; arginine and pyruvate were eventually determined to be direct precursors of CA.³⁰²

Metabolites from a mutant *S. clavuligerus* strain blocked in CA production yielded a positive Sakaguchi colour test result, thus indicating the presence of one or more guanidino groups. These metabolites were isolated, structurally determined and then synthesised with ¹³C building blocks. The labelled analogues were shown through feeding experiments to be directly incorporated into CA synthesis, proving their role as intermediates in the biosynthetic pathway.³⁰³ The structure of one of these acyclic intermediates, N²-(2-carboxyethyl)-arginine (CEA), suggested that the condensation of pyruvate and arginine take place by a mechanism different to that of a ribosomal peptide synthetase which is involved with the synthesis of penicillin and cephamycin; a lack of genetic evidence for a peptide synthetase was used to support this proposal.³⁰¹

An overview of steps from arginine and pyruvate through to clavulanic acid is given (**Figure 25**). L-Arginine and pyruvate are condensed to form CEA by the N²-(2-carboxyethyl)-arginine synthase (CEAS) enzyme, this step is dependent on a thiamin diphosphate cofactor.³⁰⁴ The β -lactam ring is next formed by the β -lactam synthetase (BLS) enzyme to make deoxyguanidinoproclavamate; this step has a stark contrast from the tripeptide intramolecular condensation to form the β -lactam ring in penicillins and cephalosporins. The structure and reactivity of BLS resembles asparagine synthetases responsible for producing asparagine in nature; BLS however, has a larger active site to accommodate the CEA substrate and favours β -lactam formation over interdomain amide formations.^{298,301}

Deoxyguanidinoproclavamate is stereoselectively hydroxylated by clavamate synthase (CAS) and then proclavamate amidinohydrolase (PAH) catalyses the removal of the guanidino group to yield the key intermediate proclavamate.^{298,303} CAS Catalyses a cyclisation reaction of proclavamate to form the oxazolidine ring and generate the bicyclic intermediate dihydroclavamate; the same enzyme then catalyses a third reaction whereby it desaturates the side chain to yield clavamate.^{301,304} Clavamate is the last common intermediate in 5S clavam and clavulanic acid synthesis; it can be elaborated on to a range of 5S clavams. In the case of CA synthesis, a double epimerisation proceeds to form clavaldehyde which has the

3R, 5R geometry on the β -lactam oxazolidine ring which is essential for β -lactamase inhibition.

The exact mechanism by which (3S,5S)-clavamate is converted to (3R,5R)-clavaldehyde is not fully understood; recent studies have suggested that this proceeds through an N-glycyl-clavaminic acid intermediate.^{305,306} Interestingly, the unstable clavaldehyde intermediate exhibits β -lactam inhibition which supports the theory this effect relies on the 3R, 5R stereochemistry.³⁰¹ The final step of the biosynthetic pathway is the reduction of clavaldehyde to clavulanic acid via the enzyme clavulanic acid dehydrogenase (CAD), which uses an NADPH cofactor and is able to reduce the aldehyde functionality without altering the β -lactam ring.³⁰⁷

Although the biological synthesis of CA is superior to total synthesis in terms of yield and efficiency, wild type *S. clavuligerus* is still not sufficient for production on a global scale. Competing metabolic pathways such as cephamycin production decrease the yield of CA and morphological differences in bacteria can lead to inconsistencies between fermentation batches. In order to circumvent these problems as much as possible, intensive strain development have been undertaken to impart more desirable properties on the CA producing *S. clavuligerus* bacteria. The biology involved with strain development is currently outside the scope of this project but a brief overview will be given.²⁹⁹

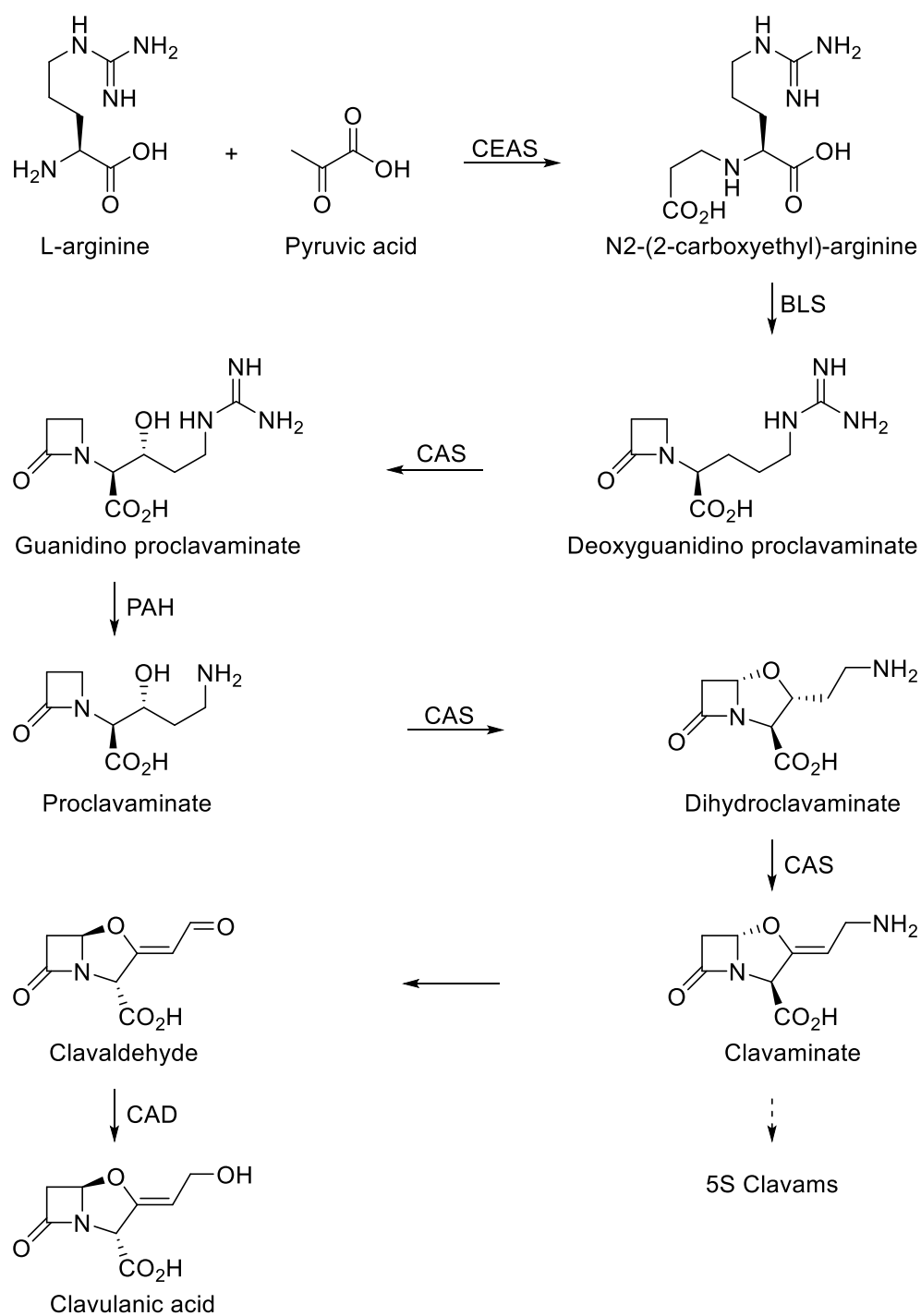


Figure 25. Overview of clavulanic acid biosynthetic pathway.^{273,298}

S. clavuligerus is capable of making CA, cephamycin C, and a range of other primary and secondary metabolites.²⁹⁸ In the industrial production of CA, it is beneficial to minimise the reactions leading to these other metabolites as they divert the overall flow of chemicals and energy away from the CA pathway.²⁹⁷ D-glyceraldehyde-3-

phosphate (G3P) is a precursor to clavulanic acid that is involved in the glycolytic pathway, in wild type *S. clavuligerus* approximately 80% of the G3P produced continues in the non-productive glycolytic pathway leaving only 20% to be elaborated into CA.³⁰⁸ It has been shown through feeding studies that G3P is a limiting factor in CA biosynthesis; a targeted approach to increasing the G3P pool in *S. clavuligerus* cultures was sought.^{308,309} Glyceraldehyde-3-phosphate dehydrogenase (GAPDH) is the enzyme responsible for the competing conversion of G3P into 1,3-biphosphoglycerate; *gap* genes are essential for GAPDH production in *S. clavuligerus*. The glycolytic pathway was genetically engineered by selectively inactivating two *gap* genes to stop GAPDH production. The result was an increased G3P pool which was responsible for an increase in CA titre compared to the wild-type strain by over 100%.^{297,308,310}

Similarly, the production of non-related 5S clavams was eradicated *via* the deletion of open reading frames essential for 5S clavam synthesis.³¹¹ The expression of positive regulatory genes has also been increased via gene modification to increase the production of CA. Aside from improvements in yield by retarding competing metabolic pathways and up regulation of CA biosynthesis, certain developments on *S. clavuligerus* strains can impart more desirable physical properties onto fermentation batches that improve the efficiency of the extraction processes subsequent to fermentation.³⁰⁸

Improved strains of *S. clavuligerus* increase the potential yield of CA but, in order for that potential to be realised, great care must be taken in the fermentation process. Consistency and repeatability between fermentation batches is often difficult to obtain due to morphological differences in bacteria.³¹² The production process can be split into 3 processes; (i) inoculum development, (ii) microbiological synthesis, and (iii) CA recovery.²⁷³ Dormant *S. clavuligerus* is activated and developed as a preculture medium to inoculate the fermentation vessel. The production of CA is strongly dependent on inoculum activity and it has been shown in previous fermentation studies that the early growth fermentation phase must be optimal in order for the remainder of the fermentation process to be successful.³¹³

On an industrial scale, multiple development steps are required to produce enough of the preculture medium to inoculate the large vessels, this is usually carried out through multiple discreet stages and it presents difficult challenges in terms of producing consistent batches between fermentation cycles. Differences in biomass concentration, cell density, and metabolic activity are usually the key contributory factors to yield variability so it is necessary for the preculture medium to be monitored before each fermentation cycle. Chromatographic analysis of the gas given off by the preculture is used to provide information about the batch and how it can be managed.³¹⁴

Though the quality of the inoculum dictates the production potential of a fermentation batch, the fermentation media must be controlled to realise that potential. The effect of different fermentation media substituents on the yield of CA has been studied by various groups in the past. Since bacteria are responsible for producing CA it is important to add the correct feedstock to a fermentation batch to maintain an environment in which they can thrive and are optimal for CA production. Factors such as pH, temperature, carbon source, nitrogen source, agitation speed, and oxygen availability have all been shown to affect the outcome of a fermentation.^{310,315–317} The optimal conditions for a fermentation batch will also depend on the strain of *S. clavuligerus* used; certain strain developments can be made in an attempt to produce CA under conditions which are cheaper or more preferable. Mutations to the wild-type *S. clavuligerus* have made it possible to utilise glucose as a carbon source, similarly strain screening programmes have been used to identify strains that are productive at the pH levels at which clavulanic acid degradation is minimal.^{308,314}

Since clavulanic acid is known to be unstable in solution, it is essential to extract and isolate it from the fermentation broth in a timely manner. The details of the extraction process used by each company are often closely guarded as the industry is competitive and any small advantage in the process can make a significant difference to operation costs or product quality. A summary will be given of the extraction process used at GSK Irvine in order to give context of the conditions that clavulanic acid is found in throughout the process; however, the detail in which each step is described will be somewhat limited due to the sensitivity of this information.

Extraction of Clavulanic Acid

After the fermentation has been carried out to give a suitable titre, the entire broth is transported to the extraction area. The broth contains the dissolved CA produced from *S. clavuligerus* but also a plethora of cell matter, proteins and other substances that need to be removed from the final product. The multi-stage process is described below and summarise in **Figure 26**.

The first stage of the process forces the fermentation broth through stacks of a semi-permeable membrane under pressure, this is known as ultrafiltration (UF). UF is designed to remove solid materials and any dissolved molecules that are 1000 Da or more in molecular weight; the UF filtrate contains CA as the free acid.³¹⁸ As the process progresses it becomes more difficult to push the broth through the membranes, when flow rate drops below a predefined level diafiltration (DF) is employed. DF is an operational mode of the UF process whereby water is added to the fermentation broth to aid separation of microsolute (those that pass through the UF membrane) and macrosolute (those that do not pass through the UF membrane).³¹⁹ The employment of DF allows an efficient separation and helps ensure a high recovery yield of CA; however, it does also result in large volumes of filtrate to be processed further downstream.³²⁰

Once the required level of UF permeate is collected, it is then subjected to a reverse osmosis (RO) step. RO processes the mixture through a membrane with appropriate porosity under pressure; the membrane can pass a small amount clavulanic acid but the vast majority is retained. The result of this process is the removal of water from the process liquor to give a concentrated CA solution on the upstream side of the membrane. The RO concentrate is directed back to RO feed vessel from which it was delivered and the flow is recycled in this manner until the mixture reaches the required concentration.³²¹

The concentrated aqueous CA solution can contain some solutes at this stage that would become insoluble upon lowering the pH of solution; these are named acid precipitable solids (APSs). The RO concentrate is passed through a hydrophobic synthetic acrylic-ester-resin which is a good adsorbent for large uncharged

compounds; the APSs are adsorbed onto the resin whilst the percolate containing CA is passed downstream towards the next stage of the process.^{322,323}

The process liquor is filtered through to a carbon column to remove further impurities but in order to do that, CA is first transferred from an aqueous to an organic medium. The post-resin aqueous sample, which is now free of APSs, is treated with sulfuric acid to lower its pH, the acidification ensures that all CA in solution is in its protonated free acid form. The rich aqueous solution is then injected into a counter current extractor (CCE) where it is rapidly mixed with methyl isobutyl ketone (MiBK); during mixing a mass transfer of CA from water to MiBK is observed.³²⁴ The disparity of density between the two immiscible solvents is exploited to separate them; rich MiBK can then be passed through a column containing activated carbon onto which impurities, particularly those that are coloured will be adsorbed.

The transfer of CA into MiBK is optimal for carbon column treatment but an aqueous solution is preferable and as such back extraction takes place. The pH of rich MiBK is raised using *tert*-butylamine: the addition of base will serve to deprotonate CA.³²⁵ Mixing between MiBK and water transfers the clavulanate anions along with *tert*-butylammonium (t-BA) cations into the aqueous phase and the two phases are separated via centrifugal force. The rich aqueous aliquots are further pH adjusted with nitric acid after back extraction is complete to aid with the removal of an impurity. The t-BA clavulanate salt is stored as an isolable intermediate as degradation is drastically slower in the solid state with an absence of moisture.³²⁶ Using organic amines other than *tert*-butylamine to isolate clavulanate has been demonstrated to leave amine traces in the final product. Addition of acetone to the aqueous t-BA clavulanate solution with cooling causes the salt to precipitate as a slurry which is then washed, dried and kegged for storage until product is required.

Potassium clavulanate is the form in which the β -lactamase inhibitor is administered hence the final stage of this process is to convert t-BA clavulanate to potassium clavulanate. To a solution of t-BA clavulanate in isopropyl alcohol (IPA) and water, potassium 2-ethylhexanoate (KEH) is added; a salt metathesis reaction occurs to yield insoluble potassium clavulanate and soluble t-BA 2-ethylhexanoate.³²⁷ The potassium

clavulanate is filtered and dried and then blended with an excipient for future processing, or amoxicillin for the production of Augmentin.

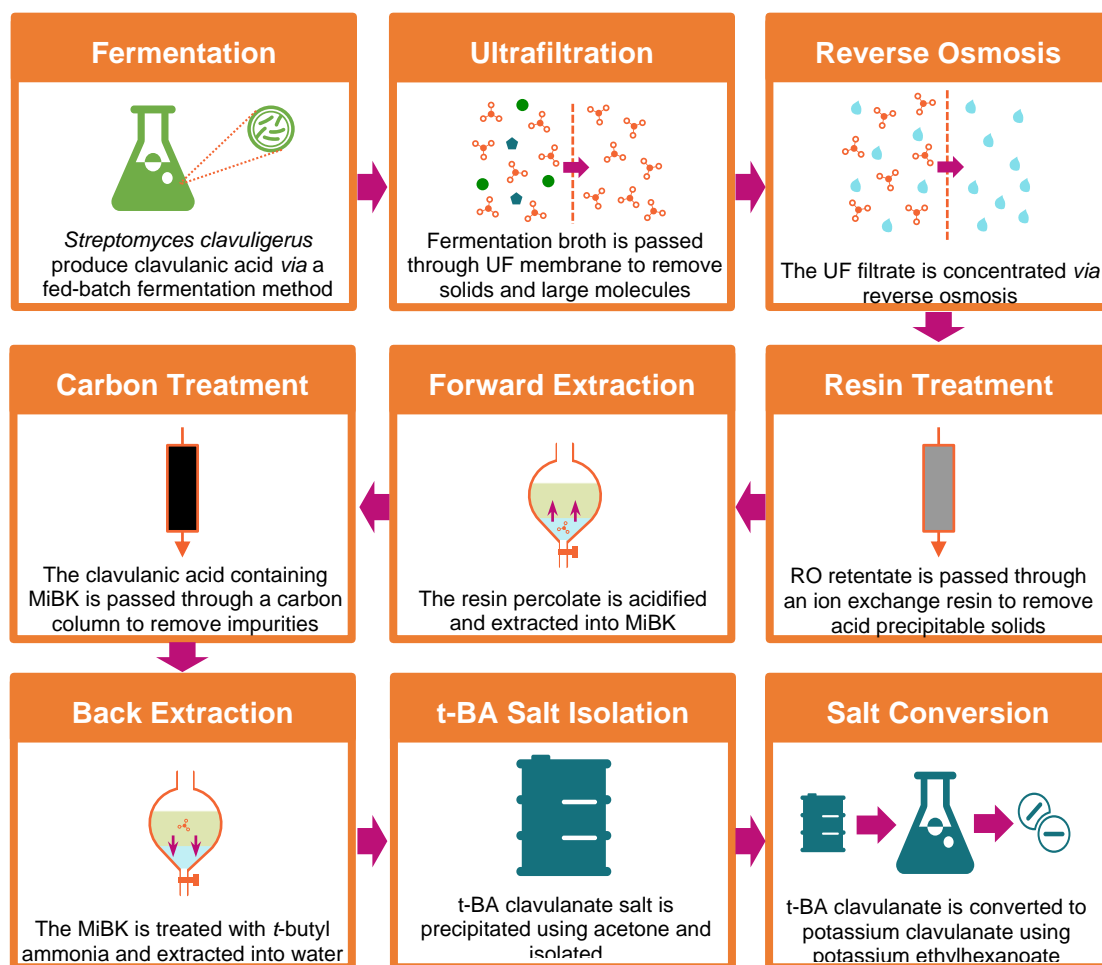


Figure 26. Summary of the clavulanic acid extraction process from fermentation broth through to the potassium clavulanate final product.

2.1.3 Degradation of Clavulanic Acid

Clavulanic acid, like most other β -lactam containing compounds, is made most efficiently by fermentation methods. As with other β -lactam containing molecules, clavulanic acid is prone to degradation under a range of different conditions.³²⁸ The fused β -lactam oxazolidine ring system leaves the molecule susceptible to nucleophilic attack which leads to ring opening of the β -lactam analogous to cases with penicillins and cephalosporins.^{235,236,329} During the fermentation and extraction processes of

clavulanic acid through to the final pure potassium clavulanate, much of the clavulanic acid and respective clavulanate salts are lost through degradation.²⁹⁶ In order to optimise the process such that degradation can be reduced, the degradation pathway and factors that affect it must be understood.

Early studies into the degradation of clavulanic acid were carried out by Haginaka *et al.*³³⁰ The group measured the effect of pH on the degradation rate of potassium clavulanate. Buffer solutions were made for pH values between the range of 3.15 and 10.10, the ionic strength of the buffer solutions was adjusted to 0.5 M with potassium chloride salt as necessary. Reverse Phase HPLC (RP-HPLC) with a UV detector set to 230 nm allowed the measurement of intact clavulanate over series of time. Pseudo-first order rate kinetics were observed for the degradation of potassium clavulanate. It was observed that ions present in buffer solutions catalysed the degradation, and as such the degradation rate was measured with a range of buffer concentrations such that extrapolation to [buffer] = 0 would provide the non-buffer-catalysed degradation rate. This was carried out at each pH. These studies demonstrated that basic conditions had a stronger catalytic effect on the degradation of clavulanate than acid conditions; it was estimated that potassium clavulanate solutions have maximum stability at pH 6.39. Activation energies were calculated using the Arrhenius equation for certain pH values.

A later study carried out by Bersanetti *et al.*³³¹ investigated the effect of temperature on the degradation of potassium clavulanate and also clavulanic acid from fermentation broth. The concentration of clavulanic acid was measured by quenching the reaction with imidazole then using a UV-Vis spectrophotometer set to a wavelength of 312 nm to measure absorbance from the CA-imidazole molecule.^{278,332} The effect of temperature on degradation rate was measured in the range of 10-40 °C at pH 6.2 and 7.0. Pseudo first order kinetics were also used in the study to derive the degradation rate law, and the Arrhenius relationship was applied to quantify the effect of temperature on reaction rate. The study found that the rate at which clavulanic acid degrades is very sensitive to temperature. Comparisons between degradation rate of potassium clavulanate and clavulanic acid in fermentation media showed that the latter degraded faster in all experiments due to other compounds present in solution.

Santos *et al.*³²⁸ carried out some similar kinetic experiments where they studied the effect of pH and temperature on clavulanic acid degradation in solution. Different inorganic salts (NaCl, MgSO₄, CaCl₂, and Na₂SO₄) were added to solution to measure their effect on the rate of degradation. A positive linear relationship was observed between the concentration of each salt in solution and the rate of clavulanic acid degradation. However, each species of salt did not give the same catalytic effect so it was deduced from the relative rates from each salt that the degradation rate could be described as a function of ionic strength. Plots of clavulanic acid concentration over a period of time showed that pseudo-first order kinetics could only describe the rate effectively during the initial stages of its degradation. After a period of time which varied with reaction conditions, the rate appears to slow down significantly in a second phase that can no longer be described by simple pseudo-first order kinetics. Although this notion was not discussed in much detail, the researchers hypothesised that the biphasic nature of degradation was due to a preliminary equilibrium between CA and an activated CA form with a higher susceptibility to degradation.

Although the majority of degradation kinetics experiments have been carried out in sterile solutions of potassium clavulanate, there have been limited studies of degradation under fermentation conditions. Mayer and Deckwer³³³ investigated the simultaneous production and decomposition rates of clavulanic acid during fermentation cultivations of *Streptomyces clavuligerus*. It was found that during periods where the bacteria were reproducing rapidly, the clavulanic acid being produced was degraded faster than periods of stagnant bacteria growth. This was postulated to have been from re-metabolism by the bacteria and the production of growth-protecting substances which can include β -lactamase enzymes. Throughout the range of conditions investigated, degradation rates of clavulanic acid *in vivo* were constantly found to be 2- to 10-fold higher than those observed *in vitro*. Roubos *et al.*³³⁴ systematically investigated the effect of individual components in fed-batch fermentation media on clavulanic acid degradation rates. Whilst many components from the cultivations were shown to have an effect on the decomposition rate, magnesium and ammonium ions in solution appeared to have the most pronounced effect.

Much of the study of clavulanic acid has revolved around the rate of degradation in aqueous solutions. Cielecka-Piontek *et al.*³³⁵ investigated the kinetic and thermodynamic parameters of solid state potassium clavulanate degradation. The rate of degradation was shown to increase in line with the relative air humidity. E_a , ΔH^\ddagger_a and ΔE^\ddagger_a were calculated from the data gathered. Computational analysis was also carried out to determine the geometry of the molecule along with the HOMO and LUMO to predict reactive sites of potassium clavulanate in the solid state.

The majority of research into the degradation of clavulanic acid and its clavulanate salts has focused on the rate of degradation. Hunt *et al.*³²⁹ carried out studies to identify some of the products of clavulanic acid degradation. It was found that the degradation reaction proceeded *via* different pathways under acidic and neutral conditions (**Figure 27**). The α -amino ketone (1-amino-4-hydroxybutan-2-one) is a major degradation product under both acidic and basic conditions. This α -amino ketone can undergo further condensation reactions in neutral and basic media to form a range of pyrazines.

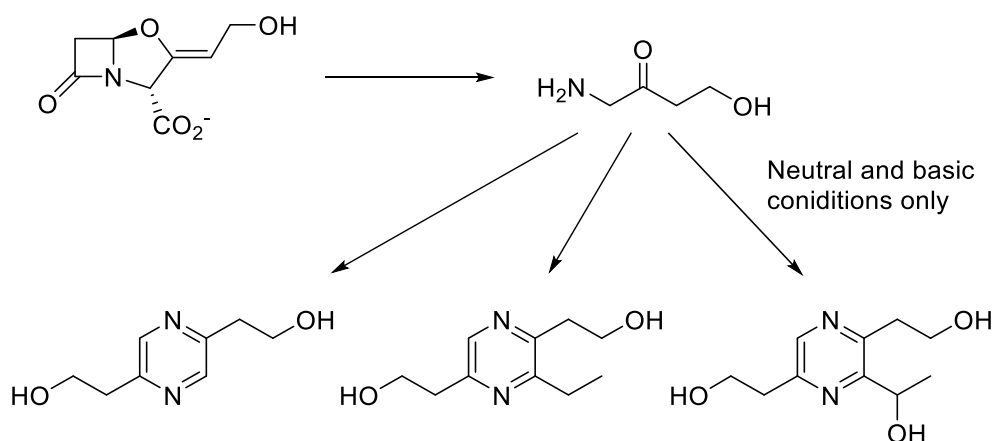


Figure 27. Main degradation products of clavulanic acid.³²⁹

In summary, there has been a number of reports in the literature that investigate the degradation of clavulanic acid. These reports have studied the rates of clavulanic acid degradation in a variety of media, and have also made some attempts to understand the degradation pathway. The knowledge gained from these studies is insightful, but a

deeper understanding of clavulanic acid degradation, particularly in the context of its process-scale manufacture, would be very valuable.

Reactivity of Clavulanic Acid Functional Groups

Clavulanic acid has a fused β -lactam-oxazolidine bicyclic core; a carboxylic acid substituent and hydroxyethylidene side chain are appended to the oxazolidine functionality.²⁷³ A brief discussion of the reactivity of β -lactams, oxazolidines, hydroxyethylidene substituents and carboxylic acids (**Figure 28**) will be discussed in this section along with their anticipated effect on the overall reactivity of clavulanic acid.

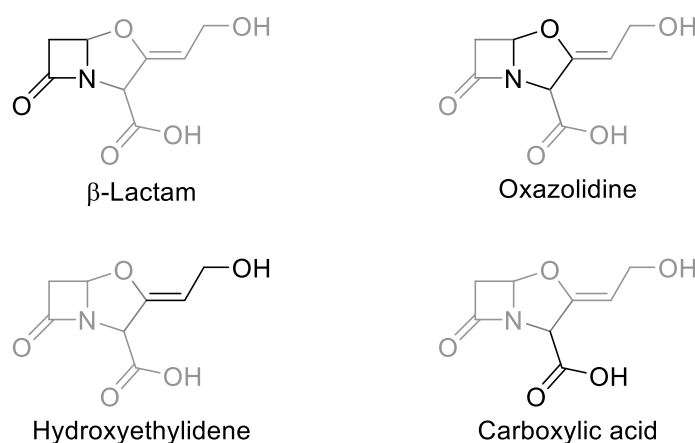


Figure 28. β -Lactam, oxazolidine, hydroxyethylidene and carboxylic acid functionalities present in clavulanic acid.

β -Lactams are four membered rings in the lactam family; lactams are cyclic amides and generally show similar reactivity to normal amides. There is an inherent instability associated with β -lactams owing to their small ring size; therefore, there is often a thermodynamic driving force for reactions leading to the opening of a β -lactam ring within a molecule. Although amides are somewhat resistant to hydrolysis in general, β -lactams (especially those which are substituted) lack the resonance stabilisation that amides possess due to conformational constraints, this is particularly true of clavulanic acid that shares a similar folded structure to penicillins (*vide supra*). Hydrolysis of the β -lactam ring is a commonly observed reaction which can each be carried out under

acidic or basic conditions.^{336,337} In acidic media (**Figure 29a**) the carbonyl oxygen atom can be protonated making the carbonyl functionality more electrophilic allowing water to act as a nucleophile attacking the carbonyl carbon. A proton transfer makes nitrogen a good leaving group and C=O double bond reforms with concomitant ring opening. In basic media (**Figure 29b**), a hydroxyl ion is sufficiently nucleophilic in nature to attack the carbonyl carbon forming an anionic tetrahedral intermediate, the four-membered ring is then opened as the carbonyl bond is restored. Nucleophiles other than hydroxide can also attack the carbonyl carbon.

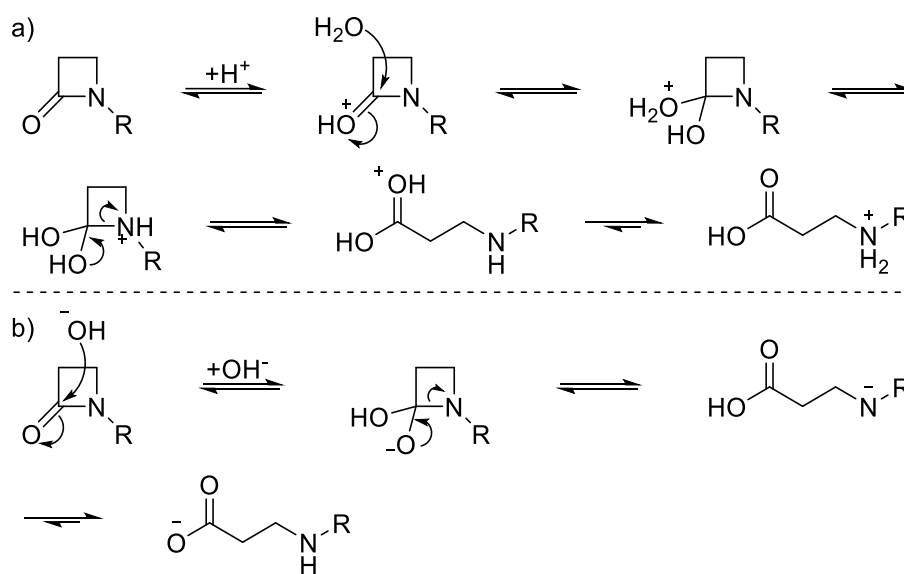


Figure 29. a) General mechanism the acid catalysed hydrolysis of β -lactams. b) General mechanism for the base catalysed hydrolysis of β -lactams.^{336,337}

Oxazolidines are five membered heterocycles containing a nitrogen and oxygen atom in the 1 and 3 positions (**Figure 28**). Oxazolidines have basic character and usually have a high susceptibility to hydrolysis. In acidic media, oxazolidine rings will be protonated, the ring opens rapidly to form a Schiff base intermediate which is then slowly hydrolysed to an aldehyde and an amine product.^{338,339} The general mechanism for the acid catalysed hydrolysis of oxazolidines is shown in **Figure 30**. Oxazolidine hydrolysis occurs more slowly under basic conditions than in acidic conditions.³⁴⁰ Oxazolidine and the hydrolysis products can feasibly undergo a range

of condensation reactions. In addition, reports of polymerisation reactions occurring in aqueous solutions have been reported.³³⁹

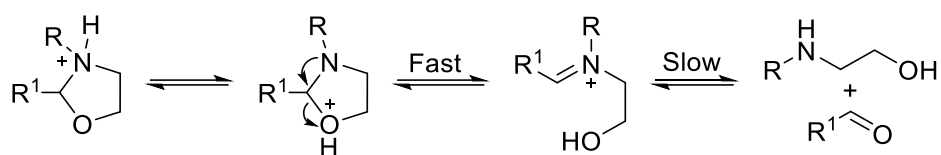


Figure 30. General mechanism for the acid catalysed hydrolysis of oxazolidines.³³⁹

The OH proton of the hydroxyethylidene side chain would be expected to be relatively acidic. Under basic conditions deprotonation could occur to yield an oxyanion. This ionic oxygen atom would be relatively unhindered so would be able to act well as a nucleophile, potentially taking part in the degradation process. Similarly, the carboxylic acid side chain can exist in solution as an anion and as such this oxygen could also act as a nucleophile in reactions such as esterifications. Nucleophilic residues on molecules within solution could react with the acid functionality such as amidation reactions happening when there is an amine present. It is also possible for the carboxylic acid moiety to be removed by a decarboxylation reaction, decarboxylations are particularly prevalent in β -keto acids (**Figure 31**).³⁴¹

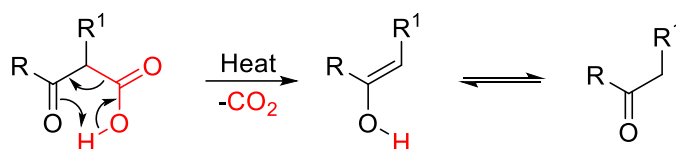


Figure 31. The general mechanism for a decarboxylation reaction in β -keto acids.³⁴⁰

Based on the reactivity of the functionalities within clavulanic acid and literature reports, the degradation pathway of clavulanic is proposed (**Figure 32**). The β -lactam ring is known to be unstable and is, as a result, the most reactive moiety on clavulanic acid. In acidic, neutral or basic media, the β -lactam ring would be expected to hydrolyse as the first step in the degradation pathway. As previously mentioned, oxazolidines have a proclivity to undergo ring opening reactions; it is expected that

the oxazolidine C-O bond could be cleaved to give an imine product. The imine contains a β -keto acid which would be liable to undergo a decarboxylation reaction as is commonly observed by this functionality (**Figure 31**). In water, imines are susceptible to hydrolysis; the hydrolysis would yield 1-amino-4-hydroxybutan-2-one and 3-oxopropanoic acid. The decarboxylation and imine hydrolysis step could, and most likely do, occur in either order. Under neutral and basic conditions, two entities of the α -aminoketone degradants could self-condense and upon oxidation, yield a pyrazine product. Both the α -aminoketone and pyrazine products have been identified in previous work. Although the products identified in **Figure 32** are thought to be the major degradants of clavulanic acid, there is the possibility for an array of more complexed products occurring from intermolecular condensation reactions to form.

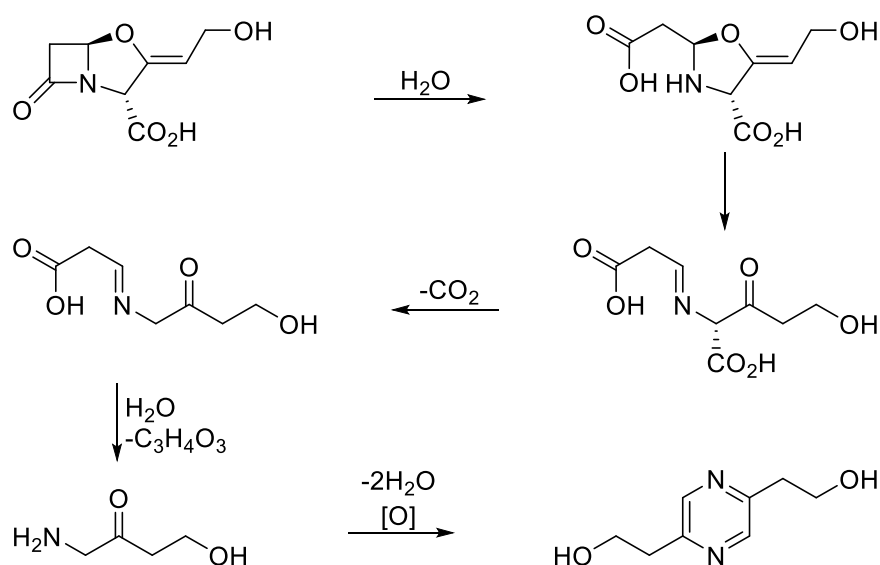


Figure 32. Proposed degradation pathway of clavulanic acid based on literature reports and reactivities of functional groups.

Reverse Phase HPLC in the Determination of Clavulanic Acid Concentration

In order to quantify the effect that pH exhibits on clavulanic acid degradation, the investigator requires a reliable method of measuring the concentration of clavulanic acid in a reaction mixture. Reverse phase high-performance liquid chromatography (RP-HPLC) coupled with UV detection is commonly used to determine the

concentration of clavulanic acid in both sterile reaction solutions, and in biological samples such as urine and human plasma.^{278,332,342}

RP-HPLC separates mixtures of molecules by exploiting their relative polarities and is a widely used technique for water soluble analytes.³⁴³ Typically a C₁₈-alkylsilica-based sorbent is attached to a support material on the RP-HPLC column wall; through this column a polar mobile phase containing the compounds to be separated is eluted.³⁴⁴ The mobile phase is usually an aqueous buffer solution and increasing proportions of a less polar organic solvent with an ionic modifier (such as acetonitrile and trifluoroacetic acid) may be used to elute less polar analytes that have an affinity for the column. Since the stationary phase is non-polar and the mobile phase is polar, it is expected that the most polar compounds will elute from the column first and the least polar compounds will elute last.³⁴³

The solution eluted from the column can be analysed using UV spectroscopy. When the separation from the column is such that no compounds which absorb light at the selected wavelength elute at the same time as the analyte, then the UV absorbance from eluting analyte peak can be directly related to the analyte concentration. A standard sample of verified purity is usually used to calibrate the UV detector response to the concentration of analyte. Previously reported methods for determining clavulanic acid concentrations via RP-HPLC have relied on the treatment of clavulanic acid containing solutions with imidazole giving a stable adduct before chromatographic analysis (**Figure 33**).^{278,332} The motivation behind this pre-column derivatization of clavulanic acid is that the stable product is retained well on the column to help with separation in biological samples and also it has a high molar absorptivity coefficient (ϵ) at 312 nm.

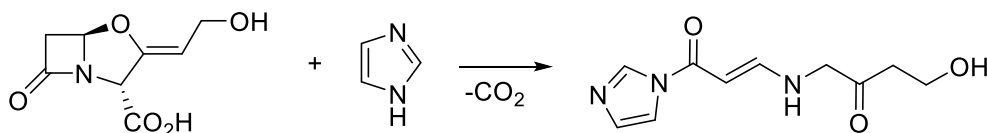


Figure 33. Reaction between clavulanic acid and imidazole for RP-HPLC clavulanic acid assay.^{278,332}

Recent investigations have developed chromatographic procedures which are able to quantify clavulanic acid in solutions without the requirement for chemical transformations to the analyte. Reports published by Hoizey *et al.*^{342,345} detail RP-HPLC methods that are capable of simultaneously determining the amount of clavulanic acid and amoxicillin in plasma for human patients treated with Augmentin.

2.2 Proposed Work

The aim of this project is to improve the current understanding of the degradation of clavulanic acid in aqueous media. The research will focus on two main areas. The first area will investigate the effect that various parameters have on the rate of clavulanic acid degradation. Whilst there have been some studies into the kinetics of clavulanic acid degradation in the past,^{323,328–331,334} much of the data is based on sterile solutions of pure clavulanates; the context of this PhD project is industrially based and, as such, much of the existing data has limited applicability on the manufacturing scale. It is important to have a good understanding of the factors that affect degradation of pharmaceutical compounds, especially in a manufacturing setting where financially-damaging loss of yield can be caused through product degradation.

The kinetic studies that will be carried out will be aimed at reflecting the conditions that clavulanic acid is found in during the industrial manufacturing process. The main objective is to improve the scientific understanding of the effect that pH has on the rate at which clavulanic acid degrades. Throughout the extraction process of clavulanic acid various pH adjustments are made; this variability in pH throughout the process is a key part of the rationale behind investigating the pH parameter.

Suitable conditions will be found to monitor the degradation of clavulanic acid under controlled acidic and basic conditions over a pH range that is relevant to the industrial manufacturing process for clavulanic acid. These conditions will be used initially to explore the effect of pH on clavulanic acid degradation rate in sterile solutions of pure clavulanates obtained as the final product of the production process used at GSK Irvine. The investigation will then extend to samples containing clavulanic acid that have been taken from various points in the aforementioned manufacturing process to identify stages that have higher degradation susceptibility than others.

The second area of research will focus on producing an in-depth mechanistic understanding of the degradation pathway of clavulanic acid. Clavulanic acid is known to degrade in solution and some of the degradants have been identified but the degradation profile has never been fully characterised. By separating, isolating, and characterising degradation products under different forced conditions such as acid- or

base-catalysed, the understanding of how clavulanic acid degrades and what factors affect this degradation will be improved.

The long-term goal of this entire project will be to apply the gained information about clavulanic acid degradation and use this to optimise the production process (**Figure 34**).

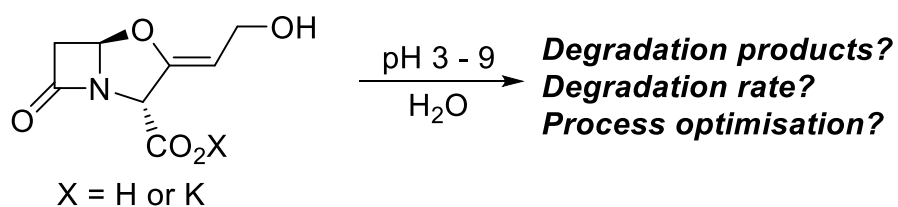


Figure 34. Summary of clavulanic acid project aims.

2.3 Results and Discussion

2.3.1 Understanding the Effect of pH on Clavulanic Acid Degradation

Determination of Suitable Reaction Conditions

Experimental investigations into the stability of clavulanic acid with respect to pH first required the development of a suitable method to quantitatively monitor degradation. Given the prevalence of RP-HPLC with UV detection used to determine clavulanic acid concentration in solutions, this technique would first be explored for its suitability in this investigation. Validated RP-HPLC conditions are used on site at GSK Irvine to calculate concentrations of clavulanic acid. One widely used method uses a C₁₈ stationary phase and a phosphate buffered aqueous-methanol mobile phase with a UV detector that measures absorbance at 230 nm; this method is referred to as the K313 method.

Aqueous solutions of potassium clavulanate were analysed using the K313 method to test the suitability of the method and also to determine a suitable starting concentration for degradation reactions to be carried out at. The concentration of potassium clavulanate in solution is required to be high enough to give a UV absorbance above the instrument detection limit. Conversely, if the concentration was too strong the UV detector would be saturated giving unreliable readings and potentially poor separation or peak shapes in the chromatograms. The potassium clavulanate used was obtained from the production process at GSK Irvine, and chromatographic analysis of the potassium clavulanate was performed to verify its authenticity. A lithium clavulanate standard of verified purity was used as a standard to quantitatively relate the UV absorbance of a sample to its concentration of potassium clavulanate.

The first potassium clavulanate solution was made with a concentration of 50 mg/mL and the HPLC for this showed a broad clavulanate peak with some tailing. A weaker solution of 0.5 mg/mL was made; however, when the area under the curve was followed as a function of time, it was observed to both decrease and increase. It is thought that error involved in measuring concentration may have been larger than the decrease in actual concentration over the time intervals of measurements. 0.5 mg/mL was therefore, considered too weak to use in this type of reaction. It was found that 0.1

g of potassium clavulanate in 50 mL water (2 mg/mL) gave a suitable peak size and shape and that the decrease in peak area could be measured over time. Owing to the uniform peak shape, and degradation rates that were suitable for monitoring with HPLC, the 2 mg/mL concentration was used consistently in degradation studies of potassium clavulanate solutions.

During the preliminary investigation for finding suitable reaction conditions, sulfuric acid (2 M) and sodium hydroxide (2 M) solutions were used to adjust the pH of the degradation reactions. A solution of 0.1 g potassium clavulanate in 50 mL deionised water was first prepared, sulfuric acid or sodium hydroxide was then added to the clavulanate solution to adjust the pH to the required level. The method used to adjust pH in these initial experiments had two major drawbacks. It was found that the addition of a small volume of sulfuric acid or sodium hydroxide solution caused a large change in the pH of the degradation solution, this made it difficult to alter the pH to a specific value in an efficient and accurate manner. It was perceived that without a method to reliably alter the pH of degradation reactions, repeatability of experiments would be problematic; preliminary experiments proved this to be true.

The second limitation associated with the use of sulfuric acid and sodium hydroxide to control pH is that the pH of clavulanate solutions changes over time. As the clavulanic acid degradation process takes place the pH of the reaction solution can rise or fall; therefore, the reaction will not be held at the pH value that it was initially adjusted to for the entire process. This phenomenon was investigated by creating three 50 mg/mL potassium clavulanate solutions in deionised water which each had a pH of 6.60; one solution was acidified to pH 4.05 using sulfuric acid, one adjusted to pH 7.02 with sodium hydroxide, and the other to pH 9.00 using sodium hydroxide. The solutions were each kept in beakers, open to air, at ambient temperature; the pH of each solution was then measured to two decimal places using a pH meter at time intervals of 30 min over a period of 4 h.

When the pH had been adjusted to 9.0 with sodium hydroxide, the solution was shown to become more acidic over time. Conversely, when the potassium clavulanate solution was adjusted to pH 4.0 *via* the addition of sulfuric acid, an increase in pH was observed over time. The solution that started at pH 7.02 rose in pH by 0.42 units over the time

period studied, but the magnitude of change was smaller than that of the two solutions which deviated further from neutrality (-1.34 and +1.44 pH units for solutions starting at pH 9.0 and 4.05, respectively). A plot of pH versus time was constructed (**Figure 35**). Each of the potassium clavulanate solutions, which were initially colourless, developed a noticeable orange hue over time after the addition of acid or base. The change in colour is indicative of clavulanic acid degradation so it is reasonable to suggest that the change in pH was a consequence of chemical transformations taking place in solution. The graph shows that for each scenario, the pH shows a faster rate of change soon after the initial pH adjustment and then slows down as the reaction progresses. This effect is more pronounced with the pH 9.0 solution; the trend is consistent with first order kinetics as the rate of clavulanic acid degradation will be expected to slow down as the starting material is consumed. It should be noted that the pH of an alkali solution may drop upon exposure to air due to the dissolution of carbon dioxide and subsequent formation of carbonic acid. A control experiment to account for this underlying pH shift was not performed.

The reason why the pH rises for a potassium clavulanate solution that is acidic whilst dropping for an alkali potassium clavulanate solution is not entirely known. The change in pH does, however, suggest that clavulanic acid degradation under acidic and basic conditions leads to different product mixtures. The acidic conditions must be consuming acidic compounds whilst basic conditions consume basic compounds.

In order to control the pH of degradation reactions accurately and to keep pH constant over the course of the study, it was decided to incorporate the use of buffer solutions.

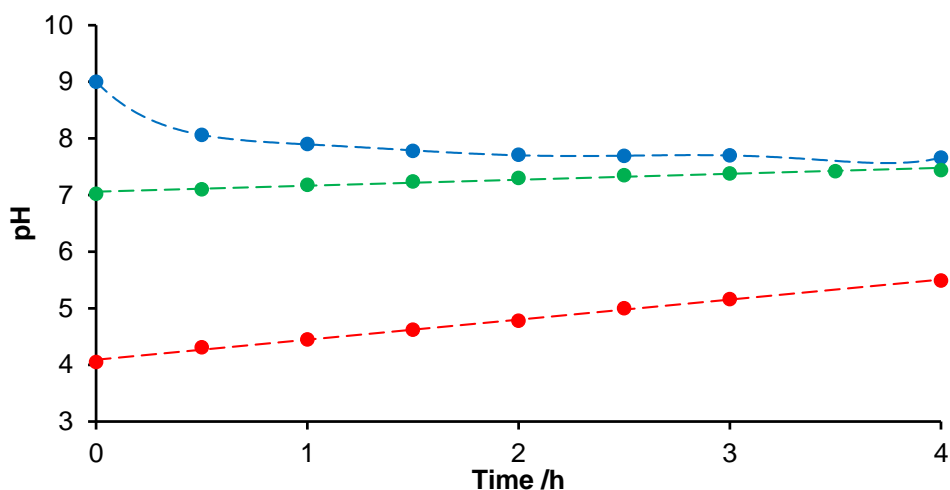


Figure 35. Change in pH of potassium clavulanate solutions over time that have been adjusted to pH 7.02 (green) and pH 9 (blue) with sodium hydroxide and pH 4 (red) with sulfuric acid. Dotted lines are presented solely as a guide to the eye.

Degradation of Clavulanic Acid in Buffered Solutions

With a suitable potassium clavulanate starting concentration and analytical technique to follow the reaction progress, the use of buffer systems to adjust and maintain the pH was investigated. The use of buffers when determining the pH profile has been widely used in the pH profiling of pharmaceutical compounds.

Buffer solutions can consist of a weak acid and its conjugate base, for example acetic acid and sodium acetate. Conversely, a buffer system can be comprised of a weak base and its conjugate acid. The dynamic equilibrium between the acidic component and its conjugate base, or *vice versa*, serves to make solutions resistant to large changes in pH upon the addition of acid or base. When choosing an appropriate buffer system, certain criteria should be fulfilled:

- (i) The buffer pK_a should be close to middle of the pH range studied; it is common to use multiple different buffer systems when investigating a wide range of pH values.
- (ii) Buffers should not give a significant response to the detection method, i.e. should not have a strong absorbance at 230 nm in this case.

- (iii) Buffers should be chemically stable under the conditions in which they are being used.

As well as the judicious selection of buffer system, it is important to consider environmental factors such as temperature when using a buffer as this can affect the pK_a of buffer components and hence the pH of the solution.

This project used multiple buffer systems in order to obtain solutions that range in pH from 3-9. In the range of pH 3-5.95 a citric acid/disodium hydrogenphosphate system was used, from pH 6-8 a sodium dihydrogenphosphate/disodium hydrogenphosphate system was used, and for pH 9-10 a glycine/sodium hydroxide buffer system was used. Whilst buffer solutions are a convenient method of controlling pH, they should be used with caution as ions in solution have been shown to catalyse the degradation of clavulanic acid.^{328,330} To that end, when using buffers to investigate the effect of pH on stability, the rate of degradation should be calculated for a series of buffer concentrations at each pH value. A plot of buffer concentration versus degradation rate can then be produced and extrapolated back to a buffer concentration of zero which gives the buffer-independent degradation rate (**Figure 36**). Each buffer solution was adjusted to an ionic strength (μ) of 0.5 M by adding the necessary amount of potassium chloride.

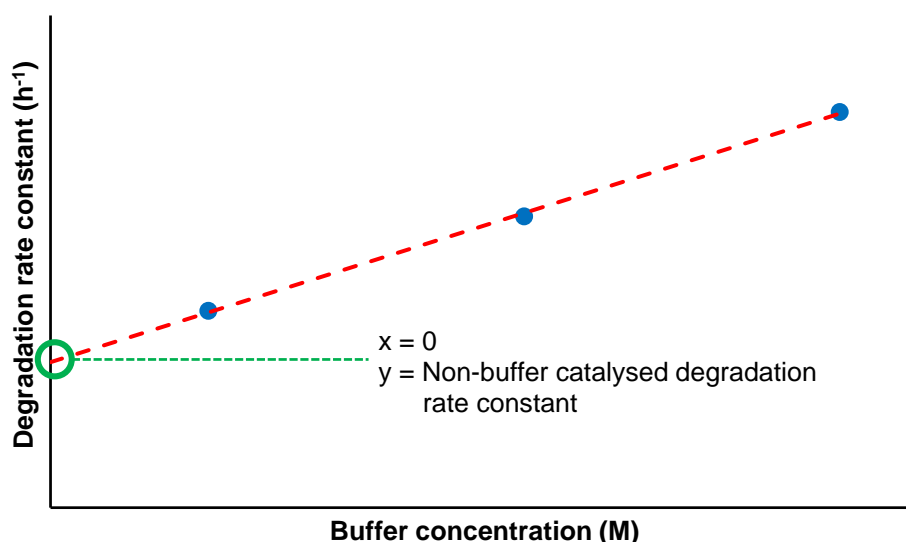


Figure 36. Diagram showing how extrapolation of rate constants at various buffer strengths can be extrapolated to the non-buffer catalysed degradation rate constant.

To measure the rate of degradation, potassium clavulanate was dissolved in the buffer solution of required pH and concentration, the degradation solution was held at 25 °C for the duration of the experiment via a temperature-controlled auto sample chamber on the HPLC instrument. A 10 μL aliquot was taken at $t=0$ and then at intervals of 1 h for a period of 20 h and the amount of undegraded clavulanate was measured using the K313 RP-HPLC method. Each data point was repeated in triplicate. Degradation of potassium clavulanate in aqueous solutions has been shown to observe pseudo-first order rate kinetics.

By plotting a graph of $\ln[\text{clavulanate}]$ versus time, the inverse of the gradient gives the pseudo-first order rate constant of degradation at the given pH and buffer concentration. The graphs and rate constants derived from this method are shown below for pH 5. Each point on **Figure 37-39** is the average of three separate data points.

Using a 0.025 M citric acid/disodium hydrogenphosphate buffer solution at pH 5, the pseudo-first order degradation rate constant of clavulanic acid was calculated to be 0.0049 h^{-1} (**Figure 37**). The process was repeated for 0.05 M and 0.1 M buffer solutions to give rate constants of 0.0056 h^{-1} (**Figure 38**) and 0.0079 h^{-1} (**Figure 39**), respectively. The R^2 value for each of these plots is 0.993 or above. This strong linear correlation indicates that the pseudo-first order rate plot used is a good model for the data obtained. The rate constants obtained increase as the concentration of buffer solution is increased, as anticipated, indicating significant background reaction involving the non-innocent buffer system. The observation that CA degradation rate depends on buffer concentration indicated that acids and bases appear in the overall degradation rate equation. This is indicative of general acid and base catalysis, as opposed to specific acid and base catalysis where protonation or deprotonation would occur rapidly before the rate determining step.

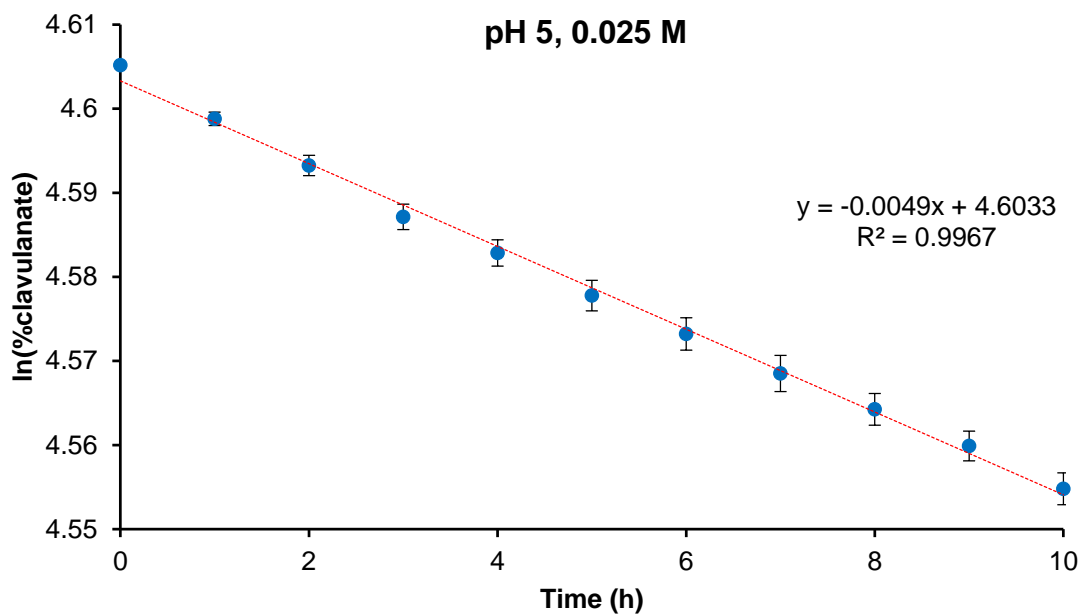


Figure 37. Pseudo-first order rate plot of potassium clavulanate degradation over time using a 0.025 M pH 5 buffer solution.

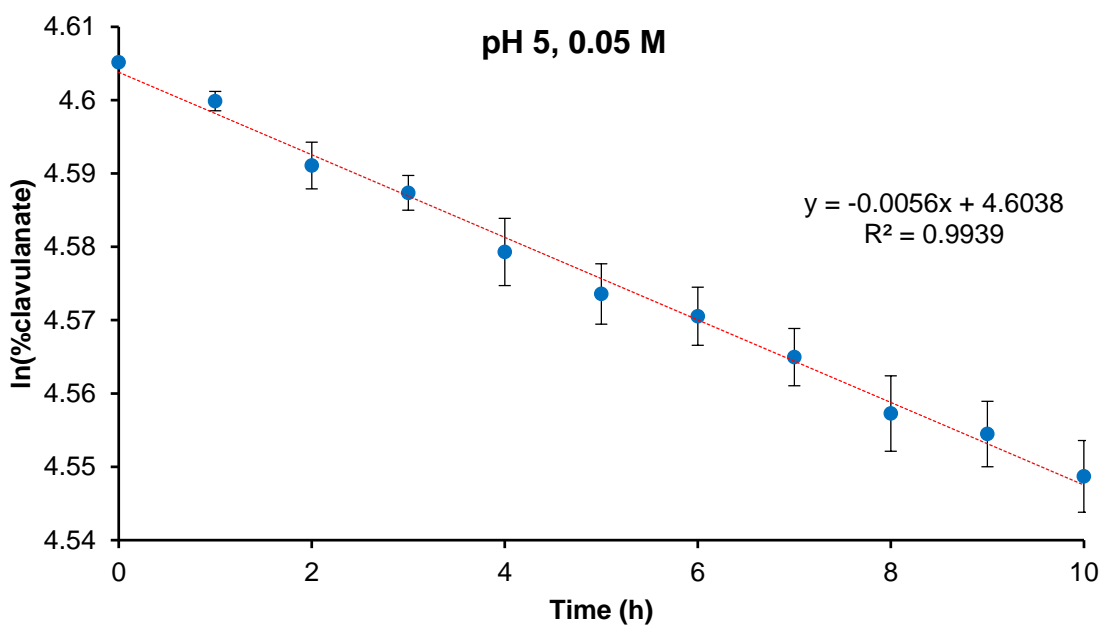


Figure 38. Pseudo-first order rate plot of potassium clavulanate degradation over time using a 0.05 M pH 5 buffer solution.

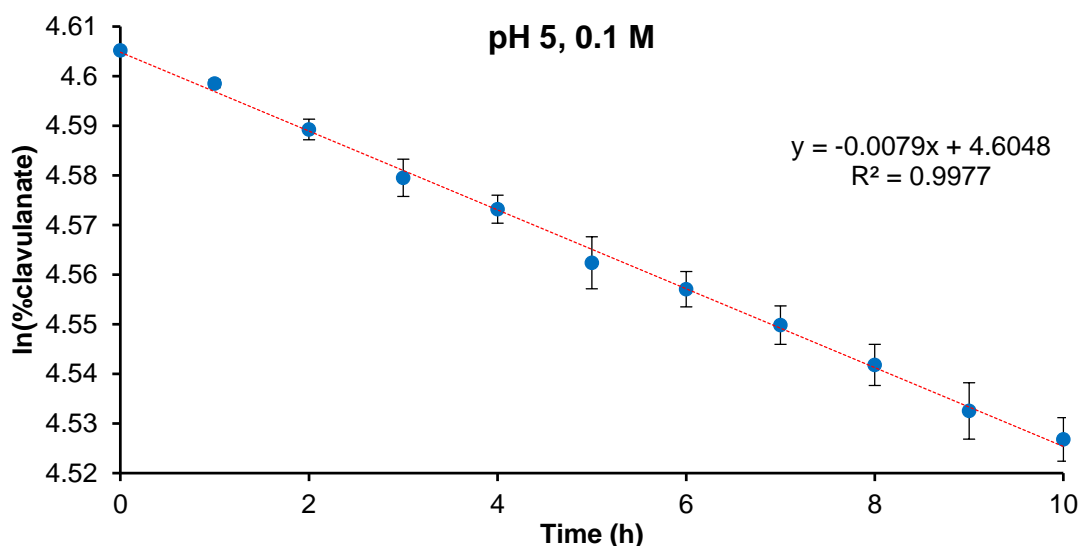


Figure 39. Pseudo-first order rate plot of potassium clavulanate degradation over time using a 0.1 M pH 5 buffer solution.

The non-buffer-catalysed rate constant was then calculated by plotting a graph of degradation rate constant *versus* buffer concentration for each of the three pH 5 buffers used (**Figure 40**). The regression line was extrapolated such that the y-intercept would give the degradation rate constant when buffer concentration was 0 M. Using this method, the non-buffer catalysed degradation rate constant at pH 5 was calculated to be 0.0038 h⁻¹.

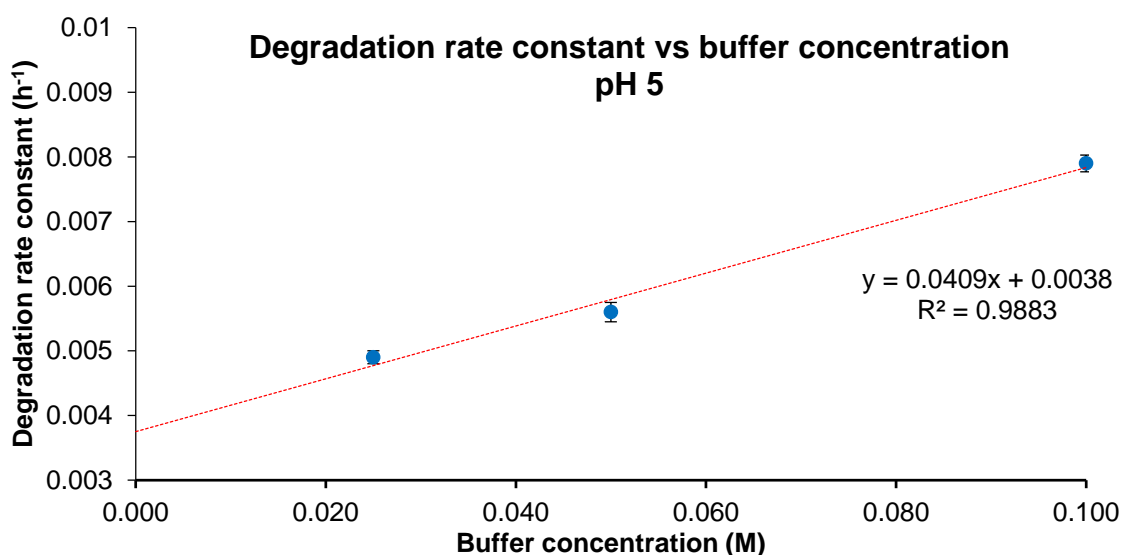


Figure 40. Plot of degradation rate constants calculated at buffer concentrations of 0.025 M, 0.05 M and 0.1 M at pH 5 to find non-buffer catalysed rate constant.

The graphs constructed to calculate the non-buffer catalysed rate constants generally showed a strong linear dependence of degradation rate on buffer concentration. The process carried out with pH 5 buffers was repeated for pH 3, 4, 6, 7, 8 and 9. It was initially planned to investigate pH 10 also but degradation rates were too fast to be determined accurately with this method. Since pH 10 is not relevant to the extraction process used on plant, it was decided that it would be an inefficient use of resources to pursue investigations at this pH. The rate constants obtained over the studied pH range are summarised in **Table 1**. A graph of non-buffer-catalysed degradation rate versus pH was produced to show the pH profile of clavulanic acid stability (**Figure 41**). This graph shows that the most stable pH of clavulanic acid solutions is around 5. The shape of the curve is indicative of different degradation mechanisms under acidic, neutral, and basic conditions. The gradient of the pH profile is 0.73 in the acidic region and 0.70 in the basic region, the reason these numbers deviate from the expected value of 1.0 for acid and base catalysed reactions is unknown.

Table 1. Degradation rate constants calculated for pH range 3-9.

| pH | Rate constant at 0.025 M / h ⁻¹ | Rate constant at 0.05 M / h ⁻¹ | Rate constant at 0.1 M / h ⁻¹ | Non-buffer catalysed rate constant /h ⁻¹ | Concentration vs rate constant slope /h ⁻¹ M ⁻¹ |
|----|--|---|--|---|---|
| 3 | 0.1130 ± 0.0044 | 0.1456 ± 0.0056 | 0.1563 ± 0.0042 | 0.1077 ± 0.0178 | 0.5250 |
| 4 | 0.0263 ± 0.0010 | 0.0303 ± 0.0022 | 0.0433 ± 0.0019 | 0.0198 ± 0.0016 | 0.2311 |
| 5 | 0.0049 ± 0.0001 | 0.0056 ± 0.0002 | 0.0079 ± 0.0001 | 0.0038 ± 0.0003 | 0.0410 |
| 6 | 0.0132 ± 0.0005 | 0.0152 ± 0.0009 | 0.0200 ± 0.0005 | 0.0108 ± 0.0003 | 0.0914 |
| 7 | 0.0148 ± 0.0009 | 0.0185 ± 0.0008 | 0.0346 ± 0.0008 | 0.0140 ± 0.0004 | 0.0267 |
| 8 | 0.0177 ± 0.0005 | 0.0239 ± 0.0006 | 0.0458 ± 0.0006 | 0.0147 ± 0.0011 | 0.0580 |
| 9 | 0.1314 ± 0.0081 | 0.3935 ± 0.0079 | 1.0278 ± 0.0046 | 0.0813 ± 0.0085 | 0.5691 |

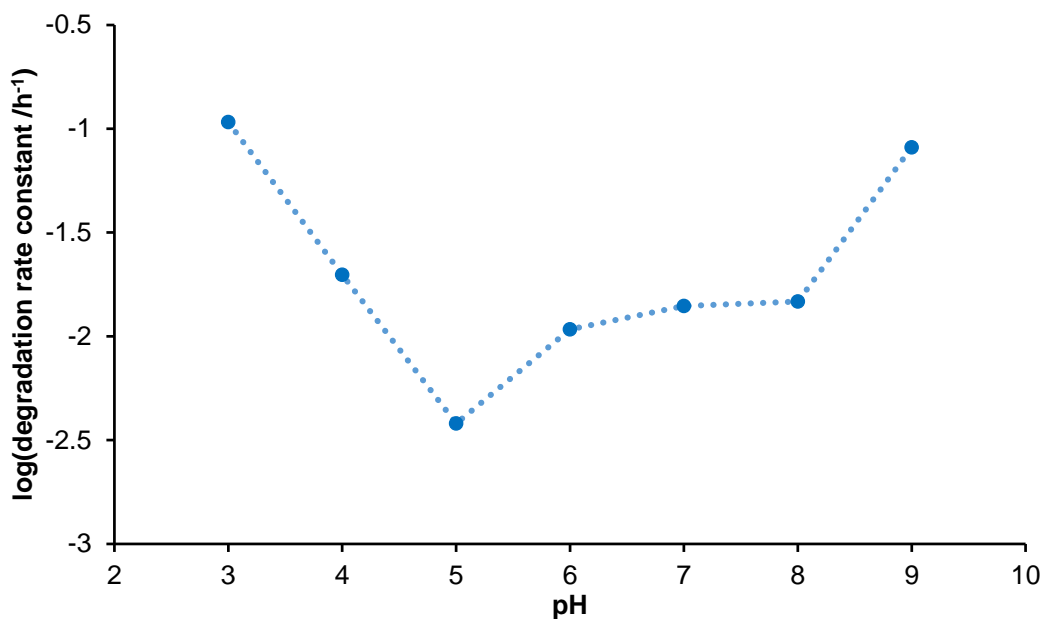


Figure 41. A graph showing the rate constants of clavulanate degradation over the pH range of 3-9. The dotted line is present solely as a guide to the eye.

Since the pH intervals studied vary by intervals of 1, the graph obtained does not show the exact pH at which clavulanic acid is most stable. The pH range 5-6 was investigated in more detail. The process used to obtain the data was the same as described for pH 3-9 with the exception that clavulanate concentration was measured in time intervals of 2 h rather than every 1 h. The data obtained from these experiments is summarised in **Table 2** and **Figure 42**, it is also shown amongst the data over the entire pH 3-9 range in **Figure 43**.

The data obtained in this pH region showed that potassium clavulanate is most stable at pH 5.9. The curve shows a steady decrease in stability as pH increases from 5 to 5.9 but towards pH 6 the increase in degradation rate is more dramatic. The buffer used to keep the pH at 6 was the sodium dihydrogen phosphate/disodium hydrogenphosphate system, whilst pH 5-5.95 all used the citric acid/disodium hydrogenphosphate system. It is possible that the difference in buffer system was contributing to the large jump in rate from one pH to another.

Table 2. Degradation rates calculated for pH range 5.1-5.95.

| pH | Rate at 0.025 M / h ⁻¹ | Rate at 0.05 M / h ⁻¹ | Rate at 0.1 M / h ⁻¹ | Non-buffer catalysed rate /h ⁻¹ |
|------|--------------------------------------|-------------------------------------|------------------------------------|---|
| 5.1 | 0.0056 | 0.0058 | 0.0086 | 0.0042 |
| 5.3 | 0.0039 | 0.0052 | 0.0072 | 0.0029 |
| 5.5 | 0.0038 | 0.0046 | 0.0069 | 0.0027 |
| 5.7 | 0.0033 | 0.0050 | 0.0075 | 0.0021 |
| 5.8 | 0.0033 | 0.0053 | 0.0081 | 0.0019 |
| 5.9 | 0.0036 | 0.0054 | 0.0094 | 0.0016 |
| 5.95 | 0.0038 | 0.006 | 0.0100 | 0.0018 |

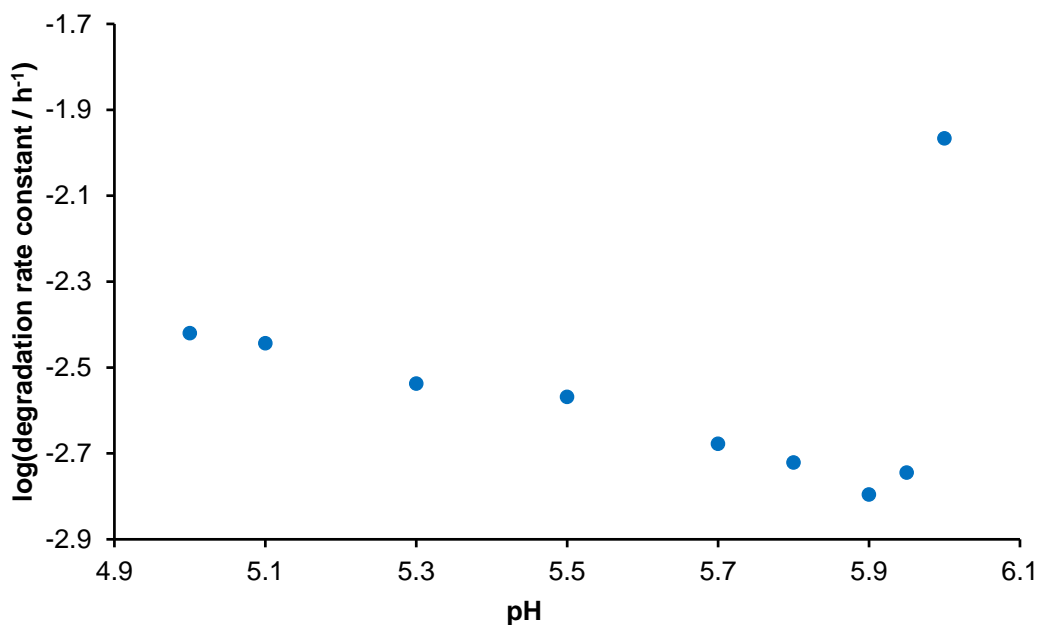


Figure 42. A graph showing the rate of clavulanate degradation over the pH range of 5-6.

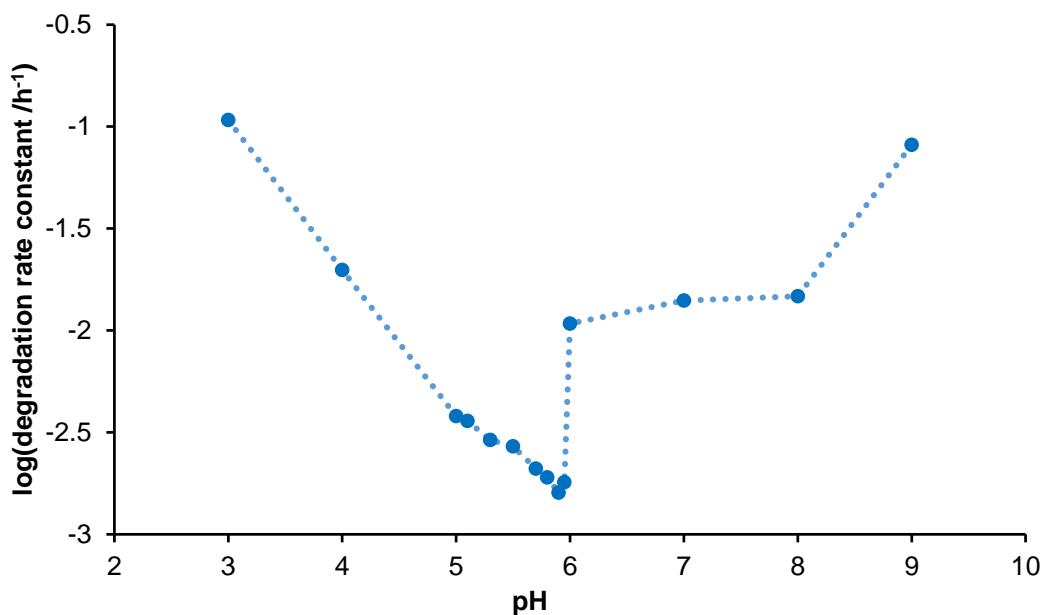


Figure 43. A graph showing the rate constants of clavulanate degradation over the pH range of 3-9. The dotted line is present solely as a guide to the eye.

To investigate this further, the citric acid buffer system was also used to calculate the non-buffer catalysed rate constant at pH 6. The value obtained with the citric acid buffer was 0.0017 h^{-1} compared to the 0.0108 h^{-1} calculated with the phosphate buffer; the reason for the large difference in calculated rate constant with each buffer system was unknown and was subject to further investigation.

To study the effect that the buffer system has on clavulanic acid degradation an additional buffer system was used. A citric acid/trisodium citrate system was chosen for its ability to buffer solutions over a large pH range. The citric acid/citrate pair can buffer effectively at pH 6 which was where the discrepancy in the degradation rate between the citric acid/phosphate and phosphate/phosphate buffers was observed.

Using the same method as has previously described, the degradation rate of clavulanic acid was measured at pH using a citric acid/ trisodium citrate buffer at concentrations of 0.025 M, 0.05 M and 0.1 M (**Figure 44-46**). The individual rates were then plotted against the buffer concentration as per the standard procedure (**Figure 47**) and extrapolated back to calculate a non-buffer catalysed degradation rate of 0.0018 h^{-1} . This value is in good agreement with the value of 0.0017 h^{-1} which was determined using the citric acid/disodium hydrogenphosphate buffer system. The degradation rate

was calculated with this method at pH 5.0, 5.5, 6.0, 6.5, 7.0, and 7.5; the results are summarised in **Table 3** and **Figure 48**. An explanation for why different rates are calculated with each buffer remained elusive, but it is unlikely that the buffers react directly with the substrate.

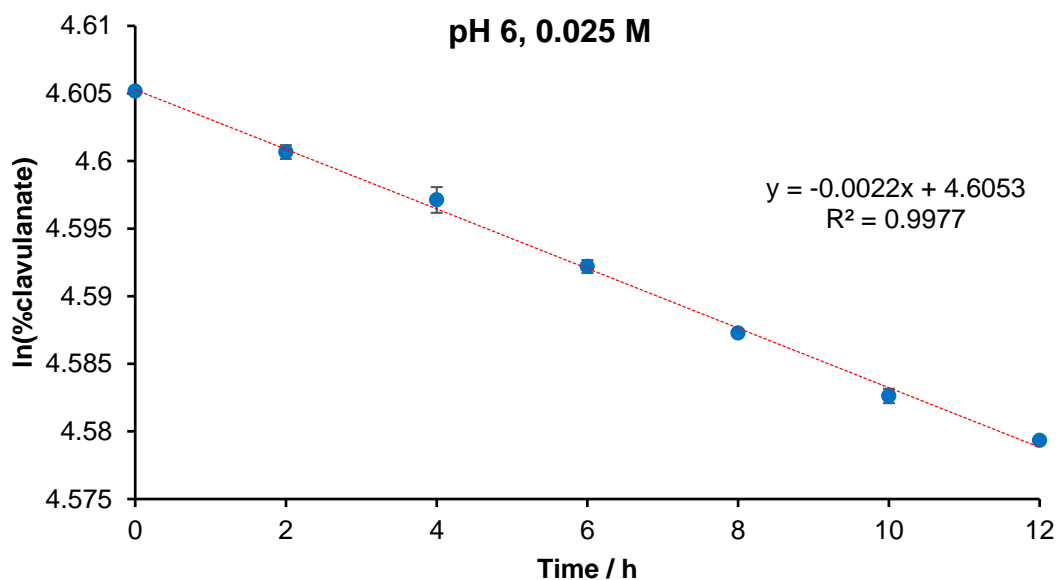


Figure 44. Pseudo-first order rate plot of potassium clavulanate degradation over time using a 0.025 M pH 6 citric acid/ trisodium citrate buffer solution.

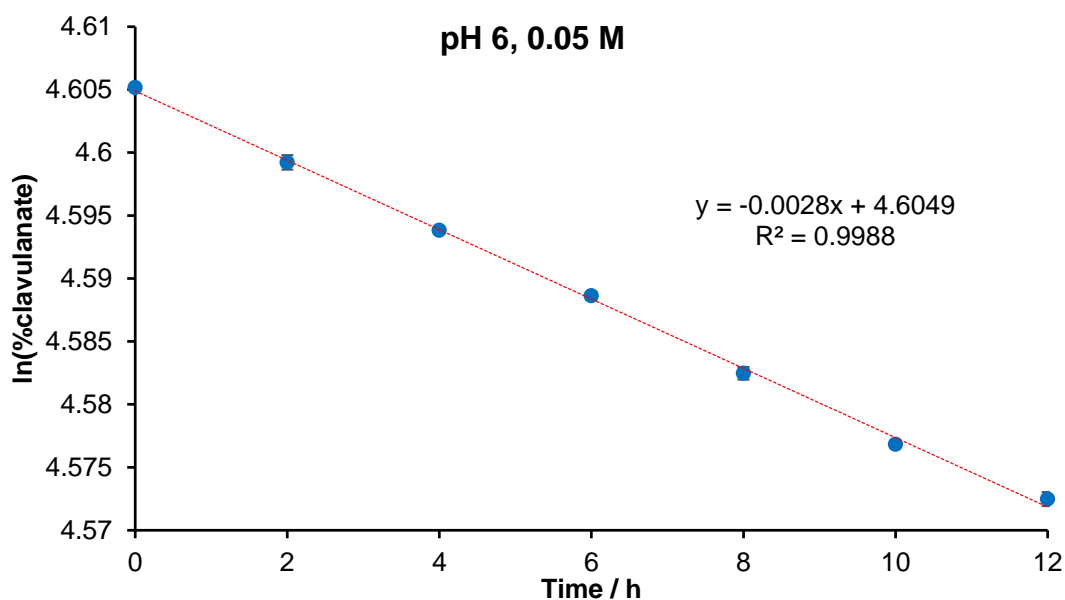


Figure 45. Pseudo-first order rate plot of potassium clavulanate degradation over time using a 0.05 M pH 6 citric acid/ trisodium citrate buffer solution.

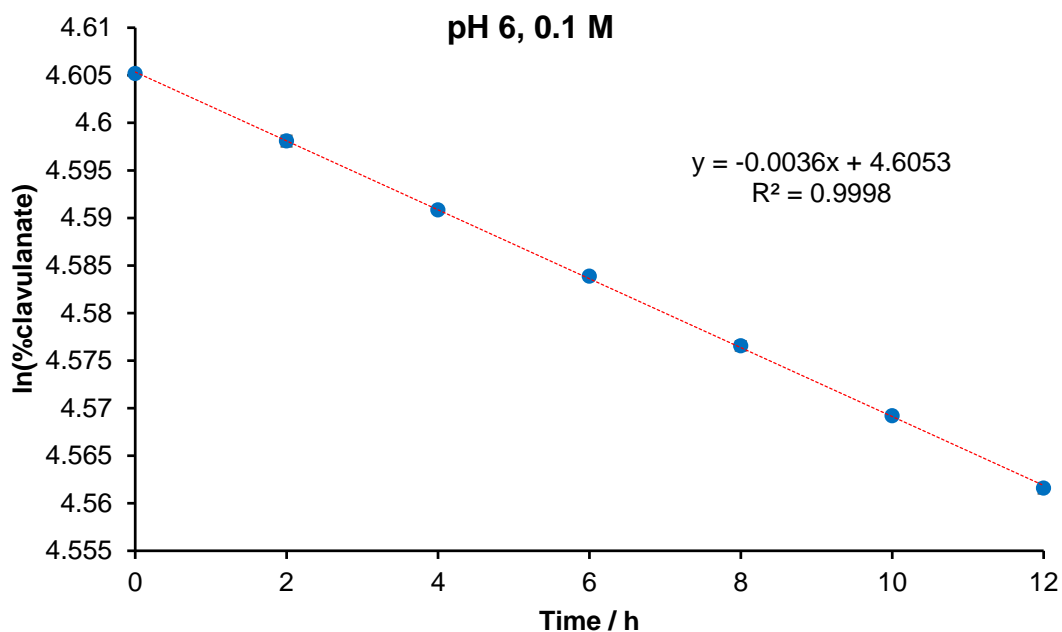


Figure 46. Pseudo-first order rate plot of potassium clavulanate degradation over time using a 0.1 M pH 6 citric acid/ trisodium citrate buffer solution.

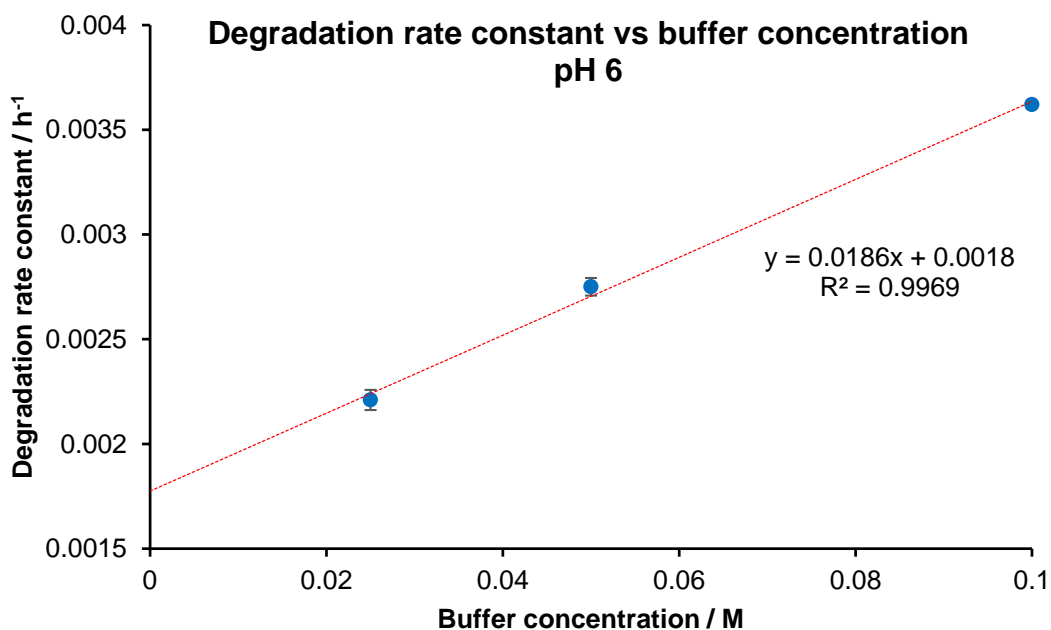


Figure 47. Plot of degradation rate constants calculated with a pH 6 citric acid/trisodium citrate buffer system at concentrations of 0.025 M, 0.05 M and 0.1 M to estimate the non-buffer-catalysed rate constant.

Table 3. Degradation rates calculated for pH range 5.0-7.5 using a citric acid/trisodium citrate buffer system.

| pH | Rate at 0.025 M / h ⁻¹ | Rate at 0.05 M / h ⁻¹ | Rate at 0.1 M / h ⁻¹ | Non-buffer catalysed rate /h ⁻¹ |
|-----|--------------------------------------|-------------------------------------|------------------------------------|---|
| 5.0 | 0.0061 | 0.0073 | 0.0107 | 0.0045 |
| 5.5 | 0.0029 | 0.0039 | 0.0057 | 0.0020 |
| 6.0 | 0.0022 | 0.0028 | 0.0036 | 0.0018 |
| 6.5 | 0.0018 | 0.0022 | 0.0028 | 0.0015 |
| 7.0 | 0.0021 | 0.0024 | 0.0028 | 0.0019 |
| 7.5 | 0.0029 | 0.0031 | 0.0035 | 0.0027 |

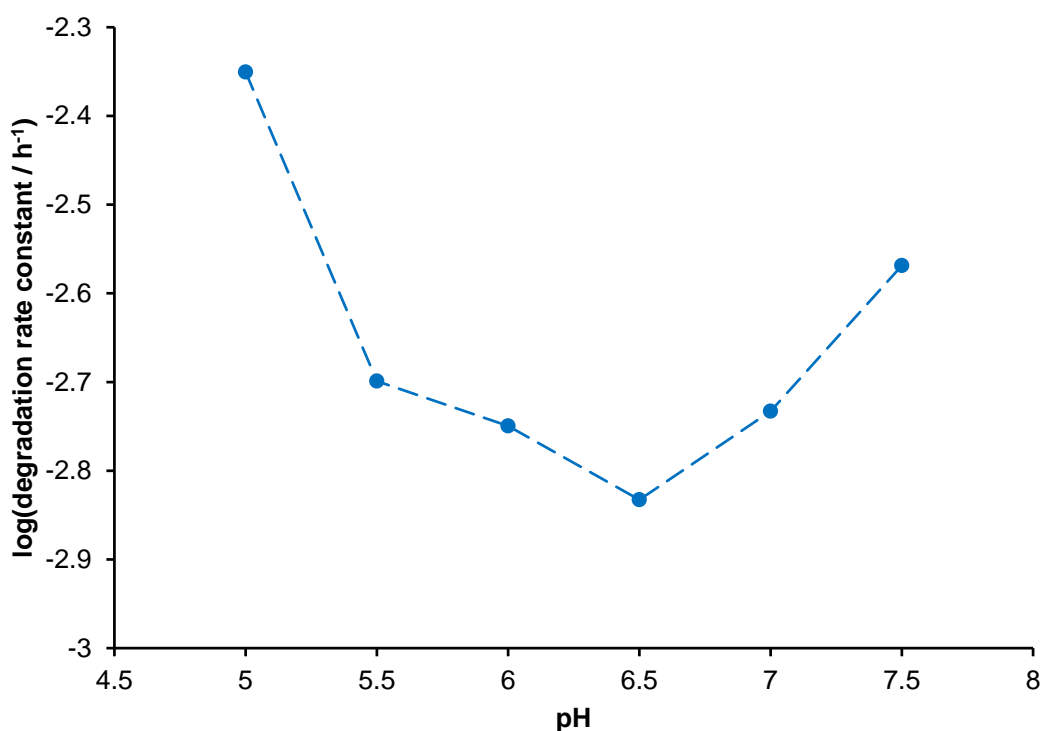


Figure 48. A graph showing the rate of clavulanate degradation over the pH range of 5-7.5 calculated with a citric acid/trisodium citrate buffer system. The dotted line is present solely as a guide to the eye.

The overall graph showing the degradation rate constant with respect to pH was reconstructed using the data obtained with the citric acid/trisodium citrate buffer in the pH range 5-7.5 and the previously obtained data outside of this range (**Figure 49**). The shape of the graph shows that clavulanic acid has a reasonably low susceptibility to degradation in the pH range 5.5-7.5 under the conditions measured. As the pH deviates from this stable region, the rate of degradation is shown to increase rapidly.

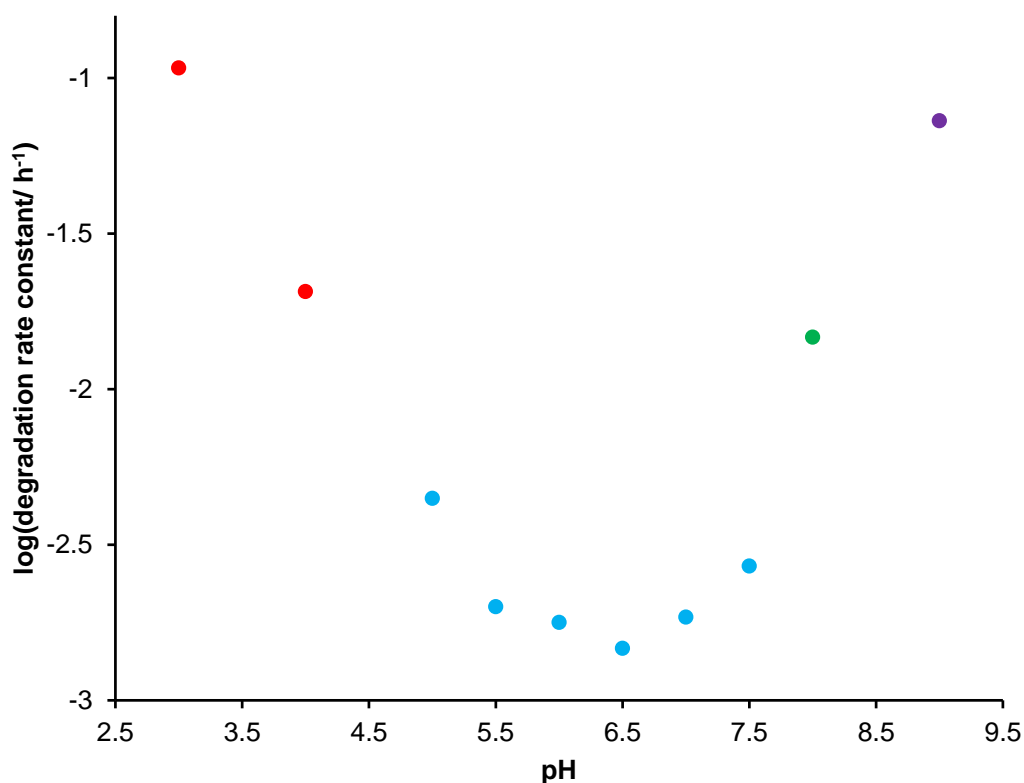


Figure 49. A graph showing the rate of clavulanate degradation over the pH range of 3-9 calculated with citric acid/disodium hydrogenphosphate (red), citric acid/trisodium citrate (blue), sodium hydrogenphosphate/disodium hydrogenphosphate (green) and glycine/sodium hydroxide (purple) buffer systems.

2.3.2 Degradation of Clavulanic Acid in Manufacturing Plant Samples

The context of this project is in an industrial setting at a global manufacturing supply site. In terms of developing a method for monitoring degradation and gaining a general knowledge of how pH affects clavulanic acid degradation, using buffered potassium

clavulanate solutions provided an informative starting point. However, the effect of pH on the degradation of clavulanic acid in samples taken directly from the manufacturing process was also to be investigated. Various stages of the extraction process were selected for sampling. A flow chart is given outlining the stages of the complete clavulanate manufacturing process (**Figure 50**), though a more descriptive overview is given in *Extraction of clavulanic acid*.

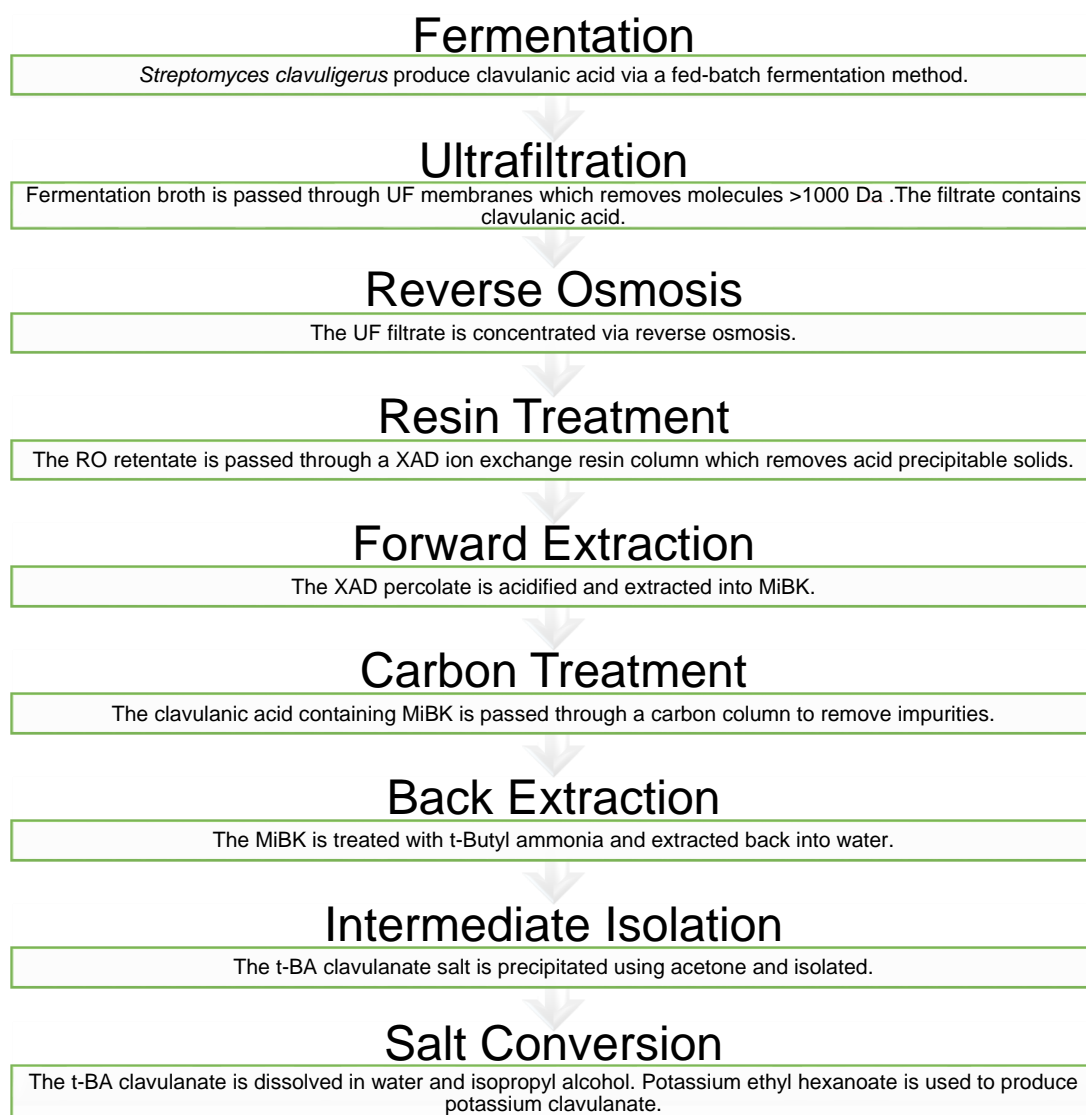


Figure 50. A flow chart giving an overview of the industrial manufacturing process of clavulanic acid from fermentation through to isolation as its final potassium salt.

Samples were taken from four different parts of the clavulanic extraction stream. Ultrafiltration (UF) was taken as the first sampling point; this stage simply passes the fermentation broth through membranes. The sample was taken directly after passing through the membrane stack. The concentration of clavulanic acid in UF flow is approximately 7-9 g/L (~0.04 M). Reverse osmosis (RO) was the second sampling point studied; this step of the process concentrates the UF filtrate by removing water through a RO membrane. The RO samples were taken from a vessel in which the concentrate is stored before transfer to the next stage of the extraction process; the concentration of clavulanic acid is not typically homogeneous throughout this vessel so the samples were taken at the point when they were the concentration of clavulanic acid was expected to be the most concentrated. The concentration of clavulanic acid in RO concentrate is approximately 40-45 g/L (~0.2 M). The third stage investigated ion exchange resin (XAD), the samples were taken directly from the percolate that had passed through the XAD column; the clavulanic concentration in XAD percolate is the same as RO concentrate (~0.2 M). The final point of the process to be studied was the back extraction (BE) step; this step transfers clavulanic acid from an organic MiBK phase back into an aqueous phase. The stage cycles the MiBK with the same tank of water until a predetermined concentration of clavulanic acid in the water is reached, the sample was taken as close to the maximum concentration as possible. The concentration of clavulanic acid in BE samples is around 200-230 g/L (~1.1 M).

For plant samples, it would not be possible to use buffer solutions to control pH effectively as diluting samples would influence the rate of degradation and the most accurate degradation rate of clavulanic acid in each sample was desired. Furthermore, pH adjustment *via* the direct addition of an acid or base, rather than using a buffer system, is more representative of the method of pH control used in the manufacturing process. Therefore, the pH of plant samples was adjusted to the required level through the addition of sulfuric acid or sodium hydroxide solutions. A smaller pH range of 3-7 (relative to earlier studies spanning pH 3-9) was investigated with samples from the manufacturing process as it reflects the pH range that would be expected throughout the process. pH adjusted solutions were stored in a water bath at 25 °C to control the temperature whilst the degradation process took place. Aliquots were taken immediately after the pH was adjusted and then subsequently at time intervals of 2 h

over a period of 8 h; aliquots were diluted appropriately for analysis depending on the stage of the process from which they were taken. The K313 reverse phase HPLC method was used to determine clavulanate concentration.

The natural log of clavulanic acid concentration was plotted against time in the same way that potassium clavulanate was in section 2.3.1. The plots were shown to be linear over the time period investigated. The rate constants determined for each of the plant samples are summarised in **Table 4**.

Table 4. Degradation rate constants calculated for pH range 3-7 for UF, RO, XAD and BE samples.

| pH | Degradation rate constant in UF samples / h⁻¹ | Degradation rate constant in RO samples / h⁻¹ | Degradation rate constant in XAD samples / h⁻¹ | Degradation rate constant in BE samples / h⁻¹ |
|-----------|---|---|--|---|
| 3 | 0.0326 | 0.0982 | 0.1042 | 0.0884 |
| 4 | 0.0158 | 0.0342 | 0.0283 | 0.0462 |
| 5 | 0.0084 | 0.0142 | 0.0126 | 0.0204 |
| 6 | 0.005 | 0.0194 | 0.0186 | 0.0127 |
| 7 | 0.0046 | 0.0294 | 0.0369 | 0.0174 |

The samples that were taken from the UF stage of the manufacturing process gave the lowest overall pseudo-first order rate constants for clavulanic acid degradation. UF filtrate most closely resembles the fermentation broth from the stages in the process studied, as a result it is expected to contain the most impurities that could potentially serve to catalyse the degradation of clavulanic acid. The stability of clavulanic acid appears to increase when the pH of a UF sample is higher. From the pH values investigated, the one that gives the slowest degradation of clavulanic acid is pH 7; however, the difference between 7 and 6 is marginal. The pH versus degradation rate constant plot for UF samples is shown below (**Figure 51**).

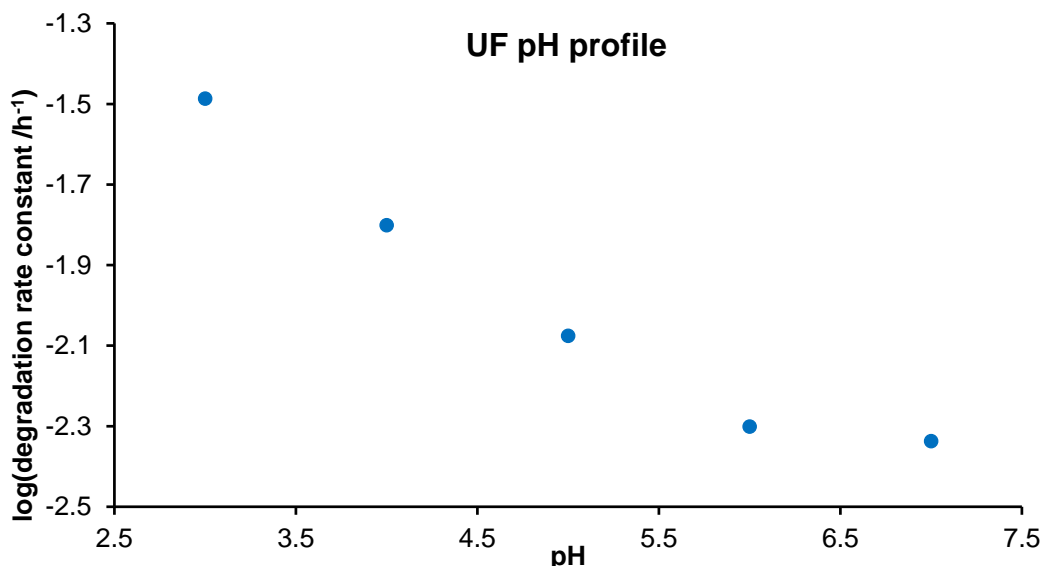


Figure 51. pH versus CA degradation rate constant plot for UF stage of manufacture.

Samples taken from the RO stage are similar to those from the UF stage in terms of chemical makeup. The RO samples are however, more concentrated than the UF samples. Comparatively, the rates of degradation in RO samples are higher for each pH measured. The pH versus degradation rate plot (**Figure 52**) does show a slightly different trend for RO than UF. It was found the most stable pH region for the RO concentrate was around pH 5. The magnitude of change in degradation rate between each pH was also higher for RO than for UF (refer to **Figure 55** for a comparison of all sample points).

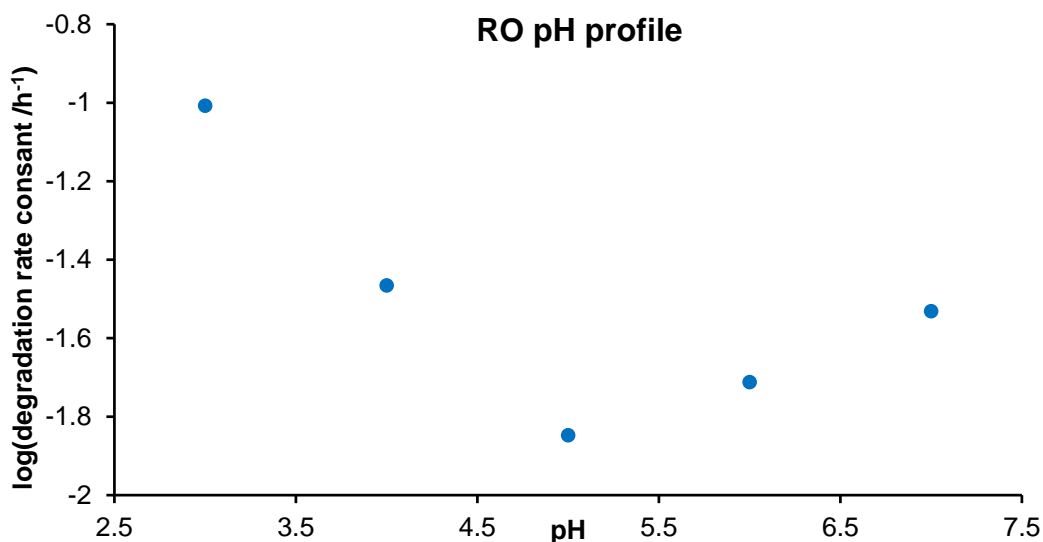


Figure 52. pH versus CA degradation rate constant plot for RO stage of manufacture.

The XAD column percolate is very similar to the RO concentrate since the step simply involves passing the batch through a XAD resin column to remove APSs from solution. Consequently, it would be expected that the degradation rates between the samples taken from each of the two stages would be comparable. The results demonstrated that that was the case; the XAD percolate was also shown to be the most stable around pH 5 (**Figure 53**). When the pH deviated further from the most stable value (at pH 3 and 7) the degradation rates from the XAD percolate were calculated to be slightly higher. The XAD columns remove acid precipitable solids from the process stream; it is possible that some of the compounds removed in this stage had a stabilising effect on clavulanic acid in solution. Alternatively, the accelerated degradation rate of the XAD percolate in comparison to the RO concentrate could be a result of clavulanic acid degradants being present in solution since clavulanic acid will have existed in solution for a longer period of time in XAD samples than RO samples. It was shown in a study by Brethauer *et al.*³⁴⁶ that clavulanic acid degradants are capable of catalysing the degradation of clavulanic acid.

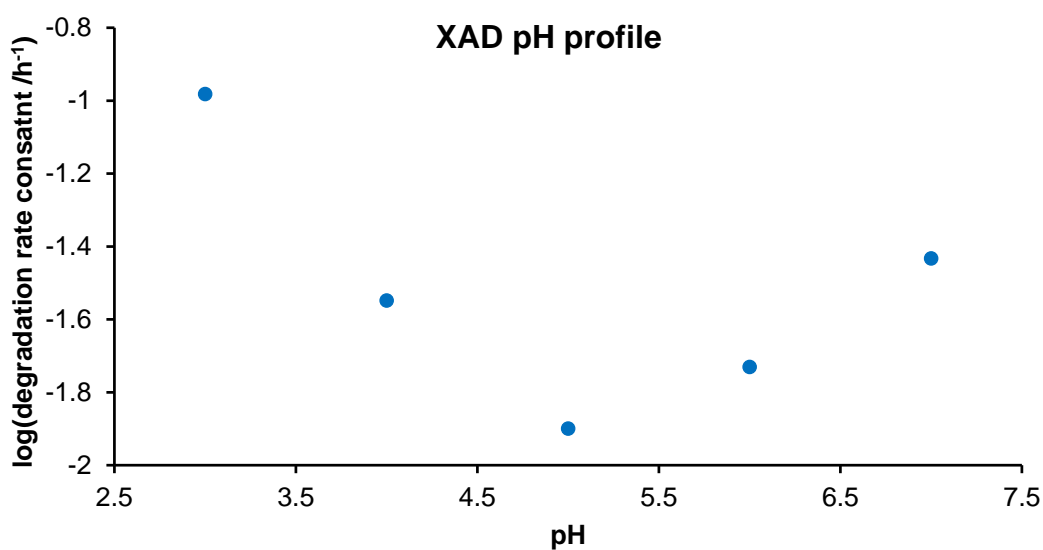


Figure 53. pH versus clavulanic acid degradation rate constant plot for XAD stage of manufacture.

Out of the four stages of the extraction process examined during this part of the project, the rich aqueous stream from the back-extraction step has the most concentrated clavulanic acid content, so faster degradation rates might be expected. However, a range of clavulanic degradants remain in the organic MiBK phase so the catalytic potential of these degradants will be reduced. The most stable pH for the back-extraction step was shown to be in the region of pH 6 showing only a slight increase in degradation rate as the pH is raised towards 7 (**Figure 54**).

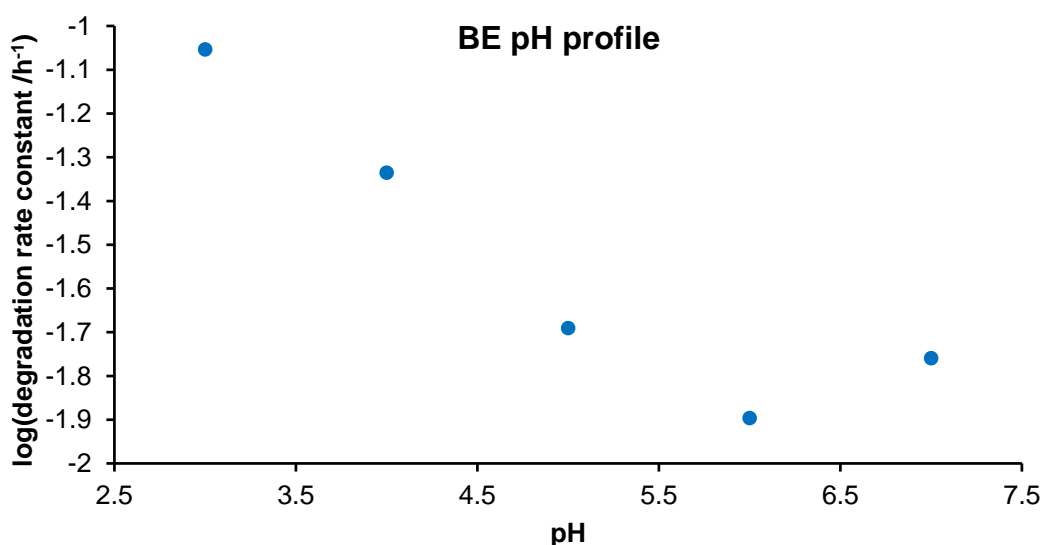


Figure 54. pH versus clavulanic acid degradation rate constant plot for BE stage of manufacture.

The pH profiles obtained for each stage of the manufacturing process have been superimposed onto a single plot to allow for a direct visual comparison (**Figure 55**). The plot makes it clear that the pH range of 5-6 is, in general, the most stable pH region for clavulanic acid. These data agree with the degradation studies carried out with potassium clavulanate in buffered solutions, suggesting that potassium clavulanate experiments are a good way of modelling the effect that pH has on other plant samples. The results do, however, show that chemicals in solution other than clavulanic acid itself appear to have an effect on the magnitude of the CA degradation rate, so the simplified potassium clavulanate model must be used with caution.

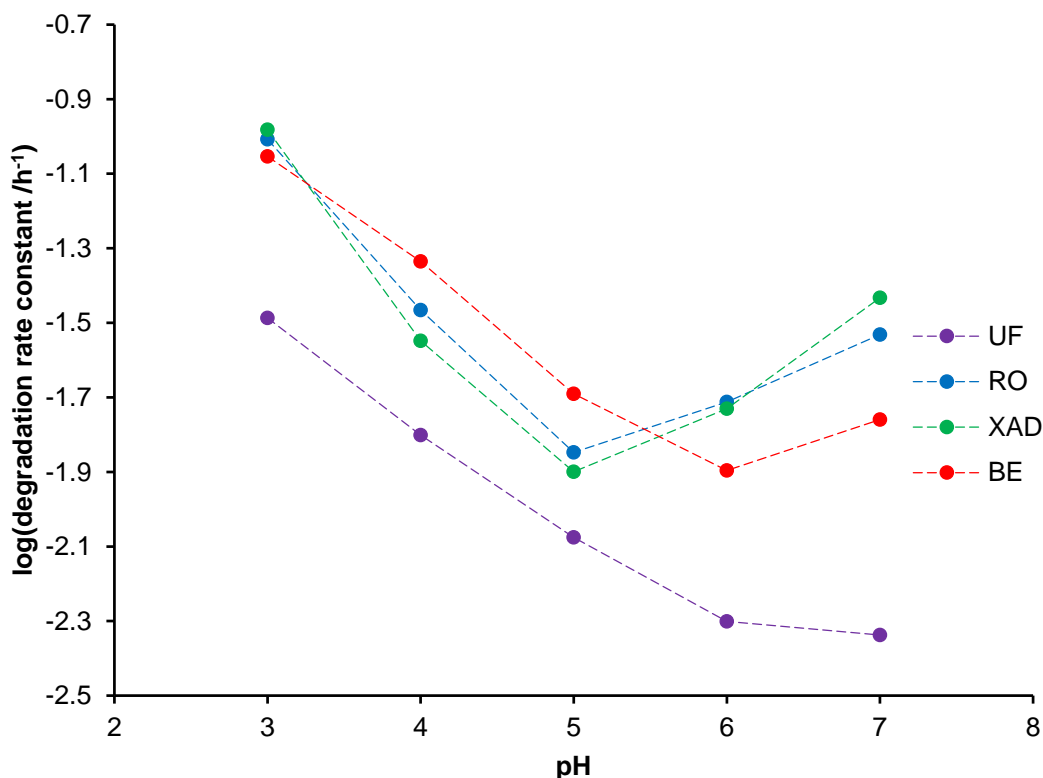


Figure 55. pH versus clavulanic acid degradation plots for UF, RO, XAD and BE stages overlaid on a single graph. Dotted lines in each data series are included solely as a guide to the eye.

Effect of Temperature and pH on the Degradation Rate of Clavulanic Acid in Reverse Osmosis Samples

The investigations up until this point have demonstrated that pH has a pronounced effect on the rate of clavulanic acid degradation in both sterile clavulanate solutions and in samples taken from various stages of its industrial manufacture. It is known that, as the temperature of a clavulanic acid-containing solution increases, the rate at which clavulanic acid degrades also increases. The following part of the project aimed to increase the understanding of how temperature affects clavulanic acid degradation. Furthermore, an appreciation for how temperature effects degradation rate over a range of pH values would be valuable as both parameters could feasibly be varied unintentionally in the manufacturing process, resulting in myriad process safety concerns.

The initial temperature-focussed experiments looked at samples taken from the RO stage of the production process. The rate of clavulanic acid degradation was determined in RO samples at integer pH values between 3-7 each at temperatures of 5, 10, 20, 25, 30, and 40 °C. The samples were pH-adjusted with either sulfuric acid or sodium hydroxide solution. Reactions at 5 °C and 10 °C were temperature controlled by containing the sample in a jacketed vessel for the duration of the study. Investigations carried out at 20, 25, 30 and 40 °C used a water bath to maintain the desired temperature throughout the course of the experiment. All experiments were carried out in triplicate using RP-HPLC to measure degradation. The results of these experiments are given in **Table 5**.

2-D plots were created of pH vs degradation rate at each individual temperature, and of temperature vs degradation rate at each individual pH. In order to aid the visualisation of the effect that pH and temperature simultaneously have on the degradation rate of clavulanic acid in RO samples, a 3-D surface plot was generated (**Figure 56**). At each temperature investigated, the pH vs degradation rate shows a similar trend with the most stable pH appearing to be around 5.

Table 5. Degradation rate constants of clavulanic acid in RO samples 5 °C, 10 °C, 20 °C, 25 °C, 30 °C and 40 °C in the pH range 3-9.

| | pH 3 | pH 4 | pH 5 | pH 6 | pH 7 |
|--------------|------------------------|------------------------|------------------------|------------------------|------------------------|
| 5 °C | 0.0291 h ⁻¹ | 0.0117 h ⁻¹ | 0.0009 h ⁻¹ | 0.0034 h ⁻¹ | 0.0039 h ⁻¹ |
| 10 °C | 0.0276 h ⁻¹ | 0.0126 h ⁻¹ | 0.0056 h ⁻¹ | 0.0092 h ⁻¹ | 0.0112 h ⁻¹ |
| 20 °C | 0.0879 h ⁻¹ | 0.0224 h ⁻¹ | 0.0079 h ⁻¹ | 0.0112 h ⁻¹ | 0.0270 h ⁻¹ |
| 25 °C | 0.0982 h ⁻¹ | 0.0342 h ⁻¹ | 0.0142 h ⁻¹ | 0.0145 h ⁻¹ | 0.0294 h ⁻¹ |
| 30 °C | 0.1536 h ⁻¹ | 0.0456 h ⁻¹ | 0.0349 h ⁻¹ | 0.0260 h ⁻¹ | 0.0436 h ⁻¹ |
| 40 °C | 0.2494 h ⁻¹ | 0.0723 h ⁻¹ | 0.0484 h ⁻¹ | 0.0811 h ⁻¹ | 0.1151 h ⁻¹ |

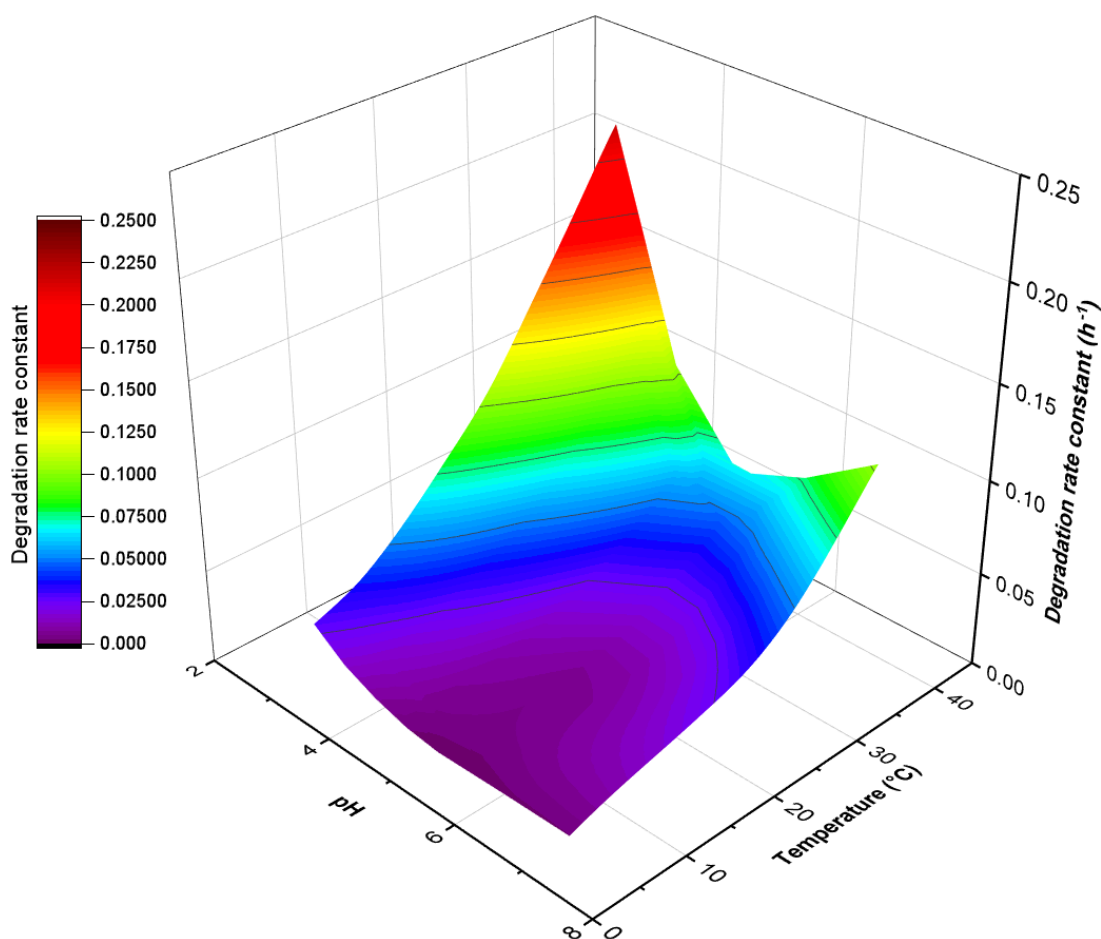


Figure 56. Surface plot showing the effect of pH and temperature on the rate of clavulanic acid degradation in RO broth.

As anticipated, the rate of degradation increased as the temperature is increases; however, the extent to which the rate is affected by temperature appears to be dependent on the pH of solution. At the stable pH region, around pH 5, degradation rate at 5 °C is 0.0009 h⁻¹ and at 40 °C it is 0.0484 h⁻¹. Outside of this stable pH region, the temperature sensitivity is more drastic, particularly at pH 3 where the rate has the steepest temperature dependence. These data are useful for identifying areas of the process where clavulanic acid could be susceptible to degradation. It demonstrates that the solution temperature is important to consider for stages of the process where the pH is outside of the stable region, for example, upon the addition of sulfuric acid for extraction into MiBK. In contrast, in the range pH 5-6, such as the RO concentrate vessels, the temperature is less important to control. These vessels are outdoors and as such are not prone to high temperatures; this would suggest that attempting to control

the temperature of broth in these vessels would outweigh the benefits in terms of degradation rate.

2.3.3 Understanding the Aqueous Degradation Pathways of Clavulanic Acid

Introduction

The previous section has focussed on the rate at which clavulanic degrades under varying pH. Together with a knowledge of how quickly clavulanic acid degrades under varied pH, it is useful to understand its degradation pathway. Some of degradation products of clavulanic acid have previously been described but the full pathway is not currently understood. It is also known that the degradation products are different when the degradation procedure takes place under acidic or basic conditions. Having a more comprehensive understanding of the degradation pathway may be useful to highlight ways in which the degradation process could be retarded and potentially even halted. Ultimately it may be possible identify development opportunities to improve the efficiency of the extraction process.

This section aims to provide an overview of methods that are useful in elucidating the pathway by which a drug compound degrades. The experimental efforts that have been carried out during this PhD towards identifying clavulanic acid degradants will then be discussed.

Identifying Drug Degradation Pathways

Understanding the degradation pathway is essential when designing a drug especially for factors such as formulation and drug storage. To this end, stress tests are carried out which subject drugs to extreme conditions to force the degradation. Stress tests are a minimum requirement from the United States Food and Drug Administration (FDA) and the International Council for Harmonisation of Technical Requirements for Pharmaceuticals for Human Use (ICH), to ensure an appropriate knowledge for drug design.³⁴⁷ In addition to identifying conditions under which drugs are susceptible to degradation, the forced stability tests also serve as a platform to identify drug degradation products. Liquid chromatography mass spectrometry (LCMS) is widely used for identifying the degradation products.^{348,349}

A theoretical degradation map is produced based on the potential degradation pathways that could be observed for the drug molecule of interest. This map considers

the functionalities within the molecule and how these might be expected to behave in a range of different reaction types such as hydrolysis, oxidation and photodegradation. Existing literature from congeners and structurally similar drugs are used along with computational chemistry to aid the prediction of how a drug might degrade.^{348,349} Molecular ions that are identified can then be correlated back to the proposed degradation map to give an insight what degradants are being formed. In some cases, MS/MS is used to provide evidence for the structure of a degradant identified by LCMS. Although the LCMS technique can provide information about the degradation products, identifying the products alone is not always sufficient. Multiple proposed pathways may lead to a common product and in some cases the occurrence of one degradation pathway could potentially set off another.³⁵⁰

Knowledge of the actual degradation pathway followed can give an insight as to what factors could be modified to improve the stability of a drug. Mass spectrometry remains key in elucidating the degradation pathway of a drug, particularly in conjunction with isotopic labelling. When investigating the hydrolysis of a drug, for example, the hydrolysis could be performed in both normal water ($^{16}\text{OH}_2$) and isotopically-enriched water ($^{18}\text{OH}_2$), a disparity in the masses generated from degradation in the two experiments can be used as evidence for the incorporation of water.^{350,351} Hydrogen/deuterium isotopes can be exploited to identify labile drug protons through the rate of ion exchange.³⁴⁹ Furthermore, mechanistic insights can be gained through the measurement of kinetic isotope effects.³⁵¹ Isotopic effects can be detected high resolution mass spectrometry (HRMS) or NMR spectroscopy when nuclei are spin active. The kinetics of degradation in non-isotopically-enriched experiments can also provide mechanistic insights to the degradation profile of a drug.^{349,352}

This Work

The objective for this part of the report is to improve the understanding of the degradation pathway(s) of clavulanic acid. Attempts will be made to identify degradation products of clavulanic acid under acidic, neutral and basic conditions. Understanding the degradation pathway(s) will be helpful to identify ways in which

the efficiency of the clavulanic extraction process may be improved. Strong acid or base, such as hydrochloric acid or sodium hydroxide, respectively, will be used to force the degradation of clavulanic acid in solution. Attempts will then be made to separate degradation mixture components from solution and identify the chemicals playing a part in the degradation process.

Results and Discussion

In addition to degradation rate studies (*vide supra*), efforts were also made to isolate and identify individual products from clavulanate degradation mixtures. The motivation for identifying degradation products was to improve the understanding of the degradation pathway of clavulanates under different conditions. Working with clavulanic acid and its clavulanates presents a number of practical complexities to be considered. The clavulanate starting materials have poor solubility in most solvents other than water: ethylacetate, diethylether, dichloromethane, and chloroform were all shown not to solvate either potassium clavulanate or t-BA clavulanate. The solubility of the clavulanates in methanol, dimethyl sulfoxide (DMSO) and combinations thereof was reasonable, albeit lower than the solubility in water. Furthermore, clavulanic acid is in aqueous media for the majority of the industrial manufacturing process. Therefore, in terms of data that would be relevant to this process, the degradations would have to be carried out in water.

A further difficulty faced is the readiness with which clavulanic acid degrades. The samples would need to be sufficiently degraded for degradation products to be present in a suitable concentration for analysis; however, the rate at which the starting material and degradants are consumed would need to be slow enough for separation and identification to be carried out during the process. The third major difficulty that has been identified is the fact the degradation products may not have chromophores for easy detection (e.g. by UV-vis). The α -amino ketone degradation product that is already known (1-amino-4-hydroxybutan-2-one), for example, would not be expected to strongly absorb UV radiation (**Figure 57**). It is plausible that other small molecule degradants are generated that will not be observed via UV detection methods.

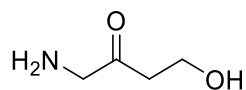


Figure 57. Structural motif of 1-amino-4-hydroxybutan-2-one, a known clavulanic acid degradant with a lack of chromophore for UV detection.

Thin Layer Chromatography

Either potassium or t-BA clavulanate were subjected to 2 M hydrochloric acid or 2 M sodium hydroxide in order to force the degradation of clavulanic acid in these experiments; therefore, all degradation experiments were carried out in aqueous media. Preliminary experiments dissolved 40 mg potassium clavulanate in 5 mL water and 1 mL 2 M HCl or 2 M NaOH were added to force the degradation process. Upon addition of acid to a solution of potassium clavulanate, the solution turned from colourless to light orange, effervescence was observed and a significant increase in temperature could be felt through the walls of the reaction vessel. Within 1-2 hours, the mixture became dark orange/brown in colour and appeared more viscous; when left for a longer period of time (ca. 10 h), a dark brown solution with a syrup-like consistency was obtained. When sodium hydroxide is added instead of acid, the solution immediately turned an intense yellow colour, over time this colour darkens to an orange and then eventually dark brown; the solution does not effervesce in the same way as the analogous experiment under acidic conditions. The difference in observations for each of the reaction conditions supports the fact that different degradation pathways are followed for acid- and base-catalysed degradations.

Thin layer chromatography (TLC) was initially trialled as a means of monitoring the clavulanic acid degradation. It was anticipated that TLC would give information about the amount of degradation products present and an insight to the ease with which degradants can be separated using a normal-phase chromatographic system. Ethyl acetate-cyclohexane (1:1) and methanol-dichloromethane (1:9) solvent mixtures were both trialled as a mobile phase. UV was first used to visualise any spots that eluted up the TLC plate; however, no spots were visible other than the original spot on the base line. As previously mentioned, the degradation products may not have exploitable

chromophores so it was deemed possible that there was adequate chromatographic separation but, ultimately, components could not be observed this method. Consequently, potassium permanganate and vanillin stains were both used to visualise any spots on TLC plates. Once again, neither method of developing the TLC plates showed any spots that had moved from the baseline. It is thought that the components in the mixture were very polar and as such showed a strong affinity for the stationary silica phase and thus did not elute up the TLC plates; another possibility to consider is that volatile degradation products could be produced that evaporate from the plate. Although there was the possibility that none of these methods detected any spots that had moved up the plate, it was thought to be more plausible that there was no separation seen via TLC.

TLC was shown to be of limited value for reasons aforementioned; it did however, suggest that reversed phase chromatography could be more suited to separating out degradants. Reversed phase HPLC was shown to be useful in the kinetic investigations into the effect of pH on clavulanic acid degradation (*vide supra*), so as a preliminary experiment, the RP-HPLC K313 method was used to obtain a chromatogram of both an acid and base degraded sample of potassium clavulanate.

Chromatograms using the reversed-phase HPLC K313 method have shown that degradation mixtures have different components depending on whether acid or base is used to catalyse degradation (**Figure 58**). Aside from the confirmation of different products, the method also showed that RP-HPLC was able to show some separation of the components in solution. The HPLC chromatograms obtained are useful for determining concentration of components with known elution times; however, in terms of identifying degradants, other means of using reversed phase chromatography were investigated.

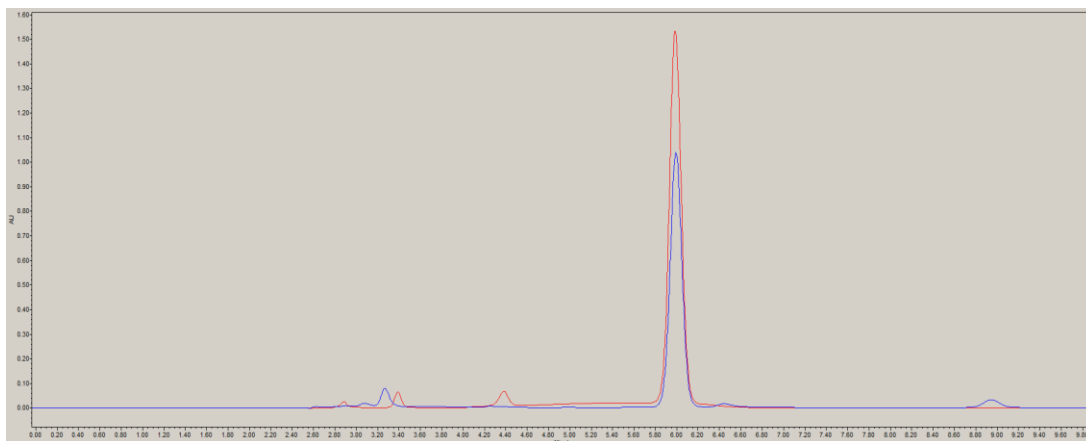


Figure 58. K313 HPLC chromatograms of acid-degraded (red) and base degraded (blue) samples of potassium clavulanate. The common peak at 6.00 minutes is due to undegraded clavulanate.

Liquid Chromatography Mass Spectrometry

LCMS has been used in attempts to gain an insight as to the chemical make-up of clavulanic acid degradation products. LCMS uses a reversed phase column whose eluents are analysed with an electron spray ionisation mass spectrometry detector (ESI-MS). Conveniently, for the reversed phase method, water can be used as the analyte matrix; this meant that samples could be taken directly from degradation reaction mixtures and analysed quickly and efficiently. LCMS data was obtained for potassium clavulanate in water (**Figure 59**) and t-BA clavulanate (**Figure 60**) in water as a reference point. Using the high pH modifier, clavulanic acid is seen to elute at 0.44 min. The clavulanate ion has a molecular mass of 199 g mol^{-1} , the spectra obtained for both potassium and t-BA clavulanate show $[M+H]^+$ ion at 200 m/z and the $[M-H]^-$ ion at 198 m/z. With the knowledge that the clavulanate ion could be identified *via* LCMS, the technique was then used to try and identify degradants in acid and base degraded samples.

The LCMS instrument employed has 3 different reversed-phase methods, each with a different eluent modifier: a trifluoroacetic acid modifier, known as the TFA method; a formic acid modifier, known as the formic method; and an ammonium bicarbonate modifier, known as the high pH method. A sample of 40 mg potassium clavulanate was dissolved in 2 mL 2 M HCl and an aliquot was analysed with the LCMS instrument on the TFA, formic and high pH method. The formic method showed the

best separation of peaks. A similar experiment was carried out using potassium clavulanate in 2 mL 2 M NaOH, and again the formic method provided the best peak separation. The formic method was used in all subsequent LCMS analysis of degraded samples. Unfortunately, although the formic method showed the best separation, the resolution was generally poor and peaks did not have clear masses associated with them. An example of an LCMS analysis carried on an acid degraded sample (**Figure 61**) and a base degraded sample (**Figure 62**) are shown; both samples were taken immediately after the addition of acid or base, as over time the samples gave a complex mixture which was difficult to extract valuable data from.

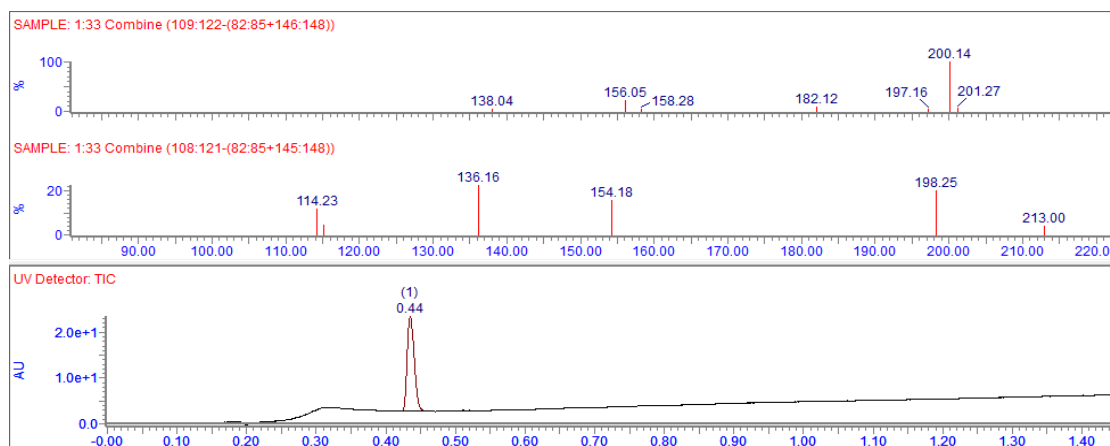


Figure 59. The LCMS spectrum data obtained for potassium clavulanate in water via the formic method. The peak at 0.44 min corresponds to the clavulanate ion.

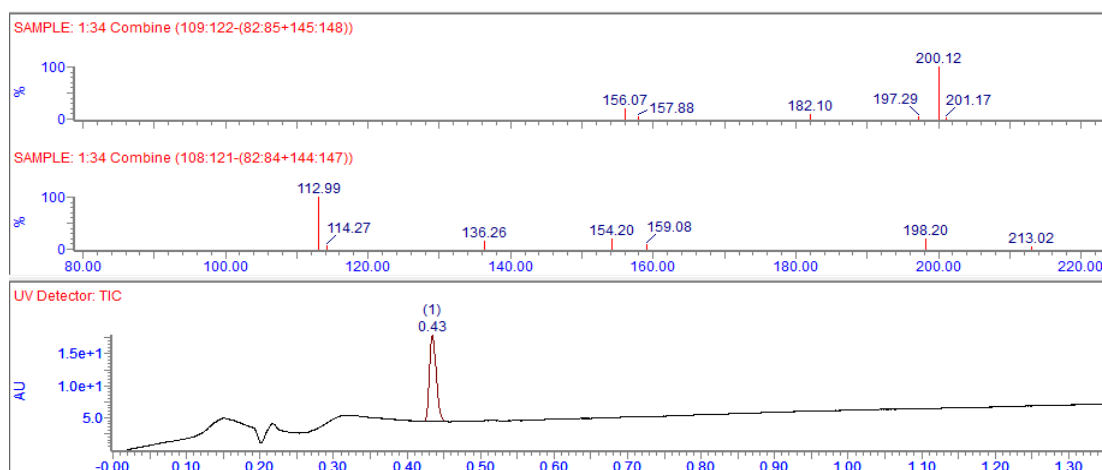


Figure 60. The LCMS spectrum data obtained for t-BA clavulanate in water via the formic method. The peak at 0.44 min corresponds to the clavulanate ion.

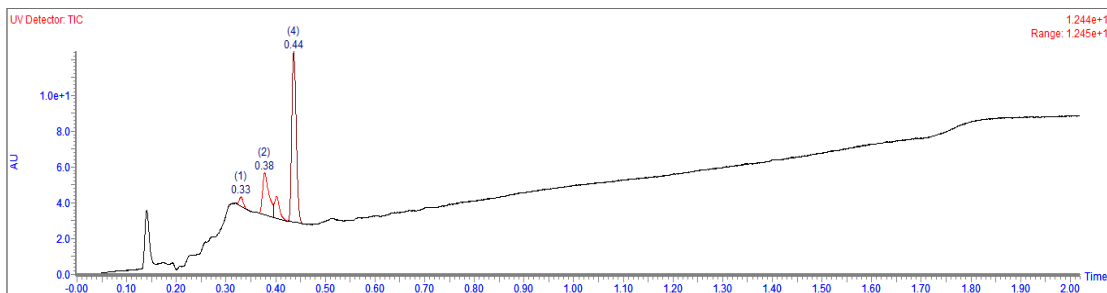


Figure 61. The UV spectrum obtained from an LCMS analysis of a HCl degraded t-BA clavulanate sample via the formic method.

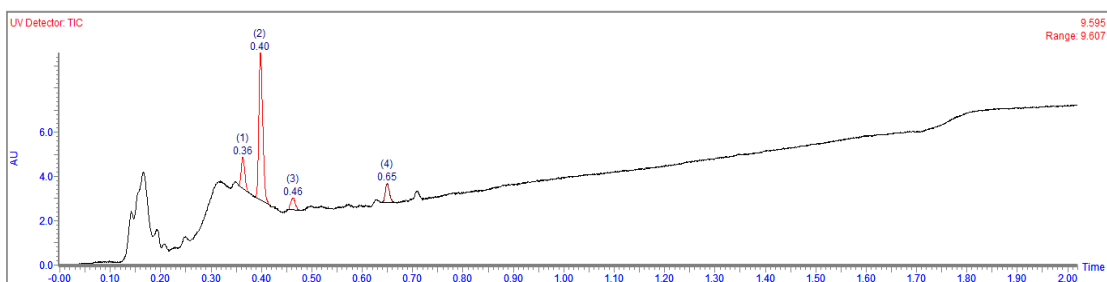


Figure 62. The UV spectrum obtained from an LCMS analysis of a NaOH degraded t-BA clavulanate sample via the formic method.

Although the data obtained from the LCMS were difficult to draw solid conclusions from as to the identity of the degradation products, it was thought that it may be useful to see if any of the peaks could be observed to shrink or grow over time. An instrument named AmigoChem was used to do this. The instrument allows a series of experiments to be set up simultaneously in separate reaction chambers. At predetermined time intervals, the instrument draws a 4 μL aliquot of the reaction mixture and dilutes it with a diluent of choice, which, in this case, was water. At the end of the run, the samples can then be analysed by the desired method.

Four reactions were set up on the AmigoChem instrument; potassium clavulanate and t-BA clavulanate were each degraded in HCl or NaOH and samples were taken every 2 h for a total period of 24 h. The samples were then analysed *via* LCMS at the end of the reaction time via the formic method. In the case of t-BA clavulanate with HCl, the

area under each of the peaks appeared to change relative to one another (**Figure 63**); however, the resolution was too poor, precluding accurate analysis of individual peak areas. Furthermore, the peaks could not be assigned a mass from the mass spectra with any certainty. For samples of both potassium clavulanate and t-BA clavulanate that were degraded with NaOH, the peaks were small and poorly separated throughout, and as such, no valuable data could be obtained.

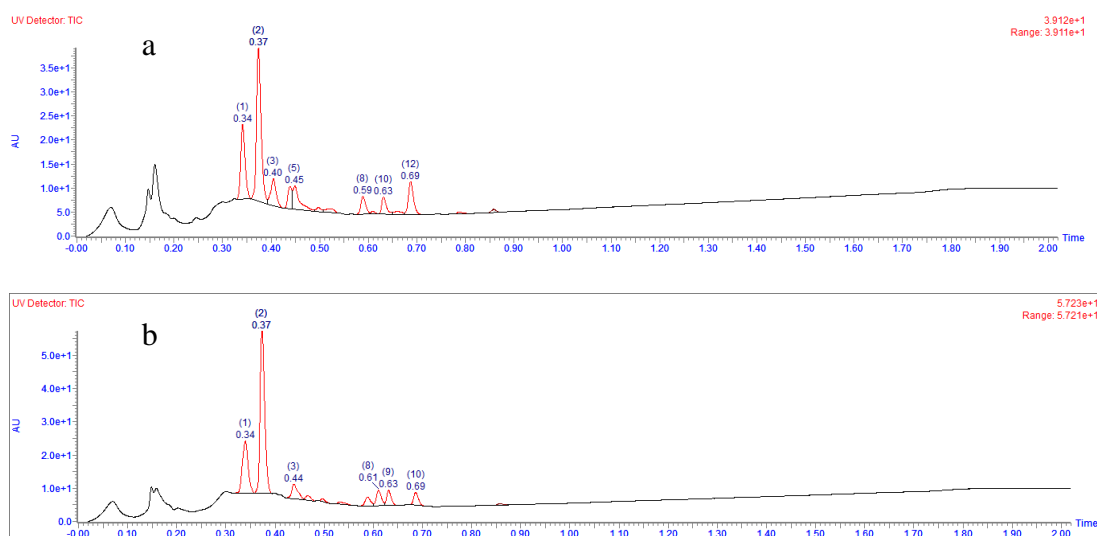


Figure 63 a) LCMS UV spectrum for HCl degraded t-BA clavulanate immediately after HCl addition. **b)** LCMS UV spectrum for HCl degraded t-BA clavulanate 16 h after addition of HCl.

One possible reason for the base-degraded sample giving poor LCMS results is that the rate of degradation was rapid on the timescale of offline sampling. It is feasible that the concentration of sodium hydroxide, and thus the pH, was too high, such that the clavulanate was degraded before the first sample was taken. Another potential issue is that after an aliquot was taken from the reaction, it was diluted with water and held at room temperature until further analysis. Clavulanic acid degradation shows first order kinetics so would be slowed down due to the dilution; however, it would not be halted entirely. Given the data showing potassium clavulanate degrades rapidly at high pH (*vide supra*), it is possible that the degradation reaction continued after sampling such that upon analysis, the degradation process was complete for all reactions.

Another factor may be that of the four reactions, three contain metal ions (Na^+ or K^+); these ions could have a deleterious effect on the mass spectra. There are no metal ions present in the t-BA clavulanate and HCl reaction. Finally, there is the possibility that some degradants do not contain chromophores so were not picked up in the UV trace.

As the resolution of LCMS spectra was generally poor in acid- and base-degraded samples, a collaboration with a specialist from the purification team at GSK Stevenage was established. A screen of various reversed-phase columns, eluents, and physical parameters was used in attempt to find conditions that could be used to separate clavulanic acid degradant mixtures with an appropriate resolution. Unfortunately, similar issues were encountered with poor resolution of peaks and a lack of confidence in assigning masses to peaks. With LCMS techniques returning data that was not conclusive in terms of identifying the degradation products, efforts were made to isolate components from degradation mixtures for identification.

In addition to the use of LCMS, mass directed automated purification (MDAP) was used in an attempt to isolate compounds. The technique utilises a reversed-phase automated column with a mass spectrometry analyser; upon detection of predetermined masses, the eluting material is collected into fractions. The potential use of MDAP was limited as the mass of products needs to be computed into the instrument and it was unknown what the expected masses would be. Unfortunately, this technique did not yield any results that were more useful than standard LCMS analysis.

Column Chromatography

Given that product separation had been observed through HPLC experiments, it was considered that using reversed phase flash column chromatography may be able to separate components from a reaction mixture on a slightly larger scale where the elutents could be collected for later analysis. A CombiFlash rf automated column system was used in the following experiments equipped with a C_{18} reversed phase column; the mobile phase consisted of water and acetonitrile, each of which had a formic acid modifier.

Potassium clavulanate was dissolved in a small volume (approximately 1 mL) of 2 M HCl and allowed to degrade until a dark orange colour was observed. LCMS was also used to check that the clavulanate had been consumed. This was then loaded onto the C₁₈ column, a solvent gradient was used from 0-100% acetonitrile over an 18-minute period and UV detection was used at 213 nm, 248 nm and 268 nm. Unfortunately, the contents of the sample eluted from the column with poor separation. The peaks were indistinguishable and as such the fractions were shown by LCMS to be mixed. The same experiment was carried out with NaOH degraded potassium clavulanate and HCl or NaOH degraded t-BA clavulanate; the t-BA clavulanate and HCl combination showed the best separation from UV trace so this reaction was used in subsequent attempts to improve the resolution of the chromatogram.

The chromatograms followed a similar pattern whereby a number of peaks would elute along with the initial aqueous solvent, suggesting the degraded compounds had a high polarity. When the acetonitrile gradient started, a number of other components would then elute in quick succession. Numerous parameters were varied to improve the separation of compounds. The volume of reaction solution was kept as low as possible to allow for a smaller loading volume on the column. The flow rate of the eluent was decreased to improve the separation of peaks. The eluent gradient was also altered; it was found that using 0% acetonitrile for the initial 10 min of a column run would allow for a slight separation of the early eluting peaks. A gradient was then used from 0-30% acetonitrile over the course of 15 min which gave some separation of the second band of eluting peaks. The instrument was programmed to automatically collect fractions when peaks were detected from the UV trace. Fractions were analysed via LCMS and typically showed multiple m/z peaks in the mass spectra suggesting either that the separation was not very efficient, or that compounds continued to degrade between the time of collection and analysis. Nonetheless, some fractions showed potential from their LCMS spectra to be an isolated compound. A range of techniques was used in the attempt to remove water from the fractions to allow the analysis of the isolate degradants.

The first technique to remove water from fractions which appeared to have a reasonable purity of unknown degradants was rotary evaporation. Water is difficult to remove *via* evaporation so the rotary evaporator water bath was heated to 40 °C.

However, the application of heat to the solution appeared to have caused further degradation of its components, this was confirmed by LCMS which now showed a mixture of products. Removal of water was carried out via rotary evaporation nonetheless and completed on a high vacuum drying line. The result was a brown solid that had a plastic-like texture. This solid was recalcitrant towards dissolution in water, DMSO and chloroform; the insolubility in water supports the argument that the solute had degraded further during the evaporation process.

As the application of heat was thought to have promoted the further degradation of the isolated degradant itself, techniques that avoided the use of harsh conditions to remove solvent were explored. A blowdown apparatus was used to remove water from a fraction obtained from the CombiFlash that LCMS suggested contained a single compound. The apparatus blows a stream of nitrogen across the surface of sample to aid with evaporation of solvent; the process is slower than rotary evaporation but removes the requirement to apply heat. The blowdown apparatus yielded a solid that appeared to be similar to that which was yielded from rotary evaporation; neither sample was soluble to analysis via NMR or LCMS. Although heat was not applied, the process was slow which allowed time for degradation of components in solution; furthermore, towards the end of the evaporation process, the solution would have been at a high concentration which could feasibly have promoted further degradation.

Freeze drying was explored as a potential method of removing water from fractions as the sample is kept at low temperature throughout. Acetonitrile had to first be removed completely so that the sample could be frozen; this was carried out via rotary evaporation at room temperature. Dry ice was then used to freeze the aqueous sample in a round bottomed flask and the sample was freeze dried overnight. The contents of the flask were a liquid when checked the next morning; likely causes for this were that the sample thawed out overnight due to a bad vacuum or incomplete removal of acetonitrile prior to freeze drying. The liquid was analysed *via* LCMS and multiple peaks were observed suggesting degradation had taken place. It was evident from these experiments that the removal of water was problematic. Two ways of circumventing this problem were proposed: (i) extracting compounds into a more volatile organic solvent and (ii) removing the need to isolate components at all by studying the degradation *via* NMR.

Fractions collected later in the reversed phase column are expected to be lower in polarity than the earlier elutents. It is possible that any compounds in these fractions could have a preference to be in a less polar organic solvent than earlier fractions. Attempts were made to perform a liquid-liquid extraction into ethyl acetate, diethylether and dichloromethane. The organic solvent could then be removed more easily *via* rotary evaporation. Analysis *via* TLC and LCMS both showed no compounds in the organic layer; the organic layers were dried to completeness. No visible product was yielded in any case but CDCl_3 was added to the round bottomed flask and a ^1H NMR spectrum was recorded in case small amount of product were left in the vessel. The NMR spectra did not show any products.

Despite not isolating any compounds suitable for analysis, the organic layer did take on a slight orange colour from the aqueous fraction when the separation was carried out. This suggests that there is mass transfer from the aqueous to the organic phase, albeit presumably limited. There was the potential that the quantity of degradants that had been extracted into the organic phase was too minimal to detect.

In response to the unsuccessful attempts to transfer the contents of reversed phase column fractions from water into an organic solvent, an alternative approach was investigated. A degradation reaction was carried out of potassium clavulanate with HCl as previously described and allowed to proceed for 1 h. The reaction mixture itself was extracted with ethyl acetate (3 x 15 mL). The colourless ethyl acetate became a pale orange colour when shaken with the degradation mixture. The organic layers were then collected and concentrated via rotary evaporation until the solution volume was reduced to approximately 2 mL.

The sample components were then attempted to be separated through a silica column on the CombiFlash instrument using a cyclohexane-ethyl acetate solvent mixture. The column did not show product peaks. TLC was used to check all fractions but no compounds were identified. It is possible that the products were transferred into the organic phase but did not contain any chromophores to be identified with, the concentration of non-polar degradants was too low to be detected, or that there was no significant transfer into the organic phase at all.

Gas chromatography (GC) has been demonstrated to be a useful technique for identifying components in chemical mixtures, especially small organic compounds. Thus, the technique would be useful if any of the clavulanic acid degradants are volatile. Water is not a suitable solvent for GC, and as such, a sample of potassium clavulanate was taken up in a methanol-DMSO 1:1 mixture. A blank sample of solvent was injected, followed by the sample containing potassium clavulanate. There was no visible peak for the clavulanate analyte, indicating that it may not be easily volatilised. Due to limitations in instrument access, the potential of this technique was not pursued further.

Nuclear Magnetic Resonance Spectroscopy

It was also attempted to use ^1H NMR spectroscopy to identify components from degradation mixtures. To avoid the necessity of removing water from the reaction mixture, a sample of potassium clavulanate was dissolved in deuterated water (D_2O) directly in an NMR tube. ^1H and ^{13}C NMR spectra as were obtained for both potassium clavulanate (**Figure 64a-d**) and t-BA clavulanate (**Figure 65a-d**). 2D Spectra: COSY, HMBC, HSQC and ROESY, were obtained also and were used to aid the NMR assignment.

t-BA clavulanate ^1H and ^{13}C NMR spectra contain peaks that correspond to acetone.³⁵³ The acetone is an artefact of the precipitation stage in the manufacturing process.

^1H NMR spectroscopy was used in attempt to follow the degradation of potassium clavulanate over time. The NMR tube was heated to $60\text{ }^\circ\text{C}$ and its ^1H NMR spectrum was recorded at 12 h and 36 h. Though there was an appearance of peaks on the baseline of the spectrum, none of these peaks had an area comparable to those belonging to clavulanic acid, even at 36 h (**Figure 66**). The lack of identifying peaks is likely due to an incomplete degradation process.

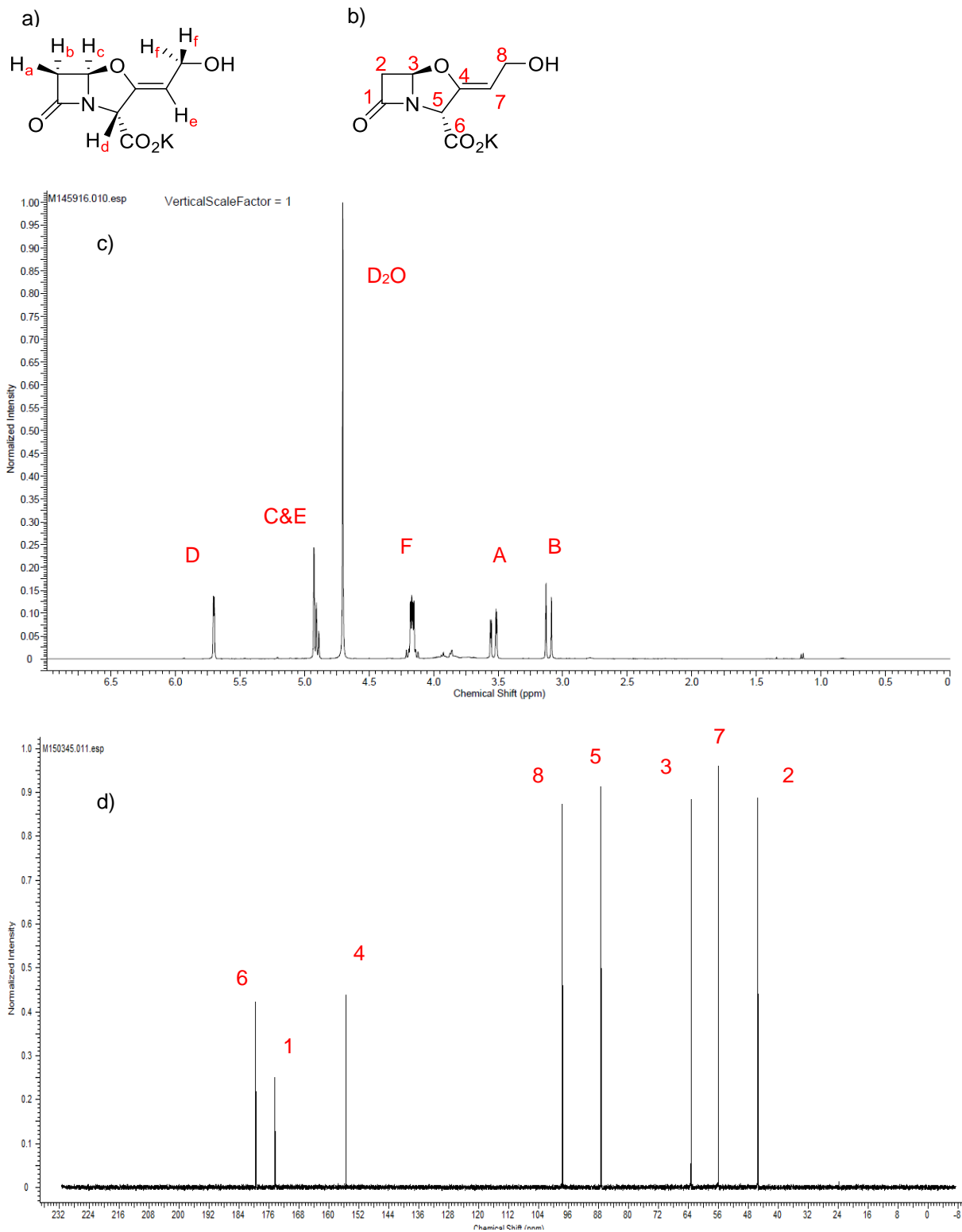


Figure 64 a) Potassium clavulanate with protons assigned letters b) potassium clavulanate with carbons assigned numbers c) ^1H NMR spectrum of potassium clavulanate in D_2O . d) ^{13}C NMR spectrum of potassium clavulanate in D_2O .

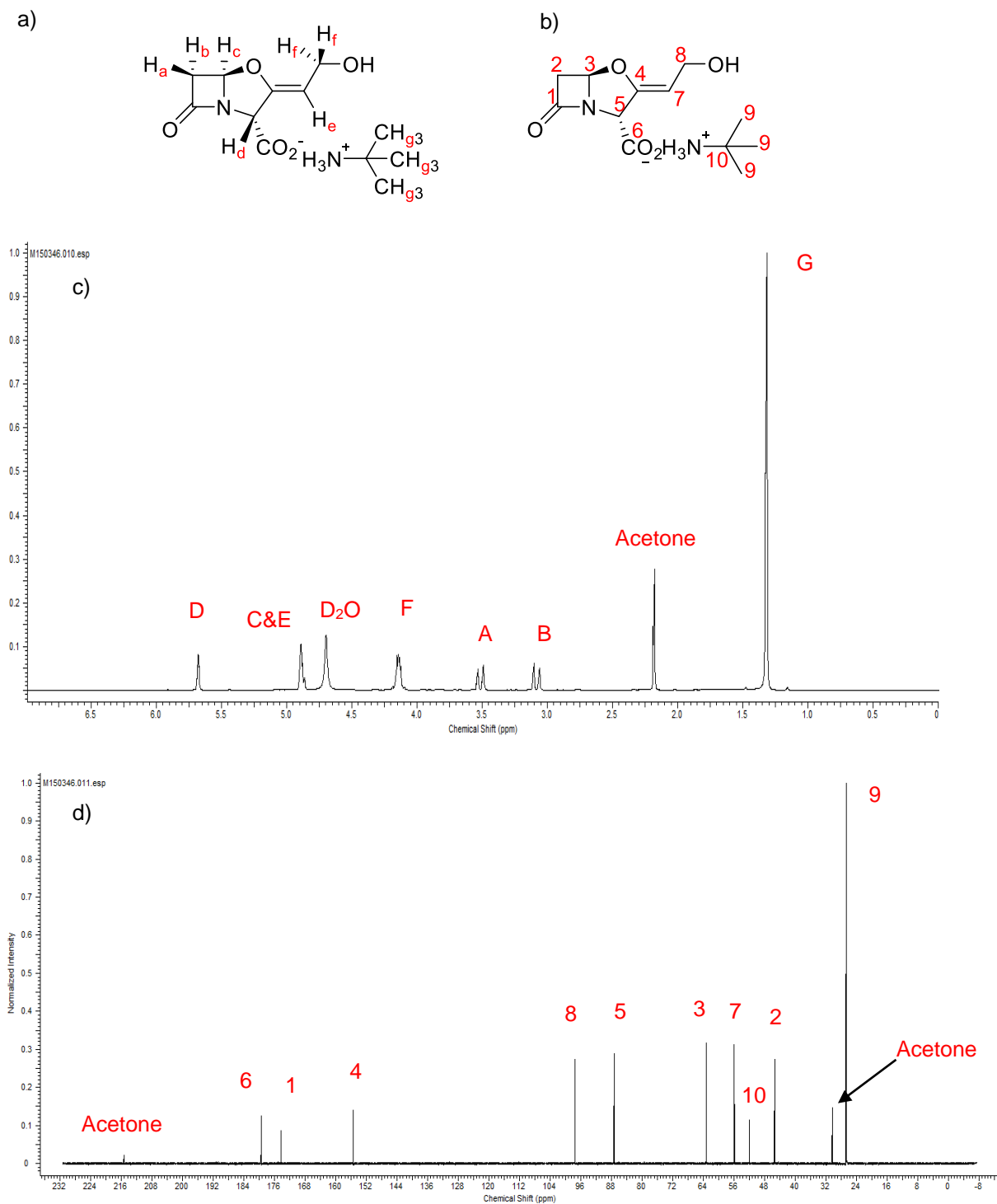


Figure 65 a) t-BA clavulanate with protons assigned letters b) t-BA clavulanate with carbons assigned numbers c) ^1H NMR spectrum of t-BA clavulanate in D_2O . d) ^{13}C NMR spectrum of t-BA clavulanate in D_2O .

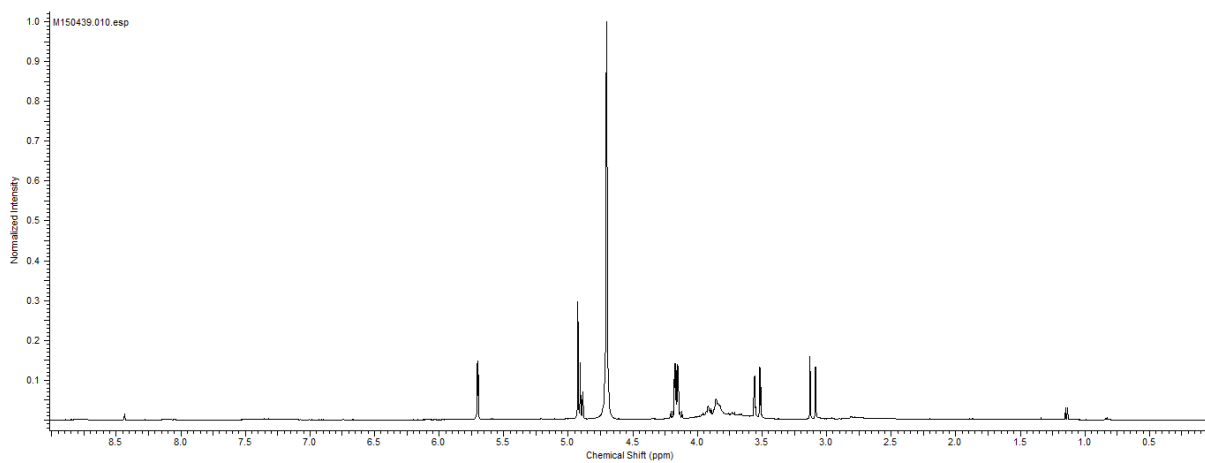


Figure 66. ^1H NMR spectrum of potassium clavulanate in D_2O after 36 h heating at $60\text{ }^\circ\text{C}$

2.4 Conclusions

From the work carried out, the following conclusions have been made:

1. A suitable method has been developed for monitoring the degradation of clavulanic acid. The method uses reversed phase HPLC with a UV detector at 230 nm to detect the quantity of clavulanic acid in solution which is then mapped over time. Buffer solutions were used to control the pH of degradation mixtures for the kinetic studies. For each pH, three concentrations of buffer could be used in order to calculate the non-buffer catalysed degradation rate.
2. Using the developed method, the degradation rates of potassium clavulanate were determined in the pH range 3-9. The results showed that between pH 5-6, the rate of potassium clavulanate degradation was the lowest. The shape of the graph suggests that degradation mechanisms are different in different pH regions but possibility of buffers influencing the shape of this curve remains to be eliminated.
3. Degradation rates of clavulanic acid in samples from the ultrafiltration, reverse osmosis, back extraction and XAD resin treatment stages of the industrial manufacturing process were calculated in the pH range 3-7. The most stable pH range appears to vary between different stages of the extraction process. Out of the stages investigated, the ultrafiltration filtrate has the lowest susceptibility to clavulanic acid degradation over the pH range studied.
4. Temperature was shown to affect the rate of clavulanic acid degradation in reverse osmosis samples. When the pH of broth was outside of the stable

pH 5-6 region, the degradation rate was particularly susceptible to change upon an increase in temperature.

5. The attempts to identify clavulanic acid degradants have been unsuccessful so far. The experiments have demonstrated that normal phase chromatography is not appropriate for separating degradation components. Separating aqueous mixtures of degradants has proven difficult owing to the high polarity of degradants and an apparent lack of chromophores with which degradants can be identified. Furthermore, removing these compounds from water is not a trivial process. The chemical composition of samples appears to change during the process, potentially due to further degradation.

2.5 Future Work

Kinetics of Clavulanic Acid Degradation

Building on the studies investigating the effect of temperature and pH on the rate of clavulanic acid degradation in RO broth, similar experiments could be carried out with other plant samples to identify areas where degradation is likely to occur. Conditions could be developed to replicate relevant parts of the plant process in the laboratory in order to carry out experiments looking at the effect of pH and temperature on the extraction efficiency. Identifying conditions where degradation is low and extraction efficiency is high may present opportunities for optimisation of the manufacturing process.

Understanding the Degradation Pathway(s) of Clavulanic Acid

Investigations into understanding the degradation pathway of clavulanic acid were largely unsuccessful. The NMR spectroscopy experiments could be continued as they allow the direct detection degradants in water and, unlike UV detection methods, do not require chromophores on the degradation products. Initially, the degradation of potassium clavulanate in D₂O would be investigated using heat to force the degradation process if necessary. An NMR spectrometer of suitable frequency would be used to obtain both one-dimensional and two-dimensional spectra in the attempt to elucidate the structure of degradants. Deuterated acid and base, such as DCl and NaOD, could also be used to compare the degradation products formed under acidic and basic conditions. Depending on the success of these experiments, carrying out the reaction in a biphasic system with deuterated organic solvent and water could be considered to identify non-polar degradants.

In addition to NMR experiments, a reactive species such as an acyl chloride could be used to modify degradants in such a way that a chromophore would be present for identification via conventional spectroscopic methods. Using a reagent with a suitably non-polar substituent may also allow for better retention on a column for purification purposes. If modifying degradation products is unsuccessful, the starting material could be appended with a substituent such as a silyl protecting group on the hydroxyl

group of the adipyl side chain such that it would be included in the degradation products.

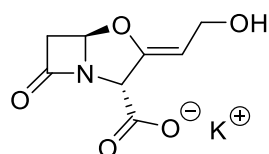
2.6 Experimental

2.6.1 General Considerations

Solvents and Reagents

Potassium clavulanate and t-BA clavulanate were obtained from the manufacturing process carried out at GSK Irvine. LCMS and NMR analysis was carried out on both clavulanate starting materials to verify their authenticity.

Potassium clavulanate

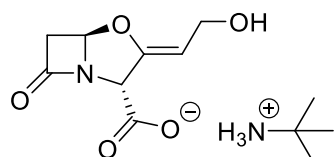


¹H NMR (400 MHz, D₂O): δ 3.11 (dd, 1H, CH₂), δ 3.54 (dd, 1H, CH₂), δ 4.17 (m, 2H, CH₂), δ 4.91 (m, 2H, CH and =CH-) δ 5.70 (s, 1H, CH).

¹³C (101 MHz, 298 K, D₂O): δ 45.4, 56.0, 63.3, 87.4, 97.6, 155.5, 174.4, 179.5

LDI-MS: [M⁻] 198.03.

t-BA clavulanate.



¹H NMR (400 MHz, D₂O): δ 1.32 (s, 9H, -(CH₃)₃), δ 3.09 (dd, 1H, CH₂), δ 3.51 (dd, 1H, CH₂), δ 4.14 (m, 2H, CH₂), δ 4.88 (m, 2H, CH and =CH-) δ 5.68 (s, 1H, CH).

¹³C (101 MHz, 298 K, D₂O): δ 26.7, 45.4, 52.0, 55.9, 63.1, 87.2, 97.6, 155.5, 174.3, 179.5

LDI-MS [M⁻] 198.03.

Deionised water was purified using a VWR Puranility TU 6 instrument with UV lamp. All other chemicals and solvents were purchased from commercial suppliers and used as received.

AmigoChem

An AmigoChem Integrity 10 reaction block was used. Samples were analysed via LCMS.

Flash Column Chromatography

Flash column chromatography was carried out using a Teledyne CombiFlash Rf+ apparatus. RediSep C₁₈ cartridges were used for reversed phase experiments whilst RediSep silica cartridges were used for normal phase experiments.

Reversed Phase High Performance Liquid Chromatography

All HPLC experiments were carried out on an Agilent 1100 Series HPLC system, results were stored and processed using Empower 3 Chromatography Data Software from Waters.

K313 HPLC Method

The K313 HPLC method was carried out on an Agilent 1100 Series HPLC system with K313 eluent (5.2.3.2) and a 25 cm x 0.5 cm C18 hypersil ODS column. 10 µL injections were made from a heat adjustable auto-sample chamber. The eluent was passed through the column at a rate of 1 mLmin⁻¹ via an isocratic pump with each analysis taking 10 min. A VWD was set to 230 nm.

Preparation of K313 Eluent

To Sodium dihydrogenphosphate (31.2 g, 26.0 mmol), deionised water (2 L) was added, phosphoric acid (85 w/w%) was added to adjust pH to 2.5. Phosphate solution (1.8 L) was mixed with HPLC grade methanol (0.2 L) and the resultant solution filtered.

Lithium Clavulanate Standard

Refrigerated lithium clavulanate (0.0500 g, 0.244 mmol) was measured and transferred into a 100 mL volumetric flask. Deionised water was added to make up a 100 mL standard solution. A 10 μ L aliquot was sampled and ran through the K313 HPLC method; the standard sample was ran in triplicate to calibrate the UV detector response to clavulanate.

Liquid Chromatography Mass Spectrometry

A Waters Acquity UPLC instrument with a BEH column (50.0 mm x 2.10 mm with 1.70 μ m packing diameter) equipped with a Waters Micromass ZQ mass spectrometer using alternate scan positive and negative electrospray ionisation, was used for LCMS analysis. A UV detector with a wavelength spectrum of 210-350 nm was equipped for detection of analytes. Three modifiers were used in LCMS experiments.

High pH LCMS

40.0 °C, 1.00 mL/min flow rate, using a mobile phase gradient of 10.0 mM aqueous ammonium bicarbonate solution, adjusted to pH 10.0 with 0.880 M aqueous ammonia and acetonitrile. Gradient conditions began at 1% acetonitrile, and increased linearly to 97% acetonitrile over 1.50 min, before remaining at this concentration for 0.40 min, and rising to 100% over 0.10 min.

Formic LCMS

40.0 °C, 1.00 mL/min flow rate, using a gradient with mobile phases of water containing 0.1% volume (v/v) of formic acid and acetonitrile with 0.1% formic acid (v/v). Gradient conditions were initially 1% of the acetonitrile mixture, increasing linearly to 97% over 1.50 min, and remaining at 97.0% for 0.40 min, before increasing to 100% over 0.10 min.

Mass Directed Auto Purification

MDAP was carried out with a Waters ZQ mass spectrometer using alternate scan positive and negative electrospray ionisation. A UV detector with a wavelength spectrum of 210-350 nm was equipped for detection of analytes. Three modifiers were used in LCMS experiments. A Sunfire C₁₈ column (100 mm x 19.0 mm with 5.00 µm packing diameter) was used with a 20.0 mL/min flow rate and a mobile phase gradient of water with 0.1% formic acid (v/v) and acetonitrile with 0.1% formic acid (v/v).

Nuclear Magnetic Resonance Spectroscopy

All ¹H NMR spectra were obtained on a Bruker AV-400 spectrometer operating at 400 MHz. ¹³C NMR spectra were obtained on the same instrument operating at 101 MHz. All spectra were recorded in deuterated solvents at ambient temperatures using standard pulse methods. Chemical shifts are reported in ppm with respect to TMS or residual solvent peak, and multiplicities are denoted as: singlet (s), doublet (d), triplet (t), quartet (q), quintet (quin), or multiplet (m).

pH Measurements

All pH measurements were made using Mettler-Toledo pH meter calibrated with pH 4.01 and pH 7.0 buffers.

Thin Layer Chromatography

TLC was carried out in a glass TLC chamber using precoated polyester-back silica plates (0.2 mm particle size). UV light λ_{max} 254 nm or 365 nm was used to visualise spots; when necessary, vanillin or potassium permanganate dip were used to develop TLC plates.

2.6.2 Experimental Procedures

Determination of Suitable Conditions for HPLC

To a volumetric flask (50 mL) potassium clavulanate was added. Deionised water was used to make potassium clavulanate solution up to a total volume of 50 mL. The solution was adjusted to pH 4.0 or pH 8.0 using sulfuric acid (50 v/v%) or sodium hydroxide (50 v/v%) and monitored via the K313 HPLC method over a period of 8 h.

Following the above procedure, data are presented as (a) quantity of potassium clavulanate, (b) Final concentration of potassium clavulanate solution

Entry 1 (a) 2.5 g, 10.5 mmol, (b) 50 mg/mL.

Entry 2 (a) 25 mg, 0.105 mmol, (b) 0.5 mg/mL.

Entry 3 (a) 100 mg, 0.422 mmol, (b) 2 mg/mL.

Monitoring pH Change Over Time

To a volumetric flask (50 mL) potassium clavulanate (2.5 g, 10.5 mmol) was added, deionised water was used to create a potassium clavulanate solution (50 mg/mL). Sulfuric acid (50 v/v%) or sodium hydroxide (50 v/v%) were used to adjust the pH to 4.0, 7.02 or 9.0. An electric pH meter was used to measure the pH in time intervals of 30 min over a period of 4 h.

General Method for Preparing 0.025 M Citric acid/Disodium hydrogenphosphate Buffer Solutions

To a volumetric flask citric acid solution and disodium hydrogenphosphate solution were added. Deionised water was used to create a buffer solution of the desired volume. The pH was measured with an electronic pH meter and adjusted to the desired level as required. Potassium chloride was added to adjust μ to 0.5 M.

Following the **general procedure**, data are presented as (a) Required pH of the buffer solution, (b) volume of buffer solution (c) quantity of citric acid added, (d) quantity of disodium hydrogenphosphate added, (e) quantity of potassium chloride added.

Entry 1 (a) 3.0, (b) 200 mL, (c) 5 mL of 1 M solution, 5 mmol, (d) 14.2 mL of a 0.2 M solution, 2.8 mmol, (e) 7.0 g, 93.9 mmol.

Entry 2 (a) 4.0, (b) 200 mL, (c) 5 mL of 1 M solution, 5 mmol, (d) 34.9 mL of a 0.2 M solution, 6.98 mmol, (e) 6.24 g, 83.7 mmol.

Entry 3 (a) 5.0, (b) 200 mL, (c) 5 mL of 1 M solution, 5 mmol, (d) 56.6 mL of a 0.2 M solution, 11.3 mmol, (e) 5.19 g, 69.9 mmol.

Entry 4 (a) 5.1, (b) 100 mL, (c) 2.1 mL of 0.5 M solution, 1.1 mmol, (d) 12.5 mL of a 0.2 M solution, 2.5 mmol, (e) 3.22 g, 43.2 mmol.

Entry 5 (a) 5.3, (b) 100 mL, (c) 2.0 mL of 0.5 M solution, 1.0 mmol, (d) 12.5 mL of a 0.2 M solution, 2.5 mmol, (e) 3.21 g, 43.1 mmol.

Entry 6 (a) 5.5, (b) 100 mL, (c) 1.8 mL of 0.5 M solution, 0.9 mmol, (d) 12.5 mL of a 0.2 M solution, 2.5 mmol, (e) 3.20 g, 42.9 mmol.

Entry 7 (a) 5.7, (b) 100 mL, (c) 1.6 mL of 0.5 M solution, 0.82 mmol, (d) 12.5 mL of a 0.2 M solution, 2.5 mmol, (e) 3.19 g, 42.8 mmol.

Entry 8 (a) 5.8, (b) 100 mL, (c) 1.56 mL of 0.5 M solution, 0.8 mmol, (d) 12.5 mL of a 0.2 M solution, 2.5 mmol, (e) 3.18 g, 42.7 mmol.

Entry 9 (a) 5.9, (b) 100 mL, (c) 1.5 mL of 0.5 M solution, 0.75 mmol, (d) 12.5 mL of a 0.2 M solution, 2.5 mmol, (e) 3.18 g, 42.7 mmol.

Entry 10 (a) 5.95, (b) 100 mL, (c) 1.44 mL of 0.5 M solution, 0.72 mmol, (d) 12.5 mL of a 0.2 M solution, 2.5 mmol, (e) 3.18 g, 42.7 mmol.

General Method for Preparing 0.025 M Sodium dihydrogenphosphate/Disodium hydrogenphosphate Buffer Solutions

To a volumetric flask sodium dihydrogenphosphate solution and disodium hydrogenphosphate solution were added. Deionised water was used to create a buffer solution of the desired volume. The pH was measured with an electronic pH meter and adjusted to the desired level as required. Potassium chloride was added to adjust μ to 0.5 M.

Following the **general procedure**, data are presented as (a) Required pH of the buffer solution, (b) volume of buffer solution (c) quantity of sodium dihydrogenphosphate added, (d) quantity of disodium hydrogenphosphate added, (e) quantity of potassium chloride added.

Entry 1 (a) 6.0, (b) 200 mL, (c) 19.7 mL of 0.2 M solution, 3.94 mmol, (d) 5.3 mL of a 0.2 M solution, 1.1 mmol, (e) 6.92 g, 92.8 mmol.

Entry 2 (a) 7.0, (b) 200 mL, (c) 6.7 mL of 0.2 M solution, 1.3 mmol, (d) 18.3 mL of a 0.2 M solution, 3.65 mmol, (e) 6.54 g, 87.7 mmol.

Entry 3 (a) 8.0, (b) 200 mL, (c) 0.87 mL of 0.2 M solution, 0.17 mmol, (d) 24.1 mL of a 0.2 M solution, 4.83 mmol, (e) 6.36 g, 85.3 mmol.

Preparation of 0.025 M pH 9 Buffer Solution

To a 200 mL volumetric flask glycine solution (0.5 M, 10 mL, 5 mmol) and sodium hydroxide (0.1 M, 13.8 mL, 5 mmol) were added, deionised water was added to make a 200 mL solution. The pH was measured using an electric pH meter and adjusted to 9.0 as necessary. Potassium chloride (7.35 g, 98.6 mmol) was then added to adjust μ to 0.5 M.

General Method for Preparing 0.025 M Citric acid/Trisodium citrate Buffer Solutions

To a volumetric flask citric acid solution and trisodium citrate solution were added. Deionised water was used to create a buffer solution of the desired volume. The pH

was measured with an electronic pH meter and adjusted to the desired level as required. Potassium chloride was added to adjust μ to 0.5 M.

Following the **general procedure**, data are presented as (a) Required pH of the buffer solution, (b) volume of buffer solution (c) quantity of citric acid added, (d) quantity of trisodium citrate added, (e) quantity of potassium chloride added.

Entry 1 (a) 5.0, (b) 200 mL, (c) 6.7 mL of 0.2 M solution, 1.3 mmol, (d) 18.3 mL of a 0.2 M solution, 3.67 mmol, (e) 6.08 g, 81.6 mmol.

Entry 2 (a) 5.5, (b) 200 mL, (c) 3.7 mL of 0.2 M solution, 0.73 mmol, (d) 21.4 mL of a 0.2 M solution, 4.27 mmol, (e) 5.70 g, 76.5 mmol.

Entry 3 (a) 6.0, (b) 200 mL, (c) 1.5 mL of 0.2 M solution, 0.31 mmol, (d) 23.5 mL of a 0.2 M solution, 4.69 mmol, (e) 5.42 g, 72.7 mmol.

Entry 4 (a) 6.5, (b) 200 mL, (c) 10.9 mL of 0.01 M solution, 0.109 mmol, (d) 24.5 mL of a 0.2 M solution, 4.89 mmol, (e) 5.29 g, 71.0 mmol.

Entry 5 (a) 7.0, (b) 200 mL, (c) 3.6 mL of 0.01 M solution, 0.036 mmol, (d) 24.8 mL of a 0.2 M solution, 4.96 mmol, (e) 5.24 g, 70.3 mmol.

Entry 6 (a) 7.5, (b) 200 mL, (c) 1.2 mL of 0.01 M solution, 0.012 mmol, (d) 24.1 mL of a 0.2 M solution, 4.83 mmol, (e) 5.23 g, 70.2 mmol.

Entry 7 (a) 8.0, (b) 200 mL, (c) 0.4 mL of 0.01 M solution, 0.004 mmol, (d) 25.0 mL of a 0.2 M solution, 5.22 mmol, (e) 5.22 g, 70.0 mmol.

General Method for Preparing 0.05 M Citric acid/Disodium hydrogenphosphate Buffer Solutions

To a volumetric flask citric acid solution and disodium hydrogenphosphate solution were added. Deionised water was used to create a buffer solution of the desired volume. The pH was measured with an electronic pH meter and adjusted to the desired level as required. Potassium chloride was added to adjust μ to 0.5 M.

Following the **general procedure**, data are presented as (a) Required pH of the buffer solution, (b) volume of buffer solution (c) quantity of citric acid added, (d) quantity of disodium hydrogenphosphate added, (e) quantity of potassium chloride added.

Entry 1 (a) 3.0, (b) 200 mL, (c) 10 mL of 1 M solution, 10 mmol, (d) 30.6 mL of a 0.2 M solution, 6.12 mmol, (e) 6.49 g, 87.1 mmol.

Entry 2 (a) 4.0, (b) 200 mL, (c) 10 mL of 1 M solution, 10 mmol, (d) 70.1 mL of a 0.2 M solution, 14.0 mmol, (e) 5.02 g, 67.3 mmol.

Entry 3 (a) 5.0, (b) 200 mL, (c) 10 mL of 1 M solution, 10 mmol, (d) 113 mL of a 0.2 M solution, 22.6 mmol, (e) 2.93 g, 39.3 mmol.

Entry 4 (a) 5.1, (b) 100 mL, (c) 4.3 mL of 0.5 M solution, 2.1 mmol, (d) 25 mL of a 0.2 M solution, 5.0 mmol, (e) 2.71 g, 36.4 mmol.

Entry 5 (a) 5.3, (b) 100 mL, (c) 3.9 mL of 0.5 M solution, 2.0 mmol, (d) 25 mL of a 0.2 M solution, 5.0 mmol, (e) 2.69g, 36.1 mmol.

Entry 6 (a) 5.5, (b) 100 mL, (c) 3.6 mL of 0.5 M solution, 1.8 mmol, (d) 25 mL of a 0.2 M solution, 5.0 mmol, (e) 2.67 g, 35.8 mmol.

Entry 7 (a) 5.7, (b) 100 mL, (c) 3.3 mL of 0.5 M solution, 1.7 mmol, (d) 25 mL of a 0.2 M solution, 5.0 mmol, (e) 2.65g, 35.5 mmol.

Entry 8 (a) 5.8, (b) 100 mL, (c) 3.1 mL of 0.5 M solution, 1.6 mmol, (d) 25 mL of a 0.2 M solution, 5.0 mmol, (e) 2.64g, 35.4 mmol.

Entry 9 (a) 5.9, (b) 100 mL, (c) 3.0 mL of 0.5 M solution, 1.5 mmol, (d) 25 mL of a 0.2 M solution, 5.0 mmol, (e) 2.63 g, 35.3 mmol.

Entry 10 (a) 5.95, (b) 100 mL, (c) 2.9 mL of 0.5 M solution, 1.5 mmol, (d) 25 mL of a 0.2 M solution, 5.0 mmol, (e) 2.63 g, 35.3 mmol.

General Method for Preparing 0.05 M Sodium dihydrogenphosphate/Disodium hydrogenphosphate Buffer Solutions

To a volumetric flask sodium dihydrogenphosphate solution and disodium hydrogenphosphate solution were added. Deionised water was used to create a buffer solution of the desired volume. The pH was measured with an electronic pH meter and adjusted to the desired level as required. Potassium chloride was added to adjust μ to 0.5 M.

Following the **general procedure**, data are presented as (a) Required pH of the buffer solution, (b) volume of buffer solution (c) quantity of sodium dihydrogenphosphate added, (d) quantity of disodium hydrogenphosphate added, (e) quantity of potassium chloride added.

Entry 1 (a) 6.0, (b) 200 mL, (c) 39.3 mL of 0.2 M solution, 7.86 mmol, (d) 10.7 mL of a 0.2 M solution, 2.14 mmol, (e) 6.39 g, 85.7 mmol.

Entry 2 (a) 7.0, (b) 200 mL, (c) 13.5 mL of 0.2 M solution, 7.31 mmol, (d) 36.6 mL of a 0.2 M solution, 7.31 mmol, (e) 5.62 g, 75.4 mmol.

Entry 3 (a) 8.0, (b) 200 mL, (c) 1.8 mL of 0.2 M solution, 0.36 mmol, (d) 48.3 mL of a 0.2 M solution, 9.66 mmol, (e) 5.27 g, 70.7 mmol.

Preparation of 0.05 M pH 9 Buffer Solution

To a 200 mL volumetric flask glycine solution (0.5 M, 20 mL, 10 mmol) and sodium hydroxide (0.1 M, 27.6 mL, 2.8 mmol) were added, deionised water was added to make a 200 mL solution. The pH was measured using an electric pH meter and adjusted to 9.0 as necessary. Potassium chloride (7.25 g, 97.2 mmol) was then added to adjust μ to 0.5 M.

General Method for Preparing 0.05 M Citric acid/Trisodium citrate Buffer Solutions

To a volumetric flask citric acid solution and trisodium citrate solution were added. Deionised water was used to create a buffer solution of the desired volume. The pH

was measured with an electronic pH meter and adjusted to the desired level as required. Potassium chloride was added to adjust μ to 0.5 M.

Following the **general procedure**, data are presented as (a) Required pH of the buffer solution, (b) volume of buffer solution (c) quantity of citric acid added, (d) quantity of trisodium citrate added, (e) quantity of potassium chloride added.

Entry 1 (a) 5.0, (b) 200 mL, (c) 13.3 mL of 0.2 M solution, 2.66 mmol, (d) 36.7 mL of a 0.2 M solution, 7.34 mmol, (e) 4.71 g, 63.2 mmol.

Entry 2 (a) 5.5, (b) 200 mL, (c) 7.3 mL of 0.2 M solution, 1.5 mmol, (d) 42.8 mL of a 0.2 M solution, 8.54 mmol, (e) 3.95 g, 53.0 mmol.

Entry 3 (a) 6.0, (b) 200 mL, (c) 3.1 mL of 0.2 M solution, 0.61 mmol, (d) 46.9 mL of a 0.2 M solution, 9.38 mmol, (e) 3.39 g, 45.5 mmol.

Entry 4 (a) 6.5, (b) 200 mL, (c) 21.8 mL of 0.01 M solution, 0.218 mmol, (d) 48.9 mL of a 0.2 M solution, 9.78 mmol, (e) 3.13 g, 42.0 mmol.

Entry 5 (a) 7.0, (b) 200 mL, (c) 7.2 mL of 0.01 M solution, 0.072 mmol, (d) 49.6 mL of a 0.2 M solution, 9.93 mmol, (e) 3.03 g, 40.6 mmol.

Entry 6 (a) 7.5, (b) 200 mL, (c) 2.3 mL of 0.01 M solution, 0.023 mmol, (d) 49.9 mL of a 0.2 M solution, 9.98 mmol, (e) 3.00 g, 40.3 mmol.

Entry 7 (a) 8.0, (b) 200 mL, (c) 0.7 mL of 0.01 M solution, 0.007 mmol, (d) 50.0 mL of a 0.2 M solution, 10.0 mmol, (e) 2.99 g, 40.1 mmol.

General Method for Preparing 0.1 M Citric acid/Disodium hydrogenphosphate Buffer Solutions

To a volumetric flask citric acid solution and disodium hydrogenphosphate solution were added. Deionised water was used to create a buffer solution of the desired volume. The pH was measured with an electronic pH meter and adjusted to the desired level as required. Potassium chloride was added to adjust μ to 0.5 M.

Following the **general procedure**, data are presented as (a) Required pH of the buffer solution, (b) volume of buffer solution (c) quantity of citric acid added, (d) quantity of disodium hydrogenphosphate added, (e) quantity of potassium chloride added.

Entry 1 (a) 3.0, (b) 200 mL, (c) 20 mL of 1 M solution, 20 mmol, (d) 63.4 mL of a 0.2 M solution, 12.7 mmol, (e) 5.47 g, 73.4 mmol.

Entry 2 (a) 4.0, (b) 200 mL, (c) 20 mL of 1 M solution, 20 mmol, (d) 140 mL of a 0.2 M solution, 28.1 mmol, (e) 2.58 g, 34.6 mmol.

Entry 3 (a) 5.0, (b) 200 mL, (c) 20 mL of 1 M solution, 20 mmol, (d) 180 mL of a 0.2 M solution, 36.1 mmol, (e) 0.22 g, 2.95 mmol.

Entry 4 (a) 5.1, (b) 100 mL, (c) 8.5 mL of 0.5 M solution, 4.3 mmol, (d) 50 mL of a 0.2 M solution, 10 mmol, (e) 1.70 g, 22.5 mmol.

Entry 5 (a) 5.3, (b) 100 mL, (c) 7.8 mL of 0.5 M solution, 3.9 mmol, (d) 50 mL of a 0.2 M solution, 10 mmol, (e) 1.65 g, 22.1 mmol.

Entry 6 (a) 5.5, (b) 100 mL, (c) 7.2 mL of 0.5 M solution, 3.6 mmol, (d) 50 mL of a 0.2 M solution, 10 mmol, (e) 1.60 g, 21.5 mmol.

Entry 7 (a) 5.7, (b) 100 mL, (c) 6.6 mL of 0.5 M solution, 3.3 mmol, (d) 50 mL of a 0.2 M solution, 10 mmol, (e) 1.57 g, 21.1 mmol.

Entry 8 (a) 5.8, (b) 100 mL, (c) 6.3 mL of 0.5 M solution, 3.2 mmol, (d) 50 mL of a 0.2 M solution, 10 mmol, (e) 1.55 g, 20.8 mmol.

Entry 9 (a) 5.9, (b) 100 mL, (c) 5.9 mL of 0.5 M solution, 3.0 mmol, (d) 50 mL of a 0.2 M solution, 10 mmol, (e) 1.54 g, 20.7 mmol.

Entry 10 (a) 5.95, (b) 100 mL, (c) 5.8 mL of 0.5 M solution, 2.9 mmol, (d) 50 mL of a 0.2 M solution, 10 mmol, (e) 1.53 g, 20.5 mmol.

General Method for Preparing 0.1 M Sodium dihydrogenphosphate/Disodium hydrogenphosphate Buffer Solutions

To a volumetric flask sodium dihydrogenphosphate solution and disodium hydrogenphosphate solution were added. Deionised water was used to create a buffer solution of the desired volume. The pH was measured with an electronic pH meter and adjusted to the desired level as required. Potassium chloride was added to adjust μ to 0.5 M.

Following the **general procedure**, data are presented as (a) Required pH of the buffer solution, (b) volume of buffer solution (c) quantity of sodium dihydrogenphosphate added, (d) quantity of disodium hydrogenphosphate added, (e) quantity of potassium chloride added.

Entry 1 (a) 6.0, (b) 200 mL, (c) 78.7 mL of 0.2 M solution, 15.7 mmol, (d) 21.3 mL of a 0.2 M solution, 5.33 mmol, (e) 5.33 g, 71.5 mmol.

Entry 2 (a) 7.0, (b) 200 mL, (c) 26.9 mL of 0.2 M solution, 5.4 mmol, (d) 73.1 mL of a 0.2 M solution, 14.6 mmol, (e) 3.78 g, 50.1 mmol.

Entry 3 (a) 8.0, (b) 200 mL, (c) 3.5 mL of 0.2 M solution, 0.7 mmol, (d) 96.5 mL of a 0.2 M solution, 19.3 mmol, (e) 3.09 g, 41.4 mmol.

Preparation of 0.1 M pH 9 buffer solution

To a 200 mL volumetric flask glycine solution (0.5 M, 40 mL, 20 mmol) and sodium hydroxide (0.1 M, 55.2 mL, 5 mmol) were added, deionised water was added to make a 200 mL solution. The pH was measured using an electric pH meter and adjusted to 9.0 as necessary. Potassium chloride (7.04 g, 94.4 mmol) was then added to adjust μ to 0.5 M.

General Method for Preparing 0.1 M Citric acid/Trisodium citrate Buffer Solutions

To a volumetric flask citric acid solution and trisodium citrate solution were added. Deionised water was used to create a buffer solution of the desired volume. The pH was measured with an electronic pH meter and adjusted to the desired level as required. Potassium chloride was added to adjust μ to 0.5 M.

Following the **general procedure**, data are presented as (a) Required pH of the buffer solution, (b) volume of buffer solution (c) quantity of citric acid added, (d) quantity of trisodium citrate added, (e) quantity of potassium chloride added.

Entry 1 (a) 5.0, (b) 200 mL, (c) 26.6 mL of 0.2 M solution, 5.32 mmol, (d) 73.4 mL of a 0.2 M solution, 14.7 mmol, (e) 1.96 g, 26.3 mmol.

Entry 2 (a) 5.5, (b) 200 mL, (c) 14.6 mL of 0.2 M solution, 2.91 mmol, (d) 85.4 mL of a 0.2 M solution, 17.1 mmol, (e) 0.44 g, 5.8 mmol.

Entry 3 (a) 6.0, (b) 200 mL, (c) 6.1 mL of 0.2 M solution, 1.2 mmol, (d) 93.9 mL of a 0.2 M solution, 18.8 mmol, (e) 0 g, 0 mmol.

Entry 4 (a) 6.5, (b) 200 mL, (c) 43.6 mL of 0.01 M solution, 0.436 mmol, (d) 97.8 mL of a 0.2 M solution, 19.6 mmol, (e) 0 g, 0 mmol.

Entry 5 (a) 7.0, (b) 200 mL, (c) 14.4 mL of 0.01 M solution, 0.144 mmol, (d) 99.3 mL of a 0.2 M solution, 19.9 mmol, (e) 0 g, 0 mmol.

Entry 6 (a) 7.5, (b) 200 mL, (c) 4.6 mL of 0.01 M solution, 0.046 mmol, (d) 99.8 mL of a 0.2 M solution, 19.9 mmol, (e) 0 g, 0 mmol.

Entry 7 (a) 8.0, (b) 200 mL, (c) 1.5 mL of 0.01 M solution, 0.015 mmol, (d) 99.9 mL of a 0.2 M solution, 20.0 mmol, (e) 0 g, 0 mmol.

Measurement of potassium clavulanate degradation rate at pH 3, 4 and 5

Potassium clavulanate stored in a freezer (0.1000 g, 0.4215 mmol) was transferred to a 50 mL volumetric flask and citrate/ phosphate buffer solution of required pH was added to make a 50 mL reaction solution. An aliquot was transferred to a HPLC vial and stored in an autosample chamber at 25°C. A 10 µL injection was taken at time intervals of 1 h and the amount of potassium clavulanate was measured with a UV detector. A lithium clavulanate standard was used to calculate the concentration of remaining potassium clavulanate in each sample.

Measurement of potassium clavulanate degradation rate at pH 6, 7 and 8

Potassium clavulanate stored in a freezer (0.1000 g, 0.4215 mmol) was transferred to a 50 mL volumetric flask and phosphate buffer solution of required pH was added to make a 50 mL reaction solution. An aliquot was transferred to a HPLC vial and stored in an autosample chamber at 25°C. A 10 µL injection was taken at time intervals of 1 h and the amount of potassium clavulanate was measured with a UV detector. A lithium clavulanate standard was used to calculate the concentration of remaining potassium clavulanate in each sample.

Measurement of potassium clavulanate degradation rate at pH 9

Potassium clavulanate stored in a freezer (0.1000 g, 0.4215 mmol) was transferred to a 50 mL volumetric flask and glycine/ sodium hydroxide buffer solution of required pH was added to make a 50 mL reaction solution. An aliquot was transferred to a HPLC vial and stored in an autosample chamber at 25°C. A 10 µL injection was taken at time intervals of 1 h and the amount of potassium clavulanate was measured with a UV detector. A lithium clavulanate standard was used to calculate the concentration of remaining potassium clavulanate in each sample.

Measurement of potassium clavulanate degradation rate at pH 5, 5.1, 5.3, 5.5, 5.7, 5.8, 5.9 and 5.95

Potassium clavulanate stored in a freezer (0.1000 g, 0.4215 mmol) was transferred to a 50 mL volumetric flask and citrate/ phosphate buffer solution of required pH was added to make a 50 mL reaction solution. An aliquot was transferred to a HPLC vial and stored in an autosample chamber at 25°C. A 10 µL injection was taken at time intervals of 3 h and the amount of potassium clavulanate was measured with a UV detector. A lithium clavulanate standard was used to calculate the concentration of remaining potassium clavulanate in each sample.

Measurement of clavulanic acid degradation rate in reverse osmosis plant samples

A sample of reverse osmosis retentate was taken at the most concentrated point. Sulfuric acid (50 v/v%) or sodium hydroxide solution (50 v/v%) was added to adjust the sample to the required pH. An aliquot of the sample (1 mL) was diluted with deionised water in a volumetric flask to 50 mL and a sample was analysed immediately via the K313 HPLC method. The remaining pH adjusted sample was stored in a water bath held at 25 °C. Aliquots were taken and analysed in the same manner at time intervals of 2 h over a period of 8 h. A lithium clavulanate standard was used to calculate the concentration of remaining potassium clavulanate in each sample.

Measurement of clavulanic acid degradation rate in post-resin samples

A sample of XAD resin percolate was taken immediately after passing through the resin. Sulfuric acid (50 v/v%) or sodium hydroxide solution (50 v/v%) was added to adjust the sample to the required pH. An aliquot of the sample (1 mL) was diluted with deionised water in a volumetric flask to 50 mL and a sample was analysed immediately via the K313 HPLC method. The remaining pH adjusted sample was stored in a water bath held at 25 °C. Aliquots were taken and analysed in the same manner at time intervals of 2 h over a period of 8 h. A lithium clavulanate standard was used to calculate the concentration of remaining potassium clavulanate in each sample.

Measurement of clavulanic acid degradation rate in ultrafiltration samples

A sample of ultrafiltration broth was taken after passing through the membrane. Sulfuric acid (50 v/v%) or sodium hydroxide solution (50 v/v%) was added to adjust the sample to the required pH. An aliquot of the sample (1 mL) was diluted with deionised water in a volumetric flask to 50 mL and a sample was analysed immediately via the K313 HPLC method. The remaining pH adjusted sample was stored in a water bath held at 25 °C. Aliquots were taken and analysed in the same manner at time intervals of 2 h over a period of 8 h. A lithium clavulanate standard was used to calculate the concentration of remaining potassium clavulanate in each sample.

Measurement of clavulanic acid degradation rate in back extraction samples

A sample of the back extraction rich aqueous was taken immediately at the most concentrated point. Sulfuric acid (50 v/v%) or sodium hydroxide solution (50 v/v%) was added to adjust the sample to the required pH. An aliquot of the sample (1 mL) was diluted with deionised water in a volumetric flask to 200 mL and a sample was analysed immediately via the K313 HPLC method. The remaining pH adjusted sample was stored in a water bath held at 25 °C. Aliquots were taken and analysed in the same manner at time intervals of 2 h over a period of 8 h. A lithium clavulanate standard was used to calculate the concentration of remaining potassium clavulanate in each sample.

Measurement of clavulanic acid degradation rate in reverse osmosis plant samples for pH vs T studies

A sample of reverse osmosis retentate was taken at the most concentrated point. Sulfuric acid (50 v/v%) or sodium hydroxide solution (50 v/v%) was added to adjust the sample to the required pH. An aliquot of the sample (1 mL) was diluted with deionised water in a volumetric flask to 50 mL and a sample was analysed immediately via the K313 HPLC method. The remaining pH adjusted sample was stored at the required temperature in a temperature-controlled jacketed-vessel for 5 °C and 10 °C, or in a water bath for 20 °C, 25 °C, 30 °C, or 40 °C. Aliquots were taken and analysed in the same manner at time intervals of 2 h over a period of 6 h. A lithium clavulanate standard was used to calculate the concentration of remaining potassium clavulanate in each sample.

Clavulanic acid degradation for AmigoChem

An AmigoChem vessel, equipped with a stirrer bar, was loaded with clavulanate salt. Acid or Base was injected into the vessel to start the degradation process. The reaction was held at 25 °C for 24 h, a 4 µL aliquot was taken from the reaction vessel at time intervals of 2 h and diluted with water (1 mL). The samples were analysed via the high pH LCMS method at the end of the 24 h reaction period.

Following the **general procedure**, data are presented as (a) type and quantity of clavulanate salt (b) type and quantity of acid or base used.

- Entry 1** (a) Potassium clavulanate, 50 mg, 2.11 mmol, (b) hydrochloric acid, 2 mL of a 2 M solution, 4 mmol.
- Entry 2** (a) Potassium clavulanate, 50 mg, 2.11 mmol, (b) sodium hydroxide, 2 mL of a 2 M solution, 4 mmol.
- Entry 3** (a) t-BA clavulanate, 50 mg, 1.84 mmol, (b) hydrochloric acid, 2 mL of a 2 M solution, 4 mmol.
- Entry 4** (a) t-BA clavulanate, 50 mg, 1.84, (b) sodium hydroxide, 2 mL of a 2 M solution, 4 mmol.

Clavulanic acid degradation for reversed phase flash column chromatography

Potassium clavulanate (40 mg, 1.69 mmol) or t-BA clavulanate (40 mg, 1.47 mmol) was dissolved in hydrochloric acid (2 M, 2 mL, 4 mmol) or sodium hydroxide (2 M, 2 mL, 4 mmol). The solution was left at room temperature, open to air for *ca.* 1 h; a dark orange colour was observed. LCMS was used with the high pH method to check that clavulanate degradation had taken place. The reaction was then subjected to flash column chromatography with a C₁₈ reversed phase column.

Clavulanic acid degradation for normal phase flash column chromatography

Potassium clavulanate (40 mg, 1.69 mmol) or t-BA clavulanate (40 mg, 1.47 mmol) was dissolved in hydrochloric acid (2 M, 2 mL, 4 mmol) or sodium hydroxide (2 M, 2 mL, 4 mmol). The solution was left at room temperature, open to air for *ca.* 1 h; a dark orange colour was observed. LCMS was used with the high pH method to check that clavulanate degradation had taken place. The reaction mixture was then extracted with ethyl acetate (3 x 15 mL), the organic layers were collected and concentrated to *ca.* 2

mL via rotary evaporation. The concentrate was then subjected to flash column chromatography with a silica column and cyclohexane-ethylacetate solvent system.

2.7 References

- (195) Bhattacharjee, M. K. Introduction to Antibiotics. In Chemistry of Antibiotics and Related Drugs; Springer International Publishing: Cham, 2016; pp 1–25.
- (196) Nicolaou, K. C.; Montagnon, T. *Molecules That Changed the World. In Molecules that changed the world*; Wiley-VCH: Darmstadt, **2008**.
- (197) Varley, A. J.; Sule, J.; Absalom, A. R. *Contin. Educ. Anaesth. Crit. Care Pain* **2009**, 9, 184.
- (198) Hamad, B. *Nat. Rev. Drug Discov.* **2010**, 9, 675.
- (199) American Chemical Society International Historic Chemistry Landmarks. Discovery and Development of Penicillin.
- (200) Kalman, D.; Barriere, S. L. *Texas Hear. Inst. J.* **1990**, 17, 203.
- (201) Zhanel, G. G.; Walkty, A.; Vercaigne, L.; Karlowsky, J. A.; Embil, J.; Gin, A. S.; Hoban, D. J. *Can. J. Infect. Dis.* **1999**, 10, 207.
- (202) Chopra, I.; Roberts, M. *Microbiol. Mol. Biol. Rev.* **2001**, 65, 232.
- (203) De la Bedoyere, G. *The Discovery of Penicillin*; Evans: London, **2005**.
- (204) Blevins, S. M.; Bronze, M. S. *Int. J. Infect. Dis.* **2010**, 14, 744.
- (205) Council, N. R. *Acute Exposure Guideline Levels for Selected Airborne Chemicals*; The National Academic Press: Washington D. C., **2009**.
- (206) Williams, K. J. *J. R. Soc. Med.* **2009**, 102, 343.
- (207) Lloyd, N. C.; Morgan, H. W.; Nicholson, B. K.; Ronimus, R. S. *Angew. Chemie Int. Ed.* **2005**, 44, 941.
- (208) Fleming, A.; Allison, V. D. *Br. J. Exp. Pathol.* **1922**, 3, 252.
- (209) Fleming, A. *Br. J. Exp. Pathol.* **1929**, 10, 226.
- (210) American Chemical Society National Historic Chemical Landmarks. Penicillin Production through Deep-Tank Fermentation.
- (211) Tan, S. Y.; Tatsumura, Y. *Singapore Med. J.* **2015**, 56, 366.

- (212) Sykes, R. *Bull. World Health Organ.* **2001**, 79, 778.
- (213) Abraham, E. P.; Chain, E.; Fletcher, C. M.; Gardner, A. D.; Heatley, N. G.; Jennings, M. A.; Florey, H. W. *Lancet*, **1941**, 238, 177.
- (214) Lobanovska, M.; Pilla, G. *Yale J. Biol. Med.* **2017**, 90, 135.
- (215) Fletcher, C. *Br. Med. J. (Clin. Res. Ed)*. **1984**, 289, 1721.
- (216) Barreiro, C.; Martín, J. F.; García-Estrada, C. *J. Biomed. Biotechnol.* **2012**, 2012, 105109.
- (217) Jami, M.-S.; Barreiro, C.; García-Estrada, C.; Martín, J.-F. *Mol. Cell. Proteomics*, **2010**, 9, 1182.
- (218) Renneberg, R.; Berkling, V.; Loroch, V. In *Biotechnology for Beginners (Second Edition)*; Academic Press: Boston, **2017**.
- (219) Elander, R. P. *Appl. Microbiol. Biotechnol.* **2003**, 61, 385.
- (220) Kardos, N.; Demain, A. L. *Appl. Microbiol. Biotechnol.* **2011**, 92, 677.
- (221) Demain, A. L. *J. Ind. Microbiol. Biotechnol.* **2006**, 33, 486.
- (222) Chain, E. *Nobel Lecture*, **1946**.
- (223) Clarke, H. T. *Chemistry of Penicillin*; Princeton University Press: New Jersey, **2015**.
- (224) Abraham, E. P.; Chain, E.; Holiday, E. R. *Br. J. Exp. Pathol.* **1942**, 23, 103.
- (225) Abraham, E. P.; Baker, W.; Chain, E.; Florey, H. W.; Holiday, E. R.; Robinson, R. *Nature* **1942**, 149, 356.
- (226) Abraham, E. P. *Nat. Prod. Rep.* **1987**, 4, 41.
- (227) Chain, E. *Annu. Rev. Biochem.* **1948**, 17, 657.
- (228) Glusker, J. P. *Protein Sci.* **1994**, 3, 2465.
- (229) Hodgkin, D. C. *Adv. Sci.* **1949**, 6, 85.
- (230) Howard, J. A. K. *Nat. Rev. Mol. Cell Biol.* **2003**, 4, 891.
- (231) Sheehan, J. C. *Ann. N. Y. Acad. Sci.* **1967**, 145, 216.

- (232) Nayler, J. H. C. *Trends Biochem. Sci.* **1991**, *16*, 234.
- (233) Saouane, S.; Buth, G.; Fabbiani, F. P. A. *Acta Crystallogr. Sect. C*, **2013**, *69*, 1238.
- (234) Matsubara, T.; Ueta, C. *J. Phys. Chem. A* **2014**, *118*, 8664.
- (235) Page, M. I. In *The Chemistry of β -Lactams*; Page, M. I., Ed.; Springer Netherlands: Dordrecht, **1992**.
- (236) Tani, K.; Stoltz, B. M. *Nature*, **2006**, *441*, 731.
- (237) Gregory, G. I. *Recent Advances in the Chemistry of β -Lactam Antibiotics*; Royal Society of Chemistry: London, **1981**.
- (238) Imming, P.; Klar, B.; Dix, D. *J. Med. Chem.* **2000**, *43*, 4328.
- (239) Sheehan, J. C.; Henery-Logan, K. R. *J. Am. Chem. Soc.* **1957**, *79*, 1262.
- (240) Benn, M. H.; Mitchell, R. E. *Can. J. Chem.* **1972**, *50*, 2195.
- (241) Woodward, R. B. *Science*. **1966**, *153*, 487.
- (242) Sheehan, J. C.; Hess, G. P. *J. Am. Chem. Soc.* **1955**, *77*, 1067.
- (243) Sheehan, J. C.; Henery-Logan, K. R. *J. Am. Chem. Soc.* **1959**, *81*, 3089.
- (244) Dunetz, J. R.; Magano, J.; Weisenburger, G. A. *Org. Process Res. Dev.* **2016**, *20*, 140.
- (245) Deshpande, A. D.; Baheti, K. G.; Chatterjee, N. R. *Curr. Sci.* **2004**, *87*, 1684.
- (246) Parmar, A.; Kumar, H.; Marwaha, S. S.; Kennedy, J. F. *Biotechnol. Adv.* **2000**, *18*, 289.
- (247) Roy, J. *An Introduction to Pharmaceutical Sciences*; Roy, J., Ed.; Woodhead Publishing Series in Biomedicine; Woodhead Publishing: Cambridge, **2011**.
- (248) Zhang, Y.-W.; Liu, R.-J.; Xu, X.-M. *Appl. Microbiol. Biotechnol.* **2010**, *88*, 49.
- (249) Geddes, A. M.; Klugman, K. P.; Rolinson, G. N. *Int. J. Antimicrob. Agents*, **2007**, *30*, 109.
- (250) Blanpain, P. C.; Nagy, J. B.; Laurent, G. H.; Durant, F. V. *J. Med. Chem.* **1980**, *23*, 1283.

- (251) Mehta, D.; Sharma, A. K. *Mol. Pharmacol.* **2016**, *1*, 1.
- (252) Bianchi, D.; Bortolo, R.; Golini, P.; Cesti, P. *Appl. Biochem. Biotechnol.* **1998**, *73*, 257.
- (253) Wright, P. M.; Seiple, I. B.; Myers, A. G. *Angew. Chem. Int. Ed. Engl.* **2014**, *53*, 8840.
- (254) King, D. T.; Sobhanifar, S.; Strynadka, N. C. J. *The mechanisms of resistance to β -lactam antibiotics*; Springer Science: New York, **2014**.
- (255) Lovering, A. L.; Safadi, S. S.; Strynadka, N. C. J. *Annu. Rev. Biochem.* **2012**, *81*, 451.
- (256) Tipper, D. J.; Strominger, J. L. *Proc. Natl. Acad. Sci.* **1965**, *54*, 1133.
- (257) Sauvage, E.; Terrak, M. *Antibiotics*, **2016**, *5*, 12.
- (258) Blumberg, P. M.; Strominger, J. L. *Bacteriol. Rev.* **1974**, *38*, 291.
- (259) Waxman, D. J.; Strominger, J. L. *Annu. Rev. Biochem.* **1983**, *52*, 825.
- (260) Yao, Z.; Kahne, D.; Kishony, R. *Mol. Cell*, **2012**, *48*, 705.
- (261) Bronzwaer, S. L. A. M.; Cars, O.; Buchholz, U.; Mölsted, S.; Goettsch, W.; Veldhuijzen, I. K.; Kool, J. L.; Sprenger, M. J. W.; Degener, J. E. *Emerg. Infect. Dis.* **2002**, *8*, 278.
- (262) Walsh, C. *Nature*, **2000**, *406*, 775.
- (263) Spratt, B. G. *Microbiology*, **1983**, *129*, 1247.
- (264) Davies, J.; Davies, D. *Microbiol. Mol. Biol. Rev.* **2010**, *74*, 417.
- (265) Bush, K. *Clin. Microbiol. Rev.* **1988**, *1*, 109.
- (266) Prashad, V. P. S.; Prashad, A. S. *Curr. Med. Chem.* **2002**, 1145.
- (267) Naas, T.; Oueslati, S.; Bonnin, R. A.; Dabos, M. L.; Zavala, A.; Dortet, L.; Retailleau, P.; Iorga, B. I. *J. Enzyme Inhib. Med. Chem.* **2017**, *32*, 917.
- (268) Surette, M. D.; Wright, G. D. *Annu. Rev. Microbiol.* **2017**, *71*, 309.
- (269) Brown, E. D.; Wright, G. D. *Nature*, **2016**, *529*, 336.
- (270) Bollenbach, T. *Curr. Opin. Microbiol.* **2015**, *27*, 1.

- (271) Reynolds, P. E. *Eur. J. Clin. Microbiol. Infect. Dis.* **1989**, 8, 943.
- (272) White, A. R.; Kaye, C.; Poupard, J.; Pypstra, R.; Woodnutt, G.; Wynne, B. J. *Antimicrob. Chemother.* **2004**, 53, 3.
- (273) Saudagar, P. S.; Survase, S. A.; Singhal, R. S. *Biotechnol. Adv.* **2008**, 26, 335.
- (274) Liras, P.; Rodríguez-García, A. *Appl. Microbiol. Biotechnol.* **2000**, 54, 467.
- (275) Brown, A. G.; Corbett, D. F.; Goodacre, J.; Harbridge, J. B.; Howarth, T. T.; Ponsford, R. J.; Stirling, I.; King, T. J. *J. Chem. Soc. Perkin Trans. 1.* **1984**, 10, 635.
- (276) Röhl, F.; Rabenhorst, J.; Zähler, H. *Arch. Microbiol.* **1987**, 147, 315.
- (277) Ambler, R. P.; Baddiley, J.; Abraham, E. P. *Philos. Trans. R. Soc. London. B, Biol. Sci.* **1980**, 289, 321.
- (278) Foulstone, M.; Reading, C. *Antimicrob. Agents Chemother.* **1982**, 22, 753.
- (279) Baggaley, K. H.; Brown, A. G.; Schofield, C. J. *Nat. Prod. Rep.* **1997**, 14, 309.
- (280) Howarth, T. T.; Brown, A. G.; King, T. J. *J. Chem. Soc. Chem. Commun.* **1976**, 7, 266.
- (281) Micetich, R. G.; Salama, S. M.; Maiti, S. N.; Reddy, A. V. N.; Singh, R. *Curr. Med. Chem.* **2002**, 1, 3.
- (282) Bush, K.; Jacoby, G. A.; Medeiros, A. A. *Antimicrob. Agents Chemother.* **1995**, 39, 1211.
- (283) Bush, K. *Antimicrob. Agents Chemother.* **1989**, 33, 271.
- (284) Richmond, M. H.; Sykes, R. B. *Adv. Microb. Physiol.* **1973**, 9, 31.
- (285) Sykes, R. B.; Matthew, M. J. *Antimicrob. Chemother.* **1976**, 2, 115.
- (286) Brem, J.; Cain, R.; Cahill, S.; McDonough, M. A.; Clifton, I. J.; Jiménez-Castellanos, J.-C.; Avison, M. B.; Spencer, J.; Fishwick, C. W. G.; Schofield, C. J. *Nat. Commun.* **2016**, 7, 12406.
- (287) Bebrone, C. *Biochem. Pharmacol.* **2007**, 74, 1686.
- (288) Walsh, T. R.; Toleman, M. A.; Poirel, L.; Nordmann, P. *Clin. Microbiol. Rev.* **2005**, 18, 306.

- (289) Page, M. I.; Badarau, A. *Bioinorg. Chem. Appl.* **2008**, *2008*, 576297.
- (290) Messerschmidt, A.; Bode, W.; Cygler, M. *Handbook of Metalloproteins*; Wiley-VCH: Weinheim, **2004**.
- (291) Therrien, C.; Levesque, R. C. *Microbiol. Rev.* **2000**, *24*, 251.
- (292) Drawz, S. M.; Bonomo, R. A. *Clin. Microbiol. Rev.* **2010**, *23*, 160.
- (293) Southgate, R. *Contemp. Org. Synth.* **1994**, *1*, 417.
- (294) Bentley, P. H.; Brooks, G.; Gilpin, M. L.; Hunt, E. *Tetrahedron Lett.* **1979**, *20*, 1889.
- (295) Bentley, P. H.; Berry, P. D.; Brooks, G.; Gilpin, M. L.; Hunt, E.; Zomaya, I. I. *J. Chem. Soc. Chem. Commun.* **1977**, *21*, 748.
- (296) Neto, A. B.; Hirata, D. B.; Cassiano Filho, L. C. M.; Bellao, A. C.; Badino, A. C.; Hokka, C. O. *J. Chem. Eng.* **2005**, *22*, 557.
- (297) Paradkar, A. *J. Antibiot.* **2013**, *66*, 411.
- (298) Song, J. Y.; Jensen, S. E.; Lee, K. J. *Appl. Microbiol. Biotechnol.* **2010**, *88*, 659.
- (299) Elson, S. W.; Oliver, R. S. *J. Antibiot.* **1978**, *31*, 586.
- (300) Flynn, E. H. *Cephalosporins and Penicillins: Chemistry and Biology*; Elsevier Science: Amsterdam, **2013**.
- (301) Jensen, S. E.; Paradkar, A. S. *Antonie Van Leeuwenhoek*, **1999**, *75*, 125.
- (302) E. Thirkettle, J.; E. Baldwin, J.; Edwards, J.; P. Griffin, J.; J. Schofield, C. *Chem. Commun.* **1997**, *11*, 1025.
- (303) Elson, S. W.; Baggaley, K. H.; Davison, M.; Fulston, M.; Nicholson, N. H.; Risbridger, G. D.; Tyler, J. W. *J. Chem. Soc. Chem. Commun.* **1993**, *15*, 1212.
- (304) Caines, M. E. C.; Sorensen, J. L.; Schofield, C. J. *Biochem. Biophys. Res. Commun.* **2009**, *385*, 512.
- (305) Ramirez-Malule, H.; Restrepo, A.; Cardona, W.; Junne, S.; Neubauer, P.; Rios-Esteva, R. *J. Theor. Biol.* **2016**, *395*, 40.

- (306) Arulanantham, H.; Kershaw, N. J.; Hewitson, K. S.; Hughes, C. E.; Thirkettle, J. E.; Schofield, C. J. *J. Biol. Chem.* **2006**, *281*, 279.
- (307) MacKenzie, A. K.; Kershaw, N. J.; Hernandez, H.; Robinson, C. V.; Schofield, C. J.; Andersson, I. *Biochemistry*, **2007**, *46*, 1523.
- (308) Li, R.; Townsend, C. A. *Metab. Eng.* **2006**, *8*, 240.
- (309) Chen, K.-C.; Lin, Y.-H.; Wu, J.-Y.; Hwang, S.-C. *J. Microb. Technol.* **2003**, *32*, 152.
- (310) Saudagar, P. S.; Singhal, R. S. *Appl. Biochem. Biotechnol.* **2007**, *136*, 345.
- (311) Barton, B.; Jensen, S.; Griffin, A. M.; Wong, A. WO2004092389, **2004**.
- (312) Neves, A. A.; Vieira, L. M.; Menezes, J. C. *Biotechnol. Bioeng.* **2001**, *72*, 628.
- (313) Hockenull, D. J. D. *Biochemistry of industrial microorganisms*; Academic Press: New York, **1963**.
- (314) Ser, H.-L.; Law, J. W.-F.; Chaiyakunapruk, N.; Jacob, S. A.; Palanisamy, U. D.; Chan, K.-G.; Goh, B.-H.; Lee, L.-H. *Front. Microbiol.* **2016**, *7*, 522.
- (315) Gouveia, E. R.; Baptista-Neto, A.; Badino Jr, A. C.; Hokka, C. O. *Biotechnol. Lett.* **2001**, *23*, 157.
- (316) Townsend, C. A.; Ho, M. F. *J. Am. Chem. Soc.* **1985**, *107*, 1066.
- (317) Rosa, J. C.; Neto, A. B.; Hokka, C. O.; Badino, A. C. *Bioprocess Biosyst. Eng.* **2005**, *27*, 99.
- (318) Alves, A. M. B.; Morão, A.; Cardoso, J. P. *Desalination*, **2002**, *148*, 181.
- (319) Li, S. Z.; Li, X. Y.; Cui, Z. F.; Wang, D. Z. *Sep. Purif. Technol.* **2004**, *34*, 115.
- (320) Ferry, J. D. *Chem. Rev.* **1936**, *18*, 373.
- (321) Sourirajan, S.; Agrawal, J. P. *Ind. Eng. Chem.* **1969**, *61*, 62.
- (322) Domínguez, J. R.; González, T.; Palo, P.; Cuerda-Correa, E. M. *Desalination*, **2011**, *269*, 231.
- (323) Barboza, M.; Almeida, R. M. R. G.; Hokka, C. O. *Biochem. Eng. J.* **2003**, *14*, 19.

- (324) Ruddick, S. EP0804441, **2004**.
- (325) Fernandez, J. L. EP0312813A2, **1985**.
- (326) Hirata, D. B.; Oliveira, J. H. H. L.; Rodrigues, M. I.; Ferreira, A. G.; Giulietti, M.; Barboza, M.; Hokka, C. O. *Brazilian J. Chem. Eng.* **2013**, *30*, 231.
- (327) Zhang, G.; McKnight, J. EP1284978, **2008**.
- (328) Santos, V. C.; Pereira, J. F. B.; Haga, R. B.; Rangel-Yagui, C. O.; Teixeira, J. A. C.; Converti, A.; Pessoa, A. *Biochem. Eng. J.* **2009**, *45*, 89.
- (329) Finn, M. J.; Harris, M. A.; Hunt, E.; Zomaya, I. I. *J. Chem. Soc. Perkin Trans. I*, **1984**, 0, 1345.
- (330) Haginaka, J. U. N.; Yasuda, H.; Uno, T.; Nakagawa, T. *Chem. Pharm. Bull.* **1985**, *33*, 218.
- (331) Bersanetti, P. A.; Almeida, R. M. R. G.; Barboza, M.; Araújo, M. L. G. C.; Hokka, C. O. *Biochem. Eng. J.* **2005**, *23*, 31.
- (332) Bird, A. E.; Bellis, J. M.; Gasson, B. C. *Analyst*, **1982**, *107*, 1241.
- (333) Mayer, A. F.; Deckwer, W.-D. *Appl. Microbiol. Biotechnol.* **1996**, *45*, 41.
- (334) Roubos, J. A.; Krabben, P.; Laat, W. T. A. M. de; Babuška, R.; Heijnen, J. J. *Biotechnol. Prog.* **2002**, *18*, 451.
- (335) Cielecka-Piontek, J.; Paczowska, M.; Zalewski, P.; Lewandowska, K.; Barszcz, B. *Pharm. Dev. Technol.* **2015**, *20*, 146.
- (336) Frau, J.; Coll, M.; Donoso, J.; Muñoz, F.; Vilanova, B.; García-Blanco, F. J. *Theor. Chem.* **1997**, *2*, 56.
- (337) Page, M. I. *Curr. Pharm. Des.* **1999**, *5*, 898.
- (338) Fife, T. H.; Hutchins, J. E. C. *J. Org. Chem.* **1980**, *45*, 2099.
- (339) Bergmann, E. D. *Chem. Rev.* **1953**, *53*, 309.
- (340) Fife, T. H.; Hagopian, L. *J. Am. Chem. Soc.* **1968**, *90*, 1007.
- (341) Hanson, R. W. *J. Chem. Educ.* **1987**, *64*, 591.

- (342) Hoizey, G.; Lamiable, D.; Frances, C.; Trenque, T.; Kaltenbach, M.; Denis, J.; Millart, H. *J. Pharm. Biomed. Anal.* **2002**, *30*, 661.
- (343) Aguilar, M.-I. *HPLC of Peptides and Proteins: Methods and Protocols*; Aguilar, M.-I., Ed.; Springer New York: New Jersey, **2004**.
- (344) Engelhardt, H.; Dreyer, B.; Schmidt, H. *Chromatographia*, **1982**, *16*, 11.
- (345) Foroutan, S. M.; Zarghi, A.; Shafaati, A.; Khoddam, A.; Movahed, H. *J. Pharm. Biomed. Anal.* **2007**, *45*, 531.
- (346) Brethauer, S.; Held, M.; Panke, S. *J. Pharm. Sci.* **2008**, *97*, 3451.
- (347) Huynh-Ba, K.; Zahn, M. *Handbook of Stability Testing in Pharmaceutical Development: Regulations, Methodologies, and Best Practices*; Huynh-Ba, K., Ed.; Springer New York: New York, **2009**.
- (348) Singh, S.; Junwal, M.; Modhe, G.; Tiwari, H.; Kurmi, M.; Parashar, N.; Sidduri, P. *Trends Anal. Chem.* **2013**, *49*, 71.
- (349) Foti, C.; Alsante, K.; Cheng, G.; Zelesky, T.; Zell, M. *Trends Anal. Chem.* **2013**, *49*, 89.
- (350) Ludvigsson, J. wu; Andersson, T.; Kjellberg, V. *J. Pharm. Biomed. Anal.* **2016**, *122*, 9.
- (351) Perry, C. S.; Charman, S. A.; Prankerd, R. J.; Chiu, F. C. K.; Dong, Y.; Vennerstrom, J. L.; Charman, W. N. *J. Pharm. Sci.* **2006**, *95*, 737.
- (352) Thormann, U.; De Mieri, M.; Neuburger, M.; Verjee, S.; Altmann, P.; Hamburger, M.; Imanidis, G. *J. Pharm. Sci.* **2014**, *103*, 3139.
- (353) Fulmer, G. R.; Miller, A. J. M.; Sherden, N. H.; Gottlieb, H. E.; Nudelman, A.; Stoltz, B. M.; Bercaw, J. E.; Goldberg, K. I. *Organometallics*, **2010**, *29*, 2176.